Structural Behaviour of Timber Concrete Composite Connections and Floors utilising Screw Connectors

A thesis submitted in fulfilment
of the requirement for the degree of
Doctor of Philosophy

By

Farzad Moshiri

Faculty of Engineering and Information Technology
University of Technology Sydney (UTS)

December 2014

To My Beloved Wife:

Azi

CERTIFICATE OF ORIGINAL AUTHORSHIP

I certify that the work in this thesis has not previously been submitted for a degree nor has it been submitted as part of requirements for a degree except as fully acknowledged within the text.

I also certify that the thesis has been written by me. Any help that I have received in my research work and the preparation of the thesis itself has been acknowledged. In addition, I certify that all information sources and literature used are indicated in the thesis.

Signature of Candidate

(Farzad Moshiri)

Sydney, December 2014

ACKNOWLEDGEMENT

I would like to express my gratitude to those who have supported me throughout my study and helped make this PhD research possible.

First of all, I am extremely grateful to my principal supervisor, Prof Keith Crews, for supporting me during the past five years. Keith has been supportive and has given me the freedom to pursue various projects without objection. He has also provided insightful discussions about the research.

I will forever be thankful to Dr Rijun Shretsha. Rijun has been helpful in providing advice many times during my journey. His encouragement, guidance and unfailing assistance throughout this study are deeply appreciated. I also thank my former co-supervisor, Dr Hamid Valipour, for his help and teaching while he worked at UTS. I am also very grateful to Dr Christophe Gerber for his scientific advice and knowledge and many insightful discussions and suggestions.

I also have to thank Prof Bijan Samali, the former head of school of Civil and Environmental Engineering at the University of Technology, Sydney for his helpful career advice, outstanding guidance, motivation, wisdom and caring support provided throughout my PhD.

I gratefully acknowledge the financial assistance provided by Structural Timber Innovation Company (STIC). Also, the financial assistance provided by University of Technology Sydney (UTS) as International Research Scholarship, and all administrative and technical support provided by the Faculty of Engineering and Information Technology at UTS is appreciated.

I wish to acknowledge my colleagues, especially those involved in this project such as Nima Khorsandnia, Zhinus Zabihi, Rajendra Rijal, Matthew Holmes and Mulugheta Hailu for providing generous help during this study.

Special thanks to the UTS laboratory staff (Rami Haddad, Peter Brown, David Dicker, David Hopper and other lab assistants) for their great efforts in providing technical support and assistance for all of my experimental tests. I would also like to thank final

year students who completed their final year theses as part of the STIC project (Chris Garvan, Jarod Wakefield, Adam Iverach, Benjamin Chen, Tim Kurniadi, Zhuoran Chen and Angus Lumsden) for their support in completing the tests.

A special thanks to my family. Words cannot express how grateful I am to my brothers, my sister, my mother, and father for all of the sacrifices that they have made on my behalf. Their steadfastness and hardworking sprit was always a source of inspiration for me to aim high and to pursue my dreams. Their prayer for me was what sustained me thus far. I would also like to thank all of my friends who supported me in writing, and incented me to strive towards my goal.

This last word of acknowledgment I have saved for my beloved wife Azi, who has been with me all these years and has made them the best years of my life. Thanks a lot and I always love you.

"In your light I learn how to love. In your beauty, how to make poems. You dance inside my chest where no-one sees you, but sometimes I do, and that sight becomes this art."
— Rumi

Farzad Moshiri
December 2014

ABSTRACT

The traditional materials such as reinforced concrete and structural steel have been widely used in the construction market. These construction materials produce a large quantity of greenhouse gases as a by-product. An environmentally sustainable solution to decrease the production of greenhouse gases is creation of composites with other materials such as timber to reduce the amount of steel and concrete used in construction.

Timber-concrete composites (TCC) structures, extends upon this by combining timber and concrete in order to form a composite structural member that utilises the properties of both materials. Since the 1990s, Timber Concrete Composite (TCC) floors have been gaining wider recognition as being a viable and effective alternative to both reinforced concrete and traditional timber floors. TCCs are a structural form whereby a concrete slab is fixed to a timber joist at the interface using a suitable shear connector which transfers shear forces and impedes slip between concrete and timber. Hence, the strength, stiffness, location and number of shear connectors used at the composite interface are the key factors in determining the composite action, the strength and stiffness of a TCC system. TCC exploits the mechanical properties of each material favourably with the concrete in compression and the timber in tension. TCCs have several advantages over full timber construction, including improved strength (double), stiffness (triple), vibration control, fire performance and thermal and sound insulation. TCCs also have advantages compared to full concrete construction, including a much higher load capacity per unit of self-weight and a lower embodied energy.

Mechanical fasteners for example screw and dowel TCC connectors are relatively simple and easy to install, cost effective and structurally efficient connectors with lower labour requirement. With these considerations, mechanical fasteners can be preassembled in prefabrication or cast in situ TCC solutions. Hence, application of mechanical fasteners in TCCs overcomes the drawbacks of alternative connection such as notch type connection and reduces the time required to construct a TCC system.

This research investigates the experimental parametric study on the effect of different types of high-performance concrete on mechanical properties of TCC connections and

floors using locally available materials in Australia to evaluate their potential for use in the construction market. A parametric study of mechanical fasteners such as crossed SFS VB, crossed SPAX and coach screws connections in different lengths (short and long SFS VB), angles (±30°, ±45° and ±60°) to the connection face and a number of crossed SFS VB and SPAX at 45° series utilising 17mm plywood formwork interlayer and different types of concrete was carried out. Hence, the effects of connector type, inclination angle and length of screw and existence of plywood interlayer on mechanical properties of the TCC connections were investigated. Moreover, two innovative TCC shear connection systems were put forward and assessed for their suitability as a substitute or replacement for existing connection systems using push-out test.

The application of high-performance concrete such as light-weight concrete and self-consolidating concrete provides a great deal of benefits in TCC technology to minimize the dead-load on the timber component or increase the concrete workability and accelerate the process of pouring. Such weight reduction and increased workability may be favourable in the renovation of old timber floors. The use of TCC technology is also advantageous in new multi-storey buildings for aspects such as prefabrication and mitigation of excess dead load – leading to saving on foundation and walls and/or column sizes.

This research investigates the effect of different types of high-performance concrete on the mechanical properties of TCC connections and floors using locally available materials in Australia to evaluate their potential for use in construction market.

Push-out test was used to determine the mechanical properties and failure modes of shear connections and once the mechanical properties of connection type were identified, full-scale TCC modules utilising different types of shear connector and concrete properties were subjected to four-point bending tests. Hence, the predictions of full beam behaviour using the connection properties were validated and the effect of shear connection and concrete type on structural behaviour of an entire floor was investigated.

Literature reports a significant lack of information on analytical closed-form equations to predict the strength and stiffness of TCC connections utilising vertical and inclined fasteners to be used in the design of timber composite beams.

This study reviewed the methodology of available analytical models for prediction of the strength and serviceability stiffness of vertically inserted single timber to timber and TCC shear connections and validated their accuracy using the experimental push-out test results. Moreover, an analytical strength model based on some adjustment to EYM to predict the strength of TCC connections utilising single and crossed screws inclined to the timber grain was proposed. This research also presented a model for the stiffness of TCC connections using crossed inclined screws. The Winkler theory of beam on elastic foundation proposed was extended to derive the serviceability slip modulus of TCC connections with inclined screws which were loaded in tension and compression.

In addition, a 3-D FE model has been put forward to simulate different TCC connections such as single and multiple wood screws and inclined coach screw utilising the commercial FE analysis software ANSYS. The findings of this part demonstrate that by using a simple numerical model, the behaviour of TCC connections can be accurately modelled and can therefore be used for parametric study of changes in end distance, edge distance, member thickness, screw diameter, screw length and number of screws.

LIST OF CONTENTS

LIST OF FIGURES

LIST OF TABLES

NOMENCLATURE

a	Unknown parameter used in mathematical model
a	Distance between support and load in four-point bending test (l/3)
a_1	Fastener spacing
a_2	Fastener spacing between rows
$a_{3,t}$	End distance in a row (loaded end)
$a_{3,c}$	End distance in a row (loaded edge)
$a_{4,t}$	Edge distance in a row (loaded edge)
$a_{4,c}$	Edge distance in a row (unloaded edge)
a_1	Distance between centroids of concrete floor and effective TCCs
a_2	Distance between centroids of timber webs and effective TCCs
a_3	Distance between centroids of timber flange and effective TCCs
A	Section area
A	Section area of steel fastener
A_t	Section area of timber member
Anal.	Analytical
AS	Australian Standards
A_α	Cross-sectional area of the fastener at the timber-concrete interface
b	Unknown parameter used in mathematical model
b_2	Width of the LVL web
B_i	Constant coefficients based on the compatibility conditions
b_w	Web width

b_{ef}	Effective width in TCC section
c	Unknown parameter used in mathematical model
CC	Conventional concrete
CoV	Coefficient of variation
$cos\alpha$	Cosine function of angle α
$cosh\alpha$	Hyperbolic cosine function of angle α
d	Diameter of screw including thread
dx	Part of a screw of length
d_1	Major diameter of screw
d_2	Core diameter of screw
d_{ef}	Effective diameter equal to 0.75 times the fastener diameter
d_k	Head diameter of screw
d_s	Shank diameter of screw
D_N	Theoretical fully non-composite deflection
D_I	Measured deflection for partially composite action
D_C	Theoretical full-composite deflection
D_f	Ductility as the ratio of ultimate to yield deformations
D_u	Ductility as the ratio of slip at maximum load to yield slip
DCA	Degree of composite action in composite system
DLWC	Dry light-weight concrete
e/d	End distance to diameter ratio of fasteners
E	Napier's constant
E	Modulus of Elasticity
EC5	Eurocode 5
E_c	Modulus of elasticity of concrete
$E_{c,m}$	Mean Modulus of Elasticity of concrete
E_s	Modulus of elasticity of steel shear connector
E_t	Modulus of elasticity of timber
E_x	Elastic modulus in the tangential direction
E_y	Elastic modulus in the longitudinal direction
E_z	Elastic modulus in the radial direction
$E_{\tau x}$	Tangent moduli (tensile and compressive) in the x direction
$E_{\tau y}$	Tangent moduli (tensile and compressive) in the y direction

$E_{\tau z}$	Tangent moduli (tensile and compressive) in the z direction
$E_{t,\alpha}$	Modulus of elasticity of timber in parallel and perpendicular directions
E_T	Tangent modulus
EI	Apparent stiffness of timber composite module
EI_{eff}	Effective bending stiffness of timber composite module
EPS	Expanded polystyrene
EPS LWC	Expanded polystyrene light-weight concrete
Exp.	Experiment/experimental
EYM	European yield model
f	Vector of surface load
F	Shear force in the connector
FE	Finite element
F_p	Shear force in the connector parallel to the grain
F_t	Shear force in the connector transverse to the grain
$f_{a,0}$	Withdrawal strength of screw inserted parallel to the grain
$f_{a,\alpha}$	Withdrawal strength of screw inserted at an angle of α to the grain
$f_{ax,k}$	Characteristic withdrawal strength perpendicular to the grain
f_b	Bending stress
f(i)	Load capacity of failure mode i
f_m	Bending strength of the timber flange in TCC section
f_t	Tension strength of the timber flange in TCC section
f_c	Uniaxial crushing stress of concrete
f_t	Uniaxial tensile cracking stress of concrete
$f_{t\text{-}t}$	Failure load at interface of timber-timber connection
f_c	Compression strength of the timber flange in TCC section
f_{cb}	Biaxial crushing stress of concrete
f_1	Biaxial crushing stress under the ambient hydrostatic stress state
f_2	Uniaxial crushing stress under the ambient hydrostatic stress state
$f_{c,m}$	Mean compressive strength of concrete
$f_{c,i}$	Mean compressive strength of concrete at age of i day (i=3,7 and 28)
$f_{ct.sp,i}$	Mean indirect tensile strength of concrete at age of i day (i=3,7 and 28)
f_p	Stress in compression perpendicular to grain
$f_{h,\alpha}$	Embedment strength of timber at an angle of α to the grain

$f_{h,d}$	Designed embedment strength of timber
$f_{h,0}$	Embedment strength of timber parallel to the grain
$f_{h,0,k}$	Characteristic embedment strength of timber parallel to the grain
$f_{h,i,k}$	Characteristic embedment strength in timber member i
$f_{h,k}$	Embedment strength of the timber and mechanical fastener
f_u	Ultimate tensile stress of fastener
$f_{c,w}$	Design compressive strength of the timber web in TCC section
f_m	Flexibility matrix of the beam on the elastic foundation
f_s	Stress in longitudinal shear LVL hySPAN project
$f_{t,w}$	Design tensile bending strengths of the timber web in TCC section
f_v	Design planar shear strength of the web in TCC section
f_y	Tangent modulus
f'_b	Bending strength of plywood
f'_c	Stress in compression in the plane of the sheet in plywood
f'_p	Stress in compression normal to the plane of the sheet in plywood
f'_s	Shear stress of plywood
f'_t	Tension strength of plywood
$F_{ax,\alpha}$	Axial withdrawal load capacity of inclined fastener
$F_{ax,Rk}$	Characteristic axial withdrawal capacity of the fastener
F_{ave}	Average load applied to the module at third-spans
$F_{LoadCell}$	Applied load in each loadcell
F_{lat}	Elastic forces acting perpendicular to the axis of fastener
F_{ax}	Elastic forces acting parallel to the axis of fastener
F_{est}	Estimated maximum load
F_{max}	Load carrying capacity
$F_{multiple}$	Load carrying capacity of the multiple fasteners
F_{single}	Characteristic load carrying capacity of single fastener
F_{ser}	Lateral load at SLS
F_u	Ultimate tensile capacity of screw
$F_{V,Rk}$	Characteristic load-carrying capacity per shear plane per fastener
FRC	Fibre reinforced concrete
Full C.	Full composite
FKN	Normal contact stiffness factor in ANSYS

FKT	Contact stiffness factor in ANSYS
FTOLN	Allowable penetration in ANSYS
h_1	Depth of the concrete slab
h_2	Depth of the timber web
h_3	Depth of the timber bottom flange
h_{ef}	Effective depth in box shape TCC section
$h_{f,c}$	Depth of compression flange in box shape TCC section
$h_{f,t}$	Depth of tension flange in box shape TCC section
HPC	High-performance concrete
HSC	High-strength concrete
I	Second moment of area of TCC section
I_s	Second moment of area of steel connector
I	With interlayer
I_c	Second moment of area for concrete slab
I_t	Second moment of area for timber joist
G	Modulus of Rigidity
G	Permanent action (self-weight or 'dead load')
G_{xy}	Shear modulus in the xy plane
G_{yz}	Shear modulus in the yz plane
G_{xz}	Shear modulus in the xz plane
Gτxy	Tangent modulus (shear) corresponding to the *xy* plane
Gτyz	Tangent modulus (shear) corresponding to the *yz* plane
Gτxz	Tangent modulus (shear) corresponding to the *xz* plane
J_i	Parameter of member i in stiffness model proposed by Kuenzi (1955)
kN	Kilo newton
k	Foundation modulus of material
k_1	Smeared slip modulus of shear connection
k_d	Minimum of $d/8$ and 1
K	Slip modulus of shear connection
K	Global stiffness of the timber composite module
K	Stiffness matrix
K_i	Parameter of member i in stiffness model proposed by Kuenzi (1955)
K_s	Serviceability slip modulus of shear connection

$K_{s,0.4}$	Serviceability slip modulus of shear connection
$K_{u,0.6}$	Ultimate slip modulus of shear connection
$K_{u,0.8}$	Slip modulus of shear connection corresponding to $0.8F_{max}$
$K_{\perp}$	Stiffness of connector for lateral loading
$K_{\parallel}$	Stiffness of connector for withdrawal loading
$\hat{K}$	Non-dimensional stiffness by Symons, Persaud and Stanislaus (2010a)
k_c	Lateral instability factor in design of timber composite in compression
k_c	Foundation modulus of concrete
k_t	Foundation modulus of timber
k_p	Foundation moduli of timber parallel to the grain
k_t	Foundation moduli of timber transverse to the grain
LVDT	Linear variable differential transformer
l	Span length of the beam
L	Screw length
L_i	Parameter of member i in stiffness model proposed by Kuenzi (1955)
l_{ef}	Penetration length of the threaded part for mechanical fastener, *t-d*
L- L_s	Threaded length of screw
LVL	Laminated veneer lumber
LWC	Light-weight concrete
mm	Millimetres
MPa	Mega Pascal
M	Bending moment transferred between timber and concrete in TCCs
M_1	Internal moment on the free end of the beam on the elastic foundation
M_{exp}	Experimental bending moment obtained from four-point bending test
M_u	Bending moment due to factored loads in TCCs
M_y	Yield moment of fastener
$M_{y,Rk}$	Characteristic fastener yield moment
MOE	Modulus of elasticity
MOR	Module of rupture
n	Number of fastener
n_{ef}	Effective number of fastener
N	Shear force transferred between timber and concrete
N	Shape function matrix

$N_{d,,j}$	Design capacity of connection
Non C.	Non-composite
NSW	New South Wales
NZS	New Zealand Standards
p	Thread pitch of screw
PVA	Polyvinyl alcohol-fibres
q	Shear flow of the TCC section
q_m	Matrix of actual displacements corresponding to the redundant
q_{om}	Matrix of actual displacements of the redundant action, due to the loads
Q_k	The 5th percentile strength
Q	First moment of area for concrete slab in TCC section
Q	Imposed action for each occupancy class
Q_k	Characteristic capacity of screw
Q_m	Matrix of redundant
R	Sample correlation coefficient
R	Collapse load in TCC connection
RH	Relative humidity
s	Connectors spacing
S	Surface
S_F	Part of the surface
s_e	Connectors spacing at the beam-ends
s_m	Connectors spacing at
$sin\alpha$	Sine function of angle α
$sinh\alpha$	Hyperbolic sine function of angle α
SCC	Self-consolidating concrete
SFRC	Steel fibres reinforce concrete
SG	Strain gauge
SLS	Serviceability limit state
STIC	Structural Timber Innovation Company
$t(x)$	Shear flow along the beam length
t	Timber thickness or the embedded length of fastener in timber
t	Traction vector
t_1	Head side thickness of fastener in a single shear connection

t_2	Point side penetration in a single shear connection
$t_{0.1}$	Value in standard for (n − 1) degrees of freedom and a probability of 0.1
T	Temperature
$tan\alpha$	Tangent function of angle α
t/d	Slenderness ratio (fastener depth/fastener diameter)
$\hat{t}$	Non-dimensional embedment (embedment depth/fastener diameter)
TCC	Timber-concrete composite
u	Displacement vector
u_d	Small slip design in design of TCC shear connector
UEA	Unequal angle
UTS	University of Technology, Sydney
ULS	Ultimate limit state
V	Shear force transferred between timber and concrete in TCC connector
V	Volume
V_1	Internal load acting on the free end of the beam on the elastic foundation
V_b	Maximum shear force at beam-end in design of TCC connectors
$V(x)$	Shear force in the cross-section of TCC along the beam
V_{sd}	Design shear force at connection in TCC modules
W_{eq}	Equivalent uniformly distributed load
W_E	External work done by the external force in a TCC connection
W_I	Internal energy in a TCC connection
WI	Without interlayer
x	Length parameter of fastener
y	Elastic transverse deformations of a connection on elastic foundation
$y_{5percent}$	5^{th} percentiles of the lower probability limit
y_{ij}	Deformation array in flexibility matrix of the beam
$y(x)$	Elastic deformations of a timber connection at point x along the fastener
y_{10}	Slip at interface of materials
Z	Foundation depth
π	pi
π	Total potential energy
β	Ratio between embedment strength of timber members
β	Factor as a function of the fastener's diameter to spacing ratio

β	Ratio of of k_t/k_p
β	coefficient in Canadian standard
θ	Inclination angle of fastener to the vertical direction (90- α)
α	Inclination angle of fastener to the horizontal direction (90- θ)
θ_{ij}	Rotation array in flexibility matrix of the beam
θ_{20}	Rotation at interface of materials
δ	Mid-span deflection of a simply supported composite beam
$\delta\perp$	Perpendicular component of slip in shear connector
$\delta \parallel$	Parallel components of slip in shear connector
Δ_p	Slip component parallel to the grain
Δ_t	Slip component transverse to the grain
Δ	Slip at interface of timber composite connection
Δ_{ax}	Axial displacement of fastener
Δ_{lat}	Slip at the interface of the concrete and timber in a TCC connection
σ	Standard deviation
σ	Stress
σ^a_h	Ambient hydrostatic stress state of concrete
σ_x	Yield stresses (tensile and compressive) in the *x* direction
σ_y	Yield stresses (tensile and compressive) in the *y* direction
σ_z	Yield stresses (tensile and compressive) in the *z* direction
σ_i	Axial stress in TCC section
$\sigma_{b,i}$	Bending stress in TCC section
$\sigma_{i,b}$	Total normal stresses in TCC section
$\sigma_{f,c,max}$	Extreme fibre flange design compressive stress in TCC section
$\sigma_{f,t,max}$	Extreme fibre flange design tensile stress in TCC section
$\sigma_{w,c,d}$	Design compressive stress of the timber web in TCC section
$\sigma_{w,t,d}$	Design tensile stress of the timber web in TCC section
$\sigma_{f,c}$	Mean flange design compressive stress in TCC section
$\sigma_{f,t}$	Mean flange design tensile stress in TCC section
$\sigma_{2,N}$	Tensile and bending stresses of timber in TCC section
$\sigma_{2,M}$	Bending stresses of timber in TCC section
σ_y	Shear yield stress of the fastener

σ_y	Yield stress
ε	Strain
Υ	Shear bond coefficient
Υ_v	Material safety factor
λi	Parameter of member i in stiffness model proposed by Kuenzi (1955)
v	slip at interface of composite materials
v	Axial deformations of a connection on elastic foundation
v_0	Axial deformations of a connection on elastic foundation at (x=0)
v_i	Slip measurement at specified points
v_y	Elastic deformation of connector
v_u	Slip corresponding to maximum load at connection
v_f	Deformation associated to load-drop (80% of the maximum load)
υ	Poisson's ratio
v_{xy}	Poisson's ratio in the xy plane
v_{yz}	Poisson's ratio in the yz plane
v_{xz}	Poisson's ratio in the xz plane
τ_{mean}	Design shear stress in TCC section
$\tau_{2,max}$	Maximum shear stress in the web of a box shape TCC section
τ_{xy}	Shear yield stress in the *xy* plane
τ_{yz}	Shear yield stress in the *yz* plane
τ_{xz}	Shear yield stress in the *xz* plane
ρ	Mass per unit volume
ρ_k	Characteristic mass per unit volume of timber
ρ_m	Mean mass per unit volume of timber
Φ	Capacity factor
2-D	Two dimensional
3-D	Three dimensional

1 INTRODUCTION

1.1 BACK GROUND

The traditional materials such as reinforced concrete and structural steel have been widely used in the construction market. These construction materials produce a large quantity of greenhouse gases as a by-product. An environmentally sustainable solution to decrease the production of greenhouses gasses is creation of composites with other materials such as timber to reduce the amount of steel and concrete used in construction.

Timber as a carbon-neutral material with low embodied energy and CO_2 emissions has a wide variety of applications in construction and engineering, from typical residential frames to its use as a decorative facade and as a structural system, such as for large-span roof trusses and floors (Yeoh et al. 2010). The key benefits of using timber in constructions such as timber floors includes significantly reduced dead-load and thus, higher efficiency in terms of the carried load per unit self-weight which leads to reduction of the gravity load on the foundation, seismic action and hence in the size or number of structural members (Branco et al. 2007; Ceccotti 2002). However, there are some limitations of timber only floors-mainly fire safety performance and thermal and noise insulations for both air-transmitted and impact noise insulation Yeoh (2010).

Medium rise residential and commercial buildings (up to eight stories) are potential markets for advanced engineered wood product and timber composite structures (Crews et al. 2010b). Timber-concrete composites (TCC) structures, extends upon this by

combining timber and concrete in order to form a composite structural member that utilises the properties of both materials.

The concept of using timber compositely with other materials has been around for centuries, with timber floor designs from the middle age being constructed from timber floors overlayed by a stone mortar mixture. However, the TCC system as it is known today, was first developed during the 1920s due to the shortage of steel following the First World War. Over the last two decades, TCC system has regained popularity as a viable alternative to existing structural systems, particularly in Europe where it has been used for the renovation of existing timber floors and as a deck system for timber bridges (Van der Linden 1999).

Composite action between timber and concrete in TCC system is achieved through the use of shear connectors between the concrete and timber interface. A stiffer connector results in a stiffer and stronger TCC system. TCCs have a number of advantages over alternative structural forms. With the push towards sustainable technologies and green design, TCCs present themselves as a viable construction material, with a lower embodied energy than that of steel or reinforced concrete structures.

Mechanical fasteners such as screw and dowel TCC connectors are relatively simple and easy to install, cost effective and structurally efficient connector with lower labour requirement. With these considerations, mechanical fastener can be preassembled in prefabrication or cast in situ TCC solutions. Hence, the application of mechanical fastener in TCCs overcomes the drawbacks of the alternative connections for example notch type connection and reduces the time required to construct a TCC system.

This research investigates the experimental parametric study on the effect of different types of high-performance concrete on the mechanical properties of the TCC connections and floors using locally available materials in Australia to evaluate their potential for use in construction market.

1.2 STRUCTURAL TIMBER INNOVATION COMPANY (STIC)

Structural Timber Innovation Company (STIC) is a research consortium which was formed to develop and commercialise new technologies to enable structural timber to compete more effectively with concrete and steel in the Australian and New Zealand construction market (STIC 2009).

STIC consists of seven shareholders: Carter Holt Harvey Ltd, Nelson Pine Industries Ltd, Wesbeam Pty Ltd, Building Research Association New Zealand Inc, NZ Pine Manufacturers Association, Auckland Uniservices Ltd (University of Auckland) and University of Canterbury. Additionally, there are two major financial stakeholders- Forest and Wood Products Australia (FWPA) and Foundation for Research Science and Technology (FRST).

STIC conducted research and development (R & D) in three parallel objectives at three universities aiming to develop design guidelines, analysis packages, and recommendations and supporting data sets for construction market in New Zealand and Australia. University of Technology, Sydney is part of STIC's R & D project with the focus on the flooring system, mainly the long-span TCC and timber only floors for multi-storey timber buildings. This thesis focuses on assessing "the structural performance of the TCC connections and modules utilising different types of shear connection and high performance concrete", which is one of the sub-objectives of the STIC project at UTS.

1.3 RESEARCH OBJECTIVES

The main focus of this doctoral research is to study and quantify the behaviour of different types of particularly screw type connections such as SFS and SPAX screws and high performance concrete for example light-weight concrete for their practical application in the medium to large span TCC floors of the multi-storey buildings.

In view of this broad aim, the main objectives of this research are as follows:

(1) Identify the alternative TCC connector designs and arrangements in terms of the basic criteria of the strength, stiffness, ductility and ease of manufacturing and deliver recommendations regarding the economy, functionality and constructability of the alternative TCC connections;

(2) Study the effect of high performance concrete including Scoria light-weight concrete, EPS light-weight concrete and self-consolidating concrete on strength, stiffness and ductility of shear connector;

(3) Investigate the short-term serviceability and ultimate limit state behaviour of the TCC modules, the effects of concrete strength and the shear connections on response of the TCC modules;

(4) Evaluate the structural efficiency of the TCC floors utilising EPS light-weight concrete;

(5) Put forward the analytical models to predict the stiffness and strength of the mechanical fastener shear connections such as the inclined screw based on the possible modes of failure;

(6) Propose and verify the numerical finite element models to predict the mechanical properties of different types of mechanical fastener shear connection based on the possible failure modes;

(7) Propose and verify the numerical finite element models to predict the mechanical properties of different types of mechanical fastener shear connection based on different possible failure modes;

(8) Study the effect of the screws spacing on the stiffness, strength, ductility and failure mode of the TCC connections for their practical application in the design of TCC floor;

1.4 SCOPE OF THE STUDY

This PhD thesis investigates the behaviour of different types of shear connection and high performance concrete for example LWC and SCC for their application in medium to large span TCC floors of the multi-storey buildings. The scope of the research is as follows:

(1) Short-term behaviour: the behavioural response of the connections and floor beams defined by the collapse test with the application of static load;

(2) Floor beams: the simply supported beam as one side pin and the other roller, single span of TCC beams, the beams can be defined as T-shape or box-shape;

(3) Connection: the connection between the timber and concrete to transfer the shear force;

(4) Timber: laminated veneer lumber (LVL);

(5) Concrete: conventional concrete, expanded polystyrene light-weight concrete (EPS LWC) (two density classes of 1600kg/m^{3}and 2000kg/m^3), Scoria light-weight concrete (density class of 2000kg/m^3), self-consolidating concrete (SCC) and high strength concrete (HSC) with the main criteria of low shrinkage and availability in Australia;

1.5 RESEARCH METHODOLOGY

LVL was utilised in this study due to its availability, feasibility and cost efficiency in Australia and New-Zealand markets for long span flooring system where other engineered wood products such as Cross Laminated Timber (CLT) and glue laminated timber (glulam) are not commonly used in Australia and New-Zealand. Moreover, the natural defects in wood are minimised for LVL and hence, the mechanical properties of LVL is improved which results in a consistent and reliable construction material. The tensile strength of LVL is approximately three times that of sawn timber from the same forest. LVL is considered to be a high strength wood product and is used primarily as structural elements such as beams, truss members, lintels and purlins. The grains of each individual veneer are aligned in the same direction prior to the lamination which provides the finished LVL product with orthotropic properties and makes it stronger in parallel to the grain direction.

Push-out test was used to determine the mechanical properties and failure mode of crossed SFS VB, crossed SPAX and coach screws connections in different lengths (short and long SFS VB), angles (±30°, ±45° and ±60°) to the connection face and a number of crossed SFS VB and SPAX at 45° series utilising 17mm plywood formwork interlayer and different types of concrete. Hence, the effects of the connector type, inclination angle and length of screw and the existence of plywood interlayer on the mechanical properties of the TCC connections were investigated utilising the push-out test results of different test series. Moreover, two innovative TCC shear connection systems were put forward and assessed for their suitability as a substitute or replacement for the existing connection systems.

Once the mechanical properties of the connection type were identified, full-scale TCC modules utilising crossed SFS screws inclined at ±45° and conventional and EPS light-weight concretes were subjected to the four-point bending tests. Hence, the predictions of the full beam behaviour using the connection properties were validated and the effects of the shear connection and concrete type on the structural behaviour of an entire floor was investigated.

This study reviewed the methodology of the analytical models for prediction of the strength and serviceability slip modulus of vertically inserted single timber to timber and TCC shear connections and validated their accuracy using experimental push-out

test results. Moreover, an analytical strength model based on some adjustment to EYM to predict the strength of TCC connections utilising single and crossed screws inclined to the timber grain has been proposed. This research also presents a model for the stiffness of TCC connections using crossed inclined screws. The Winkler theory of beam on elastic foundation proposed was extended to derive the serviceability slip modulus of TCC connections with inclined screws which are loaded in tension and compression.

Finite element (FE) method is used as a numerical technique to investigate the behaviour of structures subjected to external and internal loads by the means of dividing it into several elements. The response of each element is determined by connecting elements at nodes. The finite element (FE) as a computation tool is preferred by engineers due to its cost and time efficiency compared to the experiments.

This PhD study presented a non-linear three-dimensional FE model using flexible contact element pairs to simulate the experimental tests of the TCC connections reported in Chapters 5 and 10 utilising the commercial FE analysis software ANSYS, versions 14.5 and 15.0. A three-dimensional FE of the timber concrete composite connection is capable of predicting the effects of different parameters for example fastener slenderness ratio, fastener spacing in multiple-fastener connection, non-linear orthotropic properties of the timber composite, elasto-plastic behaviour of the fastener and concrete components.

Connections with single and multiple four wood screws with three different spacing of 50, 100 and 150mm and single medium size coach screw inclined at +45° to the horizontal face were modelled. The modelling approach can be applied to TCC connections other than simple screws only such as epoxy glue and epoxy glue reinforced with normal coach screw.

Results from FE models were validated by experimental results of push-out test. The push-out test of different TCC connection series were carried out in compliance with EN26891 (1991) to evaluate their strength, stiffness and failure mode as reported in Chapters 5 and 10.

The load capacity of multiple-fastener connections per fastener is less than that of single fastener connections. The so-called ‘‘group effects’’ of multiple fastener on the strength of connections is discussed in various codes and standards by an effective number of

fastener, n_{ef} smaller than the number of fastener, n. This thesis studied the effective number of fasteners in different codes and verifies the proposed effective number utilising push-out test results of four wood screw TCC connection spaced at 50,100 and 150mm. The effect of spacing on mechanical properties of TCC connections was also investigated.

1.6 SIGNIFICANCE OF THE RESEARCH WORK

TCC connectors exhibit mechanical properties ranging from high strength and stiffness with low ductility such as the notch connection, to lower strength and stiffness but high ductility such as the mechanical fasteners. Cost consideration and ease of fabrication are a determining factor to select connection system in the application of TCCs. Hence, the best compromise between labour cost and structural efficiency can be achieved.

Different types of shear connections have been developed in the world that can be classified into four types of (a) dowel-type, (b) tubular-type, (c) notches (shear keys) with an anchoring device (post-tensioned bolt or lag screw) and (d) (dis) continuous glued-in-wood plate (Clouston et al. 2004).

A comprehensive experimental parametric study has been carried out on notch and combination of notch and screw TCC connections using different notch geometries and inclination angles of screw at University of Technology Sydney (UTS). A comprehensive review of different types of TCC connections including the research accomplished at UTS is provided in Chapters 2 and 3. Notched connections can be relatively expensive as the fabrication of notches can be difficult due to the special conditions for example curved and angled notch. Due to these special notch requirements, the timber members would have to be fabricated off-site and can add additional cost to the construction. Glue connection in TCCs is also an expensive alternative solution due to the high cost of glue.

The mechanical fasteners for example screw, nail and bolts are identified as the common type of shear connections in TCCs. This is attributed to their availability, cost efficiency and ease of construction. Moreover, inclination of the mechanical fasteners at various angles in TCCs exploiting the axial capacity of screws increases the stiffness and strength which depends on the inclination angle, geometry of screw, tensile and withdrawal strength of screw and embedment strength of timber.

As a result, this PhD study focused on the experimental parametric study of mechanical fastener such as crossed SFS VB, crossed SPAX and coach screws connections in different lengths, angles to the connection face and with and without the formwork interlayer casted by different types of concrete. Hence, the effects of connector type, inclination angle and length of screw and existence of plywood interlayer on the mechanical properties of the TCC connections are investigated. Moreover, two innovative TCC shear connection systems are proposed for their suitability as a substitute or replacement for existing connection systems.

The application of high-performance concrete such as light-weight concrete and self-consolidating concrete provides a great deal of benefits in the TCC technology to minimize the self-weight of the concrete on the timber component or increases the concrete workability and accelerates the process of pouring. Such weight reduction and increased workability may be favourable in renovation of old timber floors. It is also advantageous in new multi-storey buildings for the aspects such as prefabrication and mitigation of excess dead load – leading to saving on foundation and walls and/or column sizes.

This research investigates the experimental parametric study on effect of different types of high-performance concrete on mechanical properties of TCC connections and floor using locally available materials in Australia to evaluate their potential for use in construction market.

The strength, stiffness and arrangement of the shear connection play a crucial role in the design parameters of a TCC system including the deflection and stiffness of the floor. Hence, the calculation of stiffness, strength and load-slip response of TCC connections is of interest to study the structural performance of TCC floor. Material properties of timber, fastener and concrete influence the overall load-displacement response of connection.

The literature indicates a significant lack of information on analytical closed-form solutions to predict the strength, stiffness and load-slip response of TCC connections utilising vertical and inclined mechanical fastener and there are only few investigations on analytical closed-form equations to predict the stiffness and strength of TCC connections as input values to design a partially composite floor. For example, Eurocode 5 recommends the use of empirical equations for the slip modulus of dowels and screws which are limited to vertically inserted fasteners only. Eurocode 5 only

recommends that the strength and stiffness of unconventional connections should be determined by push-out tests.

Hence, the development of analytical models for prediction of the strength and serviceability slip modulus of inclined screw TCC connections as the input parameter for the design of timber composite beams is of practical interest to save experimental push-out test expenses.

Alternatively, the finite element (FE) method can be used as a numerical technique to investigate the stiffness, strength and load-slip response of TCC connections subjected to external and internal loads by the means of dividing it into several elements. The 3-D FE model is also capable to investigate the influence of end distance, aspect ratio and fastener yield strength on the mechanical properties and failure of TCC shear connections.

In the case of multiple fastener timber composite connections, the end and edge distances of connections, spacing and number of fastener and different possible failure modes add to the complexity of timber composite connections. The effect of fastener spacing, number of fastener, and end and edge distances of fasteners on the mechanical properties of TCC connections utilising multiple fasteners has not been yet well investigated. This study investigates the effect of the screws spacing on the stiffness, strength, ductility and failure mode of TCC utilising single and multiple wood screws.

1.7 STRUCTURE OF THE THESIS

This dissertation consists of 11 Chapters.

In this Chapter, a background, general overview and significance of the research work, the objectives and scope of the study and the structure of the thesis are given.

Chapter 2 represents a comprehensive literature review on the history behind TCCs, the benefits that TCCs have to offer, the construction aspects and the different behaviour that shear connectors and TCC system provide. A detailed review on the previous researches into the applications of innovative high-performance concretes such as light-weight concrete (LWC), fibre reinforced concrete (FRC) and self-consolidating concrete (SCC) in TCCs was also undertaken, with a discussion based on the findings and contribution that the previous researches have presented to the TCC system.

Chapter 3 provides a review of existing TCC researches as well as the key findings and knowledge in the area of the TCC connection systems. This includes an examination of the different connection systems used as well as their advantages and shortcomings based upon the case studies.

Chapter 4 outlines the materials, apparatus and specimens used in this project. The experimental preparations that were needed in order to fabricate the specimens for the testing are also documented.

Chapter 5 focuses specifically on the short-term push-out tests of the mechanical fasteners in different lengths, angles and concrete types, with and without the plywood interlayer. The experimental results of the TCC system utilising a number of different connection solutions and concrete types are analysed and the feasibility and effectiveness of these alternative solutions are evaluated to deliver recommendations regarding the economy, functionality and constructability of these alternative TCCs.

Chapter 6 discusses the results of the experimental investigation to evaluate the effects of the concrete type on the ultimate capacities of five full-scale 8m span LVL-concrete modules constructed from conventional and expanded polystyrene light-weight concrete.

Chapter 7 reports analytical models of Gamma method and compares the experimental and analytical results for the model calibration and design recommendations. The experimental programme and results are given in Chapter 6. Moreover, a parametric study on the influence of different connections and concrete properties on the design of TCC beams in terms of shear bond coefficient and effective bending stiffness of composite section is put forward.

Chapter 8 first reviews the methodology of available analytical models for prediction of the strength and stiffness of vertically inserted single timber to timber and TCC shear connections for example screw and nail. The analytical results of the models are compared to the experimental results of single wood screw shear connection used in TCC specimens. Chapter 8 also presents two models for prediction of strength and stiffness of TCC connections utilising inclined screws.

Chapter 9 proposes a non-linear three-dimensional FE model using flexible contact element pairs to simulate the experimental tests of TCC connections reported in Chapters 5 and 10 utilising the software ANSYS, versions 14.5 and 15.0. The numerical

results of FEM simulations of different connector types are validated by experimental results of push-out test.

Chapter 10 first reviews the provision for the effective number of fasteners and verifies the proposed effective number by the experimental data of push-out test obtained from push-out test of single and multiple wood screw TCC connections. The experimental results of different series of wood screw are also used to study the effect of the screws spacing on the stiffness, strength, ductility and failure mode of TCC connections for their practical application in the design of TCC floor.

In Chapter 11, conclusions are drawn and some recommendations for future studies are given. A summary of the key findings from the investigation are presented. Recommendations are made to highlight areas for further research.

2 REVIEW OF FUNDAMENTAL BEHAVIOUR OF TCC SYSTEMS

2.1 INTRODUCTION

Timber Concrete Composite (TCC) floors have been recognised as viable and effective alternatives to reinforced concrete and/or traditional timber floors. TCC is a structural solution that combines timber and concrete into a composite system in order to exploit the mechanical properties of each material favourably. Concrete performs well in compression whilst timber is suitable to carry tension parallel to the grain and flexural forces. Consequently, the resulting structural system is stronger, stiffer, durable and has improved acoustics and fire resistance properties over a timber only system.

In TCC system, a timber joist is connected to a concrete slab using a connection system that resists shear forces and impedes slip between the members of the composite section. Hence, the strength, stiffness, location and number of connectors are identified as significant parameters for the composite action and the structural and serviceability performance of TCCs (Ceccotti et al. 2006b; Van der Linden 1999).

Sawn timber or engineered wood products such as glue laminated timber (glulam), laminated veneer lumber (LVL) or cross-laminated timber (CLT) can be used for the timber joist. In most cases, light reinforcement is placed in the concrete slab to control shrinkage cracking, rather than to act as structural reinforcement. If the chosen connector system may subject the concrete to significant tensile stresses, reinforcement will be required to prevent localised failure in the concrete (Van der Linden 1999).

This Chapter presents a comprehensive review of the literature on development and structural behaviour of TCC system. The review addresses construction aspects and shear connection concepts. The design parameters of a shear connector in TCCs such as stiffness, ductility, shape and arrangement are discussed. The influence of concrete type on structural response of TCCs is also discussed.

As recommendations, the best types of shear connection for cast in-situ and prefabricated TCC floors are put forward and assessed for criteria such as strength, stiffness, ductility and ease of manufacturing.

2.2 HISTORY OF TCC

2.2.1 General

TCC systems were first initiated due to the shortage of steel in Europe during the 1920's to 1950's. TCC systems as an alternative solution for structural applications have had a relatively slow uptake due to their unfamiliar nature and the lack of standards. However over the past two decades, they have seen a resurgence in popularity due to their relative ease of construction, economy and structural advantages in United States, New Zealand, Australia, Switzerland, Austria, and Scandinavian countries where TCC solution have been used for the construction of pedestrian or vehicle bridges, upgrading of existing (heritage) timber floors and construction of new buildings – typically public and/or multi-storey structures (Natterer et al. 1996).

TCCs have strong potential for use in rehabilitation or upgrading of existing timber floors (Jorge et al. 2011; Kieslich et al. 2010), as well as new floors (Ceccotti et al. 2006b) or even for pedestrian or vehicle bridges (Clouston et al. 2005a).

One of the first investigations on full scale TCC beams was conducted at the University of Illinois, USA, between 1938 and 1942 by Richart et al. (1943a). Their research included flexural testing of about 30 composite beams. At the same time, McCullough (1943) completed bending tests on approximately 20 full size TCC specimens for the development of cost-effective short-span highway bridges (also known as Oregon tests in the USA). From 1932 and 1952, McCullough (1943) constructed and tested many short span TCC decks.

In European countries, such as Germany and Italy, TCC technology was introduced as a way for renovation and upgrading old timber (heritage) buildings, constructed in the late

19th and beginning 20th centuries, whose traditional timber floors do not comply with acoustic and fire safety requirements of the current design codes and practices (Ceccotti 1995b; Holschemacher et al. 2002).

Application of TCC solutions in timber multi-storey residential and commercial building received particular attention in the 1980's and 1990's. Natterer et al. (1996) proposed vertical nailed planks topped by a concrete slab that is connected with shear keys and stud type fasteners. One of these developed connections as notch cut into the timber, reinforced with prestressed Hilti connectors overcame the low slip modulus of previous connectors.

Other researches for solutions applicable for floors in new multi-storey buildings have been conducted by Bathon et al. (2006), Lukaszewska (2009) and Natterer et al. (1996).

2.2.2 In Australia

Timber construction in residential and non-residential buildings has a relatively long history in Australia. This can be observed from the number of permanent timber structures such as existing industrial warehouses from the 1800's, residential buildings and in particular, timber bridges in Australia. The widespread availability of both high-quality native hardwoods and two-by-four framing material provided by softwood plantations contribute to timber construction in Australia (Crews et al. 2010b).

The most prominent application of timber in recent times has been through the use of softwood timber, used in frames and trusses for residential buildings. Although there have been innovations in a number of engineered timber products, these have hardly had any impact on the industrial and commercial construction market. This is mostly a direct result of timber being regulated to use in buildings under 3 levels in height (Crews et al. 2010b; Gerber et al. 2011).

In practical applications, TCC structures in Australia are most notably seen in the form of TCC bridges. TCC bridges are quite common and as a result the Roads and Maritime Services (RMS) publishes a TCC bridges section as part of their timber bridge manual.

Yttrup et al. (1996) reported that timber-concrete bridges have been built in Australia since at least 1945 and the oldest bridge examined in their research was built in Tasmania due to a shortage of reinforcing steel in 1949 with a service life over at least 45 years but is not regarded as a composite structure.

A three 10m span highway bridge called “Maria River bridge” was completed in 1955 as the earliest major TCC bridge in NSW. The connector was 25mm thick steel plates inserted 38mm into round timber beam and 90mm into the concrete deck (Nolan 2009).

Since then, more TCC bridges are constructed throughout NSW and Tasmania (Nolan 2009). In New South Wales, the most of the TCC bridges have been constructed from hardwood girders overlayed with a concrete slab. Coach screws and steel plates are used at the interface to provide vertical restraint and shear transfer, respectively (NSW 2008).

Since the mid-2000s, TCC structures have been gaining prominence in Australia, although this focus has been mainly through research conducted by universities. In practical applications, the utilisation of TCC solutions should improve in the future in Australia, as the design procedures become standardised and are validated by research.

2.3 ADVANTAGES OF TCC SOLUTIONS

TCCs have several advantages over full timber floor such as higher flexural strength and stiffness (up to six and three times, respectively), better vibration performance, larger in-plane rigidity acting as diaphragm, more economical in terms of the load carried per unit of self-weight (Figure 2-1a and b), improved fire safety performance and thermal and noise insulations for both air-transmitted and impact noise insulation.

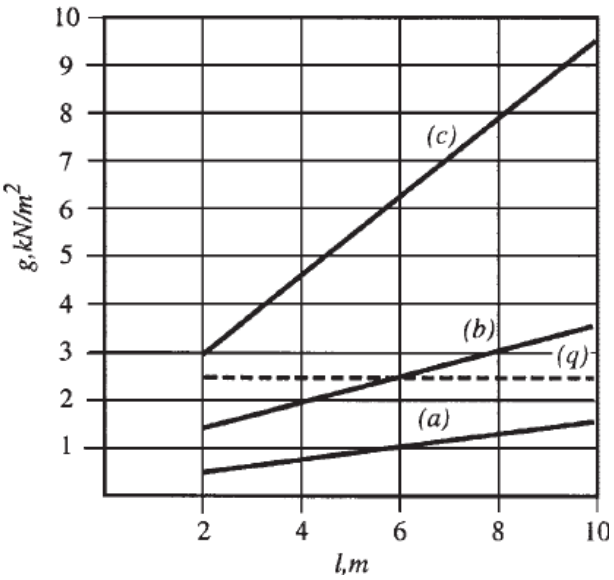

Figure 2-1 Floor self-weight (g) versus span (*l*) for a service load of 2.5kN/m^2 (a) timber structure, (b) TCC structure, (c) all concrete structure (Ceccotti 2002)

Additionally, the concrete slab used in a TCC system is more durable than alternative timber decking especially in outdoor environments where timber is prone to deterioration from natural salts, rainwater and insects.

TCCs also have advantages compared to reinforced concrete construction including significantly reduced dead-load and thus, higher efficiency in terms of carried load per unit self-weight (Figure 2-1b and c) which leads to reduction of gravity load on foundation, seismic action and hence in the size or number of structural members (Branco et al. 2007; Ceccotti 2002). Furthermore, cracks on the tensile region in reinforced concrete can cause moisture penetration and induce corrosion in the steel mesh. However, this is overcome in TCC slabs due to the concrete being in compression only (Ceccotti 2002; Gutkowski et al. 2000; Yeoh et al. 2010). TCC consists of timber as carbon-neutral material hence it has low embodied energy and reduced CO_2 emissions compared to steel and concrete (Yeoh et al. 2010).

Better thermal insulation of TCCs means its higher efficiency in reducing the energy required to heat or cool a building Yeoh (2010). The greater acoustic insulation of TCC than timber floors was verified by research conducted by Parmanen et al. (1999) which determined that TCC floor system exhibited much higher sound insulation properties compared to timber floor. This is mainly a result of the mass and density of the concrete slab which reduces the amplitude of the soundwaves. This improved acoustic performance can be attributed to the fact that a TCC system is highly damped compared to a timber floor. The viscous damping ratio of TCCs is approximately 2% over 1% for timber floors (Ceccotti 2002).

In particular TCCs have favourable fire resistance advantages over traditional timber floors. Natterer (2002) outlined the increased duration of fire resistance of a TCC slab of 90 minutes over a traditional reinforced concrete slab of 60 minutes. Natterer (2002) and Frangi et al. (2008) reiterated that in a TCC structure the concrete is a protective layer to the timber joists by delaying the start of charring and reducing speed of temperature effects and charring of the timber beam and once the timber has charred it protects the connectors from high temperatures, temperatures, thus composite action is still maintained.

O'Neill (2009) tested two full scale TCC models using an LVL joist with notched and toothed metal plate connections which were subjected to 1.56 and 3.06kN/mm^2 dead-

loads, respectively. The fire test was carried out as per ISO834 (1975) where the TCC floor collapsed after 75 minutes.

Concrete and cement in particular, require large amounts of energy to produce and leads to high carbon emissions as a by-product during their refinement whereas timber requires relatively less energy to harvest and process. A possible solution in reducing the amount of steel and concrete used in construction and consequently in greenhouse emission and embodied energy of the final product is to create composites with other materials such as carbon fibre composites and timber.

Yeoh (2010) also remarked that timber is carbon neutral product in a way that the production of timber even offsets some emissions through the growth of the tree whilst timber is also a renewable resource. Crews et al. (2010a) highlighted that if timber is assumed to permanently store carbon, the greenhouse gases emitted during its production is more than negated by the carbon removed from the atmosphere.

Crawford (2009) reported a CO_2 emission of 0.128kg, 0.014kg and 2.88kg for production of one kilogram of concrete, hardwood timber and steel, respectively whilst Ferguson (1996) noted an energy consumption of 1000, 2500 and 4500w/h for timber, concrete and steel, respectively. Timber may also be considered to provide aesthetic benefits over concrete.

2.4 CONSTRUCTION METHODS

TCC floor can be constructed utilising three different methods such as (1) wet method as common way of pouring concrete on top of timber joists addressed in most of researches; (2) semi-prefabrication method (cast in-situ); and (3) prefabrication off-site (dry-dry method) such as TCC panels prefabricated off-site and connected to the adjacent panels on site or concrete slab prefabricated off-site connected with timber joists and adjacent slabs on site (Lukaszewska 2009; Yeoh 2010).

2.4.1 Wet method in rehabilitation of existing timber floor

Most TCC systems used for the refurbishment of existing timber floors are typically half the cost of alternative new floor as outlined by Godycki et al. (1984) and Postulka (1997).

Use of TCCs also means less disruption to lower floors (Jorge et al. 2011). For an existing timber building, upgrading to TCC floor can be carried out with continued use

of the floor below whilst replacing a timber floor with a reinforced concrete floor requires the lower floor to be unused for an extended period. Time is needed to place scaffolding and formwork, then for concrete pouring and curing. The lower floor is inaccessible until concrete gained sufficient strength for the removal of the formwork and scaffolding. This will likely take at least two weeks and requires full access to the floor below. This also applies to new buildings.

In the case of TCC floor, once timber beams are erected, formwork can be placed. Beyond this there is no need for disruption of lower floors. There is no ongoing need for scaffolding, and further work can proceed on the lower floor.

For rehabilitation works, there may be limitations on construction for example the thickness of the slab should be minimised so as not to significantly reduce door and parapet heights (Clouston et al. 2005a; Kieslich et al. 2010; Meierhofer 1992; Selle et al. 2010). This is less significant for new buildings.

Typically when an existing timber floor is refurbished, formwork is constructed in order to allow for the concrete slab to be poured. However, this can be overcome by using boarding between the timber and concrete. This formwork can then be retained as a permanent part of the structure. However, it is noted that utilising the same connector system with boarding reduces the slip modulus and strength of the connectors, given the penetrations into the timber beam and concrete slab are reduced (Van der Linden 1999).

There is a general agreement that the use of a TCC floor system to refurbish an existing timber floor can increase the stiffness, strength and fire resistance of the structure Symons, Persaud and Stanislaus (2010a).

Although TCC floors can be constructed as a concrete slab over a timber beam in forms of engineered wood products or sawn timber beams as illustrated in Figure 2-2a, they can be constructed as a slab type floor using a concrete slab over laminated wooden decks of sawn timber planks nailed together with the longer side of their cross section vertical or glued laminated timber beams with the longer side of their cross section horizontal as depicted in Figure 2-2b (Frangi et al. 2003).

However, this is different to a timber beam floor which utilises boarding as formwork for the concrete, as the concrete slab in this situation bears directly onto the planks as shown in Figure 2-2b.

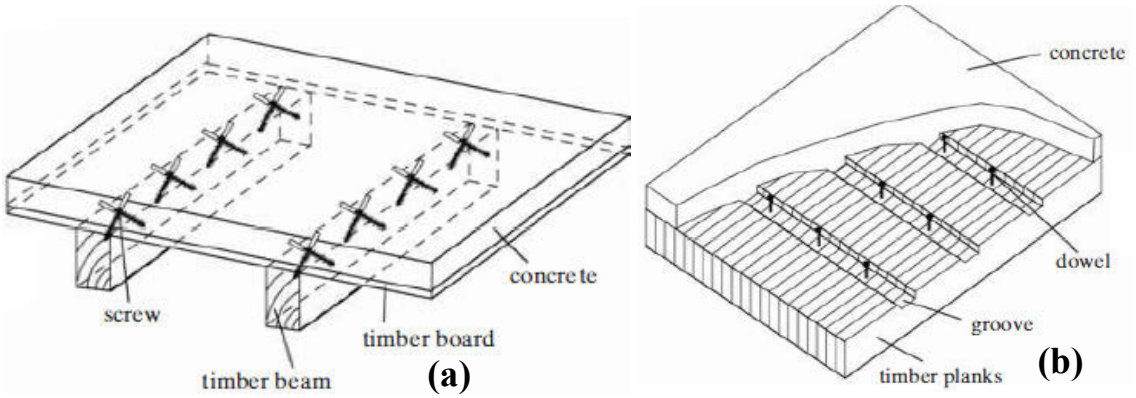

Figure 2-2 (a) Beam type floor and (b) slab type floor (Frangi et al. 2003)

The use of TCC systems is not only limited to applications such as a floor system for multistorey buildings, but also for low volume traffic bridges.

Nauta (1984) described the Mangaharakeke Stream bridge in New Zealand which features a concrete slab sitting on top of a treated nail-laminated radiata pine slab constructed from alternating boards of 250 and 300mm deep. This alternating pine slab creates a series of notches for the concrete to adhere to, with triangular steel plates at 400mm intervals and 100mm spikes driven every 600mm into the timber to mitigate uplift (Van der Linden 1999).

2.4.2 Semi prefabrication

The semi-prefabricated solution proposed by Yeoh (2010) consists of two separate parts (1) the M section wooden panel and (2) cast-in-situ concrete slab with the steel mesh to control the shrinkage (Figure 2-3a).

“M” section panel floor with the width of 2400mm consists of single 400x63mm LVL joist on the outer edges and a double LVL joist in the centre including plywood sheets as permanent form work. The specimen with span of 8 to 10m requires six to eight connectors along the joist to provide adequate composite action.

The light-weight panel with the weight of about 1kN facilitates a light-weight off-site prefabricated component. Such semi pre-fabricated element is easy to transport, crane and connect to main frame utilising designed joist hangers. Furthermore, casting monolithic concrete slab on it to connect the adjacent panels results in better in-plane strength and stiffness. In addition there is no need for additional connections between adjacent panels (Yeoh et al. 2009; Yeoh 2008).

2.4.3 Prefabrication

Application of TCC with prefabricated concrete slab overcomes the disadvantages of TCC with cast in situ concrete such as: (1) presence of concrete as a wet component in the typically dry construction of timber; (2) time interval for the setting of concrete; (3) low stiffness and high creep of concrete in curing period which needs propping of beams to sustain the self-weight of the concrete slab (Yeoh 2008); (4) high cost of cast-in-situ concrete slabs as a consequent of fresh concrete transportation, propping, extra self-weight of the floor due to application of formwork increases (Lukaszewska 2009); (5) significant increases in initial deflection and flexural stresses regarding connection of timber joist to the concrete slab with a non-fully developed shrinkage (Lukaszewska et al. 2008); and (6) potential problems of quality control (Lukaszewska 2009).

Lukaszewska (2009) developed a system with some level of prefabrication in terms of ‘‘dry’’ connections as illustrated in Figure 2-3b and c. In this novel composite system, the timber joist is connected to prefabricated concrete slab (Figure 2-3b) with the embedded mechanical connectors such as metal plates (glued or nailed), dowels and toothed metal plates (Lukaszewska 2009).

Five 4.8m span full scale TCC floors comprised of triple T-section glulam joists were tested to failure utilising four-point bending. The prefabricated concrete slab with mounted connectors was used to construct TCC floors. Three specimens consisted of coach screws surrounded by steel pipes whilst two specimens used metal plates nailed to the glulam joists.

It was concluded that prefabrication system represented equally well as conventional “wet” system. Moreover, TCC beam utilising the coach screw plus notch connector exhibited highest strength among those tested. Composite actions of only 60% and 30% were observed in the TCC beams utilising coach screws and metal plates, respectively. The use of coach screw in combination with a notched connection and steel pipe was identified to improve the connection efficiency.

From a design point of view, prefabricated TCC construction exhibits higher MOE and markedly lower shrinkage, creep and swelling compared to cast-in-situ TCCs (Lukaszewska et al. 2008). A fully prefabricated TCC panel using continuous steel mesh connector was developed by Bathon et al. (2000), Bathon et al. (2004) and Bathon

et al. (2006). The prefabricated panel competes with reinforced concrete and steel concrete composite floors (Bathon et al. 2004; Yeoh et al. 2010).

In Finland, two TCC prefabricated systems utilising nail plates connectors were developed for multi-storey buildings. The first system was a cast in-situ floor whilst the second system represented concrete casted upside down in factory without framework (Yeoh et al. 2010).

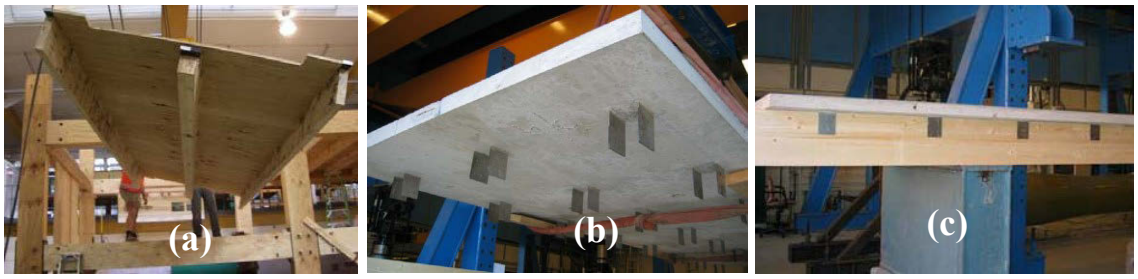

Figure 2-3 (a) Semi-prefabricated TCC (Yeoh 2010) and (b) and (c) prefabricated slab (Lukaszewska 2009)

2.5 FUNDAMENTAL BEHAVIOUR OF A TIMBER-CONCRETE COMPOSITE SYSTEM

TCCs are structural elements that are comprised of timber and concrete elements joined together by some form of shear connector which transfers the shear force between the composite components and significantly increases the strength and stiffness of the composite system over traditional timber constructions.

TCC system is considerably lighter compared to an all concrete solution (Miotto et al. 2011). This concept is well accepted in the engineering community and is backed up by Fernandez-Cabo et al. (2012). Ceccotti (1995b) states that a TCC solution can double the load capacity of a traditional timber floor whilst there is a three to four times improvement in its transversal stiffness.

Ceccotti (1995b) asserted that the stiffness of the TCC beam results from the stiffness of the timber beam and the composite action of the timber and concrete. The stiffness of the concrete typically does not add to the stiffness of the T-beam shape TCC system. The strength and stiffness of the timber beam dictate the strength and stiffness of the TCC beam. This is because there is a large variation in the mechanical properties of timber whilst TCC beams typically fail when the tensile capacity of the timber beam is reached (Van der Linden 1999). This was observed during experimental test carried out

by Frangi et al. (2003) in which the TCC systems failed due to a combined bending and tension failure of the timber joist. However, it highlighted that an increase in the bending stiffness helps to redistribute the stresses. Hence, it reduces the tensile stress on the concrete.

The design of timber composite structure is governed by displacement within serviceability limit state (SLS). Hence, the connections slip at the interface of the composite materials and consequently the slip modulus of laterally loaded shear connection has a significant influence on the overall behaviour of composite beams. The connection between timber and concrete is not fully rigid and there is some relative slip. Therefore, the assumption of plane section remaining plane and the transformed section method are not applicable in design of TCC (Clouston et al. 2008).

An efficient design of a structure is achieved by a high stiffness of cross section which can carry the higher load for minimum self-weight. Composite I and box beam type sections are the most conventional structural timber sections that can be connected to a concrete slab to achieve higher stiffness and strength through the composite action of timber and concrete. TCC system is appropriate for long span (6-8m) commercial and multi-storey residential applications.

The connector allows for composite action – that is, for the timber and concrete to act together as one entity, with the timber acting in a combined bending and tension whilst concrete is subjected to bending and compression (Branco et al. 2007). This is aligned with the natural properties and behaviours of the materials. TCCs benefit from the composite action, resulting in a significant improvement in strength and stiffness compared to the timber and concrete acting independently (Clouston et al. 2005a).

The transferred shear force is equal to the internal axial forces applied on timber and concrete. The transferred shear force, composite action and stiffness of the TCC depend on the stiffness of the connector and can range from no connection to rigid connection with the boundaries of structural efficiency determined by these theoretical limits. The lower bound refers to layers which are not connected together and work quite independently subjected to bending only (N=0) as depicted in Figure 2-4c whilst a rigid connection without slip represents the maximum transferred shear force (N=N_{max}) and minimum internal bending moment (M_i=$M_{i,min}$) as upper bound (Figure 2-4a).

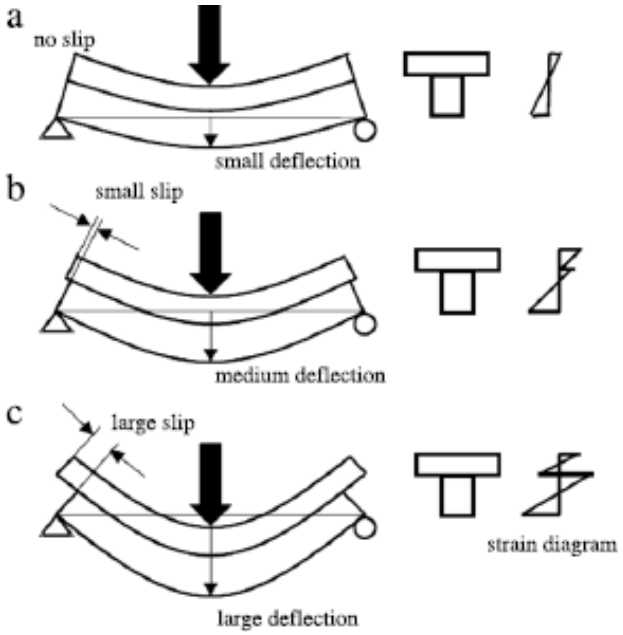

Figure 2-4 Degrees of composite action (a) full composite, (b) partial composite and (c) no composite action (Yeoh et al. 2011)

Most of commonly used shear connections in TCC exhibit a semi-rigid behaviour with some relative slip at the interface of the timber and concrete components as illustrated in Figure 2-4b. Consequently, TCC structures with semi-rigid connections exhibit partial (not full) composite action and this adds to the complexity of the system (Clouston et al. 2004). Gutkowski et al. (2008) evaluates the composite efficiency or degree of composite action, *DCA* of TCC beam by:

$$DCA = \frac{D_N - D_I}{D_N - D_C} \times 100 \qquad (2\text{-}1)$$

where, D_N is the theoretical fully non-composite deflection (calculated as a layered beam with no interlayer shear transfer), D_c the theoretical full-composite deflection (calculated by the transformed section method) and D_I is the measured deflection for partially composite action of the specimen (Gutkowski et al. 2008).

In TCC floor with larger composite efficiency, the beam depth is reduced and in contrary, the medium to long span floors (7-15m) are achieved (Yeoh 2010).

2.5.1 Beam design

To analyse timber concrete composite structure, understanding of the relationship between the strength and stiffness of all three composite components including timber, concrete and shear connections is required. TCC modules have to be designed to satisfy

the ultimate (ULS) and serviceability (SLS) limit states in both short- and long-terms. The ULS verification controls the maximum connection's shear force, maximum axial and bending stresses in concrete and combination of axial and flexural stresses in timber, flexural shear strength in timber and bearing strength of timber against the support reactions to be less than design values whilst SLS verifies that the maximum deflection is less than the design values.

2.5.1.1 Gamma method

The "Gamma method" in Eurocode 5 part 1 annex B EN (2004b) has been recognised as the only specific design provision used to analyse TCC structures, with reasonable accuracy in determining the resultant stresses and deformations. The "Gamma method" based on work done by Möhler (1956) is widely used to design a simply supported TCC using differential equation of beam with partial composite action.

Gamma method implements an elastic analysis for the short-term verifications of a simply supported TCC beam with constant slip stiffness subjected to loads giving a bending moment varying sinusoidally whilst a simplified method called "effective modulus method" has been proposed to consider the effect of creep for the long-term verification of Gamma method.

The effect of creep in long-term verification is considered by dividing the MOE of concrete and LVL and the stiffness of the connection, by one plus the creep coefficient.

The design of timber composite structure is governed by displacement within serviceability limit state (SLS). Hence, the slip at the timber connection plays a crucial role on the design of timber beams. Moreover, the linear-elastic behaviour for design of timber composite beams proposed by Gamma method employs different key parameter such as slip modulus of connection to design the TCC beams whilst inaccurate slip modulus results in unreliable design for the timber composites (EN 2004b).

To design an optimal composite beam with increased load carrying capacity and ultimate deformation capacity, the ultimate slip of shear connection should not be reached before the failure of the composite system (Dias et al. 2011).

Timber, concrete and shear connection are assumed to be linear-elastic and Bernouilli's hypothesis is valid for each composite component (Frangi et al. 2003). The free body diagram of a T shape TCC module with partial composite action including internal and external loads is illustrated in Figure 2-5.

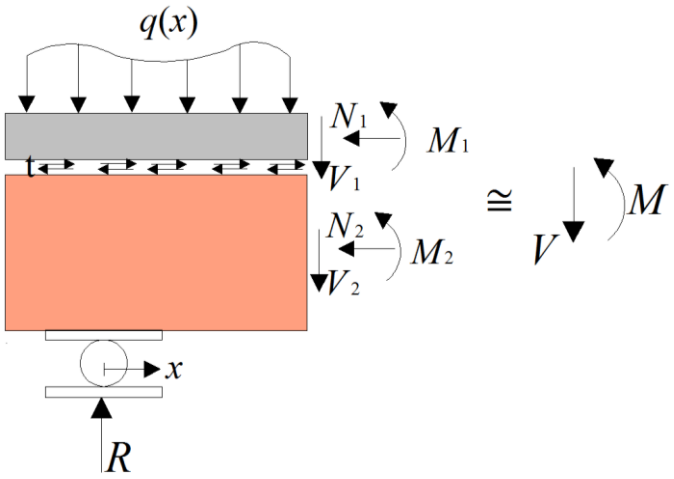

Figure 2-5 Internal and external loads applied on TCC system

In the Gamma method, it is assumed that there is no vertical separation between concrete slab and timber joist and also plane sections remain plane except for the discontinuity at the connection interface. The Gamma method evaluates effective bending stiffness, EI_{eff} using the shear bond coefficient, γ. The effective bending stiffness is used to check the design resistance of the connector and the stress values in the timber and concrete.

The shear bond coefficient depends on different input parameters such as connector properties of slip modulus and spacing whilst the ductility of the connection is neglected in its calculation and consequently in the Gamma method. As the stiffness of the shear connector increases, the shear bond coefficient and consequently, the effective bending stiffness of the TCC beam tend towards a fully composite section.

The shear bond coefficient is demonstrated in (EN 2004b):

$$\gamma_i = \frac{1}{1+\frac{\pi^2 E_i A_i s}{K_i L^2}} \qquad \text{for i=1 and 3, } \gamma_2=1 \qquad (2\text{-}2)$$

where, E_i and A_i are modulus of elasticity (MOE) and section area of the composite components; s represents spacing of the connectors; K is slip modulus of the connector; and L is span length of the beam. Usually the design parameters of shear connectors such as the serviceability and ultimate slip moduli and strength of connections are obtained from push-out shear tests (EN 2004b; Lukaszewska 2009).

Moreover, the effective bending stiffness of the composite cross-section is shown in (EN 2004b):

$$EI_{\text{eff}}=\sum_{i=1}^{3} E_{\text{i}}\, I_{\text{i}}+E_{\text{i}} A_{\text{i}} a_{\text{i}}^{2} \gamma_{\text{i}} \tag{2-3}$$

where, for a box TCC modules as shown in Figure 2-7, a_1 represents distance between centroids of concrete floor and effective TCCs whilst a_2 and a_3 indicate distance between centroids of timber webs and timber flange and effective TCCs in a TCC box system. The contribution of the formwork interlayer (if present) is neglected in the design. The distance between centroid of timber web component and centroid of TCCs section, a_2 is given by:

$$a_2=\frac{\gamma_1 E_1 A_1 (h_1+h_2)-\gamma_3 E_3 A_3 (h_2+h_3)}{2\sum_{\text{i=1}}^{3} \gamma_{\text{i}} E_{\text{i}} A_{\text{i}}} \tag{2-4}$$

where, h_1, h_2 and h_3 are depth of the concrete slab, timber web and timber bottom flange, respectively. a_1 and a_3 are calculated using a_2 by:

$$a_1=\frac{h_1}{2}+\frac{h_2}{2}-a_2 \tag{2-5}$$

$$a_3=\frac{h_2}{2}+\frac{h_3}{2}+a_2 \tag{2-6}$$

The effective bending stiffness depends on the shear bond coefficient of the interface where the shear bond coefficients of the TCC beam depends on the spacing and slip modulus of the connectors. Usually the shear bond coefficient of regular connection is within the range of 0.1-0.4. A shear bond coefficient of 0 represents the layers which behave totally independently with no force couple resisted by the composite section ($EI_{\text{eff}}=EI_{\text{ min}}=E_{\text{c}}I_{\text{c}}+E_{\text{t}}I_{\text{t}}$) whilst a shear bond coefficient of 1 indicates a fully composite beam with no slip in the interface ($EI_{\text{eff}}=EI_{\text{max}}=4EI_{\text{min}}$).

The spacing for the commercially available connectors in Europe is within the range of 100 to 500mm (Steinberg et al. 2003). Based on the values for shear force at the interface, the spacing of connectors can be variable and an effective constant spacing s_{eff} can be assumed during calculation of shear bond coefficient as shown in (Ceccotti 2002):

$$s_{\text{eff}}=0.25\, s_{\text{m}}+0.75\, s_{\text{e}} \tag{2-7}$$

$$s_e < s_m < 4s_e \tag{2-8}$$

where, s_e and s_m are the spacing at the beam-ends and mid–span, respectively (Ceccotti 2002). The span of TCC beam influences the effectiveness of connection given in form of shear bond coefficient, γ.

The total normal stresses in the concrete (i= 1) and timber (i = 2) components of a TCC is obtained by (Steinberg et al. 2003):

$$\sigma_{i,b}=\sigma_i+\sigma_{b,i} = \frac{M_u}{EI_{eff}}\gamma_i a_i E_i + \frac{M_u}{EI_{eff}}\frac{h_i}{2}E_i \tag{2-9}$$

where, σ_i and $\sigma_{b,i}$ are axial and bending stresses, respectively which are calculated by:

$$\sigma_i = \frac{M_u}{EI_{eff}}\gamma_i a_i E_i \tag{2-10}$$

$$\sigma_{b,i}=\frac{M_u}{EI_{eff}}\frac{h_i}{2}E_i \tag{2-11}$$

where, M_u indicates the moment due to factored loads as depicted in Figures 2-6 and 2-7 for T shape and box TCC modules, respectively.

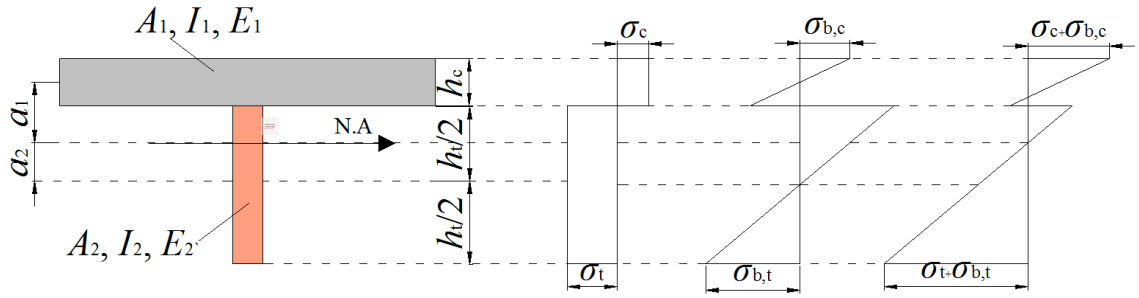

Figure 2-6 Stress distribution of a partially composite, T shape TCC beam

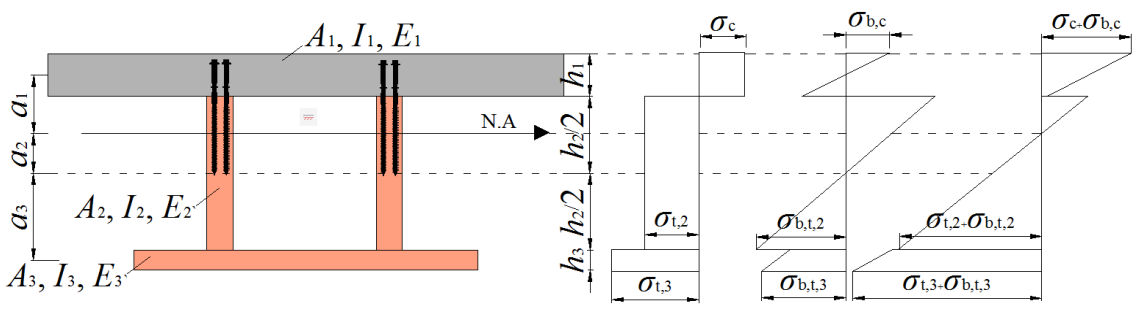

Figure 2-7 Stress distribution of a partially composite, box TCC module

The shear flow between composite components, shear force in the connector and the mid-span deflection of TCC module are given in:

$$t(\mathrm{x}) = \frac{\gamma E_{\mathrm{i}} A_{\mathrm{i}} a_{\mathrm{i}}}{EI_{\mathrm{eff}}} V(\mathrm{x}) \tag{2-12}$$

$$F(\mathrm{x}) = \frac{\gamma E_{\mathrm{i}} A_{\mathrm{i}} a_{\mathrm{i}} s}{EI_{\mathrm{eff}}} V(\mathrm{x}) \tag{2-13}$$

$$\delta = \frac{5wl^4}{384EI_{\mathrm{eff}}} \tag{2-14}$$

where, t is shear flow, W_{eq} is the uniformly distributed load, F is the shear force in the connector, V is the shear force in the cross-section of TCC beam and δ is the mid-span deflection of a simply supported composite beam (Frangi et al. 2003; Lukaszewska et al. 2008). The shear force in connector, F(x) is checked by:

$$F(x) \le F_{\max} \tag{2-15}$$

where, $F_{\max}$ is the load capacity of connector. The maximum shear stress occurs at the section with zero normal stresses. The maximum shear stress in the web, $\tau_{2,\max}$ is:

$$\tau_{2,\max} = \frac{\gamma_3 E_3 A_3 a_3 + 0.5 E_2 b_2 h_2^{\,2}}{b_2 EI_{\mathrm{eff}}} V(\mathrm{x}) \tag{2-16}$$

where, b_2 is the width of the LVL web.

In the design of fully composite timber module, Eurocode 5 (EN 2004b) recommends that the flange of a timber joist should satisfy the following equations:

$$\sigma_{\mathrm{f,c,max}} \le f_{\mathrm{m}} \tag{2-17}$$

$$\sigma_{\mathrm{f,t,max}} \le f_{\mathrm{m}} \tag{2-18}$$

$$\sigma_{\mathrm{f,c}} \le k_{\mathrm{c}} f_{\mathrm{c}} \tag{2-19}$$

$$\sigma_{\mathrm{f,t}} \le f_{\mathrm{t}} \tag{2-20}$$

where, $\sigma_{\mathrm{f,c,max}}$ and $\sigma_{\mathrm{f,t,max}}$ are the extreme fibre flange design compressive and tensile stresses, $\sigma_{\mathrm{f,c}}$ and $\sigma_{\mathrm{f,t}}$ are the mean flange design compressive and tensile stresses, f_{m}, f_{t} and f_{c} are the bending, tension and compression strength of the timber flange, respectively and k_{c} is a factor which takes into account the lateral instability.

The axial stresses in the timber webs should satisfy the following equations:

$$\sigma_{w,c,d} \leq f_{c,w} \tag{2-21}$$

$$\sigma_{w,t,d} \leq f_{t,w} \tag{2-22}$$

where, $\sigma_{w,c,d}$ and $\sigma_{w,t,d}$ are the design compressive and tensile stresses of the web and $f_{c,w}$, and $f_{t,w}$ are the design compressive and tensile bending strengths of the web, respectively.

The tensile and bending stresses of timber and concrete at the extreme fibres (the upper and lower fibres of concrete and the lower fibre of timber) ($\sigma_{2,N}$ and $\sigma_{2,M}$) must be fitted into the linear-elastic condition of:

$$\frac{\sigma_{2,N}}{f_t} + \frac{\sigma_{2,M}}{f_m} \leq 1 \tag{2-23}$$

where, f_t and f_m are the tensile and bending strength of the components, respectively.

The shear stress in web of timber beam should be as:

$$\tau_{mean} \leq \begin{cases} f_v \text{ for } h_f \leq 4b_{ef} \\ f_v \left(\frac{4b_{ef}}{h_f}\right)^{0.8} \text{for } h_f \geq 4b_{ef} \end{cases} \tag{2-24}$$

τ_{mean} is the design shear stress at the sections assuming a uniform stress distribution, f_v is the design planar shear strength of the web, h_f is either $h_{f,c}$ or $h_{f,t}$ and b_{ef} is calculated as:

$$b_{ef} \leq \begin{cases} b_w \text{ for box beam} \\ 0.5b_w \text{ for I beam} \end{cases} \tag{2-25}$$

where, b_w is width of web (EN 2004b). b_{ef} of a concrete member is defined to be its width (b). Exceeding the ultimate properties (allowable stress) in any part of the specimen leads to the failure of composite components.

The design procedure of a TCC beam consists of verifications such as (1) ULS in the short-term, the structure is subjected to maximum load after construction ($1.2G + 1.5Q$) in compliance with the AS/NZS1170.0 (2002); (2) SLS in the short-term, the deflection due to imposed load is verified (i.e. only Q); (3) ULS in the long-term, the structure is subjected to the permanent load condition (i.e. G+0.4Q) in compliance with AS/NZS1170.0 (2002) during the service life, and the remaining part of the ultimate load (i.e. $0.2G + 1.1Q$) at the end of the service life; and (4) SLS in the long-term at the

end of the service life; creep in the materials is evaluated under the permanent load condition (G + 0.4Q) during the service life, and the instantaneous effects are considered by the difference between the rare (G+ Q) and the quasi-permanent (G + 0.4Q) load condition (0.6Q) (Ceccotti 2002; Yeoh 2010).

2.5.1.2 Elasto-Plastic model

TCC systems are typically modelled as demonstrating linear elastic behaviour. In most instances, the connectors become plastic and as a result the linear elastic model has to be modified to take into account the plasticity of the connectors. Moreover, by crack initiation in concrete the linear elastic model is no longer valid.

Frangi et al. (2003) developed an elasto-plastic model for TCC system in order to account for the non-linear behaviour of connectors. This new model considers parameters such as the ductile behaviour of the connectors. It is highlighted that the shear force developed within the connectors is in equilibrium with the internal normal force of the timber and concrete. The magnitude of this shear force depends on the stiffness of the connectors. When a rigid connection is used, no slip should develop between the timber and concrete and the system can be theoretically analysed as a single unit as illustrated in Figure 2-8. Figure 2-9 highlights that the shear connector experiences a linear-elastic load-slip at lower loads.

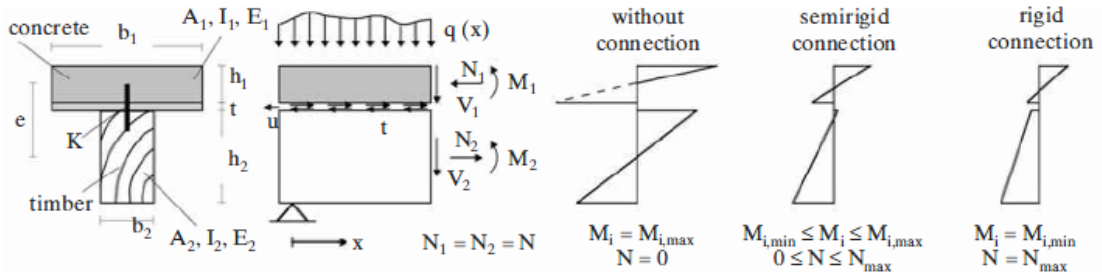

Figure 2-8 The effect of connector rigidity on TCC beam (Frangi et al. 2003)

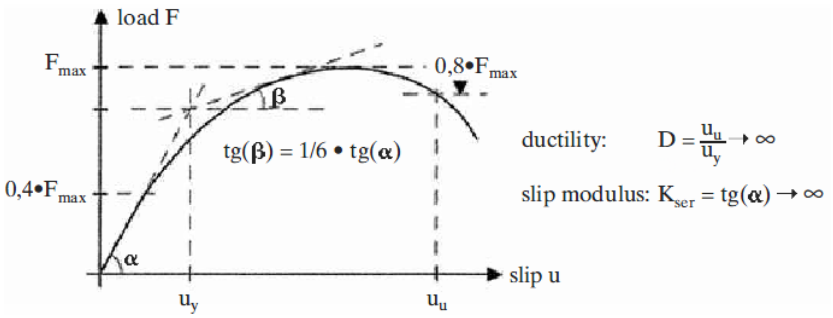

Figure 2-9 Typical elastic-plastic load-slip of shear connector (Frangi et al. 2003)

Frangi et al. (2003) assumes a rigid-perfectly plastic load-slip relationship for connections. As the load is increased, a plastic behaviour is observed which results in the connections deforming to an irreversible state. After reaching the maximum load capacity, the connector continues to deform in a plastic manner depending on the ductility.

Although the elasto-plastic model developed by Frangi et al. (2003) is more relevant and accommodates a number of factors which affect a TCC system's behaviour, the linear-elastic model is still commonly used for TCC design (Yeoh et al. 2010).

2.5.2 Connection design based on deformation control

Gelfi et al. (2002) proposed a method to design connection of TCC beams based on a designed deformation in connection. The connection design of TCC system includes calculation of diameter and length of mechanical fastener for example nail, bolt and screw and its spacing.

The minimum fastener spacing is determined based on the deflection control under service load. The mid-span deflection of TCC beam depends upon the slip at the connections. Hence, to control the connection slip, a minimum stiffness of composite system should be imposed by employing appropriate combination of connection stiffness and spacing (Dias et al. 2011). Ronca et al. (1991) and Gubana (1995) proposed a deflection increase due to partial composite action of eight to ten times of maximum slip at connection for a simply supported TCC beams under uniform load. Hence, the minimum spacing is found by a designed maximum slip at connection.

A small slip design (u_d) for example 0.2-0.3mm leads to a limited increment of the deflection compared to full-composite beam. The design shear force at connection (V_{sd}) for the connector located near to the support is defined to be:

$$V_{sd} = K_s u_d \tag{2-26}$$

where, K_s is the serviceability slip modulus of shear connection. The spacing of shear connection, S is calculated by:

$$S = \frac{V_{sd}}{q} = \frac{K_s u_d}{q} \tag{2-27}$$

where, q is shear flow of the section and can be approximated by:

$$q=\frac{V_b Q}{I} \tag{2-28}$$

where, V_b is the maximum shear force at beam-end, Q is first moment of area for concrete slab and I represents the second moment of area of TCC section. Thus, Gelfi et al. (2002) calculates the spacing of shear connection, S by:

$$S=\frac{K_s I}{V_b Q} u_d \tag{2-29}$$

2.6 INFLUENCE OF CONNECTIONS

The concept of utilising a connection system to achieve uniform composite action between the concrete and timber interface dates back to the 1920s when Muller (1922) patented a connection system of nails and steel braces between the timber and concrete.

This idea was further built upon in 1943 when Richart et al. (1943b) tested some composite beams utilising different types of connectors. Richart et al. (1943b) stated that the bond failure between the concrete and timber was greatest when the connectors utilised were spikes and/or triangular plates (Van der Linden 1999).

Research conducted by Pincus (1969, 1970) found that either the timber element failed under tensile stresses or the concrete failed in shear or crushing prior to the epoxy resin compound used as the connector (Van der Linden 1999).

The connection between the timber and concrete is a key part of the composite, with the stiffness of the TCC depending on the level of stiffness in the interfacial connection (Ceccotti et al. 2006b; Clouston et al. 2005a). A significant amount of research into TCC systems has been focused on assessing the effectiveness of shear connections in terms of their strength, stiffness, ductility and failure mode utilising push out tests.

The strength refers to maximum load capacity whilst the failure mode examines connection ductility. In addition, the stiffness of the connection indicates the resistance to slip at the interface of timber and concrete.

In the case of a simply supported TCC with neutral axis located at the interface of timber and concrete components, the forces developed on the fasteners at the interface are related to the slip in the fasteners at that location when loaded. In other words, the shear forces transmitted through the beam are equal to the shear forces resisted by the connectors.

Concrete and timber members exhibit quite brittle behaviour in tension and compression, respectively. Hence, the shear connection is the only contributor to ductile behaviour of TCCs (Ceccotti et al. 2006b; Van der Linden 1999). The strength, stiffness, location and number of connectors thus play a crucial role in the composite action and structural performance of TCC floor system.

The effectiveness of shear connection solutions are evaluated in terms of their strength, stiffness and failure mode utilising shear test. Herein the maximum load carrying capacity and slip at interface of composite materials are measured precisely then plotting the load-slip curve, the slip modulus or stiffness of the connection is determined (Kuhlmann et al. 2004).

Shear tests are undertaken with either asymmetrical or symmetrical specimens. In asymmetrical specimen, one concrete slab is connected to timber joist whilst in symmetrical specimen, timber joist is connected to two concrete slabs placed on two sides of the timber joist. Comparing these two types of specimen, the asymmetrical one is lighter and cheaper. Furthermore, in asymmetrical specimen, overturning moment of the axial forces due to eccentricity increases the compression force at interface. Hence, higher compression force results in larger stiffness and strength (Van der Linden 1999).

A variety of connector types are utilised depending upon the structural requirements including notches, glues, dowel type fastener, nail plates, notches combined with mechanical fastener, continuous slotted sheets, novel connection and proprietary devices, and each of these has different mechanical properties, as well as cost and ease of use (Clouston et al. 2005a). Connectors should be relatively simple, cost effective and structurally efficient. With these considerations, connectors can be preassembled thus the time required to construct a TCC system is reduced.

The level of connection can range from no connection to rigid connection, and this obviously affects load bearing behaviour (Kieslich et al. 2010).

While the failure of a TCC system can theoretically occur in any of the three materials (timber, concrete or connection), Clouston et al. (2005a) stated that it is desirable to design the failure to occur in the connection rather than timber and concrete. Steel connectors represent moderate stiffness and ductile response through elasto-plastic failure which leads to overt warning ahead of failure.

The design of the shear connection should therefore provide a stiff connection between the timber and the concrete while undergoing loading and provide a ductile response while undergoing stresses in the plastic range. Further, designing for failure in steel will likely lead to greater reliability in results, due to the more consistent properties and behaviour of steel compared to timber and concrete (Ceccotti et al. 2006b). In this Section the design parameters of a shear connector in TCCs such as stiffness, ductility, shape and arrangement are discussed.

2.6.1 Connection stiffness

The slip between timber and concrete in TCC connection and consequently the slip modulus of laterally loaded shear connection for a linear elastic model is proportional to the overall behaviour of composite beams including displacement, stiffness, load carrying capacity and distribution of internal forces (Dias et al. 2011). However Santos et al. (2010) and Mascia et al. (2009) reported that the stresses are not so sensible to the behaviour of the connection for plywood composite beams.

Non-linear load-slip response of a connection and its stiffness within the linear range of response (slip modulus) characterises the overall behaviour of composite beams. A connection within the non-linear range results in non-linear behaviour of the TCC beam (Mascia et al. 2009). Thus, the design of TCCs is governed by displacement within serviceability limit state and the slip at the interface of timber and concrete.

The linear-elastic approach for design of timber composite proposed by the Eurocode 5 "Gamma method" employs different input parameter such as slip modulus of connector to design the TCC beams where inaccurate slip modulus results in unreliable design for the timber composite beams (EN 2004b; Mascia et al. 2008).

Hence, the calculation of stiffness is of interest to design and study the structural performance of TCC floor. Material properties of timber, fastener and concrete influence the overall load-displacement response of shear connection. As a result, a stiffer connection typically reduces the slip at the interface of timber and concrete. However, stiffer connectors also tend to fail in a brittle manner and this must be taken into consideration when selecting a connector.

2.6.2 Ductility

Ductility is an important consideration in the design of connectors. Van der Linden (1999) mentioned the necessities of a moderate bending stiffness property in TCCs, as it

allows the structure to deflect and therefore induces adequate warning to inhabitants of the building prior to failure. This ductile failure can be achieved through the use of a ductile connection system that becomes plastic prior to the timber or concrete failing. As a result, TCCs utilising ductile connections fail in a manner that the catastrophic failure is prevented.

Ceccotti et al. (2006b) and Clouston et al. (2005a) highlight the importance of balancing stiffness and ductility. Connection is required to be stiff enough to obtain high composite efficiency. Moreover, not too resistant shear connections with elasto–plastic behaviour are desirable to provide overall ductility in TCC systems.

Dias et al. (2011) simulated numerically the behaviour of non-linear connectors and found that ductile connectors increase the strength and serviceability of a TCC system by increasing the load carried and the maximum safe deflection. Moreover, it was stated that ductile connections are the safest connector type which has an ultimate deformation capacity greater than the highest slip demand of the composite system and allows the loads to be redistributed.

Yeoh et al. (2009) highlighted that the plasticity in the connector is the only mechanism for introducing ductility into a TCC system due to the brittle behaviour of timber in tension and concrete in compression.

Steel represents an elasto-plastic failure exhibiting a high stiffness in the elastic range with more ductile behaviour in the plastic range. Moreover, designing for failure in steel connector leads to higher reliability due to more consistent properties and behaviour of steel compared to timber and concrete (Clouston et al. 2005a).

2.6.3 Inclined and crossed fasteners

Previous investigations reported that the inclination of a fastener significantly increases the initial stiffness and strength of the connections and consequently composite floor. The strength of a vertically inserted fastener is calculated based on the flexural capacity of the fastener and the embedding strength of the timber.

The inclination of the fastener to the grain increases the strength of the connection by taking into account the withdrawal and tensile capacity of the fastener and as a consequence, a more economic connection is achieved.

Van der Linden (1999) reported an experiment conducted by Küng (1987), which highlighted that by positioning the dowel connectors at an angle of 60 degrees, rather than 90 degrees from the horizontal face, the load capacity of the connection was increased by a factor of two. The slip modulus of the connectors also increased.

Symons, Persaud & Stanislaus (2010a & b) tested 16mm threaded diameter, 230mm long coach screws in a set of push out tests aimed at validating their analytical strength and stiffness models of an inclined screw shear connector. Each TCC specimen was fabricated from a 1000x600x100mm concrete slab fixed to a 1000x270x160mm grade GL28 glulam joist.

Each specimen featured an interlayer utilising a trough shaped steel decking fixed to the joist with self-drilling, self-tapping screws. Each trough had a coach screw drilled 120mm into the timber with a total of 5 coach screws per specimen. Two specimens were prepared for each screw inclination from 0 to 50° to the vertical face, in increments of 10° (Symons et al. 2010a).

Figure 2-10 highlights the load-slip diagram per screw for selected screw angles of 0°, 20° and 40°. Symons et al. (2010b) stated that by inclining screws, the connectors act to resist slip by axial loading rather than just in bending. Symons et al. (2010a) mentioned that the screws failed either through the development of single or double plastic hinges in the glulam or in both the glulam and concrete, respectively.

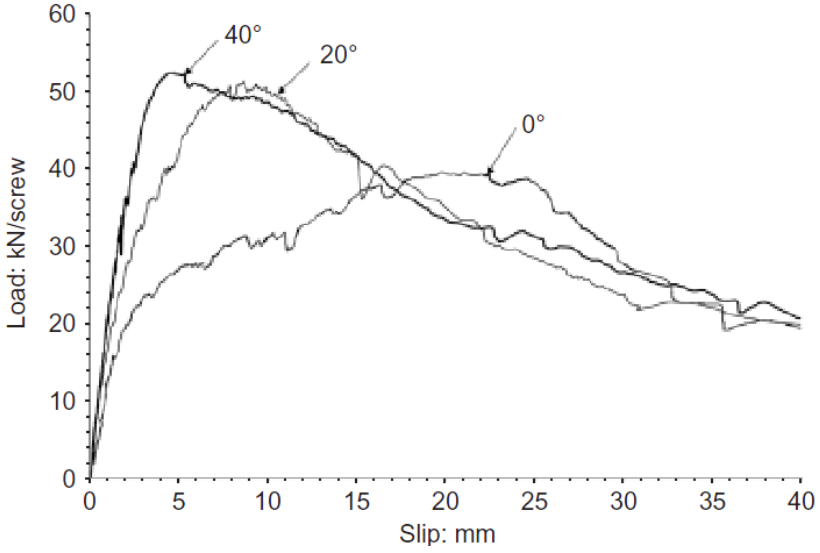

Figure 2-10 Load-slip of varying angles (Symons et al. 2010a)

The results clearly indicate that inclining the screw increased the strength and stiffness of the connection. It was concluded that increasing the inclination angle to the vertical face increases both the stiffness and strength of inclined screws whilst it reduced the slip at F_{max}.

Dias et al. (2011) tested angled screw connections utilising different grades of light-weight concrete with and without presence of an interlayer. SFS screws were used in both parallel (45°) and crossed (±45°) arrangements. The crossed arrangement has one screw carry shear forces in tension whilst the other screw takes forces in compression. In the parallel layout, both screws are under tension.

Results showed that on average, parallel screws withstood slightly higher strength and slip moduli. Additionally, in the case of parallel screws there was less reduction in strength due to the interlayer.

Elsewhere, Fernandez-Cabo et al. (2012) stated that inclined connectors produced better efficiency of the composite structures.

2.6.4 Embedment depth

Proper embedment is required to ensure that there is enough contact between the shear connector and the timber and concrete interfaces. If the depth of embedment is insufficient, the connector typically fails either by being withdrawn from the timber or being distorted.

Van der Linden (1999) noted that the embedment depth of screws was a factor in determining their failure mode, stiffness and strength of TCC connection. Yeoh (2010) reinforced this idea, stating that the depth of a concrete notch affects the connector's behaviour. A theoretical model developed by Symons et al. (2010b) highlighted that for a greater non-dimensional embedment depth ($\hat{t}$), the non-dimensional stiffness ($\hat{K}$) of a vertical screw shear connector increased as illustrated in Figure 2-11.

The non-dimensional stiffness ($\hat{K}$) is slip modulus of screw (K) divided by foundation modulus of timber parallel to the grain and diameter of screw shank whilst non-dimensional embedment depth ($\hat{t}$) represents the ratio of screw's embedment length in timber (t) to screw diameter (d) as given in Figure 2-11.

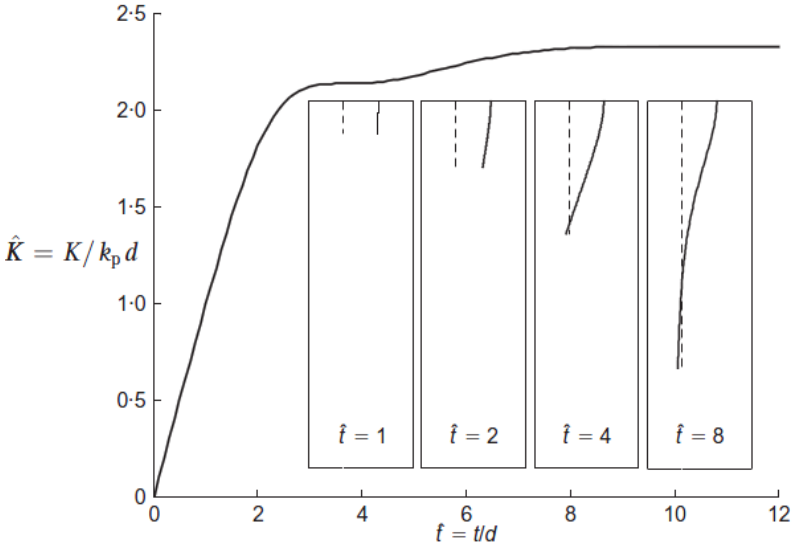

Figure 2-11 Non-dimensional stiffness of a vertical screw ($\hat{K}$) as a function of the non-dimensional embedment depth ($\hat{t}$) (Symons et al. 2010b)

2.6.5 Spacing and positioning

The greater the number of shear connectors and hence, a tighter spacing increase the strength of connectors. However, codes such as Eurocode 5 present minimum spacing requirements to ensure the elements are not overstressed and to prevent splitting of the timber.

Dias et al. (2011) stated that for a given slip modulus demand at ULS, the slip of the composite members is less when the spacing is closer, as shown in Figure 2-12. Shear is typically maximum at the ends of a simply supported beam and as a result, the shear and consequently slip are maximum at the ends of a TCC system (Ceccotti 2002).

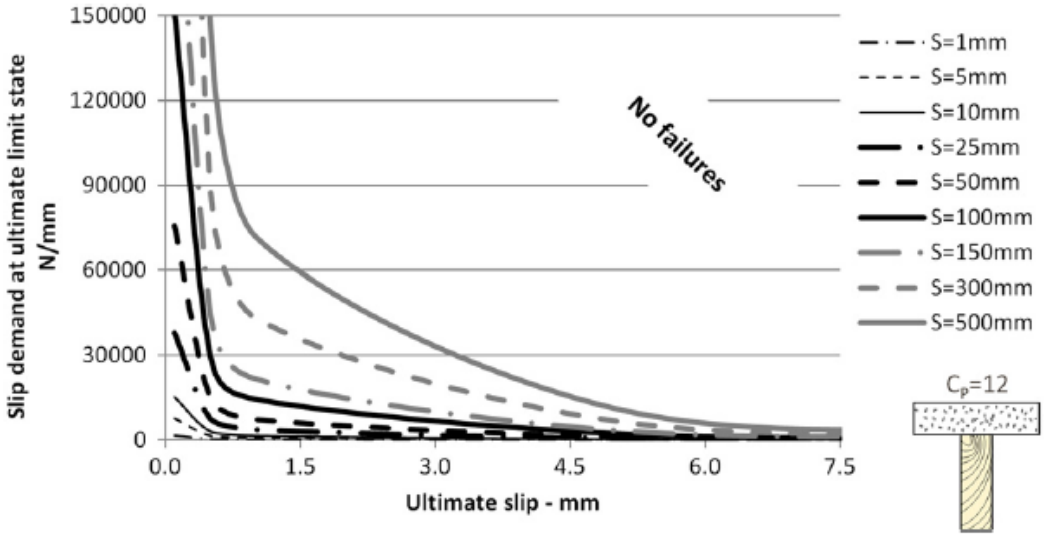

Figure 2-12 TCC slip behaviour as a function of fastener spacing (Dias et al. 2011)

This concept is reinforced in literature where Postulka (1983) and Postulka (1997) report the use of Nails 6.3 x 180mm, as connectors spaced equally at 250mm at the mid-span and 100mm near the supports for TCC floors. Frangi et al. (2003) also supported this concept and stated that the end shear connectors reached their maximum capacity first during their laboratory tests.

2.6.6 Connector shape

Dias et al. (2010b) also concluded that the shape or strength of the steel dowel does not have a significant impact on the slip modulus although the nominal diameter of the dowel does have an impact on the stiffness and strength of shear connections.

In notch connectors, the shape of the notch can have a significant impact on how the connector fails, either through crushing of the timber or brittle failure of the concrete For example, Gerber et al. (2011) stated that polygonal shaped notched connections have a much more desirable behaviour than trapezoidal notch designs.

2.6.7 Effect of timber and concrete dimensions

Van der Linden (1999) remarked that there is an optimum ratio between the dimensions of the concrete slab and timber beam to achieve a desirable bending stiffness.

The span of the TCC beam also influences the effectiveness of the connector in transmitting complete composite action. Figure 2-13 highlights the effect of span on the connector through the use of a combination factor (shear bond coefficient) which denotes effectiveness of the composite action with varied smeared slip modulus k_1.

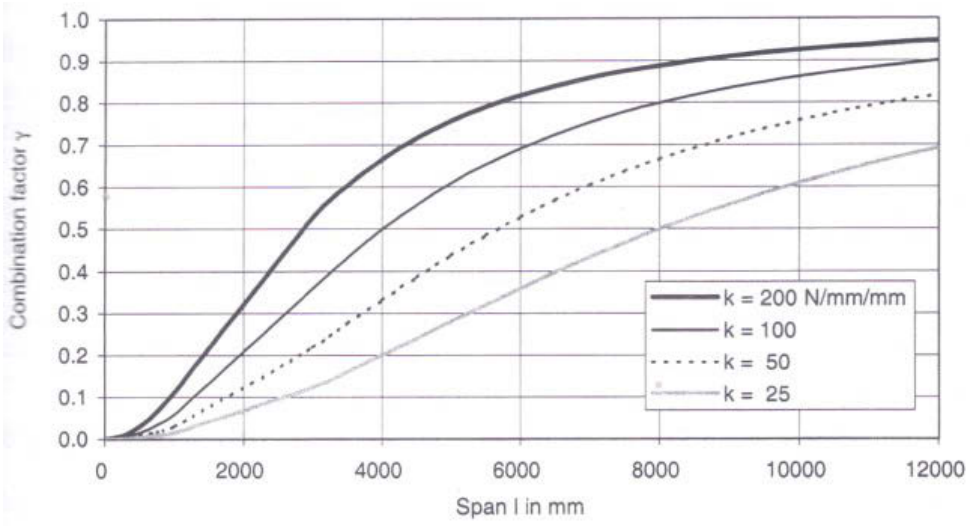

Figure 2-13 Beam span-combination factor of various stiffness (Van der Linden 1999)

The concrete slab and timber joist had dimensions of 600x70mm and 100x200mm, respectively. For example, at a span of 2000mm and a smeared slip modulus, k1 of 100N/mm/mm, the combination factor is 0.2, which means that only 20% of the possible ultimate stiffness is achieved through composite action.

2.7 INFLUENCE OF HIGH-PERFORMANCE CONCRETE PROPERTIES ON TCC CONNECTIONS

To-date, conventional concrete (CC) has been applied in most investigations on TCCs. There are only few investigations to study the effect of concrete properties on the structural behaviour of TCC system. Today, with the advance in admixtures and additives, concrete mixes can be designed to new requirements of strength and serviceability with modified fresh and hardened properties.

High-performance concrete (HPC) is an enhanced concrete with new technique that mainly improves in durability, workability, strength, early age strength, toughness, light density, volume stability economic and suitability of some special environmental situation. The water reducer is used to decrease the water cement ratio to increase the strength and workability; fly ash and silica fume increase the durability of concrete; air entrained agent used to produce bubbles in concrete which prevent the freezing and thawing, as the air density is very low the density of concrete reduces. However, strength of concrete is not a governing parameter in TCCs, properties of concrete such as workability, lower shrinkage and durability play an important role in structural performance of TCCs.

Kieslich et al. (2010) highlighted the variety of high-performance concretes available such as light-weight concrete (LWC), fibre reinforced concrete (FRC), self-consolidating concrete (SCC), high-strength concrete (HSC) and the ways in which these can be used in TCCs.

For example, steel fibres concrete might be beneficial for TCCs in confined spaces (for example building rehabilitations). Holschemacher et al. (2002) investigated application of steel fibre reinforced concrete (SFRC) without any conventional reinforcement in TCCs.

The major difference between high-strength concrete (HSC) and conventional concrete is its compression strength which ranges between 50-100MPa (EN 2004a). Although the material used to produce high-strength concrete is very similar to the material of

conventional concrete, the key issue is to increase the strength of concrete, by controlling the factors that affect the strength. The HSC is produced utilising different methods such as improving the hydration condition of cement by increasing high-strength aggregate content or increasing the fineness of grinding to achieve high specific surface, mixing with different type of high-strength aggregate, using admixture such as water reducer, fly ash and silica fume and increasing the compaction of concrete.

Holschemacher et al. (2002) tested 160mm normal screws in 3 test series such as (1) conventional concrete with concrete key; (2) fibre-reinforced concrete with concrete key (notch) and (3) fibre-reinforced concrete to study the effect of shear key and SFRC compared to steel mesh reinforced concrete. Comparing conventional concrete and SFRC, the application of SFRC with concrete key increased the ultimate load capacity by 30% whilst the initial slip was reduced by about 60%. Steel fibres did not need any concrete cover. Thus, the thickness of concrete slab was reduced to 35mm. This is a particular advantage for rehabilitation works where floor heights are limited.

It was concluded that the application of steel fibres has no important effect on strength and stiffness of TCC connections. Furthermore, the crack initiation and development in concrete was delayed and the stresses distributed more uniformly (Holschemacher et al. 2002). As a drawback, steel fibres may wear out the concrete pump and pump-line (Kieslich et al. 2010).

The fresh properties of concrete in upgrading of old timber floor to TCC are of interest for two reasons, first the concrete needs to be workable and compactable in order to fill the formwork in confined spaces and complex forms properly. Moreover, concrete needs to be pumpable as some locations, particularly in retrofits, it may not be able to be delivered by crane. Given that concrete in TCCs is likely to be primarily under compressive stress, FRC presents a strong opportunity to reduce conventional reinforcement (Kieslich et al. 2010).

SCC has been used increasingly for more than two decades in pre-cast concrete technology whilst its application in TCC provides a potential development to enhance the workability and flow ability of concrete without the need for an external vibration (Kieslich et al. 2010; Ramezanianpour et al. 2012).

The components of SCC and CC are identical, consisting of cement, water, aggregates, admixtures, and mineral additions but the composition of the mixture, fresh and

hardened properties are different. SCC includes larger amount of mineral fillers (i.e. finely crushed limestone or fly ash) and water-reducing admixtures. Moreover, the maximum size of coarse aggregate is smaller than that in CC. Water reducer, superplasticiser and viscosity modifying admixture were used to adjust the SCC mix.

SCC may be advantageous for upgrading of old timber floor with complex formworks and little space for compacting measures. SCC typically has appropriate workability and flowability and is self-venting. SCC generally has a high content of cememtitious material which can lead to higher heat of hydration and shrinkage. It can also lead to lower strength which may require higher levels of reinforcement. For these reasons, Kieslich et al. (2010) suggested application of a highly workable concrete but not self-consolidating concrete in TCCs.

Leborgne et al. (2010) studied the negative effect of poor consolidation, moisture loss, transverse shrinkage cracks of the concrete and swelling of the timber on composite action of TCC floor. Moisture absorption from the concrete into timber was reduced by painting the specimens with water proofing paint and as a consequence the swelling of the timber was mitigated.

Furthermore, a self-levelling concrete was utilised with a design compressive strength of 34.5MPa and a slump of 279.4mm to modify consolidation. Two types of Nylon and Type I steel fibres admixtures were utilised in ultimate bending test on twelve full-size specimens constructed with Hilty shear key connectors and notch connections. The dominant failure mode was observed as a combination of bending and tensile failure at mid span. The composite efficiency of specimens did not vary significantly. The average composite efficiency of twelve specimens was 83.4% (Leborgne et al. 2010).

The application of LWC provides an interesting development in TCC technology to minimize the dead-load on timber component. Such reduction may be favourable in renovation of old timber floor. It is also advantageous in new multi-storey buildings for aspects such as prefabrication and mitigation of excess dead load – leading to saving on foundation and walls and/or column sizes.

Comparing LWC and conventional concrete, LWC causes larger shrinkage strain and lower MOE (due to lower MOE of light-weight aggregates). Hence, the serviceability deflection of TCC is expected to be larger. In contrast, the nominal reduced creep coefficient and lower dead-load of LWC may reduce the serviceability deflection of

TCCs. Hence, the question of influence of LWC on structural response of TCC beams has no direct answer and needs to be verified by experiment (Jorge et al. 2010).

LWC exhibits the advantages of higher strength/weight ratio, energy absorption, better tensile strain capacity, lower coefficient of thermal expansion and superior heat and sound insulation characteristics due to air voids of the light-weight aggregate (Al-Khaiat et al. 1998; Topçu 1997; Yasar et al. 2003).

Light-weight aggregates are categorised into two broad categories as natural (crushed basaltic pumice, scoria, diatomite, volcanic cinders, etc.) and artificial (perlite, clay, sintered fly ash, expanded shale, Polystyrene) (Miled et al. 2004) (Al-Khaiat et al. 1998; Ghavami 1995; Hossain 2006).

The LWCs are classified by their mass per unit volume ranging from 300kg/m^3 to 1900kg/m^3 and application including low mass per unit volume, moderate strength and structural concrete as illustrated in Figure 2-14 (ACI213R 1987).

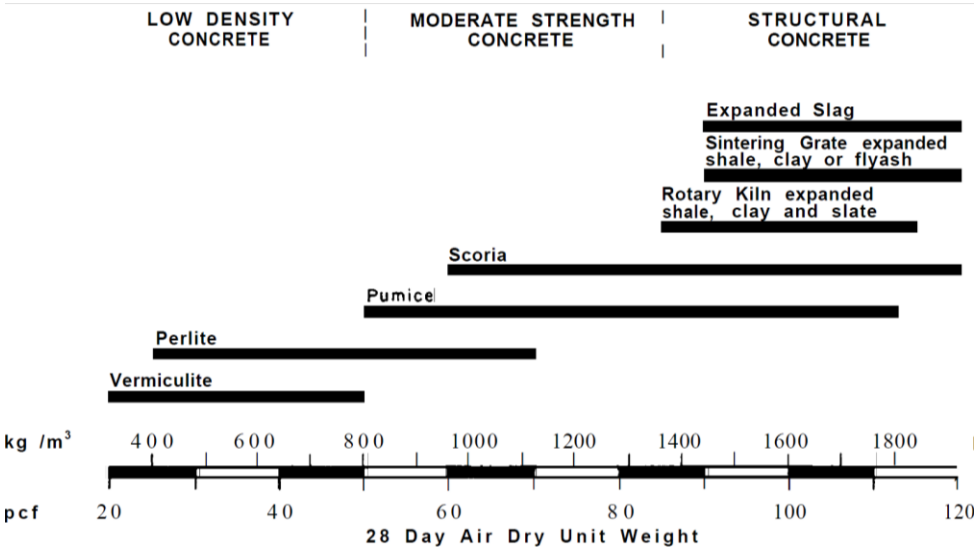

Figure 2-14 Mass per unit volume and use classification of LWC (ACI213R 1987)

Steinberg et al. (2003) reported that application of a LWC with a mass per unit volume of 1600kg/m^3 instead of conventional concrete in TCC reduces its dead-load approximately 15%. Steinberg et al. (2003) carried out push-out tests on five different types of shear connection utilising LWC. It was concluded that the MOE of LWC reduced the composite efficiency and effective bending stiffness of TCC floor. Therefore, the spacing of connectors in LWC must be less than conventional concrete.

The design depends upon the compromise between the lower spacing of the connectors (higher cost) and the reduction in permanent load (Steinberg et al. 2003).

TCC specimens utilising LWC slab exhibited concrete failure whilst most of TCC connections utilising conventional concrete and mechanical fastener in literature experienced predominant failure mode of shearing off or withdrawal of the connectors. The failure in connection allows that altering dimensions of the fastener governs the failure. Moreover, the application of LWC in TCC requires an evaluation of the anchorage potential of the connectors in concrete (Steinberg et al. 2003).

Haiman et al. (2004) tested four TCC beams utilising different connection types and Expanded polystyrene LWC with mass per unit volume grade of 1200-1400kg/m^3.

Expanded polystyrene is a stable low density foam as an artificial ultra light-weight aggregate with the mass per unit volume of 12-32kg/m^3 which can replace part of coarse aggregate in the concrete - to obtain a light-weight concrete with a significantly reduced mass per unit volume ranging 1600-2000kg/m^3 allowing for large self-weight reductions (Chen et al. 2004; Cook 1983; Miled et al. 2004).

Increasing the content of polystyrene beads in EPS LWC reduces the density and compressive strength of LWC. However, adding polystyrene beads creates segregation problems and requires special mix design method to prevent segregation (Choi et al. 2006). Over vibration of the EPS mixtures causes the beads to rise to the surface which significantly affects the uniformity of strength. (Ravindrarajah et al. 1997).

The failure of EPS LWC under compression is different from conventional concrete and represents a more gradual failure with retaining the load after failure, without full disintegration which proves the high energy absorbing capacity (Chen et al. 2004). The energy absorption capacity and ductility of concrete increased with increased polystyrene aggregate content (Sabaa et al. 1997).

The TCC connector types tested by Haiman et al. (2004) were type 1 ⌀25mm steel dowels placed in pairs at 200mm spacing and type 2 ⌀25mm steel dowels placed alternatively 200mm apart that were both epoxied. Type 3 ⌀6mm nails driven in threes to a depth of 100mm, 50mm exposed 100mm apart. Type 4 connected the two materials with epoxy glue. Haiman et al. (2004) found that TCC beams utilising glued connections (type 4) experienced the highest stiffness and load carrying capacity whilst TCC beams with nails (type 3) exhibited the worst stiffness and load carrying capacity.

Grantham et al. (2004) investigated TCC connections (short SFS screws inclined at 45° placed in tension) and beams utilising LWC produced from recycled sewage sludge. The existing timber floor was upgraded by casting a LWC slab with a mass per unit volume of 1760kg/m^3. TCCs were subjected to long-term and collapse tests. It was concluded that a LWC floor exhibited a favourable lower self-weight and higher strength. In contrast, LWC floor in long-term test represented a larger sensitivity to rheological phenomena compared to TCC with conventional concrete (Grantham et al. 2004; Yeoh 2010).

Fragiacomo et al. (2007) investigated mechanical properties of "Tecnaria" connectors utilising eighteen specimens made from light-weight and conventional concretes. It was found that application of LWC rather than conventional concrete did not affect the stiffness.

Kieslich et al. (2010) studied TCC modules utilising different types of high-performance concretes including SCC, FRC, LWC, HSC or combinations of them in TCC -aiming to study easy workable mixture with lower dead-load and shrinkage strain. Moreover, the effect of the MOE of different conventional and light-weight concretes on the effective stiffness, EI_{eff} of TCC beam versus shear bond coefficient, γ was investigated. It was found that the LWC slab with higher value of MOE and same thickness increased the effective stiffness of TCC compared to LWC with lower MOE. The proposed values of the MOE for concrete were obtained from the German standard DIN1045 (2008) whilst the real values strongly depend upon the type and MOE of aggregates. The main drawback of the LWC is the characteristic of sucking some part of the concrete's water which has to be considered in the mixing ratio (Kieslich et al. 2010). Moreover, the higher compressive strength of the cement matrix rather than the light-weight aggregates causes high brittleness in LWC. In contrast to LWC, the cement matrix of conventional concrete exhibits a lower compressive strength compared to its aggregates (Kieslich et al. 2010).

Kieslich et al. (2010) proposed a mix of polyvinyl alcohol-fibres (PVA) into dry light-weight concrete (DLWC), aiming to modify high brittleness. The important concerns about the combined high-performance concrete are summarised as problematic pumpability using porous light-weight aggregates and difficulties for a uniform fibres distribution in concrete. Five different mixtures of two types of fibres with the dry mass per unit volume of 1600kg/m^3 were tested using bending test of small TCC beams. It

was concluded that increasing the fibre content using both fibres improved the load carrying capacity of TCC modules compared to using only one type or control series (without fibre) (Kieslich et al. 2010).

Jorge et al. (2011) studied the influence of the interlayer on the structural properties of TCC connections and beams utilising different grades of LWC and arrangement of inclined short SFS screws. Jorge et al. (2011) reported that inclusion of interlayer in a TCC specimens reduced strength and stiffness and proposed strength reduction factors of approximately 30-50% and 10-30% for short SFS screws test series utilising conventional concrete and light-weight concrete, respectively.

The application of LWC instead of conventional concrete led to a strength reduction of 30% and 50% for the specimen without an interlayer whilst in presence of an interlayer, the reductions were smaller. This is promising for renovation and strengthening purposes utilising LWC where the floor board acts as an interlayer.

In the case of TCC beams, application of LWC reduced the strength, but the stiffness is maintained approximately constant. The stiffness is more relevant to design compared to load capacity. Therefore, the difference between light-weight and conventional concrete seems to be negligible in the short term (Jorge et al. 2010).

In addition to suggesting a reduction factor for samples with an interlayer, Jorge et al. (2011) also investigated and quantified two different shear connection layouts. From their results conclude that screws in parallel at +45° provide higher strength results than screws crossed at ±45°. Both screw arrangements utilising different LWCs exhibited a tensile failure of screws.

2.8 CONCLUSIONS

Interest in TCC floors as a viable and effective alternative to conventional reinforced concrete and/or traditional timber floors in multi-storey buildings has increased over the last 20-30 years. In TCC technology, a timber beam is connected to a concrete slab using a connection system that resists shear forces and impedes slip between the composite materials. The strength, stiffness, location and number of connectors play a crucial role for the composite action and determine the structural and serviceability performance of the floor system.

This Chapter describes the state of the art of TCC structures. A comprehensive review of literature about the development and structural behaviour of TCC structures is presented. The history behind and various advantages of TCC were introduced.

The advantages of TCCs are numerous, including the improved durability over reinforced concrete and timber floors, as well as improved fire retention and thermal and sound insulation properties. They carry a much higher live-load per unit self-weight and have a lower embodied energy than reinforced concrete solutions.

Three different construction methods of TCC such as (1) wet method; (2) semi-prefabrication method (cast in-situ) and (3) prefabrication off-site (dry-dry method) have been discussed. The specific design methods of TCCs such as the Gamma method proposed in Eurocede 5 part 1 annex B and elasto-plastic were introduced.

A review on previous research into the applications of innovative high-performance concretes such as LWC, FRC and SCC in TCCs was also undertaken, with a discussion based on the findings and contribution that the previous research has presented to TCCs.

3 REVIEW OF CONNECTION TYPES FOR TCC

3.1 INTRODUCTION

The first Section of this Chapter is a discussion of different classifications of TCC connection and case studies to demonstrate, in detail, the behaviour achieved from a wide variety of shear connector systems. Each case studies first introduces shear connection classification and compares the experimental results of different types of TCC connection utilising push-out and four-point bending tests.

In the second Section, the TCC shear connections have been broken up into categories based on the type of classification although, at certain times, an overlap may occur. Each category of TCC connection is investigated more thoroughly by undertaking case studies on previous experimental investigations on similar connections.

3.2 CONNECTION CLASSIFICATION AND CASE STUDIES

A review of different classifications and case studies of TCC connections conducted by previous academics is presented in this Section. The case studies compare the experimental results of different types of TCC connection to demonstrate, in detail the behaviour achieved from a wide variety of connector systems as shown in Figure 3-1.

The TCC connectors can be classified into different groups such as discrete/continuous, glued/non-glued, vertical/inclined and prestressed/non-prestressed (Yeoh et al. 2010).

Clouston et al. (2004) presented an example of this classification and categorised the shear connections into four types of (a) dowel-type, (b) tubular-type, (c) notches with an anchoring device and (d) (dis)continuous glued-in-wood plate.

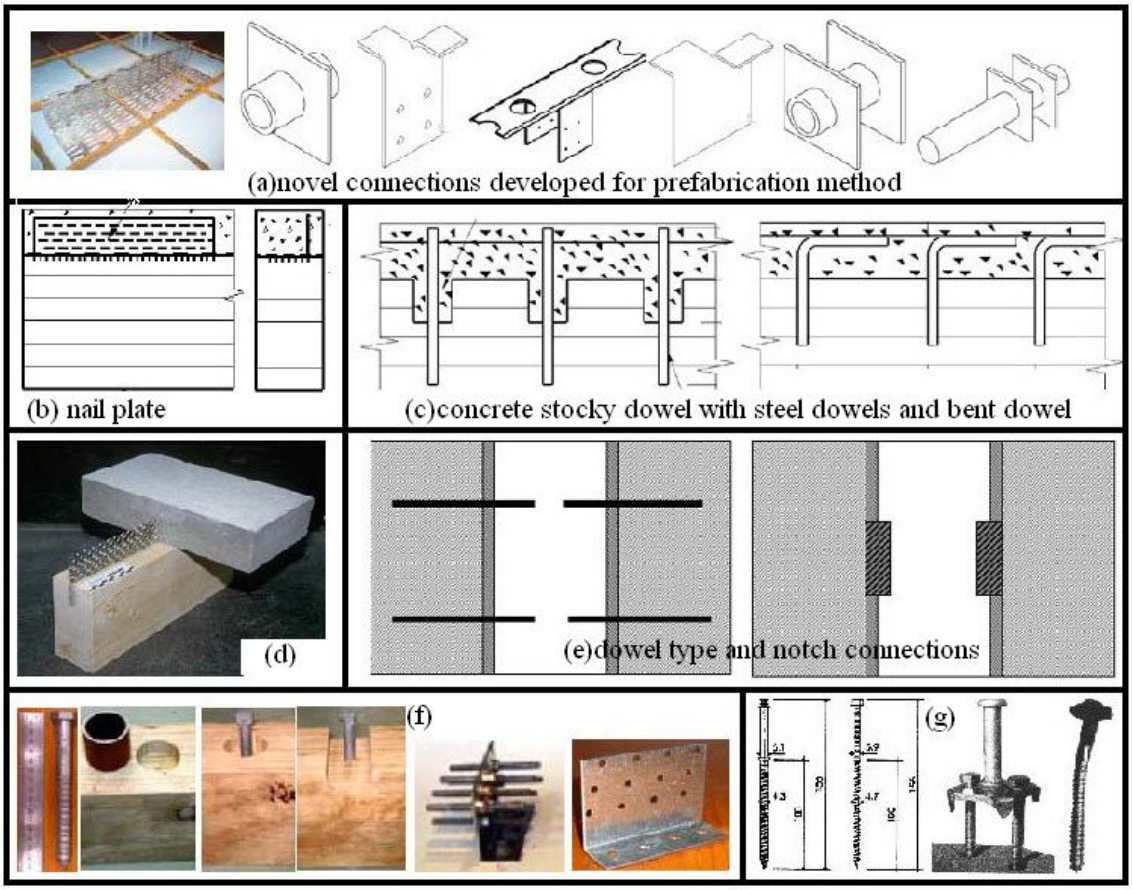

Figure 3-1 Different connection systems (a) Lukaszewska (2009), Van der Linden (1999), (c) Piazza et al. (2000), (d) Bathon et al. (2000), (e) Dias (2005), (f) Deam et al. (2008) and (g) Steinberg et al. (2003)

3.2.1 Van der Linden (1999) case studies

Van der Linden (1999) tested four connector types which were screws fixed at ±45° nail plates bent at 90° (Figure 3-1b), concrete notches and reinforcement bar with concrete notches in laminated veneer lumber (LVL).

Shear tests of the screws highlighted that the embedment depth of screws was a factor in determining their failure mode. In the case of the presence of interlayer between the timber and concrete, the majority of screws pulled out of the timber whilst the screws failed due to rupturing of the steel shaft in test series without interlayer (Van der Linden 1999). Van der Linden (1999) stated that the application of an interlayer for example timber board between the timber beam and concrete slab significantly affects the behaviour of the connector.

The primary failure mode of the nail plates was through the partial-rupture and bending of the nails that were connected into the timber beam.

Van der Linden (1999) tested the concrete notches in LVL joist across a range of configurations including the use of different coating treatments between the timber and concrete interface. The key findings noted that through the use of a LVL joist with two layers perpendicular to the remaining seven layers, the bending stiffness of the timber were increased. When LVL had been dried for 74 days, the concrete notches were able to carry a significantly higher shear load, before failing in a brittle manner due to the shear forces induced between the concrete slab and the notch (Van der Linden 1999).

Van der Linden (1999) stated that the reinforcement bar with concrete notch connection allowed the reinforcement bar to transmit its force into the timber beam and thus increased the strength and slip of the connector. On the other hand, the reinforcement bars displayed very plastic behaviour. The reinforcement bar with concrete notch was forced through the timber beam as the applied load approached the embedding strength of the timber. The reinforcement bar was also bent as the maximum load was attained with visible crushing of the concrete notch evident. The key findings from the reinforcement bar tests highlighted that the size of the concrete notch plays a significant role in increasing the shear capacity of the connection system (Van der Linden 1999).

Once the notch was reinforced with an adequate amount of steel reinforcement, a plastic behaviour could be achieved. When the connector displaced by 2mm, the maximum load capacity of the connector had already been reached. The load was further increased up to a displacement of 15mm until the timber had reached a plastic state, although the connection was still capable of further loading.

Further tests by Van der Linden (1999) showed that as the amount of notch reinforcement was reduced, the concrete failed around the edges of the notch resulting in the distorted notch slipping out of the LVL.

It is difficult to draw definite conclusions after undertaking an evaluation of the efficient connector types given they all had different mechanical properties, costs, dimensions and utility. An assessment of the results by Van der Linden (1999) however, showed that the screws are more efficient than the nail plates given their smaller area of connection. Nearly all four connector types failed in a plastic manner except for some of the screws and the concrete notches which failed by rupturing of the screw shaft and through crushing of the concrete.

In terms of strength, it can be demonstrated that the nail plate, reinforcement bar and concrete notch exhibit far greater shear strength capacity than the screws (Van der Linden 1999). It was found that the TCC beams exhibited a plastic behaviour before ultimate collapse contrary to the timber beam with brittle failure in tension zone. Ductility of connectors resulted in the occurrence of the plastic hinges in outer connectors, hence the load redistributed to the adjacent connectors until they behaved as plastic hinge. The dominant failure mode of TCC beams was combined bending and tensile failure of the timber component (Lukaszewska 2009; Van der Linden 1999).

3.2.2 Piazza et al. (2000) case studies

Piazza et al. (2000) identified the mechanical properties of TCC samples constructed from eight different types of connection and subjected to push-out and bending tests. Moreover, some numerical analyses were carried out to verify the influence of the connection systems on the behaviour of the composite beams. Full scale TCC beams utilising two types of glued-in connections including 16mm diameter bent dowels and concrete stocky dowels coupled with 16mm diameter steel ribbed dowels (Figure 3-1c) were tested to failure.

The connectors exhibited a linear response up to 50% of the failure load followed by a post-elastic hardening branch. The composite efficiency of 70% and 85% was obtained by hardening branch of bent dowels and concrete stocky dowels, respectively. The bending strength of bent and concrete stocky dowels applied in TCC were measured about 2.0 and 2.5 times larger than that of timber beams, respectively (Lukaszewska 2009; Piazza et al. 2000).

3.2.3 Ceccotti (2002) case studies

Ceccotti (2002) also presented an overview of the most commonly used shear connections based on their shape and structural efficiency to achieve composite action between the concrete and the timber members as shown in Figure 3-2.

The selected shear connectors were tested using push-out tests and classified according to their stiffness into four classes of (a) nails, screws or dowel shaped fasteners with the lowest stiffness (Figure 3-2a); (b) the rigidity can be increased by surface connectors (Figure 3-2b); (c) or by cutting the notches along the timber joist (Figure 3-2c); and (d) continuous glued to timber connector which presents the highest stiffness with full composite action and neglected slip as depicted in Figure 3-2d (Ceccotti 2002).

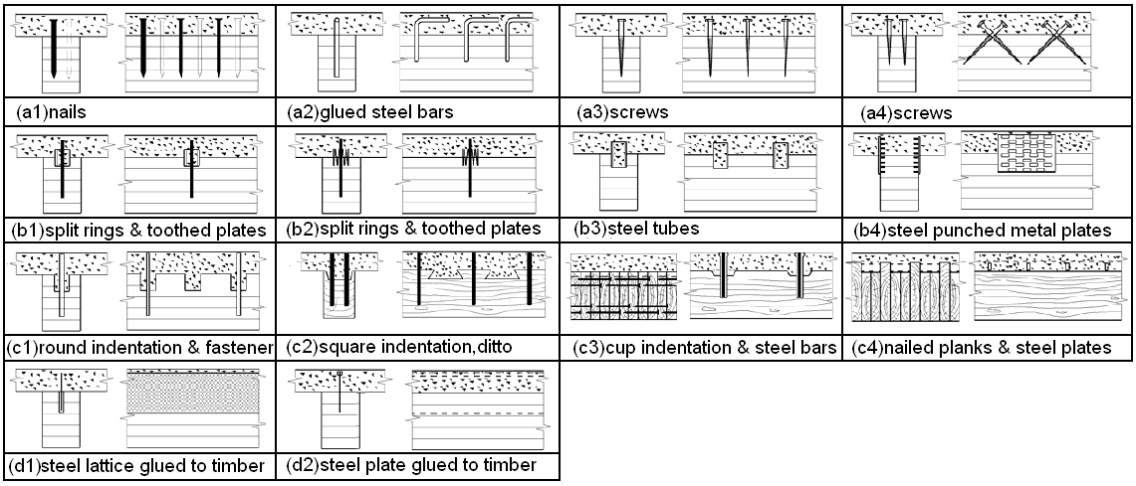

Figure 3-2 TCC connectors (Ceccotti 2002; Lukaszewska 2009; Van der Linden 1999)

3.2.4 Lukaszewska et al. (2008) case studies

Lukaszewska et al. (2008) tested different shear connections for example continuous steel mesh, steel tube, two folded steel plates, dowel with flanges embedded into the concrete and long steel tube combined with coach screw and notch cut in timber developed for prefabricated TCC system utilising push-out test as illustrated in Figure 3-1a.

It was concluded that a steel mesh and long steel tube in combination with coach screw and concrete notch represented the highest strength and stiffness among those tested as shown in Figure 3-3 (Lukaszewska et al. 2008).

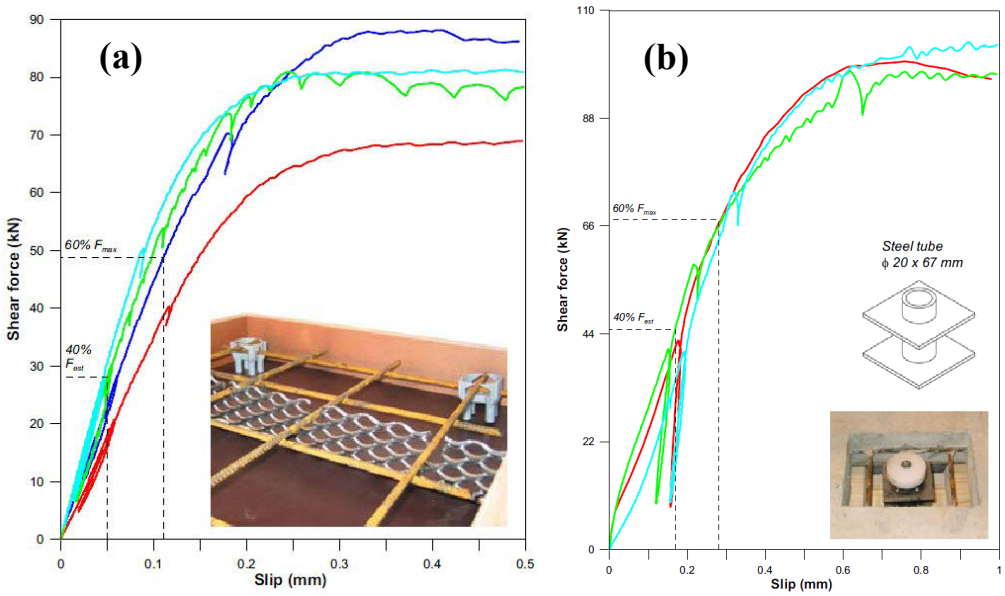

Figure 3-3 Load-slip of (a) steel mesh and (b) steel tube and notch (Lukaszewska 2009)

3.2.5 Deam et al. (2008) case studies

Deam et al. (2008) studied the feasibility of a composite structure, consisting of LVL joists, concrete slab and connectors, in order to identify the most cost effective connections. A number of connections such as round and rectangular concrete plugs with and without steel pipe or screws reinforcement, SFS screws, coach screws with different diameters, sheet brace anchors, and framing brackets (Figure 3-1f) were tested using push-out tests (Deam et al. 2008).

Deam et al. (2008) summarised the main conclusions of the experimental program as: (1) concrete plugs reinforced with a screw or steel pipe exhibited the highest stiffness, strength, and post-peak behaviour. Screw reinforcement enhanced the strength and post-peak behaviour; (2) strength and stiffness of these connections depended upon the bearing area, hence a rectangular plug exhibited higher composite action compared to a smaller round plug; and (3) rectangular concrete plug reinforced by a coach screw spaced 500mm along the beam was found as a capable solution with highest stiffness and ductility for 8m span floor.

3.2.6 Dias et al. (2011) case studies

Dias et al. (2011) compared the behaviour and capacity of a number of common connectors as illustrated in Figure 3-4. The glued and notch connections exhibited the highest stiffness whereas the mechanical fasteners for example nails and dowels were identified to experience the lowest stiffness (Dias et al. 2011).

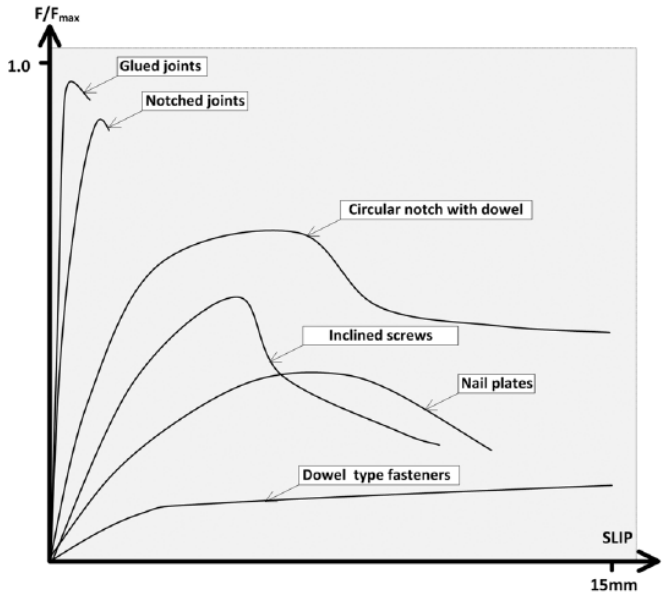

Figure 3-4 Load-slip responses for common TCC connectors (Dias et al. 2011)

3.2.7 Fernandez-Cabo et al. (2012) case studies

Fernandez-Cabo et al. (2012) presented a connection classification based on their structural performance in TCC beams which includes dowels, ring and shear plates, notches and dowels, nail plates and continuous slotted sheets. Dowels typically achieve an efficiency of 65-75%, whilst rings and shear plates achieve an efficiency of 90%. Notches and dowels on average demonstrate 75-85% efficiency for beam floor systems, whilst nail plates can achieve a composite efficiency of 80%.

3.3 CONNECTION TYPES

In this Section, the TCC shear connections have been broken up into categories based on the type of classification although, at certain times, an overlap may occur. Each category of TCC connection is investigated more thoroughly by undertaking case studies on previous experimental investigations on similar connections.

3.3.1 Dowel type fastener

Dowel type fasteners for example bolt, nails and screws have a long history of use in timber structures due to their relatively cheaper price and ease of fabrication and there are a number of different types of dowel connectors available for TCCs ranging in effectiveness, price and labour requirement.

The slender dowel type fasteners indicate a significant nonlinearity and ductility prior to the failure in their load-slip responses due to geometric nonlinearity of the fastener-to-hole contact, inelastic strain in the timber at low-load levels and inelastic strain in timber and fastener associated with high level of loading (Tan et al. 1999).

Ahmadi et al. (1993) identified the feasibility of a TCC floor constructed from high-strength nails in residential and commercial building. In this investigation, ten types of high-strength nail were tested using push out, bending, and long-term tests on full scale specimens. In addition, a finite element model was implemented to verify the results of the experimental tests. Comparison of non-composite and partially composite TCC, proposed partially composite beams exhibited two times higher load carrying capacity and one-fifth of deflection than non-composite system. It was concluded that application of appropriate connections in TCCs increases the stiffness and load carrying capacity of floor. Hence, at least a 50% saving in the cost of the timber joists compared to non-composite floors was achieved (Ahmadi et al. 1993).

Steinberg et al. (2003) tested five different connectors utilising push-out test as illustrated in Figure 3-1g. Connector A is a cross pair of screws similar to a SFS screw and connector B is a parallel pair of screws. Connectors C and D are the 'Tecnaria' with head stud and a steel plate with two side screws whilst connector E is a screw with a washer. The screws in connectors A, B and D connectors were installed at an angle of 45 degrees to shear plane. Connectors B and D experienced strength slightly above 20kN within the 5mm slip whilst connection C and D represented the highest stiffness at approximately 20kN/mm.

Dias (2005) carried out an extensive experimental investigations on dowel type TCC connections subjected to eight series of short-term and long-term shear tests (Figure 3-1e) to assess their behaviour over a wide range of practical applications. In addition, a numerical model was developed to predict the mechanical properties of TCC connections. The TCC test series involved connectors made from ungraded smooth steel reinforcement bars with a diameter of 8mm and 10mm and a mean ultimate strength of 476MPa. Two additional test series using profiled S500 quality steel reinforcement bars were tested. In addition to varying the dowels used, three timber species including spruce, maritime pine (MP) and chestnut (C) were used as the joists whilst three types of concrete including high-strength concrete (C50/60), conventional concrete (C20/25) and light-weight concrete (LC16/18) were considered. A 20mm interlayer fixed with two nails to the joist was used in one test series (INT) (Dias et al. 2010b).

The dimensions of the timber varied depending on the timber species. Pre-drilling was carried out at the nominal diameter of the dowel and to a depth of 80mm for the 8mm series, 120mm for the 10mmB and INT series and at 100mm for all other series. The dowels were cast 60mm into the concrete for the 10mm, B and INT series whilst for the remaining series the depth of anchorage was 40mm. The dowels were hammered into the timber joists (Dias et al. 2010b). The samples were tested in shear using a double sided shear test with a concrete slab fixed to two timber joists on either side. Although, Eurocode 4 stipulates that a double sided specimen achieves higher strength and this is attributed to the shear force being distributed among a larger number of connectors.

Dias et al. (2010b) found that the load capacity of a connection depends upon the material properties of timber, connections and concrete whilst the stiffness of the connection is influenced by the timber species due to the embedment strength having a significant impact on the stiffness behaviour of the connector. Among the series tested,

10mmB series exhibits highest strength and stiffness of 68.6kN and 34.2kN/mm, respectively. The interlayer reduced the slip modulus of the connector although the strength did not vary as much as it was observed in previous studies such as the one by Van der Linden (1999).

3.3.2 Proprietary devices

Other connection types may include proprietary systems such as that mentioned by Van der Linden (1999) and Martin et al. (1999).

Van der Linden (1999) highlighted the development of a double headed screw produced by SFS intec Company. This type of connector allows the first head to be driven into the timber beam whilst the second head is fixed into the concrete slab.

Martin et al. (1999) developed a flexible tubular connector which was developed by INSA–Hilti company. The INSA–Hilti consists of a hollow cylinder with varying cross-section and wall thickness as depicted in Figure 3-5.

Three connection types were tested including (a) a flexible connector, which is commonly used in connection of steel concrete composite beam called Hilti HVB, (b) a tubular connector, with a drilled head, where the holes are filled by mortar in TCC called Hilti Tubular and (c) a hollow cylinder with varying cross-section size and wall thickness in the part which penetrates into the wooden matrix, generated by galvanized heat-treated anti-corrosion steel called INSA-Hilti as depicted in Figure 3-5. The connection type b experienced the highest strength whilst the type c represented a significant ductility as illustrated in Figure 3-5 (Martin et al. 1999). The experiments showed that a flexible tubular connector with dowel type behaviour has a high ductility.

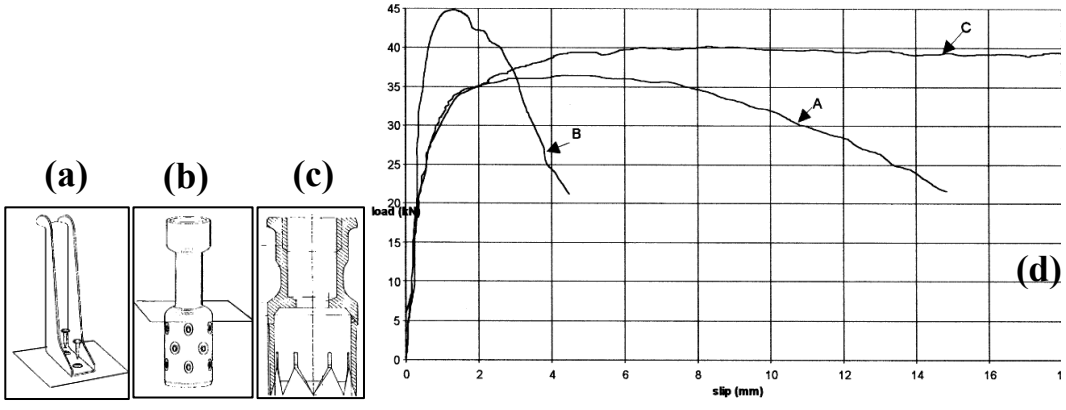

Figure 3-5 Hilty connectors: (a) Hilti HBV, (b) Hilti-Tubular, (c) INSA-Hilti and (d) load-slip graph (Martin et al. 1999)

The slips were 16 and 22mm while the maximum loads per four connectors were 163 and 160kN as shown in Figure 3-5 (Martin et al. 1999).

Gurkšnys et al. (2005) tested the response of sleeved connectors (Figure 3-6) in a TCC floor system utilising I shaped joists as illustrated in Figure 3-7.

The timber web of the orientated strand board (OSB) I-shaped joist had 25mm holes drilled through it which was then embedded into the concrete slab to form concrete dowels. Previous research highlighted that the concrete dowel fails as a result of cutting action from the web. Thus, a steel sleeved connector 25mm in diameter (Figure 3-6) was inserted into the hole of the timber web before the concrete was poured.

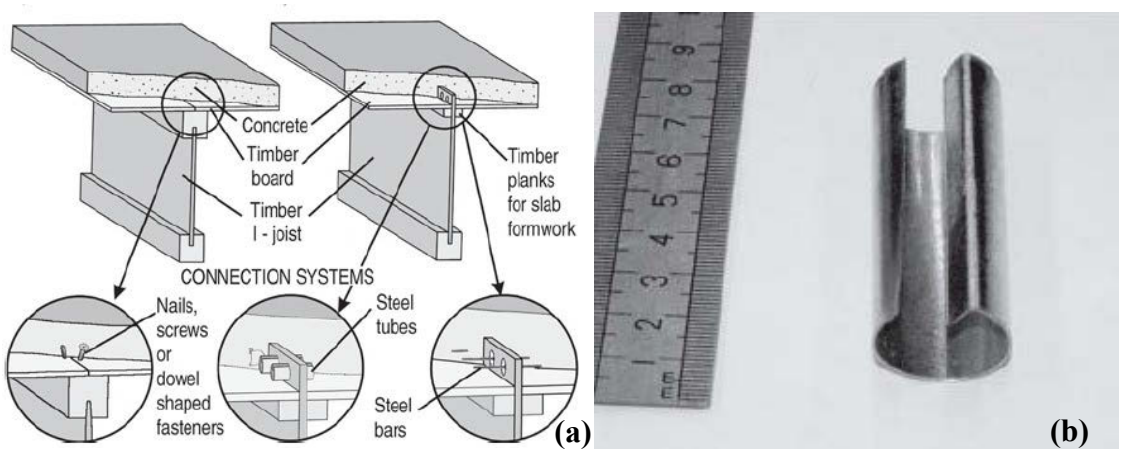

Figure 3-6 (a) Timber I joist with the web acting as a connector and (b) Sleeved steel connector (Gurkšnys et al. 2005)

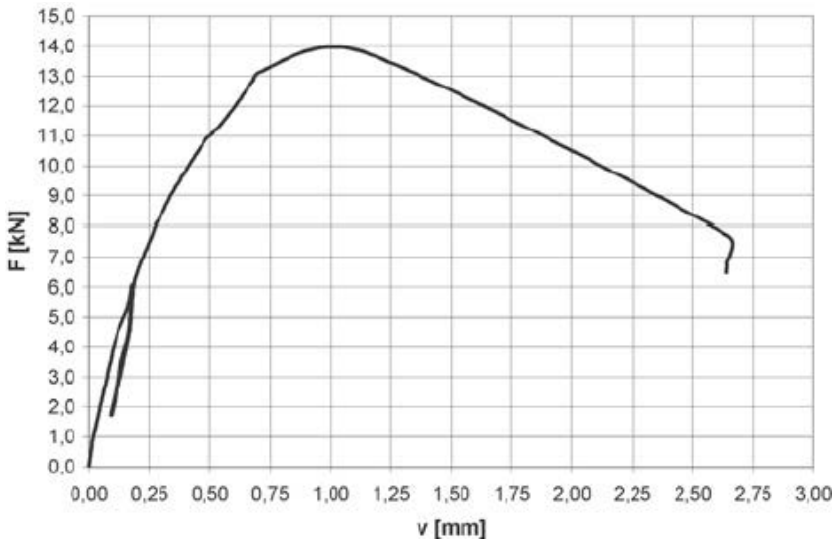

Figure 3-7 Load-slip of sleeved connector (Gurkšnys et al. 2005)

The main failure mode was a result of the shear pressure from the concrete dowels imposed on the OSB web causing it to fracture. Compared to previous tests on alternative shear connectors in TCC systems, the sleeved connector demonstrated a relatively low shear capacity. However, the behaviour of the connector was quite ductile with 2.5-3mm displacement before the connector failed as depicted in Figure 3-7.

Tecnaria connection (Figure 3-1g) investigated by Fragiacomo et al. (2007) was tested to short- and long-term push-out tests utilising light-weight and conventional concretes. It was concluded that the Tecnaria connection presented a very stiff behaviour with limited relative slips for low values of the shear force ($F < 0.2\ F_{max}$). This refers to the contribution of the crampons of the steel plate. Also by increasing the loads, some larger slip occurred with a consequent reduction in stiffness up to the collapse of the specimen due to the withdrawal of the screws.

Fernandez-Cabo et al. (2012) tested eight Habitat System Beton (HSB) TCC connectors in a short term experimental investigation. The aluminium alloy HSB System comprised of a 26mm diameter bar, 70mm long which is formed onto a 65mm diameter base plate as illustrated in Figure 3-8. The aluminium bar is embedded in the concrete slab whilst its length allows an interlayer to be used for formwork. The base plate is connected to the timber beam using a threaded nail, although this has no bearing on shear load capacity. Although this may be considered an alternative connection system, it may also be regarded as a mechanical fastener due to the fact that the HSB shear plate can be idealised as a dowel type connector. Each test specimen was double sheared tested with two HSB connectors per shear plane as depicted in Figure 3-8b.

The results from the shear tests highlighted that the connectors were relatively stiff up to the service load and all depicted similar behaviour as shown in Figure 3-9. Fernandez-Cabo et al. (2012) also observed that most of the deformations as a result of shear loading occurred within the local region surrounding the connector and could not be visibly observed on the outside of the specimen.

Closer analysis of the connectors after testing showed that the specimens failed either as a result or combination of: (1) the connector shear plates failing in a brittle manner; (2) due to the embedment failure in which the timber was crushed by a compressive force in front of the connector; (3) shear failure of the wooden cup that sits inside the connector's base; (4) shear failure of the test specimen between the connectors; and (5) shear failure on the loaded side of the test specimen (Fernandez-Cabo et al. 2012).

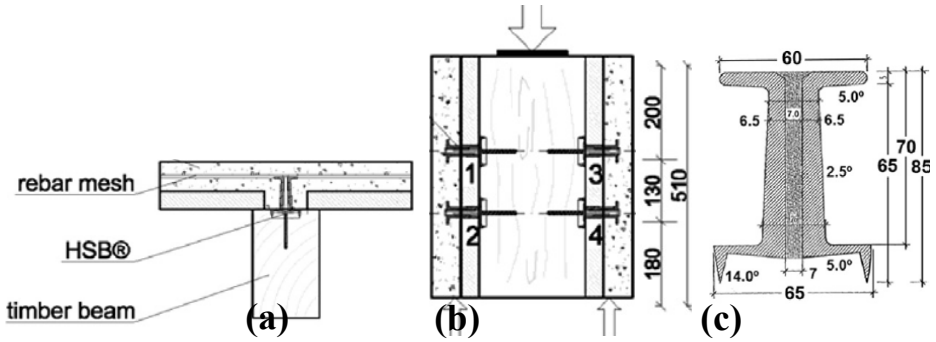

Figure 3-8 (a) HSB flooring system, (b) shear test arrangement, (c) HSB dimensions and HSB connector (Fernandez-Cabo et al. 2012)

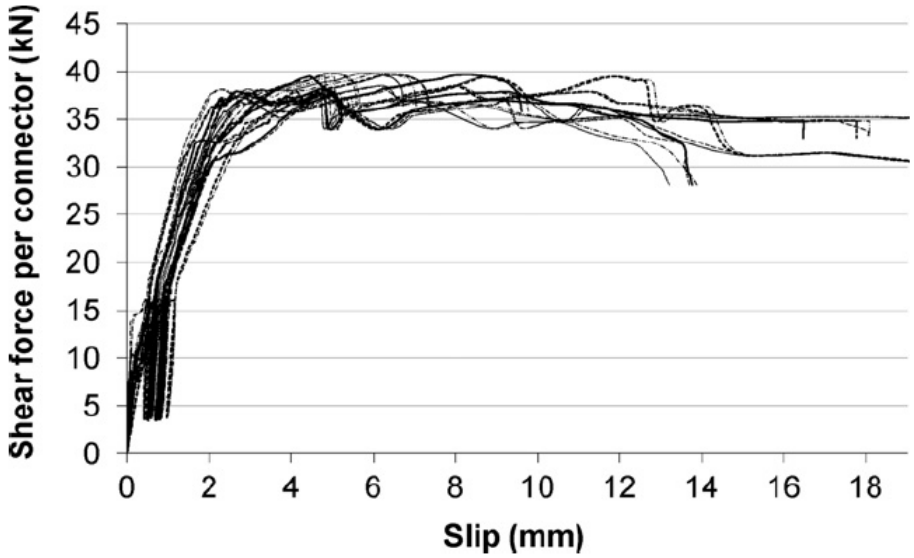

Figure 3-9 Load-slip diagram of the HSB connectors (Fernandez-Cabo et al. 2012)

Fernandez-Cabo et al. (2012) recommended that a less brittle alloy should be used for the shear connector given its fracture failure mode. Eurocode 5 stipulated that the strength of the connector is dependent on the formation of a single plastic hinge in the fastener (failure mode 4) and as a result, the distance between the connectors should be increased. The HSB connector was relatively stiff relative to alternative connectors.

3.3.3 Continuous glued in metallic solutions

Bathon et al. (2000) introduced the continuous glued-in metal plate. In this novel connection, the steel mesh embedded in a concrete slab was inserted into a continuous slot in the timber beam and bonded by an adhesive (Figure 3-1d). Continuous slotted sheet, on average, obtains full composite action. The connections demonstrate planar behaviour and a linear strain distribution across the TCC cross section corresponding to full composite action.

Clouston et al. (2004) tested TCC beams utilising continuous steel mesh connectors. This research however was aimed towards adapting the use of a continuous steel mesh to TCC systems in the US, whereas previously these were only used in Germany. A 305x100x2.5mm steel plate was glued 45mm deep into the wood and embedded 55mm into the concrete. The timber joist of 305x133x89mm Parallam southern pine was fixed to a concrete slab of 305x305x89mm. A number of two part epoxies were tested to glue the mesh to the timber, with the best performing adhesive used for bending tests.

The experiment results from the shear tests highlighted that 3M Scotch-Weld 2216 B/A Gray and Devcon 2-Ton Epoxy were the strongest and most ductile glues with very consistent results across a number of tests. The failure mode of these two glues was as a result of the steel mesh failing in shear. Due to steel being used, the connectors were still able to demonstrate favourable performance with the steel yielding and having high strength and ductility (Clouston et al. 2004). Two of the five glue samples tested were inconsistent in their results and demonstrated unfavourable behaviour with the glues failing along the glue line or at the interface of the timber and steel.

Clouston et al. (2004) concluded that the desired behaviour of TCC system depends upon the glue to transfer the shear forces to the steel mesh connector. Furthermore, they stated that the working times of the glue are an important factor in determining the final bond strength of the adhesives. A longer adhesive working time is particularly necessary when used in a commercial application, where the adhesive needs to be applied to a large surface area.

The initial failure mode of TCC beams utilising the 3M Scotch-Weld 2216 B/A Gray adhesive with continuous connectors arranged along the length of the beam was again through yielding of the steel mesh. This mode of failure was preferred, as a ductile response utilising the full capacity of the steel was achieved. Horizontal displacement was visibly observed between the timber beam and the concrete slab prior to failure in the shear zones of the beam (Clouston et al. 2004). Similar to previous tests, the ultimate failure of the beam in bending was a result of the timber beam failing in tension at the ultimate load.

It was found that use of continuous steel mesh as a connection, secured in the timber with structural adhesives (such as epoxy resin) led to a rigid stiffness in the elastic branch followed by a ductile post peak. Furthermore, a transformed analysis of the theoretical capacity of a TCC beam utilising continuous steel mesh glued to the timber

with full composite action highlighted that the steel mesh connector achieved an approximately full composite action with 97% effective stiffness and 99% strength of that of a fully composite beam (Clouston et al. 2005b).

Similar to Clouston et al. (2004), Miotto et al. (2011) investigated the performance of a continuous perforated steel plate as a TCC connector. However, they improved upon the previous design by utilising a steel plate which had a considerably higher yield strength compared to the steel used by Clouston et al. (2004).

Five double sided TCC specimens were tested in shear with each specimen comprised of a central glulam joist of 500x322x82mm connected on both sides to a concrete slab of 500x150x70mm as illustrated in Figure 3-10. The connector was fabricated from flat steel plates with a minimum yield strength of 500MPa and was connected to the joist by epoxy adhesive (Miotto et al. 2011).

The results indicated that the connector had a very high strength and serviceability slip modulus of 153.4kN and 339kN/mm, respectively with CoV values of 10.5% and 42.7%. Such high strength and stiffness are only obtained from notch type connection systems. Similar to Clouston et al. (2004), the serviceability slip modulus was very high. However, the connectors failed through concrete cracking around the region of the steel plates, whereas Clouston et al. (2004) stated that the steel connector failed due to yielding of the steel. No deformation in the steel plates was observed and the adhesive bond remained perfectly intact (Miotto et al. 2011).

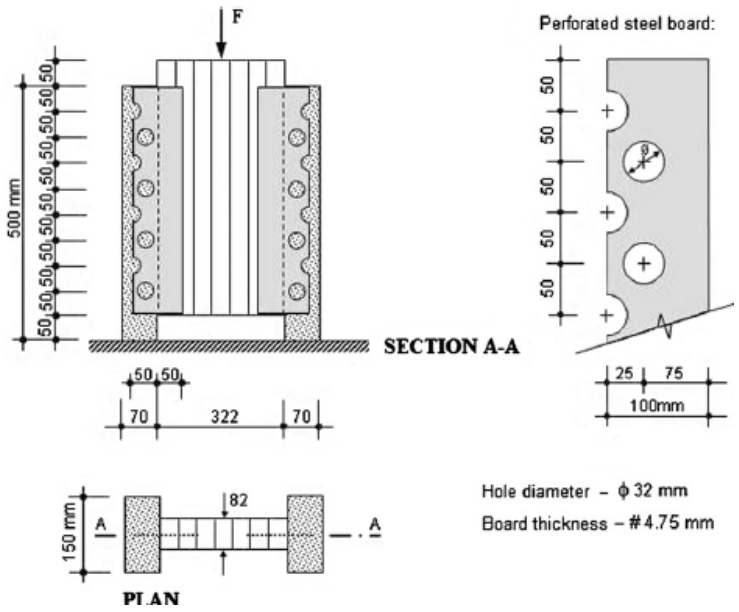

Figure 3-10 TCC specimen setup of perforated steel plate (Miotto et al. 2011)

3.3.4 Notches & fasteners

There are other studies which highlight possible solutions to further increase the strength of a TCC connection. Holschemacher et al. (2002) introduced a timber key to the TCC design. With the inclusion of a timber key, similar to a triangle notch, an increase in the strength and stiffness of the TCC connection was expected. It is noted that the added shape requires further concreting, which could lead to potential failures due to the concrete. However, the results from this study conclude that the strength of the TCC sample was not dependent on the concrete strength and therefore such systems could be further explored.

Crocetti. R et al. (2010) considered the application of wooden shear anchors. These work similarly but in opposite fashion to concrete keys and involve a timber block rigidly connected to the beam extending into the concrete. There were also additional fastener between this block and the surrounding concrete. The results highlighted that TCCs utilising wooden shear anchors are likely to gain improved strength and stiffness values, as some of the testing samples experienced only 1mm of vertical displacement at failure. However, the benefits are highly dependent on the type of shear anchor and the particular timber used. Furthermore, while increased stiffness and strength is highly desirable in TCCs, the lack of ductility presents numerous problems in terms of failure modes behaviours. As a result, such designs is undesirable in real world applications (Ceccotti et al. 2006b).

As part of Frangi et al. (2003) investigations into developing an elasto-plastic model for TCCs, push-out test on some shear connectors was carried out to verify the elasto-plastic model. Spruce timber beams had 20mm deep by 150mm long groves cut into their upper face. M12 threaded steel dowels were imbedded 80mm into the timber beam with a special adhesive. Each test specimen that underwent push out tests had two grooves and steel dowels used as the connector between the timber beam and the concrete slab. Frangi et al. (2003) observed a high serviceability stiffness, however, noted that the connector plastically deformed under ultimate loads as shown in Figure 3-11. The steel dowels deformed plastically and the timber near the grooves compressed during the ductile failure. Frangi et al. (2003) noticed very small slip deformations up to a load of 25kN in TCC beam. However, as the load level was increased and plastic failure was induced in the TCC beam, the connectors also displaced at a faster rate. This agreed with the behaviour observed in the push-out tests.

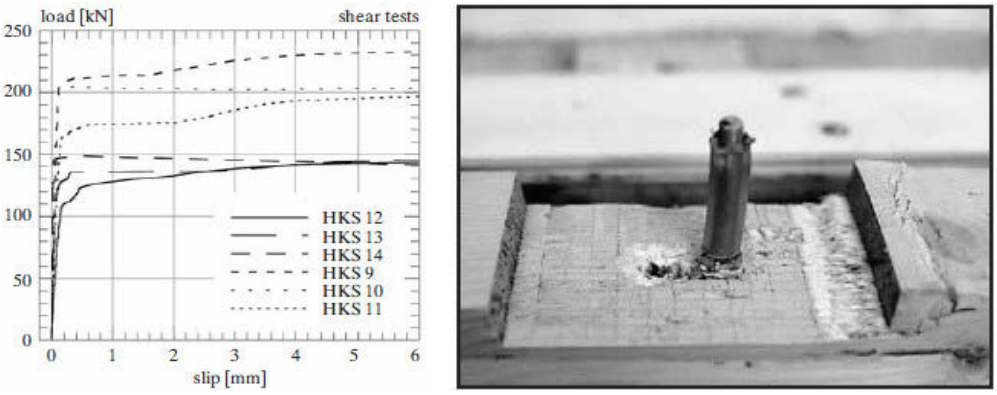

Figure 3-11 Load-slip diagram and failure of the connector (Frangi et al. 2003)

Yeoh et al. (2009) assessed notched designs to determine the most effective connection shape for use in long-span TCC floors. The notch design with the highest strength and stiffness values allow for a reduction in the number of connectors required and as a result reduce the cost of implementing a TCC floor. Double sided push out tests were performed on a range of notch designs with the two main parameters being the shape and inclusion of a coach screw.

In general, Yeoh et al. (2009) found that a longer notch length improves the strength of the connector considerably with all specimens failing in shear in the concrete. Triangle notches performed similar to rectangular notch and this has important implications due to the ease of construction of a triangular notch. The presence of a coach screw increases the ductility of the connection whilst the penetration depth of the screw into the timber improved the stiffness of the connection significantly.

Yeoh (2010) tested 11 LVL-concrete composite T-beams with 8 and 10m span, 600 and 1200mm widths utilising notched coach screw and toothed metal plate connections to failure under four-point bending. Among those, 6 beams were well-designed whilst 5 beams were under-designed. TCC beams were designed for the non-structural permanent load of 1kN/m^2 and imposed load of 3kN/m^2. A composite action of 87.6 to 99.2% at SLS was observed.

Another worthwhile alternative to traditional crossed shear connections would be to introduce a triangle notch in the LVL joist and then insert a shear connection. Ooi (2011) studied the performance of different connections systems in TCCs. The results of the investigation propose the use of a triangle notch with diagonal nail connection as it exhibited the highest strength and stiffness compared to vertical screw connection. This presents another connection arrangement that has the potential for further investigation.

Crews et al. (2010b) tested the behaviour of various TCC notch connections under shear push-out tests as illustrated in Figure 3-12. The types of connections included a coach screw placed centrally inside a notch with each of the notches having different geometrical properties. Approximately, hundred samples were fabricated with various configurations and concrete type implemented within the experimental set-up.

The study aimed to provide a parametric study to find the most suitable shape and material in terms of structural capability and cost effectiveness for long-span non-residential construction market. The results concluded that birds-mouth connections are easier to manufacture and generally exhibit higher strength and similar stiffness compared to rectangular notches. It was also found that the material characteristics of concrete influence the structural behaviour of the connection.

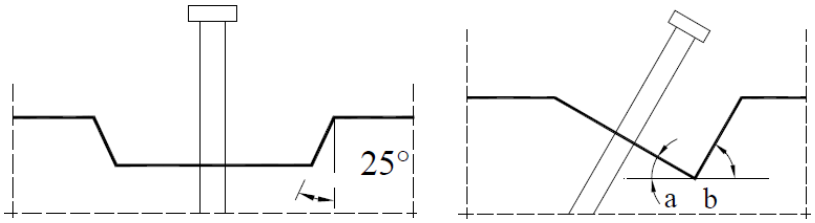

Figure 3-12 Trapezoidal (T series) and triangular (B Series) notches

3.3.5 Adhesives connections

Glues were recognised as an attractive material in order to mitigate slip at the TCC interface. However, the thermo hygrometric behaviour between the adhesives and the composite elements are challenging to determine and as a results adhesives are rarely considered over alternative connector designs. For example timbers hysteretic response to moisture can cause delamination at the interface (Negrão et al. 2010a).

Application of adhesive material at the interface of timber and concrete has been addressed and investigated in many researches for example Pincus (1969, 1970), Schober et al. (2006), Ceccotti et al. (2006b), Brunner et al. (2007a), Brunner et al. (2007b), Negrão et al. (2010a) and Negrão et al. (2010b). The main drawbacks of a mechanical fastener including limited stiffness of the connectors, extensive drillings and mountings, force concentration may be overcome by application of adhesive bound as a slip-free and force distributed connection Negrão et al. (2010b). However, adhesives are typically not preferred due to quality control issues that arise from applying adhesives (Yeoh 2010).

Pincus (1969) investigated on feasibility of an epoxy resin compound in TCC. It was found that pouring fresh concrete on wet adhesive resulted in an efficient rigid connection with negligible slip before final failure. Furthermore, application of nail fastener in bounded TCC increased the shear capacity of connection up to 50% (Lukaszewska 2009).

Brunner et al. (2007a) and Brunner et al. (2007b) studied the possible displacement of the adhesive when the fresh concrete was poured onto the wet adhesive. In this delicate process, important factors such as concrete type, falling height and adhesive stiffening time were investigated and optimised.

In order to determine the performance of adhesives, Negrão et al. (2010a) tested eighteen test series of twenty TCC specimens in double shear tests. Both cast in-situ and prefabricated concrete slabs were utilised. The glue was also not the weakest point of failure, with the shear strength at the glue interface being one fold greater than the shear strength of unreinforced concrete as provided by Eurocode 2 (EN 2004a). A thinner application of adhesives proved to provide greater shear strength for the prefabricated concrete slab although this was not the case for the cast in-situ slabs with the primary explanation being that adhesive was partially removed when vibrating the concrete.

In general, it was concluded that an adhesive bond between timber and concrete performs best in a stable and dry environment. Under these conditions the shear strength was very adequate with the prevailing failure mode being the concrete.

Negrão et al. (2010b) listed the major reasons of limited investigations on adhesives connections as the brittle failure of bonded layers, delamination damage due to different hygroscopic behaviour of composite components and the fire behaviour of adhesives.

3.4 COMPARISON OF SHEAR CONNECTIONS

It is not accurate to compare the mechanical properties of different shear connector systems in literature utilising different timber and concrete specifications. However, in general it is widely accepted that TCC connections can be classified based on their stiffness and strength.

Table 3-1 summarises some key results from the case studies reviewed. It is concluded that notches and dowels along with continuous connector systems provide the highest strength and stiffness whilst dowels and screws have lower structural capacities.

Table 3-1 Summary of the strength and stiffness of reviewed shear connectors

Connector System	Load capacity (kN)	Serviceability slip modulus (K_{ser}) (kN/mm)
Wood screws fixed at ±45 degrees Frangi et al. (2003)	15.0	N/A
10mm vertically fixed dowel Dias et al. (2010b)	22.6	15.2
HSB Connector System Fernandez-Cabo et al. (2012)	37.0	19.5
20mm deep by 150mm long grooves with a M12 dowel Frangi et al. (2003)	110.0	N/A
Rectangular notch 150x50x63 with a 16mm diameter coach screw Yeoh et al. (2009)	73.0	80.2
2.5mm thick steel mesh continuous metal connector Clouston et al. (2004)	51.7	21.2
Continuous steel perforated plate Miotto et al. (2011)	153.4	339.0
Sleeved steel connector Gurkšnys et al. (2005)	14.2	29.8

3.5 CONCLUSIONS

In this Chapter, different classifications of TCC connection and case studies to demonstrate, in detail the behaviour achieved from a wide variety of shear connector systems were discussed. The TCC shear connections have been broken up into categories based on the type of classification although, at certain times, an overlap did occur. Each category of TCC connection is investigated more thoroughly by undertaking case studies on previous experimental investigations on similar connections.

A variety of shear connectors can be used including dowels, nails, screws, nail plates, alternative mechanical fasteners, notches, glues, continuous systems and proprietary designs. There has been a large amount of research on the strength and stiffness of TCC shear connectors in recent years. The most important different shear connection solutions in literature were quoted.

It is concluded that notches and dowels along with continuous connector systems provide the highest strength and stiffness whilst dowels and screws have lower structural capacities.

4 MATERIAL PROPERTIES

4.1 INTRODUCTION

This Chapter presents details of a series of laboratory based and desk-top investigations into the material properties of the composite components of TCC system including timber, concrete and shear connectors.

The material properties (fresh and hardened) of six types of concretes, conventional concrete (CC), high-strength concrete (HSC), self-consolidating concrete (SCC), expanded polystyrene light-weight concrete (EPS LWC2000 and 1600) and Scoria light-weight concrete (Scoria LWC2000), are reported. The specifications of plywood and two types of LVL used as timber joists in TCC are presented. Finally, the material properties and geometry of different types of screws used in this research are stated. The material properties of the composite component have been used extensively for both analytical and FE modelling of the TCC connections and modules.

4.2 CONCRETE

Six sets of concrete mixes were prepared to be used as a concrete slab for TCCs. The mix designs of different concrete types are listed in Table 4-1. Normal-weight concretes such as conventional and high-strength concretes were prepared as control series. Two types of light-weight concrete also were tested- expanded polystyrene (EPS) and Scoria. These concretes replace the heavy aggregates of conventional concrete with polystyrene beads and light-weight pumice rock. LWC has a lower density, a higher ductility, as well as reduced modulus of elasticity, compressive and tensile strength compared to conventional concrete. LWC is generally specified by mass per unit volume.

Table 4-1 Concrete mix designs

Mix	Gravel (20mm)(kg)	Gravel (10mm)(kg)	Coarse Sand(kg)	Fine Sand(kg)	Cementitious content (kg)	Water (kg)	Scoria Sand	Scoria 14mm (kg)	EPS beads (kg)
HSC	755	406.5	355.6	355.7	350.4	130.1	-	-	-
CC	700	260	562	236	320	180	-	-	-
SCC	-	820	660	221	400	208	-	-	-
Scoria	-	-	91.5	91.5	420	526.4	428	612	-
EPS2000	-	800	310	310	500	180	-	-	4.7
EPS1600	-	550.7	260.4	260.4	450.6	170.3	-	-	9.3

Finally, self-consolidating concrete was mixed. The mechanical property of SCC is similar to the conventional concrete or need to be reduced by the factor within 0.85 to 0.9. The main difference between the SCC and CC is that the external vibration is not required for SCC which is compacted by its self-weight.

The fresh properties of concrete such as fresh mass per unit volume, slump and air content were measured in accordance with AS1012.5 (1999), AS1012.3.1 (1998) and AS1012.4.3 (1999), respectively as reported in Table 4-2.

The air content of LWC is much higher than the conventional concrete and increased by adding more EPS beads or Scoria LWC aggregates into concrete as shown in Table 4-2 whereas increasing EPS beads or Scoria LWC aggregates into concrete leads to a decrease in concrete workability. The mixes achieved the desired 100-150mm slump specification with the exception of EPS LWC1600. It was observed that the slump test is not a suitable method to measure workability of ultra LWC. For example EPS LWC1600 experienced 20mm slump but it exhibited a desired workability.

Table 4-2 Fresh properties of different types of concrete

fresh property	HSC	CC	SCC	Scoria LWC	EPS LWC2000	EPS LWC1600
fresh mass per unit volume (kg/m^3)	2570	2405	2390	2027	2059	1645
Slump (mm)	60	120	-	150	165	20
Air content (%)	1	1	1.3	4.5	8.5	11

The hardened properties of the test series including mean mass per unit volume, compressive and splitting tensile strengths, static chord modulus of elasticity (MOE) and module of rupture (MOR) at different ages of 3, 7 and 28 days were measured in compliance with AS1012.12 (1998), AS1012.9 (1999), AS1012.10 (2000), AS1012.17 (1997) and AS1012.11 (2000), respectively as listed in Table 4-3. Compressive and indirect tensile strength developments from 3 to 7 and 7 to 28 days of different concrete types are illustrated in Figure 4-1.

Table 4-3 Hardened properties of different types of concrete

material hardened property (Mpa)	HSC	CC	SCC	Scoria LWC	EPS LWC 2000	EPS LWC 1600
Hardened mass per unit volume (kg/m^3)	2478	2360	2340	1997	2029	1603
$f_{c,3}$	22.5	13.0	12.5	12.2	15.2	7.0
$f_{c,7}$	37.0	19.8	21.8	17.5	15.9	9.0
$f_{c,28}$	55.0	37.0	35.4	28.1	23.4	12.1
$f_{ct.sp,3}$	2.5	1.8	1.6	1.8	1.8	0.8
$f_{ct.sp,7}$	4.7	2.4	2.3	2.3	2.0	0.9
$f_{ct.sp,28}$	5.7	3.7	3.6	3.3	2.8	1.2
MOE	37000	33239	35400	17933	27621	11783
MOR	8.6	8.0	7.8	5.8	5.9	2.8

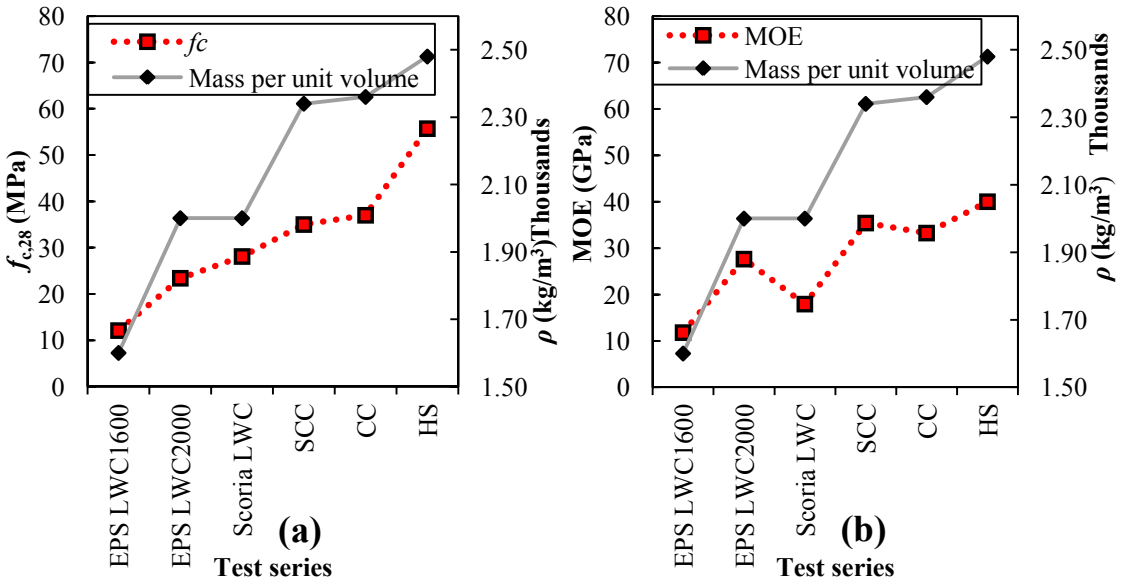

Figure 4-1 (a) 28-day compressive strength versus mass per unit volume and (b) MOE versus mass per unit volume of different mixes

Results show that LWC mixes have lower hardened properties rather than other mixes and its hardened properties of EPS LWC concrete were significantly reduced by increasing the amount of EPS beads to the mixes. The splitting tensile strength of EPS LWC1600 and 2000 were 68% and 46% less than CC series and significantly reduced by increasing EPS beads into the LWC mix whereas HSC series represented maximum $f_{ct.sp,28}$ values of all series, 54% higher than that of conventional concrete. EPS LWC1600 and Scoria LWC series experienced 67% and 52% lower MOE than CC series, respectively. LWC series exhibits significantly lower MOR than CC series.

Figure 4-1 illustrates that the LWC with scoria aggregate and EPS has lower strength and MOE compared to other types of concrete and within LWC MOE and compressive strength decrease with reduction in mass per unit volume.

4.3 TIMBER (LVL)

Laminate veneer lumber (LVL) was selected as timber joist of the TCC connections and modular specimens.

Table 4-4 Timber Design Properties

Mechanical property	Mean values	CoV(%)
mass per unit volume hySPAN project LVL	600.0 kg/m^3	2.4
mass per unit volume cross-banded LVL	550.0 kg/m^3	3.0
Modulus of Elasticity hySPAN project LVL (E)*	13746.0MPa	6.4
Modulus of Elasticity cross-banded LVL (E)*	11525.0 MPa	8.1
Modulus of Rigidity (G)$^+$	660.0MPa	N/A
Stress in flat-wise bending hySPAN project LVL (f_b) *	76.6Mpa	14.7
Stress in flat-wise bending cross-banded LVL (f_b)*	57.1 Mpa	5.4
Stress in tension parallel to grain LVL hySPAN project (f_t)*	38.2Mpa	1.4
Stress in tension parallel to grain cross-banded LVL (f_t)*	33.7Mpa	7.0
Stress in compression parallel to grain hySPAN projectLVL (f_c)	53.4MPa	6.8
Stress in compression parallel to grain cross-banded LVL (f_c)*	42.6MPa	2.8
Stress in compression perpendicular to grain (f_p)$^+$	12.0MPa	N/A
Stress in longitudinal shear LVL hySPAN project (f_s)*	6.7MPa	3.8

$^+$ Characteristic values reported in(CHHWA) (2011)
*Mean values reported in Zabihi et al. (2012)

Two types of LVL, that is, hySPAN Cross-banded and hySPAN project produced by Carter Holt Harvey Wood Products Australia were used in this investigation to form the bottom flange and two webs of the structural section of the timber-only modules, respectively as discussed in Chapter 6. LVL hySPAN project produced by Carter Holt Harvey Wood Products Australia was selected to fabricate the joist section of the TCC connections as reported in Chapter 6.

LVL was tested and mean values were measured in accordance with AS4357.0 (2005) and design characteristic values was calculated in compliance with AS4063.2 (2010). The properties of different types of LVL are tabulated in Table 4-4. The LVL used in the push-out and four-point bending tests indicated a moisture content of 8.5% which is within the acceptable range of 8%-15% as proposed by AS2098.1 (2006). The mass per unit volume of timber specimens was measured in compliance with AS1080.3 (2000).

4.4 TIMBER (PLYWOOD)

F17 grade plywood (as per AS2269 2004 classification) was used in the fabrication of the interlayer in the TCC series with interlayer. Characteristic properties of F17 grade plywood based on AS1720.1 (2010) are given in Table 4-5.

Table 4-5 Characteristic values of structural plywood F17 AS1720.1 (2010)

Mechanical property	Value (MPa)
mass per unit volume	710kg/m^3
Mean Modulus of Elasticity (E)	14000
Modulus of Rigidity (G)	700
bending strength (f'_b)	45
tension strength (f'_t)	27
Stress in compression in the plane of the sheet (f'_c)	36
Stress in compression normal to the plane of the sheet(f'_p)	20
Shear stress (f'_s)	6

4.5 SHEAR CONNECTION

A number of different types of screw ranging in diameter, length and material properties such as SFS VB (long and short), SPAX (flat countersunk head (large) and cylindrical head (small)), medium coach and wood screws were selected as TCC connector in this study as shown in Figure 4-2.

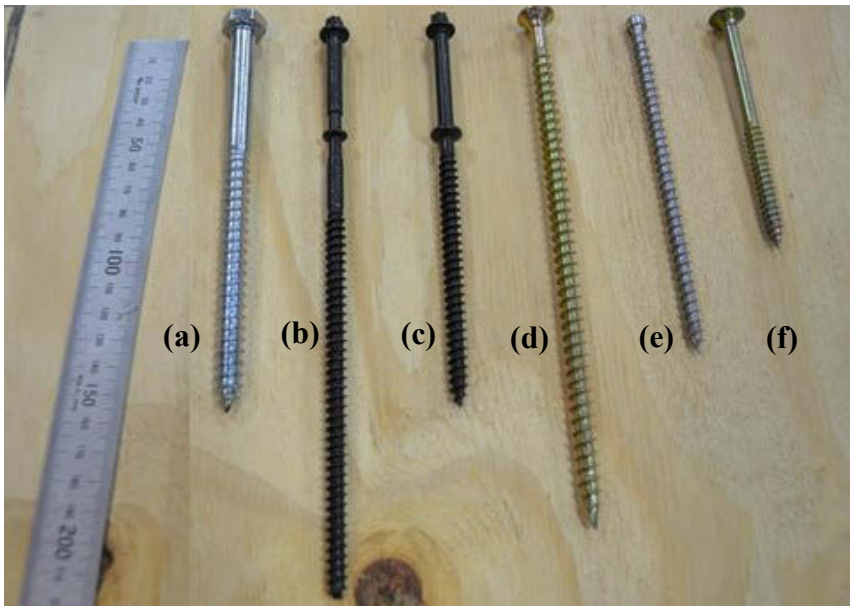

Figure 4-2 Different screw connection(a) medium coach, (b) long SFS , (c) short SFS, (d) SPAX, (e) small SPAX screws and (f) type17 wood screw used in the experiment

The holes for the screws embedded in the timber members were pre-drilled. Table 4-6 lists the geometrical and material properties of different types of screw used in TCC connection and modular specimens.

Table 4-6 Characteristic dimensions and material properties of the screws

Description	coach	Long SFS	short SFS	Long SPAX	small SPAX	Wood 17
Major diameter, d_1 (mm)	9.3	7.6	7.6	8.1	6	6.6
Head diameter, d_k (mm)	18	12	12	15.1	8.4	14.5
Core diameter, d_2 (mm)	7.3	4.6	4.6	5	4	4.8
Shank diameter, d_s (mm)	9.3	6	6	5.7	6	5.2
Threaded length, L- L_s (mm)	95	135	100	160	125	50
Thread pitch, p (mm)	4	3.2	3.2	4	3	2.5
Head height, k (mm)	7	1.4	1.4	4.4	6	4
Screw length, L(mm)	157	220	160	200	140	100
Characteristic yield moment, $M_{y,Rk}$ (Nmm)*	15074	33815.2	27251	38172	15937	18093
Ultimate tensile strength (MPa)*	461	1221	984	1168	1064	943

*Set-up and results of these tests were reported in Appendix D

4.5.1 SFS VB screw

The SFS screw connectors were developed in 1992 by Meierhofer (1992) and were proprietary system for TCC structures, either in the construction of new flooring systems or the rehabilitation of existing timber floors. The double headed screw consists of two parts with a diameter of 6mm as an anchor in the concrete and another threaded 100mm or 165mm long with a diameter of 7.5mm as an anchor in the timber as shown in Figure 4-3 (Lukaszewska 2009).

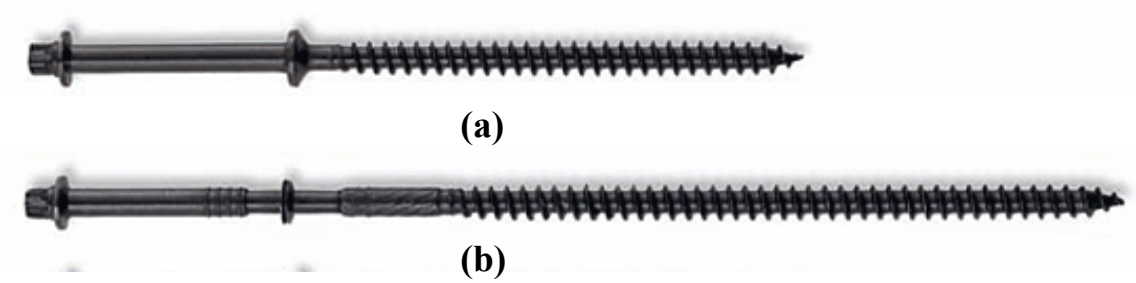

Figure 4-3 SFS VB-48-7.5(a) x100mm (b) x165 threaded parts

The screw had a measured total length of 160 or 220mm and a measured thread length of 100 or 135mm (Figure 4-3) and their characteristic dimensions and material properties are listed in Table 4-6. Screws were inserted so that the thread was in the timber/interlayer. This meant a vertical length of approximately 55mm was embedded in the concrete (as such, samples with interlayer had less length within the LVL as screws also had to penetrate through the interlayer).

Application of SFS screws in TCC system were extensively investigated in literatures such as Blass et al. (1995), Van der Linden (1999), Frangi et al. (2003), Steinberg et al. (2003), Grantham et al. (2004), Lukaszewska (2009) and Jorge et al. (2010).

The first type of shear connection used throughout this investigation comprised of dual VB-48-7.5 x 100/165 carbon fibre SFS VB screws and the threaded part of a pair of screws were installed laterally reversed at an angle of ±30°, ±45°(short), ±45°and ±60° with embedding length of 120, 60, 142 and 156 mm as shown in Figure 4-4. The inclination angles were measured from the horizontal. The cross screws were positioned at the centre of composite material's interface.

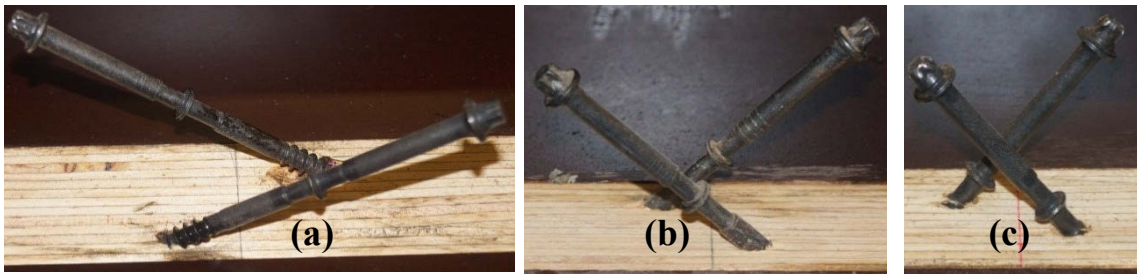

Figure 4-4 Long SFS screws installed at an angle of (a) ±30°, (b) ±45° and (c) ±60°

4.5.2 SPAX screw

The SPAX international, founded in 1823, was the first German company to manufacture screws at an industrial level. SPAX international has recently entered the Australian and New Zealand market. SPAX screws are not designed specifically for use in TCCs, however its material properties presents them as a worthy alternative to the SFS screws. Two types of SPAX screw were used in this investigation and their characteristic dimension and material properties are listed in Table 4-6.

The first SPAX screw was a full threaded, flat countersunk head, SPAX T-Star screw with milling ribs and a hardened synthetic coating. This large SPAX screw had a total length of 200mm and a measured diameter of 8.1mm as shown in Figure 4-2d.

The pair of screws was installed laterally reversed at an angle of ±30°, ±45°and ±60° with embedding length of 100, 120 and 136 mm as shown in Figure 4-5. The crossed screws were positioned at the centre of composite material's interface. As they are not designed specifically for TCC use, there is no anchor section for the concrete as there is with the SFS screws. As a result, the thread travels the entire length of the screw.

The second chosen SPAX screw with cylindrical head was used for U and L profile connection designs. This small SPAX screw had a total length of 140mm and a measured diameter of 6mm as depicted in Figure 4-2e.

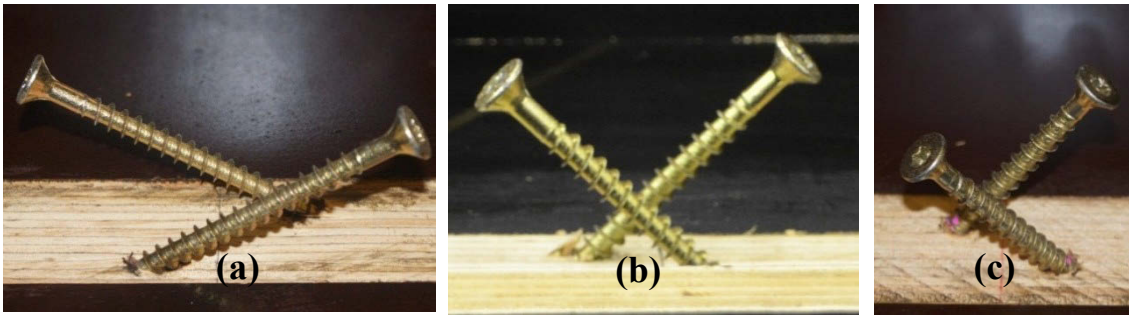

Figure 4-5 Crossed SPAX screws installed at an angle of (a) ±30°, (b) ±45° and (c) ±60°

The screws were screwed into the LVL joist at an angle of 45° for the entire length of the thread until the cylinder head of the screws sat tight and flush against the bottom face of the connectors. The screws were placed in tension rather than in bending to improve the strength and stiffness of the connection in push-out test. Both types of SPAX screws comprised of cold rolled wire of high-carbon steel screws.

4.5.3 Wood screw (type 17)

A commercially available wood screw (type17) with outer diameter, *d* of 6.6mm was used as shear connections. The embedding length of screw in LVL was 65mm in all test series and was installed in pre-drilled holes whilst a length of 35mm with the shank diameter of 4.8mm was embedded in the concrete as shown in Figure 4-6.

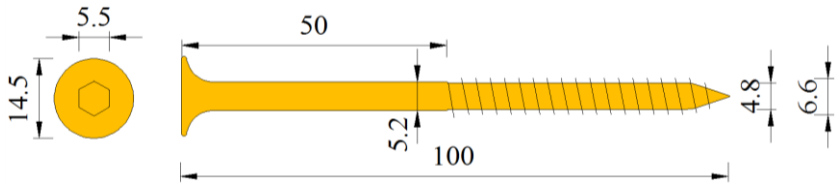

Figure 4-6 Geometry of wood screws

4.5.4 Coach screw

A 9.30mm diameter partially threaded coach screw with a thread length of 95mm and nominal length of 157mm was selected as a benchmark in the assessment of mechanical properties of two innovative solutions of the L and U profile shear connectors (Figure 4-2a). The coach screws were screwed into the timber joist at an angle of 45° to the horizontal face of the LVL joist, for the full length of the thread (Figure 4-7c). Hence, 95mm of the screw was fixed into the timber whilst 62mm of the screw shank and coach head was embedded into concrete. Figure 4-7 depicts the coach screw shear connector and TCC specimen utilising coach screw.

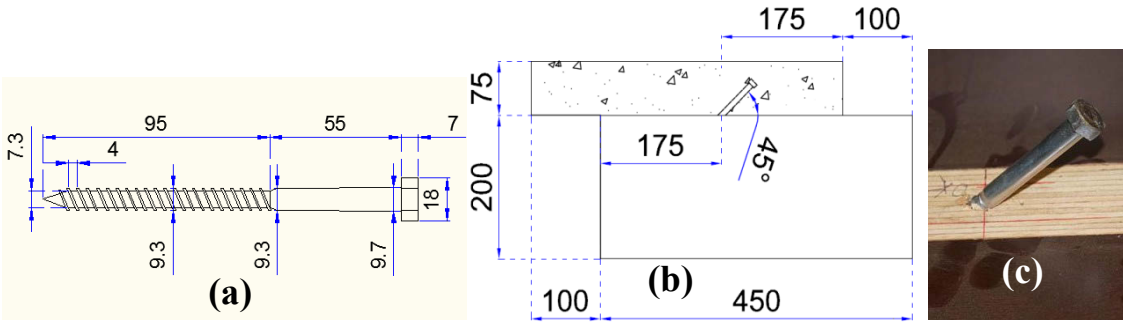

Figure 4-7 (a) Coach screw dimensions, (b) and (c) TCC specimen utilising coach screw

Table 4-6 lists the characteristic dimensions and material properties of coach screws. The coach screws were produced from mild carbon steel due to the ductile necking evident in the failure zone.

4.5.5 L profile and three small SPAX screws at 45°

Based on the criteria discussed in Chapter 2, two connector designs were developed. The first shear connector which is referred to as the "L connector", comprised of a steel equal angle with a minimum yield strength of 250MPa, cut into 65x40x4.7mm as the unequal angle with a length of 150mm with the long edge embedded into the concrete. Additionally, 3 Small SPAX screws inclined at 45° were screwed into L connector for their entire thread as displayed in Figure 4-8b. 3 equally spaced 30mm diameter perforations were drilled into the long edge of the L connector as shown in Figure 4-8 The concrete mix design of conventional concrete specified a maximum nominal aggregate size of 20mm. Hence, 30mm diameter perforations were selected to give the connector mechanical interlock by allowing the larger aggregates to embed inside the perforation, thereby providing lateral and uplift restraint.

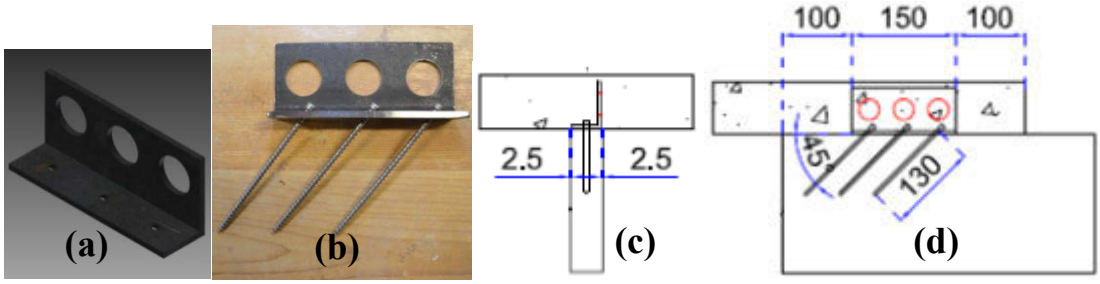

Figure 4-8 (a) L connector profile (b) L profile and SPAX screws, (c) and (d) dimentions of TCC specimen utilising L connector

Figure 4-8 depicts the L profile connector combined with three small SPAX screws and TCC specimen utilising L connector. Table 4-6 lists the characteristic dimensions and material properties of the small SPAX screws.

4.5.6 U profile and three small SPAX screws at 45°

The second shear connector design was referred to as the "U connector" and was fabricated from a 150mm long galvanised surface coating Unistrut P1000 channel made from low carbon steel with a width and height of 41.3mm and a wall thickness of 2.5mm as shown in Figure 4-9a.

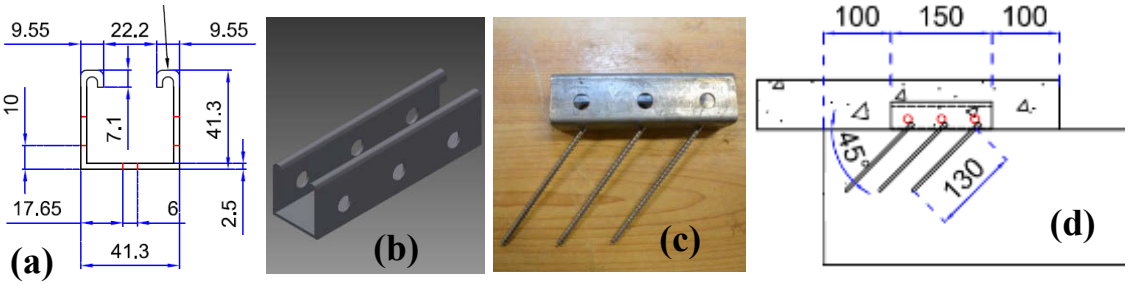

Figure 4-9 U connector (a) dimensions (b) and (c) UniStrut profile and (d) TCC specimen

Both U and L connectors had 3 equally spaced 6mm diameter holes drilled at 45° to the bottom face of the connector. 3 small fully threaded SPAX screws inclined at 45° were screwed to the connector and LVL joist for the entire length of the thread, 130mm until the cylinder head of the screws sat tight and flush against the bottom face of the connectors as illustrated in Figures 4-8 and 4-9. Inclination of the connector improved stiffness, strength and ductility of the connector where the screws were placed in tension rather than in bending. The screws used to connect the U and L connectors to the timber joist were the critical factor in determining the strength of the connections. Hence, three wood screws were used to fix the connectors to the timber joist to improve the strength of the L and U connectors.

3 equally spaced 12mm diameter perforations were drilled into each wall of the channel. Due to the physical size of this channel, it was impracticable to create 30mm perforations in the channel walls to accommodate the maximum aggregate size without compromising the structural integrity of the connector. Hence, a 12mm diameter sized perforation design was selected as it created an adequate bond between the connector and the concrete. Additionally by selecting a different perforation size to the L connection, a comparative assessment was carried out to study the effect of perforation size on the overall stiffness and strength of the connectors.

Figure 4-9 depicts the U profile connector combined with three small SPAX screws and TCC specimen utilising the U connector. Unistrut channel members were accurately rolled from strip steel in compliance with AS1594 (2002) and AS1365 (1996).

There is no Australian design procedure for TCC structures and only the Australian Standard for timber, AS1720.1 (2010) specifies the minimum spacing for wood screws to be $10d_s$ along the grain, where d_s is the shank diameter of the screw. Fastener spacing in L and U connectors was designed to be 50mm to accommodate this minimum spacing requirement and meet the constraints of the connector dimensions.

4.6 CONCLUSIONS

In this Chapter, the material properties of the composite components of a TCC system including timber, concrete and shear connections were discussed.

The material properties of six types of concretes including conventional concrete (CC), high-strength concrete (HSC), self-consolidating concrete (SCC), EPS light-weight concrete (EPS LWC2000 and 1600) and Scoria light-weight concrete (Scoria LWC2000) were reported.

Moreover, specifications and design properties of plywood and two types of LVL including hySPAN Cross-banded and hySPAN project were introduced in this Chapter.

Finally, characteristic dimensions and material properties of different types of screws used as shear connector in TCC push-out and modular specimens were given.

The material properties of the composite component were widely used in analytical and FE modelling of the TCC connections and modules.

5 CONNECTION PUSH-OUT TESTS

5.1 INTRODUCTION

The aim of the short-term push-out tests program was to investigate the mechanical properties and failure mechanism of different types of mechanical fastener used as shear connector in long-span non-residential timber-concrete composite floor. Different types of available screws and two novel types of connectors utilising various types of concrete, inclination angles and with and without plywood interlayer between timber and concrete were tested to determine the mechanical properties of connector such as stiffness (slip modulus), shear strength, ductility and failure mode.

This Chapter focuses specifically on short-term push-out test of mechanical fastener such as crossed SFS VB, crossed SPAX and coach screws connections in different lengths (short and long SFS VB), angles (±30°, ±45° and ±60°) to the connection face and a number of crossed SFS VB and SPAX at 45° series utilising 17mm plywood formwork interlayer and different types of concrete. Hence, the effects of concrete properties, connector type, inclination angle and length of screw and existence of plywood interlayer on mechanical properties of the TCC connections were investigated.

Moreover, two innovative TCC shear connection systems in the form of a perforated grade 250MPa steel unequal angle (UEA) and a perforated Unistrut P1000 channel were fixed into LVL joist by 3 SPAX wood screws at 45 degrees. The alternative connections were assessed for their suitability as a substitute or replacement for existing connection systems using push-out test.

In addition to conventional concrete, expanded polystyrene light-weight concrete (two density classes of 1600kg/m^{3}and 2000kg/m^3), Scoria light-weight concrete (density class of 2000kg/m^3), self-consolidating concrete and high-strength concrete were employed for experimental parametric study on effect of concrete type on mechanical properties of TCC connections using locally available materials in Australia to evaluate their potential for use in construction market. The findings were compared to the similar results of same connection types obtained from literature.

The experimental results of the TCC system utilising a number of different connection solutions and concrete type were analysed and the feasibility and effectiveness of these alternative solutions were evaluated to deliver recommendations regarding the economy, functionality and constructability of these alternative TCC systems.

The mechanical properties of connection such as stiffness (slip modulus) and shear strength were used in the design of the TCC floor as discussed in Chapter 6. Hence, based on the push-out test results and experience of constructing the specimens, efficient solution of mechanical fastener was selected for four-point bending test.

The stiffness and strength of TCC connections obtained from push-out test results were compared to that of derived from proposed analytical models as discussed in Chapter 8.

5.2 EXPERIMENTAL PUSH-OUT TEST PROGRAMME

A comprehensive parametric study on TCC shear connections utilising different variables was conducted to investigate the effect of these variables on the strength, stiffness, ductility and failure mode of the TCC connections. The variables addressed in the programme included:

• Shear connectors such as screws, L and U profiles in combination with multiple screws;

• Concrete type including conventional concrete (CC), expanded polystyrene light-weight concrete (EPS LWC2000 and 1600), Scoria light-weight concrete (Scoria LWC), self-consolidating concrete (SCC), high-strength concrete (HSC);

• Inclination angle of crossed screw including: ±30°, ±45° and ±60°;

•With and without presence of plywood interlayer between timber and concrete;

• Length of screw for example short and long SFS screws;

A total of 170 TCC connection specimens divided into 33 different test series utilising six different concrete types were prepared and 5 specimens of each series were constructed with the exception of CC SFS WI30 series with 4 samples (loss of data) and EPS LWC2000 SFS WI45 series with 10 samples (repeating the series) as listed in Table 5-1. In naming of the test series first the concrete and connector types are given and then it indicates the presence of interlayer (I) or (WI) for without interlayer series and finally the inclination angle to horizontal is mentioned.

Table 5-1 Experimental test series

	Inclination angle SFS						SPAX				New connectors		
Concrete	WI30	WI45	WI60	I45	short WI45	short I45	WI30	WI45	WI60	I45	coach45	L	U
CC	4	5	5	5	5	5	5	5	5	5	5	5	5
EPS LWC2000	5	10	5	5	5	-	5	5	5	5	-	-	-
EPS LWC1600	-	5	-	5	-	-	-	-	-	-	-	-	-
Scoria LWC	-	5	-	5	-	-	-	5	-	5	-	-	-
HSC	-	5	-	5	-	-	-	5	-	-	-	-	-
SCC	-	5	-	5	-	-	-	-	-	-	-	-	-

5.3 TEST PREPARATION AND CONNECTION DESCRIPTION

The TCC push-out test specimens consisted of a 450x300x75mm concrete slab which was connected to a 200mm deep by 45mm wide by 450mm long LVL joist using a shear connection as depicted in Figure 5-1. In Figure 5-1, a crossed long SFS screws inclined at ±45° is used to schematically depict the push-out test specimen.

For the specimens with interlayer, an interlayer of 17mm plywood was placed as permanent formwork between the concrete slab and the LVL joist (Figure 5-1b). A 45x350mm slot was cut centre of the formwork base to provide direct contact of the concrete and the LVL joist in specimens without interlayer. The plywood used for the formwork and interlayer was F17 grade plywood classified by AS2269 (2004). The hySPAN range LVL produced by Carter Holt Harvey Australia was used as timber joist in TCC specimens and its material properties were given in Chapter 4.

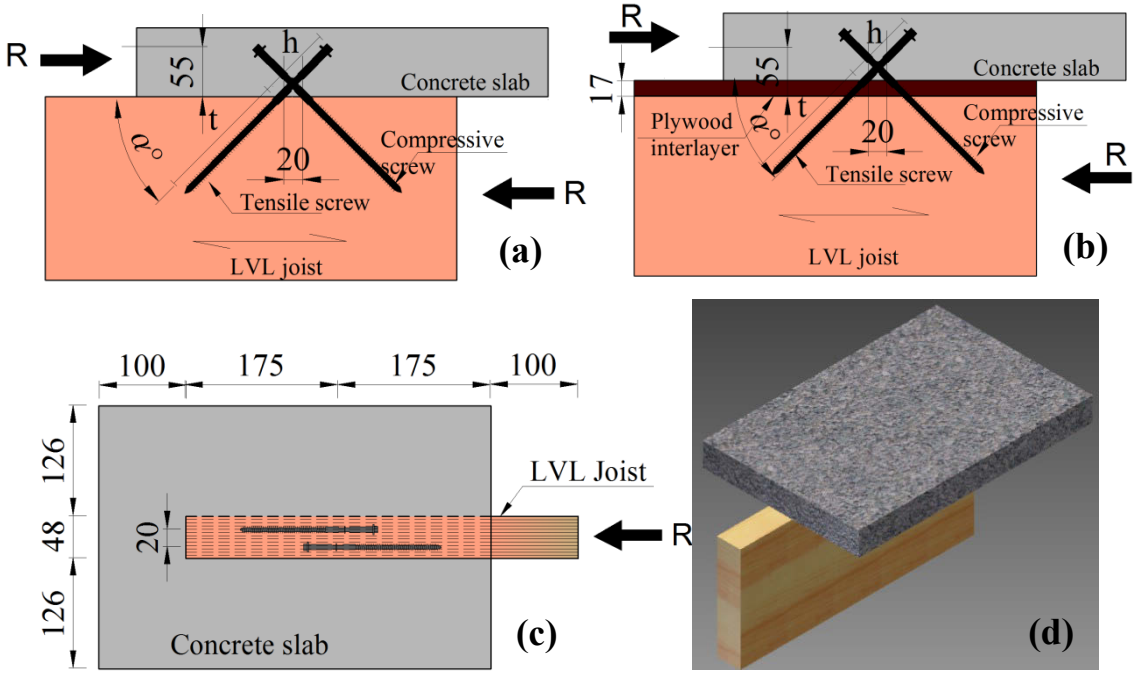

Figure 5-1 Typical geometry and components of specimens: (a) cross-section of specimen without interlayer (WI series), (b) cross-section of specimen with interlayer (I series) (c) plan and (d) 3D view TCC Specimen (in mm)

The timber was assembled to the pre-fabricated formwork using small scraps of plywood, nailed to both the timber and plywood (this was removed before testing).

After assembling the form work and prior to pouring of the concrete slab, the shear connectors were inserted. Various types of screws were embedded into the LVL joist at angles of ±30°, ±45° and ±60°. The screws were placed at the midpoint of the timber-concrete interface. A guide was used to ensure consistent placement and precise angling of the screws. Each hole was predrilled the majority of the length of insertion. Screws were inserted so that the thread was in the timber/interlayer.

A vertical anchorage length of approximately 58mm was embedded in the concrete (as such, samples with interlayers had less length within the LVL as screws also passed through a plywood interlayer). 58mm embedment of connector in a concrete slab with 75mm thickness leads to 17mm concrete cover which satisfies the limitations provided by the Australian concrete standards. Once the concrete was poured into the specimens, they were covered by plastic sheets to cure in a controlled environment and reduce speed of the hydration process. After 7 days, the formwork was removed and the specimens were exposed to an indoor laboratory environment (T=20°, RH=65%) until testing.

5.3.1 Test set-up, test procedure and data recording

The push-out tests were undertaken to test the connection in shear, as a representative behaviour of the composite and the effectiveness of the shear connection in terms of its strength, stiffness and ductility was evaluated. The applied load and the slip at the interface between the timber and the concrete were measured using a load cell and three linear variable differential transformers (LVDTs). Consequently, three slip moduli of shear connection corresponding to different load levels were obtained from the load-slip response of connections. The push-out test was carried out after 28 days of concrete curing. In the push-out tests, a steel test rig was used to hold the TCC specimens upright and load was applied to the free end of the timber as depicted in Figure 5-2.

The test rig was fabricated to accommodate for a variety of TCC specimen concrete slab sizes and as a result, metal packers were used to support the TCC specimen. Schematic drawing of the details of the test rig, as well as the test setup is shown in Figure 5-3. Two LVDTs were attached on either side of the LVL timber to measure the slip at the centre of the interface of timber and concrete (Figures 5-2 and 5-3). The third LVDT was placed at the centre of the TCC specimen, between the LVL joist and concrete offset as shown in Figure 5-2. The centre LVDT was fixed to the LVL whilst the contact tip rested against the concrete slab. A steel packer was placed between the top face of the LVL joist and the loading piston joist to transfer a uniform load and to concentrate the load close to the plane of connection in order to achieve pure shear. The recorded slip of the centre LVDT is plotted against the applied load in all series.

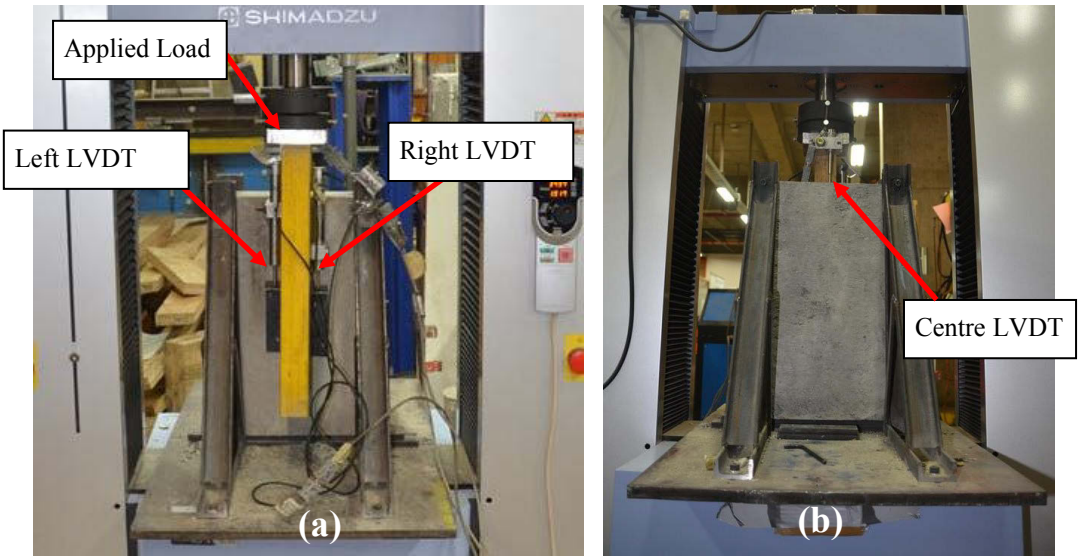

Figure 5-2 Set-up of a specimen in the test rig: (a) front and (b) back views

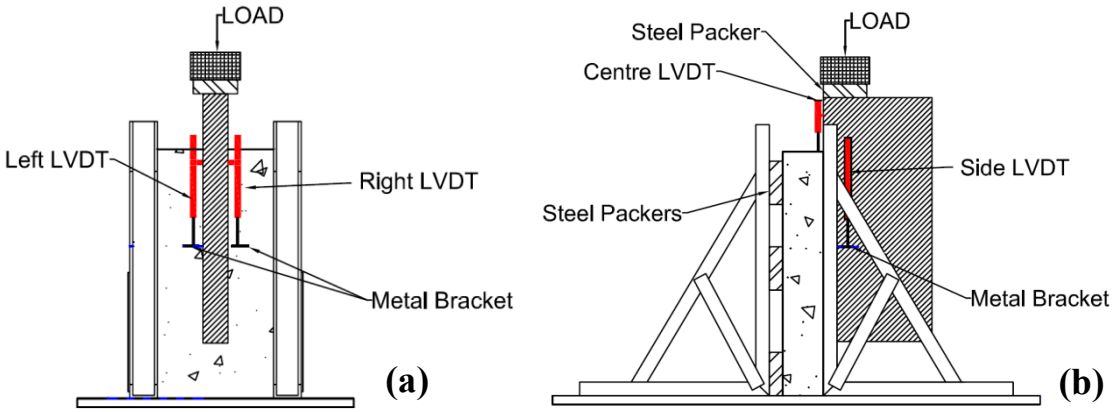

Figure 5-3 Schematic drawing:(a) front and (b) elevation views of test set up

The loading procedure for the push-out tests was conducted in accordance with EN26891 (1991) which sets a required loading sequence as illustrated in Figure 5-4. The loading procedure consists of five distinct stages. The application of load was speed controlled by monitoring the rate of the loading and checking that each of the loading phases was applied in the corresponding time interval. The preloading and then unloading are carried out to eliminate any internal friction in the connections and to prevent any premature failure due to initial slip or slack in the connection. However, the peak load occurs at a small slip between the timber joist and the concrete slab, the loading were continued to failure which happened at higher slip to study the post-peak behaviour, ductility and failure mode. Failure of the specimens was considered to be the point when the LVL joist separated physically from the concrete slab or when the connector had failed to such a point, that no further load could be applied onto the LVL.

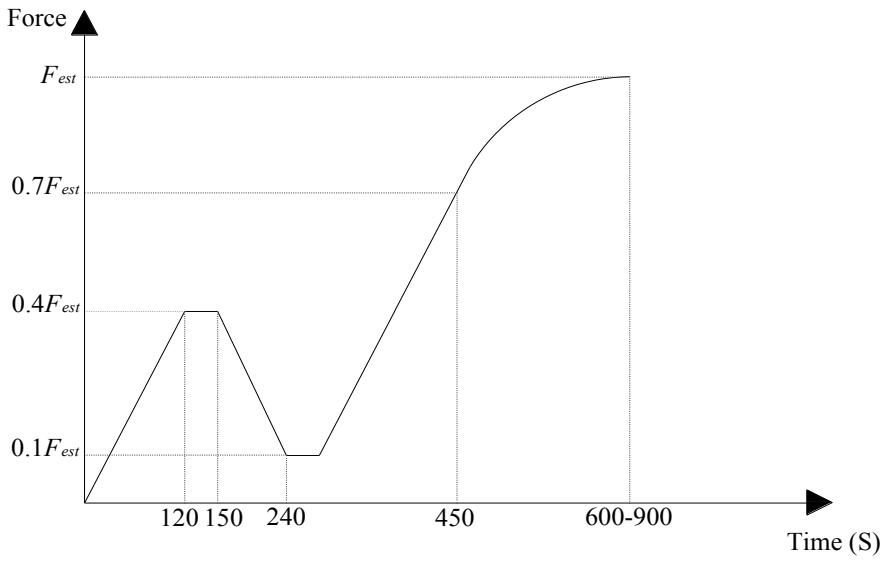

Figure 5-4 Loading regime in compliance with EN26891 (1991)

5.3.2 Stiffness analysis

Stiffness of the shear connection is proportionally related to the stiffness of the TCC system.

The serviceability slip modulus was calculated based on $0.4F_{max}$ (F_{max} is the load carrying capacity), whilst the ultimate slip modulus was calculated based on $0.6F_{max}$. Finally, the near collapse slip modulus was calculated based on $0.8F_{max}$.

These slip moduli are defined to be the slope of the load-slip curve within 10–40%, 10–60% and 10–80% of the load carrying capacity, respectively. The slip moduli of the connectors were derived from the load-slip responses using two different methods.

The first method to calculate the slip modulus of the connections is based on EN26891 (1991), using the slip measurements at specified points as shown in Figure 5-5. EN26891 (1991) proposes the first loading cycle to estimate the slip moduli of connections whilst the modified method calculates the serviceability slip moduli using the second reloading cycle to avoid the inconsistency of the results.

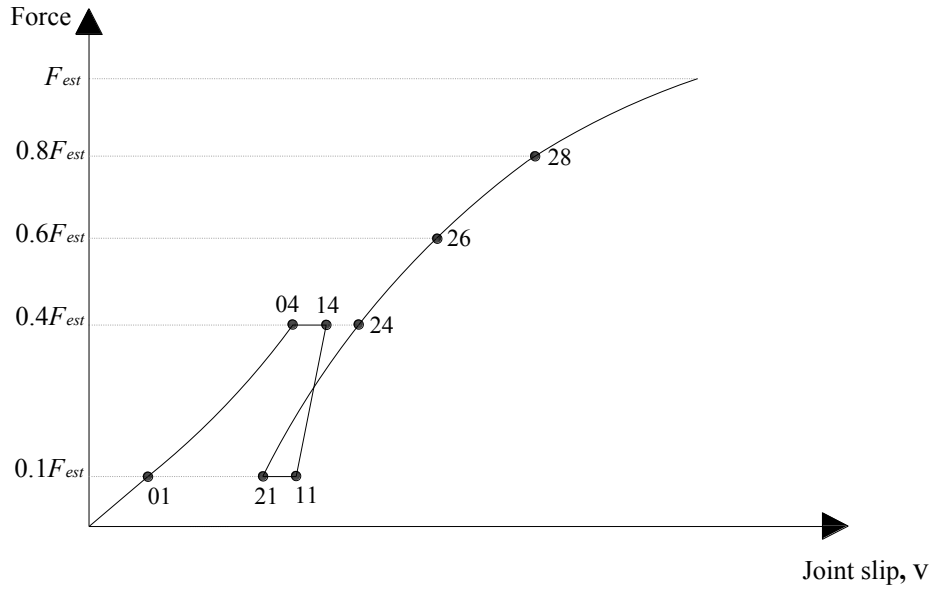

Figure 5-5 Idealised load-slip curve from push-out test based on EN26891 (1991)

Plotting load slip responses of the connections, the serviceability slip modulus, $K_{s,0.4}$ was calculated based on $0.4F_{max}$ (F_{max} is the load carrying capacity) as given in Equation (5-1) whilst the ultimate slip modulus, $K_{u,0.6}$ was calculated based on $0.6F_{max}$ as given in Equation (5-2). Finally the near collapse slip modulus, $K_{u,0.8}$ was calculated based on $0.8F_{max}$ as shown in Equation (5-3).

$$K_{s,0.4}=\frac{0.4F_{max}}{\frac{4}{3}(\upsilon_{04}-\upsilon_{01})} \tag{5-1}$$

$$K_{u,0.6}=\frac{0.6F_{max}}{\frac{4}{3}(\upsilon_{04}-\upsilon_{01})+\upsilon_{26}-\upsilon_{24}} \tag{5-2}$$

$$K_{u,0.8}=\frac{0.8F_{max}}{\frac{4}{3}(\upsilon_{04}-\upsilon_{01})+\upsilon_{28}-\upsilon_{24}} \tag{5-3}$$

where, υ_i is the slip measurement at specified points as depicted in Figure 5-5. The second method to calculate the slip modulus was based on a modified formula. The EN26891 (1991) formulas are adjusted by:

$$\frac{4}{3}(\upsilon_{24}-\upsilon_{21})=\frac{4}{3}(\upsilon_{04}-\upsilon_{01}) \tag{5-4}$$

From assessing the slip modulus across all states, it is evident that the modified method is less conservative than the EN26891 (1991) method. This is primarily attributed to the fact that the EN26891 (1991) method utilises the initial slip in the linear elastic range whereas the modified method utilises the slip values after it has been loaded to $0.4F_{max}$, unloaded and reloaded.

During the initial loading to $0.4F_{max}$, the connector is settled in and any initial slippage is overcome. However after it is unloaded and reloaded to failure, the slip is much lower in the linear elastic range due to the initial loading. Thus, the slip modulus based upon the modified method is much higher as it neglects the initial loading phase.

Effectively, the modified method is a longer term calculation of the slip modulus as it disregards the initial slip during the initial loading of the TCC system. For consistency the slip modulus derived using EN26891 (1991) were used for comparison of shear connectors since this method has been used widely in literature.

The slip moduli values calculated across both the modified and EN26891 (1991) methods experienced a much higher CoV compared to strength and ductility and it is attributed to the fact that a minor change in the slip values has a large impact on the resulting slip moduli. A higher CoV reduces the reliability which in turn leads to lower characteristic value.

5.3.3 Ductility

If other failure mechanisms rather than brittle failure of timber governs the resistance of timber composite, mechanical fastener exhibit a semi rigid plastic behaviour and it is attributed to high slenderness ratio, *t*/*d* (fastener length/fastener diameter) and embedding strength behaviour of timber itself and ductile behaviour of fastener (Johnsson 2004). A ductile connection exhibits large plastic deformation capacity without a significant strength reduction.

The ductility of a timber connection is measured in different ways as a relation between the yield and the ultimate deformations whilst the definitions of yield and ultimate deformations differ (Johnsson 2004).

For cyclic loading European standards, EN12512 (2001) defines ductility as the ratio of ultimate to yield deformations, D_f by:

$$D_f = \frac{\upsilon_f}{\upsilon_y} \tag{5-5}$$

where, υ_f is the deformation associated to load-drop (80% of the maximum load) and υ_y is the elastic deformation of connector (EN12512 2001).

Ductility has also been defined as the relative deformation capacity associated with the maximum load (Karacabeyli et al. 1996):

$$D_u = \frac{\upsilon_u}{\upsilon_y} \tag{5-6}$$

where, υ_u represents the slip corresponding to maximum load at connection and υ_y is the elastic deformation of connector. The schematic υ_y, υ_u and υ_f used in ductility calculations are depicted in Figure 5-6. Two different types of ductility, D_f and D_u were calculated using υ_y, υ_u and υ_f for each test series. For consistency, D_f were used for comparison of ductility in different test series since this method has been adopted in literature.

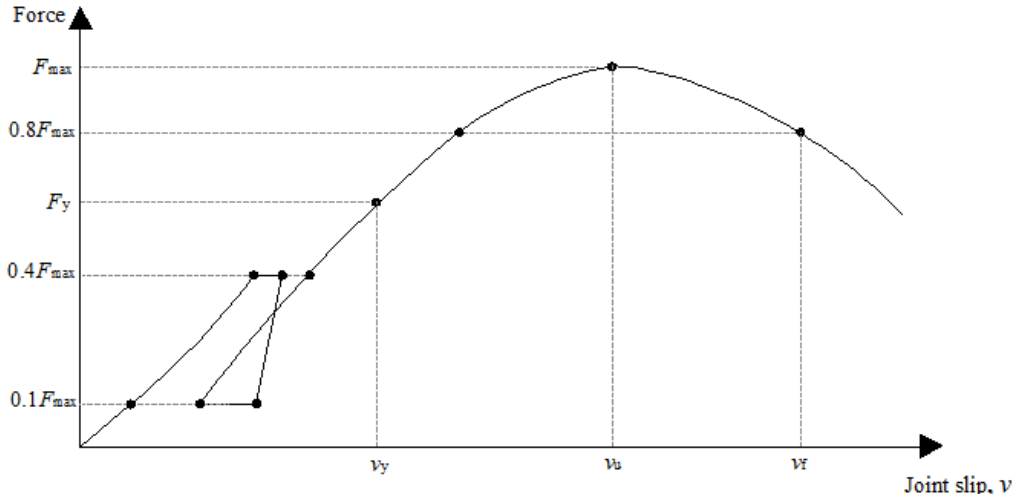

Figure 5-6 Different slip values at yield, F_{max} and ultimate points used in ductility

5.3.4 Failure mode analysis

The failure of connectors, as well as angle of screws at the plane of connection and state of concrete and timber around connection as failure mechanism of specimen was of interest. The general failure modes and observatory notes of each test series were separately discussed. Following the failure of the specimens, they were removed from the test rig and were split to determine the failure mode.

5.3.5 Mathematical model for responses of the test series

The mathematical descriptive model of each connections test series was proposed using the load-slip response of the connections and non-linear regression. The load-slip response of most of the test series is divided into two part as the pre-peak and post-peak. The load increased quite steadily, slowing slightly before peak load, F_{max} was reached whilst after reaching the peak, the load gradually reduced to around 50-90% F_{max} before a sudden failure of the screw placed in tension occurred. The pre-peak and post-peak parts of the load-slip responses of different series (before the sudden failure) were considered for mathematical expression. Equation (5-7) indicates the exponential function with three unknown parameters (a, b and c) which is fitted into each test series whilst υ indicates slip at interface of composite materials.

$$P = a(e^{-b\upsilon} - e^{-c\upsilon}) \qquad (5\text{-}7)$$

The mathematical expression and its square of the sample correlation coefficient between the experimental results and the mathematical expressions, R^2 of each test series were proposed. Mathematical expressions and load-slip responses of

different test series were plotted together. This exponential function is a suitable representative of load-slip response for mechanical fastener as shear connector in TCCs.

5.3.6 Interlayer

TCC construction is a possible solution for construction of new floor slabs. However, it is most competitive in rehabilitation works, where an existing timber floor is present. In upgrading of old timber floors using TCC construction, existing floorboards is used as a permanent formwork in form of an interlayer between the timber beams and concrete slab. Mechanical shear connections are mounted into timber joists at regular spacing and concrete is then poured over existing timber floorboard.

The pouring of a concrete slab on top of an existing timber floor is a simple operation, requiring minimal work. Such permanent formworks are advantageous in terms of savings on labour costs associated with demolishing the existing floor and construction of new formwork. Moreover, it creates less disturbance to the building. The only concern is to prevent any wetting of the timber and leakage to the lower floors which can be accommodated by inclusion of a thin film layer (Jorge et al. 2011).

Another form of an interlayer is the use of formwork for constructing a TCC floor. The formwork is laid on top of the timber sections and used to provide the needed edge restraints to cast the slab.

Inclusion of an interlayer to a TCC has no structural effect for bending stiffness and thus, the cross section analysis should only consider the concrete and timber members and neglect the middle layer of timber floorboards.

Previous investigations includingVan der Linden (1999) and Jorge et al. (2011) identified that the interlayer component of the TCC is generally a weak or non-structural element which creates a gap between the timber and concrete members. Hence, TCC connections with the presence of interlayer exhibit lower slip modulus and load capacities (Jorge et al. 2011).

Nevertheless, comparing the cross-section of two types of TCC beams, without and with interlayer, the additional section depth due to the interlayer compensates for the lack of stiffness created by the interlayer. Further investigations on influence of interlayer on mechanical properties of TCC connections and floors utilising different types of concrete can improve design codes and its practical applications in upgrading of old timber floor.

5.4 PUSH-OUT TEST RESULTS

The experimental and analytical load-slip diagrams of the test series utilising different types of concrete and shear connector are given in Appendix B. Appendix B also reports the stiffness, ductility and failure mode of different test series categorised into CC, EPS LWC, Scoria LWC, HSC and SCC series.

Figures 5-7 and 5-8 plot analytical load-slip graphs obtained from curve-fitting of experimental response of CC and EPS LWC series utilising crossed SFS and SPAX screws. Further discussions on varying the parameters in the experimental series including screw types, the inclination angle of screws, the existence of interlayer, LWC concrete types, influence of concrete properties and alternative connection design are given in discussions Section of this Chapter.

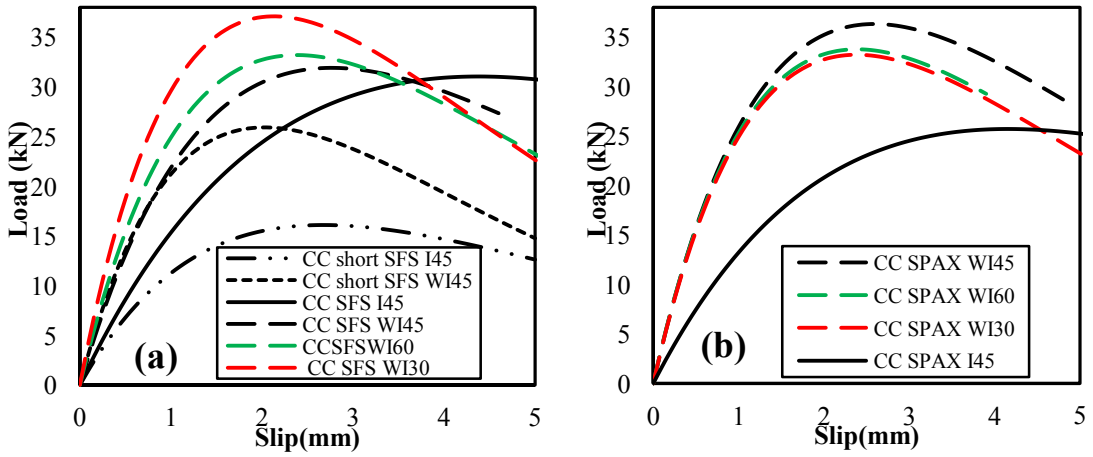

Figure 5-7 Analytical graphs of (a) CC SFS series, (b) CC SPAX series and

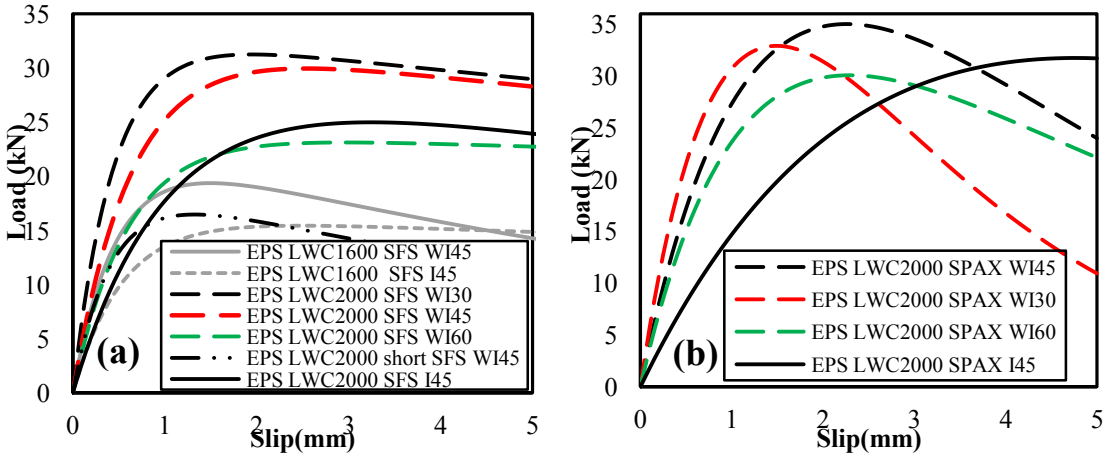

Figure 5-8 Analytical graphs of (a) EPS LWC SFS series, (b) EPS LWC SPAX series

Figures 5-9 and 5-10 represent analytical load-slip graphs obtained from curve-fitting of the experimental response of Scoria LWC, HSC and SCC series.

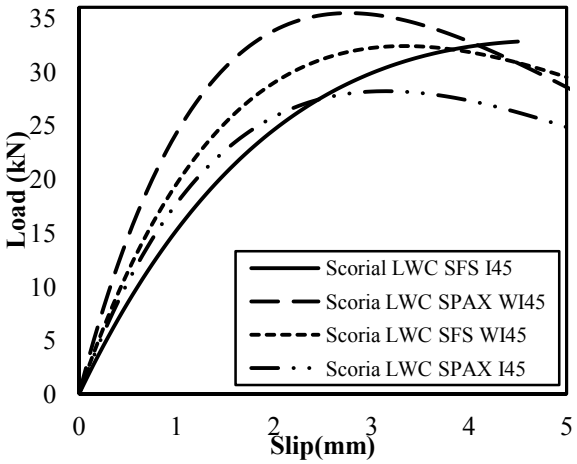

Figure 5-9 Analytical graphs of crossed SFS and SPAX screws Scoria LWC series

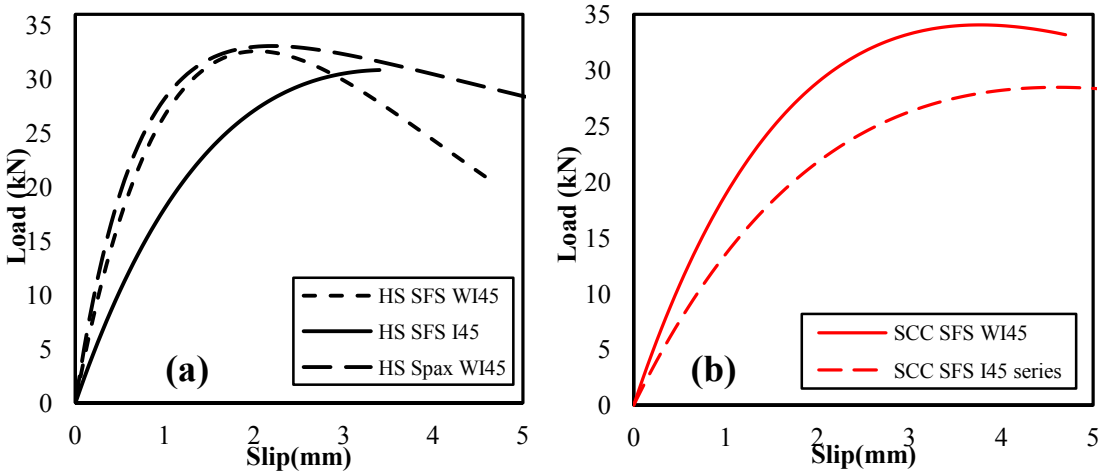

Figure 5-10 Analytical graphs of (a) HSC and (b) SCC series

5.5 DISCUSSION

The effect of different varying parameters such as screw types, the inclination angle of screws, existence of interlayer, LWC concrete types and influence of concrete properties are discussed from the experimental results explored through this Chapter.

5.5.1 Effect of inclination angle of screws

The effect of the inclination angle of SFS and SPAX screws utilising CC and EPS LWC2000 on their load-slip responses obtained from regression analysis is shown in Figure 5-11.

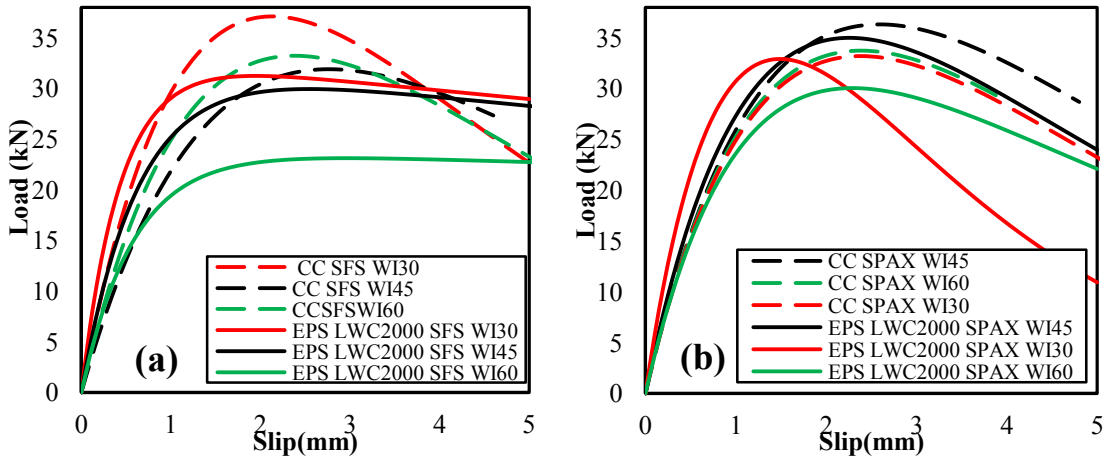

Figure 5-11 Graphs showing the effect of inclination angle of (a) SFS and (b) SPAX screws utilising CC and EPS LWC2000 on their load-slip responses

The effect of the inclination angle of SFS and SPAX screws on the serviceability and ultimate slip moduli of TCCs utilising CC and EPSLWC2000 is shown in Figure 5-12.

The inclination angle of connector has a significant influence on its serviceability and ultimate stiffness. Increasing the angle of connector beyond 30° reduces serviceability and ultimate stiffness proportionally and the lowest slip moduli were recorded at an angle of 60° and 45° for EPS LWC and CC series, respectively. This may be due to the fact that the flexural deformation of slender fastener is limited in lower inclination angles which results in higher slip moduli and this is aligned with other researches for example Symons et al. (2010a). In the EPS series, SFS and SPAX screws show nearly identical serviceability and ultimate stiffness at their given angle.

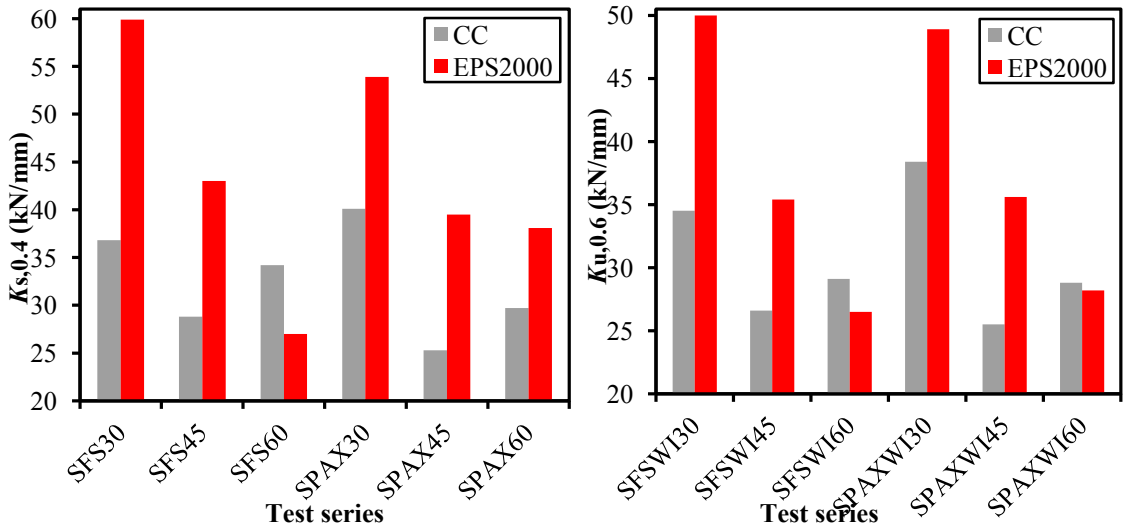

Figure 5-12 Stiffness comparison of shear series utilising different concrete and angles

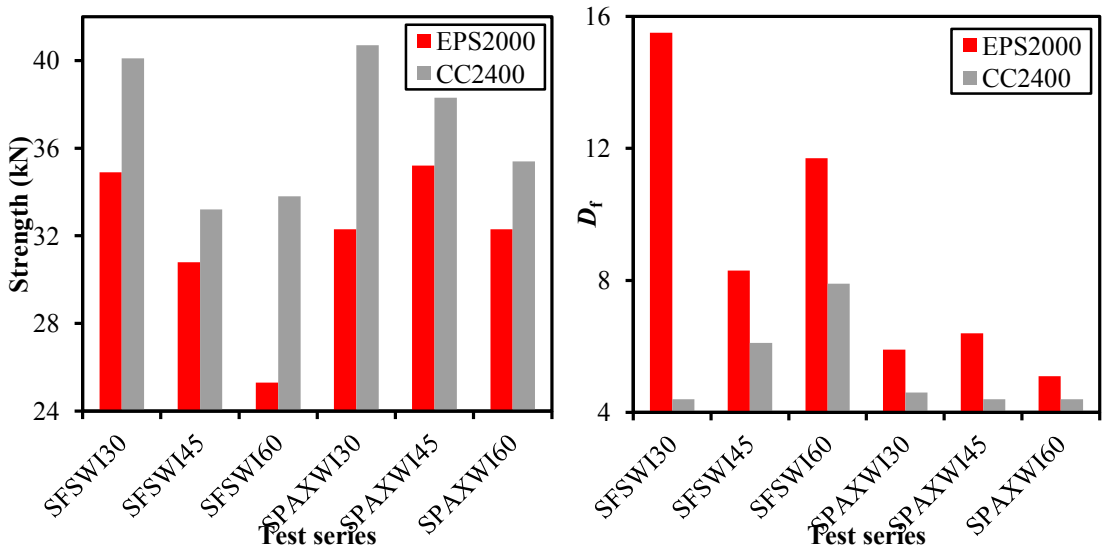

Figure 5-13 Strength and ductility of shear series with different concrete and angles

The effect of the inclination angle of SFS VB and SPAX screws on the strength and ductility of a TCC connection utilising CC and EPSLWC2000 is illustrated in Figure 5-13. There is a relationship between the angle of shear connector and strength as a smaller angle to the timber results in greater strengths. The highest strength in both CC and EPS LWC with varied inclination angles was experienced by CC SPAX WI30 with a mean value of 40.7kN. Shear connectors at an angle of 60° exhibited the lowest strength with the exception of CC SFSWI60° that is slightly higher than CC SFSWI45°.

For strength, SPAX screws have slightly outperformed SFS VB screws in both CC and EPS LWC series. Comparing EPS LWC2000 series with different inclination angle, EPS LWC SPAX WI45 experienced highest strength a value of 35kN.

EPS LWC2000 SPAX screws series with inclination angles of 30°, 45°, and 60° experienced 0.1%, 14.4% and 27.9% higher strength than similar series using SFS VB, respectively. This is an interesting observation as SFS VB has designed specifically for use in TCC. The SPAX screw does have a slightly larger diameter, 8.1mm compared to 7.6mm and 5mm at the bottom section of the SFS screw. The larger diameter provides a greater axial strength and yield moment.

EPS LWC2000 SFS WI60 series initially experienced premature localised failure of concrete around the tensile screw on all samples due to deformation of screws. Then all the specimens ultimately were failed by tensile failure of screw placed in tension. The failure mechanism including premature and ultimate failure results in a much lower strength compared to the other EPS LWC series.

Comparing EPS LWC2000 and CC series with different inclination angle, EPS LWC indicates much higher ductility than similar CC series. For ductility, SFS screws outperformed SPAX screws in both CC and EPS LWC series. There is no relationship present between the angle of shear connector and ductility.

5.5.2 Effect of screw type

The effect of the screw types and inclination angle on the load-slip responses of series utilising CC and EPS 2000 obtained from regression analysis is shown in Figure 5-14.

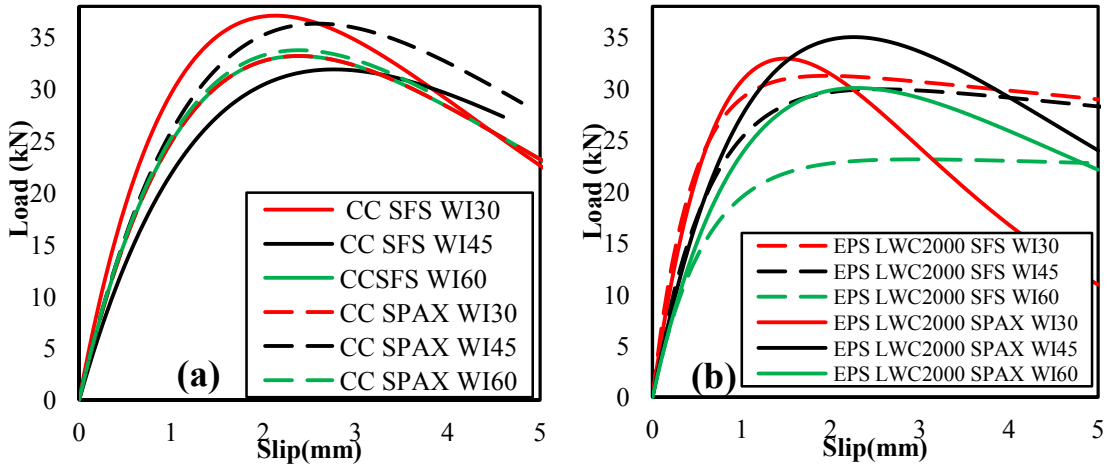

Figure 5-14 Graphs showing the effect of screw and inclination angle on (a) CC and (b) EPS 2000 series

Figure 5-15 shows the slip moduli comparison of SFS and SPAX screws.

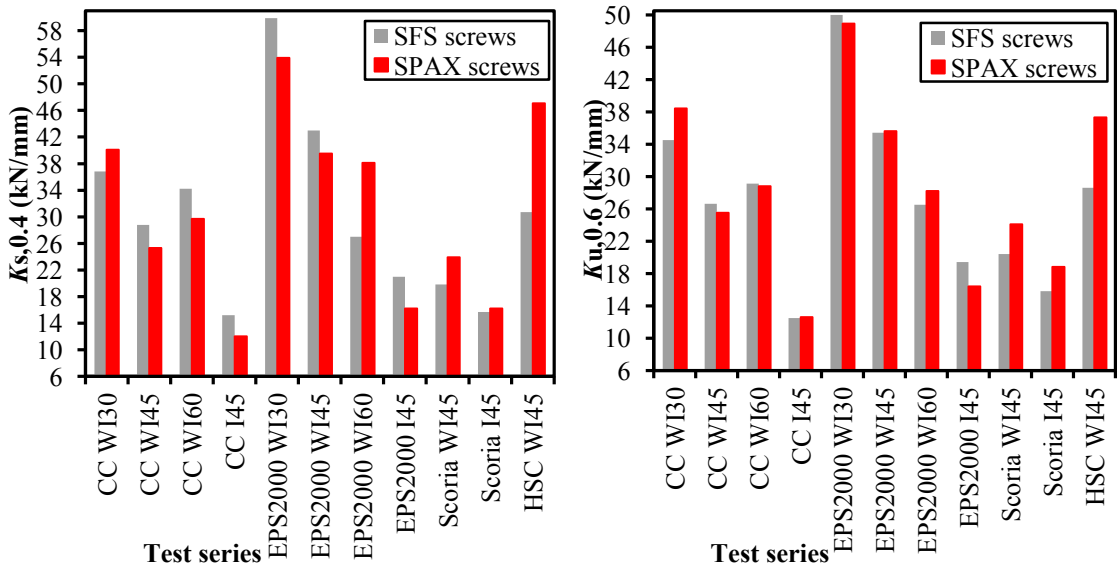

Figure 5-15 Serviceability and ultimate stiffness comparison of SFS and SPAX screws

In terms of stiffness, SFS VB screws exhibited 8-20% higher serviceability and ultimate slip moduli than SPAX screws utilising CC and EPS LWC2000 series whereas for Scoria and HSC series, SPAX screws obtained 3-53% higher stiffness compared to SFS VB screws. This trend is identical for both serviceability and ultimate slip moduli.

Figure 5-16 depicts the strength and ductility comparison of SFS and SPAX screws. In terms of strength for different series, SPAX screws highlighted 0-15% higher strength than SFS VB screws with the exception of CC SPAX I45, EPS 2000 SPAX WI30 and HSC SPAX WI45 series where SFS VB screws represented 2-8% higher strength than SPAX screws (Figure 5-16). SPAX series exhibited lower or similar ductility compared to SFS series with an exception of HSC SPAX WI45 series which represented approximately 90% higher ductility than similar SFS series (Figure 5-16).

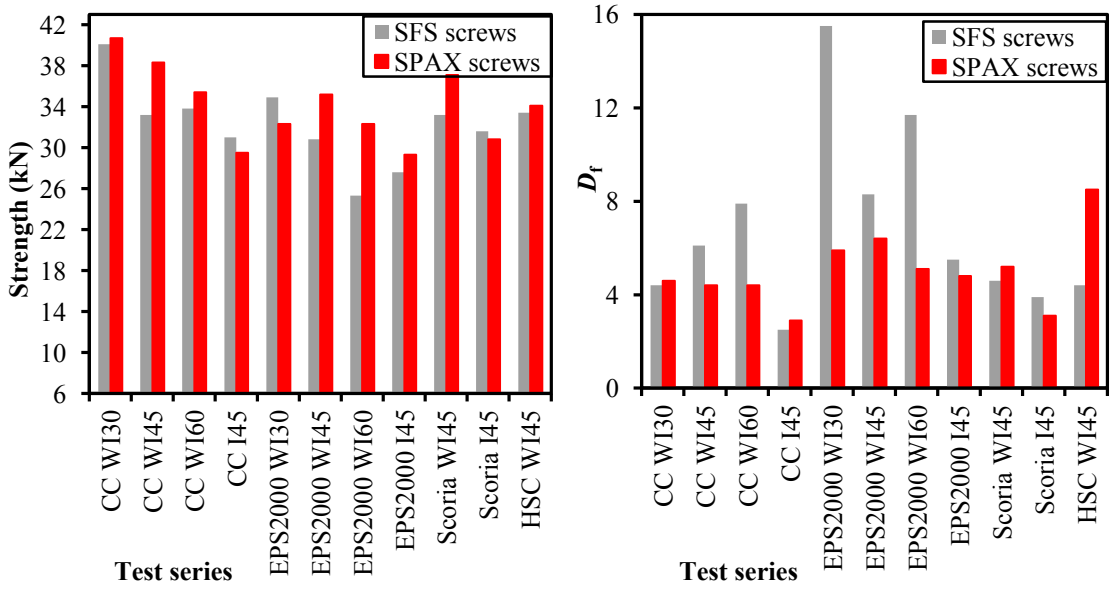

Figure 5-16 Strength and ductility comparison of the SFS and SPAX screws series

5.5.3 Effect of Interlayer

Previous investigations such as Van der Linden (1999), Jorge et al. (2010) and Jorge et al. (2011) identified the effect of interlayer on stiffness and strength of TCC connections utilising light-weight concrete or conventional concrete.

Though similar in nature and intent, there were a number of differences between tests for this research and those aforementioned as illustrated in Table 5-2.

Table 5-2 Differences in specimens and test configuration for different investigations

Property	This research	Jorge et al. (2010),(2011)	Steinberg et al. (2003)
28 day compressive strength of concrete	37MPa	30MPa	22.5MPa
	22-28MPa	16-18MPa	
	12MPa	12-13MPa	
Density of concrete	2350kg/m^3 (CC)	2400 kg/m^3 (CC)	2400 kg/m^3 (CC)
	2000kg/m^3 (EPS LWC)	1400 – 1600kg/m^3 (LWC)	
	1600kg/m^3 (EPS LWC)	1200 – 1400kg/m^3 (LWC)	
light-weight aggregate	Expanded polystyrene beads (25kg/m^3)	LECA (500kg/m^3)	N/A
Bulk density	25kg/m^3	500kg/m^3	N/A
Sample size	450 x 300 x 75mm (concrete)	(2x) 300 x 160 x 160mm (concrete)	400 x 360 x 70mm (concrete)
	450 x 200 x 48mm (LVL)	300 x 160 x 160mm (glulam)	400 x 140 x 100 mm (glulam)
Thickness of inter layer	17mm	25 mm	19,28 mm
interlayer species	Plywood	sawn Maritime pine	Particleboard
push-out set-up	Asymmetrical	Symmetrical	Symmetrical
Screws	SFS VB 48 _ 7.5 × 160 (crossed)	SFS VB 48 _ 7.5 × 100 (parallel and crossed)	SFS VB 48 _ 7.5 × 100 (crossed)
No of screw	2	2	4
species	Radiata Pine, Douglas Fir	Spruce	Spruce

Figure 5-17 illustrates the serviceability and ultimate slip moduli of different test series with and without the inclusion of an interlayer.

The presence of an interlayer significantly reduced the serviceability and ultimate slip as depicted in Figure 5-17.

It is attributed to the fact that the interlayer of plywood allowed for additional deformations at F_{max} and after reaching F_{max}. Test series with interlayer exhibited low reduction in load capacity after reaching F_{max}. The amount of stiffness reduction varied among the test series and no particular trend was observed.

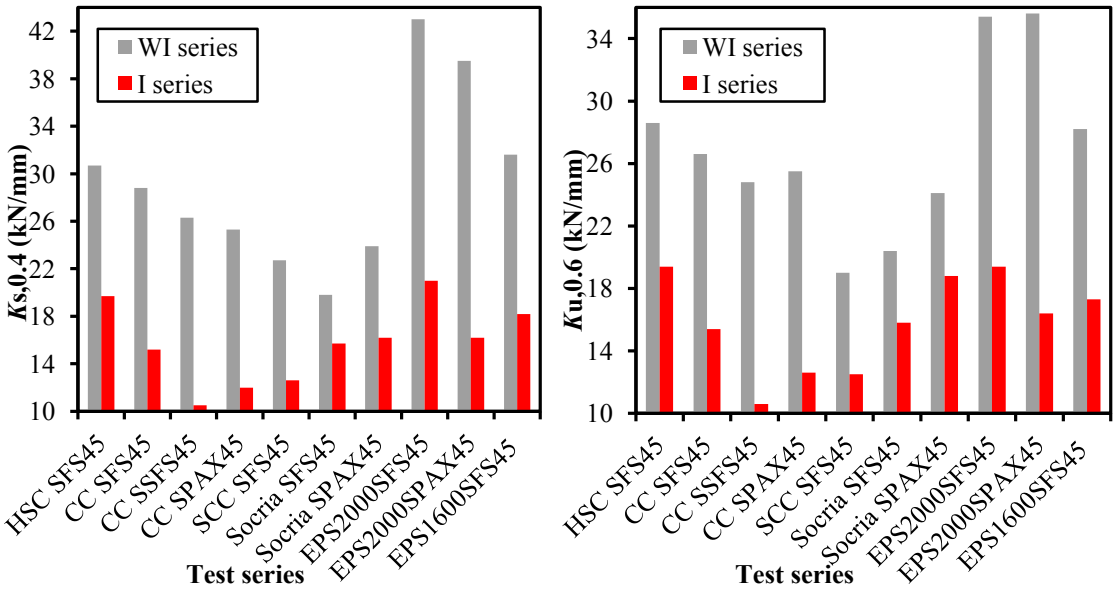

Figure 5-17 Serviceability and ultimate stiffness comparison of the WI and I series

The experimental result agrees with result from Jorge et al. (2011). Jorge et al. (2011) proposed a serviceability slip modulus reduction for short SFS ±45°crossed screws samples utilising two compressive-strength grades of LWC 20-22MPa (ρ=1600kg/m^3) and 16-18MPa (ρ=1400kg/m^3) to be 33% and 30%, respectively whilst Scoria LWC2000 SFS45 (f_c=28.1MPa) and EPS LWC2000SFS45 (f_c=23.4MPa) and EPS LWC1600 SFS45 (f_c=12.1MPa) series demonstrated 21%, 50% and 42% reduction in serviceability slip modulus, respectively.

Elsewhere, Van der Linden (1999) tested short SFS screws TCC connections utilising conventional concrete in specimens with and without interlayer and concluded 55% and 45% reductions in $K_{s,0.4}$ for the specimens with 19 and 28mm interlayers, respectively and these reductions are in agreement with this study where inclusion of interlayer in both CC short SFS45and CC SFS45 series leads to a reduction of approximately 60% and 47% in the serviceability slip modulus, respectively.

CC short SFS45 series exhibited most significant reduction in both serviceability and ultimate slip moduli due to the presence of the interlayer, approximately 60% whilst the Scoria SFS45 series showed a minimum serviceability slip moduli reduction of approximately 21% for both serviceability and ultimate slip moduli in presence of an interlayer.

This trend was continued throughout different slip moduli. However, by approaching F_{max} the difference in stiffness values became smaller. However, the results highlighted

that samples with an interlayer experienced a greater linear relationship than those without an interlayer, as the difference percentages when approaching F_{max} were significantly smaller. The difference percentages in serviceability slip modulus due to the presence of interlayer were 2%- 10% higher than that of ultimate slip modulus.

Moreover, a reduction of 35-40% is suggested for the stiffness of CC series. Whilst the results suggest individual reduction factors, there is not enough evidence to conclude an overall reduction for capacity and slip modulus of CC and LWC series with interlayer compared to without interlayer series, as proposed by Jorge et al. (2011).

The effect of the interlayer on the strength and ductility is shown in Figure 5-18. The test results depict that the inclusion of an interlayer into the TCC samples reduced its strength and led to greater average slip at F_{max}. The experimental result indicated almost similar trend compared to experiments investigated by Jorge et al. (2011).

Jorge et al. (2011) reported strength differences for short SFS ±45° crossed screws samples utilising two compressive-strength grades of LWC 20-22MPa (ρ=1600kg/m^3) and 16-18MPa(ρ=1400kg/m^3) to be -6% and +11%, respectively whilst Scoria LWC2000 SFS45(f_c=28.1MPa) and EPS LWC2000SFS45 (f_c=23.4MPa) and EPS LWC1600 SFS45(f_c=12.1MPa) series demonstrated 5%, 11% and 15% strength reduction in presence of interlayer.

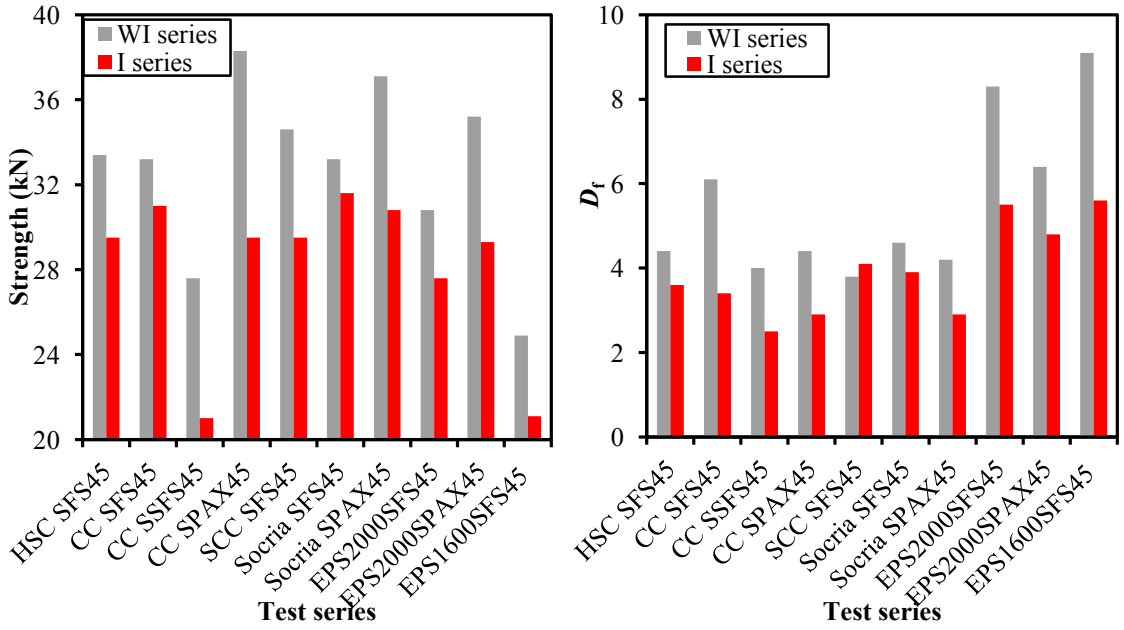

Figure 5-18 Graphs showing that the strength and ductility comparison of the series with and without an interlayer

The experimental results conclude that a strength reduction of 6-24% is suggested for CC samples, as well as a strength reduction of 12% and 15% for HSC SFS45 and SCC SFS45 series in presence of interlayer.

CC short SFS45 series exhibited maximum strength reduction in presence of interlayer, approximately 24% whilst Scoria SFS45 series showed minimum strength reduction of about 5% in presence of interlayer.

Figure 5-18 illustrates no apparent link between the amount of strength reduction from the inclusion of an interlayer and the strength of the concrete mixes or the strength of the connections as the degree of strength reduction varies among the mixes.

For example, no significant differences between the strength reduction of CC and LWC series (both EPS and Scoria LWCs) due to the presence of an interlayer were observed as 13% compared to 17.5%, respectively.

As a result, considering all the test series, a reduction factor of 5-20% was more appropriate as there are significant differences between the strength capacities results. However, it is clear that the strength of the specimens utilising the CC mix is less affected by the inclusion of an interlayer and the presence of an interlayer in short SFS series had the largest impact on strength reduction.

The inclusion of an interlayer into the TCC specimens leads to an increase in the slip experienced at F_{max} in all cases. For the specimens with the long SFS screws, the amount of slip increase was approximately 20-50%. The CC, SCC and EPS LWC2000 mixes experienced similar slip increases in the range of approximately 40-50%.

However, the slip at F_{max} of the EPS LWC1600 specimens was least affected by the inclusion of an interlayer and showed significantly less slip at F_{max} than the other series with a slip increase of only 22.80%.

Unlike the F_{max}, the slip at F_{max} experienced by CC short SFSWI series was similar to the other series. However, the CC short SFS series was most affected by the inclusion of an interlayer with an increase in slip at F_{max} of 52.5%.

Figure 5-18 also shows the ductility for each series with and without of plywood interlayer. The experiments concluded that the use of interlayer in samples decreased the ductility approximately 18%-44% as shown in Figure 5-18.

There was one exception, SCC SFS45 which represented 7% higher ductility in presence of interlayer. The CC short SFS45 series exhibited maximum ductility reduction in presence of an interlayer, approximately 37% whilst the Scoria SFS45 series showed minimum ductility reduction of approximately 15% in presence of an interlayer. The EPS LWC 1600 SFSWI45 series exhibited maximum ductility of 9.1 and CC short SFS I45 series demonstrated minimum ductility of 2.5.

5.5.4 Effect of concrete properties

Figures 5-19 and 5-20 demonstrates the effect of compressive strength of concrete on serviceability and ultimate slip moduli of different series, respectively.

Due to visual inspection of the variables before regression analyses and also inspection of residuals in quadratic relationship compared to linear one, quadratic relationships were selected to represent the scatter data in this Section.

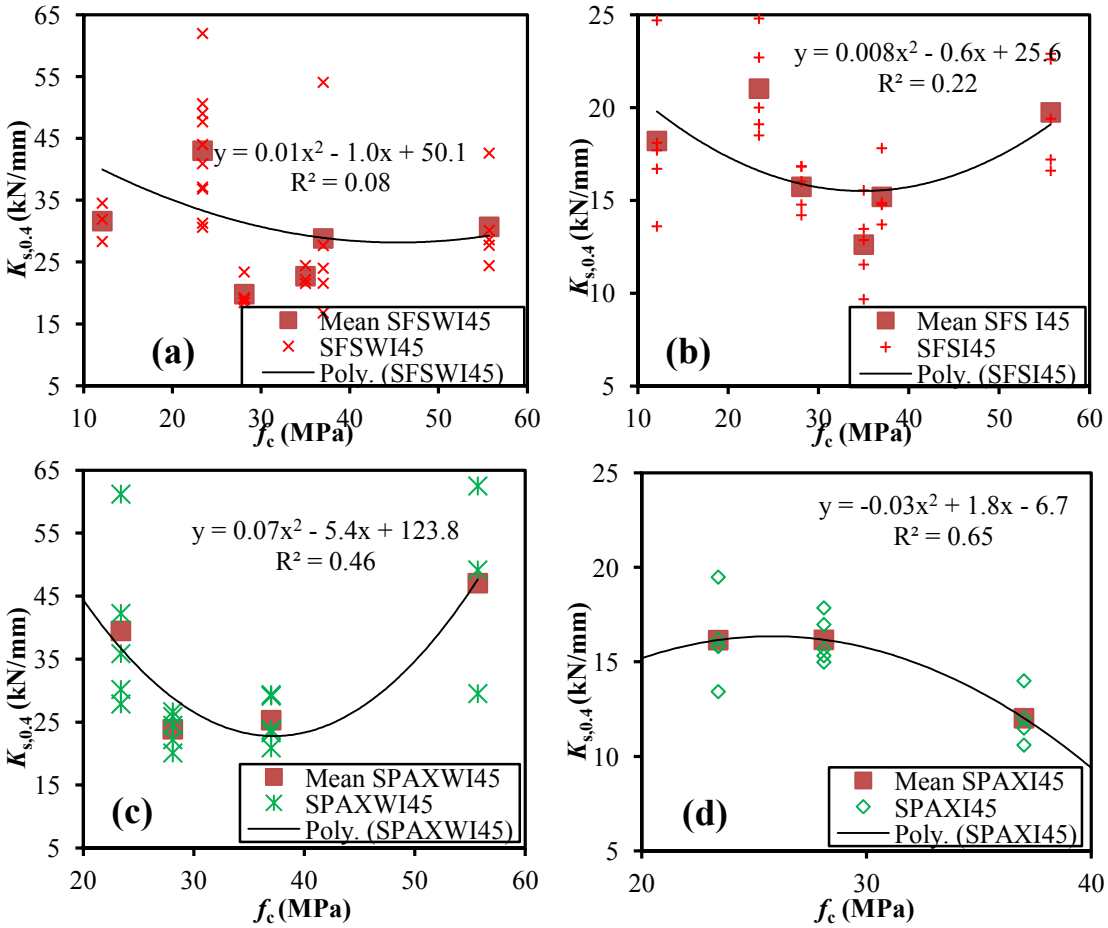

Figure 5-19 Effect of compressive strength of concrete on serviceability slip modulus of TCC (a) SFS WI45 , (b) SFS I45 series, (c) SPAX WI45 and (d) SPAX I45 series

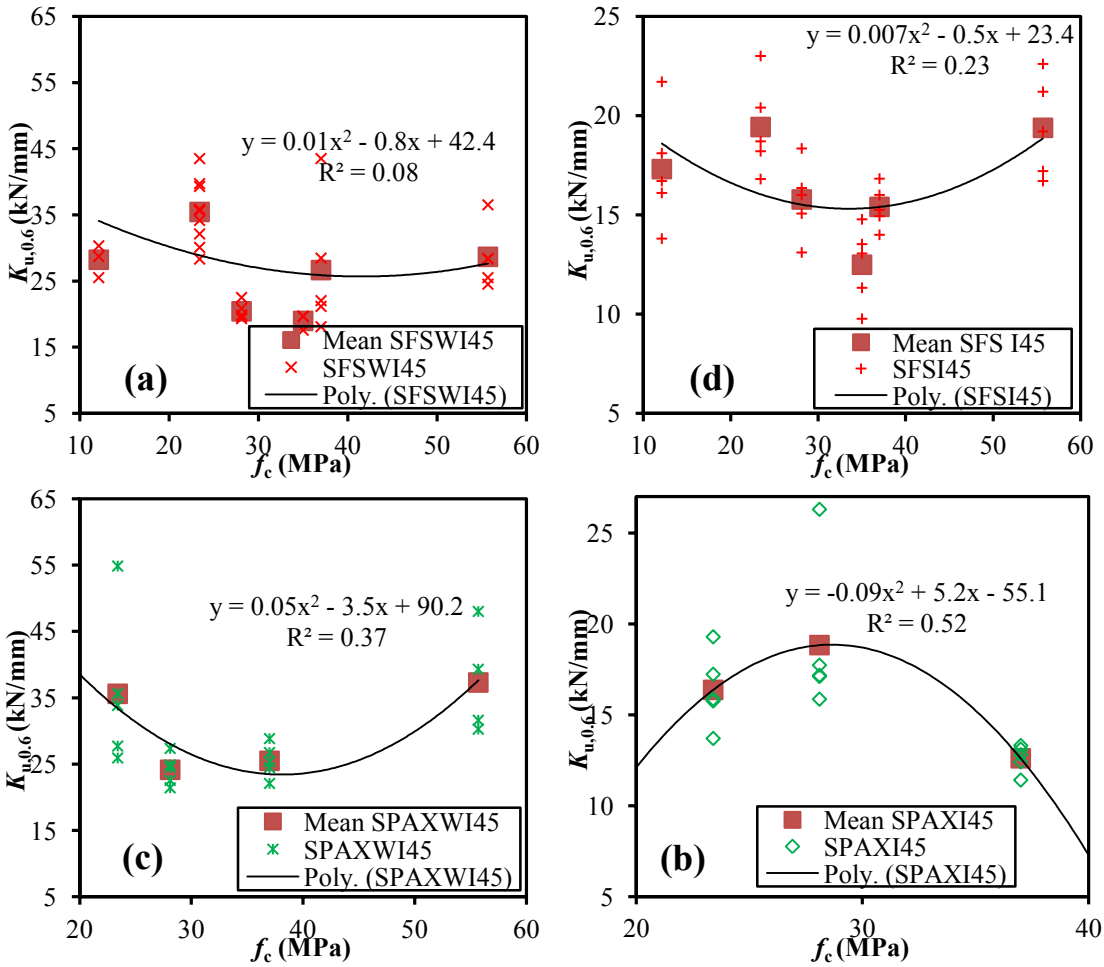

Figure 5-20 Effect of compressive strength of concrete on ultimate slip modulus of TCC (a) SFS WI45 , (b) SFS I45 series, (c) SPAX WI45 and (d) SPAX I45 series

An initial localised failure in the EPS LWC concrete at the connection caused the first drop, before the ultimate failure of the screws. Failure in EPS series was more ductile than similar series utilising CC with a greater deflection following F_{max} before failure.

Jorge et al. (2011) noted that the mortar matrix of EPS LWC is stronger than in CC whereas light-weight aggregate has lower compressive strength than conventional aggregates. This may result in higher anchor strength of LWC mortar after the initial crushing of light-weight aggregate, leading to the recovery of the load level after an initial drop at low slip value and consequently a higher serviceability and ultimate slip moduli. The EPS LWC1600 mix, however, did not follow the same trend and although it had the lowest density and compressive strength out of all the mixes, it displayed a decreased serviceability and ultimate slip moduli of approximately 15% and 30% than EPS LWC2000 series, respectively.

Conversely, comparing to CC and HSC series, any increase of the compressive strength of the concrete accompanied higher serviceability and ultimate slip moduli of the test series as depicted in Figures 5-19 and 5-20. HSC series which has an increased density and compressive strength, exhibited higher serviceability and ultimate slip moduli of approximately 6-80% and 7-46%, respectively compared to that of CC series.

Comparison of serviceability and ultimate slip moduli of different series such as CC vs. EPS LWC2000, CC vs. EPS LWC1600, CC vs. Scoria LWC and Scoria LWC vs. EPS LWC1600 implies that an increase of the compressive strength of the mixes decreases the stiffness of TCC SPAX and long SFS screws. This agreed with Jorge et al. (2011) , however, one discrepancy when comparing these results was that literature compared two grade of LWC as 16-18 and 20-22 utilising short SFS screws. Figure 5-21 shows the effect of compressive strength of concrete on connection strength of different TCC series. The polynomial descriptive model and the sample correlation coefficient, R^2 are Illustrated in same Figure.

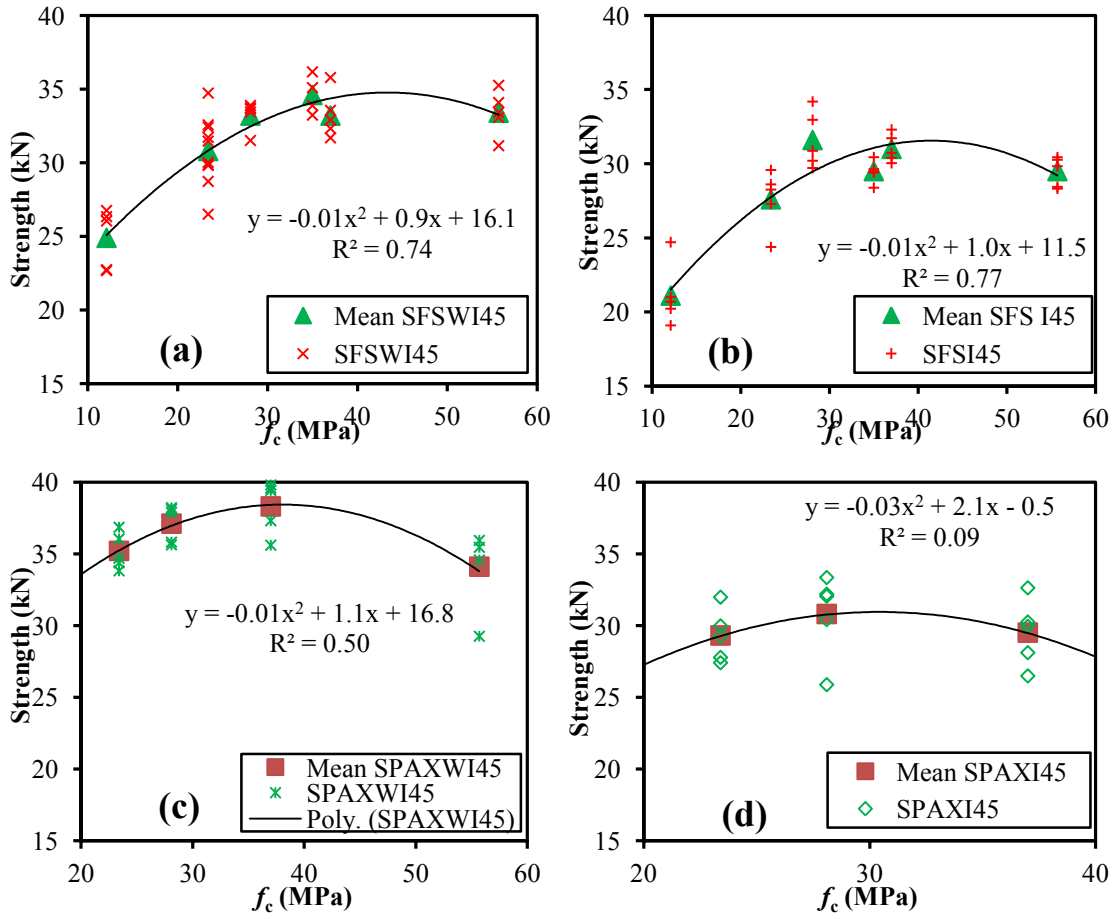

Figure 5-21 Effect of compressive strength of concrete on strength of TCC (a) SFS WI45 , (b) SFS I45 series, (c) SPAX WI45 and (d) SPAX I45 series

Comparing to CC series, the reduction in density and compressive strength within the mixes decreased the strength of the SFS and SPAX screws series with and without interlayer as shown in Figure 5-21.

However, comparing CC and Scoria LWC series, the strength of Scoria LWC series remained almost unchanged. SCC mix, with a lower mass per unit volume and compressive strength of 2340kg/m^3 and 35MPa compared to the CC series with those of 2360kg/m^3 and 37MPa, respectively experienced 4% higher strength.

Although the compressive strength of the concrete directly influenced the strength of the connections, for both the EPS LWC2000 and 1600 mixes, the reduction in connection strength was not proportional to the decrease in concrete strength.

This is observed in the LWC2000 mix ($f_{c=}$23.4MPa), with a decrease of concrete compressive strength of 37% compared to the CC series ($f_{c=}$37.0MPa) decreased the connection strength of SFS45 and SPAX 45 series only 7-11% and 1-8%, respectively. Similarly, the EPS LWC1600 SFS WI45 and I45 with a reduced compressive strength of 12.1MPa, resulted in a connection strength reduction of 25-32% compared to the CC mix.

This trend agrees with Jorge et al. (2011) where comparing CC and LWC (strength grade of 20-22) with short SFS screws, 24% reduction in connection strength was observed.

For the concrete with higher compressive strength than conventional concrete, an increase in concrete strength does not increase the connection strength and the connection strength remains almost constant. Changing the failure from a ductile failure in LWCs to brittle failure of CC or HSC limits the strength of connector.

Figure 5-22 demonstrates the effect of compressive strength of concrete on ductility of different TCC series, respectively. The polynomial descriptive model and the sample correlation coefficient R^2 are illustrated in same Figure.

Comparing to CC series, the decrease in density and compressive strength within the concrete mixes increased the ductility of the SFS and SPAX screws with and without interlayer as depicted in Figure 5-22. However, comparing CC and Scoria LWC series, the ductility of Scoria LWC series remained almost unchanged whereas, HSC SPAX WI45 series with maximum compressive strength of concrete had highest ductility.

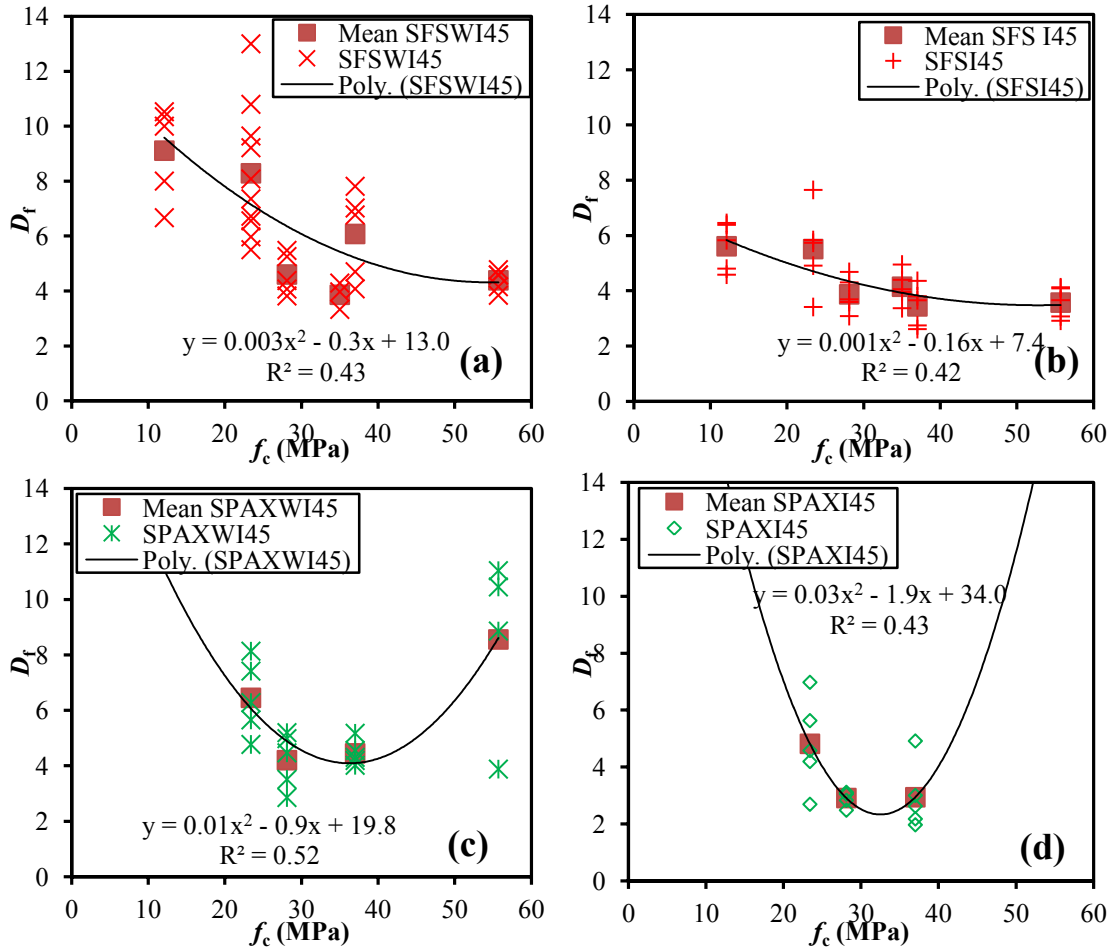

Figure 5-22 Effect of compressive strength of concrete on ductility of TCC (a) SFS WI45 , (b) SFS I45 series, (c) SPAX WI45 and (d) SPAX I45 series

5.5.5 Effect of Light-weight concrete (LWC) type

The serviceability and ultimate slip moduli comparison of different series utilising different types of LWC and CC with and without interlayer are depicted in Figure 5-23.

Comparing CC and different types of LWC series, EPS2000 SFSWI45 series was the stiffest connection at 40%, 60% and 80% F_{max}.

Scoria and EPS LWC with interlayer series exhibited higher serviceability and ultimate slip moduli than similar CC series. However, Scoria LWC SFSWI45 series experienced less stiffness than similar series utilising conventional concrete.

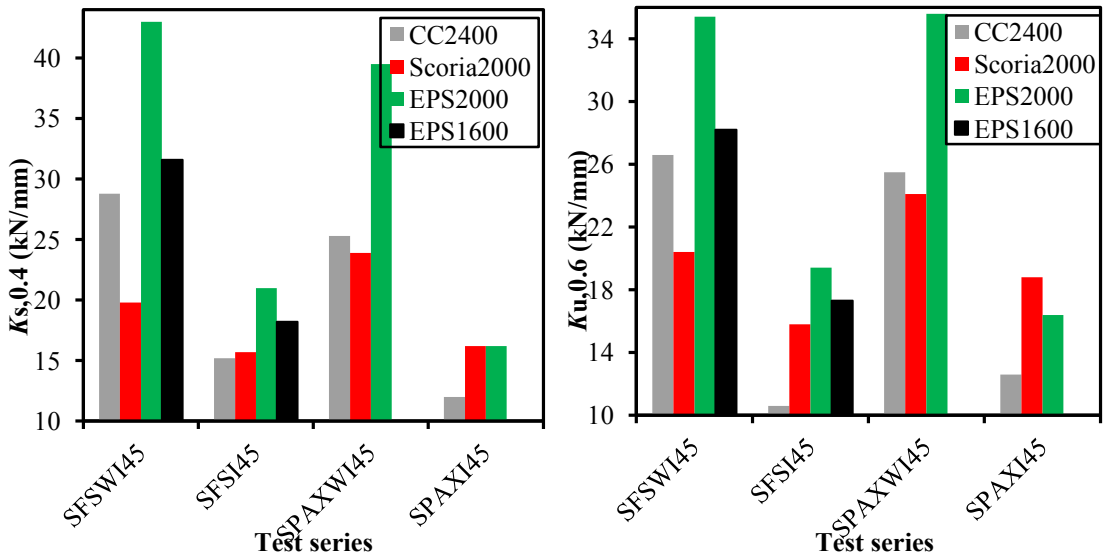

Figure 5-23 Stiffness comparison of different series using different LWC and CC

The strength and ductility comparison of different series utilising different types of LWC and CC with and without interlayer are presented in Figure 5-24.

Figure 5-24 depicts the reduction in strength of TCCs accompanying the lowering of concrete compressive-strength, however SPAX WI45 series shows an exceptional behaviour as Scoria LWC SPAX WI45 produced 4% higher strength than that of CC series.

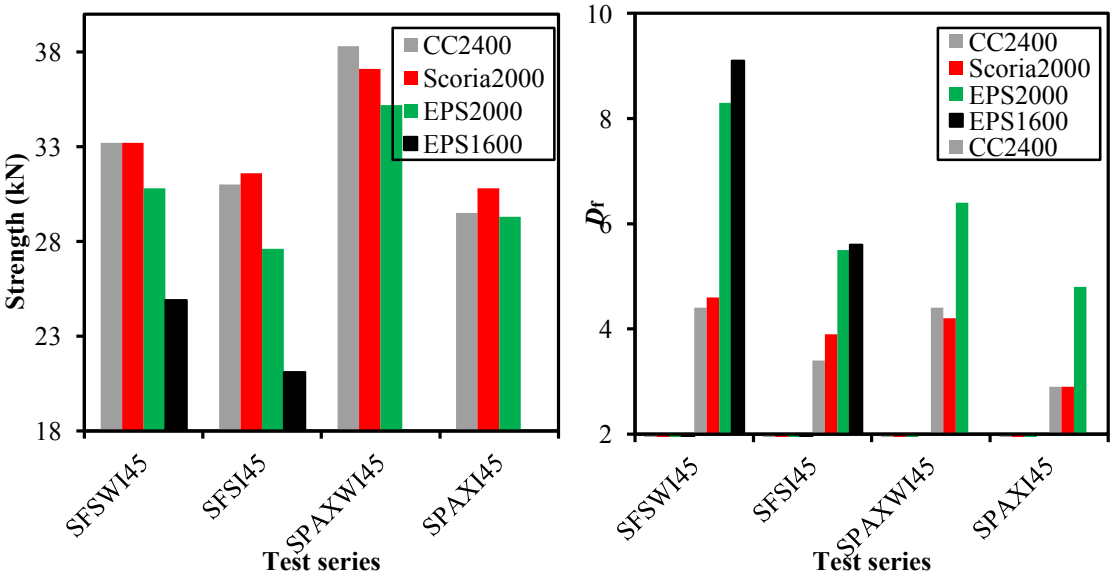

Figure 5-24 Strength and ductility comparison of the test series utilising different LWC

The use of EPS LWC 2000 reduced the strength of the connection up to 11% compared to similar CC series, and the use of EPS LWC 1600 reduced the strength by 25-32% compared to similar CC series whereas the strength of Scoria LWC series remained unchanged or in some series experienced slightly higher strength than that of CC series.

Hence, application of Scoria LWC with reduced density of 2000kg/m^3 results in similar, if not greater strength out of the SFS and SPAX connection which highlights that the strength of a TCC connection sample is predominately dependent on the shear connection and the presence of an interlayer, not the strength of concrete.

Comparing the conventional concrete (CC series) and low density expanded polystyrene light-weight concrete with low 28 day compressive strength of concrete (EPS LWC1600 series), the reduction in strength of the connection in samples using EPS LWC1600 was significantly less than the reduction in compressive strength of concrete.

This means that their strength in the connection is unlikely to be a limiting factor on the use of EPS LWC1600 in TCCs. Rather, the bending, compressive and crushing behaviour of LWCs is more likely to be a limiting factor. As such, it can be concluded that where LWCs are adequate for use in terms of general structural performance, they are likely to be acceptable for use in terms of their behaviour at the connection of TCCs.

In terms of average slip at F_{max}, CC SFSWI45 was the most effective connection for application, producing an average slip at F_{max} value of 2.4mm, 15% less than the Scoria LWC series. It is expected that the higher F_{max} increases the slip at F_{max}.

Figure 5-24 shows the average ductility for each series utilising different concrete types. Samples with EPS LWC2000 and EPS LWC1600 concrete experienced 20-25% and 40-60% less slip at F_{max}, respectively compared to similar samples of CC series.

EPS LWC series also experienced significant slip after initial localised failure of concrete. Hence, the ductility of the EPS LWC series increased approximately 65-100% compared to similar series using CC. EPS LWC series exhibited maximum ductility ranging 4.8-15.5 among the different concretes tested due to localised concrete failure at the connections.

Comparing the failure modes, EPS LWC 1600 and 2000 series exhibited dual peak responses as shown in Appendix B (Figures B-17 and B-31) whilst similar series utilising other types of concrete experienced single peak behaviour.

The dual peak response of the EPS LWC2000 SFS WI45 series was agreed upon by Jorge et al. (2011) who attributed the first drop in load to the low compressive strength of the light-weight aggregate which allowed for the localised failure in the LWC.

It is noted that an increase in strength of the mortar matrix exists in LWC compared to CC series, which results in higher anchor strength, allowing for the recovery of the load after the initial drop. Higher compressive strength of concrete decreased the localised failure of concrete at connections in CC, HSC and SCC series than EPS LWC2000 which leads to a single peak response with much lower ductility.

5.5.6 Alternative connection design

In terms of alternative connections, two novel connectors in the form of L and U connector were developed based on their wide availability and structural properties. Figure 5-25 plots analytical load-slip graphs obtained from curve-fitting of experimental response of CC L and U profiles and coach screw inclined at 45°series.

The L series of connectors exhibited highest average strength of 54.6kN which was 36.6% higher than the U series and 109% higher than the coach screw series.

This was anticipated as the L connector was the most rigid design being fabricated from a structural section with a relatively high moment of inertia compared to the U connector, and thus it was less susceptible to bending and deflection. Additionally, 3 small SPAX screws used increased load capacity than a single coach screw.

The L series connectors had the highest average serviceability and ultimate slip moduli. Compared to the other connection designs in literature, the L connector exhibited a relatively high serviceability slip modulus, however it does not achieve the same stiffness values such as the perforated steel plate connector system tested by Miotto et al. (2011) and Miotto et al. (2012) or concrete notches investigated by Yeoh (2010).

The L connector design can be further optimised and refined to achieve a better result in terms of economy and mechanical behaviour.

The U connector has no advantages over the L connector with exception of ductility and due to its higher cost, it cannot be recommended as a viable shear connector with advantages over existing shear connections.

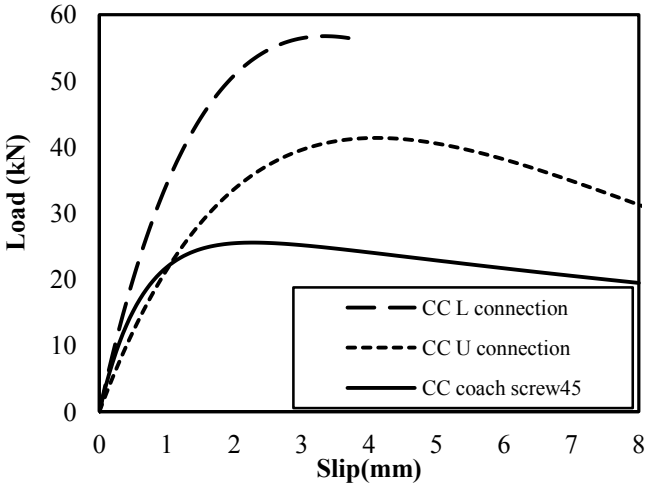

Figure 5-25 CC inclined coach scrw, L and U connector series

5.6 CONCLUSION

The scope of the research was to increase the understanding on the parameters that affect the mechanical properties and failure mode of the TCC connections. Experimental results of test series also have a positive contribution to achieve reliable design codes.

This Chapter included experimental testing of composites of laminated veneer lumber (LVL) and different concrete types to assess mechanical properties and failure mechanism of different types of mechanical fastener including available screws and two novel types of shear connectors inclined at various angles and with and without plywood interlayer between timber and concrete.

The slip moduli calculated across both EN26891 (1991) and the modified methods experienced a much higher CoV compared to strength and ductility and it is attributed to the fact that a minor change in the slip has a large impact on the resulting slip moduli. A higher CoV reduces the reliability which in turn leads to lower characteristic value.

5.6.1 Effect of screw type (SFS VB and SPAX screws)

Comparing CC and EPSLWC 1600 and 2000 series, it was found that SFS VB screws exhibited a greater stiffness than SPAX screws. However, Scoria LWC SPAX series represented higher stiffness than similar SFS series. SPAX screws series indicated higher strength than SFS VB screws whereas the ductility of SFS was higher than similar series of SPAX series. The use of SPAX screws as a shear connector in TCC beam should be further investigated as the presented results highlight sizable potential.

5.6.2 Effect of inclination angle

In CC and EPS LWC2000 series utilising SFS and SPAX crossed screws at different angle, an angle of 30° offers the greatest stiffness and strength compared to others. Overall, these results are very conclusive in finding that the angle of connector significantly influenced the strength and slip moduli. In terms of strength, both EPS and conventional concrete series exhibited a strong relationship between strength and inclination angle.

5.6.3 Effect of light-weight concrete type

Lower compressive strength and density of Scoria LWC had minor impact on the connection strength. CC and Scoria LWC series experienced greater strength than EPS LWC 1600 and 2000 series with minor difference between Scoria LWC and CC series whereas EPS LWC 1600 and 2000 series produced greater serviceability and ultimate stiffness than CC and Scoria LWC. An initial localised failure in the EPS LWC concrete at the connection caused the first drop, before the ultimate failure of the screws. Failure in EPS LWC series was more ductile than similar CC series with a greater deflection following F_{max} before failure. This result may be based on the fact that the mortar matrix of EPS LWC is stronger than in CC whereas light-weight aggregate has lower compressive strength than conventional aggregates. This may result in higher anchor strength of LWC mortar after the initial crushing of light-weight aggregate, leading to the recovery of load level after an initial drop at low slip value and consequently a higher serviceability and ultimate stiffness. Scoria LWC series showed higher ductility than the similar CC series which is beneficial in construction applications.

The application of LWC represents an innovative solution when combined with TCC technology to further minimise the dead loads of structures. Such a system is a favourable alternative for both the renovation of existing timber floors and the construction of new ones. This research suggests that there is strong potential for moderate light-weight concrete to be used in TCC systems, with limited effect on strength or behaviour whilst for very light-weight concretes, EPS LWC1600 series, low compressive strength of LWC may limit their application in TCCs.

5.6.4 Effect of interlayer

Comparison of different test series utilising different concrete types of and shear connections with and without plywood interlayer implies that inclusion of an interlayer significantly reduced stiffness, strength and ductility of the series.

5.6.5 Alternative connection design

Two novel connectors in the form of L and U connectors were developed based on their wide availability and structural properties. The results of the push-out tests highlighted that the L connector had the highest strength and stiffness while U connector achieved lower values. Overall, the L connector has a relatively high strength and stiffness although alternative connectors such as concrete notch or a continuous steel plate achieve higher values. However, the L connector design can be further optimised and refined to achieve a better result in terms of economy and mechanical behaviour. The U connector has no advantages over the L connector and due to its higher cost, it cannot be recommended as a viable connector with advantages over existing shear connections.

6 EXPERIMENTAL FLEXURAL TEST

6.1 INTRODUCTION

This chapter reports the details and results of short-term four-point bending tests at serviceability (SLS) and ultimate (ULS) limit states of five simply-supported LVL-concrete composite modules constructed from conventional and light-weight concretes to evaluate the effect of light-weight concrete on the flexural stiffness, strength at service and ultimate loads and failure mode. The short-term serviceability and collapse four-point bending tests of three LVL modules used in TCC modules are also discussed.

Once the mechanical properties of connection are identified and quantified from push-out tests, a full-scale floor sample can be tested to assess the structural behaviour of an entire floor system. This is significant to identify any problems or complications that might arise which might have been overlooked or not foreseen in the small scale tests.

Based on the outcomes of push-out tests for various shear connections given in Chapter 5, ±45° crossed SFS screws were selected to connect LVL and concrete slab. In terms of connection, ±45° crossed SFS screws in EPS LWC exhibits higher serviceability and ultimate stiffness compared to similar connections using conventional concrete.

The dimensions of composite components represent a realistic secondary beam in a typical non-residential building in Australia which was designed in compliance with the Gamma method given by Eurocode 5 EN (2004b).

These specimens were loaded to failure after 28 days from casting using a four-point bending test. This Chapter reports the experimental programme and results. The

experimental test methods and instrumentations are stated. The characteristics of the composite materials and push-out tests results of shear connections were reported in Chapters 4 and 5, respectively.

Extensive data including deflection at one and two thirds and mid-span points, strain readings at mid-span and slips between composite components at the beam ends and the first three pairs of connection at beam end are reported.

6.2 TCC DESIGN

An efficient design of a structure is achieved by a high stiffness of cross section which can carry the higher load for minimum self-weight. Composite I and box beam type sections are the most conventional structural timber sections that can be connected to a concrete slab to achieve higher stiffness and strength through the composite action of timber and concrete.

The LVL modules used in the current TCC design initially formed the top part of a timber module designed as a timber-timber non-residential floor designed by STIC as reported in Zabihi et al. (2012) (Figure 6-1a).

The timber-timber module was attached to two bottom LVL flanges which were removed by a TCC module. The remaining part of the timber-timber module was placed upside down and a top layer of concrete cast on it to study an alternative non-residential floor using the initial fabricated timber-timber modules (Figure 6-1b).

The box module has a void between webs and bottom flange which can be used for the insulation and some other services (plumbing and wiring).

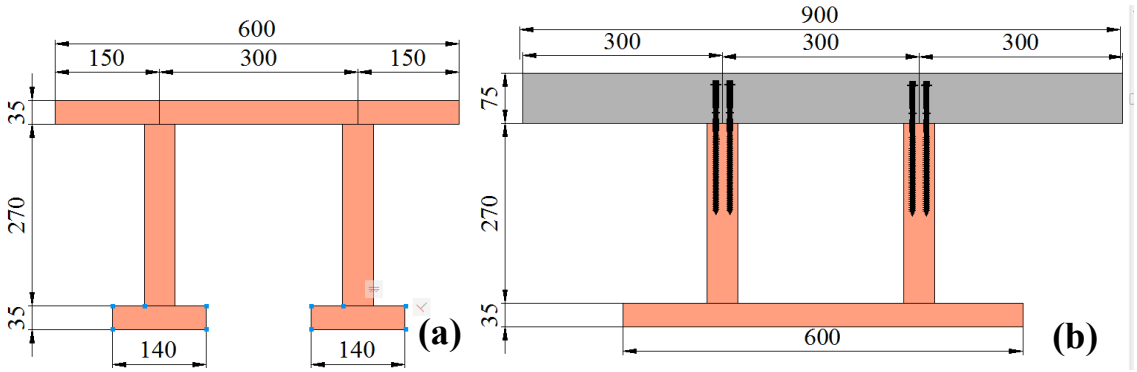

Figure 6-1 (a) Timber-timber and (b) TCC modules designed for non-residential floor

The design procedure of the TCC module was discussed in Chapter 2. The Gamma method based on the formulas for composite beams with flexible connections was used to design the TCC modules under the design loads in compliance with AS/NZS1170.1 (2002). The design loads consisted of an imposed action, Q of 3kN/m^2 for office buildings and a total permanent action, $G = G_1 + G_2$ of 3.24kN/m^2, with G_1 and G_2 including the self-weight and the superimposed permanent load, assumed as 2.24 and 1kN/m^2, respectively.

A concentrated live-load equal to 3.50kN is imposed for office building. The live-load is a variable load according to the use and occupancy of the building and consists of all loads applied by humans, machines, or movable objects. The TCC modules were in compliance with the design requirements at SLS and ULS.

6.3 EXPERIMENTAL PROGRAM

6.3.1 Timber modular systems

Five timber modules, consisting of two LVL webs, glued and screwed to a cross banded LVL flange, were subjected to full-scale four-point bending tests to serviceability loads. The serviceability behaviour of the timber module was studied by the responses of the specimens including deflection, slip and strain to the service loads. Also the apparent and global stiffness of the system and strain at mid-span were investigated.

After the serviceability tests, the TCC modules were constructed using these timber modules. Upon completion of three cycles of serviceability loading, the TCC modules were tested to failure using two different types of concrete.

The linear-elastic characteristics of the specimens including apparent and global stiffness of TCC modules were assessed using the deflection, slip and strain responses of the specimens versus service load. The applied load in each jack and the deflection at mid-span were recorded. In addition, the relative slip at the interface of timber and concrete and the first three pairs of cross screws at beam-end were measured. Moreover, the strain responses at mid-span were used to assess the composite action of the TCC modules.

The TCC modules exhibited linear-elastic behaviour and the dominant failure mode was observed in the shear connections as tensile and flexural failures of SFS screws in tension and compression, respectively whilst the timber modules remained sound and

undamaged. Hence, the concrete slabs were removed after the ULS tests of the TCC systems and the timber-only modules were subjected to serviceability and ultimate tests. Strength, stiffness, failure modes, condition of shear connections and ductility of the specimens were assessed by serviceability and ultimate loading tests.

6.3.2 TCC modules

Five full-scale simply-supported TCC modules were constructed. Their dimensions and details represent a secondary composite beam of a non-residential building which was designed in compliance with Eurocode 5 EN (2004b) and Australian standards.

In order to assess the effects of light-weight concrete on structural response of TCC beams , two specific concrete mix designs were used- (i) conventional concrete, CC grade 32Mpa with a density of 2400kg/m^3 and (ii) expanded polystyrene light-weight concrete, EPS LWC with a density of 2000kg/m^3.

Three TCC modules were constructed using the CC mix design whilst two modules were poured using LWC. The mix designs were specified to the supplier and the CC and LWC mixes were batched and delivered to UTS by external supplier. Each individual mix was supplied in accordance with AS1379 (2007). The gravels were replaced by expanded polystyrene beads in the LWC mix design.

Both mixes achieved the desired 100mm slump specification. The air content of LWC concrete is much higher than the conventional concrete. The mix designs and fresh and hardened properties of the concrete mixes including drying shrinkage were reported in Chapter 4 and Appendix A. Three cylinder tests were performed at 28 days and three more were tested upon completion of the beam test at 35 days. The delivered mixes had higher strength than specified. The concrete cylinders and prisms were moist cured.

These modules, referred to as CC1, CC2 and CC3, were constructed using conventional concrete whilst the modules LWC1 and LWC2 represent a TCC modules cast using expanded polystyrene light-weight concrete (EPS LWC). Based on the outcomes of a parametric experimental study of push-out tests with criteria of structural efficiency, lower cost and availability in NSW, Australia as reported in Chapter 5, expanded polystyrene light-weight concrete with a density of 2000kN/m^3 was selected for TCCs.

The geometry of the five beams was nominally identical and each was 8.4m long. The concrete slab on top was 0.9m wide and had a slab thickness of 0.075m. Two types of LVL, that is, hySPAN Cross-banded and hySPAN project were used to form the bottom

flange and two webs of the structural section of the timber-only modules, respectively. There were three web stiffeners in each beam which were located at approximately 2m intervals. The material properties of different types of LVL and plywood formwork were listed in Chapter 4.

A layer of square mesh N6 reinforcement spaced at 200mm in both directions with 35mm concrete cover was used to control cracks in the concrete slab. Plastic chairs were used to support the mesh and to hold it at the correct height.

The first three beams were poured on the same day using conventional concrete whilst as a second series, two modular beams were poured on the same day with expanded polystyrene light-weight concrete with a density of 2000kg/m^3.

The plywood formwork had to be designed for carrying self-weight of concrete and cut to the correct dimensions accordingly. Formwork was also required for the inner segments of the LVL between the stiffeners to ensure no concrete was able to fill these sections during pouring.

Long crossed SFS connectors were selected based on the outcomes of a parametric experimental study of push-out tests carried out on different connections with different arrangement, lower cost, labour requirement and time for fabrication as discussed in Chapter 5. The push-out test methodology and the material properties of two connection test series of CC SFS WI45 and EPS LWC2000 SFS WI45 including strength, slip moduli, ductility and failure mode were obtained from push-out tests conducted in compliance with EN26891 (1991) as reported in Appendix B.

Comparing these two series, application of EPS LWC decreased the strength about 8%. Application of EPS LWC instead of conventional concrete series increased different slip moduli including $K_{s,0.4}$, $K_{u,0.6}$ and $K_{u,0.8}$ about 62%, 38% and 18%, respectively.

The TCC module was constructed with 50 pairs of long SFS screws; each web had 25 pairs of screws, pre-drilled and screwed at (±45°) with symmetrical shear connection spacing of 220, 330 and 850mm as depicted in Figure 6-2.

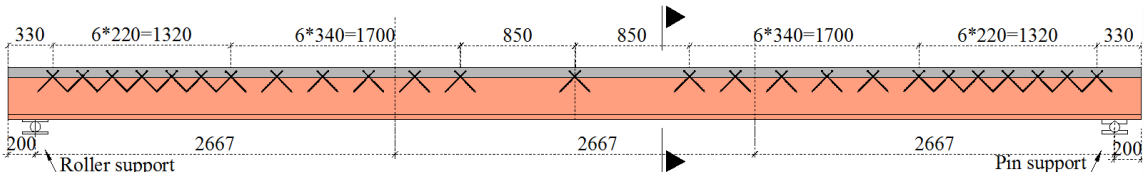

Figure 6-2 TCC beam lay-out

HBV 5.0.16 commercial package provided by SFS intec Co. was used to design the spacing details of SFS screws based on the expected amount of shear force in compliance with Eurocode 5 EN (2004b). The maximum shear force occurs at beam-ends, hence a closer spacing was required to increase the shear resistance at the ends of the TCC beams. As minimal shear force is experienced at the centre of the beam, the connections were spaced at far greater centres.

The design span of the beams was 8metres, the distance between each support when undergoing load. As a result, there was a 200mm overhang at each support since the beams were constructed at 8.4m. The beams were designed with no interlayer at the interface of the concrete and LVL. As a result, the concrete was in direct contact with the top of the LVL webs.

The modules were cast propped and the self-weight of the modules and wet concrete was carried by timber joists and plywood formwork as shown in Figure 6-3.

TCC modules were cured by a moist sponge material and were covered by plastic sheets to cure in a controlled environment and reduce the speed of the hydration process. Once the concrete hardened and reached sufficient strength to support its self-weight in day 14, formwork was removed and the TCC modules were moved to the supports. Before the bending test, the concrete slabs of modular beams exhibited shrinkage. The beams were exposed to lab conditions and the average temperature and humidity were 19°C and 65% RH, respectively before the test.

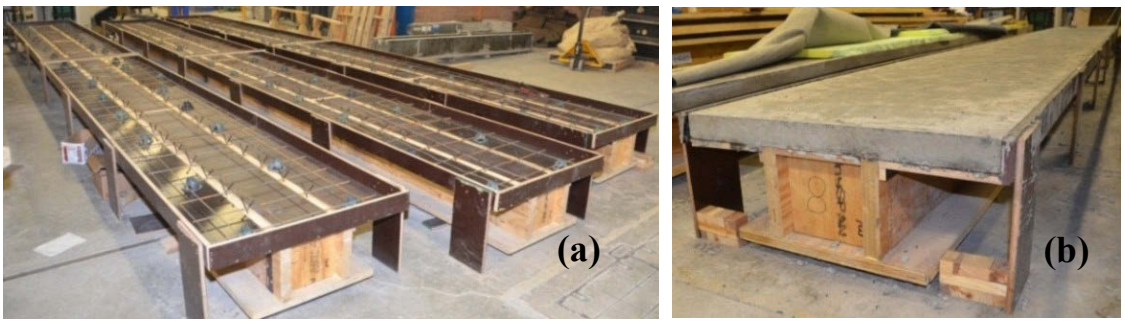

Figure 6-3 Propped TCC form works: (a) before and (b) after concrete pouring

6.3.3 Experimental set-up

The simply-supported condition of roller and pinned supports placed on top of two concrete blocks was used in the four-point bending test as shown in Figure 6-4. The specimens were deflected vertically.

Figures 6-5 and 6-6 indicate the layout of the specimens under the loading system. The data was captured through connection of strain gauges and LVDTs to a data taker.

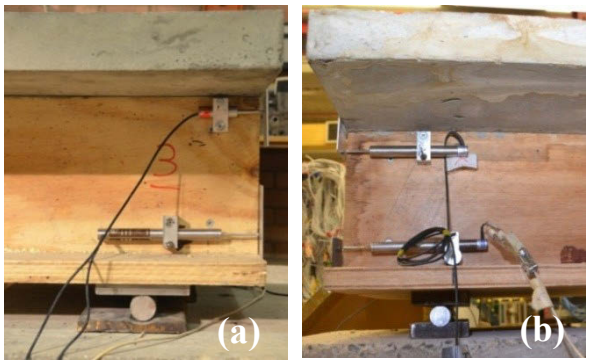

Figure 6-4 Simply-supported supporting condition: (a) pinned and (b) roller supports

Figure 6-5 The layout of specimens: (a) the timber-only and (b) TCC modules

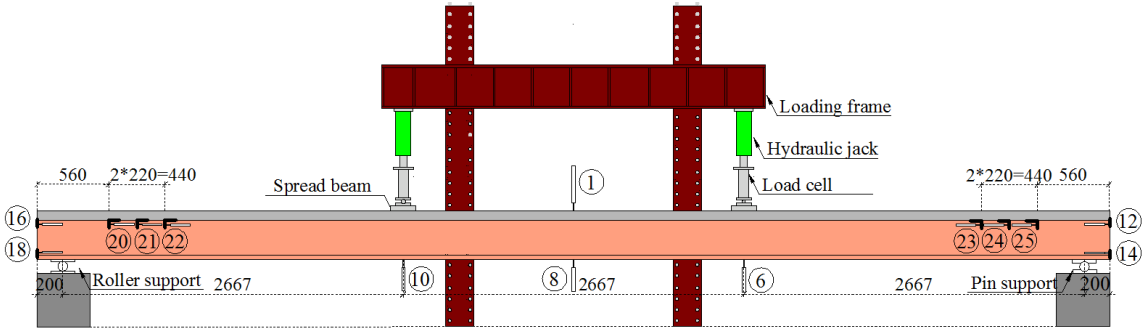

Figure 6-6 The lay-out of four-point bending test (in mm)

Figure 6-7 Load frame, hydraulic jacks, load cells and TCC specimen

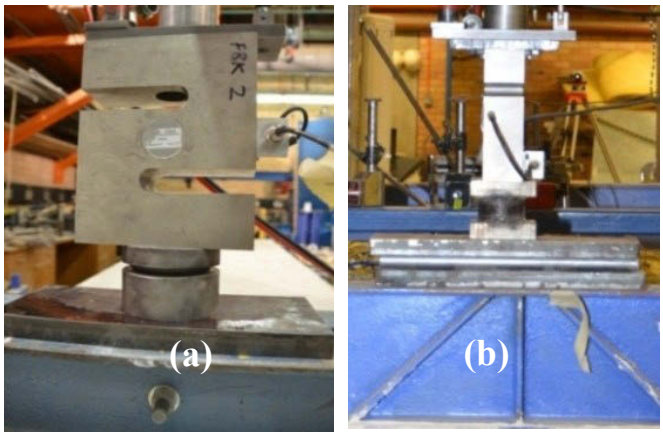

Figure 6-8 Load cell supports: (a) pinned and (b) roller

Load was applied to the beams through two hydraulic jacks supported on a reaction frame including four columns and two beams which carried a 3m beam (Figure 6-7). A pair of controlled hydraulic oil jacks was accommodated in each third span of the beams span away from each support to apply the load on the spreader beam with roller and pinned supports as shown in Figures 6-6 and 6-7.

The spreader beam was installed directly underneath each loading jack to spread the load evenly across the modules as depicted in Figure 6-8. The loading pin has a spherical shape to prevent any restraint of torsional movement across the beam (Figure 6-8a).

6.3.4 Instrumentation

LVDTs were used to measure the deflection of each beam at various locations as shown in Figure 6-9.

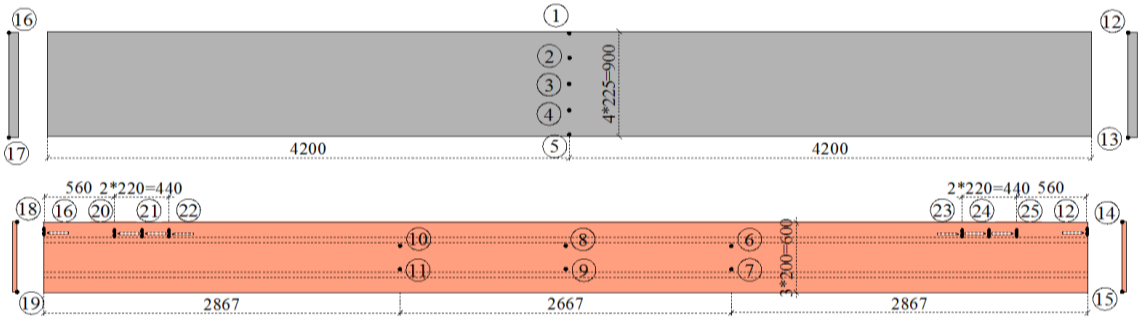

Figure 6-9 Location of LVDTs for deflection and slip measurement

Six LVDTs (LVDT 6-11) were located underneath the specimens (Figure 6-12b) at thirds- and mid-spans of each module as depicted in Figure 6-9 whilst for serviceability and ultimate loading tests, five LVDTs (LVDT 1-5) were placed on top of the concrete slab at the mid-span as illustrated in Figure 6-12a. For ultimate tests, the LVDTs located underneath the specimens were removed to avoid any possible damage to the LVDTs. The LVDTs were used to evaluate the apparent and the global stiffness of the specimens through analysing vertical deflection of the specimens versus load.

Eight LVDTs (LVDT 12-19) were also located at each beam-end to measure the interface slip of composite components. Two LVDTs measured the slip of timber and concrete on each beam-end and two remaining ones were placed at each end to measure the slip of the LVL webs and the bottom flange as shown in Figure 6-9.

In addition, six LVDTs (LVDT 20-25) were placed at the shear connectors to measure the interface slips of LWC modules. The support of LVDT was screwed into the LVL webs and a steel angle was attached to the underside of the concrete slab by double-sided sticky tape and then touched the moving head of LVDT; the slip at the shear connections was measured.

Strain gauges were employed to measure deformations at the mid-span cross-section. Strain gauge type PL-60-11 with 60mm gauge length was used on the LVL joists and the concrete slab. The locations of the strain gauges are shown in Figures 6-10 and 6-11. The strain gauges were used to verify the linear characteristics of the specimens by assessing the strain of the specimens versus load. Moreover, the strain gauges were used to investigate the composite behaviour of the system.

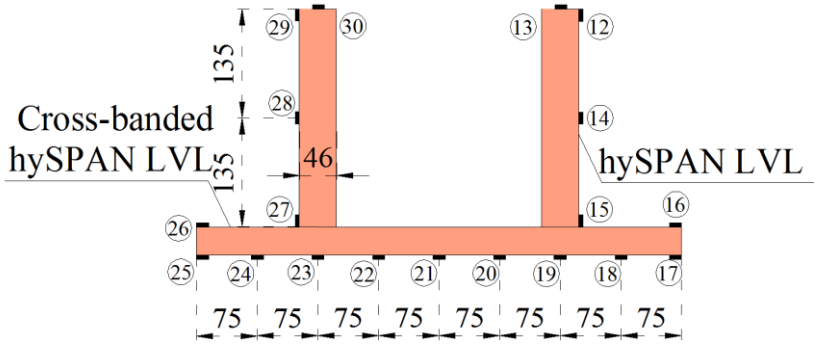

Figure 6-10 Cross-sectional geometry and arrangement of strain gauges for timber-only

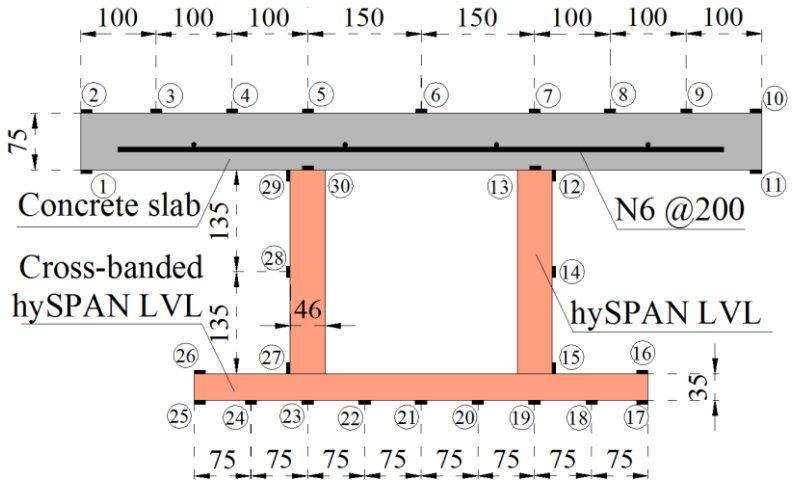

Figure 6-11 Cross-sectional geometry and arrangement of strain gauges for TCC

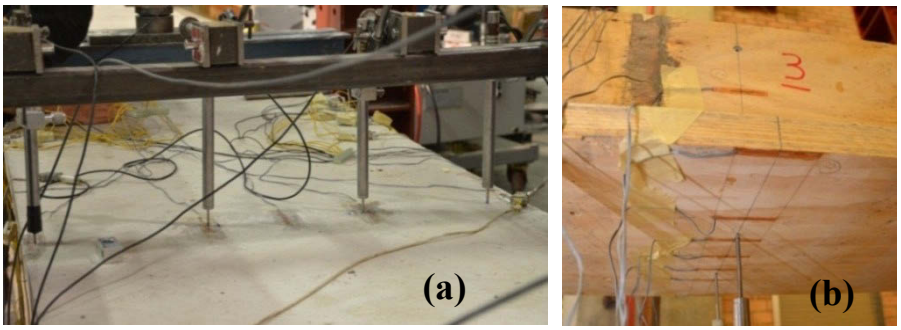

Figure 6-12 The LVDTs and strain gauges: (a) on top (b) underneath the module

The strain gauges must be attached to the smooth flat surface. For the timber beam surface, the timber surface was sanded before attachment of strain gauges whilst for the concrete surface a plastic-bond was used on the concrete surface and was sanded before attachment of strain gauges. There were 9 strain gauges on top of the concrete slab at mid-span, the strain gauge 6 was at the centre, strain gauges 5 and 7 were located at 1/3 of the width of beam, the strain gauges 2 and 10 were located at the edge of the beam,

the strain gauges 3, 4, 8 and 9 were located at the 1/9 and 2/9 width from the edge. There were 9 strain gauges on the bottom of the beam mid span, the strain gauge 21 was at the centre, strain gauges 20 and 22 were located at 1/3 of the width of beam, the strain gauges17 and 25 were located at the edge of the beam, the strain gauges 18, 19, 23 and 24 were located at the 1/9 and 2/9 width from the edge. The instrumentation at the mid-span of the timber-only and TCC modules are depicted in Figures 6-10 and 6-11, respectively.

6.3.5 Test methodology

The loading protocol of the four-point bending test was to some extend similar to that proposed by EN26891 (1991) for connection push-out test. The four-point bending test of timber modules consisted of a point load at third spans of the specimens. During the experiment, the timber-only modules were subjected initially to three cycles of 10kN corresponding to two times of the design service load of a non-residential floor.

The TCC modules were first subjected to serviceability loads of 22-26kN in each jack causing a 16-20mm deflection over a period of 90 sec. AS/NZS1170.0 (2002) proposes a load corresponding to the deflection limit equal to $L/300$ for the serviceability test, that is 26mm for 8m span specimens.

The serviceability tests were under displacement control where ultimate loading was conducted under force control. The loads were applied at a constant rate 0.3mm/sec in both SLS and ULS loading tests. The serviceability load maintained for 30 sec, then unloaded to zero. The serviceability loadings were repeated three more times and finally the TCC modules were loaded up to failure at a constant rate as used in the serviceability test. The load and stroke of the hydraulic jack were recorded. The TCC modules were failed at shear connections and hence, timber modules remained sound. To assess the structural response of timber-only modules, after removal of the concrete slabs of CC1-3, the timber-only modules were again loaded to 10kN, reaching a deflection of 33-38mm, after which they were unloaded. This process was repeated three times before loading the modules to failure. F_{est} was the estimated failure load of each composite beam which was calculated by the Gamma method.

6.4 EXPERIMENTAL RESULTS AND DISCUSSION

The experimental test includes serviceability and ultimate testing of timber-only and TCC modules utilising two different concrete types of CC and EPS LWC2000.

6.4.1 Serviceability tests of timber-only modules

The responses of the timber-only modules to service load were studied using the deflection and the strain responses to identify the linear-elastic behaviour of the system. Moreover, the global stiffness of the timber-only modules was investigated using load-deflection responses of the specimens. The load-slip graphs of timber-only modules were reported in Appendix C. Timber modules indicated a linear response in the range of 0-10kN at SLS. The range of maximum mid-span deflection of CC and LWC TCC modules in the serviceability limit state was 33mm to 38mm (approximately L/300).

Flexure formulas for beams with solid rectangular homogeneous cross-section through their length is given in AS4063.1 (2010). The formula is applicable for timber composite beams. The apparent stiffness of modular systems, *EI* was determined in compliance with AS4063.1 (2010) using the measurement of the vertical deflection at mid-spans of the specimen as given in:

$$EI = \frac{23L^3}{648}K \tag{6-1}$$

where, *K* is the global stiffness of the module as the slope of the linear portion of load-displacement (*F*- δ) graph for a load range of 10- 40% of the average load capacity as:

$$K = \frac{F_{\text{Ave}}}{\delta} \tag{6-2}$$

$$F_{\text{Ave}} = \frac{F_{\text{LoadCell1}} + F_{\text{LoadCell2}}}{2} \tag{6-3}$$

The apparent stiffness of the beam, *EI* was measured for mid-spans. A uniform rated load, *F* was applied to the module at third-spans and the failure was observed. Table 6-1 lists the results of *K* (global stiffness) and *EI* (apparent stiffness) of timber-only modules with calculations based on Equations (6-1) and (6-2) at serviceability loads.

Table 6-1 Global stiffness, *K* and apparent stiffness, *EI* of the timber modules at SLS

Timber module	Global stiffness (kN/m)	Mean (kN/m)	σ	CoV(%)	Apparent stiffness (kNm^2)	Mean (kNm^2)	σ	CoV(%)
T1	286.3				5202.3			
T2	295.5				5369.7			
T3	294.1	286.8	7.8	2.7	5344.0	5212.4	142.3	2.7
T4	279.1				5071.9			
T5	279.2				5074.3			

The stiffness of LVL timber modules used in the CC and LWC series were very similar. Therefore, for ease of comparison, the difference in timber components of CC and LWC series was ignored in the numerical model discussed in Chapter 7.

The strain gauge reading at serviceability limit state corresponding to a deflection of 10mm for timber-only joists is shown in Figure 6-13. It is evident that the timber-only modules exhibited a fully composite behaviour at SLS (Figure 6-13).

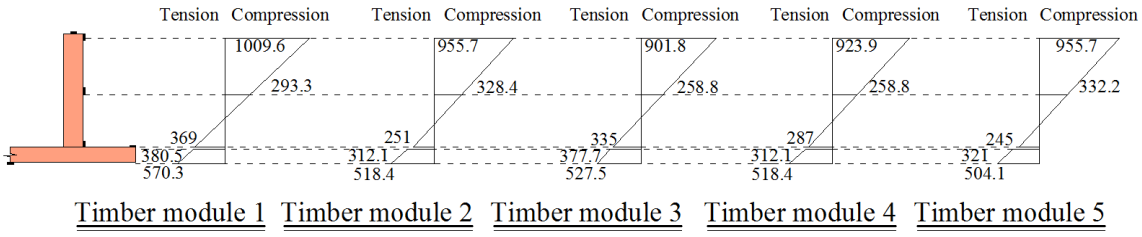

Figure 6-13 Stress distribution in the LVL- module corresponding to $0.4F_{max}$, in (με)

6.4.2 ULS test of timber-only modules

6.4.2.1 Ultimate flexural capacities of timber-only modules

Upon completion of ultimate test on TCC modules, the concrete slabs were removed and the timber modules were subjected to serviceability and ultimate tests. Strength, stiffness, failure modes, condition of shear connections between bottom flange and web and ductility of the modules were assessed by ultimate loading test. The load–deflection responses at mid-span of the timber-only modules are depicted in Figure 6-14.

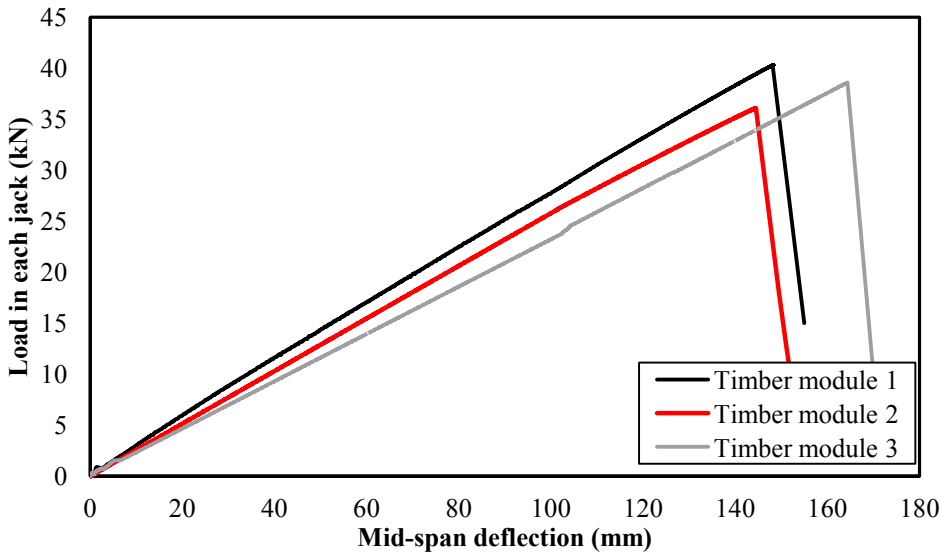

Figure 6-14 Load-mid span deflection responses of timber-only modules

The load-deflection graphs of timber-only modules represent a linear response up to failure. The maximum load capacity, F_{max}, corresponding to summation of two point loads, ultimate moment capacity and the mid-span deflection at maximum load capacity, are listed in Table 6-2. Moreover, the equivalent uniformly distributed load (W_{eq}) and bending moment (M_{exp}) were reported by the equation $M_{exp}=W_{eq}L^2/8 =F_{max}L/3$. F_{max} and the deflection at F_{max} show consistent results with CoV of 5.6% and 7%, respectively.

Table 6-2 Strength and deflection at F_{max} capacity of the timber modules

Timber module	Strength (kN)	Mean (kN)	σ	CoV(%)	M_{exp} (kNm)	W_{eq} (kN/m)	Deflection at F_{max} (mm)	Mean (kN)	σ	CoV(%)
T1	80.1				106.8	13.3	148.1			
T2	71.7	75.5	4.2	5.6	95.6	12.0	144.5	152.3	10.6	7.0
T3	74.7				99.6	12.4	164.4			

6.4.2.2 Global and apparent stiffness of timber-only modules

Table 6-3 tabulates the results of *K* (global stiffness) and *EI* (apparent stiffness) as the slope of the linear portion of load-displacement graph for a load range of 10% to 40% of the load carrying capacity for timber-only modules at ULS. The global stiffness of beams indicates an acceptable consistency.

Table 6-3 Global stiffness, *K* and apparent stiffness, *EI* of the timber modules at ULS

Timber module	Global stiffness (kN/m)	Mean (kN/m)	σ	CoV(%)	Apparent stiffness (kNm^2)	Mean (kNm^2)	σ	CoV(%)
T1	275.7				5010			
T2	256.5	254.3	22.6	8.9	4660.4	4620.3	411.2	8.9
T3	230.6				4190.5			

Table 6-4 compares *K* (global stiffness) and *EI* (apparent stiffness) as the slope of the linear portion of the load-displacement graph of timber-only modules subjected to serviceability loads before and after TCCs' ULS test. The serviceability test carried out on timber modules before and after ultimate test of TCC shows 5% and 6% stiffness loss in timber modules 2 and 3, respectively whilst the stiffness of the first module remained approximately unchanged.

Table 6-4 Stiffness in timber-only modules tested before and after TCCs' ULS test

Timber module	Global stiffness (kN/m)	Mean (kN/m)	σ	CoV(%)	Apparent stiffness (kNm^2)	Mean (kNm^2)	σ	CoV(%)
T1before TCC	286.3				5202.3			
T2 before TCC	295.5	292.0	5.0	1.7	5369.7	5305.3	90.1	1.7
T3 before TCC	294.1				5344.0			
T1 after TCC	289.4				5259.4			
T2 after TCC	279.9	281.7	7.0	2.5	5086.6	5118.5	54.6	2.5
T3 after TCC	275.7				5009.4			

Table 6-5 tabulates the theoretical and experimental apparent stiffness of timber-only modules. Theoretical apparent stiffness of timber modules based on a fully composite section assumption represents accurate prediction for the timber-only modules.

Table 6-5 theoretical and experimental apparent stiffness at SLS for timber modules

Apparent stiffness	Timber1	Timber2	Timber3	Timber4	Timber5
EI_{eff} Experiment (kNm^2)	5202.3	5369.7	5344.0	5071.9	5074.3
EI_{eff} Full-composite(kNm^2)	5188.6	5188.6	5188.6	5188.6	5188.6
Error (%)	-0.3	-3.3	-2.9	+2.1	+2.2

6.4.2.3 Failure modes of timber-only modules

The observed failure mechanism in timber modules 2 and 3 was local buckling in the compressive zone of LVL webs close to the load jack as a combination of bending and twisting of a member as shown in Figures 6-15 and 6-16 whilst module 1 exhibited too much twisting at 37kN in each jack without failure.

Figure 6-15 Local buckling of web underneath load cell at timber module 2

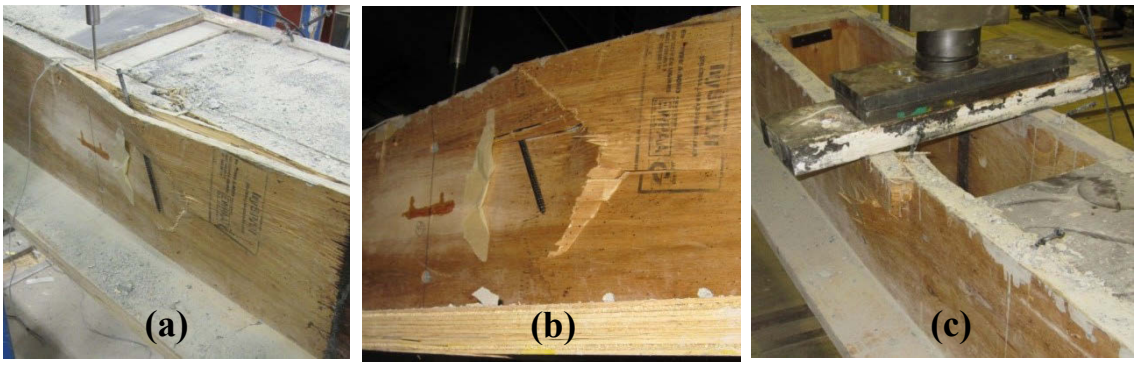

Figure 6-16 Lateral buckling of web (a) and (b) near mid-span and (c) underneath load cell in timber module 3

The shape and cross section of the module is a key-parameter in this failure mode. Hence, cross sections such as channels, structural tees, double-angle shapes, and equal-leg single angles must be designed for lateral buckling. The timber-only module was insufficiently supported in the lateral direction. Hence, by reaching a critical flexural load, the beam failed due to the compression web buckled laterally and the cross section began twisting in torsion as illustrated in Figures 6-15 and 6-16.

6.4.3 Serviceability tests of TCC modules

The responses of the TCC modules to 25kN load at SLS were investigated using the deflection and the strain responses to identify the linear-elastic behaviour of the system. The load-slip graphs of TCC modules were plotted in Appendix C. The LVLs, screw and concrete exhibited linear-elastic behaviour during the cyclic loading at SLS. Hence, the results of the third and mid-span highlight the TCC modules exhibited a linear relationship when loaded to serviceability loads. The linear behaviour experienced by the TCC modules at SLS is similar to that of push-out test results of the connections at SLS. Hence, there are similarities between the beams and the connection responses.

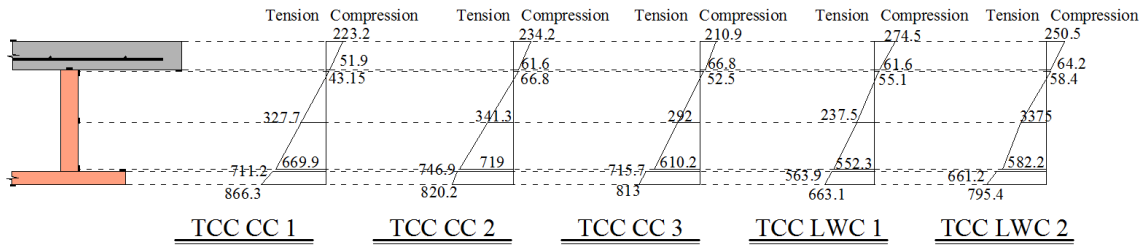

Figure 6-17 Stress distribution in the TCC module corresponding to $0.4F_{max}$, in (με)

Figure 6-17 shows the mid-span strain gauge reading of TCC modules at serviceability limit state corresponding to a deflection of 16-20mm. TCC modules indicated a close to fully composite behaviour at SLS and this agreed with the high composite efficiency of the TCC modules under serviceability loads.

6.4.4 ULS test of TCC modules

6.4.4.1 Strain gauge data and slip at shear connections and beam-ends analysis

Slip at shear connections and beam-ends of the TCC modules were plotted in Appendix C. In addition, the reading results of the strain gauges were reported in Appendix C. Figure 6-13 shows the mid-span strain gauge reading at ULS of the TCC modules.

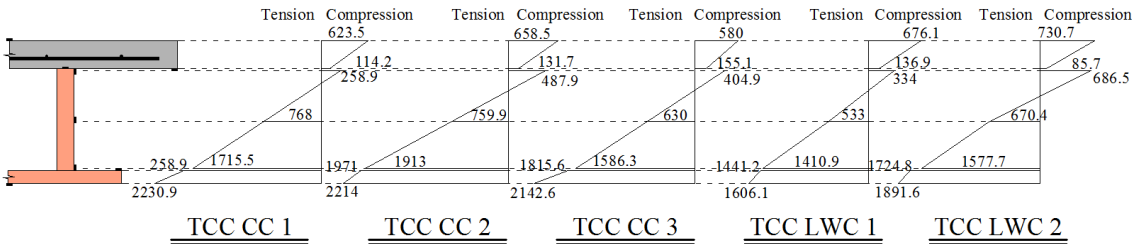

Figure 6-18 Stress distribution in the TCC module corresponding to F_{max}, in (με)

6.4.4.2 Ultimate flexural capacities of TCC modules

The behaviour of the TCC modules up to the failure point was investigated by loading the system to ultimate load. The ultimate flexural capacity, the linear-elastic characteristics and failure mode of the system were studied. Moreover, the global stiffness of the system and composite efficiency were assessed. The load–deflection responses at mid-span of the TCC modules are depicted in Figure 6-19.

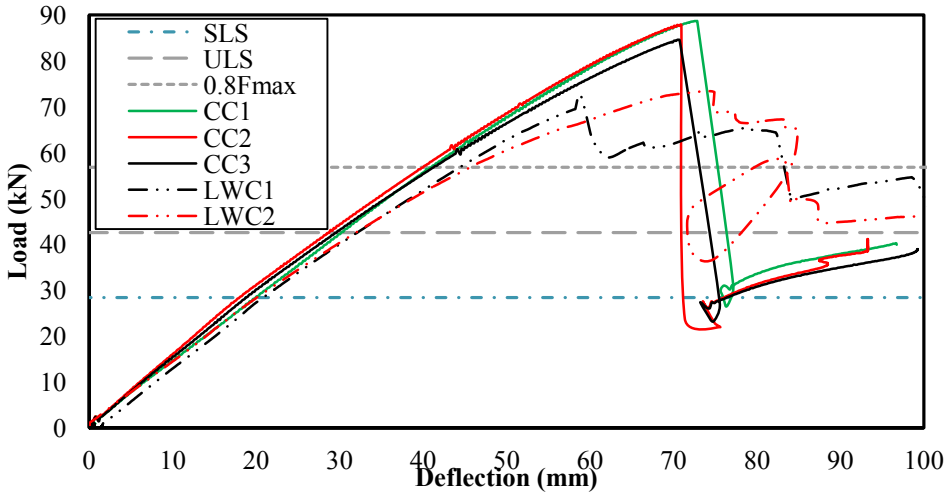

Figure 6-19 Load-mid span deflection responses of TCC modules

These mid-span deflections are vertical displacements due to the four-point bending test and did not include deflections due to self-weight. The CC modules behaved linearly until the first series of connections reached its maximum strength (mid-span deflection at 69-71mm) whilst in LWC modules a non-linearity and small load drop due to localised crushing in LWC concrete were observed before reaching the maximum strength of the connectors and modules. Moreover, some localised failure of concrete at shear connections close to the beam-ends were also observed in LWC modules.

Higher plastic capacity and ductility of EPS LWC connection series after localised crushing of LWC compared to CC series are attributed to pronounced non-linear load-deflection response up to failure in LWC TCC modules. Throughout the loading process, a number of noises were recorded. As a maximum capacity was reached a 'bang' noise was observed and then a sudden failure was the subsequent result. The sudden failure in the modules was the tensile failure of the SFS screws working in tension and flexural deformation of screws in compression.

The modules then continued to carry an approximate load of 25%-50% of their corresponding F_{max} until the test was ceased. The continuation of loading after the connection failure was due to the LVL having the ability to maintain the load. After being tested, it was noted that cracks had formed through the concrete slab directly underneath the load jacks. Initially, the TCC modules experienced a linear behaviour to a load of approximately 40-50kN in each load cell -and then the beam began to deflect nonlinearly beyond 50kN.

The responses of TCC modules CC series within linear range were almost identical where near failure CC3 failed at a slightly lower ultimate deflection. Although these beams were constructed from different types of concrete they showed very similar global and apparent stiffness. A small level of noise caused by the deformation of the SFS screws appears after the yielding point in the Figure 6-19. LWC2 indicated a decrease in stiffness before reaching the ultimate load.

The maximum load capacity, F_{max}, corresponding to summation of two point loads, ultimate moment capacity and the mid-span deflection at maximum capacity, are listed in Table 6-6. The degree of composite action, *DCA* at SLS was calculated based on Equation (2-1) using the experimental deflection corresponding to SLS load and non-composite and full-composite analytical models.

Table 6-6 Strength and deflection of TCC modules at ultimate loading

TCC module	Strength (kN)	Mean (kN)	σ	CoV (%)	M_{exp} (kNm)	W_{eq}* (kN/m)	SLS DCA(%)	Deflection at F_{max} (mm)	Mean (mm)	σ	CoV (%)
CC1	176.2				234.9	29.4	97.0	73.6			
CC2	175.2	173.5	3.9	2.2	233.5	29.2	96.7	75.3	73.5	1.9	2.6
CC3	169.0				225.3	28.2	93.9	71.5			
LWC 1	137.6	142.1	6.4	4.5	183.4	22.9	94.5	76.0	68.2	11.0	16.2
LWC2	146.6				195.4	24.4	94.4	60.4			

* $W_{eq}L^2/8 = F_{max}L/3$

The average strength observed for TCC modules constructed from conventional concrete was 173.5kN with a CoV of 2.2% whilst the ultimate strength of TCC modules utilising LWC were 137.6 and 146.6kN with a CoV of 4.5% as listed in Table 6-6. The self-weight of the modules were excluded from the ultimate capacities. The strength of the TCC modules was highly consistent, shown by the significantly low CoV values. The average deflection at the F_{max} point of CC is 73.5mm (≈span/109), and the average deflection at the F_{max} point of EPS LWC is 68.2mm (≈span/117). The maximum deflection of CC series is 97.5mm (≈span/82) while the maximum deflection of EPS LWC is 116.7mm (≈span/69). The deflection of EPS LWC at F_{max} is smaller than CC. However, the maximum deflection of EPS LWC series is larger than CC series. The deflections measured at thirds of the span along the beam indicated a symmetric deflection profile for both SLS and ULS tests, up to failure.

The results of the ultimate testing for the TCC beams were very consistent as shown in Table 6-6 with CoV values of 2.2% and 4.5% for strength of CC and LWC series, respectively. However, the corresponding deflection of LWC series indicates a higher CoV of 16.2%. CC and LWC series exhibited high efficiency at SLS equal to 95.9% and 94.5%, respectively. The high degree of composite action exhibited by both CC and LWC implied that the vertical deflection in the TCC modules is minimal.

6.4.5 Global and apparent stiffness of TCC modules

Table 6-7 lists the results of the K (global stiffness) and EI (apparent stiffness) for the TCC modules. The deflection value used was calculated by taking the average of all the centre LVDTs at mid span which corresponding to a load range of 10% to 40% of the load carrying capacity. The apparent and global stiffness of the five TCC modules exhibited highly consistent values, shown by low CoV values as listed in Table 6-7.

Table 6-7 Global stiffness, *K* and apparent stiffness, *EI* of the TCC modules

TCC module	Global stiffness (kN/m)	Mean (kN/m)	CoV(%)	Apparent stiffness (kNm^2)	Mean (kNm^2)	σ	CoV(%)
CC1	1366.8			24837.7			
CC2	1403.5	1398.6	2.1	25302.9	25348.7	535.3	2.1
CC3	1425.5			25905.4			
LWC 1	1390.1	1376.7	1.4	25262.1	25019.0	343.8	1.4
LWC2	1363.4			24775.9			

The apparent and global stiffness of the LWC series were 99% of the CC series. Hence, the effect of LWC slab on stiffness of TCC modules is identified to be negligible The influence of concrete properties on stiffness of TCC system agrees with Van der Linden (1999) who conducted parametric studies on the effect of different concrete properties such as tensile strength, compressive strength, MOE and slab width on strength and stiffness of a TCC system. Van der Linden (1999) concluded that the MOE(varied between 2500 and 30000MPa), tensile strength(varied between3.3 to 8.3MPa), compressive strength(varied between class 15 and 35) and plasticity of concrete had minor influence on structural behaviour of a TCC beam.

Comparing stiffness of timber-only and TCC modules utilising CC and EPS LWC slabs, the TCC system exhibited approximately 5 times higher apparent stiffness.

6.4.6 Failure modes of TCC modules

Previous investigations highlight tension fracture of timber with no apparent failure in connections as a common failure in TCC specimens whereas this research indicates tensile failure of screws in tension with flexural deformation of screws in compression and some crushing of concrete around screws in both CC and LWC series. The failure pattern of cross inclined SFS screw was similar to that detected in push-out tests. The results agree with Dias et al. (2011) which states greater connection slip demand of TCC beam with higher width/height ratio of timber component leads to connection failures before reaching maximum strain in timber. Hence, the ultimate deformation capacity of connections as the governing factor in design leads to lower load capacity of a TCC system. In this case a smaller spacing limits the slip between timber and concrete and results in tensile failure of timber.

The failure mechanism was as: (1) tensile failure of multiple screws placed in tension; (2) redistribution of the shear force and tensile failures of the other screws close to mid-

span and plastic deformation of screws placed in compression; and (3) some localised crushing failure at under-side of the concrete slab close to shear connectors at the beam-ends; these observations were observed as shown in Figure 6-24.

By increasing the load, the TCC modules began to show deflection and the concrete and LVL exhibited slip at their interface. The flexural and axial deformation of screws embedded in the concrete formed concrete crushing while showing no sign of bearing failure and horizontal movement was observed in the screw embedded in the LVL web. The experiments were stopped after reaching the load capacity and the failure of the first set of screws had clearly occurred. Upon removal of the load and breaking of the concrete slab, tensile and flexural failures of SFS screws in tension and compression for the 5 to 10 first pairs of screws from one beam-end were observed (Figure 6-21).

All the TCC modules exhibited tensile and flexural failures of the screws in tension and compression near to one beam-end, respectively (Figures 6-20 and 6-21) and the crossed screws at other side of beam-end remained sound as depicted in Figure 6-22. An observation that was consistent across all the TCC modules was uplift slip of the concrete slab relative to the timber joist at the interface of concrete and LVL close to the end-ends supports close to failed screws, shown in Figure 6-23. Last specimen TCC LWC 2 exhibited lateral buckling on the compressive side of the web close to mid-span as indicated in Figure 6-25.

LWC series indicated a redistribution of shear force after the first connection yielding where a recovery of strength occurred after the load decreased to about 50kN following the yielding of a connector. High ductility of SFS screws in EPS LWC (see Chapter 5) and ductile behaviour of EPS light-weight concrete (see Chapter 4) lead to the ductile behaviour of LWC modules with the ability to sustain high plastic deformation. Hence, LWC modules provide significant warning before failure occurs though visible deflections in the system. Such recovery was not observed in the CC series.

Figure 6-20 (a) Failed tensile screw, (b) bent screw in compression and (c) sound one

Figure 6-21 Failure of the first six pairs of SFS screws

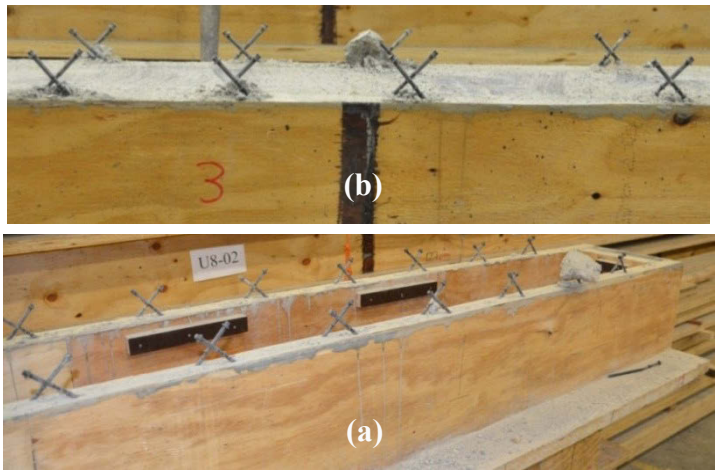

Figure 6-22 Sound pairs of SFS screws in TCC CC modules (a) 1 and (b) 3

Figure 6-23 Uplift of the concrete slab relative to the timber joist

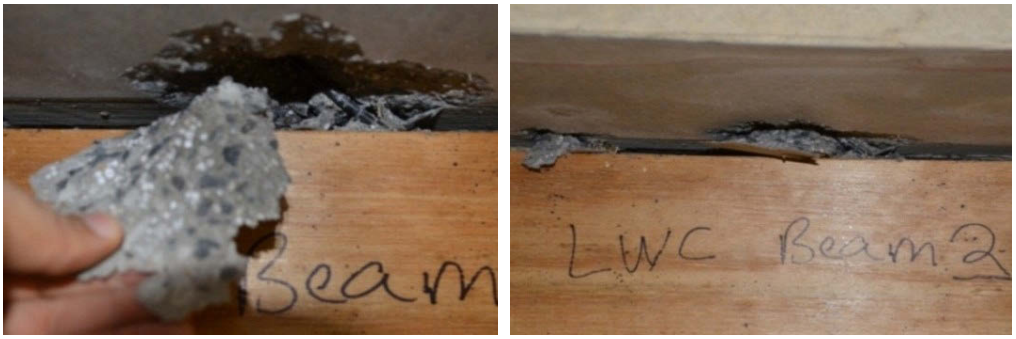

Figure 6-24 Localised failure of concrete at shear connectors in TCC LWC2 module

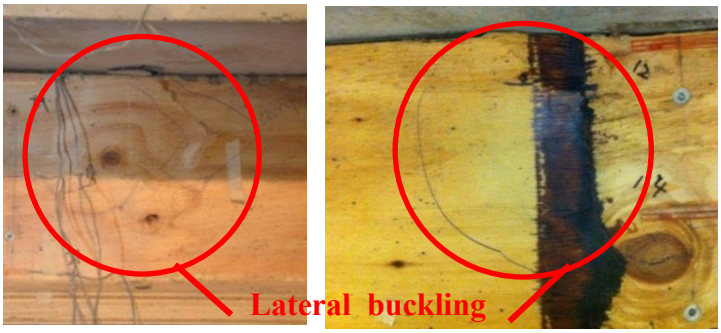

Figure 6-25 Lateral buckling of top part of LVL webs with localised crushing in concrete around connections at mid-span for TCC LWC2 modules

6.4.6.1 The load applied to TCC modules versus the load in connections

The load applied to TCC modules versus the load in connections were obtained using the slip between the concrete and LVL at the first three pairs of screws from beam-end, together with the corresponding shear force obtained from load-slip curves of the connection push-out tests as shown in Figure 6-26. Figure 6-27 depicts the load in the TCC module versus the load in the virtual connections at the beam-ends of different series. The load in shear connection is indicated for different load levels applied to the module at SLS, ULS and $0.8F_{max}$.

The largest load in TCC modules occurred at maximum load capacity of connection and hence, the dominant failure of TCC modules was tensile and flexural failures of SFS screws placed in tension and compression, respectively. Both CC and LWC series exhibited a high initial stiffness before SLS load level and the slip markedly increased beyond ULS load indicating load-slip responses of the screws.

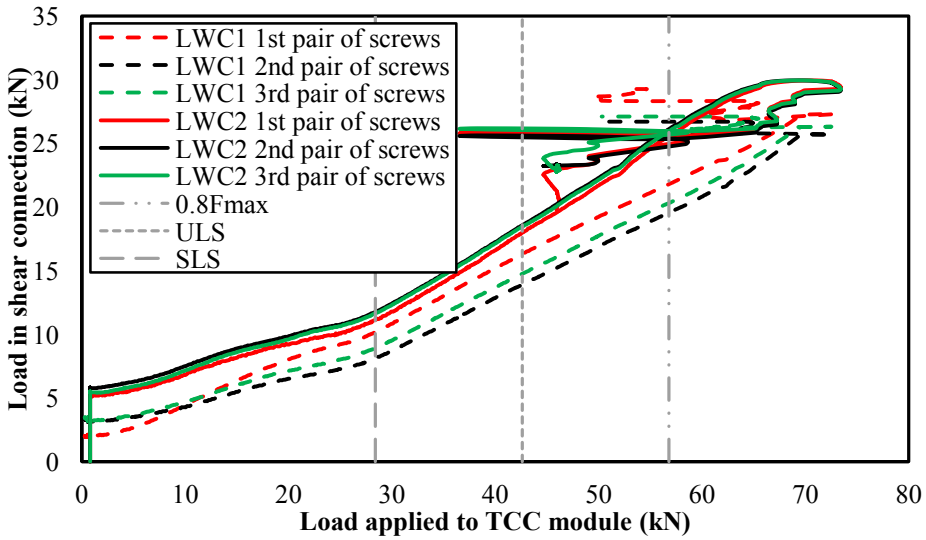

Figure 6-26 Load in each jack vs load in connector of first three pairs of screws in LWC

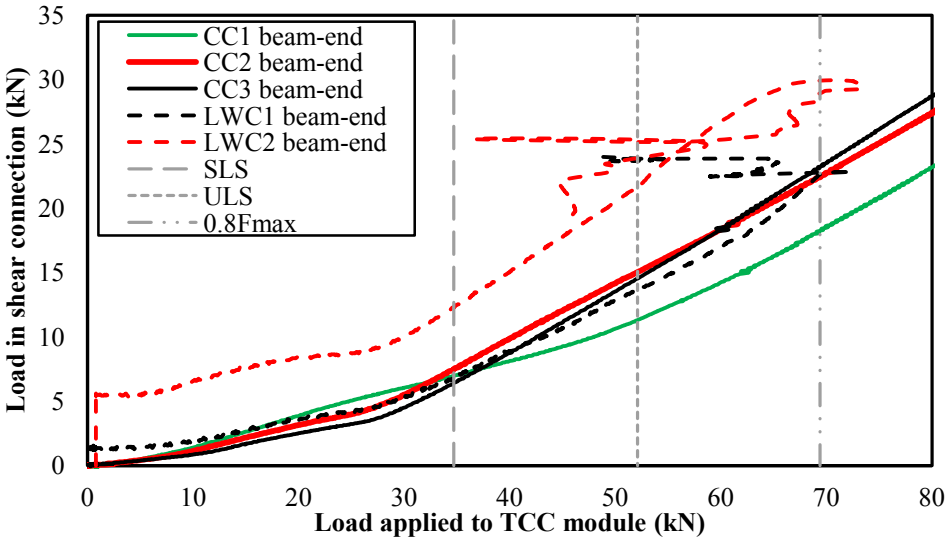

Figure 6-27 Load in each jack vs load in the virtual connector at the beam-ends

The shear force in the virtual connectors of TCC modules reached a plateau and suddenly dropped indicating axial failure in the connections and consequently in the TCC modules as depicted in Figure 6-27.

6.4.7 Residual deflection due to self-weight and shrinkage

A survey was undertaken for TCC modules before and after loading as shown in Table 6-8.

Table 6-8 TCC modules survey results

Specimen	distance(mm)	Left End(mm)	Mid Span(mm)	Right End(mm)	Sag (mm)	Difference (mm)
TCC CC1	before loading	672	695	679	19.5	35.5
	after loading	670	728	676	55	
TCC CC2	before loading	791	811	801	11	27.5
	after loading	789	833	800	38.5	
TCC CC3	after loading	623	643	627	18	37.5
	before loading	621	676	620	55.5	
TCC LWC1	before loading	575	590	575	15	40
	after loading	560	605	540	55	
TCC LWC2	before loading	528	540	533	9.5	108.5
	after loading	521	642	527	118	

After 28 days of casting concrete and 14 days of unpropping, the self-weight of TCC modules (1.9kN/m for CC and 1.7kN/m for LWC series) caused 11-20mm and 10-15mm initial deflection at mid-span for CC and LWC modules, respectively. However, the propping of both series were identical, under the permanent load (self-weight), the initial deflections of TCC modules have shown small differences.

The small difference in initial deflection of the two series (about 3mm) is not enough to conclusively show the better stiffness of the LWC series. Under the self-weight there was a minor shear force in the connections which lead to negligible slip in between composite components. Such negligible values are not capable of representing the differences in stiffness of the different TCC series.

The survey results of the CC series after the testing highlighted a mid-span residual deflection of approximately 27-37mm whilst the LWC series indicated a mid-span deflection of approximately 40-108mm after the testing. The difference between the two records of before and after the test indicates the deformation due to the four-point bending test. In LWC series, the difference between the two recordings of TCC LWC2 exhibited a significant deformation during the bending test which agreed with the ultimate failure of lateral buckling in the LVL web.

6.5 CONCLUSIONS

The results of an experimental investigation to evaluate the effects of the concrete type on the ultimate capacities of five full-scale 8m span LVL-concrete modules constructed from conventional and expanded polystyrene light-weight concrete were presented in this Chapter. The dimensions of the TCC module represent a realistic secondary beam in a typical non-residential building in Australia. TCC modules specimens were tested to serviceability and then, to failure after 28 days from casting. Extensive data including deflection at one and two thirds and mid-span points, strains at mid-span and slips between composite components at the beam-ends and the first three pairs of connection from beam-ends were measured during the tests.

The TCC modules were designed based on the Gamma method proposed by Eurocode 5 EN (2004b) under an imposed load Q of 3kN/m^2 for office buildings and a total permanent load $G = G_1+G_2$ of 3.24kN/m^2, with G_1 and G_2 including the self-weight and the superimposed permanent load, assumed as 2.24 and 1kN/m^2, respectively.

Timber composite structures generally exhibit linear-elastic behaviour. All the TCC modules exhibited more than 94% degree of composite efficiency at SLS.

LWC indicated a recovery of strength occurred after the load in each jack decreased to about 50kN following the yielding of a connector. This strength recovery might be attributed the ductile behaviour of SFS screws in the EPS LWC and higher ductility and plasticity of the EPS LWC slab. Such ductile behaviour in the LWC series might save some time for evacuation in an emergency. The apparent and global stiffness of the LWC series were very close to that of the CC series. Hence, the effect of LWC slab on stiffness of TCC modules is identified to be negligible compared to the CC series.

7 ANALYTICAL MODELS OF TCC MODULES

7.1 INTRODUCTION

This Chapter reported the analytical model and compared the experimental and analytical results for model calibration and design recommendations. The experimental programme and results were explained in Chapter 6. The dimensions of the TCC module represents a realistic secondary beam in a typical non-residential building in Australia.

The TCC modules were designed based on the Gamma method proposed by Eurocode 5 EN (2004b) under an imposed load Q of 3kN/m^2 for office buildings and a total permanent load $G = G_1+G_2$ of 3.24kN/m^2, with G_1 and G_2 including the self-weight and the superimposed permanent load, assumed as 2.24 and 1kN/m^2, respectively. The Gamma method was used to obtain different analytical results including live-load capacity, deflection and degree of composite action (*DCA*) and apparent stiffness of full-composite, partially composite and non-composite TCC modules at ultimate (ULS) and serviceability (SLS) limit states. The analytical results were also compared to the similar results obtained from experimental tests.

Finally, a parametric study on the influence of different connections and concrete properties (discussed in Chapter 5) on design of TCC beams in terms of shear bond coefficient and effective bending stiffness of composite section was presented.

7.2 COMPARISON OF EXPERIMENTAL AND ANALYTICAL RESULTS

7.2.1 Live-load capacities at SLS

Figure 7-1 shows the analytical and experimental imposed live-load capacities of CC, LWC and timber-only test series corresponding to the deflection limit at SLS. The effective bending stiffness, EI_{eff}, calculated by Eurocode 5 EN (2004b) with connection serviceability slip modulus and MOE of concrete and LVL was used to obtain the analytical imposed loads. The experimental and analytical SLS loads (F) in kN were changed to kN/m^2 using equivalent deflection formula as:

$$\frac{5wl^4}{384EI_{eff}} = \frac{Fa(3l^2 - 4a^2)}{24EI_{eff}} \qquad (7\text{-}1)$$

Where, a is the distance between support and load in four-point bending test (l/3) and then by dividing the calculated uniformly distributed load, w by the concrete width (900mm).

The Gamma method with γ_1=1 was used to calculate the fully composite live-load capacity at SLS. Moreover, the load of timber-only modules at SLS was used to calculate timber-only imposed SLS load using the formula above. The load of full-composite modules was substituted in the same formula to obtain imposed live-load capacity of full-composite modules as a benchmark for further comparison. The Gamma method underestimated the experimental live-load of CC and LWC series by 24% and 22%, respectively. Hence, it predicts the deflection limit state at SLS corresponding to a lower imposed load which is conservative for the series.

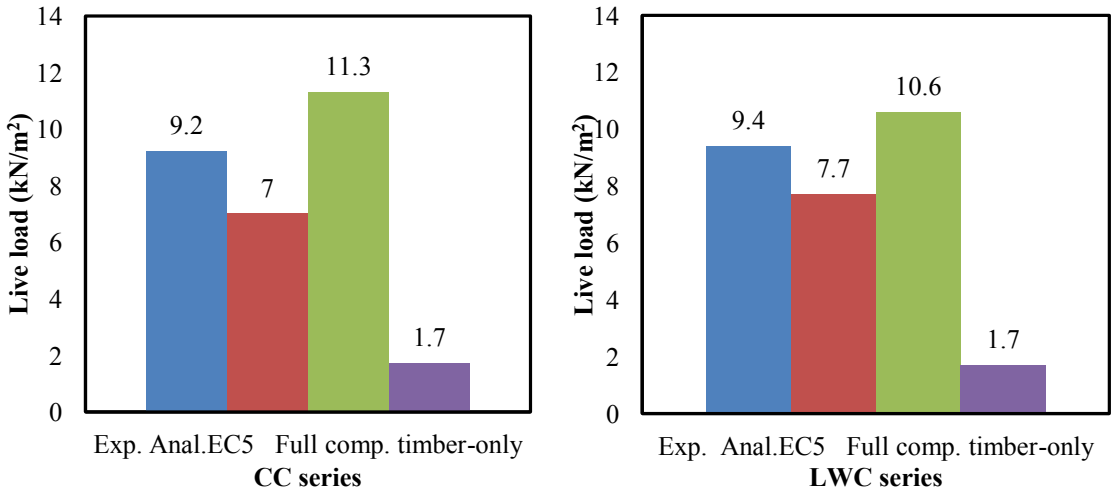

Figure 7-1 Experimental and analytical SLS live-load capacity of test series

The experimental imposed load capacity of CC and LWC series indicates only 18.5% and 11.5% lower values comparing to that of fully-composite modules. The design live-load of 4.53kN/m^2 consisted of 3kN/m^2 distributed live-load and a 3.5kN concentrated live-load at mid-span is about 50% of the experimental imposed live-load at SLS. Hence, other design criteria such as long-term deflection are highlighted as governing design criteria of TCC.

7.2.2 Live-load capacities at ULS

Experimental ULS live-load capacity of CC, LWC and timber-only series and analytical Eurocode 5 EN (2004b) and fully-composite modules are depicted in Figure 7-2.

The effective bending stiffness, EI_{eff}, calculated by the Gamma method with connection ultimate slip modulus and MOE of concrete and LVL was used to obtain the analytical design imposed load in kN/m^2 at ULS. The experimental and analytical ULS load, F_u in kN was changed to w_u in kN/m^2 using equivalent bending moments formula as:

$$\frac{w_u l^2}{8} = \frac{F_u l}{3} \qquad (7\text{-}2)$$

where, w_u is the ultimate design distributed load as a combination of the dead- and live-loads (w_u= 1.2G +1.5Q). The corresponding load combination was used to calculate Q where G is 3.24kN/m^2, divided by the module spacing (900mm) as w_u= 1.2(3.24 ×0.9) + 1.5(Q×0.9) = 3.5 + 1.35Q. The Gamma method with γ_1=1 was used to calculate the fully composite live-load capacity at ULS. The strength of timber-only modules (Table 6-2) was used to gain the imposed load capacity of timber-only modules.

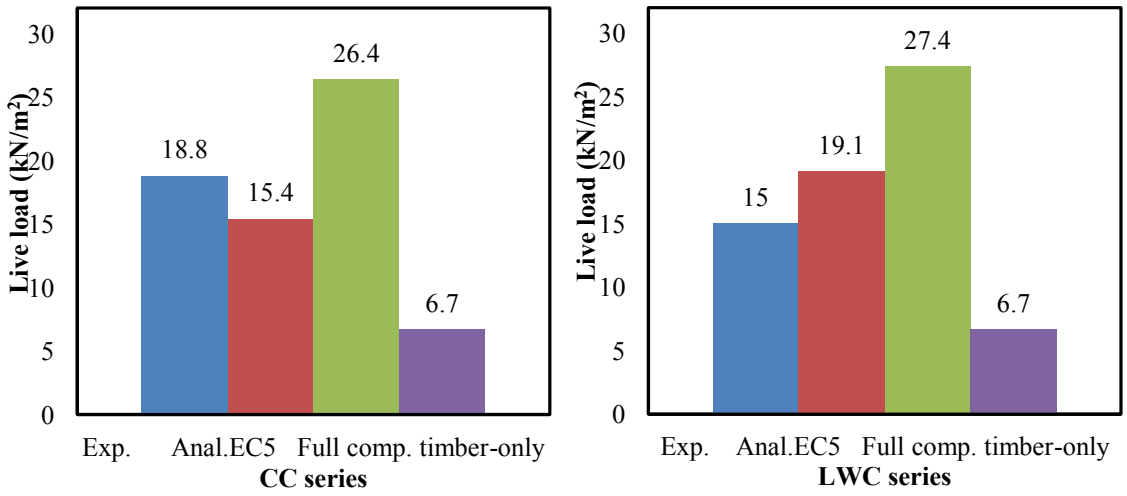

Figure 7-2 Experimental and analytical ULS live-load capacity of CC and LWC series

7.2.3 Deflection and degree of composite action (DCA) at SLS

In order to approximate the accuracy of the Gamma method, experimental and analytical deflections given by the Gamma method using $K_{s,0.4}$ and *DCA* at SLS and ULS of different test series were compared in Tables 7-1 and 7-2. For LWC series, the experimental deflection at SLS was about 1.12 times the full-composite deflection at SLS and 0.78 times the analytical deflection at SLS whilst CC series indicates a 1.22 times the full-composite SLS deflection and 0.76 times the SLS analytical deflection.

The deflections ratios and *DCA*s trends at ULS agreed with that of SLS with the exception of high experimental to full composite deflection ratios of LWC modules which are 1.21-1.26 at ULS compared to SLS values of 0.76-0.81. Moreover, *DCA*s of modules at ULS were 7%-9% less than similar values at SLS.

Table 7-1 Experimental and analytical deflections and *DCA* at SLS of different series

Deflection (mm)						Ratio		
TCC	Full comp.	Exp.	Anal. EC5	Non. comp.	SLS *DCA*(%)	Exp./Anal.	Exp./Full C.	Exp./Non C.
CC1	12.9	15.9	20.7	63.5	93.9	0.77	1.23	0.25
CC2	14.5	17.6	23.4	71.7	94.5	0.75	1.21	0.25
CC3	15.7	19.2	25.3	77.7	94.4	0.77	1.22	0.25
LWC1	15.6	17.4	21.5	76.1	97	0.76	1.12	0.23
LWC2	15.0	16.9	20.8	73.5	96.7	0.81	1.13	0.23

Table 7-2 Experimental and analytical deflections and *DCA* at ULS of different series

Deflection (mm)						Ratio		
TCC	Full comp.	Exp.	Anal. EC5	Non. comp.	ULS *DCA*(%)	Exp./Anal.	Exp./Full C.	Exp./Non C.
CC1	49.9	71.5	83.7	246.1	89.0	0.85	1.43	0.29
CC2	42.2	76.0	83.2	206.5	79.4	0.91	1.8	0.37
CC3	44.9	60.4	80.3	219.7	91.1	0.75	1.35	0.27
LWC1	52	73.6	58.3	256.5	89.4	1.26	1.42	0.29
LWC2	51.7	75.3	62.2	255.1	88.4	1.21	1.46	0.3

7.2.4 Stiffness of composite module at SLS and ULS

The theoretical apparent stiffness of TCC modules was calculated using Gamma method proposed by Eurocode 5 design provision EN (2004b). The serviceability slip moduli for two of the CC and LWC extracted from the push-out results were applied to the equations to determine γ_i. The theoretical values of apparent stiffness for TCC CC and LWC series are listed in Tables 7-3 and 7-4, respectively.

The CC and LWC series indicated an experimental load capacity of 71% and 55% compared to that of a fully composite system. The experimental live-load capacities of CC series at ULS was 22% larger than the analytical capacities obtained from the Gamma method which means the Gamma method underestimated the short-term ULS capacity whereas, experimental live-load capacity of LWC series indicated a 27% lower values compared to the values calculated by the Gamma method.

Comparing timber-only and TCC modules, casting a top layer of conventional and light-weight concrete slabs leads to 2.8 and 2.2 times higher live-load capacity, respectively.

Table 7-3 Apparent stiffness of TCC CC series using Eurocode 5 EN (2004b)

TCC module Components	E_iI_i(kNm^2)	γ_i	$\gamma_i E_iA_ia_i^2$	EI(kNm^2)
CC Concrete slab	1051.7	0.18	7457.7	8527.4
LVL web	2029.2	1.0	449.8	2479
LVL flange	23.1	1.0	8095.7	8118.8
			Total EI_{eff} =	19125.2

Table 7-4 Apparent stiffness of TCC LWC series using Eurocode 5 EN (2004b)

TCC module Components	E_iI_i(kNm^2)	γ_i	$\gamma_i E_iA_ia_i^2$	EI(kNm^2)
LWC Concrete slab	873.9	0.3	7673.1	8547
LVL web	2029.2	1.0	1032.8	3062
LVL flange	23.1	1.0	9795	9818.1
			Total EI_{eff} =	21427.1

It is noted that after conducting short-term SLS and ULS tests, the TCC modules satisfied the specified design criteria. Hence, it is concluded that other design criterion such as long-term deflection is highlighted to be a governing design criterion of TCCs.

Table 7-5 lists the theoretical and experimental apparent stiffness of TCC modules. Theoretical apparent stiffness of different test series corresponding to full and non-composite actions were calculated in accordance with the transformed section method and introducing a shear bond coefficient of 0 to the Gamma method calculations, respectively, as listed in Table 7-5. In addition, the experimental apparent stiffness of TCC modules calculated in compliance with AS4063.1 (2010) were compared to the theoretical apparent stiffness by the Gamma method and apparent stiffness of full and non-composite sections as tabulated in Table 7-5.

Theoretical apparent stiffness of the CC series calculated based on the Gamma method represents the results that are approximately 73.8-77% accurate whilst the theoretical apparent stiffness of the LWC series is more accurate as the comparison percentage is approximately 84.8–86.5%.

The average experimental apparent stiffness of CC and LWC series are 17.7% and 15.6% lower than the theoretical full-composite apparent stiffness, respectively. As a result of this inaccuracy, the design model has to be revised. To propose a correction factor for design of TCC at SLS, the increment correction factors of 22% and 13% were proposed to the deflection of CC and LWC series obtained from fully-composite section or alternatively, 18% and 16% reductions to the flexural stiffness, EI_{eff} calculated by transformed section method were proposed for CC and LWC series, respectively.

Table 7-5 Theoretical full and non-composite and experimental apparent stiffness

	EI_{eff} (kNm^2)				Ratio		
TCC	Full comp.	Exp.	Anal.EC5	Non. comp.	Exp./Anal.	Exp./Full C.	Exp./Non C.
CC1	30800.4	24837.7	19125.2	6062.5	1.3	0.81	4.1
CC2	30800.4	25302.9	19125.2	6062.5	1.32	0.82	4.17
CC3	30800.4	25905.4	19125.2	6062.5	1.35	0.84	4.27
LWC1	29663.5	25262.1	21427.1	6240.3	1.18	0.85	4.05
LWC2	29663.5	24775.9	21427.1	6240.3	1.16	0.84	3.97

The load-mid span deflection curves of the CC and LWC series are shown in Figures 7-3 and 7-4, respectively. In the same figures, also the upper and lower limits corresponding to fully-composite beam and non-composite conditions and the case of timber-only beams with no concrete slab were plotted. An additional line represented the load-deflection response of partial composite action was drawn using Eurocode 5.

A trend is evident as the difference between analytical model (Gamma method) and experimental results are significantly low until the load approaches maximum load capacity. As the load passes maximum capacity the model begins to underestimate the deflection. This response can be attributed to the modules experiencing a non-linear response after reaching maximum capacity as depicted in Figures 7-3 and 7-4.

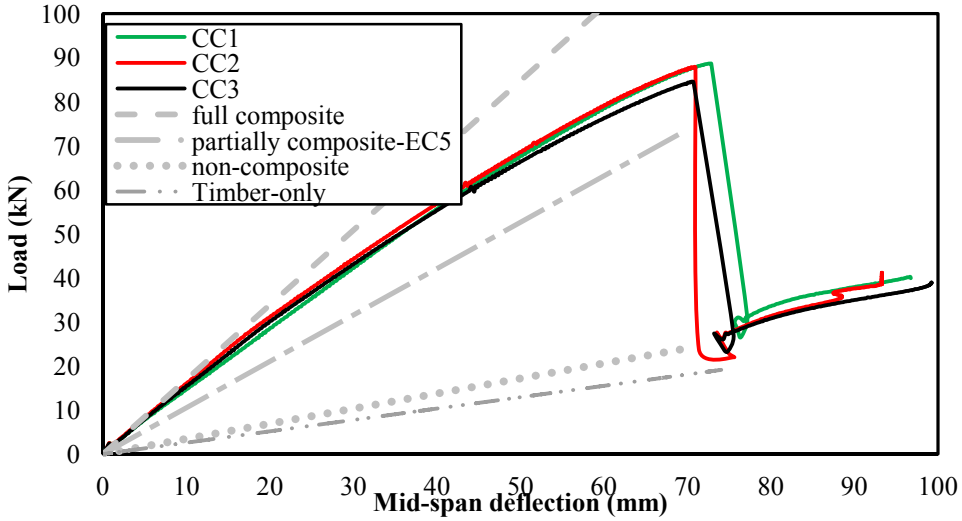

Figure 7-3 Comparison of experimental and theoretical responses of TCC CC series

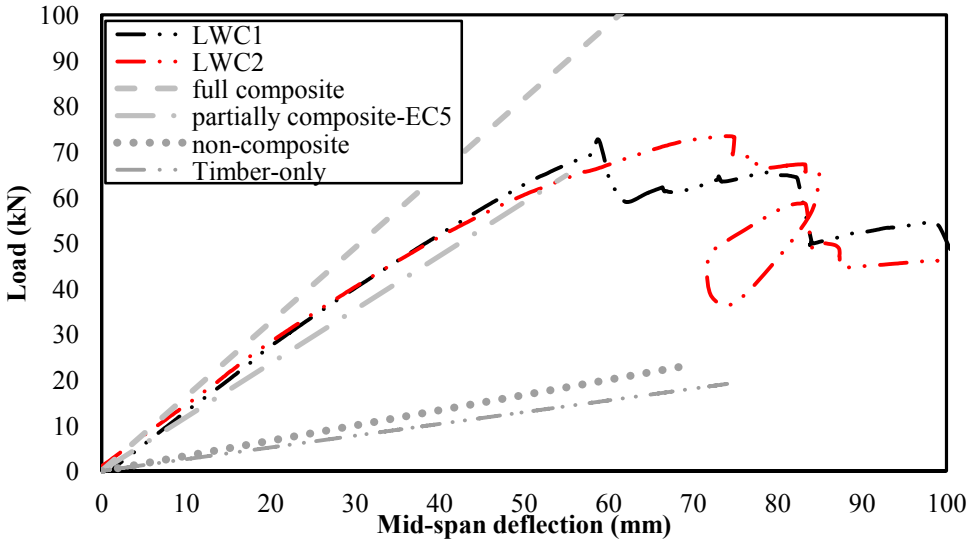

Figure 7-4 Comparison of experimental and theoretical responses of TCC LWC series

7.3 EFFECT OF CONNECTOR AND CONCRETE TYPES ON EFFECTIVE STIFFNESS OF TCC MODULES

In this Section, the influence of different connection and concrete properties reported in Chapter 5 on design parameters of TCC beams is presented. The Gamma method was used to calculate the shear bond coefficient and effective flexural stiffness of the TCC modules utilising different connection and concrete types. The span of TCCs influences the effectiveness of connection given in form of shear bond coefficient, γ as a design parameter defined in Chapter 2.

Figures 7-5:7-7 represents shear bond coefficient, γ versus span for the discussed geometry of TCC modules with different concrete (conventional concrete, EPS light-weight concrete and others including Scoria light-weight concrete, high-strength concrete and self-consolidating concrete) and connection properties (SFS screws, SPAX screws and L and U connectors). The varied parameters of concrete MOE and serviceability slip modulus of connections result in different shear bond coefficient of the TCC section with a 900x75mm concrete and 378mm spacing of connections as discussed in Chapter 6.

Having the identical connections spaced every S, the shear bond coefficient, γ is increased by the length of the TCC modules. For the 8m long TCC module application of CC SPAX I45 results in the lowest efficiency of connection (γ=0.08) whilst EPS LWC2000 SFS WI30 series indicates the highest shear bond coefficient (γ=0.35).

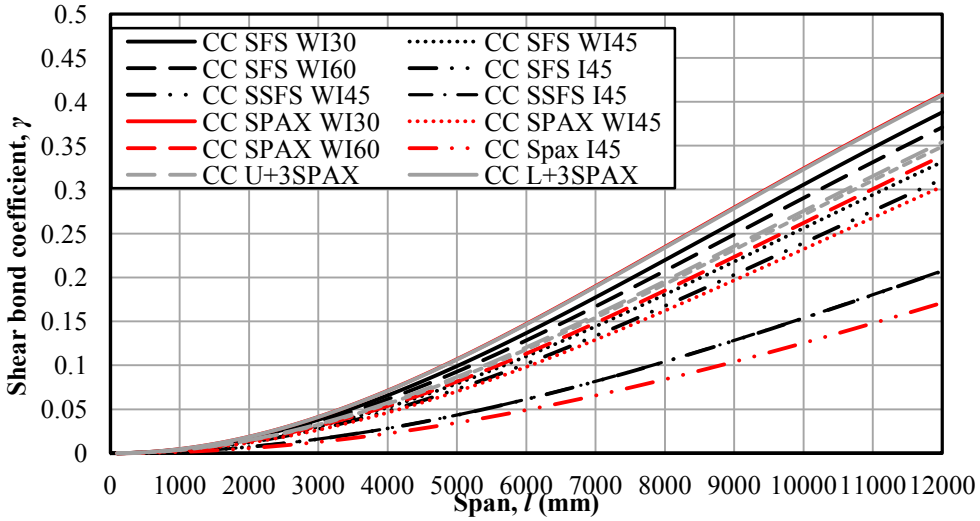

Figure 7-5 Shear bond coefficient, γ vs. span, l for CC test series

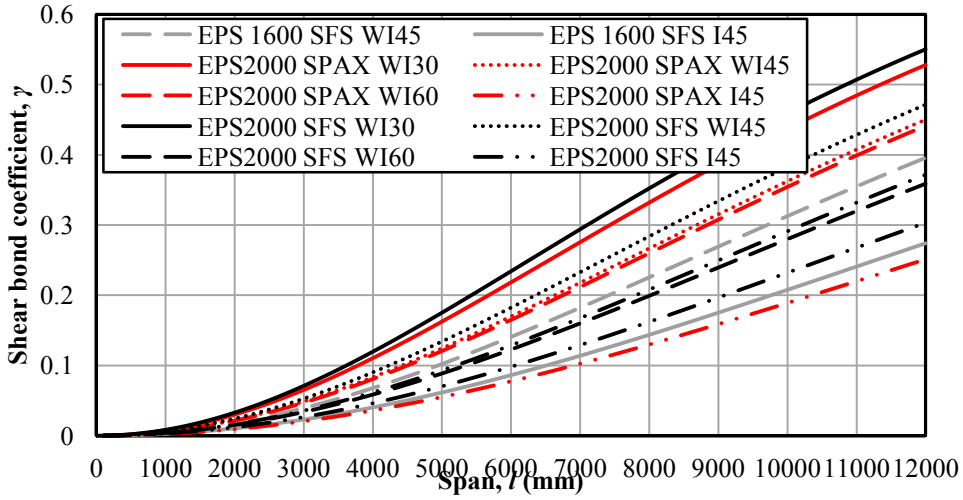

Figure 7-6 Shear bond coefficient, γ vs. span, l for EPS LWC test series

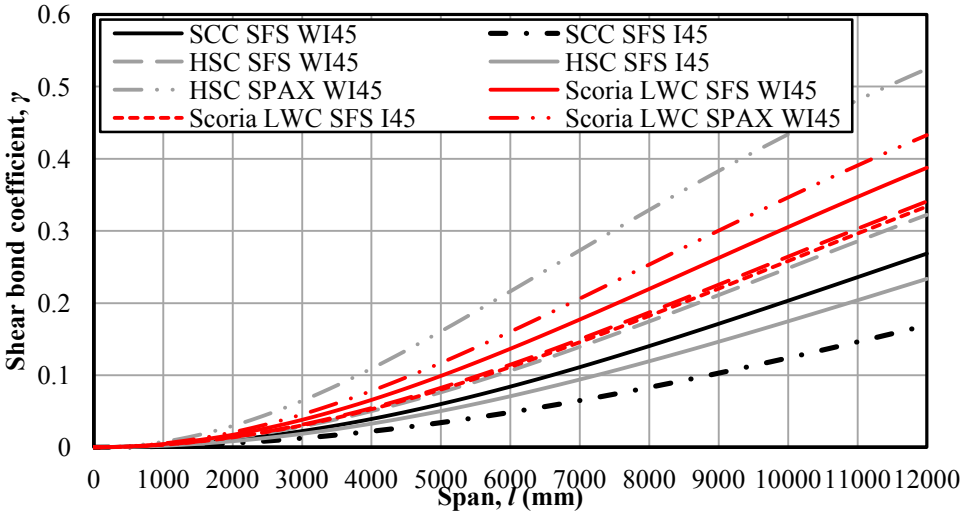

Figure 7-7 Shear bond coefficient, γ vs. span, l for HSC, SCC and Scoria LWC series

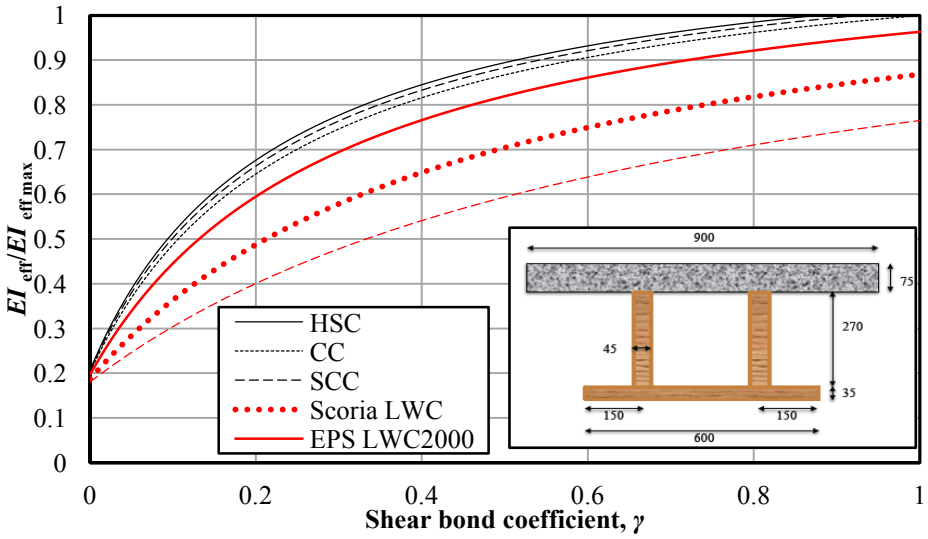

Figure 7-8 Effective bending stiffness vs. shear bond coefficient, γ

Figure 7-8 depicts the effect of MOE of six types of concrete used in the experiment on the effective bending stiffness of a TCC modular beam, depending on different shear bound coefficient. The geometry and material properties of composite components used in TCC modules were reported in Chapters 4 and 6. HSC series with highest MOE indicates maximum effective stiffness whereas EPS LWC1600 represents the minimum one as shown in Figure 7-8.

The interlayer had no contribution to the flexural stiffness of the TCC section. Thus, LVL and concrete only were considered in the model. The plywood interlayer slightly increased the height of the TCC compared to a TCC without interlayer which compensates for the lack of stiffness in the connection due to the interlayer (Jorge et al. 2011).

7.4 CONCLUSIONS

This Chapter reported analytical models of the Gamma method and compared the experimental and analytical results for model calibration and design recommendations. The experimental programme and results were explained in Chapter 6. The dimensions of the TCC module represent a realistic secondary beam in a typical non-residential building in Australia.

The TCC modules were designed based on the Gamma method proposed by Eurocode 5 EN (2004b) under an imposed load Q of 3kN/m^2 for office buildings and a total permanent load $G = G_1+G_2$ of 3.24kN/m^2, with G_1 and G_2 including the self-weight and the superimposed permanent load, assumed as 2.24 and 1kN/m^2, respectively.

The Gamma method was used to obtain different analytical results including live-load capacity, deflection and degree of composite action (*DCA*) and apparent stiffness of full-composite, partially composite and non-composite TCC modules at ultimate (ULS) and serviceability (SLS) limit states. The analytical results were also compared to the similar results obtained from experimental tests.

The experimental live-load capacity at SLS was close to that of a full- composite system in both the CC and LWC series whilst the experimental live-load capacity at ULS showed higher differences to that of a fully-composite system in the both series.

To propose a correction factor for design of TCC at SLS, the increment correction factors of 22% and 13% can be proposed to the deflection of CC and LWC series

obtained from the fully-composite section or alternatively, 18% and 16% reductions to the flexural stiffness, EI_{eff} calculated by the transformed section method can be proposed for CC and LWC series, respectively. It is important to note that the correction factors were obtained from the experimental test carried out in this investigation; thus, further experimental investigation with different connections and concrete properties are recommended to calibrate these correction factors.

The Gamma method underestimates the imposed live-load by approximately 20% at SLS (CC and LWC series) and ULS (CC series) whereas LWC series highlights 27% overestimation at ULS. The experimental stiffness of the CC and LWC series were 20% and 30% greater than those calculated in compliance with the Gamma method.

The TCC system exhibited 2.5 and 5 times higher live-load capacity and apparent stiffness comparing to timber-only modules, respectively.

In terms of deflection, the Gamma method overestimated the experimental deflections at both SLS and ULS by 23%-33% for CC series whilst the Gamma method deflection of LWC series indicated a 10%-33% overestimation at SLS and 21%-26% underestimation compared to the experimental deflections.

The experimental live-load capacity of TCC modules at SLS were approximately two times the design live-load requirement of 4.53KN/m^2 which consisted of 3KN/m distributed live-load and a 3.5KN concentrated live-load at mid-span. Hence, other design criteria such as long-term deflection are highlighted as governing design criteria of TCC. This information is useful for the model calibration and design guideline.

The application of LWC represents an innovative solution when combined with TCC technology to further minimise the dead loads of structures. Such a system can be seen as a favourable alternative for both the renovation of old timber floors and the construction of new ones. Furthermore, experimental results of LWC series have a positive contribution to improve reliable design codes.

Finally, a parametric study on the influence of different connections and concrete properties discussed in Chapter 5 on design of TCC beams in terms of shear bond coefficient and effective bending stiffness of composite section has been presented where for the 8m TCC module the maximum shear bond coefficient was found to be four times higher when fabricated with EPS LWC2000 SFS WI30 compared to CC SPAX I45 which represented the minimum one.

8 ANALYTICAL MODELS OF TCC CONNECTOR

8.1 INTRODUCTION

The literature highlights a significant lack of information on analytical closed-form equations to predict the strength and stiffness of TCC connections to be used in the design of timber composite beams.

There are only a few references in the literature for stiffness prediction of timber to timber and TCC shear connections which include simplified models and also the models based on the theory of beam on elastic foundation where Johansen yield theory and Eurocode 5 are available to predict the strength of timber composite connections. However, the equations are limited to vertically inserted fasteners and Eurocode 5 EN (2004b) recommends that the strength and stiffness of unconventional connections should be determined by push-out tests. In the case of TCC, the predicted stiffness can be used as input parameter for the design of composite structure.

Previous investigations reported that the inclination of fastener significantly increases the initial stiffness and ultimate strength of the TCC connections and floor, exploiting the axial capacity of shear connections (Bejtka et al. 2002).

This Chapter consists of two separate Sections of strength and stiffness models of TCC connections. Each Section first reviewed the methodology of available analytical models for prediction of the strength or stiffness of vertically inserted single timber to timber and TCC shear connections for example screw and nail. Then, the available strength and stiffness models of vertically inserted fasteners were verified by experimental data of single wood screw shear connection used in TCC specimens. Due

to availability, lower cost, labour requirement and time for fabrication, the wood screw was selected as the shear connection to verify the models.

In the strength models Section, a kinematic plastic collapse model adopted for strength prediction of TCC connections utilising crossed screws inclined at various angles is proposed. The Johansen yield theory has been extended to derive the strength model of TCC connection with crossed screws which are loaded in tension and compression.

Finally, in the stiffness model Section, an analytical stiffness model of crossed screws is presented. The model assumes the behaviour of an inclined screw as a beam on a two-dimensional elastic foundation, and considers the timber as the elastic foundation consisting of orthogonal springs with differing stiffness in the parallel to and transverse to the grain directions. To compare the accuracy of the stiffness model, a relatively simple model with fewer variables proposed by Tomasi et al. (2010) for inclined screws in timber-timber connection was used and its results were verified by experimental data.

The experimental data of stiffness, strength and failure mode obtained from push-out test of TCC connections with crossed (±30°, ±45°, ±60°) SFS VB and SPAX screws utilising different concrete types (discussed in Chapter 5) were used to examine the accuracy of the strength and stiffness models of TCC connections for their practical application in the design of a TCC floor.

The methodology of the required experimental tests to characterise the input parameter of the models and their results are presented in Appendix D.

8.2 STRENGTH MODEL OF TCC CONNECTION

In this Section, available strength models of vertical fastener in TCC are reviewed and verified utilising experimental data. Moreover, an analytical strength model to predict the strength of TCC connections utilising single and crossed screws inclined to the timber grain is proposed.

8.2.1 Strength model of vertical fastener

European yield model (EYM) presumes a ductile failure for multiple fasteners timber composite connections, provided that an adequate end distance, spacing, and member thickness are employed (Smith et al. 2001). The accuracy of EYM is examined using the experimental results. EYM simulates the fastener and timber by elastic perfectly

plastic behaviour. Hence, the initial yield and fully plastic capacities of the composite components coincide (Smith et al. 2001).

EYM only predicts the load carrying capacity of timber connections without any prediction of the stiffness or displacement of connection during loading before failure and at failure (Dias 2005; Mascia et al. 2009).

In EYM, some possible failure modes were postulated whilst the equations of equilibrium were employed to find the location of plastic hinge. EYM proposed a limit state load corresponding to each possible failure mode. Consequently, the failure mode with the lowest estimated load governs the load carrying capacity of the connection which is loaded monotonically up to failure in shear force parallel to the timber grain. The dominant failure mode and yield load of the connection depend on the geometry of the composite components, yield moment of fastener and embedding strength of the composite materials (Patton-Mallory et al. 1997b).

Johansen (1949) proposed a minimum required end distance to diameter ratio (e/d) of 7 and 10 for pinned and bolted connections, respectively to reach the "yield load". This model is called the "yield theory" or "yield model" which implies the contribution of yielding of fastener to load carrying capacity of the timber connections.

In the case of TCC connections where the concrete component is assumed to remain rigid and undamaged, the possible failure modes of dowelled timber connections proposed by Johansen's theory are limited to the equations where screw crushing the surrounding timber (Equation (8-1)) and the formation of single (Equation (8-2)) and double plastic hinges (Equation (8-3)) in screw.

$$f_{t\text{-}t}\ (a)=f_{h,1,k}\ t_1\ d \tag{8-1}$$

$$f_{t\text{-}t}\ (b) = f_{h,1,k}\ \ t_1\ d[\sqrt{2+\frac{4M_{y,Rk}}{f_{h,1,k}\ d\ t^2}}\text{-}1] \tag{8-2}$$

$$f_{t\text{-}t}\ (c) = 2.3\sqrt{M_{y,Rk} f_{h,1,k} d} \tag{8-3}$$

where, $f_{h,1,k}$ is the embedding strength of the timber components;

d is the fastener diameter;

t is the timber thickness or the embedded length of fastener in timber;

$M_{y,Rk}$ is the yield moment of the fastener;

Although Eurocode 5 recommends push-out tests to calculate the serviceability stiffness and load capacity of timber connections, Eurocode 5 Part 2 modified the EYM's equations to approximate the characteristic load capacity of the timber connection per shear plane per fastener ($F_{v,Rk}$) as a minimum of six failure modes as shown in Figure 8-1 (EN 2004b; Heine et al. 2001; Johnsson 2004). The failure modes are:

$$f_{t\text{-}t}\ \text{(a)}=f_{h,1,k}\ t_1\ d \tag{8-4}$$

$$f_{t\text{-}t}\ \text{(b)}=f_{h,2,k}\ t_2\ d \tag{8-5}$$

$$f_{t\text{-}t}\ \text{(c)}=\frac{f_{h,1,k}\ t_1\ d}{1+\beta}\left[\sqrt{\beta+2\beta^2\left[1+\frac{t_2}{t_1}+\left(\frac{t_2}{t_1}\right)^2\right]+\beta^3\left(\frac{t_2}{t_1}\right)^2}-\beta\left(1+\frac{t_2}{t_1}\right)\right]+\frac{F_{ax,Rk}}{4} \tag{8-6}$$

$$f_{t\text{-}t}\ \text{(d)}=1.05\frac{f_{h,1,k}\ t_1\ d}{2+\beta}\left[\sqrt{2\beta(1+\beta)\frac{4\beta(2+\beta)M_{y,Rk}}{f_{h,1,k}\ t_1^{\,2}\ d}}-\beta\right]+\frac{F_{ax,Rk}}{4} \tag{8-7}$$

$$f_{t\text{-}t}\ \text{(e)}=1.05\frac{f_{h,1,k}\ t_2\ d}{1+2\beta}\left[\sqrt{2\beta^2(1+\beta)\frac{4\beta(1+2\beta)M_{y,Rk}}{f_{h,1,k}\ t_2^{\,2}\ d}}-\beta\right]+\frac{F_{ax,Rk}}{4} \tag{8-8}$$

$$f_{t\text{-}t}\ \text{(f)}=1.15\sqrt{\frac{2\beta}{1+\beta}}\sqrt{2M_{y,Rk}f_{h,1,k}d}+\frac{F_{ax,Rk}}{4} \tag{8-9}$$

where,

$$\beta=\frac{f_{h,1,k}}{f_{h,2,k}} \tag{8-10}$$

$f_{h,i,k}$ are the characteristic embedding strength of the timber member i;

d is 0.75 times the outer diameter of fastener;

t_i is the timber thickness or the embedded length of fastener in member i;

$M_{y,Rk}$ is the characteristic yield moment of fastener;

$F_{ax,Rk}$ is the characteristic axial withdrawal capacity of the fastener;

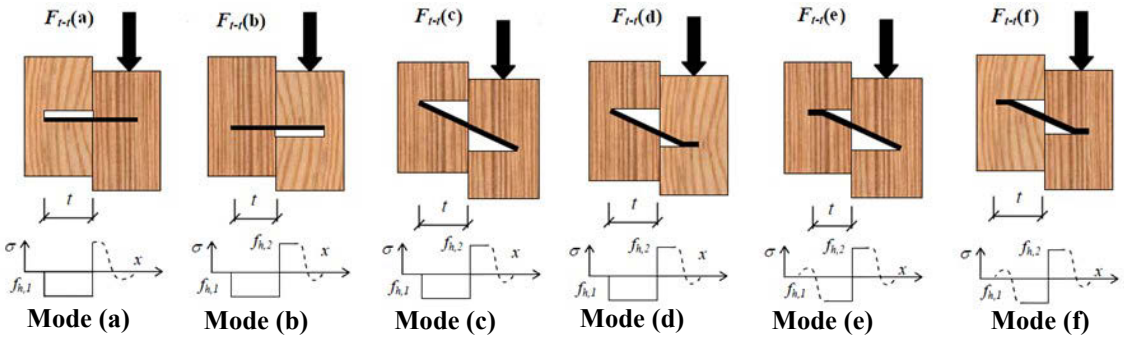

Figure 8-1 Six possible failure modes for timber-timber connections (Dias 2005)

The possible failure modes of dowelled timber connections proposed by Eurocode 5 EN (2004b) (Figure 8-1) include modes (a), (b) and (c) where the fastener crushes timber components 1, 2 and both (Equations (8-4):(8-6)) and modes (d) and (e) correspond to formation of a single plastic hinge in components 1 or 2 as given in Equations (8-7) and (8-8) and finally mode (f) represents the formation of double plastic hinges, one in each timber component (Equation (8-9)).

The second term in Equations (8-6):(8-9) represents the 'rope effect' which considers the friction between the timber components. Hence, the rope effect is written as 0.25 of the axial withdrawal strength of the connection where 0.25 represents the coefficient of friction in a timber-timber composite. The rope effect is neglected in the failure modes proposed by Johansen's theory.

The characteristic axial withdrawal capacity of the fastener is determined using either experimental test in compliance with the codes for example EN1382 (1999) or analytical approximations proposed by Eurocode 5 EN (2004b) as:

$$F_{\mathrm{ax,Rk}} = f_{\mathrm{ax,k}} d l_{\mathrm{ef}} k_{\mathrm{d}} \tag{8-11}$$

where,

$$f_{\mathrm{ax,k}} = 0.52 d^{-0.5} {l_{\mathrm{ef}}}^{-0.1} {\rho_{\mathrm{k}}}^{0.8} \tag{8-12}$$

$f_{\mathrm{ax,k}}$ is the characteristic withdrawal strength perpendicular to the grain whilst l_{ef} is the penetration length of the threaded part and k_{d} is the minimum of d/8 and 1.In the case of TCC connection, the concrete component is assumed to remain rigid and undamaged. Hence, the possible failure modes are limited to three cases of Figure 8-1 (a), (d) and (f) as depicted in Figure 8-2. Failure mode (a) represents the screw crushing the surrounding timber as a low ductile failure mode whereas failure modes (d) and (f) illustrate the formation of single (at the interface of the timber and concrete) and double plastic hinges (one at interface of the composite materials and one inside timber), respectively and are ductile failure modes.

In the case of TCC, Eurocode 5 (EN 2004b) proposes a modification factor of 1.2 for load capacity to consider the effect of concrete (Ceccotti et al. 2006a). The material properties of timber affect the load carrying capacity of the timber composite connections by the embedding strength of timber which is defined as the local compressive capacity of timber (Gehri 2009).

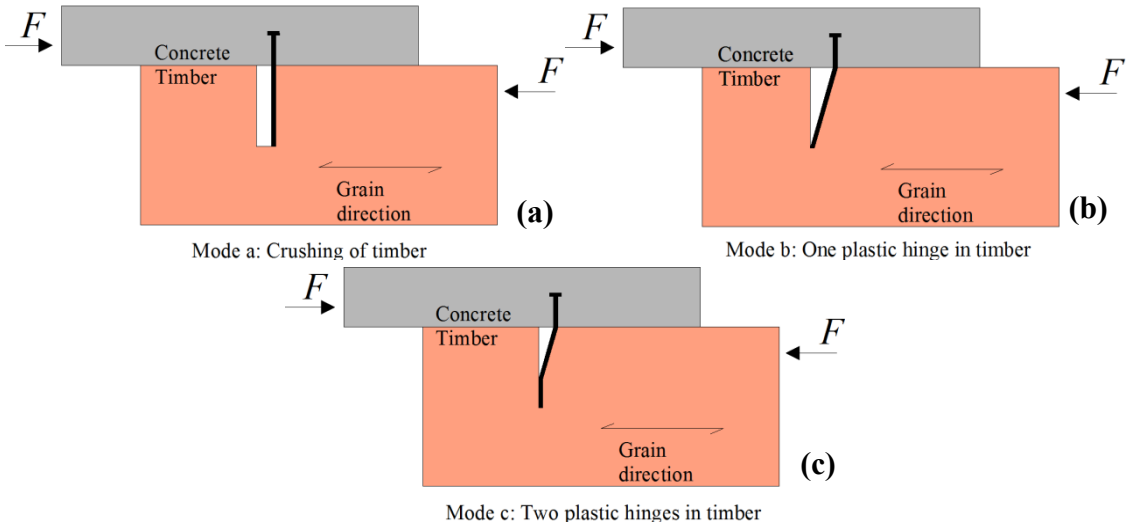

Figure 8-2 Failure modes of TCC connections (a) crushing of timber (mode (a)), (b) formation of one plastic hinge (mode(d)) and (c) two plastic hinges in timber (mode(f))

The embedment strength of the timber and fastener, $f_{h,k}$ is determined directly according to available codes for example ASTM5764 (1997) and EN383 (2007). Alternatively, analytical equations given by the literature predict the embedment strength of the timber. Eurocode 5 predicts the characteristic embedment strength of a screw with pre-drilled hole and the diameter up to 8mm embedded in the timber and LVL as:

$$f_{h,k}=0.082\rho_k(1-0.01d) \qquad (8\text{-}13)$$

where, d_{ef} is the effective diameter equal to 0.75 times the fastener diameter and ρ_k is the characteristic mass per unit volume of timber in kg/m^3.

In addition to the discussed failure modes proposed by European yield theory, the shear failure of connection contributes to the failure of timber connections and should be checked. The shear failure is approximated by Eurocode 4, part .1.1 EN (1994) as:

$$f_{shear}=\frac{0.8\sigma_y A}{\gamma_v} \qquad (8\text{-}14)$$

where, σ_y is shear yield stress of the fastener and Υ_v is material safety factor. σ_y is approximated as $0.6f_u$ and Υ_v is assumed to be 1.25.

8.2.2 Comparison of analytical and experimental strength results

The experimental data carried out by Khorsandnia et al. (2012) is used for verification of the models. The push out test consists of four TCC connection specimens utilising single wood screw, LVL joist and conventional concrete slab. The push-out

methodology and results were given in Chapters 5 and 10, respectively. The push-out test was undertaken in compliance with EN26891 (1991).

Johansen's Yield and Eurocode 5 EN (2004b) provides characteristic values of strength. In order to compare the characteristic values of analytical strength models with experimental strength, Ceccotti et al. (2006b) suggested calculating mean analytical values by dividing the characteristic values by 0.7. Hence, in this Section, the mean analytical strength values were calculated by dividing the characteristic values of strength obtained from Johansen's Yield and Eurocode 5 EN (2004b) by 0.7. The comparisons of Johansen's Yield and Eurocode 5 strength models (characteristic values divided by 0.7) and the experimental data are listed in Table 8-1.

The strength of connection approximated by Johansen's Yield and Eurocode 5 EN (2004b) are multiplied by 1.2 to be adjusted for TCC. Theoretically, reaching failures mode (f) with the formation of two plastic hinges is of interest as the most ductile failure regarding the safety of timber Structures (Johansen 1949).

In some of experiments, the penetration depth of the connectors in both concrete and timber added to slenderness of connectors which lead to the formation of two plastic hinges – one inside the timber and the other near the interface between timber and concrete in the concrete. Eurocode 5 EN (2004b) and Johansen strength models predict the strength of TCC connection utilising the wood screw with a relatively high underestimation errors of 32.1% and 21.1%, respectively and this agrees with previous investigations such as Ceccotti et al. (2006b) where a significant underestimation error of 42% between the strength model of Eurocode 5 and the push-out test of glued re-bar connections was reported. Hence, this study recommends further investigation on modification of the available strength models for TCC connections.

Table 8-1 Comparison of analytical and experimental results of single wood screw TCC

	Single screw(kN)	Johansen's theory(kN)	Eurocode 5 (kN)
Failure mode (a)	-	28.7	28.7
Failure mode (d)	-	12.5	23.2
Failure mode (f)	-	7.4	8.6
Screw Shear failure	-	10.2	10.2
Experimental result	10.9	-	-
Error (%)		-32.1	-21.1

Figure 8-3 illustrates the experimental data and the failure modes versus embedding depth of 100mm long wood screw in LVL in compliance with Eurocode 5 models. Figure 8-4 indicates the experimental data and the failure modes based on Eurocode 5 versus diameter of a wood screw with 65mm embedding depth in hySPAN LVL.

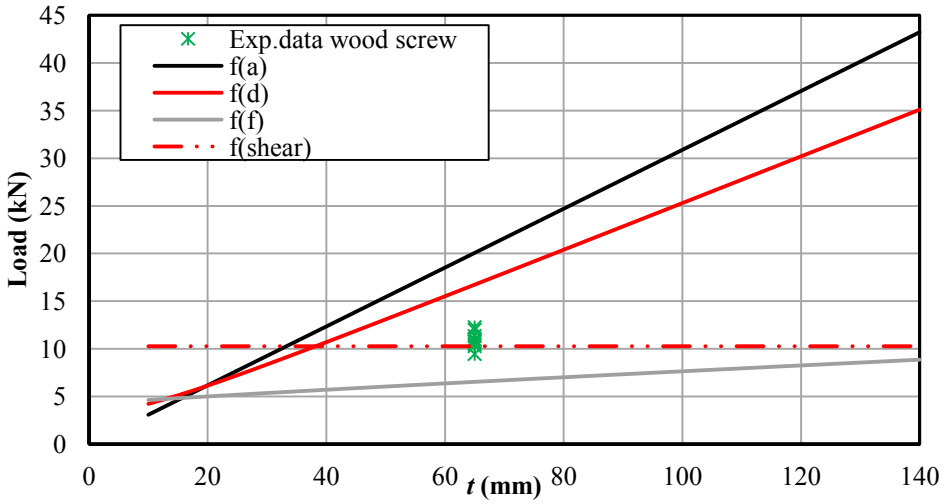

Figure 8-3 Failure modes versus embedded depth of wood screw based on Eurocode 5

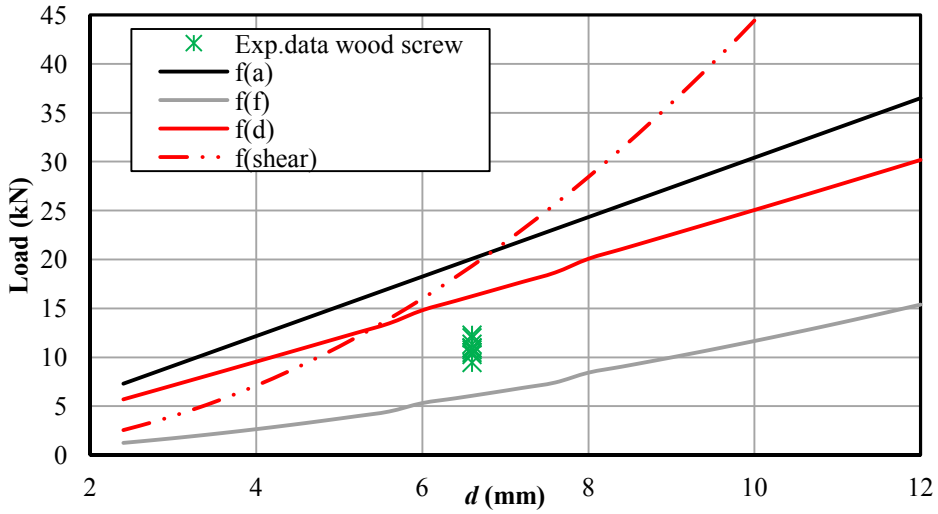

Figure 8-4 Failure mode vs. diameter of wood screw based on Eurocode 5

These failure maps are in agreement with the dominant failure mode in the experimental test as a combination of shear failure and the formation of plastic hinges in the screw. Persaud et al. (2006) plotted a non-dimensional parameter of $f/\sqrt{M_y f_{h,d} d}$ against the non-dimensional fastener penetration, $t/\sqrt{M_y / f_{h,d} d}$ to show the failure map of different failure modes proposed by Johansen theory as shown in Figure 8-5. At

$t/\sqrt{M_y/f_{h,d}d}$ =1.4, the governing failure mode changes from mode (a) to mode (d) whilst at $t/\sqrt{M_y/f_{h,d}d}$ =4.9, the dominant failure mode changes to mode (f). Hence, for a 100mm wood screw embedded in hySPAN LVL and conventional concrete the optimum penetration depth in timber corresponding to $t/\sqrt{M_y/f_{h,d}d}$ =4.9 is 41mm.

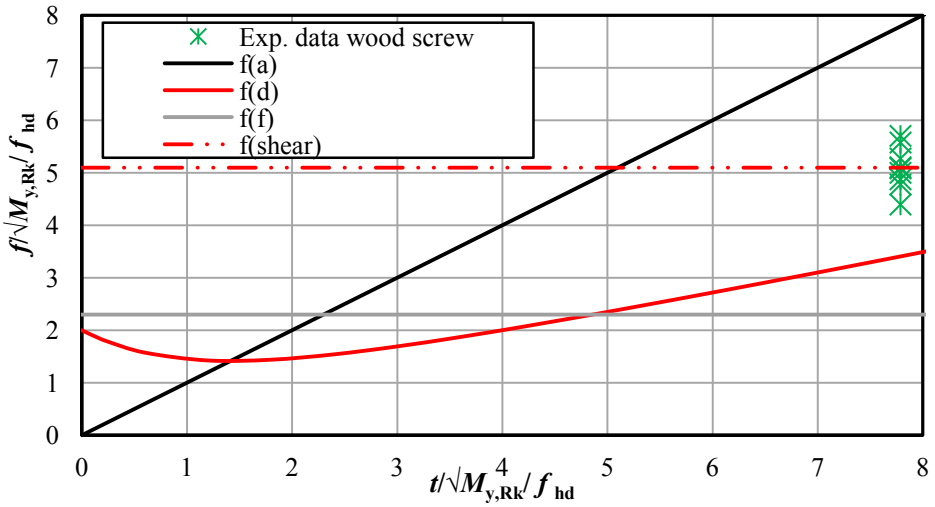

Figure 8-5 Failure modes vs. non-dimensional embedded depth of screw in compliance with Johansen model

Similar non-dimensional parameters were plotted utilising failure modes obtained from Eurocode 5 EN (2004b) which indicates slight differences particularly in modes (d) and (f) compared to Johansen yield theory as depicted in Figure 8-6.

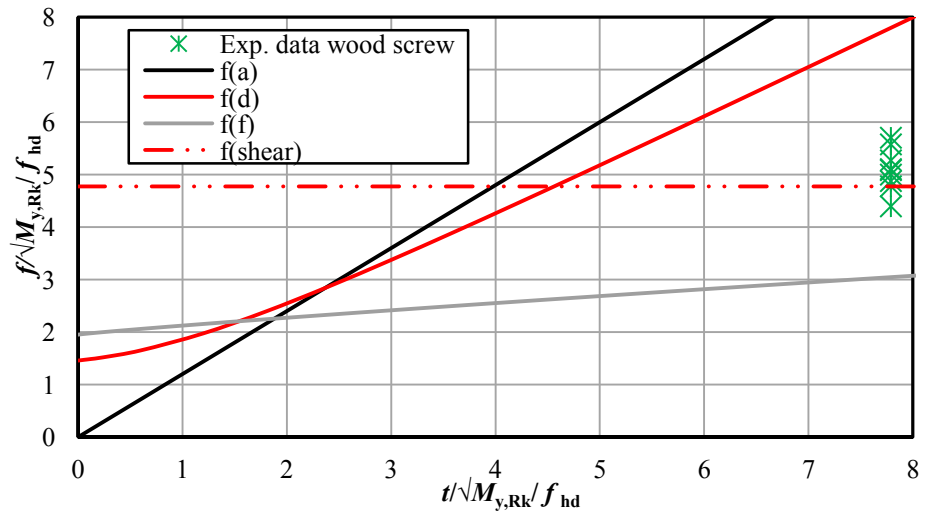

Figure 8-6 Failure modes versus non-dimensional embedded depth of screw in compliance with Eurocode 5Comparing the experimental data of single wood screw

connections and the failure maps, the non-dimensional failure maps particularly, the one using Eurocode 5 model agrees with the experimental strength and dominant failure mode as a combination of shear failure and the formation of plastic hinges in the screw. Further verification using more experimental data is required to make a comprehensive statement.

8.2.3 Strength model of inclined fastener

In order to overcome the limitations of Eurocode 5 for predicting the strength of inclined connections, a new model has been developed for predicting the strength of inclined crossed screws in TCCs. The strength model of crossed inclined fastener used in TCC connection consists of six failure modes which are derived based on some modification to the European yield model taking into account the embedment strength of the timber at an angle to the grain, the extra contribution of the withdrawal strength of the screw and alternative tensile and shear failure modes in the screw.

The aforementioned model assumes an upper bound collapse load and the failure strength is taken as the minimum of loads associated with the six failure modes. The failure modes consider the yield of screw in tension or shear, and some combined modes assume screw withdrawal, lateral crushing of the timber and the development of plastic hinges in the screw embedded in timber.

In order to apply the kinematic plastic method using the principle of virtual work, the presumed shape at collapse is postulated as part of the compatible displacement set whilst the external and internal loads are considered as the equilibrium set. In order to derive the equations, the kinematic plastic method of TCC connections assumes that the work done by the external applied load is equated with the energy dissipated during plastic deformation in either the screws, the timber or both. The external work done by the external force, W_E is the multiplication of collapse load, R by the corresponding slip at the interface of the concrete and timber, Δ_{lat} as shown in Equation (8-15) whilst the internal energy W_I dissipated by each failure mode is the internal work equal to the internal force times the localised displacement associated with each failure mode (Symons et al. 2010b).

$$W_E = R\Delta_{lat} \tag{8-15}$$

Equating the external work and internal dissipated energy, an upper bound on the collapse load of each supposed failure mode is obtained. Therefore, the lowest collapse load and the corresponding failure mode govern the behaviour of the connection.

$$W_E = W_I \tag{8-16}$$

The model assumes that the concrete remains undamaged whilst the screws and timber behaviour is perfectly plastic. Hence, the model neglects the effect of concrete properties. The model considers that one of crossed screws is inclined in the direction of slip acting in tension shear whilst the second one resists compression and shear forces. In addition, the model assumes that the screw does not fail in the concrete due to it being rigidly embedded within.

The friction forces between the timber and concrete for crossed screws balance each other. Hence, the friction forces are neglected in the case of crossed screws (Tomasi et al. 2010). The material properties of screw and timber such as embedment strength of timber, withdrawal and ultimate tensile strength of screw are required to predict the load carrying capacity of the connection.

8.2.3.1 Modes (a) and (b) – lateral displacement of screw and withdrawal of screw

Mode (a) indicates the horizontal displacement of the screw which crushes the timber without forming a plastic hinge (Figure 8-7a). The load carrying capacity in failure mode (a) is governed by the embedding strength of the surrounding timber. Eurocode 5, section 8.3 (EN 2004b) calculates the characteristic embedment strength of nails and screws embedded in timber and LVL with predrilled holes by:

$$f_{h,o,k} = 0.082\rho_k(1 - 0.01d) \tag{8-17}$$

where, d is 0.75 of screw diameter. Hence, the internal dissipated energy is found as:

$$W_I = f_{h,0,k} dt\Delta_{lat} \sin\alpha \tag{8-18}$$

Again, equating the external work, Equation (8-15) and internal dissipated energy, Equation (8-18), the load carrying capacity in failure mode (a) is obtained as:

$$f(a) = f_{h,0} dt \sin\alpha \tag{8-19}$$

where, d is 0.75 of the screw diameter, in mm. In the case of crossed screws, the right hand side of Equation (8-19) is multiplied by 2 to take into account the embedding failure of the second screw placed in compression.

Mode (b) states the withdrawal failure of the threaded part of the screw from the timber component without any sign of crushing in the timber as depicted in Figure 8-7b. In mode b, the screw is withdrawn from the timber without developing any embedding failure of the surrounded timber. Eurocode 5 EN (2004b) calculates the withdrawal strength, $f_{\alpha,0}$ of a screw perpendicular to the timber grain by:

$$f_{a,0}=0.0036\rho_k^{1.5} \tag{8-20}$$

where, ρ_k is the characteristic mass per unit volume of timber, in kg/m³.

In addition, Eurocode 5 derives the withdrawal strength of a screw inserted at an angle to the grain by:

$$f_{a,\alpha}=\frac{f_{a,0}}{1.5\cos^2\alpha+\sin^2\alpha} \tag{8-21}$$

where, α is inclination angle of screw axis to the grain. Eurocode 5 determines withdrawal load capacity of the inclined screw by introducing Equation (8-21) into:

$$F_{ax,\alpha}=(\pi dl_{ef})^{0.8}tf_{a,\alpha} \tag{8-22}$$

where, t is the embedded length of the screw in the timber and effective length, l_{ef} is t – d and d is the outer diameter of the screw. Thus, the internal dissipated energy is as:

$$W_I=F_{ax,\alpha}\Delta_{ax} \tag{8-23}$$

where, Δ_{ax} is the axial displacement of the fastener. Equating the external work, Equation (8-15) and internal dissipated energy, Equation (8-23), the load-bearing capacity in failure mode (b) is obtained as:

$$f(b)=\frac{F_{ax,\alpha}}{\cos\alpha} \tag{8-24}$$

It is noteworthy that the lateral and axial displacements are related together by:

$$\Delta_{axial}=\frac{\Delta_{lat}}{\cos\alpha} \tag{8-25}$$

The values of embedding and withdrawal stresses vary with the inclination angle of the screw to the grain direction of the timber. At an angle of 90°, the embedding stress is equal to the embedding stress parallel to the grain without any withdrawal stress, whilst at an angle of 0°, the embedding stresses reaches zero with the maximum withdrawal stress (Kavaliauskas et al. 2010).

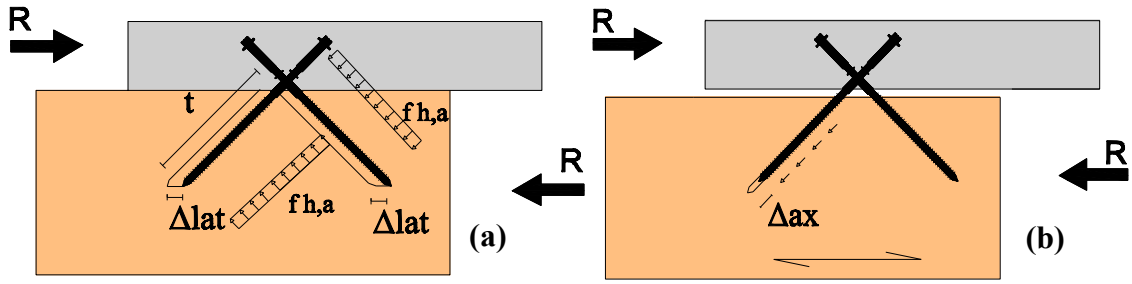

Figure 8-7 (a) Lateral displacement of screw and (b) screw withdrawn from timber

8.2.3.2 Modes (c) and (e) - tensile and shear failure of screw

The two failure modes (c) and (e) are presumed to only involve the fastener as tensile and shear failure of the screw at the interface of timber and concrete, respectively and depend on the tensile strength of the fastener. The tensile strength of the fastener is calculated by:

$$f(c)=\frac{F_{\mathrm{u}}}{\cos\alpha} \tag{8-26}$$

where, F_{u} is the ultimate tensile capacity of the screw which is measured by ultimate tensile test. Hence, the strength of the connection is governed by the tensile strength of the screw as:

$$f(c)=\frac{f_u \pi d^2}{4\cos\alpha} \tag{8-27}$$

where, f_{u} is the ultimate tensile strength of the screw.

The shear failure of the screw at timber-concrete interface is identified to be the second failure mode which involves only the fastener. Lower inclination the angle of screw to the grain, α, increases the cross-sectional area of the fastener at the timber-concrete interface, A_α as proposed by:

$$A_\alpha=\frac{\pi d^2}{4\sin\alpha} \tag{8-28}$$

Assuming that the shear yield stress of the screw is $0.6f_{\mathrm{u}}$, the strength corresponding to shear failure of the screw, mode (e) is calculated by:

$$f(e)=0.6f_{\mathrm{u}}A_\alpha=\frac{0.6f_{\mathrm{u}}\pi d^2}{4\sin\alpha} \tag{8-29}$$

In the case of crossed screws, a factor of two is used to take into account the shear failure of two screws simultaneously.

8.2.3.3 Modes (d) and (f)-single and double plastic hinges in screw

Considering the dowel effect in modes (d) and (f), mode (d) represents the formation of a single plastic hinge at the timber-concrete interface (Figure 8-8a) whilst mode (f) exhibits double plastic hinges, one at the timber-concrete interface and one along the portion of the screw embedded in the timber (Figure 8-8b). The free body diagram of part of the screw is also shown in Figure 8-8.

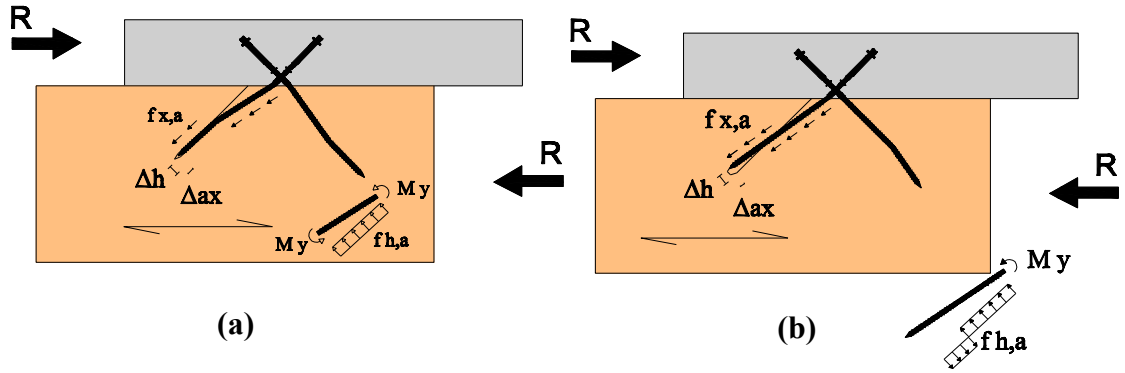

Figure 8-8 (a) Single plastic hinge and (b) double plastic hinges of screw

Eurocode 5 section 8.3 EN (2004b) calculates the yield moment M_y for round fasteners produced from wire with a minimum tensile strength of 600N/mm² by:

$$M_y = 0.3 f_u d^{2.6} \qquad (8\text{-}30)$$

where, d is the fastener diameter, in mm and f_u is the tensile strength of the wire, in N/mm². The appropriate embedded length and distribution of the embedment stress along the screw results in the formation of the plastic hinge at the timber-concrete interface. This failure coincides with a rigid rotation of the fastener about some point along the fastener which crushes the timber in front of the screw above the point of rotation and behind the screw below the point of rotation as illustrated in Figure 8-8 (Kavaliauskas et al. 2007; Symons et al. 2010b).

Two equations proposed by Symons et al. (2010b) were adjusted to calculate failure modes (d) and (f) associated with the formation of plastic hinges in crossed screws. Symons et al. (2010b) derived these equations based on some modification to EYM in the case of an inclined screw.

Satisfying the equilibrium of the moment about the timber-concrete interface, the distance between the rotation point and the interface of materials, x is calculated using:

$$x=\sqrt{\frac{M_{\mathrm{y}}}{f_{\mathrm{h},\alpha}}+\frac{t^2}{2}} \tag{8-31}$$

The lateral displacement of the tip of the screw Δ_{tip} is then calculated as the function of lateral displacement and x as given in:

$$\Delta_{\mathrm{tip}}=\frac{\Delta_{\mathrm{lat}}(t-x)}{x} \tag{8-32}$$

The internal energy which is dissipated by the embedment capacity of the timber, withdrawal of the screw and rotation of the fastener is shown in:

$$W_{\mathrm{I}}=f_{\mathrm{h},\alpha}d\sin\alpha\frac{\Delta_{\mathrm{lat}}}{2}+f_{\mathrm{h},\alpha}d(t-x)\sin\alpha\frac{\Delta_{\mathrm{tip}}}{2}+F_{\mathrm{ax},\alpha}\Delta_{\mathrm{axial}}+M_{\mathrm{y}}\sin\alpha\frac{\Delta_{\mathrm{lat}}}{x} \tag{8-33}$$

where, Eurocode 5 EN (2004b) determines the embedment strength of timber at an angle, α to the grain direction, $f_{\mathrm{h},\alpha}$ by:

$$f_{\mathrm{a},\alpha}=\frac{f_{\alpha,0}}{\cos^2\alpha+k_{90}\sin^2\alpha} \tag{8-34}$$

where, k_{90} is a modification factor calculated for LVL joist using:

$$k_{90}=1.3+0.015d \tag{8-35}$$

The internal dissipated energy equation (Equation 8-33) is equated to the external work done by the external force (Equation 8-15). Then, Δ_{lat} is cancelled out and Δ_{axial}, x and Δ_{tip} are substituted by the Equations (8-25), (8-31) and (8-32) into the Equation (8-33). Hence, the load carrying capacity in failure mode (f) is calculated by:

$$f(d)=f_{\mathrm{h},\alpha}d\sin\alpha\left(2\sqrt{\frac{M_{\mathrm{y}}}{f_{\mathrm{h},\alpha}}+\frac{t^2}{2}}-t\right)+F_{\mathrm{ax},\alpha}\cos\alpha \tag{8-36}$$

The embedding strength of timber and yield moment of the fastener govern the load-carrying capacity in modes (d) and (f) as the fastener displaces laterally and axially due to withdrawal and embedment forces. In mode (f) the point of rotation defines the second plastic hinge. The distance between the plastic hinges x is thus calculated in a similar way to that explained in mode (d), using:

$$x=\sqrt{\frac{M_{\mathrm{y}}}{f_{\mathrm{h,a}}}} \tag{8-37}$$

The internal energy which is dissipated by the embedment of timber, withdrawal of the screw and rotation of the plastic hinge is shown in Equation (8-38).

$$W_{\mathrm{I}}=f_{\mathrm{h},\alpha} d \sin\alpha \frac{\Delta_{\mathrm{lat}}}{2} + F_{\mathrm{ax},\alpha}\Delta_{\mathrm{axial}} + M_{\mathrm{y}} \sin\alpha \frac{\Delta_{\mathrm{lat}}}{x} \quad (8\text{-}38)$$

The internal dissipated energy, Equation (8-38) is equated to the external work done by the external force, Equation (8-15). Then, as stated in mode (d), Δ_{lat} is cancelled out and Δ_{axial} and x are substituted by Equations (8-25) and (8-37) into Equation (8-38). Hence, the load carrying capacity of mode (f) is represented by:

$$f(f)=2\sin\alpha\sqrt{f_{\mathrm{h},\alpha} M_{\mathrm{y}} d} + F_{\mathrm{ax},\alpha}\cos\alpha \quad (8\text{-}39)$$

In the case of crossed screws, a factor of two is used to take into account the formation of plastic hinges in compressive screws for modes (d) and (f). Using the equations above the failure load of six failure modes were calculated as listed in Table 8-3.

8.2.4 Comparison of analytical and experimental strength of inclined screws

The connection geometry and material properties used in the strength model are listed in Table 8-2. The material properties of the TCC components were discussed in Chapter 4.

Table 8-2 Material properties of TCC connections used in the model

Material properties of TCC connections	SPAX	Long SFS	Short SFS	coach
embedment in timber, t (mm) at α=30°, 45°,60°	100,120,136	120,142,152	100	95
diameter of screw, d (mm)	8.1	7.6	7.6	9.3
Measured embedment strength, $f_{\mathrm{h},0}$ (kN) based on ASTM5764 (1997)	46.2	46.4	46.4	45.8
Calculated withdrawal strength, $f_{\mathrm{a},0}$ (N/mm^2) based on EN (2004b)	52.9	52.9	52.9	52.9
Calculated withdrawal load, $F_{\mathrm{a},0}$ (kN) based on EN (2004b)	35.0	38.3	25.0	27.7
Measured tensile strength of screw, f_{u} (N/mm^2) based on EN1383 (1999)	1167.9	1221	984	461.2
Calculated yield moment of screw, M_{y} (N.mm) based on EN (2004b)	38172	33815	27251	15074
Measured mass per unit volume of LVL, ρ_{k} (kg/m^3) based on AS1080.3 (2000)		600		

Table 8-3 Summary of push-out test results and predictions of different test series

	crossed SPAX			crossed long SFS			crossed Short SFS			Single coach		
Load (kN)	WI30	WI45	WI60	WI30	WI45	WI60	WI30	WI45	WI60	WI30	WI45	WI60
Mode (a)	28.1	47.6	66.1	31.7	53.1	69.9	26.4	37.4	45.8	15.2	21.4	26.2
Mode (b)	22.0	34.7	60.7	24.6	38.2	63.6	21.0	28.3	44.5	23.3	31.3	49.2
Mode (c)	26.5	32.4	45.9	23.4	28.7	40.6	18.9	23.1	32.7	22.3	27.3	38.6
Mode (e)	55.0	38.9	31.8	48.7	34.4	28.1	39.2	27.7	22.6	23.2	16.4	13.4
Mode (d)	44.9	54.6	59.1	49.0	58.9	60.9	41.9	44.0	43.0	22.9	24	23.4
Mode(f)	38.7	43.1	41.1	42.1	45.9	41.6	36.2	35.2	31.1	19.3	18.5	15.9
governing mode	(b)	(c)	(e)	(c)	(c)	(e)	(c)	(c)	(e)	(a)	(e)	(e)
governing load	22.0	32.4	31.8	23.4	28.7	28.1	18.9	23.1	22.6	15.2	16.4	13.4
meanExp. CC2400	40.7	38.3	35.4	40.1	33.2	33.8	-	21.0	-	-	26.1	-
observed mode	(a)&(f)	(c)	(c)	(c)	(c)	(c)	-	(c)	-	-	(c)	-
Error (%)	-45.9	-15.4	-10.2	-41.6	-13.5	-16.7	-	10.0	-	-	-37.2	-
meanExp. EPS2000	32.3	35.2	32.3	34.9	30.8	25.3	-	17.3	-	-	-	-
observed mode	(a)&(f)	(c)	(c)	(c)or (a)&(f)	(c)	(c)	-	(a)&(f)	-	-	-	-
Error (%)	-31.9	-7.9	-1.5	-32.9	-6.8	11.1	-	33.5	-	-	-	-

The push-out test results of 90 TCC connector specimens using crossed SFS VB and SPAX screws inclined at an angle of 30°, 45° and 60° and single coach screws inclined at 45° which connect LVL joists and conventional concrete and EPS LWC2000 slabs were used to validate the analytical strength model of inclined screws. The push-out test methodology and the experimental results were reported in Chapter 5.

Table 8-3 illustrates the experimental and analytical results of strength for the different series. Failure modes observed in the push out test and dominant failure mode obtained from the model are also tabulated in Table 8-3.

The failure map of different failure modes of the strength model and experimental load capacity results of the CC and EPS LWC 2000 series utilising a single coach screw,

crossed short SFS, long SFS and SPAX inclined at 30°, 45° and 60° are plotted in Figures 8-9:8-12.

The influence of screw geometry (t/d) and effect of compressive screws in crossed screws compared to single tensile screws can be seen in different failure maps of crossed slender screws for example SPAX and SFS compared to coach screws or long SFS compared to short SFS screws as depicted in Figures 8-9:8-12.

It is observed that the experimental values were placed close to the dominant failure mode curves obtained from the analytical model. However, the experimental results especially the CC series are higher than the dominant failure modes. This variation in results could be due to the fact that the compression screw provides some resistance and contributes to the load carrying capacity during the push out test where a tensile failure of a screw in tension was identified as the dominant failure mode.

The predicted failure mode according to the model is tensile failure of a screw placed in tension for most of the cases and hence, tensile failure governs the strength of inclined TCC connections.

As seen in Chapter 5, a tensile failure of the tensile screw and the flexural deformation of the compressive screw with timber crushing at the compressive screw were observed as the dominant failure mode of the push out test in most of the test series and as tabulated in Table 8-3. This reinforced the good agreement between the experimental failure modes and the prediction.

However, the experimental results demonstrated different failure modes in the test series such as single coach screw at 45° and crossed screws inclined at ±60°. In most of these cases, the analytical model indicated a shear failure as the dominant failure mode whilst the observed failure in the experiment was tensile failure of the screw. This is attributed to the fact that the difference between tensile and shear failure modes in the experimental test of TCC connections with inclined screws is not obvious and in most of the cases the observed failure mode could be a combination of both failure modes.

The model was able to predict the shear strength of the crossed screws inclined at ±45° and ±60° accurately with a difference of 10-15% between the analytical and experimental results. However, the model was not accurate in strength prediction of crossed screws inclined at ±30°.

The analytical model underestimates the strength of TCC connections in most of the cases and the differences between the experimental and analytical results of crossed screws appear to follow a trend as an increasing of inclination angle to the grain results in the higher accuracy of the strength model for prediction of both the CC and EPS LWC series.

The underestimation is attributed to the fact that the analytical model has not taken into account the contributions of the compressive screw in the load carrying capacity of the tensile failure and the withdrawal of tensile screw (failure modes (c) and (b)). Hence, the model is purely reliant on the tensile screw.

However, the load is distributed between the tensile and compression screws before failure which enables the connection to carry more load. This is significantly highlighted at angles of 30° in both SPAX and SFS screws, where the load carrying capacity of the experimental test was noticeably higher than the analytical model as listed in Table 8-3. The effect of concrete properties is neglected in the calculations.

In this investigation, the effect of different types of concrete for example Scoria light-weight concrete, self-consolidating concrete and high-strength concrete on mechanical properties of crossed screws inclined at only ±45° were studied. Hence, further verification tests utilising these concrete types inclined at various angles such as ±30°, ±45° and ±60° are essential to include the influence of concrete types on the model calculations.

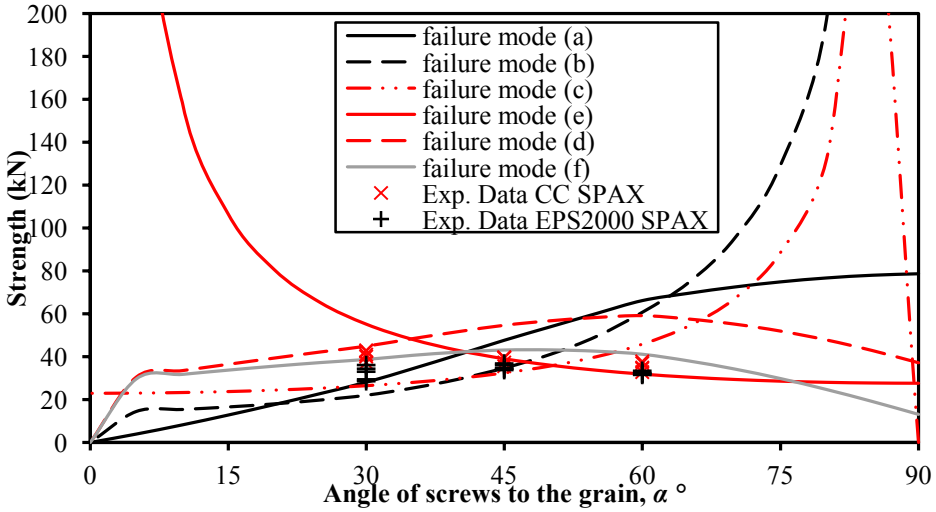

Figure 8-9 Failure map and strength of inclined crossed SPAX screws

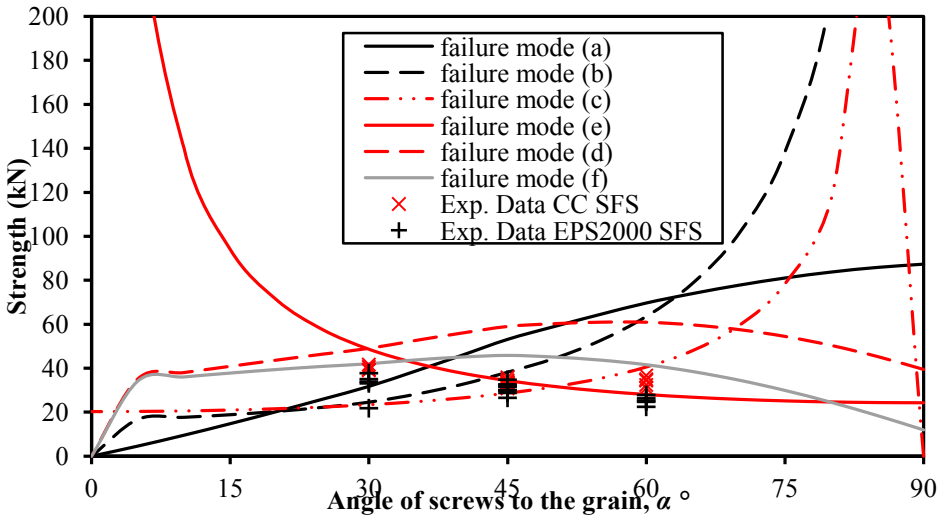

Figure 8-10 Failure map and strength of inclined crossed long SFS screws

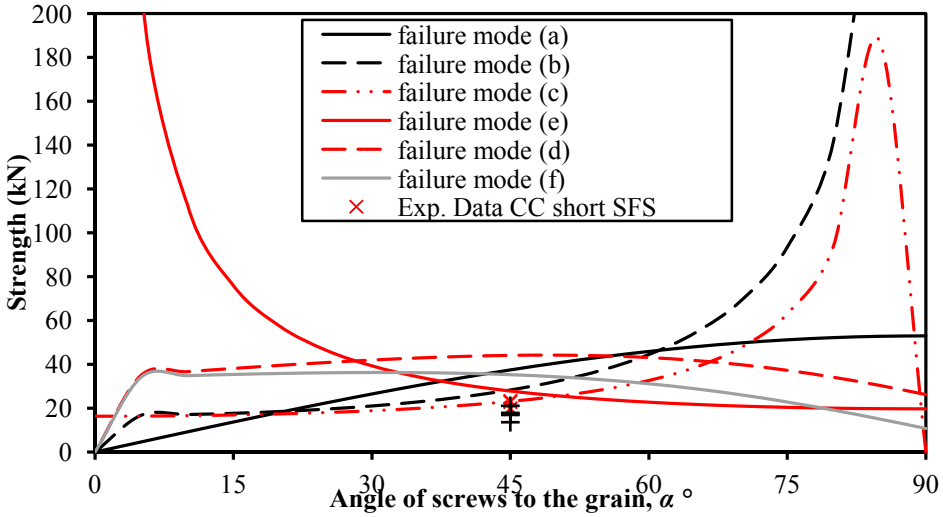

Figure 8-11 Failure map and strength of inclined crossed short SFS screws

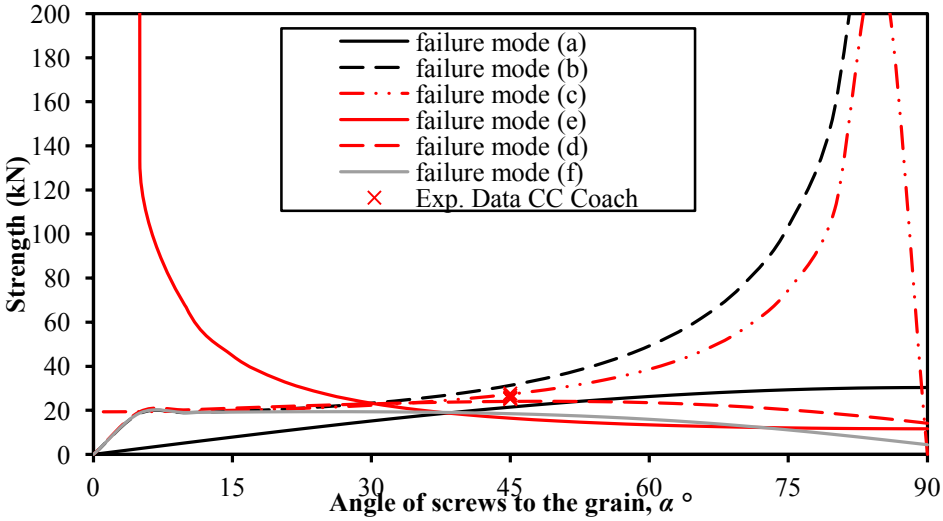

Figure 8-12 Failure map and strength of inclined single coach screw

8.3 STIFFNESS MODEL OF TCC CONNECTION

In this Section, available stiffness models of vertical and inclined fastener in TCC are reviewed and verified utilising experimental data.

8.3.1 Stiffness models of vertically inserted fastener

Herein, different available analytical models for the serviceability stiffness of vertically inserted timber composite connections such as simplified models and the models based on Winkler theory are discussed. Their methodology and required input parameters are also analysed.

The input parameters of the simplified models are limited to fastener diameter and mass per unit volume or modulus of elasticity (MOE) of timber whilst in addition to aforementioned parameters, the effect of the bearing behaviour of concrete and the length of fastener are taken into account in the models based on the Winkler theory.

Lack of appropriate verification of the available models seems to be a major limitation for their practical application in the design of a TCC floor. The available analytical models of the foundation modulus of timber and concrete are also discussed.

8.3.1.1 Stiffness model: Eurocode 5 EN (2004b)

Eurocode 5 EN (2004b) proposes an empirical equation to predict the characteristic serviceability stiffness, K_s of vertically inserted dowel-type fasteners such as dowels, bolts without clearance, screws and nails without pre-drilling in timber-timber connection.

In the case of TCC, a modification factor of two is taken into account to consider the presence of a concrete slab instead of one of the timber components as:

$$K_s = \rho_m^{1.5} \frac{d}{23} \tag{8-40}$$

where, ρ_m is the mean mass per unit volume of timber and d is the outer thread diameter of the fastener as defined in EN14592 (2008). The stiffness is approximated based on the fastener diameter and mass per unit volume of timber, and is valid for loading parallel to the grain whilst the effect of length of fastener is neglected.

8.3.1.2 Stiffness model: Zahn (1991)

Elsewhere, Zahn (1991) proposed a similar equation to the work proposed by Eurocode 5 EN (2004b) to approximate the serviceability stiffness of the single bolt timber-timber connector which was adopted by NDS (1997) as:

$$K_s = 246d^{1.5} \tag{8-41}$$

Similar to the model proposed by Eurocode 5 EN (2004b), a modification factor of two is adopted by the author to use the model for verification of the experimental data of wood screws used in a TCCs.

8.3.1.3 Stiffness model: Turrini et al. (1983) and Ceccotti (1995a)

Based on the experimental works, Turrini et al. (1983) and Ceccotti (1995a) proposed Equations (8-42) and (8-43), respectively to approximate the serviceability stiffness of timber composite connections using diameter of fastener, d and MOE of timber, E_t.

$$K_s = 0.08E_t d \tag{8-42}$$

$$K_s = 0.125E_t d \tag{8-43}$$

8.3.1.4 Stiffness model: Kuenzi (1955)

Previous investigations such as Hetényi (1946), Kuenzi (1955), Larsen (1975), Patton-Mallory et al. (1997b) and Gelfi et al. (2002) employed generic solutions of an elastic beam on an elastic foundation to approximate the elastic range of load-slip response and stiffness of vertically inserted fastener for timber composite connection (Patton-Mallory et al. 1997b). The beam on an elastic foundation under the acting external loads was studied first by Winkler (1867).

The Winkler theory of a beam on an elastic foundation simulates a vertically inserted fastener by a beam with flexural deforming whilst elastic foundations of distributed springs model timber and/or concrete components resisting the deformation of fastener. The Winkler theory states that the design values of timber composite connection with a single fastener depends on several parameters such as the material properties of timber and fastener. Moreover, the slip at interface of composite components, slip modulus, internal forces and moments and the deformation profile of the fastener along with the embedded length in timber associated with each stage of loading are approximated.

Kuenzi (1955) first employed the Winkler theory to introduce a differential equation to approximate the load carrying capacity and the elastic deformations of a single and double shear planes timber-timber connection by modelling the nail as a linear-elastic beam on an elastic foundation by:

$$EI\frac{d^4y}{dx^4}+ky=0 \tag{8-44}$$

where, k (k_t for timber, k_c for concrete) is the foundation modulus of the underestimation material whilst E and I are the MOE and second moment of area for the fastener. Equation (8-44) results in a general solution represented in:

$$y_t\ (x)=(B_{1t}\ \cos\lambda_t x+B_{2t}\ \sin\lambda_t x)e^{-\lambda_t x}+(B_{3t}\ \cos\lambda_t x+B_{4t}\ \sin\lambda_t x)e^{-\lambda_t x} \tag{8-45}$$

where,

$$\lambda_t=\sqrt[4]{\frac{k_t}{4E_s\ I_s}} \tag{8-46}$$

$$\lambda_c=\sqrt[4]{\frac{k_c}{4E_s\ I_s}} \tag{8-47}$$

B_i are constant coefficients based on the compatibility conditions.

Kuenzi (1955) assumed the stiffness of attached springs to be linear elastic. The reaction forces act perpendicular to the fastener axis and opposing the deflection of the fastener. Thus, there is compression in the surrounding timber and concrete in front of the fastener. These forces distributed along the fastener are proportional at every point to the deflection of the fastener at this point, $y(x)$ multiply by the foundation modulus, k as:

$$P(x)=ky(x) \tag{8-48}$$

Using compatibility conditions, Kuenzi (1955) approximated the slip at the interface of the timber composite connection by:

$$\Delta = F[2(L_1+L_2)-\frac{(J_1-J_2)^2}{K_1+K_2}] \tag{8-49}$$

where, L_1, L_2, J_1, J_2, K_1 and K_2 are calculated by:

$$L_1=\frac{\lambda_1}{k_1}[\frac{\sinh\lambda_1 t_1\cosh\lambda_1 t_1-\sin\lambda_1 t_1\cos\lambda_1 t_1}{\sinh^2\lambda_1 t_1-\sin^2\lambda_1 t_1}] \tag{8-50}$$

$$L_2 = \frac{\lambda_2}{k_2}[\frac{\sinh\lambda_2 t_2 \cosh \lambda_2 t_2 - \sin \lambda_2 t_2 \cos \lambda_2 t_2}{\sinh^2 \lambda_2 t_2 - \sin^2 \lambda_2 t_2}] \quad (8\text{-}51)$$

$$J_1 = \frac{\lambda_1^{\ 2}}{k_1}[\frac{\sinh^2\lambda_1 t_1 + \sin^2 \lambda_1 t_1}{\sinh^2\lambda_1 t_1 - \sin^2 \lambda_1 t_1}] \quad (8\text{-}52)$$

$$J_2 = \frac{\lambda_2^{\ 2}}{k_2}[\frac{\sinh^2\lambda_2 t_2 + \sin^2 \lambda_2 t_2}{\sinh^2\lambda_2 t_2 - \sin^2 \lambda_2 t_2}] \quad (8\text{-}53)$$

$$K_1 = \frac{\lambda_1^{\ 3}}{k_1}[\frac{\sinh\lambda_1 t_1 \cosh \lambda_1 t_1 + \sin \lambda_1 t_1 \cos \lambda_1 t_1}{\sinh^2 \lambda_1 t_1 - \sin^2 \lambda_1 t_1}] \quad (8\text{-}54)$$

$$K_2 = \frac{\lambda_2^{\ 3}}{k_2}[\frac{\sinh\lambda_2 t_2 \cosh \lambda_2 t_2 + \sin \lambda_2 t_2 \cos \lambda_2 t_2}{\sinh^2 \lambda_2 t_2 - \sin^2 \lambda_2 t_2}] \quad (8\text{-}55)$$

where, t_i is the embedded length of fastener in each component. The serviceability stiffness of the timber composite connection is approximated as load capacity (F) divided by slip at interface of composite materials (Δ) as shown in:

$$K = \frac{F}{\Delta} = [2(L_1 + L_2) - \frac{(J_1 - J_2)^2}{K_1 + K_2}]^{-1} \quad (8\text{-}56)$$

In the case of TCC connection, the timber and concrete components are assumed to be a Winkler foundation where elements of continuous beam displace perpendicular to the axis of fastener parallel to the compressive force without shear interactions between the adjacent elements.

The stiffness of the surrounded concrete and timber can be idealised by the springs attached to the fastener embedded in timber and concrete. The deformed shape of the fastener in timber and concrete is modelled by a continuous beam which is laid on the springs over its length.

8.3.1.5 Stiffness model: Gelfi et al. (2002)

Based on the Winkler theory, Gelfi et al. (2002) proposes a theoretical approach to predict serviceability stiffness of vertically inserted screws in TCC beams. In this model, a timber plank interlayer simulates the upgrading of an old timber floor by inserting the fastener into the timber plank as permanent formwork and casting a thin concrete slab. The interlayer is simulated as a gap between composite components then the transmitted loads are ignored as illustrated in Figure 8-13a and b.

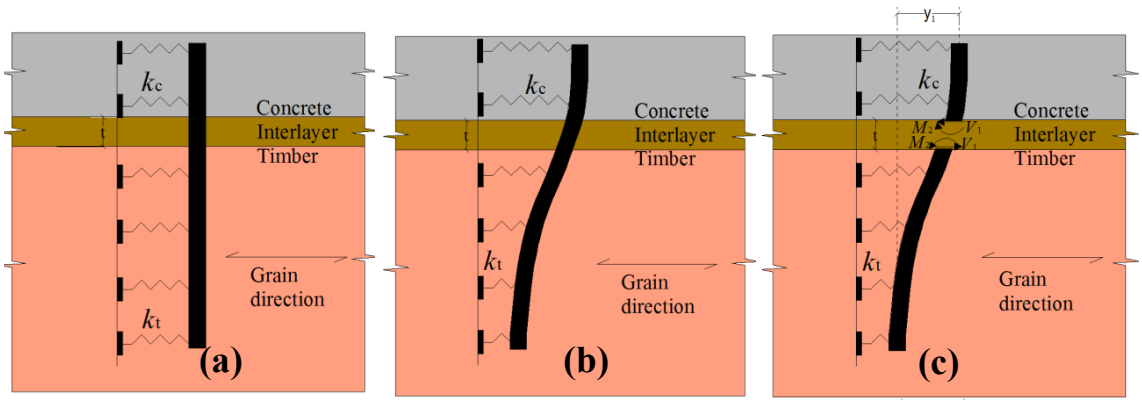

Figure 8-13 Stiffness model of vertically inserted fastener in TCC (a) undeformed, (b) deformed fastener and (c) internal forces of fastener

The material properties of concrete and timber are accounted by their foundation moduli whilst the bending stiffness of fastener indicates its material properties (Dias et al. 2010a). The fastener is assumed to behave as a Winkler beam with unlimited length in the concrete and timber.

The Winkler theory of the beam on elastic foundation assumes the following assumptions for simulation of TCC connection (Gabr et al. 1995; McLain et al. 1983; Patton-Mallory et al. 1997b):

• The behaviour of fastener is elastic perfectly plastic

• Winkler foundation (ignores shear strain)

• The connector fits tightly in the hole (no clearance)

• No friction between members or along the fastener

• Small displacement theory is valid

• The governing failure mode is crushing of timber beneath fastener (no splitting)

• Constant material properties through the thickness

The serviceability stiffness is calculated by the continuity of the flexural deformations for the fastener as the ratio of shear force to slip at interface of materials (y_{10}) in:

$$K_s = \frac{V_1}{y_{10}} \tag{8-57}$$

The compatibility equations of the fastener are calculated using the flexibility method approach assuming the timber and concrete components as elastic materials as:

$$q_{\mathrm{m}} = f_{\mathrm{m}} Q_{\mathrm{m}} + q_{\mathrm{om}} \tag{8-58}$$

$$\begin{bmatrix} y_{11} & y_{12} \\ \theta_{21} & \theta_{22} \end{bmatrix} \begin{bmatrix} V_1 \\ M_2 \end{bmatrix} + \begin{bmatrix} y_{10} \\ \theta_{20} \end{bmatrix} = 0 \tag{8-59}$$

where, Q_{m} is matrix of redundant and q_{m} and q_{om} represent the matrices of actual displacements corresponding to the redundant and actual displacements corresponding to the redundant action and due to the loads, respectively. The flexibility matrix, f_{m} size (2x2) and its flexibility coefficient of y_{11}, y_{12}, θ_{21} and θ_{22} are determined from the solution of the beam on elastic foundation formula whilst V_1 and M_2 indicate the internal loads acting on the free end of the beam as depicted in Figure 8-13c.

Moreover, the rotation and deformation of the fastener at the very end distance from interface are assumed to be zero. The flexibility coefficients of the flexibility matrix are determined by summation of the displacements and rotations of the beam embedded in the elastic foundation of concrete, timber and interlayer as given in Equations (8-60):(8-63).

$$\theta_{20} = 0 \tag{8-60}$$

$$y_{11} = \frac{2\lambda_{\mathrm{c}}}{k_{\mathrm{c}}} + \frac{2\lambda_{\mathrm{t}}}{k_{\mathrm{t}}} + \frac{4\lambda_{\mathrm{t}}^{\,2}}{k_{\mathrm{t}}} t + \frac{4\lambda_{\mathrm{t}}^{\,3}}{k_{\mathrm{t}}} t^2 + \frac{t^3}{3E_{\mathrm{s}}I_{\mathrm{s}}} \tag{8-61}$$

$$\theta_{21} = y_{21} = \frac{2\lambda_{\mathrm{c}}^{\,2}}{k_{\mathrm{c}}} - \frac{2\lambda_{\mathrm{t}}^{\,2}}{k_{\mathrm{t}}} - \frac{4\lambda_{\mathrm{t}}^{\,3}}{k_{\mathrm{t}}} t - \frac{t^2}{2E_{\mathrm{s}}I_{\mathrm{s}}} \tag{8-62}$$

$$\theta_{22} = \frac{4\lambda_{\mathrm{c}}^{\,3}}{k_{\mathrm{c}}} - \frac{4\lambda_{\mathrm{t}}^{\,3}}{k_{\mathrm{t}}} + \frac{t}{E_{\mathrm{s}}I_{\mathrm{s}}} \tag{8-63}$$

Eliminating M_2 in Equation (8-59), the stiffness of connection is obtained from:

$$K_{\mathrm{s}} = \frac{12\lambda_{\mathrm{t}}\lambda_{\mathrm{c}}\, E_{\mathrm{s}}I_{\mathrm{s}}}{3(\lambda_{\mathrm{t}}^{\,2} + \lambda_{\mathrm{c}}^{\,2})(\lambda_{\mathrm{t}} + \lambda_{\mathrm{c}}) + 3t\lambda_{\mathrm{t}}\lambda_{\mathrm{c}}(\lambda_{\mathrm{t}} + \lambda_{\mathrm{c}})^2 + 3(t\lambda_{\mathrm{t}}\lambda_{\mathrm{c}})^2(\lambda_{\mathrm{t}} + \lambda_{\mathrm{c}}) + (t\lambda_{\mathrm{t}}\lambda_{\mathrm{c}})^3} \tag{8-64}$$

where, t is thickness of the interlayer.

8.3.2 Foundation modulus models

Herein, the available models to approximate the foundation moduli of timber and concrete are reviewed.

8.3.2.1 Foundation modulus model of timber: Kuenzi (1955)

Kuenzi (1955) approximates the foundation modulus of timber in parallel and perpendicular to the grain directions using:

$$k_t = E_{t,\alpha} \frac{d}{Z} \tag{8-65}$$

where, d is the diameter of the fastener, Z is the foundation depth, and $E_{t,\alpha}$ is the modulus of elasticity of timber in parallel and perpendicular directions whilst Z is a constant and assumed to be about 25mm.

8.3.2.2 Foundation modulus model of concrete: Gelfi and Giuriani (1987)

There are few experimental data available for the foundation modulus of concrete. Gelfi et al. (1987) estimates the foundation modulus of concrete, k_c by:

$$k_c = \frac{E_c}{\beta} \tag{8-66}$$

where, E_c is the MOE of the concrete and β is a factor as a function of the fastener's diameter to spacing ratio ranging between 2.5-3.3.

The foundation modulus of concrete is much stiffer than engineered wood whilst the embedded head of screw in concrete component provides additional interlocking (Symons et al. 2010a).

8.3.3 Comparison of models and experimental results

The experimental data carried out by Khorsandnia et al. (2012) is used for verification of the models. The push out test consists of four TCC connection specimens utilising a single wood screw, LVL joist and conventional concrete slab. The push-out methodology, stiffness analysis and results were given in Chapters 5 and 10.

Different available models for serviceability stiffness of timber composite connections connected with mechanical fastener were discussed.

Table 8-4 lists the connection geometry and material properties of a wood screw connection used in TCC. A summary of the push-out test results and predictions of the available stiffness models of TCC connections using wood screw is shown in Table 8-5. The stiffness results of simplified models were calculated by dividing the characteristic values by 0.7.

Table 8-4 Summary of material properties of TCC connection with wood screw

Material properties of TCC connection	Value
Outer thread diameter of screw, d (mm)	6.6
Shank diameter of screw, d (mm)	5.2
MOE of screw, E_s (MPa)	210000
MOE of LVL, E_t(MPa)	13746
Measured mass per unit volume of LVL, ρ_k (kg/m^3)	600
Embedment depth in timber, t_1 (mm)	65
Embedment depth in concrete, t_2 (mm)	35
Foundation modulus of LVL, k_t (MPa)$^+$	384
Foundation modulus of concrete, k_c (MPa)*	7160

$^+$Obtained from Franke et al. (2011)
*Obtained from Dias et al. (2010b)

Table 8-5 Summary of experimental and analytical data of serviceability stiffness

Results	K_{ser} (kN/mm)	Error (%)
Experiment (CoV=35.7)	12.3	-
Eurocode 5 EN (2004b)	8.4	-31.6
Zahn (1991)	8.3	-32.4
Turrini et al. (1983)	7.1	-42.2
Ceccotti (1995a)	11.1	-9.7
Kuenzi (1955)	4.5	-63.6
Gelfi et al. (2002)	4.5	-63.6

The simplified stiffness models that is Eurocode 5 EN (2004b), Turrini et al. (1983) and Zahn (1991) underestimated the experimental data of wood screw with an error ranging approximately 10-40% whereas the models based on Winkler theory that is Kuenzi (1955) and Gelfi et al. (2002) calculated a much lower stiffness compared to that of the experimental test with an error of approximately 60%.

The low foundation moduli of wood screw obtained from the experimental test as listed in Table 8-4 is attributed to this high underestimation. However, if the foundation modulus value calculated by the foundation modulus model of Kuenzi (1955) (Equation (8-65)) is employed, a suitable agreement between experimental and analytical stiffness results will be achieved. It is noted that the models based on Winkler theory are not

suitable to calculate the stiffness of TCC connections utilising a screw with small diameter. The accuracy in simplified stiffness models is different where Ceccotti (1995a) indicates appropriate agreement with the experimental data whereas other simplified models show notable difference between analytical and experimental data.

The under estimation error of simplified stiffness models is as expected and agrees with literature. For example Ceccotti et al. (2006b) reported a high difference of 40% for analytical and experimental serviceability stiffness of glued re-bar TCC connections.

The underestimation of simplified stiffness models is due to the fact that these models only consider limited parameters such as fastener diameter and MOE of timber whereas, the important parameters such as foundation moduli of timber, slenderness of fastener, its embedding length and MOE are ignored.

The underestimated stiffness and strength lead to the larger resistance but brittle failure of the composite beam whilst an accurate approximation of stiffness and strength by push-out test or some modifications of the predictive models are crucial in order to have a ductile design.

8.3.4 Stiffness of inclined screw based on Winkler theory

Herein, for TCC connection, the timber and concrete components are assumed to be a Winkler foundation where elements of a continuous beam displaces vertically perpendicular to the axis of the fastener and parallel to the compressive forces. The stiffness and deformation of the fastener in the surrounding concrete and timber can be idealised by a continuous beam which is attached to the springs over the entire length of the fastener. Assuming the stiffness of attached springs to be linear elastic, Kuenzi (1955) proposed Equation (8-44) to predict the slip modulus of the timber connection whilst Foschi (1974) extended the stiffness of spring to non-linear range assuming an ideal elastic–plastic steel for the fastener and smooth elastic–plastic for nail.

A large number of shear connections including bolts and screws indicate non-linear responses even during the early stages of loading hence, the non-linear assumption seems to be more applicable (Gabr et al. 1995; Patton-Mallory et al. 1997b).

The reaction forces act perpendicular to fastener axis and opposing the deflection of the fastener. Thus, there is compression in the surrounding timber and concrete in front of the fastener. These compressive forces that are distributed along the fastener are proportional at every point to the deflection of the fastener at this point multiplied by

Symons et al. (2010a) the constant k (foundation modulus expressed in kN/mm^2) which is calculated in compliance with different codes such as ASTM5764 (1997) and EN383 (2007).

Symons et al. (2010a) extends the model of vertical to the inclined fastener assuming a two-dimensional elastic foundation by additional springs resisting vertical translation of screws which is perpendicular to the grain direction as shown in Figure 8-14a and b.

The timber is considered as the elastic foundation consisting of orthogonal springs with different stiffness in the parallel and transverse to the grain directions. The screw is inclined at an angle of θ to the vertical direction whilst the grain direction is horizontal. The timber is assumed to be an elastic material whilst rigid concrete clamps the fastener at the interface of timber and concrete. Hence the portion of screw embedded in timber is only considered for the model. The shear force at the interface leads to a horizontal slip at the interface of composite materials.

Figure 8-14c shows part of a screw of length of dx from a whole length of t embedded in timber whilst y and υ represent the transverse and axial displacements of the part in the timber. The vertical and horizontal springs simulate the foundation moduli of timber transverse and parallel to the grain direction impeding the vertical and horizontal displacements of the screw. The foundation moduli of timber parallel and transverse to the grain k_p and k_t account for the stiffness of the spring per unit length in the vertical and horizontal directions. Axial force, shear force and bending moment are indicated by means of the variables N, V and M, respectively. The effect of friction between composite components is neglected in calculation of the equilibrium of the screw.

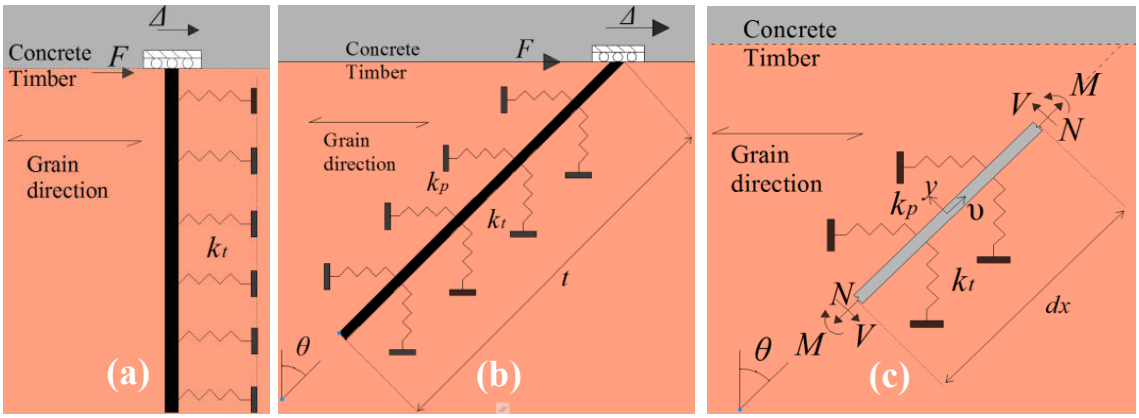

Figure 8-14 Stiffness model of (a) vertical and (b) inclined fastener TCC connection with rigid behaviour of concrete and (c) internal forces in element of inclined fastener

Foundation modulus of timber in Equation (8-44) can be given in the form of:

$$k=\frac{dV}{dy}\frac{1}{dx} \tag{8-67}$$

Hence, Equation (8-44) is written as:

$$EI\frac{d^4y}{dx^4}+\frac{dV}{dx}=0 \tag{8-68}$$

The horizontal and vertical forces which act on the part of the screw are determined as foundation moduli of timber multiplied by the associated resisting displacements as indicated in:

$$F_P=k_p\,\Delta_p=k_p\,dx\cos\theta(y\cos\theta+\upsilon\sin\theta) \tag{8-69}$$

$$F_t=k_t\,\Delta_t=k_t\,dx\sin\theta\,(\upsilon\cos\theta-y\sin\theta) \tag{8-70}$$

Satisfying the equations of equilibrium of the fastener, the shear and axial forces acting on the part of screw are calculated in the form of a combination of horizontal and vertical forces in the springs as given in:

$$N=EA\frac{d\upsilon}{dx}=F_t\cos\theta+F_P\sin\theta=k_p\,dx\cos\theta(y\cos\theta+\upsilon\sin\theta)\sin\theta+ k_t\,dx\sin\theta\,(\upsilon\cos\theta-y\sin\theta)\cos\theta \tag{8-71}$$

$$V=F_t\sin\theta-F_P\cos\theta=k_p\,dx\cos\theta(y\cos\theta+\upsilon\sin\theta)\cos\theta+ k_t\,dx\sin\theta\,(\upsilon\cos\theta-y\sin\theta)\sin\theta \tag{8-72}$$

The friction between composite components is neglected in the calculations. The derivations of shear and axial forces are determined by:

$$\frac{dV}{dx}=-EI\frac{d^4y}{dx^4}=(y\cos\theta+\upsilon\sin\theta)\,k_p\cos^2\theta-(\upsilon\cos\theta-y\sin\theta)\,k_t\sin^2\theta \tag{8-73}$$

$$\frac{dN}{dx}=EA\frac{d^2\upsilon}{dx^2}=-[(y\cos\theta+\upsilon\sin\theta)\,k_p+(\upsilon\cos\theta-y\sin\theta)\,k_t]\sin\theta\cos\theta \tag{8-74}$$

The shear force at the interface of timber and concrete is given as a combination of axial and shear forces acting on the part of screw at the interface by:

$$F=N\sin\theta-V\cos\theta \tag{8-75}$$

Symons et al. (2010a) proposed that in the case of a long screw with higher *t*/*d* ratio for example 30, the axial deformation of the screw is important where the shear force for most of the length of screw is zero. Hence, for a very long screw, Equation (8-72) is

equal to zero and the relation between the axial and lateral displacement of the screw is changed to:

$$y = -\upsilon \frac{(1 - \beta \tan\theta)\tan\theta}{(1 + \beta \tan^3 \theta)} \tag{8-76}$$

where, β is ratio of k_t/k_p. Symons, Persaud and Stanislaus (2010a) stated that substitution of Equation (8-76) in Equation (8-74) leads in the differential equation of:

$$y = \frac{d^2\upsilon}{dx^2} - \frac{d\upsilon}{\frac{(1 + \beta \tan^3 \theta)EA}{k_p \beta \tan\theta} \cos\theta} \tag{8-77}$$

Compatibility condition enforces that the axial deformation of the fastener at the very end distance from the interface is zero. Hence, Equation (8-77) leads to Equation (8-78) as the axial force acting on the screw at the interface of timber and concrete.

$$N(x = 0) = \frac{\upsilon_0}{\sqrt{\frac{(1 + \beta \tan^3 \theta)EA}{k_p \beta \tan\theta} \cos\theta}} EA \tanh \frac{t}{\sqrt{\frac{(1 + \beta \tan^3 \theta)EA}{k_p \beta \tan\theta} \cos\theta}} \tag{8-78}$$

Substitution of Equation (8-78) into Equation (8-75) gives the force at the interface. Consequently the slip modulus of a long slender inclined screw as used in the TCC is approximated by:

$$K = \frac{F}{\Delta} = \frac{EA}{\sqrt{\frac{(1 + \beta \tan^3 \theta)EA}{k_p \beta \tan\theta} \cos\theta}} \tanh\left(\frac{t}{\sqrt{\frac{(1 + \beta \tan^3 \theta)EA}{k_p \beta \tan\theta} \cos\theta}}\right) \sin^2 \theta \tag{8-79}$$

It is noteworthy to state that a factor of two takes into account the contribution of the second screw placed in tension in the stiffness of crossed screws TCC connections.

8.3.5 Comparison of models and experimental results

The push-out test results of 65 TCC connector specimens using crossed SFS VB and SPAX screws inclined at an angle of 30°, 45° and 60° inserted in LVL joists and conventional concrete or EPS LWC2000 slabs were used to validate the analytical stiffness model of crossed screws. The material properties of SFS VB screw, LVL and concrete were given in Chapter 4. Table 8-6 lists the input parameters of stiffness models for SFS and SPAX screws embedded in hySPAN LVL.

Table 8-6 Summary of mechanical properties of TCC connection used in the model

Material properties of TCC connections	Value
embedment depth of SFS screw in timber t (mm) for θ=±30°,±45°, ±60°	152, 142, 120
embedment depth of SPAX screw in timber t (mm) for θ=±30°,±45°, ±60°	136, 120, 100
Shank diameter of SFS screw, d (mm)	6.0
Shank diameter of SPAX screw, d (mm)	5.7
MOE of SFS and SPAX screws (N/mm^2)	210000
Foundation modulus of LVL parallel to the grain (bolt dia 6mm) (N/mm^2)*	384.5
Foundation modulus of LVL transverse to the grain (bolt dia 6mm) (N/mm^2)*	129.0
Foundation modulus of LVL parallel to the grain (bolt dia 8mm) (N/mm^2)*	444.8
Foundation modulus of LVL transverse to the grain (bolt dia 8mm) (N/mm^2)*	193.1

* based on embedding test carried out by Franke et al. (2011)

A summary of the push-out test results and predictions of serviceability slip modulus of crossed (±30°, ±45° and ±60°) SFS VB and SPAX screws is listed in Table 8-7.

Table 8-7 Experimental and analytical stiffness results of SFS and SPAX screws

Test series	Mean exp. $K_{s,0.4}$ (kN/mm)	CoV (%)	Analytical $K_{s,0.4}$ (kN/mm)	Error (%)
CC SFS WI60 (Θ=30)	34.2	41.3%	43.5	27.1%
CC SFS WI45 (Θ=45)	28.8	51%	49.7	72.5%
CC SFS WI30 (Θ=60)	36.8	10.1%	38.4	4.3%
CC SPAX WI60 (Θ=30)	29.7	17.9%	37.1	24.9%
CC SPAX WI45 (Θ=45)	25.3	14.9%	45.1	78.3%
CC SPAX WI30 (Θ=60)	40.1	18.6%	33.3	-16.9%
EPS LWC SFS WI60 (Θ=30)	27.0	9.6%	43.5	61.1%
EPS LWC SFS WI45 (Θ=45)	43.0	22.5%	49.7	15.6%
EPS LWC SFS WI30 (Θ=60)	59.9	24%	38.4	-35.9%
EPS LWC SPAX WI60 (Θ=30)	38.1	49.8%	37.1	-2.6%
EPS LWC SPAX WI45 (Θ=45)	39.5	33.8%	45.1	14.2%
EPS LWC SPAX WI30 (Θ=60)	53.9	27%	33.3	-38.2%

Figures 8-15:8-18 plot the analytical and experimental serviceability stiffness of CC and EPS LWC series using crossed SFS and SPAX screws inclined at ±30°, ±45° and ±60°.

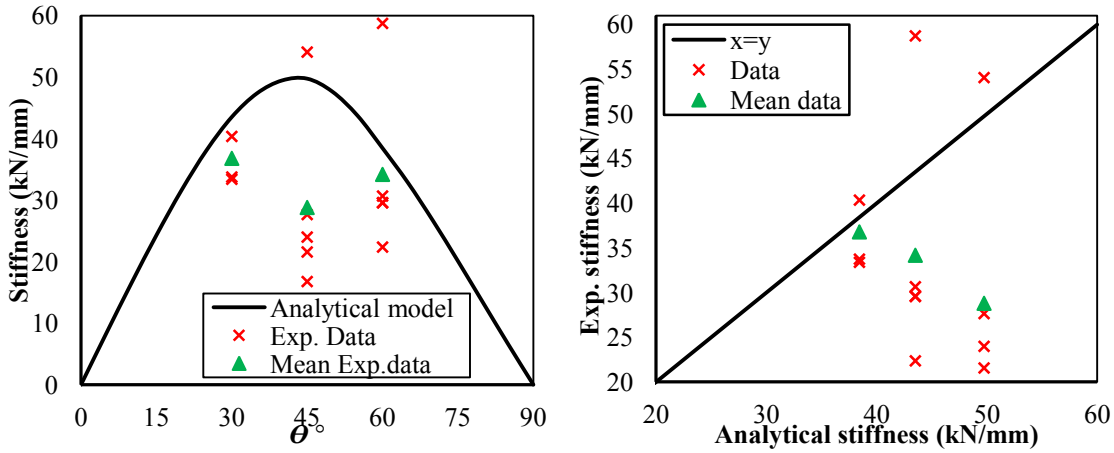

Figure 8-15 Analytical model vs. experimental results of CC SFS series

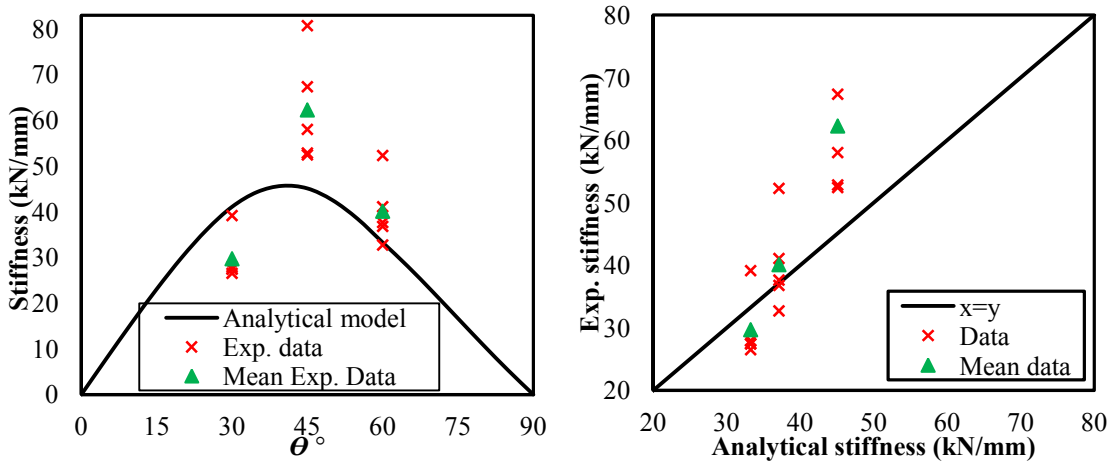

Figure 8-16 Analytical model vs. experimental results of CC SPAX series

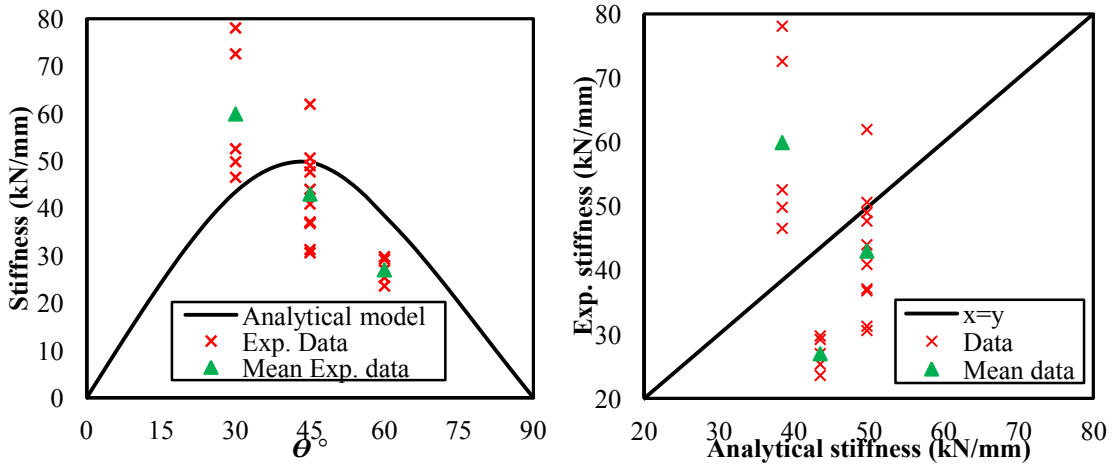

Figure 8-17 Analytical model vs. experimental results of EPS LWC2000 SFS series

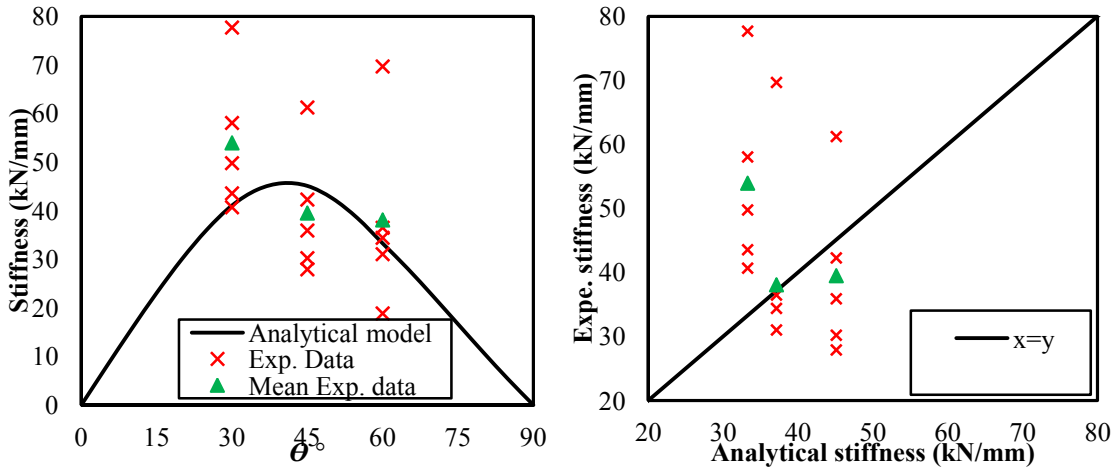

Figure 8-18 Analytical model vs. experimental results of EPS LWC2000 SPAX series

The experimental serviceability stiffness was calculated in compliance with EN26891 (1991) as given in Chapter 5. The analytical model considers only axial deformation of screw which agrees with the tensile failure of screw in tension as reported in Chapter 5.

The experimental test of the CC series quantified the serviceability slip modulus of the different test series specimens representing less differences to the predicted value for Θ=60° and 30° series ranging between -16.9-4% and 24.5-27.1%, respectively whilst a maximum difference of 72.5-78.3% was observed for the stiffness of the Θ=45° series.

The experimental test of EPS LWC exhibits a less difference to the predicted value for Θ=45° ranging between 14.2%-15.6% whereas a maximum difference of 61.1% was observed for the stiffness of the SFS Θ=30° series (Table 8-7). The medium difference of 35.9%-38.2% was observed in Θ=60° series.

Among different experimental series, the Θ=60° series indicates the maximum serviceability slip modulus of both the CC and EPS LWC series whereas the Θ=30° and Θ=45° series represent the minimum stiffness of the CC and EPS LWC series, respectively (Table 8-7).

In the case of the conventional concrete series utilising inclined screws, the factor of two is an upper limit and it was observed that the modification factor of two overestimates the stiffness of some experimental test series.

In the case of the EPS light-weight concrete series utilising inclined screws, the serviceability stiffness is 28-63% higher than similar conventional concrete series.

It adds to the complexity of the verification and it leads to underestimation of the experimental results in some series such as EPS LWC SFS WI30 and EPS LWC SPAX WI30.

Hence, to derive a more precise model in future study, revision of the modification factor utilising more experimental series is recommended. The load-slip response and failure of the series were reported in Chapter 5.

8.3.6 Stiffness of inclined screw based on Tomasi et al. (2010)

Elsewhere, Tomasi et al. (2010) proposed an analytical model to predict stiffness of single and crossed screws inclined at an angle to the grain of timber-timber connections.

Two different forces of F_{lat} and F_{ax} are defined to be the elastic forces acting perpendicular and parallel to the axis of the fastener placed in tension and assuming a linear-elastic behaviour of the screw at serviceability limit state(SLS), lateral and axial forces are written in the form of displacements by:

$$F_{lat}=K_{\perp}\delta_{\perp} \tag{8-80}$$

$$F_{ax}=K_{\parallel}\delta_{\parallel} \tag{8-81}$$

where, $K\perp$ and $K\parallel$ are the stiffness of connector for lateral and withdrawal loadings and $\delta\perp$ and $\delta\parallel$ represents perpendicular and parallel components of slip. The slip at the interface of composite components, δ of an undeformed fastener resolves into:

$$\delta\perp=\delta\cos\theta \tag{8-82}$$

$$\delta_{\parallel}=\delta\sin\theta \tag{8-83}$$

For crossed screws inclined at an angle of $\pm\theta$ to the vertical direction, the equilibrium of lateral load at SLS, F_{ser} is written as the sum of the load-carrying contribution of the tensile and compressive screws as:

$$F_{ser}=F_{lat}\cos\theta+F_{ax}\sin\theta \tag{8-84}$$

And consequently the stiffness is given by:

$$K_{ser}=\frac{F_{ser}}{\delta}=K_{\perp}\cos^2\theta+K_{\parallel}\sin^2\theta \tag{8-85}$$

$K_{\perp}$ can be calculated using the analytical models of vertically inserted fastener as discussed in Section 6.6 whilst German Institute for Building Technology approximates $K_{\parallel}$ by:

$$K_{\text{ser,ax,i}}=30td \tag{8-86}$$

where t is the embedment length, in mm, of the threaded part of the screw, and d is the outer diameter of the screw thread, in mm (Bautechnik 2006).

8.3.7 Comparison of models and experimental results

A summary of the push-out test results and stiffness predictions based on the Tomasi et al. (2010) model for crossed (±30°, ±45° and ±60°) SFS VB and SPAX screws utilising CC and EPS LWC2000 is listed in Table 8-8.

Table 8-8 Experimental and analytical stiffness results of SFS and SPAX screws

Stiffness values	θ=±30°	θ=±45°	θ=±60°
$K_{\perp}$ SFS(kN/mm)	10.3	10.3	10.3
$K_{\parallel}$ SFS(kN/mm)	36.9	34.5	29.2
$K_{\perp}$ SPAX (kN/mm)	9.7	9.7	9.7
$K_{\parallel}$ SPAX (kN/mm)	31.0	27.4	22.8
K_{ser} SFS(N/mm) (analytical stiffness)	17.0	22.4	24.5
$K_{\text{s,0.4}}$ CC SFS WI (experimental stiffness)	34.2	28.8	36.8
Error(%)	-50.3	-22.1	-33.5
$K_{\text{s,0.4}}$ EPS LWC2000 SFS WI	27.0	43.0	59.9
Error(%)	-37.0	-47.8	-59.2
K_{ser} SPAX (N/mm) (analytical stiffness)	15.0	18.5	19.5
$K_{\text{s,0.4}}$ CC Spax WI (experimental stiffness)	29.7	25.3	40.1
Error(%)	-49.4	-26.8	-51.3
$K_{\text{s,0.4}}$ EPS LWC2000 SPAX WI	38.1	39.5	53.9
Error(%)	-60.5	-53.0	-63.8

The analytical stiffness of crossed SFS and SPAX screws underestimated the experimental values of both the CC and EPS LWC2000 series exhibiting significant differences ranging approximately 20-60%. The differences were less for the CC series comparing to the EPS LWC series.

This model is proposed for stiffness prediction of inclined fasteners inserted in a timber-timber connection. Hence, in a similar manner to the stiffness model of a vertically inserted fastener given by Eurocode 5 EN (2004b), a modification factor can take into account the effect of the presence of a rigid concrete slab in TCC compared to timber-timber connections and adjust the underestimation of experimental values for TCC connections.

However, it was observed that considering a modification factor of two overestimates the stiffness of some experimental test series and it is concluded that a modification factor of two is a bit strong. Hence, to derive a more precise model in future study, revision of modification factor utilising more experimental series is recommended.

8.4 CONCLUSION

The literature indicates a significant lack of information on analytical closed-form equations to predict the strength and stiffness of TCC connections to be used in the design of timber composite beams. Inclination of the mechanical fasteners at various angles in TCCs exploiting the axial capacity of screws increases the stiffness and strength which depends on the inclination angle, geometry of the screw, tensile and withdrawal strength of the screw and embedment strength of timber.

This Chapter consisted of two separate Sections of strength and stiffness models of TCC connections. The methodology of available analytical models for prediction of the strength and serviceability slip modulus of vertically inserted single timber to timber and TCC shear connections for example screw and nail were separately reviewed in this Chapter. The analytical results of the models were compared to the experimental results of single vertically inserted wood screw shear connection used in TCC specimens.

Eurocode 5 EN (2004b) and Johansen strength models predict the strength of TCC connection utilising vertical wood screw with a notable errors of 32.1% and 21.1%, respectively whilst the stiffness models represent a wide range of errors.

The simplified stiffness models such as Eurocode 5EN (2004b), Turrini et al. (1983) and Zahn (1991) underestimated the experimental data of vertically inserted wood screw with an error ranging approximately 10-40% whereas the models based on Winkler theory such as Kuenzi (1955) and Gelfi et al. (2002) were inaccurate and calculated a much lower stiffness compared to that of the experimental test with an error of approximately 60%. The reasons attributed to the inaccuracy of the stiffness models were discussed.

This investigation recommends further investigation on the prediction of foundation moduli of timber and concrete as the main input parameters of the models based on the Winkler theory. It is noteworthy to state that the fewer required input parameters for the simplified models of vertically inserted fasteners compared with those of the models based on the Winkler theory makes them more practical for application in the design of TCC floor. However, further examination of the simplified stiffness models of vertically inserted fasteners using experimental data of different types of mechanical fastener with various lengths and diameters is required to propose the models for the design of a TCC floor.

An analytical strength model based on some adjustment to EYM to predict the strength of TCC connections utilising single and crossed screws inclined to the timber grain is proposed. The model is an upper bound plastic collapse model that assumes that the behaviour of the timber and screw is perfectly plastic and the concrete remains undamaged. The failure modes consider yield of the screw in tension and/or shear, and a series of combined failure modes such as screw withdrawal, lateral crushing of the timber and the development of plastic hinges in the screw.

This Chapter also presents a model for the stiffness of TCC connections using crossed inclined screws. The Winkler theory of beam on elastic foundation proposed is extended to derive the serviceability slip modulus of TCC connections with inclined screws which are loaded in tension and compression. To compare the accuracy of the stiffness model , a relatively simple model with fewer variables proposed by Tomasi et al. (2010) for crossed screws inclined at timber-timber connection was explained and its results were verified.

In the case of TCC, a modification factor needs to be introduced to Tomasi et al. (2010) to take into account the effect of the presence of a rigid concrete slab in TCC compared to timber-timber connections and adjust the underestimation of experimental values for

TCC connections. However, it was observed that considering a modification factor of two overestimates the stiffness of some experimental test series and it is concluded a modification factor of two is a bit strong. Hence, to derive a more precise model applicable for the TCCs, revision of modification factor utilising more experimental series is recommended.

The experimental data of stiffness, strength and failure mode obtained from push-out test of TCC connections with crossed (±30°,±45°, ±60°) SFS VB and SPAX screws utilising different concrete types are used to examine the accuracy of the strength and stiffness models of TCC connections for their practical application in the design of a TCC floor. It is concluded that the strength model is a realistic model for predicting the failure mode and strength of inclined screws in TCC structures. This research suggests the model is reliable and can be used for the design of a TCC floor with crossed inclined screws. Comparing analytical and experimental results, the stiffness model based on Winkler theory seems to be reasonably accurate in predicting the slip modulus of TCC connections at SLS. This research suggests the model to facilitate the design of inclined screw shear connections for TCC construction.

9 FINITE ELEMENT MODELS OF TCC

9.1 INTRODUCTION

Some key results of finite element (FE) analysis of timber concrete composite connections and beams from literature are first reviewed in this Chapter.

This Chapter also presents a non-linear three-dimensional FE model using flexible contact element pairs to simulate the experimental tests of TCC connections reported in Chapters 5 and 10 utilising the commercial FE analysis software ANSYS, versions 14.5 and 15.0. A three-dimensional FE of timber concrete composite connection is capable of predicting the effects of different parameters for example fastener slenderness ratio, fastener spacing in multiple-fastener connection, non-linear orthotropic properties of the timber composite and elasto-plastic behaviour of the fastener and concrete components.

Connections with single and multiple four wood screws with three different spacings of 50, 100 and 150mm and single medium size coach screw inclined at +45° to the horizontal face were modelled. The modelling approach can be applied to TCC connections other than simple screws only such as epoxy glue and epoxy glue reinforced with normal coach screw.

Results from FE models were validated by experimental results of push-out test. The push-out tests of TCC connectors were carried out in compliance with EN26891 (1991) to evaluate their strength, stiffness and failure mode as reported in Chapters 5 and 10.

The accuracy of models is influenced by the quality of the input data such as material properties, element type, boundary conditions and mesh size. An orthotropic behaviour

was adopted to model the timber using Hill's criterion which utilises different plasticity stresses in three x, y and z directions of material whilst the von Mises yield criterion associated with an isotropic work hardening was used to simulate a steel fastener. In addition, the "concrete" model in the ANSYS material library was used to reproduce the cracking associated with tensile stresses in concrete.

A model calibration was performed to set friction coefficients of materials contacts and contact element parameters. The model calibration was carried out using the failure load obtained from experimental tests. The model was validated comparing the load–slip response, load capacity and their serviceability slip moduli, K_{ser}. The calibrated FE model can be used for parametric study of TCC connections and beams.

9.2 FINITE ELEMENT ANALYSIS OF TCC SYSTEMS

Anisotropic and inhomogeneity property of wood and different layouts of shear connector used in TCC floors results in complex interaction of timber, concrete and shear connection which indicates the concentrated stresses followed by different patterns of crack growth in any of the timber and concrete components.

FE studies of TCC connections (in shear) and beams utilising mechanical fastener can be classified into two main categories: (1) simplified 2-D and 3-D FEM using linear or nonlinear spring elements at fastener location and (2) 3-D FEM of detailed modelling of connector using 3-D solid elements (Oudjene et al. 2013).

The 2-D models of TCC connections and beams were employed to decrease the computational time of analysis.

3-D FE modelling of detailed TCC connections can predict the strength, stiffness and failure mode of different shear connections as input values for standard procedure to design a partially composite TCC floor such as the Gamma method proposed by Eurocode 5.

In addition, Moss (1997b) stated that a detailed analysis of a single fastener timber connection is required to study the effect of the number of rows of fastener and its slenderness ratios. The 3-D model is capable of investigating the influence of end distance, aspect ratio and fastener yield strength in timber composite connections (Patton-Mallory et al. 1997a).

Modelling the stress calculations, failure mechanisms, strength and load-slip of a timber composite requires non-linear material modelling and failure prediction of timber composite components (Moses 2000; Patton-Mallory 1996). Crushing behaviour of timber in compression leads to non-linear stress-strain behaviour in its three orthotropic material directions (Patton-Mallory et al. 1997a). Stress concentrations of each normal and shear stress of timber composite connections in the vicinity of the hole are evident in the stress field of the three-dimensional model (Patton-Mallory et al. 1998a, 1998b).

Investigations on 3-D FE modelling of TCC connections connected by mechanical fastener are limited to bolt with large diameter and glued steel plate connections (Oudjene et al. 2013). Hence, a 3-D numerical analysis of TCC screw connections facilitates parametric study on different types and geometry of screw, screw spacing, materials and their effect on the load carrying capacity, stiffness and failure behaviour of composite connections in an efficient time and cost compared to experiment.

9.3 FINITE ELEMENT ANALYSIS OF TCC SYSTEMS IN LITERATURE

This Section summarises some key results of FE analysis of timber concrete composites from literature reviewed. TCC connections and beams under shear and flexural tests have been simulated by available commercial packages such as ANSYS or ABAQUS.

Kuhlmann et al. (2004), Kuhlmann et al. (2006) and Kuhlmann et al. (2008) investigated grooved connection in TCCs. The numerical simulation of groove connections exhibited a good agreement with experimental failure mechanism but the stiffness and the ultimate load capacity of the connector were overestimated by the numerical results. Lack of softening in the timber material model probably led to this deviation in load capacity (Kuhlmann et al. 2008; Kuhlmann et al. 2004).

Dias et al. (2007) used 3D non-linear FEM models to predict the mechanical properties of dowel type fasteners. An isotropic model was employed to model steel and concrete behaviours whilst the timber component was modelled utilising an orthotropic model. In addition the interaction between materials was modelled by frictional contact elements. Comparing the experimental and numerical results, it was concluded that the initial stiffness and maximum load capacity were overestimated by the numerical models. The assumption of a yielding strength equal to the embedding strength of timber might cause the overestimation in load carrying capacity. Furthermore, the

assumption of perfect linear elastic behaviour probably resulted in higher linear stiffness (Dias et al. 2007).

Elsewhere, Lukaszewska (2009) implemented FEM to simulate experimental tests of TCC beams utilising four connectors including a U-shaped steel plate welded to a long punched metal, coach screwed into steel tubes, long punched metal plate and inserted steel tubes as shown in Chapter 3 (Figure 3-1a). The results of nonlinear FE modelling were very similar to the results of experimental tests. Hence, it was concluded that FE models are useful to extend the experimental results of a composite floor with different geometrical and mechanical properties (Lukaszewska et al. 2010).

Miotto et al. (2011) modelled a continuous perforated steel plate as a TCC connector using ANSYS 10.0. A good agreement with the experimental tests was noted. The numerical model failed in the concrete due to the compressive stress being reached. However, this accuracy is most pertinent in the linear elastic range with the results deviating once the materials become plastic. This was attributed to the assumptions made in the numerical model to simplify the analysis.

9.4 MATHEMATICAL PROCEDURE

TCC connection is discretised with a number of elements and then the elements are assembled at nodes. Different elements type and shape with boundary conditions are utilised in the FE model. The finite element equation of variational principle related to total potential energy (π) is given by:

$$\pi = \int_V \sigma^{\mathrm{T}} \varepsilon \mathrm{d}V - \int_{S_{\mathrm{F}}} u^{\mathrm{T}} \bar{t} \mathrm{d}S = 0 \qquad (9\text{-}1)$$

where, V is a volume bounded by a surface, S with the traction vector t on a part of the surface S_{F} whilst σ, ε and u are stress, strain and displacement vectors, respectively (Kim et al. 2007). The first order variation of Equation (9-1) results in:

$$\delta\pi = \int_V \sigma^{\mathrm{T}} \delta\varepsilon \mathrm{d}V - \int_{S_{\mathrm{F}}} \delta u^{\mathrm{T}} \bar{t} \mathrm{d}S = 0 \qquad (9\text{-}2)$$

Constitutive equation of $\sigma = D\varepsilon$ and strain–displacement relation of $\varepsilon = Bu$ changes Equation (9-1) to:

$$\delta u^{\mathrm{T}} \left[\int_V B^{\mathrm{T}} DB \mathrm{d}V \right] \mathrm{u} - \delta u^{\mathrm{T}} \int_{S_{\mathrm{F}}} N \bar{t} \mathrm{d}S = 0 \qquad (9\text{-}3)$$

where, N is the shape function matrix. Equation (9-3) is used as basic formulation of finite element and can be written in the forms of:

$$f = Ku \tag{9-4}$$

9.5 TEST SPECIMEN CONFIGURATION

Different types of TCC connection specimens used in experimental push-out test were modelled and analysed utilising ANSYS versions 14.5 and 15.0. Table 9-1 lists the geometry of TCC connection samples.

Table 9-1 Finite element used in FE modelling of the specimen (in mm)

Series	No. of fastener	LVL (hySPAN project)			Conventional concrete		
		Length	width	depth	Length	width	depth
Single wood screw	1	550	48	200	550	300	75
4WS spaced at 50mm	4	450	48	200	450	200	75
4WS spaced at 100mm	4	600	48	200	600	200	75
4WS spaced at 150mm	4	750	48	200	750	200	75
Inclined coach screw	1	450	46	200	450	300	75
Epoxy glue	0	450	48	200	450	300	75
Epoxy glue and coach screw	1	450	48	200	450	300	75

9.6 ELEMENT TYPE

The linear and non-linear structural elements in ANSYS range from simple spars and beams to complex layered shells and large strain solids. TCC connection models are comprised of three different materials of timber, concrete and steel connected together utilising contact surfaces. Therefore, the element types for each component of the TCC connection model were defined using the most suitable elements available in the ANSYS library.

The fastener, timber and concrete components were modelled using SOLID elements whilst the contact between the fastener and the hole in the timber and concrete components were simulated using contact elements as listed in Table 9-2. In this Section, these element types are discussed.

Table 9-2 Finite element used in FE modelling of the specimen

Type	Material	Finite element
1	Concrete	Solid65
2	hySPAN project LVL	Solid45
4	Steel	Solid45
5	Target surface	Target170
6	Contact surface	Contact173

9.6.1 SOLID45

Timber and steel fastener were simulated utilising SOLID45 which is capable of modelling plastic deformation, creep, large deflection and strain of solid elements. Figure 9-1 depicts the geometry, node location, and coordinate system of SOLID45.

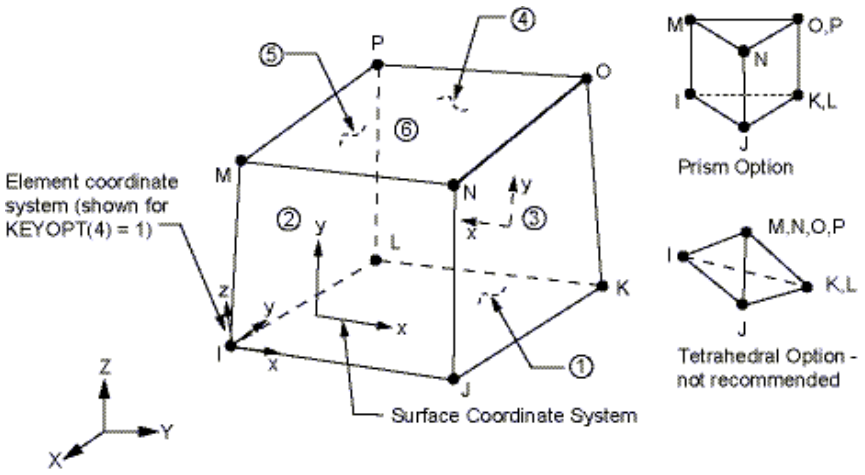

Figure 9-1 Geometric properties of SOLID45 Wood (ANSYS 2010)

The element consists of eight nodes with three degrees of freedom per node and allows for the material's plasticity and orthotropic behaviour. Orthotropic material directions are defined corresponding to the element coordinate directions.

9.6.2 SOLID65

SOLID65 consists of eight nodes which include three degrees of freedom at each node (Figure 9-2). The capability of SOLID65 in simulation of cracking in tension and crushing in compression is beneficial to 3-D modelling of solids with or without rebar reinforcement e.g. reinforced concrete and rocks. The concrete simulates the cracking (in three orthogonal directions), crushing, plastic deformation and creep. The rebar can model tension and compression , plastic deformation and creep (ANSYS 2010).

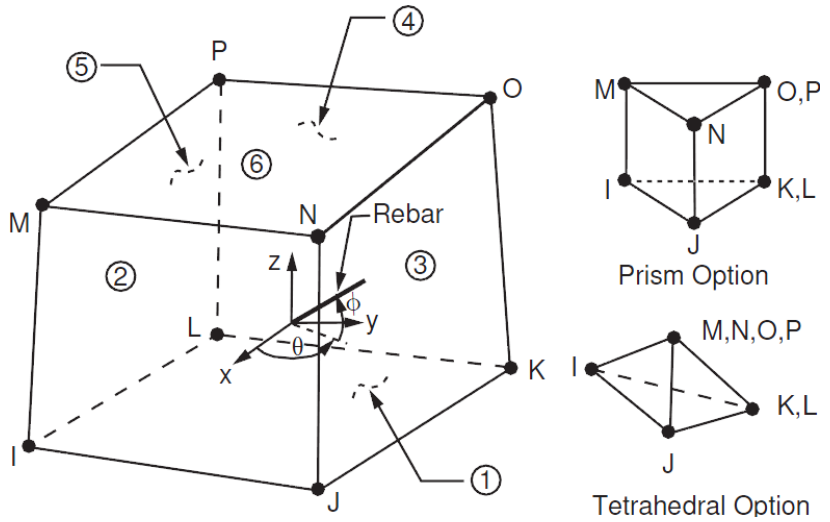

Figure 9-2 Geometric properties of SOLID65 concrete (ANSYS 2010)TARGE170 and CONTA173

TARGE170 and CONTA173 were used for three-dimensional analysis of surface-to-surface contact between concrete slab, timber joist and steel fastener. These elements can simulate the existence of pressure or separation between the composite components in the case of contact and no contact, respectively.

TARGE170 simulates various 3-D target surfaces for the associated contact elements (CONTA173). The contact elements are in contact with the target surface which is discretised by a set of target segment elements (TARGE170). TARGE170 and CONTA173 are paired by a shared real constant set. The contact elements overlay the solid element to consider the boundary of a deformable body as shown in Figure 9-3.

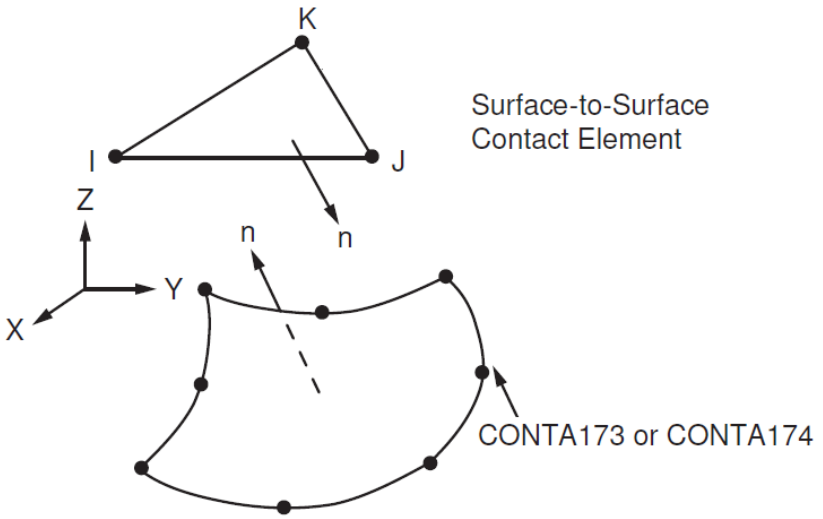

Figure 9-3 Geometric properties of TARGA170 and CONTA173 (ANSYS 2010)

CONTA173 placed on the surfaces of 3-D solid represents contact and sliding between 3-D target surfaces and a deformable surface. Figure 9-3 depicts the geometry, node locations, and the coordinate system of TARGA170 and CONTA173 elements.

CONTA173 surface penetrates TARGE170 element on a specified target surface to produce contact. Coulomb friction, shear stress friction, and user defined friction utilising subroutine are possible to model. Moreover, CONTA173 enables separation of bonded contact to model delamination.

9.7 CONSTITUTIVE RELATIONS AND MATERIAL PROPERTIES

Different material properties such as linear or non-linear, isotropic or orthotropic, and constant or temperature dependent can be adapted to model material behaviour in ANSYS. The material models of each component in the TCC specimen were defined utilising material properties of composite components as reported in Chapter 4 (Tables 4-3:4-6). In this Section, the constitutive relations and material properties of TCC models are given.

9.7.1 Timber

Mechanical properties of wood are complex and this is attributed to the variable behaviour with direction, time, temperature, moisture or loading rate (Mackerle 2005).

Wood is an anisotropic material and under appropriate conditions, is assumed to be an orthotropic material in FEM which consists of three planes of symmetry defined by longitudinal, radial and tangential directions. Wood contains natural defects in the form of irregular grains and knots which lead to high variation in its material properties (Mackerle 2005).

An orthotropic behaviour was adopted to model the timber using criterion reported by Hill (1948) which is associated with an isotropic work hardening utilising different plasticity stresses in three x, y and z directions of the material. Hill criterion is produced utilising the von Mises yield criterion to consider the anisotropy of the material (Dias 2005). Each direction of an orthotropic material exhibits its own properties which are different from the others in tension and compression.

Equations (9-5):(9-7) reported by Dias (2005) and Flores et al. (2007) were used to calculate the plastic properties of the timber model in other directions rather than the grain direction as listed in Table 9-4.

The material properties of timber in the radial and tangential directions were assumed to be identical. The tensile and compressive behaviours of timber were assumed to be identical to reduce the number of different properties.

$$\frac{\sigma_x}{\sigma_y} = \frac{\sigma_z}{\sigma_y} = 0.19 \tag{9-5}$$

$$\tau_{xz} = \tau_{xy} = 0.38\sigma_z \tag{9-6}$$

$$\tau_{yz} = 0.038\sigma_z \tag{9-7}$$

The behaviour of timber is relatively plastic and can thus be reasonably approximated by an elasto-plastic law with hardening whereas in tension it exhibits a brittle behaviour. An elasto-plastic constitutive model was used to model the timber component of TCC connections.

Figure 9-4 illustrates the bi-linear stress–strain diagram of timber in compression. The initial slope of the stress–strain diagram represents the MOE of material in x, y and z directions. The second slope of the stress–strain diagram after reaching yield stress, f_y indicates the tangent modulus.

The material properties of timber reported in Chapter 4 were adopted to obtain linear orthotropic and plastic properties of the timber as listed in Tables 9-3 and 9-4, respectively.

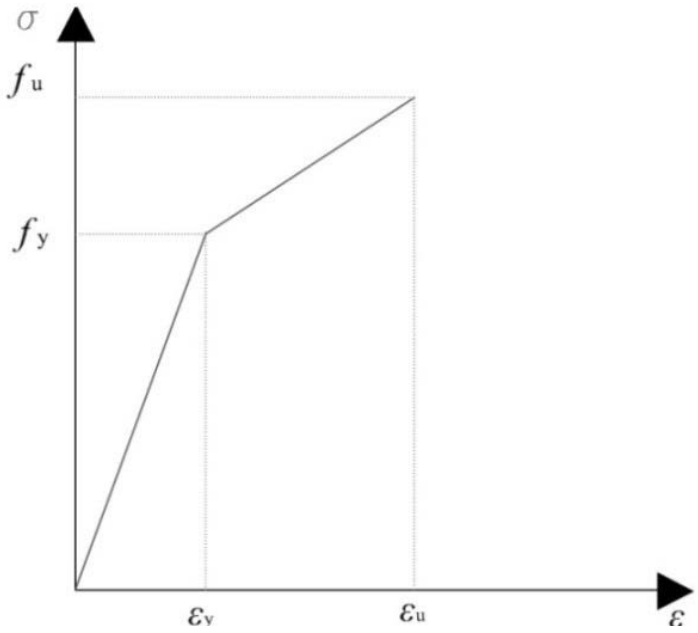

Figure 9-4 Constitutive model utilised for timber in compression

Table 9-3 Linear orthotropic properties of the timber (LVL)

Elastic parameters	Value
Elastic modulus in the tangential direction, E_x(MPa)	1400
Elastic modulus in the longitudinal direction, E_y(MPa)	14000
Elastic modulus in the radial direction, E_z(MPa)	1400
Shear modulus in the xy plane, G_{xy}(MPa)	700
Shear modulus in the yz plane, G_{yz}(MPa)	700
Shear modulus in the xz plane, G_{xz}(MPa)	700
Poisson's ratio in the xy plane, υ_{xy}	0.013
Poisson's ratio in the yz plane, υ_{yz}	0.013
Poisson's ratio in the xz plane, υ_{xz}	0.23

Table 9-4 Plastic properties of the timber (LVL)

Elastic parameters	Value(MPa)
Yield stresses (tensile and compressive) in the *x* direction, σ_x	10.2
Yield stresses (tensile and compressive) in the *y* direction, σ_y	53.4
Yield stresses (tensile and compressive) in the *z* direction, σ_z	10.2
Tangent moduli (tensile and compressive) in the *x* direction, $E_{\tau x}$	2.05
Tangent moduli (tensile and compressive) in the *y* direction, $E_{\tau y}$	140.0
Tangent moduli (tensile and compressive) in the *z* direction, $E_{\tau z}$	2.05
Shear yield stress in the *xy* plane, τ_{xy}	20.3
Shear yield stress in the *yz* plane, τ_{yz}	2.03
Shear yield stress in the *xz* plane, τ_{xz}	20.3
Tangent modulus (shear) corresponding to the *xy* plane, Gτxy	12.0
Tangent modulus (shear) corresponding to the *yz* plane, Gτyz	0.012
Tangent modulus (shear) corresponding to the *xz* plane, Gτxz	12

9.7.2 Steel

A linear-elastic isotropic material was assumed to model a steel fastener in numerical simulations. A bi-linear curve with isotropic work hardening and von Mises yield criterion was used to simulate steel shear connectors.

Figure 9-5 illustrates the bilinear stress–strain curve assumed. The isotropic behaviour of steel fasteners was characterised utilising the values listed in Table 9-5.

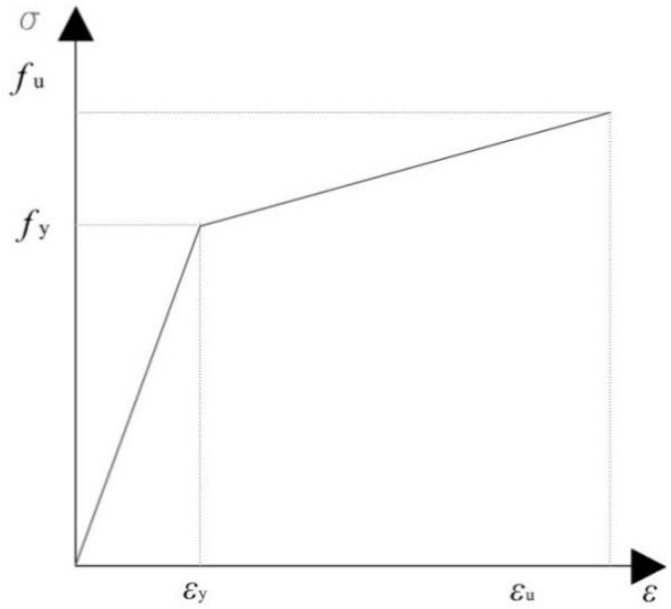

Figure 9-5 Constitutive model utilised for steel fastener

Due to the complexity of screw geometry, the screw was modelled as a cylindrical rod with frictional contact which was presumed to model the interaction of the threaded part of the screw and timber. Rigid deformation of the screw in concrete and the interlocking of its head were modelled by bonded contact between concrete and screw.

Table 9-5 Steel fastener ptoperties

Mean mechanical property	Wood 17 screw	Medium coach	Large coach
Modulus of Elasticity, E (MPa)	210000	210000	210000
Yield stress, σ_0 (MPa)	700	300	300
Tangent modulus, E_T (MPa)	7600	5000	5000
Poisson's ratio, υ	0.3	0.3	0.3

9.7.3 Concrete

A multi-linear constitutive model with isotropic hardening proposed by Eurocode 2 (EN 2004a) was used to model the concrete slab as given in:

$$\sigma = f_{cm} \frac{k\eta - \eta^2}{1 + (k-2)\eta}, \text{for } 0 < \varepsilon < \varepsilon_{c1} \quad (9\text{-}8)$$

where,

$$\eta = f_{cm} \frac{\varepsilon}{\varepsilon_{c1}} \quad (9\text{-}9)$$

$$\varepsilon_{c1} = 0.7 f_{cm}^{0.31} < 2.8 \quad (9\text{-}10)$$

$$k = \frac{1.1 E_{cm} |\varepsilon_{c1}|}{f_{cm}} \quad (9\text{-}11)$$

And $f_{c,m}$ and $E_{c,m}$ are mean compressive strength and MOE of concrete, respectively.

Figure 9-6 shows the constitutive model (in compression) adopted for a conventional concrete slab of TCC connections.

The adopted model was similar to the graphs obtained from the uni-axial compressive test of 100x200mm concrete cylinders as reported in Appendix A.

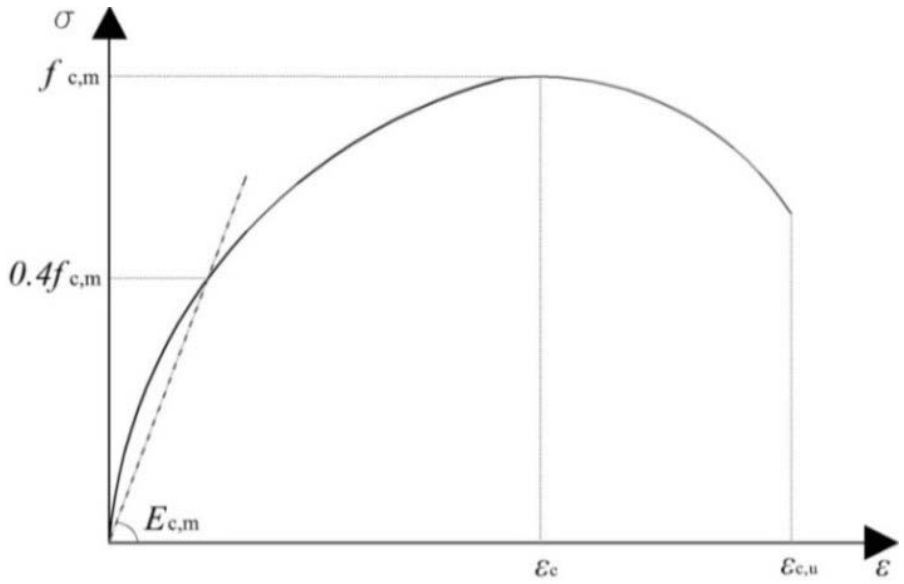

Figure 9-6 Constitutive model utilised for conventional concrete

The concrete model developed by Willam and Warnke (1975), available in the ANSYS library was selected to model nonlinear behaviour of the concrete.

Based on the work carried out by Kotinda (2004), the values of 0.2 and 0.6 were used for the shear transfer coefficient of open and closed cracks, respectively. Uniaxial tensile cracking stress was approximated as 10% of the compressive strength of concrete Kotinda (2004).

This model simulates the tensile cracking of concrete subjected to tensile stresses. The crushing capability of concrete is ignored utilising a uniaxial crushing stress constant of -1. Hence, exceeding the uniaxial tensile ultimate strength, f_t leads to cracking of the concrete (Miotto et al. 2012). There is no need to define some parameters of Table 9-6 as ANSYS can use its default values.

The material properties of conventional concrete such as MOE and uniaxial tensile cracking stress, reported in Chapter 4 (Table 4-3) were used as input parameters of the model. Table 9-6 lists the coefficients and strength input parameters of the concrete model used in the simulations.

Table 9-6 Coefficients and strength properties of the concrete used in the model

Parameters	Value
Mean modulus of elasticity, E_{mean}	33239MPa
Poisson's ratio, υ	0.2
Shear transfer coefficient for an open crack	0.2
Shear transfer coefficient for a closed crack	0.6
Uniaxial tensile cracking stress, f_t	3.39MPa
Uniaxial crushing stress, f_c	-1
Biaxial crushing stress, f_{cb}	$1.2\,f_c$
Ambient hydrostatic stress state, σ^a_h	default
Biaxial crushing stress under the ambient hydrostatic stress state, f_1	$1.45\,f_c$
Uniaxial crushing stress under the ambient hydrostatic stress state, f_2	$1.75\,f_c$
Stiffness multiplier for cracked tensile condition	default

9.8 FINITE ELEMENT MESH DEFINITION

Due to the slender screw hole inside the concrete and timber components in TCC connections utilising screw connector, it was not possible to use mapped brick mesh. Hence, in the case of complex geometry particularly in TCC connections utilising screw connector, a free mesh was employed. Some adjustments in the shapes and dimensions of the finite elements were carried out to consider the influence of the hole in the geometry of connections. The mesh for each model is illustrated in the results and discussion Section.

9.9 CONDITIONS OF SYMMETRY, SUPPORTS AND LOADING

The stability of the model during loading was obtained by considering two types of boundary conditions (i) symmetry conditions and (ii) support, as shown in Figure 9-7.

In order to save computation time, the symmetry of TCC specimen was considered and only half of the geometry of the specimen used in the experiment was modelled as depicted in Figure 9-7a.

The nodes of the elements used consist of three degrees of freedom corresponding to the translations in the *x*, *y* and *z* directions. The support conditions of experimental push-out test were adopted in the numerical model as illustrated in Figure 9-7b. Hence, the displacement constraint in the perpendicular to the grain direction was applied to the nodes at the back of the concrete slab whilst the nodes at the bottom of the concrete slab were fixed to all degrees of freedom which include translations in x, y and z directions.

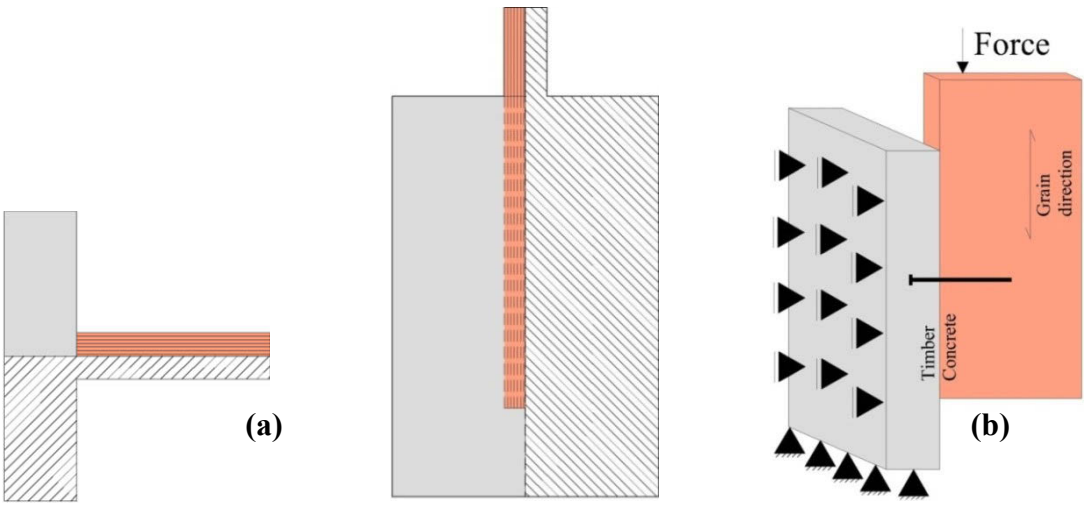

Figure 9-7 (a) Symmetry in plan and section and (b) support condition of TCC models

9.10 CHARACTERISTICS OF CONTACT ELEMENT

ANSYS can analyse the most complex assemblies including nonlinear contact to determine stresses, temperatures, displacements and contact pressure distributions on all component and assembly designs by the most comprehensive set of solvers available (Kim et al. 2007). ANSYS can model surface-to-surface contact and frictional sliding using contact elements which use Lagrange multiplier, penalty function and direct constraint approaches (ANSYS 2009; Kim et al. 2007).

The contact surfaces between timber, concrete and steel fastener were defined utilising TARGE180 and CONTA173 elements available in the ANSYS library. The stiffness between target and contact surfaces was defined utilising different parameters including contact stiffness factor (FKN, FKT) and allowable penetration (FTOLN).

Normal contact stiffness, FKN controls the depth of penetration and the distance between target and contact surfaces which has a considerable influence on convergence of the model. The value entered for the parameter FKN, in this case, was equal to 1.0 (default ANSYS) for the models. The contact stiffness factor, FKN was found to affect the initial stiffness of the load-slip response of the models. ANSYS automatically defines tangential contact stiffness, FKT which depends upon the coefficient of friction and the normal stiffness, FKN. Allowable penetration, FTOLN indicates the status of the contact, open or closed. For example a contact with minimum penetration value is considered closed. The value adopted for the FTOLN parameter was 0.1 (ANSYS default) for most of the models.

A model calibration was carried out to set contact parameters such as friction coefficient of the contact surfaces of timber joist–concrete slab, concrete slab-steel fastener and timber joist-steel fastener. It was found that the frictional contact between the screw and the timber in TCC models has no significant influence on the linear elastic behaviour whereas, it has a considerable impact on the convergence of the FE models and its nonlinear part of response and this finding agrees with previous research of timber-timber connection such as Nishiyama et al. (2003).

Based on previous investigations such as Molina (2008) and Miotto (2009), the coefficient of friction values between timber-concrete, timber-steel and steel-concrete for most of the models were selected to be 0.1, 0.6 and 0.5, respectively which led to convergence of the models and also a good agreement with experimental results.

9.11 MODEL VERIFICATION

The model was validated comparing load-slip responses of experimental and numerical results. Moreover strength, serviceability stiffness and failure mode of models were verified utilising experimental results and observation as reported in Chapters 5 and 10 and Appendix B.

In order to capture the non-linear load-slip response of TCC connections, a displacement was applied in place of the external load by load jack in the experiment. The applied load was measured by summation of reaction forces in each node placed at the bottom face of the concrete slab. The applied load was reported versus the displacement at the interface of timber and concrete components close to the shear connection. The geometry of the verified model can be modified for parametric study of changes in end distance, edge distance, member thickness, screw diameter, screw length and number of screws.

9.12 RESULTS AND DISCUSSION

The TCC connection models include single and multiple slender wood screws (WS) and inclined medium size coach screws. The modelling approach can be applied to TCC connections other than simple screws such as epoxy glue and epoxy glue with coach screw connections. The load-slip response of each connection model was compared to that of the experimental test. The deformation pattern provides information on the location and amount of the maximum slip between composite components.

The stress pattern in timber as an orthotropic material is defined utilising six components of stress such as normal stresses σ_x, σ_y, σ_z and shear ones σ_{xy}, σ_{yz}, and σ_{xz}. In TCC connections models, the connection is only subjected to vertical force parallel to the grain direction. Hence, the normal stress graphs, parallel to the grain direction were plotted to provide information on the possible location of stress concentrations and failures in the TCC connections.

The serviceability slip modulus, K_s representing the resistance to the relative displacement between the timber joist and the concrete slab in push-out test was used to verify the stiffness of the numerical model which is calculated by:

$$K_s = \frac{0.4F_{mean}}{\frac{4}{3}(\upsilon_{40} - \upsilon_{10})} \qquad (9\text{-}12)$$

where, F_{mean} is the mean experimental strength and v_{40} and v_{10} are the slip corresponding to 40% and 10% F_{mean} of numerical load-slip response.

9.12.1 Single and multiple wood screws

The experimental tests of TCC connections series connected by single and four 100mm long wood screws with screw spacing of 50, 100 and 150mm were selected to verify the single and multiple screw models. The geometry of TCC connection specimens utilising single and multiple wood screws are discussed in Chapter 10. The mesh used in the FEM models of single and multiple screws are illustrated in Figures 9-8:9-11. Figures 9-8:9-11 compare the number of elements around each screw and between screws for single and multiple screw series utilising four screws spaced at 50, 100 and 150mm, respectively.

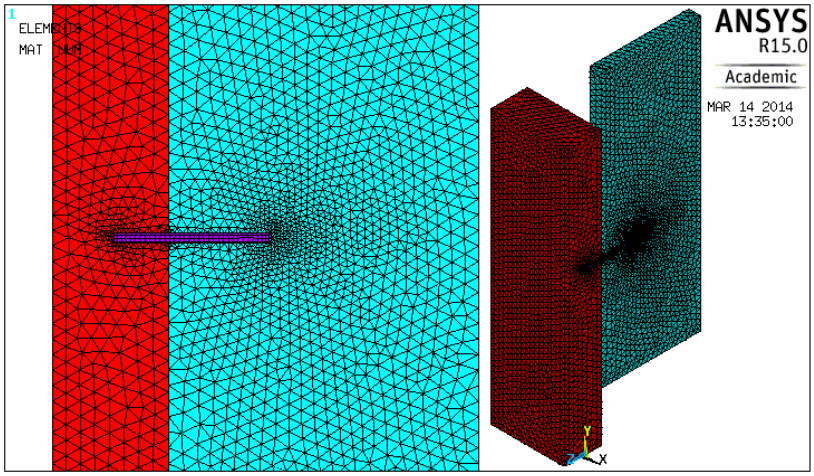

Figure 9-8 Mesh of single wood screw model TCC connection model

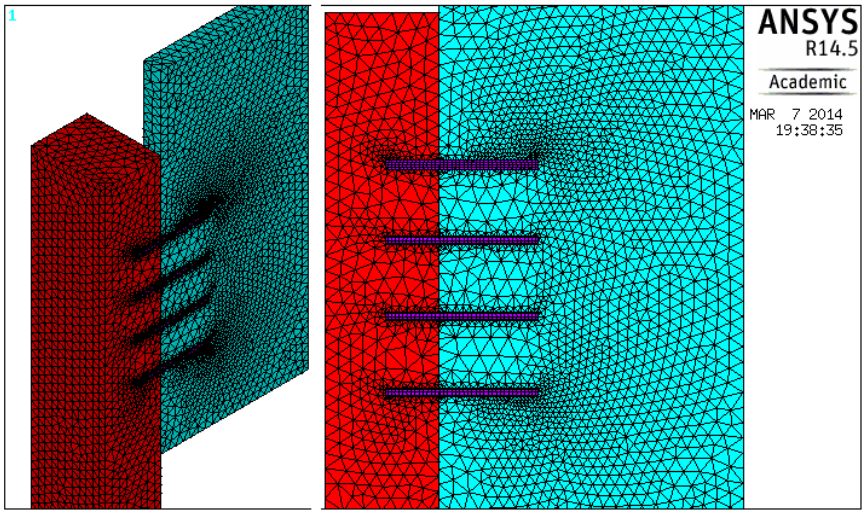

Figure 9-9 Mesh of four wood screw model spaced at 50mm

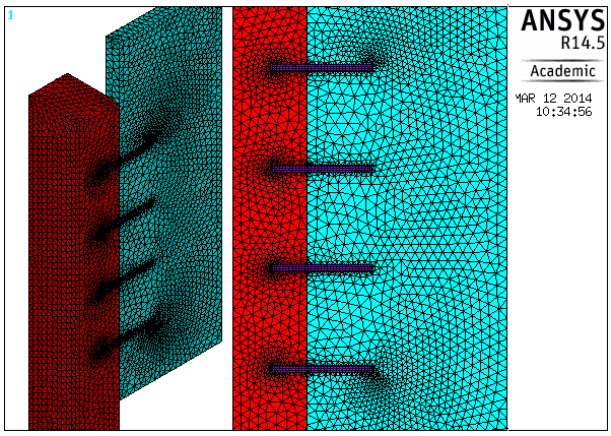

Figure 9-10 Mesh of four wood screw model spaced at 100mm

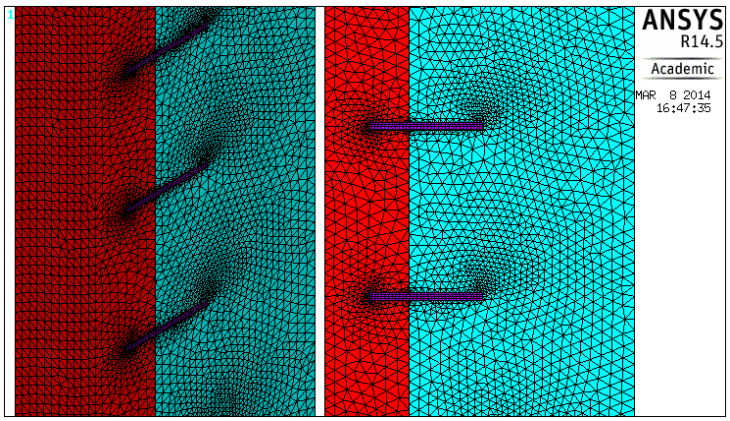

Figure 9-11 Mesh of four wood screw model spaced at 150mm

Figures 9-12:9-15 plot the numerical and experimental load-slip responses of single and multiple wood screw series. In the screw connection series, the screws were subjected to direct shear force and bending moment resulted from embedding behaviour of timber due to relative slip of composite members. The axial withdrawal force in screws is caused by the frictional contact condition between timber-screw and concrete-screw.

The model was processed considering the materials' nonlinear behaviour and the result was in good agreement with experimental results, particularly in the elastic-linear behaviour of materials. However, slight overestimations were observed in the post-elastic regions of the numerical models compared to experimental responses as depicted in Figures 9-12:9-15 where materials experience plastic deformation. This deviation might be attributed to the fact of variation in parameters such as the screw geometry, material properties of timber, screws and concrete influence the load-slip curve of the TCC connection. Thus, slight inaccuracy in FE models and variation in experimental properties influence load-slip response of numerical and experimental results.

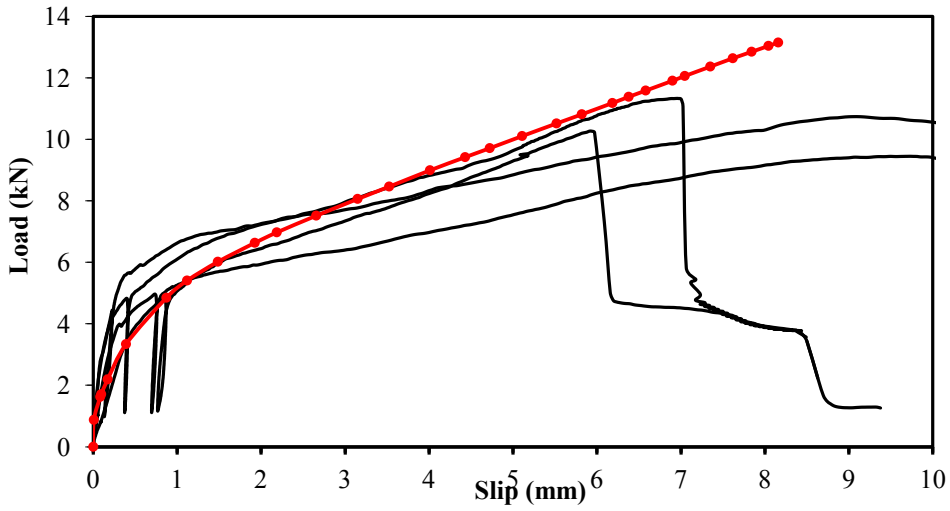

Figure 9-12 Experimental (black) and FEM (red) results of single wood screw test series

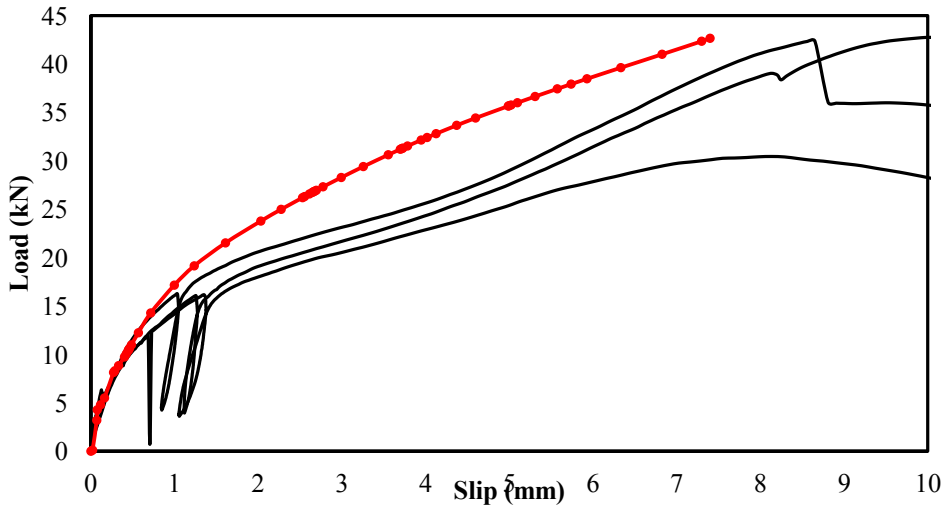

Figure 9-13 Experimental (black) and FEM (red) results of 4 WS-50mm test series

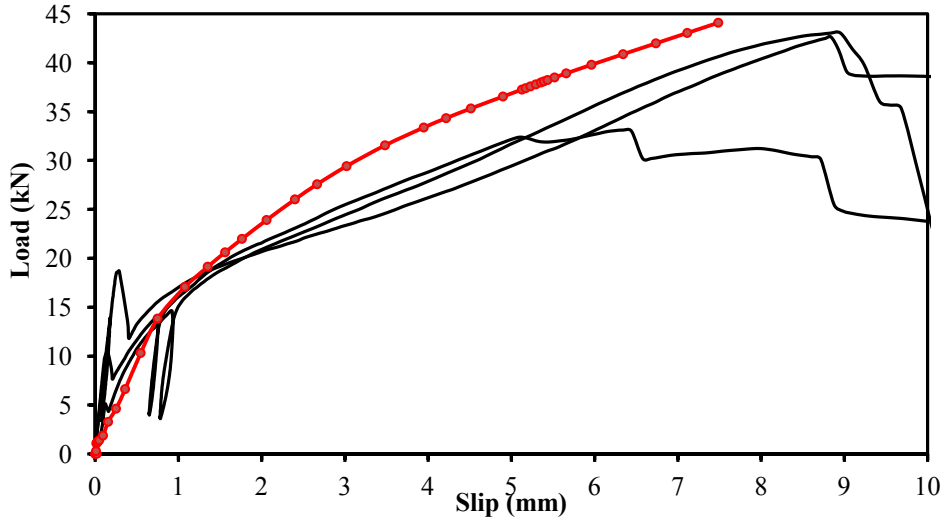

Figure 9-14 Experimental (black) and FEM (red) results of 4 WS-100mm test series

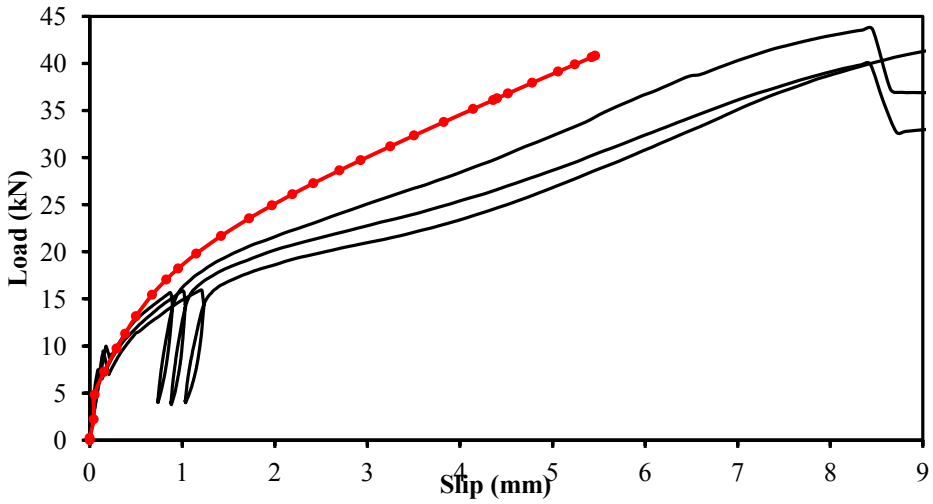

Figure 9-15 Experimental (black) and FEM (red) results of 4 WS-150mm test series

The strength of the numerical model for single and multiple wood screw series confirms a fairly good agreement with experimental results, shown by a difference of -3.5 to 20.2% between the experimental and numerical strength.

Figures 9-16:9-23 illustrate the numerical and experimental ultimate displacement and normal stress in loading direction of single and multiple wood screw series. The stress distribution within different types of TCC connections at the end of the simulation, that is under ultimate vertical displacement are depicted in the stress diagrams. The ultimate failure of numerical models in single and multiple wood screw series indicates a similar failure pattern to experimental failure mode where a combination of crushing in timber and concrete due to flexural deformation of the screws and formation of plastic hinges in the screws were observed as illustrated in Figures 9-16:9-23.

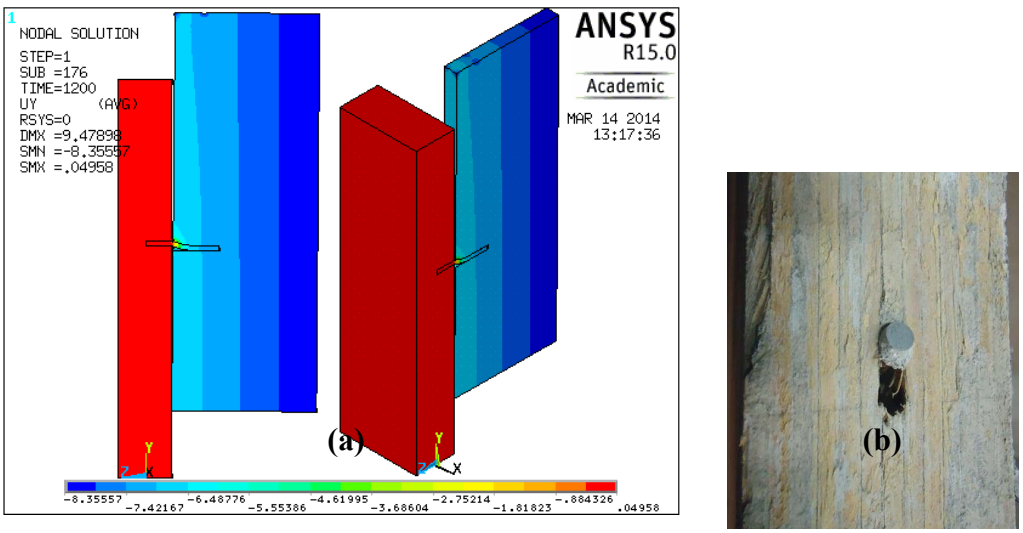

Figure 9-16 (a) FEM displacement in y direction and (b) failure of single wood screw

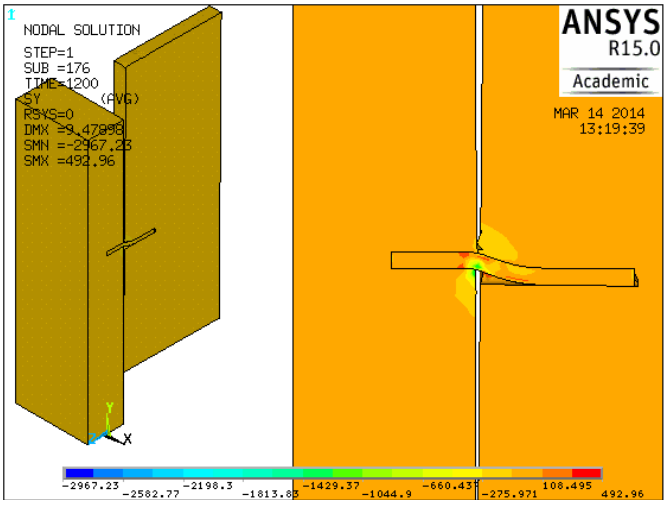

Figure 9-17 Normal stress in y direction at last sub-step of single wood screw model

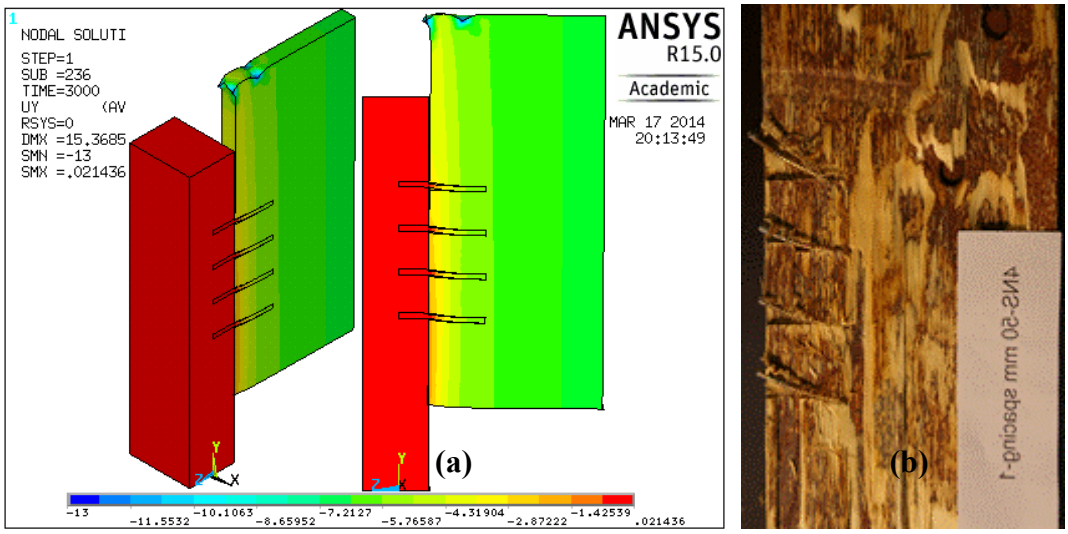

Figure 9-18 (a) FEM displacement in y direction and (b) exp. failure of 4 WS 50mm

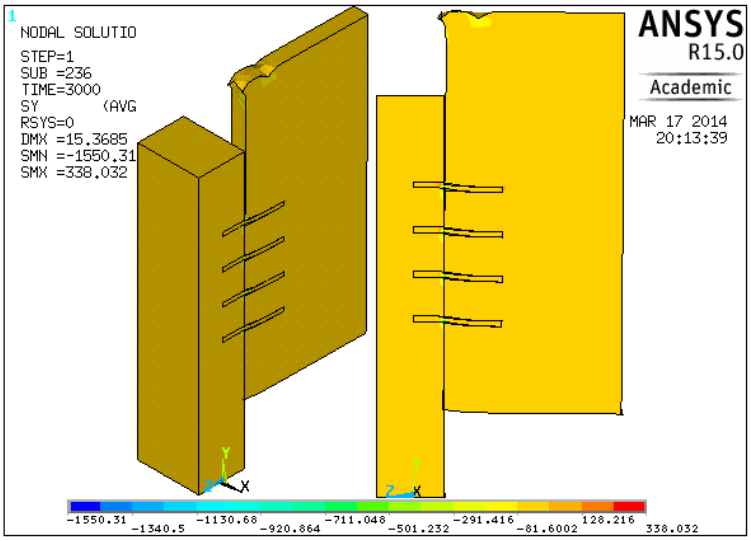

Figure 9-19 Normal stress in y direction at last sub-step of 4 WS 50mm model

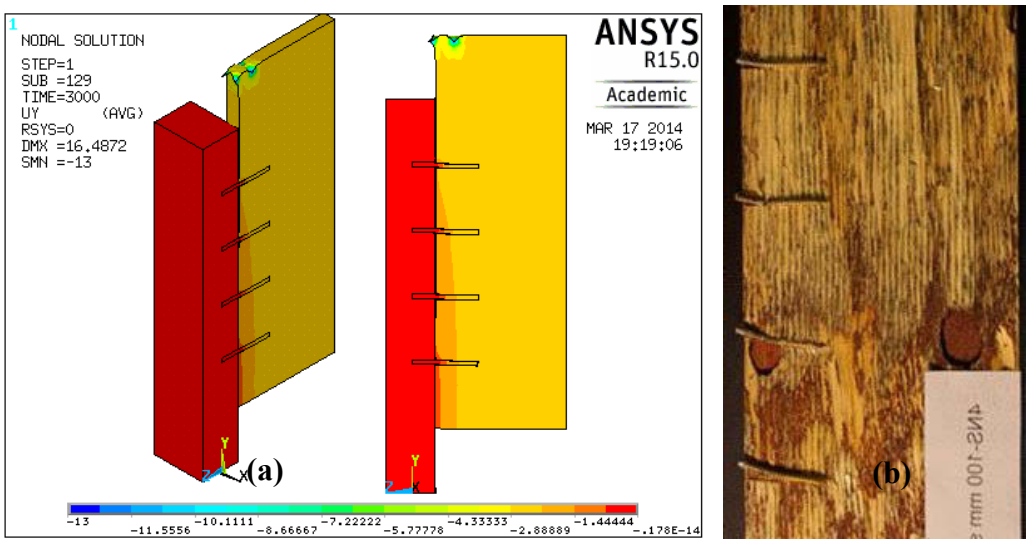

Figure 9-20 (a) FEM displacement in y direction and (b) exp. failure of 4 WS 100mm

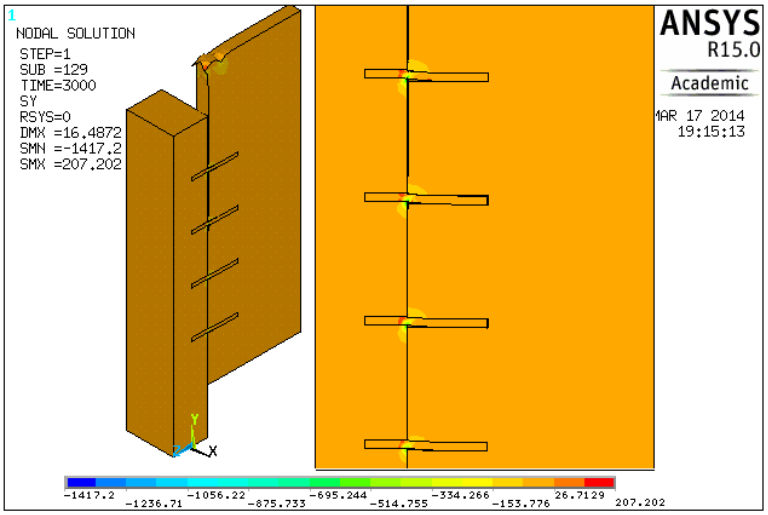

Figure 9-21 Normal stress in y direction at last sub-step of 4 WS 100mm model

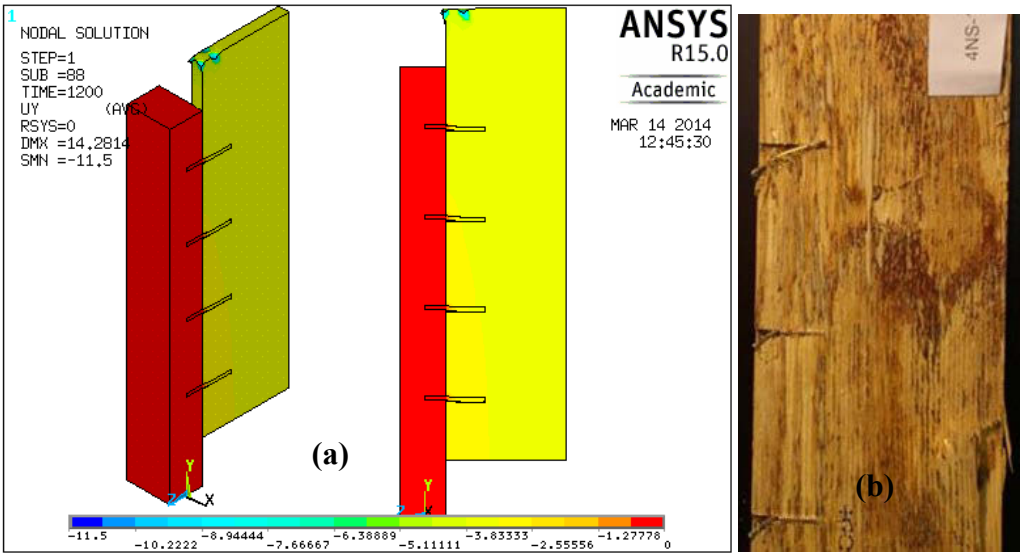

Figure 9-22 (a) FEM displacement in y direction and (b) exp. failure of 4 WS 150mm

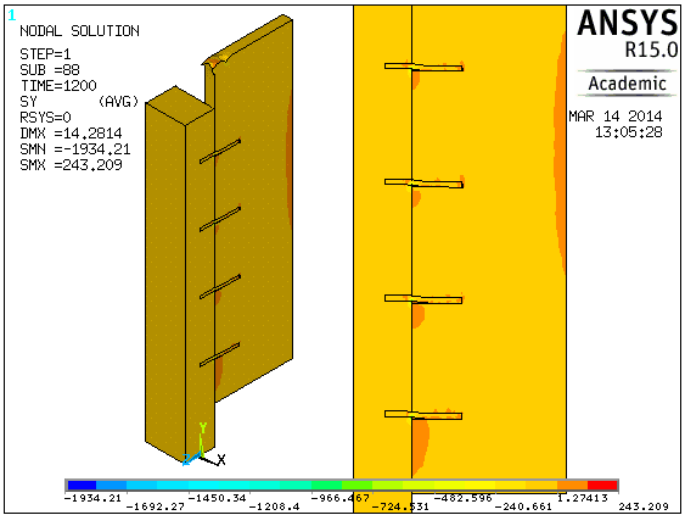

Figure 9-23 Normal stress in y direction at last sub-step of 4 WS 150mm model

The stress concentration in the vicinity of the screw holes at the interface of timber and concrete agrees with localised crushing of timber and concrete around the screws in the experimental series. The LVL joists under the load jack experienced the highest compressive stress parallel to the grain close to its average compressive strength (53.4MPa) as plotted in Figures 9-16:9-23.

Figure 9-24 illustrates the contact condition such as far open (no contact), near contact, sliding (no separation) and sticking (full contact) in the ultimate load step of different series utilising single and four wood screws at 50, 100 and 150mm. The near contact and far open contact between timber and concrete in numerical simulation agree with experimental observations of contact surface at failure whilst a sticking contact between concrete and screw condition shows the rigid motion of a screw clamped by concrete.

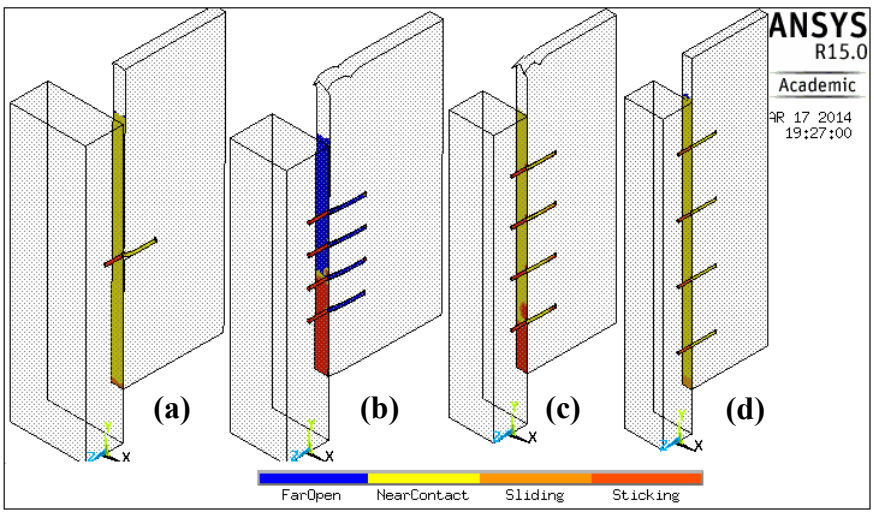

Figure 9-24 Contact condition in (a)single and four screws at (b)50, (c)100 and (d) 150

9.12.2 Inclined coach screw

The model of a single coach screw inclined at 45° was verified by the experimental results of CC coach at 45° series. The geometry of the coach screw and TCC connection specimens are discussed in Chapter 4. The mesh used in the FE model of inclined coach screw is illustrated in Figure 9-25. Figure 9-26 plots the numerical and experimental load-slip responses of TCC connection utilising an inclined coach screw.

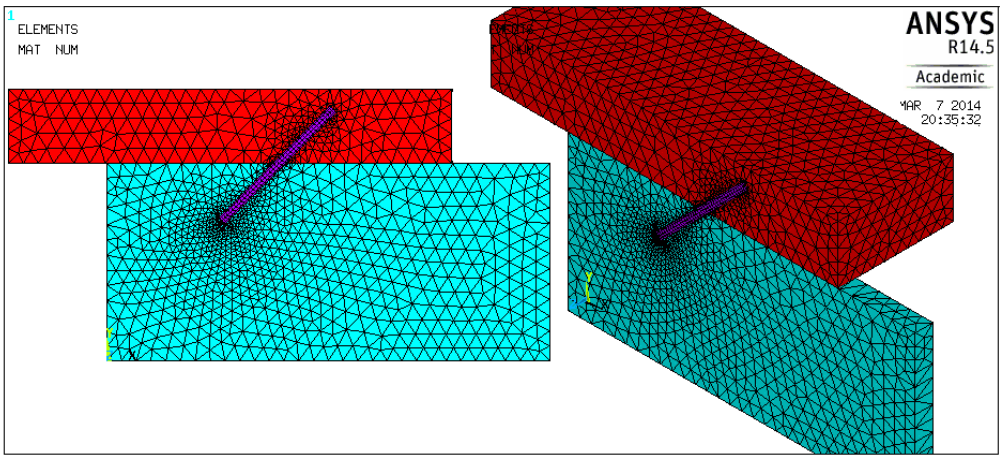

Figure 9-25 Mesh of 45° inclined coach screw TCC connection model

Figure 9-26 illustrates a relatively good agreement between the numerical and experimental results of the inclined coach screw series. However, slight underestimation was observed in both linear and post-elastic regions of the FE model compared to the experimental results (Figure 9-26). The numerical model of inclined coach screw TCC connection has a similar strength compared to that of the experimental series.

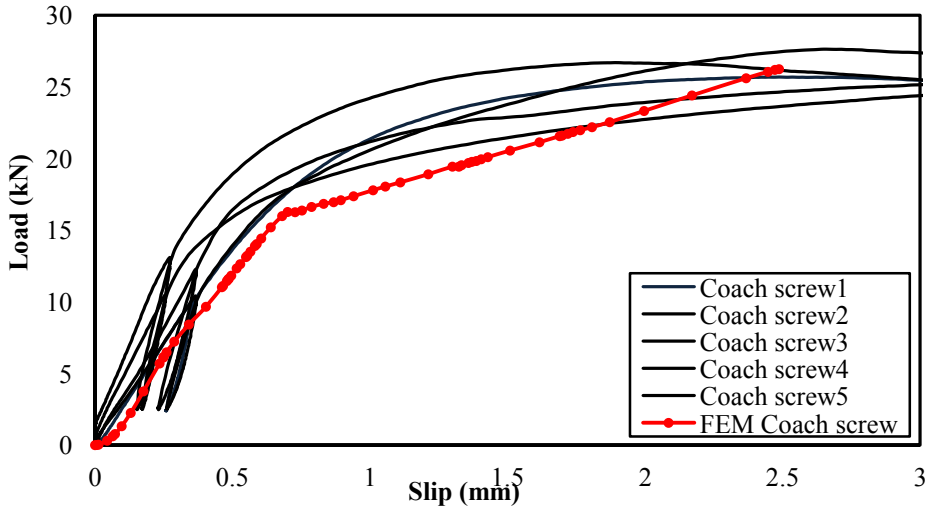

Figure 9-26 Experimental and FEM results of inclined coach screw test series

Figures 9-27 and 9-28 illustrate the numerical and experimental ultimate displacement and normal stress in loading direction of inclined coach TCC connection series.

The ultimate failure for numerical models of inclined coach screw as yielding of screw in tension agrees with experimental failure where coach screws failed in a combination of shear and tension at the TCC interface with no signs of a plastic hinge as shown in Figure 9-27. The screw in numerical model undergoes high levels of stress at the interface of timber and concrete reaching a 400-500MPa stress peak; hence its necking and yielding is evident as depicted in Figure 9-27a.

The stress concentration in the vicinity of the screw hole at the interface of timber and concrete agrees with localised crushing of timber and concrete around the screws in the experimental series as shown in Figure 9-28.

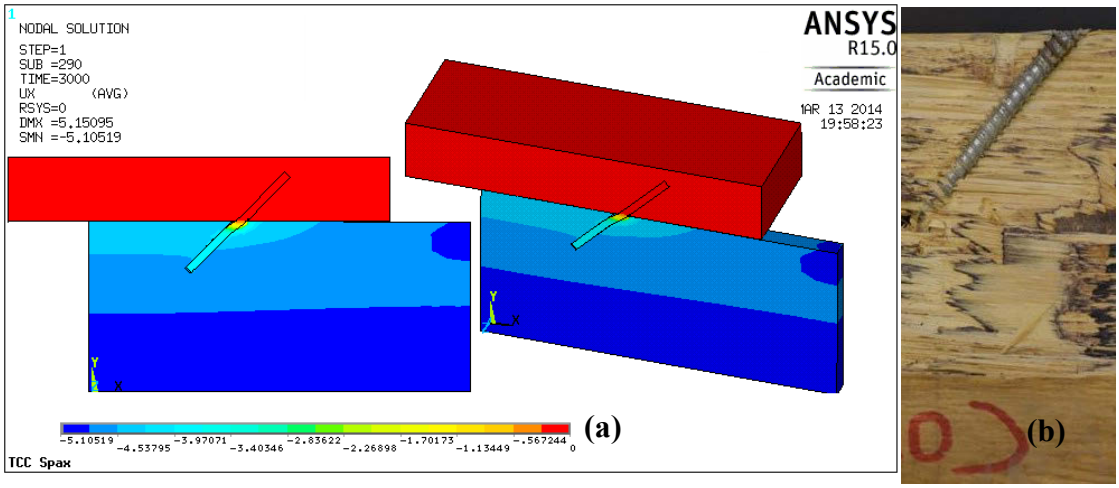

Figure 9-27 FEM displacement in x direction and (b) failure of inclined coach screw

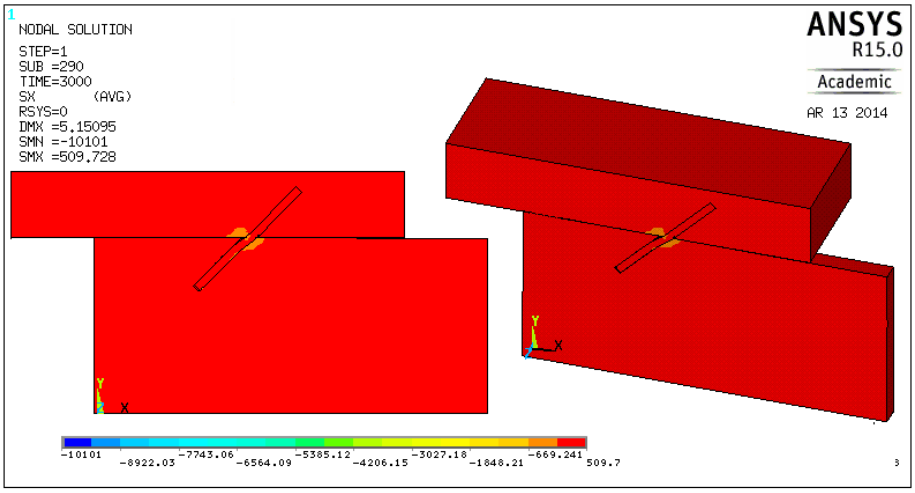

Figure 9-28 Normal stress in x direction at last sub-step of inclined coach screw model

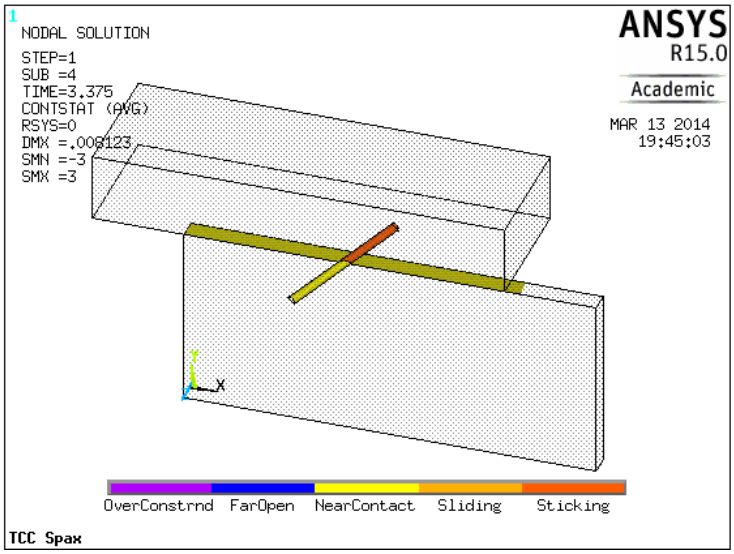

Figure 9-29 Contact condition of inclined coach TCC connection

Figure 9-29 illustrates the contact condition in ultimate load step of inclined coach TCC connection series. The sliding condition of timber-concrete and timber-screw pairs and also rigid bond of screw-concrete pairs follow the experimental observations.

9.12.3 Glue and glue in combination with normal coach screw

The modelling approach can be applied to connections other than simple screws only for example epoxy glue and epoxy glue reinforced with normal coach screw.

The experimental test of epoxy glue with and without a vertical 12mm diameter coach screw carried out by Shrestha et al. (2012) was selected to verify the model.

A set of ten connection samples comprised of a 450x200x45 LVL joist and a 450x300x75 concrete slab were tested to failure utilising push-out test. Five of the specimens (epoxy glue series) had concrete slab and LVL joist bonded together using epoxy glue only whilst for the remaining five specimens (epoxy glue with coach series), a 12mm diameter and 200mm long coach screw were subsequently installed through a pre-drilled hole in the concrete slab and into the joist following the application of the epoxy glue as illustrated in Figure 9-30.

The mesh used in the FE model of epoxy glue and epoxy glue combined with coach TCC connections are shown in Figure 9-31. The glued interface was modelled utilising always bonded contact type.

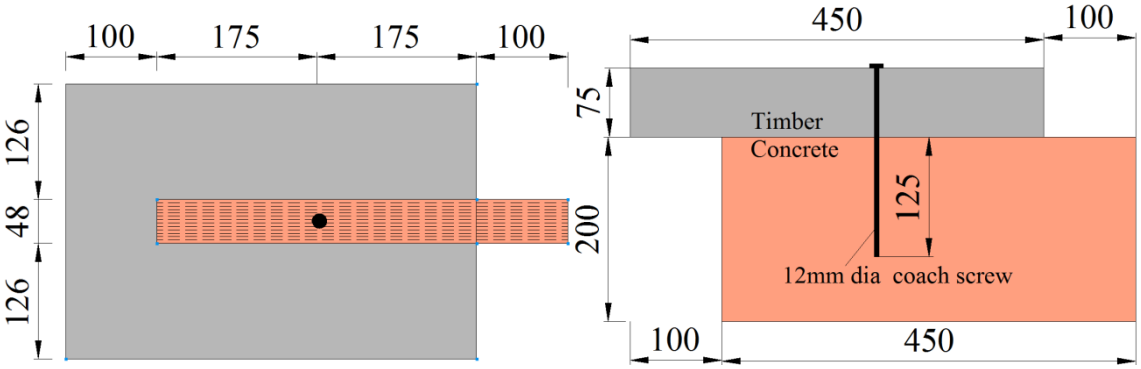

Figure 9-30 Geometry of epoxy glue TCC connection combined with coach screw

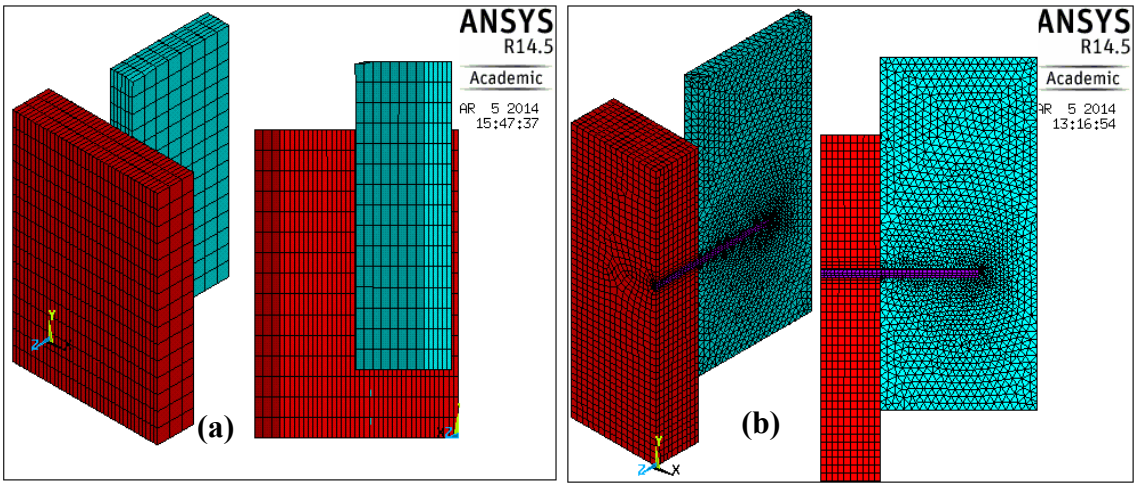

Figure 9-31 Mesh of (a) glue TCC connection and (b) coach screw and glue models

Figures 9-32 and 9-33 plot the numerical and experimental load-slip of TCC connection utilising epoxy glue and epoxy glue combined with coach screw, respectively.

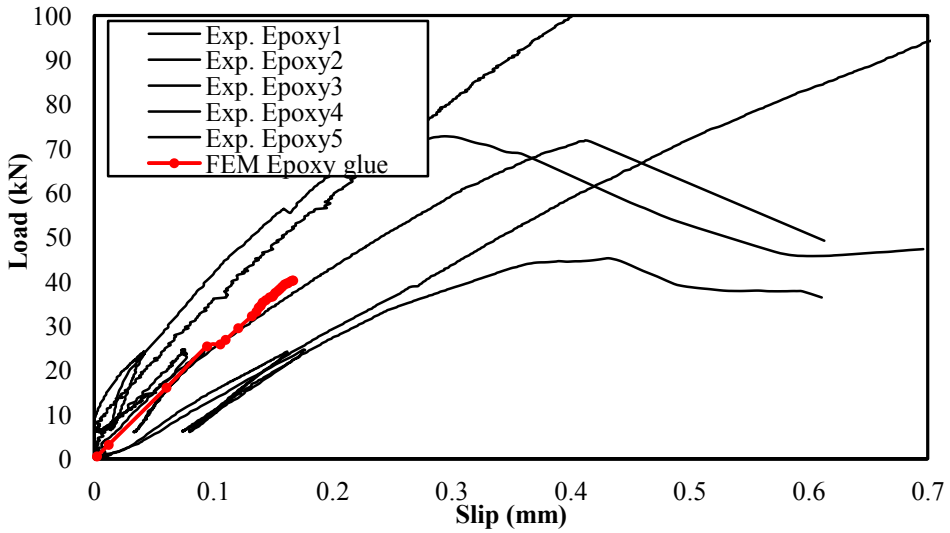

Figure 9-32 Experimental and FEM results of glued connection test series

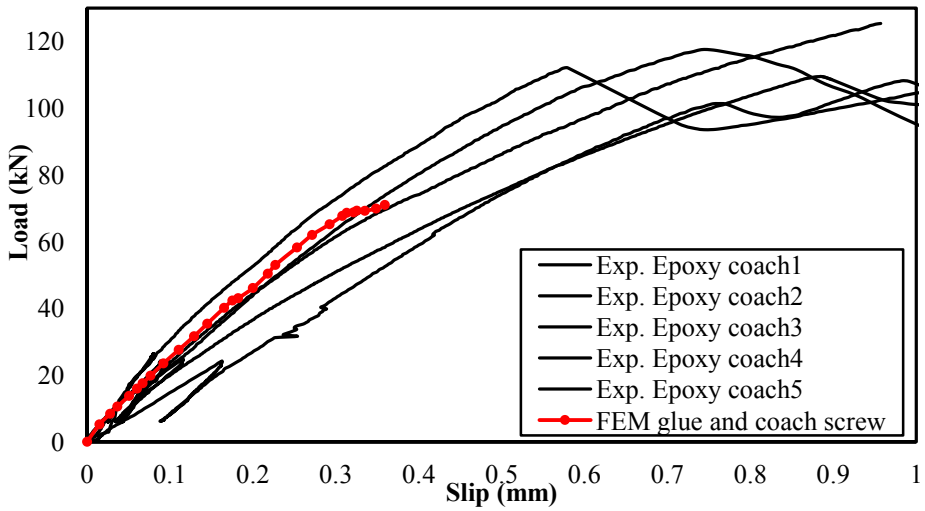

Figure 9-33 Experimental and FEM results of glued 12mm coach screws series

The numerical load-slip graphs were in good agreement with the elastic-linear part of the experimental results for the load level up to 40kN and 70kN for epoxy glue only and epoxy glue reinforced with coach screw, respectively as depicted in Figures 9-32 and 9-33. However, the models were not able to determine the non-linear post-elastic regions and ultimate strength of the experimental test series.

The linear elastic behaviour of the connections was observed for a significant portion of the load-slip curve. Hence, utilising the strengths of both materials, epoxy bonded connections with and without coach screw are effective in obtaining significant improvements in composite action between concrete and timber. By combining epoxy glue with a anchor results showed increased strength and stiffness compared to the epoxy glue alone series, but the only drawback was that the holes had to be pre-drilled.

The strength and stiffness results of epoxy glue series with and without coach screw show that connections with high strength and stiffness, comparable to that of notch type connections or continuous steel plate, were achieved by using epoxy glue for bonding timber and concrete. By combining epoxy glue with a mechanical anchor, results showed increased strength and stiffness compared to the epoxy glue only series.

Epoxy glue connections are advantageous and effective, especially for use in pre-fabricated TCCs, where a pre-cast concrete slab can be bonded to a timber joist. Figures 9-34:9-37 illustrate the numerical and experimental ultimate displacement and normal stress in the loading direction of TCC connection utilising epoxy glue only and epoxy glue reinforced with coach screw.

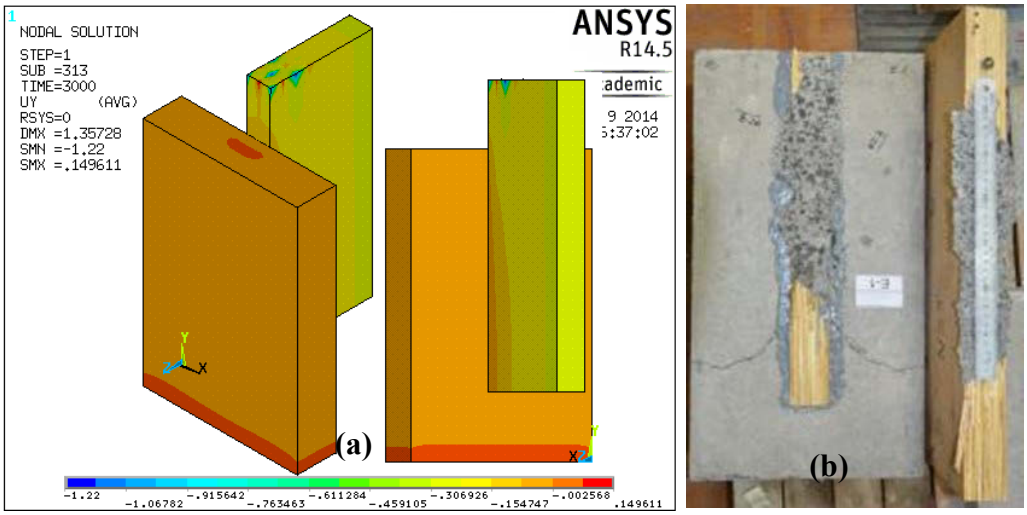

Figure 9-34 (a) FEM displacement in y direction and (b) exp. failure of epoxy glue

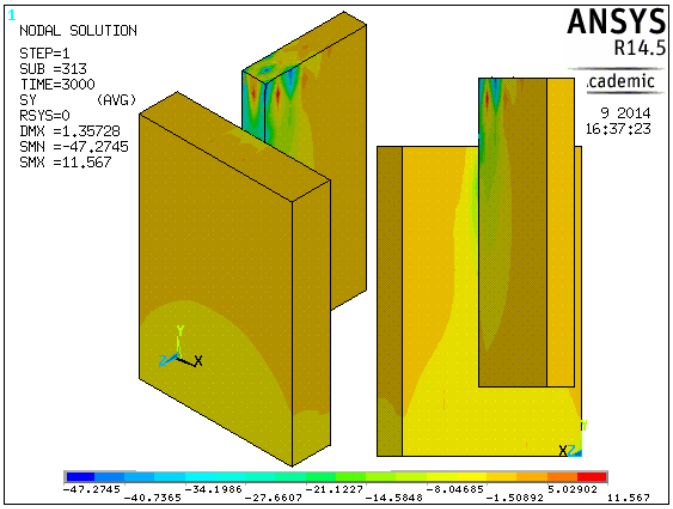

Figure 9-35 Normal stress in y direction at last sub-step of epoxy glue model

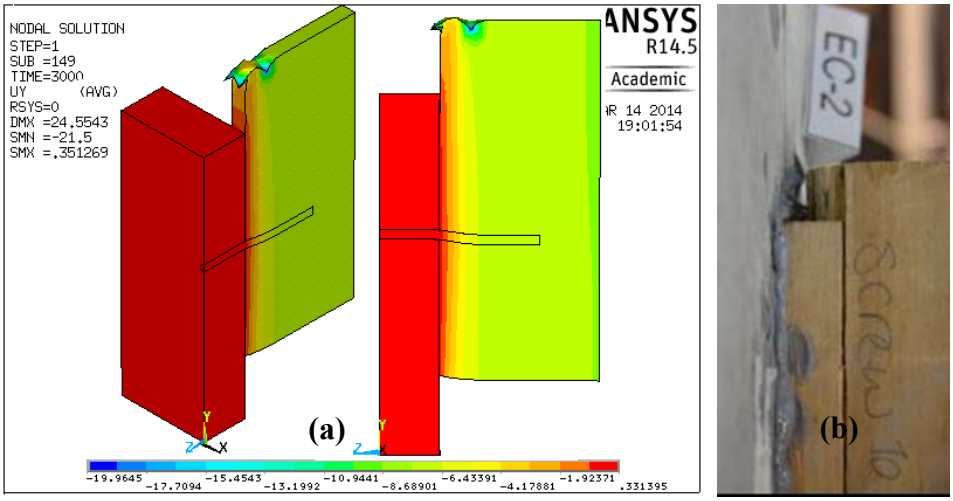

Figure 9-36 (a) FEM displacement in y direction and (b) exp. failure of epoxy glue combined with coach screw

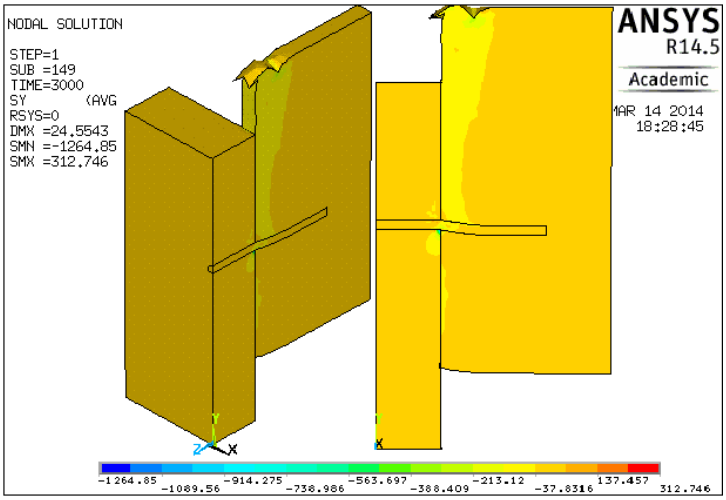

Figure 9-37 Normal stress in y direction of epoxy glue combined with coach screw

Experimental failure modes for all connections with epoxy glue only (epoxy series) were similar, characterised by sudden and brittle failure. The failure in all connections was located either in concrete or in LVL. The chunks of concrete attached to the LVL joist and LVL attached to concrete slab is depicted in Figure 9-34b. Considering a 53.4MPa average compressive strength parallel to the grain of the timber used in the TCC connection model, it is concluded that the failure of numerical models occurred on top of the timber joist in the place of the load jack where the compressive stress parallel to the grain reached a value of 53.4MPa as illustrated in Figures 9-35 and 9-37.

The epoxy bonded connections with coach screw (epoxy glue with coach screw series) facilitated in maintaining a good bond between timber and concrete as the experimental failure mode was governed by the strength of the LVL joist. Adding coach screw to the epoxy bonded connection delayed the failure of the connection, as well as avoiding brittle failure of epoxy glued connections and the connections still had some load carrying capacity following the peak load. The LVL joist failed in shear and split away from the bond surface as depicted in Figure 9-36b. Similar to the epoxy glue connection model, the epoxy bonded with coach screw model exhibited no failure in the bond interface and the coach screw remained perfectly glued to the LVL joist. Slight stress concentration around the screw at the interface of timber and concrete was observed in the numerical model of epoxy glue with coach screw series as shown in Figure 9-37.

9.12.4 Stiffness verification of the numerical models

Table 9-7 compares the mean experimental and numerical slip modulus of the connections that were modelled.

Table 9-7 Comparison of experimental and numerical serviceability slip modulus

Series	Experimental		Numerical	Error (%)
	K_{ser} (kN/mm)	CoV(%)	K_{ser} (kN/mm)	
single wood screw	12.3	35.7	4.8	60.9
4WS spaced at 50mm	13.0	13.5	15.4	18.5
4WS spaced at 100mm	14.9	8.8	15.8	6.0
4WS spaced at 150mm	14.3	18.7	16.7	16.8
Inclined coach screw	31.1	11.5	26.5	-15.9
Epoxy glue	250.3	45.0	291.4	16.4
Epoxy glue and coach screw	346.3	29.0	218.7	-36.8

The comparison of numerical and experimental stiffness for the modelled TCC connections exhibits a relatively good agreement between numerical and experimental results. However, for two models of epoxy glue combined with coach screw and single wood screw, there are relatively high differences between experimental and numerical serviceability stiffness. This can be attributed to the high variation of the stiffness results in these experimental series.

9.13 CONCLUSION

This Chapter presents a non-linear three-dimensional FE model using flexible contact element pairs to simulate the experimental tests of TCC connections reported in Chapters 5 and 10 utilising the software ANSYS, versions 14.5 and 15.0.

The modelled connections included single and multiple four wood screws with three different spacing of 50, 100 and 150mm. Moreover, a single medium size coach screw inclined at +45° to the horizontal face was simulated.

The numerical results of FEM simulations of different connector types in terms of strength, stiffness and failure behaviour were validated by experimental results obtained from push-out test as explained in Chapters 5 and 10.

The comparison of the load-slip responses, stiffness and strength of single and multiple wood screw models confirms that the numerical models are reasonably accurate to simulate TCC connections, particularly in the elastic-linear behaviour of materials. However, for two models of epoxy glue combined with coach screw and single wood

screw, there are relatively high differences between experimental and numerical serviceability stiffness. Moreover, minor overestimations were observed in the post-elastic regions of numerical models compared to those of experimental responses.

The load-slip response of the medium size coach screw inclined at 45° demonstrates the ability to simulate experimental response of inclined screws. However, slight underestimation was seen in both linear and post-elastic regions of the FE model compared to the experimental response.

The modelling approach can be applied to connections other than simple screws only such as epoxy glue and epoxy glue reinforced with normal coach screw. The numerical load-slip graphs of epoxy glue connections with and without coach screw were in good agreement with the elastic-linear part of the experimental results obtained from literature. However, the models were not able to determine the non-linear post-elastic regions and ultimate strength of experimental test series.

The findings of the Chapter demonstrates that by using the numerical model, the behaviour of TCC connections can be accurately modelled and can therefore be used for parametric study of changes in end distance, edge distance, member thickness, screw diameter, screw length and number of screws.

10 EFFECT OF SCREW SPACING ON SHEAR CONNECTIONS PROPERTIES

10.1 INTRODUCTION

In the case of multiple fastener timber composite connections, end and edge distances of connections, spacing and number of fastener and different possible failure modes add to the complexity of timber composite connections. The effect of fastener spacing, number of fasteners, and end and edge distances of fasteners on mechanical properties of TCC connections utilising multiple fasteners has not been yet well investigated.

The load capacity of multiple-fastener connections per fastener is less than that of single fastener connections. The so-called ‘‘group effects’’ of multiple fastener on the strength of connections is discussed in various codes and standards by an effective number of fastener, n_{ef} smaller than the number of fastener, n. This Chapter represents the effective number of fasteners in different codes and verifies the proposed effective number by the experimental data of push-out test.

The experimental aspect of this Chapter consists of push-out tests on TCC connections utilising single and multiple wood screws (WS) to study the effect of the screws spacing on stiffness, strength, ductility and failure mode of TCC connections. Four different types of specimens were fabricated using single and four wood screws (4WS) spaced at 50, 100 and 150mm. The strength and stiffness of the test series was analysed and the results were compared to the available group effect models for timber-timber composite connections for their practical application in the design of TCC. The failure modes observed was also compared between the specimens.

10.2 MULTIPLE-FASTENER CONNECTION

The mechanical properties of multiple fastener timber composite connections including stiffness, strength, ductility, stress distribution and failure modes depend on various parameters including wood species, fastener properties, geometry of composite components, end and edge distances of connections, spacing and number of fasteners, concrete properties if present, fastener/hole clearances, friction and loading configuration (Gattesco et al. 2004; Santos et al. 2010).

The available analytical models of load carrying capacity of timber composite connections for example the European yield model (EYM) evaluate the capacity of single fastener connections as discussed in Chapter 8.

To study the mechanical properties of multiple fasteners timber composite connections which are vertically inserted in a row parallel to the loading direction, the available analytical models of single fastener need to be extended to the multiple fasteners.

Generally the failure modes of a multiple-fastener timber composite connection is categorised into three categories of ductile, low ductile and brittle failures.

The low ductile failure is showed by plastic deformation for example the bearing failure in timber beneath the fastener whilst the formation of plastic hinges in the fastener represents the ductile failure. The brittle failures always occurs in the timber components are such as net tension, group tear-out, plug shear and splitting which are associated with rigid body motion of the fasteners (Figure 10-1) (Quenneville 2009).

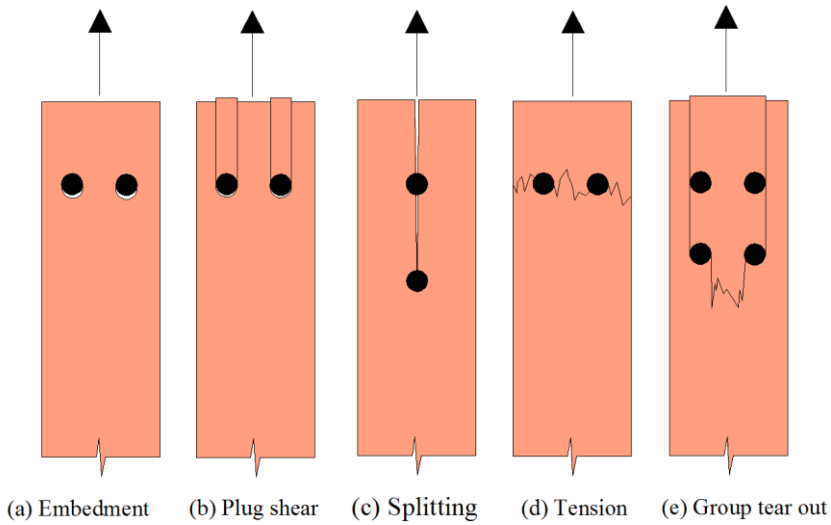

Figure 10-1 Failure modes for bolted connections (after Jorissen (1998))

In contrast to the ductile failure which is studied in the literature, the brittle failure modes are not well investigated. The ductile failure modes of timber connections are discussed by Johansen (1949) and European yield model (EYM) as given in Chapter 8.

10.3 GROUP EFFECT OF THE MULTIPLE FASTENERS

In an optimal multiple connection, the load carrying capacity of the timber connection is equal to the sum of the load carrying capacity of each single fastener. However, the strength of multiple fasteners timber composite connections is generally not equal to the strength of single fastener timber connection multiplied by the number of fastener due to unequal load distribution among the fasteners (Gattesco et al. 2004).

Such reduction in load carrying capacity depends on different parameters such as number of fasteners, fastener spacing, end and edge distances, dimensions of the composite members, the material properties of wood species, the construction tolerances, the load-slip characteristics of single fastener (Moss 1997a). Moreover, splitting of timber and/or softening of timber following complicated stress distribution around the fastener decrease the load carrying capacity of the multiple connections compared to that of the single fastener timber connection (Jorissen 1998).

Previous investigations indicate that using an adequate spacing and consequently longer connections, the reduction of load carrying capacity may be neglected. The literature indicates that the fastener spacing has a significant influence on the load carrying capacity of the fasteners whilst an adequate spacing minimises such negative implication. In practical application, sometimes the shorter spacing and consequently shorter connection is preferred which lowers the load carrying capacity, hence a larger number of fasteners is required to compensate for it (Gehri 2009).

Smaller spacing may lead to splitting of timber. Hence, in the case of multiple fastener connection, some codes such as Eurocode 5 propose minimum fastener dimensions, spacing and edge and end distances to avoid overstressing of composite components and to maximise the capacity of a fastener with a more ductile failure (Dias et al. 2011).

This reduction in load carrying capacity of multiple screw connections is stated in different design codes e.g. Eurocode 5, DIN1052 (2004), CSA086-01 (2001) and NDS (1997) by introducing a reduction factor as the effective number of fasteners, n_{ef} which is smaller than the number of fasteners, n. Hence, the effective load carrying capacity of one row of fasteners which are loaded parallel to the grain is approximated by:

$$F_{\text{multiple}} = n_{\text{ef}}\ F_{\text{single}} \tag{10-1}$$

where, F_{multiple} is the load carrying capacity of the multiple fasteners where F_{single} represents the characteristic load carrying capacity of a single fastener. In this Section, different equations proposed by various codes for approximation of the effective number of fasteners in multiple-fastener timber composite connections are introduced.

It is noted that the ductility of connection as a contributor to safety is not reflected in the standards. The fastener spacing may influence the ductility of connection (Gehri 2009).

10.3.1 Eurocode 5

Based on the experimental investigation by Jorissen (1998), Eurocode 5 (EN 2004b) approximates the effective number, n_{ef} for dowel-type fasteners with the diameter d less than 6mm for one row of fasteners which is loaded parallel to the grain as:

$$n_{ef} = \min\begin{cases} n \\ n^{\sqrt{\frac{a_1}{14d}}} \end{cases} \tag{10-2}$$

where, n_{ef} and n are the effective number of fasteners in the row and number of fasteners in the row respectively where a_1 is the spacing of the fasteners. Moreover, Eurocode 5 approximates the load carrying capacity of dowel-type fasteners which are loaded parallel to the grain with the outer thread diameter, d greater than or equal to 6mm by:

$$n_{ef} = \min\begin{cases} n \\ n^{0.9\ \sqrt[4]{\frac{a_1}{13d}}} \end{cases} \tag{10-3}$$

where, n_{ef} and n are the effective and actual number of fasteners in the row while a_1 is the fastener spacing.

10.3.2 Germany code DIN1052 (2004)

DIN1052 (2004) proposes the same equation of Eurocode 5 but instead of $13d$ a value of $10d$ is replaced as:

$$n_{ef} = \min\begin{cases} n \\ n^{0.9\ \sqrt[4]{\frac{a_1}{10d}}} \end{cases} \tag{10-4}$$

where, n_{ef} and n are the effective number of fasteners in the row and number of fasteners in the row respectively where a_1 is the fastener spacing.

10.3.3 Australian Standards AS1720.1 (2010)

AS1720.1 (2010) calculates the design capacity, $N_{d,j}$ for lateral loading in a single shear plane timber connection consisting of n screws by:

$$N_{d,j}=\phi n Q_k \tag{10-5}$$

where, Φ is the capacity factor equal to 0.95 and n indicates the total number of screws whilst Q_k represents the characteristic capacity of screw given as a function of shank diameter of fastener (Q_k is 4kN for wood screw with shank diameter of 5.1mm).

10.3.4 Canadian Standard Association CSA086-01 (2001)

CSA086-01 (2001) estimates the effective number of fastener, n_{ef} in a row in compliance with the experimental research carried out by Smith (1994) by:

$$n_{ef}=0.25\beta\left(\frac{t}{d}\right)^{0.5}\left(\frac{a_1}{d}\right)^{0.2} n^{0.7} \tag{10-6}$$

where, t is the thickness of the timber member and the coefficient β is considered to be 1 for a single row of fastener whilst the values of 0.8 and 0.6 are proposed for two and three rows of fasteners, respectively.

10.3.5 The National Design Specification for wood construction, US NDS (1997)

NDS (1997) gives an equation represented by Zahn (1991) to consider the group effect of fasteners taking into account the deformability of timber and fastener, the stiffness of fastener, modulus of elasticity and cross sectional area of timber and steel as:

$$n_{ef}=\frac{m(1-m^{2n})}{(1+r\,m^{n})(1+m)-1+m^{2n}}\frac{1+r}{1-m} \tag{10-7}$$

where,

$$r=\min\left\{\frac{E_{t1}\,A_{t1}}{E_{t2}\,A_{t2}},\ \frac{E_{t2}\,A_{t2}}{E_{t1}\,A_{t1}}\right. \tag{10-8}$$

$$m=u-\sqrt{u^2-1} \tag{10-9}$$

$$u=1+K\frac{a_1}{2}\left(\frac{1}{E_{t1}A_{t1}}+\frac{1}{E_{t2}A_{t2}}\right) \quad (10\text{-}10)$$

where, E_{t1}, A_{t1}, E_{t2}, A_{t2} are MOE and the sectional area of main and side timber members, respectively and K is the stiffness of the single fastener connection. It is noted that n and a_1 represent the number and the spacing for fasteners. Zahn (1991) approximates the stiffness of the single fastener timber-timber connections which was adopted by Forest et al. (1997) by:

$$K=246\,d^{1.5} \quad (10\text{-}11)$$

where, d is the outer thread diameter of the fastener. The linear elastic response is assumed for composite connections.

Figure 10-2 plots graphs of the effective number of fastener given by different standards associated with the material properties of different series utilising wood screw.

The effective number of fasteners depends on the number of fasteners which takes into account uneven distribution of load along fasteners and the fastener spacing, a_1 which considers the influence of spacing on the splitting strength of timber. The effect of fastener spacing, a_1 on the load carrying capacity of timber composite connections is neglected by increasing the spacing, a_1 to 13d or 14d as n_{ef} becomes 1.

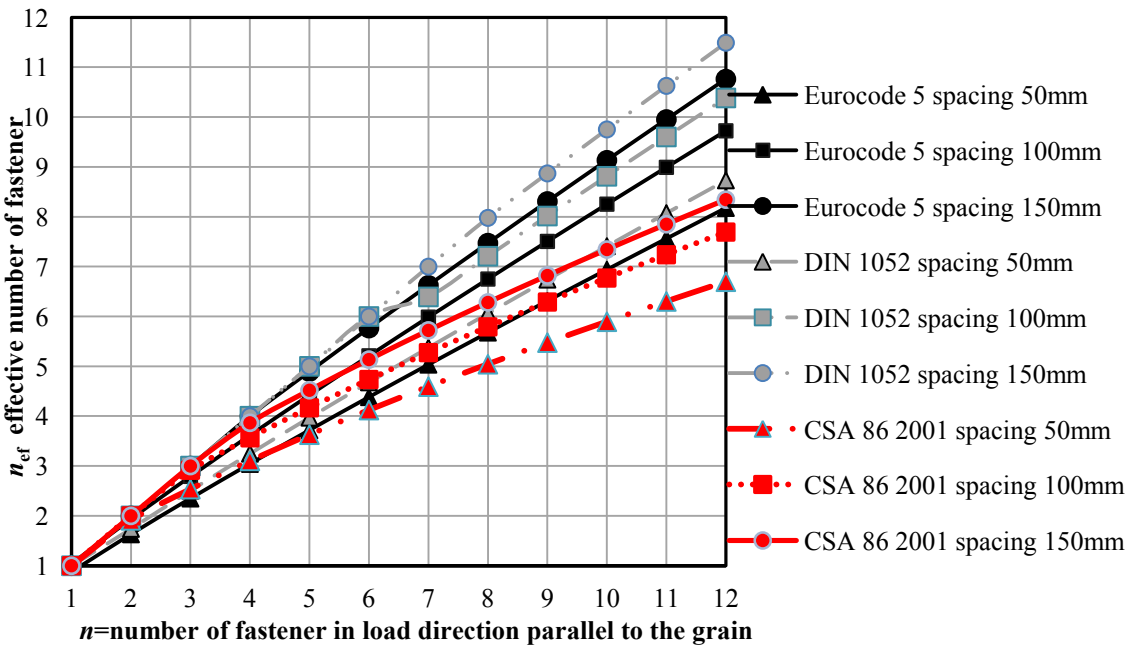

Figure 10-2 Effective number of fasteners proposed by different codes

Strength in both single and multiple-fastener connections is obtained by sufficient spacing, end and edge distances, as given by different codes. Table 10-1 tabulates the minimum spacing, edge and end distances for screws given by different codes in terms of the shank or outer thread diameter of fastener for timber composite connections.

Table 10-1 Minimum spacing and edge and end distances of screw (d is outer diameter)

Spacing or end/edge distance	AS 1720.1:2010	Eurocode 5	DIN 1052:2004	CSA86:2001
a_1 , fastener spacing in a row	$10d_{shanks}$	5*d*	5*d*	4*d*
a_2, fastener spacing between rows	$3d_{\text{shanks}}$	4*d*	3*d*	2*d*
$a_{3,t}$, End distance in a row (loaded end)	$10d_{\text{shanks}}$	max(7*d*,80)	max(7*d*,80)	max(7*d*,50)
$a_{3,c}$, End distance in a row (unloaded end)	$10d_{\text{shanks}}$	max(4*d*,40)	3*d*	-
$a_{4,t}$, Edge distance in a row (loaded edge)	$5d_{\text{shanks}}$	4*d* for *d*<8mm 40mm for 8mmβ*d*<10mm 3d for *d*ρ10mm	3*d*	-
$a_{4,c}$, Edge distance in a row (unloaded edge)	$5d_{\text{shanks}}$	-	3*d*	-

10.4 STIFFNESS OF MULTIPLE SCREW CONNECTION

There is a gap of knowledge in the literature to explain the effect of spacing on the stiffness of the multiple-fastener timber connections. Moreover, no obvious trend is observed in the experimental results to explain the effect of the number of screws on stiffness of multiple-screw timber composite connections compared to single screw connections. The stiffness of multiple-fastener connections is much lower than the stiffness of the single fastener connection multiplied by the number of fasteners.

10.5 PUSH-OUT TEST

The push-out tests were undertaken on TCC samples connected by single and multiple wood screws with different fastener spacing to determine load-slip, slip moduli, load capacity, ductility and failure modes. A total of eighteen specimens including nine samples of multiple-screw series, three per each series with different screw spacing of 50, 100 and 150mm were fabricated for the push-out tests. The results of multiple screw series were compared to the similar single wood screw series reported by Khorsandnia et al. (2012). The geometry of the different series is shown in Figures 10-3:10-6.

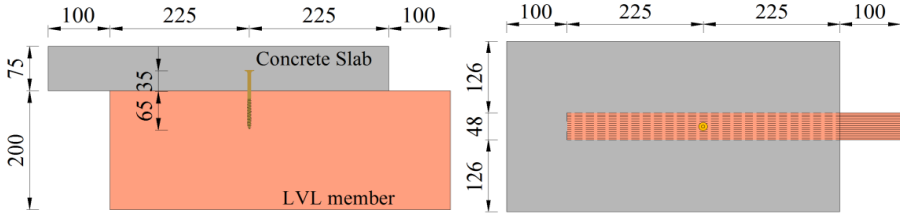

Figure 10-3 Single WS specimen: (a) cross-section, (b) plan view (in mm)

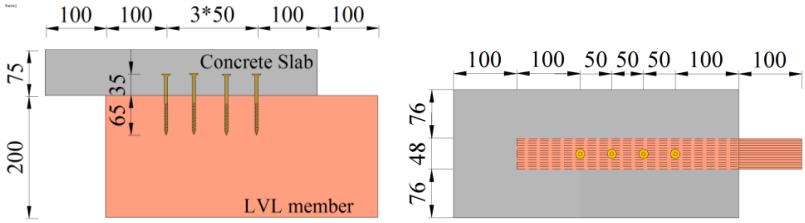

Figure 10-4 4WS spaced at 50mm specimen: (a) cross-section, (b) plan view (in mm)

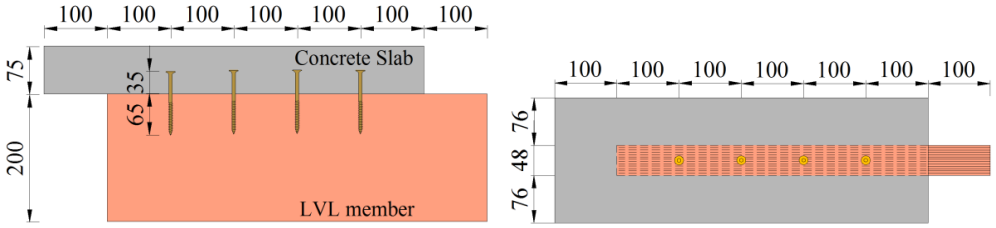

Figure 10-5 4WS spaced at 100mm specimen: (a) cross-section, (b) plan view (in mm)

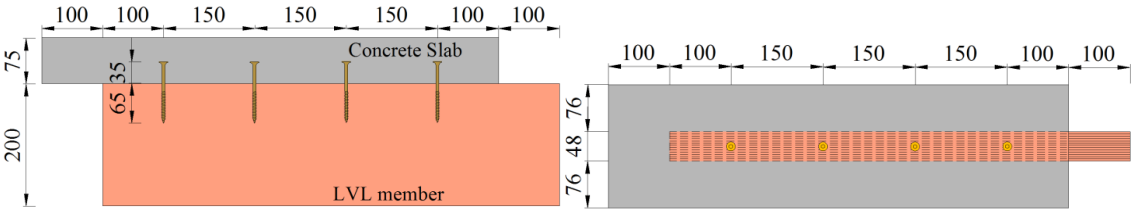

Figure 10-6 4WS spaced at 150mm specimen: (a) cross-section, (b) plan view (in mm)

Due to availability and lower cost, labour requirement and time for fabrication, wood screw were selected as shear connections in the experiment.

As tabulated in Table 10-1, AS1720.1 (2010) proposes that the minimum screw spacing in a row parallel to the loading is $10d_{\text{shank}}$. Hence, a wood screw with the shank diameter of 5.2 requires a minimum of 50mm spacing. The spacing should be more than 50mm, thus three different spacings of 50, 100 and 150mm were selected to study the effect of fastener spacing on the mechanical properties of TCC connections.

The testing machine limits the length of the LVL joist to be 850mm which can include a maximum of four wood screws spaced at 150mm and it agrees with the literature such

as Soltis et al. (1987) which reviews many other experimental investigations on the effect of spacing in timber connections employing four screws.

Since this investigation aims only to study the effect of spacing on the mechanical properties of TCC connections, other parameters such as timber joist, screw type and concrete batch are considered to be identical in different test series. The conventional concrete was used for the concrete slab. The material properties of hySPAN LVL and wood screw and the mix design and fresh and hardened properties of concrete and were reported in Chapter 4. The push-out test methodology was given in Chapter 5.

10.6 PUSH-OUT TEST RESULTS AND DISCUSSION

The load-slip responses of different series including single and four wood screw connections with various spacing are depicted in Figure 10-7. The load-slip response of each TCC series is separately graphed in Figure 10-16.

The pre-peak load-slip responses of the series were reasonably consistent and which consisted of two distinct regions of a bilinear graph as depicted in Figure 10-7. The load increased steadily in first part, then slowing without any significant drop up to the peak load following which the connections lost most of their stiffness. Sample 4WS100-2, however, showed an unusual high load. After reaching peak load, load gradually reduced to around 50-60% F_{max}, before a sudden failure in multiple screws series while single screw series represents a sudden drop of load after the peak load.

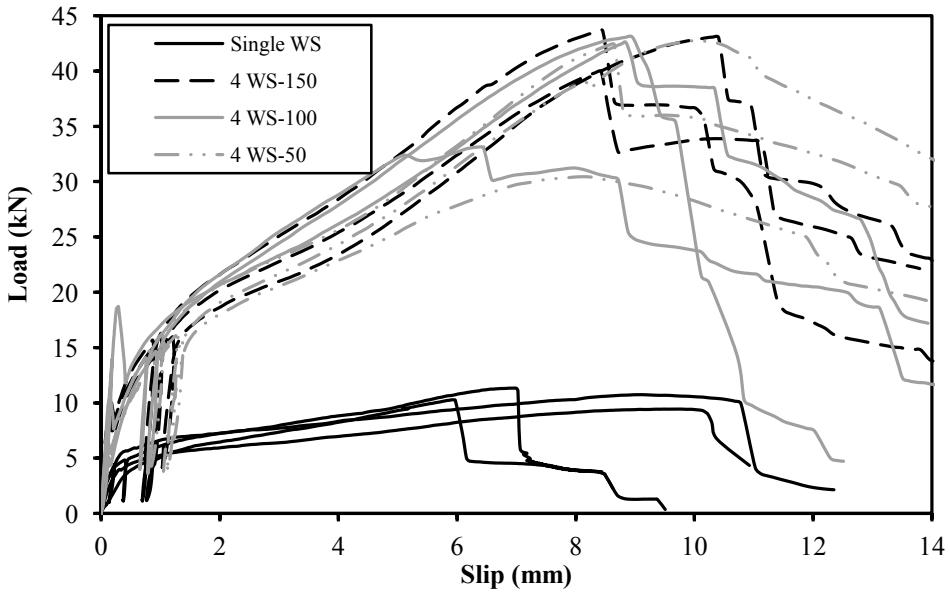

Figure 10-7 Load-slip respons of different test series

Stiffness and the 5th percentile strength of the TCC connections were calculated in compliance with EN26891 (1991) and AS1649 (2001), respectively. Comparing different series, the influence of the screw spacing on mechanical properties of the TCC connections were investigated whilst the mechanical properties of multiple screws series were compared to those of single screw series to study the group effect of wood screws in TCC specimens.

10.7 STRENGTH ANALYSIS

The values of maximum load carrying capacity, the 5th percentile strength (Q_k) as well as the mean, the standard deviation σ and coefficient of variation (CoV) of four different test series are tabulated in Table 10-2. The 5th percentiles of the lower probability limit for strengths of the test series were determined in compliance with Appendix B AS1649 (2001) as:

$$y_{5\text{percent}} = \bar{y} - t_{0.1}\sigma\sqrt{(1+\frac{1}{n})} \qquad (10\text{-}12)$$

where, σ is standard deviation and $t_{0.1}$ is the value listed in standard texts for (n − 1) degrees of freedom and a probability of 0.1.

As listed in Table 10-2 the reduction in the screw spacing accompanies the lowering of the strength with higher value of slip at failure whilst four wood screws spaced at 50mm and 100mm series represent a strength reduction of 9% and 7% compared to four wood screws at 150mm series, respectively. However, increasing the screw spacing increases the load capacity carried by each screw for the test series, the results of the student's t-test showed that the differences of the load capacities for different multiple-fastener series are not statistically significant.

Table 10-2 The load carrying capacity for different test series

Test series	No. of Specimen	Range(kN)	Mean(kN)	5th Strength Q_k (KN)	σ	CoV(%)
single wood screw	9	9.4-12.2	10.9*4=43.6	10.5	0.9	7.9
4WS-150	3	39.9-43.6	42.2	40.6	2	4.7
4WS-100	3	33.1-43.0	39.6	37.9	5.6	14.2
4WS-50	3	30.5-42.7	38.5	36.9	7	18.1

The observed splitting of timber in 4WS 50mm series contributes to the strength reduction of that series compared to other multiple screw series.

The relative capacities of each test series are presented graphically by means of a strength ratio in Figure 10-8. Figure 10-9 illustrates the load carrying capacity per screw-spacing of different series.

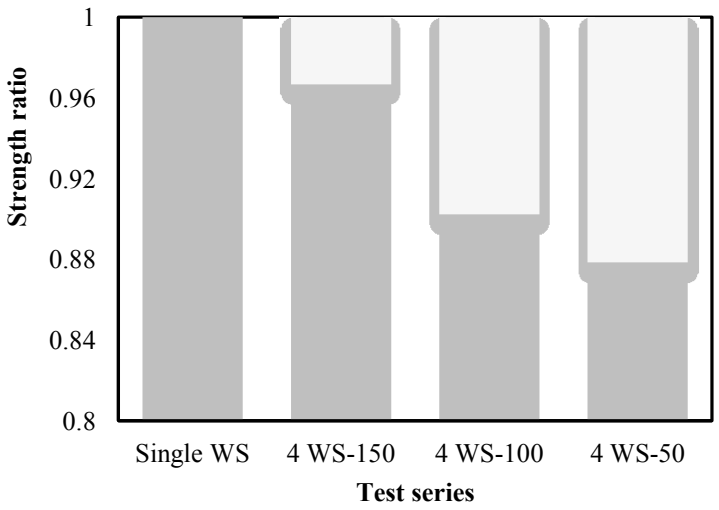

Figure 10-8 Strength comparison for different test series

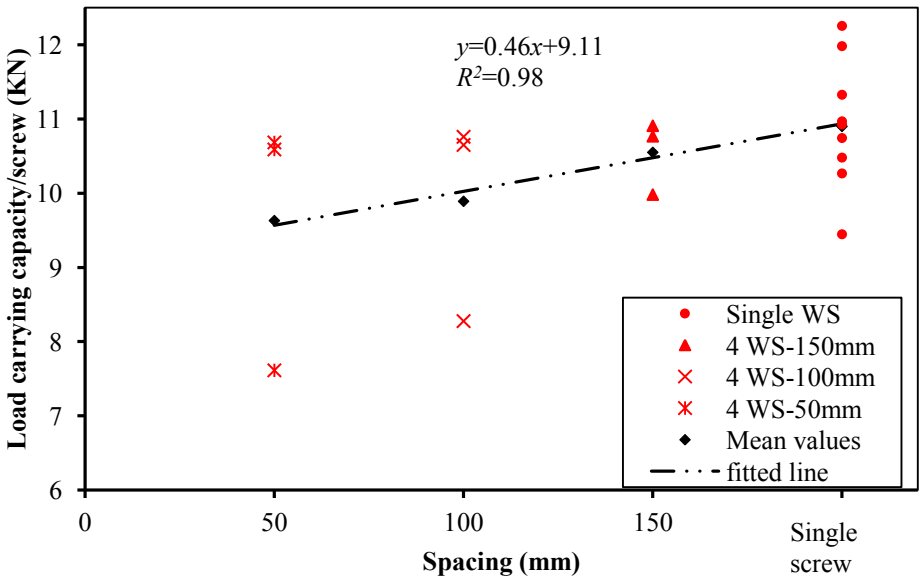

Figure 10-9 Load carrying capacity per screw-spacing of the test series

Table 10-3 Load carrying capacity per screw in the multiple fastener series

series	No.	Mean load capacity(kN)	Mean load capacity per screw (kN)	n_{ef} Exp. data	n_{ef} Eurocode 5:2004	n_{ef} DIN1052: 2004	n_{ef} CSA86:2001
Single crew	9	10.9*4=43.6	10.9	-	-	-	-
4WS-150	3	42.2	10.5	3.87	4	4	3.86
4WS-100	2	39.6	9.9	3.63	4	4	3.56
4WS-50	3	38.5	9.6	3.53	2.77	3.24	3.10

Table 10-3 lists the load capacity per screw of the series and different n_{ef} given by the codes and tests. Comparing different equations of the codes, CSA086-01 (2001) indicates a good agreement with experimental data of wood screw TCC connections.

10.8 STIFFNESS AND DUCTILITY ANALYSIS

Three different slip moduli based on EN26891 (1991) and modified methods as discussed in Chapter 5, are tabulated in Tables 10-4 and 10-5, respectively.

Table 10-4 Slip moduli of different series based on EN26891 (1991)

Series	No	Slip moduli (kN/mm)								
		$K_{s,0.4}$			$K_{u,0.6}$			$K_{u,0.8}$		
		Range	Ave	σ(CoV)	Range	Ave	σ(CoV)	Range	Ave	σ(CoV)
Single Screw	4	6.9-17.6	12.3	4.4(35.7)	4.4-7.2	5.4	1.2(23)	1.6-2.2	2	0.2(12.8)
4WS-150mm	3	11.3-16.4	14.3	2.7(18.7)	5.5-8.1	6.9	1.3(18.6)	5.1-6.4	5.7	0.7(12.3)
4WS-100mm	2	14-15.8	14.9	1.3(8.8)	8.0-11.3	9.7	2.3(23.9)	6.2-7.6	6.9	1.0(14.5)
4WS-50mm	3	11-14.2	13	1.8(13.5)	5.8-11	7.7	2.8(36.9)	5.1-5.8	5.4	0.3(5.2)

Serviceability and ultimate Slip moduli of the series shows high variability. As listed in Table 10-5, different slip moduli calculated in compliance with the modified method represent a similar trend with optimised stiffness of multiple screw series spaced at 100mm. However, the EN26891 (1991) method is much more conservative than the modified method with much lower values for serviceability and ultimate slip moduli.

Table 10-5 Slip moduli of different series based on the modified method

Series	No	Slip moduli (kN/mm)								
		$K_{s,0.4}$			$K_{u,0.6}$			$K_{u,0.8}$		
		Range	Ave	σ(CoV)	Range	Ave	σ(CoV)	Range	Ave	σ(CoV)
Single Screw	4	32.5-62.4	45.0	12.9(66.9)	5.8-8.0	7.1	0.8(28.8)	1.7-2.7	2.2	0.4(17.8)
4WS-150mm	3	23.6-32.0	31.5	7.7(24.4)	6.6-9.6	8.3	1.5(18.0)	5.7-7.0	6.3	0.6(10.1)
4WS-100mm	2	27.9-84.6	61.8	30.0(48.5)	6.8-20.0	12.0	7.0(58.2)	5.5-9.8	7.3	2.2(30.0)
4WS-50mm	3	29.5-38.0	34.2	4.3(12.7)	7.4-15.9	10.5	4.8(45.6)	6.3	0.3	0.3(5.7)

The stiffness of multiple screw connections is much lower than the stiffness of the single screw connection multiplied by the number of screws and no proportional trend is observed to explain the effect of the number of screw on stiffness of multiple screw connections compared to single screw connections.

Comparing to the single screw series, the serviceability slip modulus of multiple screw series calculated in compliance with EN26891 (1991) increased by 6%, 21% and 16% for four wood screw series spaced at 50, 100 and 150mm respectively. The increase in serviceability slip modulus is greatest with the multiple screw series with 100mm spacing and it is least with the multiple screw series spaced at 50mm.

The same trend is observed in ultimate slip modulus ($K_{u,0.6}$) of different test series based on EN26891 (1991) where ultimate slip modulus of multiple screw series increased by 42%, 80% and 28% compared to single screw series.

However, it was observed that an optimum spacing might maximise the stiffness of multiple screw series and the spacing lower or higher than the optimised spacing reduces serviceability and ultimate stiffness of multiple screw series; the results of the student's t-test proved that the differences of the serviceability and ultimate slip moduli for different series are not statistically significant.

The relative serviceability slip moduli ($K_{s,0.4}$, $K_{u,0.6}$ and $K_{u,0.8}$) of each test series are shown graphically in Figure 10-10.

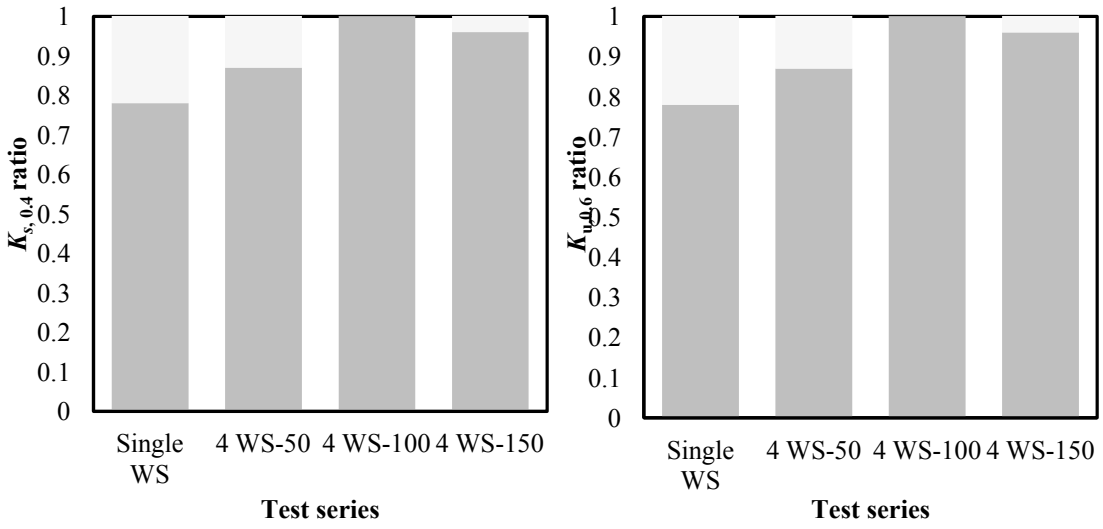

Figure 10-10 Serviceability and ultimate stiffness ratios based on EN26891 (1991)

Table 10-6 Ductility of the test series with different spacing

series	u_y(mm)	u_u(mm)	u_f(mm)	D_u		D_f	
	Ave(CoV)	Ave(CoV)	Ave(CoV)	Range	Ave(CoV)	Range	Ave(CoV)
Single Screw	0.3(34.4)	7.9(23.7)	8.2(32.2)	15.7-47.1	33.4(41.1)	16.4-49.2	33.8(39.9)
4WS-150mm	0.2(16.1)	8.9(13.1)	10.8(4.8)	45.8-78.5	58.4(30.1)	62.2-83.7	69.9(17.2)
4WS-100mm	0.4(35.6)	7.9(18.1)	9.7 (8.8)	27.6-41.7	34.6(20.4)	30.3-58.7	43.7(32.6)
4WS-50mm	0.4(2.8)	8.7(10.8)	12.2(9.5)	18.6-23.9	21.0(12.8)	27.4-32.9	29.3(10.7)

Table 10-6 lists the ductility of the test series utilising different spacing calculated in compliance with the definitions explained in Chapter 5.

Comparing the single and multiple screw spaced at 100 and 150mm series, the ductility of the multiple screw series increased whereas the single screw has a higher ductility rather than multiple screw spaced at 50mm. The reduction in the screw spacing accompanies the lowering of the ductility as listed in Table 10-6.

The observed splitting of timber in 4WS50 series contributes to the ductility reduction of that series compared to other multiple screw series.

10.9 FAILURE MODE ANALYSIS

The failures of screws as well as angle of screws at the plane of connection and state of concrete and timber around the connection were of interest. The possible failure modes of different test series have been discussed before. Following the failure of the specimens, they were removed from the test rig and were split to determine the failure mode as illustrated in Figures 10-11:10-14. The failure of the multiple screw series was due to a combination of plastic deformation and shear failure of screws and crushing and splitting of LVL connections.

The failure mode in all series was initiated by some sign of crushing in the timber and the concrete which was caused by bending of the screws. The plastic deformation of screws is followed by the formation one or two plastic hinges developing in the screws inside the timber and the concrete members whilst the ultimate failure of the connection was governed by the shearing of the screws at the interface of timber and concrete as depicted in Figures 10-11:10-14.

Shear failure of the screws at the interface of timber and concrete occurred in all the test series at ultimate load. Specimen 4WS150-2, however, was an exception where the screws were pulled out from the LVL joist.

Moreover, observation of the failed specimen revealed that the splitting of the LVL joist in the four wood screw spaced at 50mm series was an additional failure mode but the same was not observed for screw spacing of 100 and 150mm as shown in Figures 10-11:10-14.

The ductility of the connection is provided by the crushing of timber around the screw, the formation of a plastic hinge and yielding of the screw has a negligible effect on the failure mode of the connection.

Figure 10-11 Opened specimens and failure mode of single wood screw

Figure 10-12 Opened specimens and failure mode of four wood screws at 150mm

Figure 10-13 Opened specimens and failure mode of four wood screws at 100mm

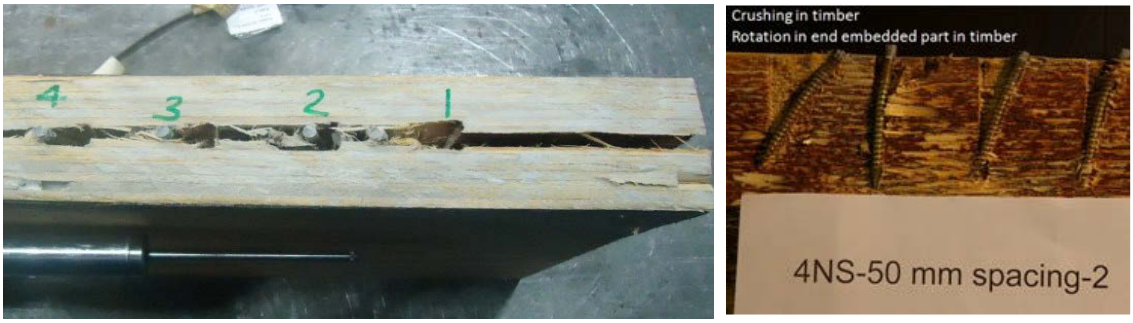

Figure 10-14 Opened specimens and failure mode of four wood screws at 50mm

The series exhibited minor signs of concrete crushing with no visible concrete cracks which indicates that the screw and timber were the weakest points of the sample where the conventional concrete component resisted the embedding forces due to rotation of the fastener at the interface of composite materials (Figure 10-15).

The reduction in the screw spacing accompanies the lowering of the crushing in concrete as shown in Figure 10-15.

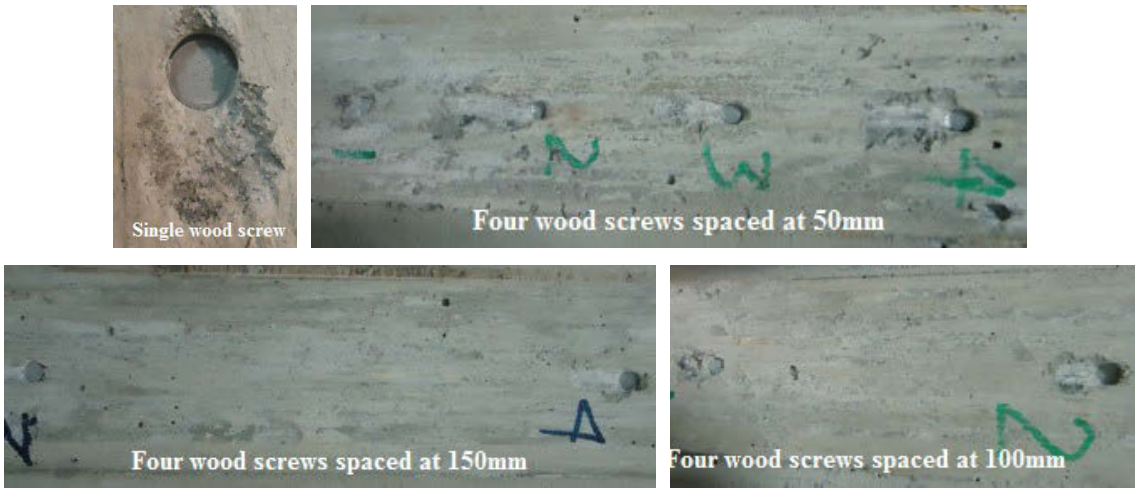

Figure 10-15 Concrete crushing in different series

10.10 MATHEMATICAL EXPRESSION FOR THE LOAD-SLIP RESPONSE

The mathematical descriptive model of each connection series is proposed using the load-slip response of the series and non-linear regression.

The load-slip responses of the series with wood screw (pre-peak and post-peak responses) consist of three distinct parts where the post-peak part varies slightly in single and multiple screws series. In all series, the load increased quite steadily, slowing slightly before peak load is reached. Single screw indicates a sudden fall after reaching the peak due to failure of screw whilst the load in multiple screw series gradually reduced to around 30% F_{max} which is due to higher ductility of multiple screws.

The pre-peak and post-peak parts of the load-slip responses of different series are considered for the mathematical expression. Due to variability of post-peak responses, the mathematical expression of single wood screw only consists of pre-peak expression. Richard–Abbott model given in Chan et al. (2000) with four parameters (a, b, c and d) is fitted into each series whilst v indicates slip at interface of composite materials as shown in Equation (10-13). Post-peak linear expression consists of two parameters.

$$\begin{cases} F = \dfrac{(a-b)\,|\upsilon|}{\left[1+\left[\left|\dfrac{(a-b)\,|\upsilon|}{c}\right|^{d}\right]^{\frac{1}{d}}\right]} + b|\upsilon| \\ F = a'\upsilon + b' \end{cases} \qquad (10\text{-}13)$$

High value of a represents the initial stiffness of the test series where low value of b shows a gradual increase in the load corresponding to deformability of the fasteners and

a large slip. The mathematical expression and its R^2 of each test series are proposed in Equations (10-14):(10-17).

R^2 indicates the square of the sample correlation coefficient between the experimental and mathematical data.

Single wood screw:

$$\begin{cases} F=\dfrac{(96.8-0.3)|\upsilon|}{[1+\left[\left|\dfrac{(96.8-0.3)|\upsilon|}{9.6}\right|^{0.50}\right]^{2}}+0.3|\upsilon|,(R^2=0.93) & \text{pre-peak response} \end{cases} \tag{10-14}$$

Four wood screws with 50mm spacing:

$$\begin{cases} F=\dfrac{(42.9-2.9)|\upsilon|}{[1+\left[\left|\dfrac{(42.9-2.9)|\upsilon|}{13.9}\right|^{1.3}\right]^{\frac{1}{1.3}}}+2.9|\upsilon|,(R^2=0.98) & \text{pre-peak response} \\ F=-1.5\upsilon+46.2,(R^2=0.72) & \text{post peak response} \end{cases} \tag{10-15}$$

Four wood screws with 100mm spacing:

$$\begin{cases} F=\dfrac{(106.9-3.6)|\upsilon|}{[1+\left[\left|\dfrac{(106.9-3.6)|\upsilon|}{12.9}\right|^{1.5}\right]^{\frac{1}{1.5}}}+3.6|\upsilon|,(R^2=0.96) & \text{pre-peak response} \\ F=-3.2\upsilon+61.0,(R^2=0.55) & \text{post peak response} \end{cases} \tag{10-16}$$

Four wood screws with 150mm spacing:

$$\begin{cases} F=\dfrac{(156.6-3.0)|\upsilon|}{[1+\left[\left|\dfrac{(156.6-3.0)|\upsilon|}{16}\right|^{0.7}\right]^{\frac{1}{0.7}}}+3.0|\upsilon|,(R^2=0.99) & \text{pre-peak response} \\ F=-2.7\upsilon+59.5,(R^2=0.73) & \text{post peak response} \end{cases} \tag{10-17}$$

Figure 10-16 indicates the mathematical expressions (red line) and load-slip responses for different series, separately.

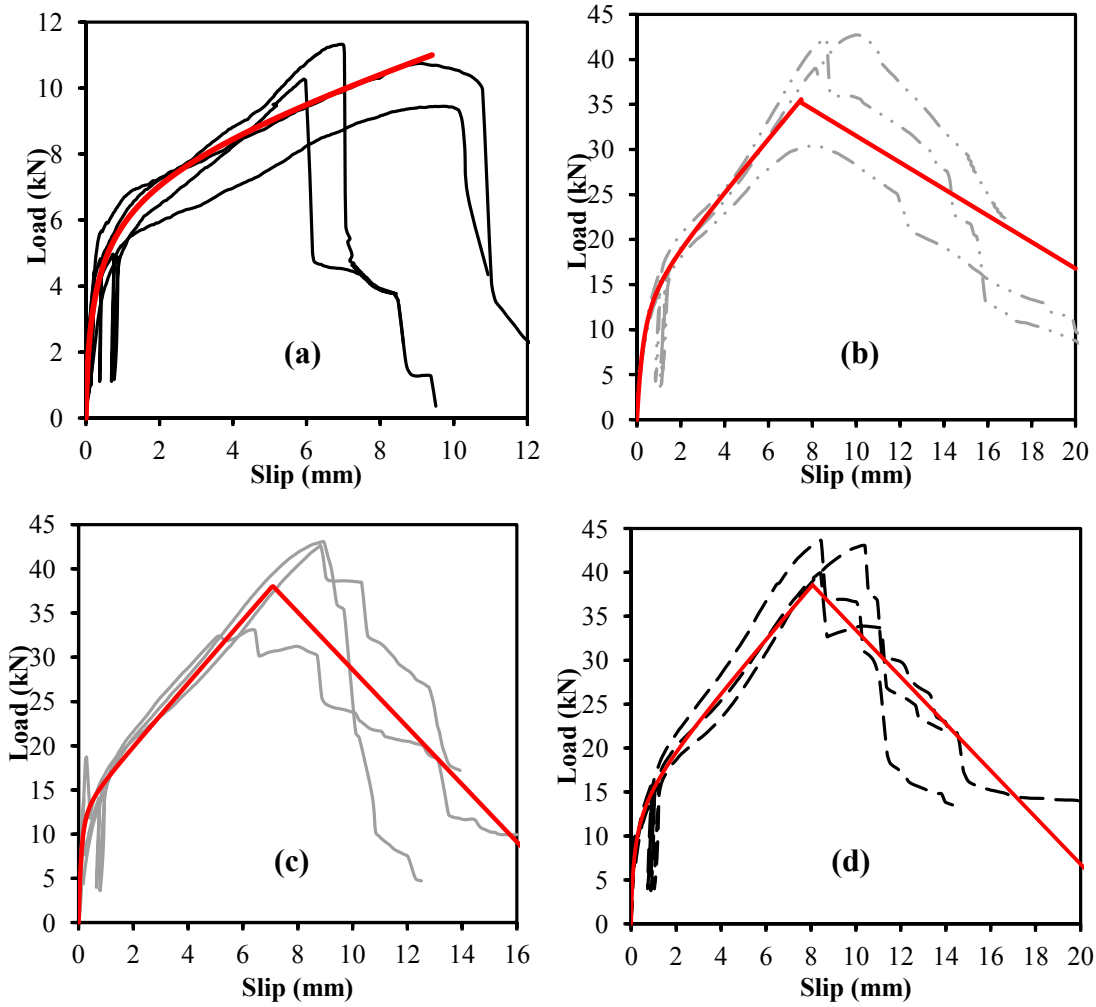

Figure 10-16 Load-slip responses (black lines) and mathematical expression (red lines) of (a) single WS, (b) 4WS at 50mm, (c) 4WS at 100mm and (d) 4WS at 150mm series

10.11 CONCLUSIONS

This Chapter first reviewed the effective number of fasteners in different codes and verifies the proposed effective number by the experimental data of push-out test obtained from push-out test of single and multiple wood screw TCC connections. The comparison was only made for 100mm wood screw series comprised of single and four-wood screw TCC connection spaced at 50, 100 and 150mm series and the effective number of fasteners in different codes has not been verified for a larger number of screws.

The push-out test determined the mechanical properties of TCC specimens; these are load carrying capacity, stiffness, ductility and failure modes which were used to examine the accuracy of the available models. Moreover, the experimental results were

used to study the effect of the screws spacing on stiffness, strength, ductility and failure mode of TCC connections for their practical application in the design of a TCC floor.

Different equations and values of n_{ef} given by the design codes show the discrepancies of the design codes. Hence, the necessity of further research on estimation of design parameters of multiple fastener connections is highlighted.

The load-responses of different series of wood screw consist of three different parts where the post peak part slightly varies in single and multiple screws series. The strength of multiple screw TCC connections is lower than the strength of single screw specimen multiplied by the number of screws due to unequal load distribution among the fasteners. However, the reduction is greatest at lowest screw spacing, four wood screw 50mm series whilst it is least with the multiple fastener series spaced at 150mm. The results of the student's t-test showed that the differences of the load capacities for different multiple-fastener series are not statistically significant.

Different slip moduli of each test series were calculated in compliance with EN26891 (1991) and modified method. The serviceability and ultimate slip moduli of multiple fasteners series are higher than the single screw series. The increase in serviceability and ultimate slip moduli is greatest with the multiple fastener series with 100mm spacing and it is least with the multiple fastener series spaced at 50mm. However, it was observed that an optimum spacing might maximise the stiffness of multiple screw series and the spacing lower or higher than the optimised spacing reduces serviceability and ultimate stiffness of multiple screw series; the results of the student's t-test showed that the differences of the serviceability and ultimate slip moduli for different multiple-fastener series are not statistically significant.

Moreover, no proportional trend is observed in the experimental stiffness results to explain the effect of number of fasteners on stiffness of multiple-fastener timber composite connections in comparison with the single fastener connections. For example, serviceability stiffness of the four wood screw100mm series is just 30% higher than the single wood screw test series.

The observed failure modes of all series include some crushing in timber and concrete which was caused by bending of the screws. The plastic deformation of the screws is followed by the formation of one or two plastic hinges whilst the ultimate shear failure of the screws at the interface of timber and concrete were observed in all the test series.

Moreover, multiple screw series spaced at 50mm revealed splitting of the LVL joist as the additional failure mode. The failure modes of the test series indicated a consistent behaviour. Finally, the mathematical descriptive model of each test series was proposed using the load-slip response of the connections and non-linear regression.

It was found that the screw spacing influences the strength, stiffness and failure of TCC connections; however the results of the student's t-test showed that the differences of the strength and stiffness results of different multiple-fastener series are not statistically significant.

11 CONCLUSIONS

11.1 CONCLUSIONS

The main focus of this PhD dissertation has been to study and quantify the behaviour of different types of particular screw type connections and high performance concrete such as light-weight concrete for application in medium to large span TCC floors of multi-storey buildings. The following conclusions can be drawn from the experimental and analytical results explored and analysed through this investigation.

11.1.1 **Experimental part**

1. The material properties of the composite components of TCCs including timber, concrete and shear connectors have been measured as reported in Chapter 4. The material properties were widely used in analytical and FE modelling of the TCC connections and modules.

2. A parametric study on 170 TCC connection specimens divided into 33 different test series utilising six different concrete types was undertaken in Chapter 5 to study the mechanical properties of shear connector such as stiffness, strength, ductility and failure mode. The experimental results of different screws (such as crossed SFS VB, crossed SPAX and coach screws and two novel types of connector) utilising various concrete types (conventional concrete, expanded polystyrene light-weight concrete, Scoria light-weight concrete, self-consolidating concrete and high-strength concrete), inclination angles (±30°, ±45° and ±60°) and with and without plywood interlayer between timber and concrete were analysed. Hence, the effects of aforementioned parameters on mechanical properties of TCC shear connections were investigated and the feasibility

and effectiveness of these alternative solutions were evaluated to deliver recommendations regarding the economy, functionality and constructability of these alternative TCCs.

- The mathematical expressions model of each series was also proposed using the load-slip response of the connections and non-linear regression.
- Based on the criteria discussed in Chapter 3 for example stiffness, strength and ductility, two novel connector designs of L and U profile in combination with three small SPAX screws were developed. The push-out test results of the L connector indicated higher strength and stiffness. Overall, the L connector has a relatively high strength and stiffness although alternative connectors such as concrete notch or steel plate achieve higher values. The U connector has no advantages over the L connector and due to its higher cost, it cannot be recommended as a viable shear connector.
- In terms of screw types, conventional concrete and EPS light-weight concrete 1600 and 2000 series showed that SFS VB screws exhibited a greater stiffness compared to SPAX screws. However, Scoria LWC SPAX series represented higher stiffness compared to similar SFS series. SPAX screws series indicated higher strength than SFS VB screws whereas the ductility of SFS was higher than the similar series of SPAX series. This research concludes that the use of SPAX screws as a shear connector in TCC module represents sizable potential compared to other slender screw connector such as SFS screw and should be further investigated.
- In terms of inclination angle of crossed SFS and SPAX screws, an angle of 30° offers the greatest stiffness and strength compared to other series. Overall, these results are very conclusive in finding that SFS VB and SPAX screws exhibited almost identical serviceability and ultimate stiffness. However, angle of shear connector significantly influenced the strength and stiffness. In terms of strength, a strong relationship between strength and inclination angle was observed.
- In terms of interlayer, comparison of different series utilising different types of concrete and shear connections with and without plywood interlayer implies that inclusion of an interlayer significantly reduced stiffness, strength and ductility of the test series.

- In terms of application of LWC, lower compressive strength and density of Scoria LWC had minor impact on the connection strength. The CC and Scoria LWC series represented greater strength than the EPS LWC 1600 and 2000 series with minor difference between Scoria LWC and CC series whereas EPS LWC 1600 and 2000 series produced greater serviceability and ultimate slip moduli compared to CC and Scoria LWC series. Failure in EPS LWC series was much more ductile than similar series utilising CC with a greater deflection following F_{max} before failure. Scoria LWC series represented higher ductility compared to similar CC series which is beneficial in construction applications. This research points to strong potential for use of moderate LWC in TCCs, with limited effect on strength or behaviour whilst for very light-weight concretes, low compressive strength, higher shrinkage and crushing behaviour of LWC may limit their application in TCCs. Application of moderate LWC in TCC is a favourable alternative for both the renovation of old timber floors and the construction of new ones.

3. Based on the short-term four-point bending tests at serviceability (SLS) and ultimate (ULS) limit states of five simply-supported TCC modules constructed from conventional and light-weight concretes utilising ±45° crossed SFS screws, the effect of LWC on the flexural stiffness, strength at SLS and ULS was evaluated. The short-term serviceability and collapse four-point bending tests of three LVL modules used in TCC modules have been also studied.

- It was found that all the TCC modules exhibited more than 94% degree of composite efficiency at SLS.
- The TCC system exhibited 2.5 and 5 times higher live-load capacity and apparent stiffness compared to timber-only modules, respectively.
- The LWC showed a recovery of strength after the load in each jack decreased to about 50kN following the yielding of a connector and after the peak load was reached. Higher ductility of SFS screws in EPS LWC in shear compared to that of CC series and ductile behaviour of EPS light-weight concrete lead to the strength recovery of the LWC modules with the ability to sustain high plastic deformation. The apparent and global stiffness of the LWC series were very close to that of the CC series. Hence, the effect of LWC slab on stiffness of TCC

modules is identified to be negligible compared to CC series. Hence, it is concluded that EPS LWC is adequate for use in terms of general structural performance in TCCs.

11.1.2 **Analytical part**

1. The Gamma method was used to obtain different analytical results including live-load capacity, deflection and degree of composite action (*DCA*) and apparent stiffness of full-composite, partially composite and non-composite TCC modules at ultimate (ULS) and serviceability (SLS) limit states. The analytical results were also compared to the similar results obtained from experimental tests.

- The experimental live-load capacity at SLS was close to that of a full-composite system in both CC and LWC series whilst the experimental live-load capacity at ULS exhibited higher differences to that of a fully-composite system in CC and LWC series. To propose a correction factor for design of TCC at SLS, the increment correction factors of 22% and 13% can be proposed to the deflection of CC and LWC series obtained from fully-composite TCC or alternatively, 18% and 16% reductions to the flexural stiffness, EI_{eff} calculated by transformed section method can be proposed for CC and LWC series, respectively.
- The Gamma method underestimates the imposed live-load approximately 20% at SLS (CC and LWC series) and ULS (CC series) whereas LWC series highlights 27% overestimation at ULS. The experimental stiffness of the CC and LWC series were 20% and 30% greater than those calculated in compliance with the Gamma method. In terms of deflection, the Gamma method overestimated the experimental deflections at both SLS and ULS by 23%-33% for CC series whilst the Gamma method deflection of LWC series indicated a 10%-33% overestimation at SLS and 21-26% underestimation compared to the experimental deflections.
- The experimental live-load capacity of TCC modules at SLS were approximately two times the design live-load requirement of 4.53kN/m^2 consisted of 3kN/m distributed live-load and a 3.5kN concentrated live-load at mid-span. Hence, other design criteria such as long-term deflection are highlighted as governing design criteria of TCC. This information is found to be useful for the model calibration and design guideline.

- Based on a parametric study on the influence of different connections and concrete properties discussed in Chapter 5 on design of TCC beams in terms of shear bond coefficient and effective bending stiffness, it was found that for the 8m TCC module the maximum shear bond coefficient was four times higher when fabricated with EPS LWC2000 SFS WI30 compared to CC SPAX I45 which represented the minimum shear bond coefficient.

2. The analytical results of available stiffness and strength models of vertically inserted screws were compared to the experimental results of the single wood screw TCC shear connection. Eurocode 5 EN (2004b) and Johansen strength models predict the strength of TCC connection utilising wood screw with a notable errors of 32.1% and 21.1%, respectively whilst the stiffness models represent an error ranging approximately 10-60%. For the simplified stiffness models such as Eurocode 5 EN (2004b), Turrini et al. (1983) and Zahn (1991) underestimated the experimental data of wood screw with an error ranging approximately 10-40% whereas the models based on Winkler theory such as Kuenzi (1955) and Gelfi et al. (2002) were inaccurate and calculated a much lower stiffness compared to that of the experimental test with an error of approximately 60%. The reasons attributed to inaccuracy of the stiffness models were discussed.

- An analytical strength model based on some adjustment to the European yield model (EYM) to predict the strength of TCC connections utilising single and crossed screws inclined to the timber grain was proposed. The failure modes considered were yield of the screw in tension and/or shear, and a series of combined failure modes such as screw withdrawal, lateral crushing of the timber and the development of plastic hinges in the screw. Comparing analytical and experimental results of crossed SFS VB and SPAX screws at various inclination angles to the vertical face, it was found that the strength model is a realistic model for predicting the failure mode and strength of inclined screws in TCC structures. This research suggests the model is reliable and can be used for the design of a TCC floor with crossed inclined screws.

- A model for the stiffness of TCC connections using crossed inclined screws was also presented. The Winkler theory of beam on elastic foundation was extended to derive the stiffness of TCC connections with inclined screws which were loaded in tension and compression. To compare the accuracy of the stiffness model, a relatively simple model with fewer variables proposed by Tomasi et al.

(2010) for crossed screws inclined at timber-timber connection was explained and its results were verified. In the case of TCC, a modification factor needs to be introduced to Tomasi et al. (2010) to take into account the effect of the presence of a rigid concrete slab in TCC compared to timber-timber connections and adjust the underestimation of experimental values for TCC connections.

It was concluded that the stiffness model of inclined screw based on Winkler theory was reasonably accurate in predicting the stiffness of TCC connections at SLS. This research suggests the model to facilitate the design of inclined screw shear connections for TCC construction.

3. A non-linear three-dimensional FE model using flexible contact element pairs was developed to simulate the experimental tests of TCC connections reported in Chapters 5 and 10 utilising the software ANSYS, versions 14.5 and 15.0. The modelled connections were single and multiple four wood screws with three different spacings of 50, 100 and 150mm. Moreover, a single medium size coach screw inclined at +45° to the horizontal face was simulated.

- The comparison of the numerical and experimental results for load-slip responses, strength, stiffness and failure mode of single and multiple wood screw models concluded that the numerical models were reasonably accurate to simulate TCC connections, particularly in the elastic-linear behaviour of materials. However, minor overestimations were observed in the post-elastic regions of numerical models compared to those of experimental responses.
- The comparison of numerical and experimental load-slip response of medium size coach screw inclined at 45° demonstrated the ability to simulate experimental response of inclined screws. However, slight underestimation was seen in both linear and post-elastic regions of the FE model compared to the experimental response.
- The modelling approach can be applied to connections other than simple screws only for example epoxy glue and epoxy glue reinforced with normal coach screws. The numerical load-slip graphs of epoxy glue connections with and without coach screws were in good agreement with the elastic-linear part of the experimental results obtained from literature. However, the models were not

able to determine the non-linear post-elastic regions and ultimate strength of the experimental test series.

- The verified FE models can be used for parametric study of changes in end distance, edge distance, member thickness, screw diameter, screw length and number of screws.

4. The proposed effective number of fastener in different codes were verified by the experimental data of push-out test obtained from push-out test of single and multiple wood screw TCC connections. The experimental results of different series of wood screw were also used to study the effect of the screws spacing on stiffness, strength, ductility and failure mode of TCC connections for their practical application in the design of a TCC floor.

- Different equations and values of effective number of screws (n_{ef}) given by the design codes show the discrepancies of the design codes for multiple fastener TCC connections.

- The strength of multiple screw TCC connections is lower than the strength of single screw specimen multiplied by the number of screw due to unequal load distribution among the screws. The reduction is greatest at lowest screw spacing, four wood screw 50mm series whilst it is least with the multiple screw series spaced at 150mm.

- The serviceability and ultimate slip moduli of multiple screw series are higher than the single screw series. The increase in serviceability and ultimate slip moduli is greatest with the multiple screw series spaced at 100mm and it is least with the multiple screw series spaced at 50mm. Hence, an optimum spacing might maximise the stiffness of multiple screw series whilst spacing lower or higher than that the optimised spacing might reduce serviceability and ultimate slip moduli of multiple screw series.

- No proportional trend is observed in the experimental stiffness to explain the effect of number of screws on stiffness of multiple-screw TCC connections in comparison with the single screw connections.

- The mathematical expressions model of each series was also proposed using the load-slip response of the connections and non-linear regression.

- The results of the student's t-test showed that the differences of the load capacities for different multiple-fastener series are not statistically significant.

11.2 RECOMMENDATIONS FOR FUTURE STUDY

As a result of undertaking this PhD study, a number of recommendations can be made for further investigations on the timber concrete composite system:

- The use of SPAX screws as a shear connector in TCC module can be further investigated as the presented results highlight sizable potential and suggest they are a suitable and practical TCC shear connection.
- The L connector design can be further optimised and refined to achieve a better result in terms of economy and mechanical behaviour compared to alternative connectors such as concrete notch or a continuous steel plate.
- Further investigations on the influence of the interlayer on mechanical properties of TCC connections and floors utilising various thicknesses of the interlayer, connectors and inclination angles can provide design recommendations for its practical applications in upgrading of old timber floors.
- Use of high performance concrete for example SCC can be further investigated by additional push-out and four-point bending tests; this can determine their influence on the stiffness, strength and failure of TCCs.
- the correction factors to transformed section and Gamma methods were obtained from the experimental four-point bending tests carried out in this investigation; thus, further experimental tests utilising different connections and concrete types are recommended to calibrate these correction factors.
- The application of Scoria LWC in TCC modules should be further investigated as the presented results highlight sizable potential. Investigation on further reduction of the EPS LWC density (<2000kg/m^3) in a TCC module can be undertaken to study the effect of low compressive strength and higher shrinkage of LWC on the structural behaviour of TCCs. The experimental results of LWC series also contribute to improve reliable design code.
- Investigation on the prediction of foundation moduli of timber and concrete as the main input parameters of the models based on Winkler theory can be carried out. Moreover, investigation of the withdrawal and embedding capacities of

TCC connections upon variation of the inclination angle can result in a more reliable strength model. Further examination of the available stiffness and strength models using a greater number of experimental data relating to different types of mechanical fastener with various lengths and diameters can increase the reliability of the models for the design of a TCC floor.

- The verified FE models given in Chapter 9 can be used for parametric study of changes in end distance, edge distance, member thickness, screw diameter, screw length and number of screws. Moreover, the FE model of TCC modules utilising different concretes and connectors can be put forward and be verified using the four-point bending test results concluded from this investigation.
- Different equations and values of effective number of screws (n_{ef}) given by the design codes show the discrepancies of the design codes. Hence, the necessity of further research on estimation of design parameters of multiple screw TCC connections is highlighted.

REFERENCES

(CHHWA), C.H.H.W.A. 2011, *Span Guide for Residential Framing*, in C.H.H.W.A. (CHHWA) (ed.)CHHWA, Australia.

ACI213R 1987, *Guide for Structural Lightweight Aggregate Concrete*, American Concrete Institute, USA.

Ahmadi & Saka 1993, 'Behavior of composite timber-concrete floors', *Journal of Structural Engineering*, vol. 119, no. 10, pp. 3111-3129.

Al-deen, S., Ranzi, G. & Vrcelj, Z. 2011, 'Shrinkage effects on the flexural stiffness of composite beams with solid concrete slabs: An experimental study', *Engineering Structures*, vol. 33, no. 4, pp. 1302-1315.

Al-Khaiat, H. & Haque, M. 1998, 'Effect of initial curing on early strength and physical properties of a lightweight concrete', *Cement and Concrete Research*, vol. 28, no. 6, pp. 859-866.

ANSYS 2009, *ANSYS 12.0*.

ANSYS, I. 2010, *ANSYS Mechanical APDL Element Reference* ANSYS.

AS1012.3.1 1998, *Methods of testing concrete Determination of properties related to the consistency of concrete - Slump test*, Standards Australia.

AS1012.4.3 1999, *Methods of testing concrete Measuring air volume when concrete is dispersed in water*, Standards Australia.

AS1012.5 1999, *Methods of testing concrete Determination of mass per unit volume of freshly mixed concrete*, Standards Australia.

AS1012.8.1 2000, *Methods of testing concrete Method of making and curing concrete - Compression and indirect tensile test specimens*, Standards Australia.

AS1012.9 1999, *Methods of testing concrete Determination of the compressive strength of concrete specimens*, Standards Australia.

AS1012.10 2000, *Methods of testing concrete Determination of indirect tensile strength of concrete cylinders (Brasil or splitting test)*, Standards Australia.

AS1012.11 2000, *Methods of testing concrete Determination of the modulus of rupture*, Standards Australia.

AS1012.12 1998, *Methods of testing concrete Determination of mass per unit volume of hardened concrete - Rapid measuring method*, Standards Australia.

AS1012.13 1992, *Methods of testing concrete Determination of the drying shrinkage of concrete for samples prepared in the field or in the laboratory*, Standards Australia.

AS1012.17 1997, *Methods of testing concrete Determination of the static chord modulus of elasticity and Poisson's ratio of concrete specimens*, Standards Australia.

AS1080.3 2000, *Timber-Methods of test*, *Method 3: Density*, Standards Australia.

AS1141.4 2000, *Methods for sampling and testing aggregates*, *Bulk density of aggregate*, Standards Australia.

AS1141.5 2000, *Methods for sampling and testing aggregates*, *Particle density and water absorption of fine aggregate*, Standards Australia.

AS1365 1996, *Tolerances for flat-rolled steel products*, Standards Australia.

AS1379 2007, *Specification and supply of concrete*, Standards Australia.

AS1594 2002, *Hot-rolled steel flat products*, Standards Australia.

AS1649 2001, *Methods of test for mechanical fasteners and connectors*, *Basic working loads and characteristic strengths*, Standards Australia.
AS1720.1 2010, *AS 1720.1—2010 Timber structures*, *Part 1: Design methods*, Standards Australia.
AS2098.1 2006, *Methods of test for veneer and plywood Moisture content of veneer and plywood*, Standards Australia.
AS2269 2004, *Plywood—Structural* Standards Australia.
AS2758.1 1998, *Aggregates and rock for engineering purposes*, *Concrete aggregates*, Standards Australia.
AS4063.1 2010, *Characterization of structural timber Test methods* Standards Australia.
AS4063.2 2010, *Characterization of structural timber Determination of characteristic values*, Standards Australia.
AS4357.0 2005, *Structural laminated veneer lumber*, *Specifications*, Standards Australia.
AS/NZS1170.0 2002, *Structural design action*, *General principles*, Australian/New Zealand Standard™.
AS/NZS1170.1 2002, *Structural design actions*, *Permanent, imposed and other actions*, Australian/New Zealand Standard™.
ASTM5764 1997, *Standard Test Method for Evaluating Dowel-Bearing Strength of Wood and WoodBased Products*, *D 5764-97a*, American Society for Testing and Materials, West Conshocken, PA.
ASTMC143 2012, *Standard Test Method for Slump of Hydraulic-Cement Concrete*, ASTM International West Conshohocken, PA.
Bathon, L., Bletz, O. & Schmidt, J. 2006, 'Hurricane proof buildings—An innovative solution using prefabricated modular woodconcrete-composite elements.', paper presented to the *World Conference on Timber Engineering WCTE*, Portland, Ore.
Bathon, L. & Graf, M. 2000, 'A continuous wood-concrete-composite system', *World Conference on Timber Engineering WCTE*.
Bathon, L.A. & Clouston, P. 2004, 'experimnetal and numerical results on semi prestressed wood-concrete composite floor systems for long span application', paper presented to the *World Conference on Timber Engineering WCTE*, Lahti, Finland.
Bautechnik, D.I.f. 2006, Deutsches Institut für Bautechnik, Berlin, Germany.
Bejtka, I. & Blaß, H.J. 2002, 'Joints with Inclined Screw', paper presented to the *International council for research and innovation in building and construction-workinfg commision W18-timber structures*, Kyoto, Japan.
Blass, H.J., Ehlbeck, J., Van der Linden, M. & Schlager, M. 1995, 'Trag- und Verformungsverhalten von Holz-Beton-Verbundkonstruktionen'.
Branco, J.M., Cruz, P. & Piazza, M. 2007, 'Experimental analysis of laterally loaded nailed timber-to-concrete connections', *Construction and Building Materials*, vol. 23, no. 1, pp. 400-410.
Brunner, M., Romer, M. & Schnüriger, M. 2007a, 'Timber-concrete-composite with an adhesive connector (wet on wet process)', *Materials and Structures*, vol. 40, no. 1, pp. 119-126.
Brunner, M. & Schnüriger, M. 2007b, 'Timber-concrete-composite with adhesive interface', *Practical Solutions for Furniture and Structural Bonding International Workshop*.
Ceccotti, A. 1995a, *Lecture E13: Timber–concrete composite structures*, Netherlands.

Ceccotti, A. 1995b, 'Timber-concrete composite structures', in, *Timber engineering*, edn Centrum Hout, The Netherlands.
Ceccotti, A. 2002, 'Composite concrete–timber structures', *Struct. Engng Mater.*
Ceccotti, A., Fragiacomo, M. & Giordano, S. 2006a, 'Behaviour of a timber-concrete composite beam with glued connection at strength limit state', *World Conference on Timber Engineering (WCTE)*, Portland, OR, USA.
Ceccotti, A., Fragiacomo, M. & Giordano, S. 2006b, 'Behaviour of a Timber-Concrete Composite Beam with Glued Connection at Strength Limit State', paper presented to the *World Conference on Timber Engineering*, USA.
Chan, S.-L. & Chui, P.-T. 2000, *Non-linear static and cyclic analysis of steel frames with semi-rigid connections*, Elsevier.
Chen, B. & Liu, J. 2004, 'Properties of lightweight expanded polystyrene concrete reinforced with steel fiber', *Cement and Concrete Research*, vol. 34, no. 7, pp. 1259-1263.
Choi, Y.W., Kim, Y.J., Shin, H.C. & Moon, H.Y. 2006, 'An experimental research on the fluidity and mechanical properties of high-strength lightweight self-compacting concrete', *Cement and Concrete Research*, vol. 36, no. 9, pp. 1595-1602.
Clouston, P., Bathon, L.A. & Schreyer, A. 2005a, 'Shear and Bending Performance of a Novel Wood--Concrete Composite System', *Journal of Structural Engineering*, vol. 131, no. 9, pp. 1404-1412.
Clouston, P., Bathon, L.A. & Schreyer, A. 2005b, 'Shear and Bending Performance of a Novel Wood–Concrete Composite System', *Journal of Structural Engineering*.
Clouston, P., Civjan, S. & Bathon, L. 2004, 'Experimental behavior of a continuous metal connector for a wood-concrete composite system', *Forest Products Journal*, vol. Vol. 54.
Clouston, P. & Schreyer, A. 2008, 'Design and Use of Wood–Concrete Composites', *PRACTICE PERIODICAL ON STRUCTURAL DESIGN AND CONSTRUCTION*, vol. 13, no. 4, pp. 167-174.
Cook, D.J. 1983, 'Expanded polystyrene concrete, concrete technology and design', *New Concrete Materials*, pp. 41– 69.
Crawford, R.H. 2009, 'Using life cycle assessment to inform infrastructure decisions: the case of railway sleepers', *6th Australian Conference on Life Cycle Assessment, Melbourne, Australia*, pp. 16-20.
Crews, K., John, S., Gerber, C., Buchanan, A., Smith, T. & Pampanin, S. 2010a, 'Innovative engineered timber building systems for non-residential applications, utilising timber concrete composite flooring capable of spanning up to 8 to 10m', *Report prepared for Forest & Wood Products Australia, Victoria*.
Crews, K.I. & Gerber, C. 2010b, 'Development of Design Procedures for Timber Concrete Composite Floors in Australia and New Zealand - Part 1: Design Methods', paper presented to the *CIB W18 WORKING COMMISION w18 timber structures*, New Zealands.
Crocetti. R, Sartori. T & Flansbjer, M. 2010, 'Timber concrete composite structures with prefabricated FRC slab', paper presented to the *world conference on timber engineering(WCTE)*, Italy.
CSA086-01 2001, *Engineering Design of Wood*, Canadian Standard Association, Ontario, Canada.
Deam, B., Fragiacomo, M. & Buchanan, A. 2008, 'Connections for composite concrete slab and LVL flooring systems', *Materials and Structures*, vol. 41, no. 3, pp. 495-507.

Dias, A.M.P.G. 2005, 'Mechanical behaviour of timber concrete joints', university of Delf.

Dias, A.M.P.G., Cruz, H.M.P., Lopes, S.M.R. & van de Kuilen, J.W. 2010a, 'Stiffness of dowel-type fasteners in timber-concrete joints', *Proceedings of the Institution of Civil Engineers: Structures and Buildings*, vol. 163, no. 4, pp. 257-266.

Dias, A.M.P.G., Cruz, H.M.P., Lopes, S.M.R. & van de Kuilen, J.W. 2010b, 'Stiffness of dowel-type fasteners in timber–concrete joints', *Proceedings of the Institution of Civil Engineers Structures and Buildings*, vol. 163, no. SB4, pp. 257–266.

Dias, A.M.P.G. & Jorge, L.F.C. 2011, 'The effect of ductile connectors on the behaviour of timber-concrete composite beams', *Engineering Structures*, vol. In Press, Corrected Proof.

Dias, A.M.P.G., Van de Kuilen, J.W., Lopes, S. & Cruz, H. 2007, 'A non-linear 3D FEM model to simulate timber-concrete joints', *Advances in Engineering Software*, vol. 38, no. 8-9, pp. 522-530.

DIN1045 2008, *Tragwerke aus Beton, Stahlbeton und Spannbeton – Teil 1: Bemessung und Konstruktion (Concrete, reinforced and prestressed concrete structures – part 1 design*, Beuth Verlag, Berlin ,Germany.

DIN1052 2004, *Entwurf, Berechnung und Bemessung von Holzbauwerken*, Beuth Verlag, Berlin ,Germany.

EFNARC 2005, *European guidelines for self-compacting concrete: specification, production and use*.

EN383 2007, *Determination of embedment strength and foundation values for dowel type fasteners*, *Timber Structures —Test methods* European Committee for Standardization, Brussels, Belgium.

EN409 2009, *Timber structures Test methods —Determination of the yield moment of dowel type fasteners*, European Committee for Standardization, Brussels, Belgium.

EN1382 1999, *Test methods Withdrawal capacity of timber fasteners*, *Timber structures*, European Committee for Standardization, Brussels, Belgium.

EN1383 1999, *Timber structures-Test methods*, *Pull-through resistance of timber fasteners*, European Committee for Standardization, Brussels, Belgium.

EN12512 2001, *Cyclic testing of joints made with mechanical fasteners*, *Timber structuresTest methods*, European Committee for Standardization, Brussels, Belgium.

EN14592 2008, *Dowel-type fasteners —Requirements*, *Timber structures* European Committee for Standardization, Brussels, Belgium.

EN26891 1991, *Timber structures - joints made with mechanical fasteners general principles for the determination of strength and deformation characteristics*, European Committee for Standardization, Brussels, Belgium.

EN, B. 1994, *Eurocode 4-Design of composite steel and concrete structures*, *Part 1-1: General rules and rules for buildings*, European Committee for Standardization, Brussels, Belgium.

EN, B. 2004a, *Eurocode 2- Design of Concrete Structures*, *Part 1-1: General Rules and Rules for Buildings*, British Standards Institution.

EN, B. 2004b, *Eurocode 5-Design of Timber Structures-Part 1-1 General rules and rules for buildings*, European Committee for Standardization, Brussels, Belgium.

Fernandez-Cabo, J.L., Arriaga, F., Majano-Majano, A. & Iñiguez-González, G. 2012, 'Short-term performance of the HSB® shear plate-type connector for timber–

concrete composite beams', *Construction and Building Materials*, vol. 30, pp. 455-462.
Flores, E., Rioseco, C. & Matamal, A. 2007, 'Calibración del modelo de Hill modificado para el Pino Radiata cileno en conexiones de cizalle doble sometidas a compressión paralela', *II Jornadas Chilenas de Estructuras de Madera. Santiago, Chile*, pp. 12-15.
Forest, A. & Association, P. 1997, 'National Design Specification for Wood Construction, (ANSI/NFoPA NDS-1997)', *Washington, DC*.
Foschi, R.O. 1974, 'Load-slip characteristics of nails', *Wood science*, vol. 7, no. 1, pp. 69-76.
Fragiacomo, M., Amadio, C. & Macorini, L. 2007, 'Short- and long-term performance of the ''Tecnaria'' stud connector for timber-concrete composite beams', *Materials and Structures*, vol. 40.
Frangi, A., Erchinger, C. & Fontana, M. 2008, 'Charring model for timber frame floor assemblies with void cavities', *Fire Safety Journal*, vol. 43, no. 8, pp. 551-564.
Frangi, A. & Fontana, M. 2003, 'Elasto-Plastic Model for Timber-Concrete Composite Beams with Ductile Connection', *Structural Engineering International*, vol. 13, pp. 47-57.
Franke, S. & Quenneville, P. 2011, 'Bolted and dowelled connections in Radiata pine and laminated veneer lumber using the European yield model', *Australian Journal of Structural Engineering*, vol. 12, no. 1, p. 13.
Gabr, M.A. & Valero, S.N. 1995, 'Geotechnical properties of municipal solid waste', *ASTM geotechnical testing journal*, vol. 18, no. 2, pp. 241-251.
Gattesco, N. & Toffolo, I. 2004, 'Experimental study on multiple-bolt steel-to-timber tension joints', *Materials and Structures*, vol. 37, no. 2, pp. 129-138.
Gehri, E. 2009, 'Influence of fasteners spacings on joint performance - Experimental results and codification', paper presented to the *CIB - W18 working commission w18 -Timber Structures*, Dübendorf, Switzerland.
Gelfi, P. & Giuriani, E. 1987, 'Shear force-slip relationship for stud connectors. Studi e Ricerche', *Corso di Perfezionamento per le Costruzioni in Cemento Armato F.lli Pesenti*, vol. 9.
Gelfi, P., Giuriani, E. & Marini, A. 2002, 'Stud Shear Connection Design for Composite Concrete Slab and Wood Beams', *Journal of Structural Engineering*, vol. 128, no. 12, pp. 1544-1550.
Gerber, C. & Crews, K. 2011, 'Development of a design procedure for Timber Concrete Composite floors in Australia and New Zealand'.
Ghavami, K. 1995, 'Ultimate load behaviour of bamboo-reinforced lightweight concrete beams', *Cement and concrete composites*, vol. 17, no. 4, pp. 281-288.
Godycki, T., Pawlica, J. & Kleszczewski, J. 1984, 'Verbunddecke aus holzrippen und Betonplatte', *Bauingenieur*, vol. 59, no. 1984, pp. 477-483.
Grantham, R., Enjily, V., Fragiacomo, M., Nogarol, C., Zidaric, I. & Amadio, C. 2004, 'Potential upgrade of timber frame buildings in the UK using timber-concrete composites', paper presented to the *World Conference on Timber Engineering WCTE* Lathi,Finland.
Gubana, A. 1995, 'Un approccio analitico per il calcolo delle deformazioni di travi miste con connessione a comportamento non lineare', *Proc., 2nd Italian Workshop on Composite Structures*, pp. 259-272.
Gurkšnys, K., Kvedaras, A. & Kavaliauskas, S. 2005, 'Behaviour evaluation of "sleeved" connectors in composite timber-concrete floors', *JOURNAL OF CIVIL ENGINEERING AND MANAGEMENT*, vol. 11, no. 4, pp. 277-282.

Gutkowski, R., Balogh, J., Natterer, J., Brown, K., Koike, E. & Etournaud, P. 2000, 'Laboratory tests of composite wood-concrete beam and floor specimens', paper presented to the *international wood engineering conference*, New Orleans US.

Gutkowski, R., Brown, K., Shigidi, A. & Natterer, J. 2008, 'Laboratory tests of composite wood-concrete beams', *Construction and Building Materials*, vol. 22, no. 6, pp. 1059-1066.

Haiman, M., Rak, M., Krolo, B., Herceg, L. & Calogivic, V. 2004, *EPS Conrete Compostie Structures Lab testing and FEA modelling*, Department of Structures, Faculty of Civil Engineering University of Zagreb, Zagreb.

Heine, C.P. & Dolan, J.D. 2001, 'A New Model to Predict the Load-Slip Relationship of Bolted Connection', *Wood and Fiber Science*, vol. 33, no. 4, pp. 534-549.

Hetényi, M. 1946, *Beams on elastic foundation: theory with applications in the fields of civil and mechanical engineering*, vol. 16.

Hill, R. 1948, 'A theory of the yielding and plastic flow of anisotropic metals', *Proceedings of the Royal Society of London. Series A. Mathematical and Physical Sciences*, vol. 193, no. 1033, pp. 281-297.

Holschemacher, K., Klotz, S. & Weiße, D. 2002, 'Application of Steel Fibre Reinforced Concrete for Timber-Concrete Composite Constructions', *LACER*, vol. 7, pp. 161-170.

Hossain, K.M.A. 2006, 'Blended cement and lightweight concrete using scoria: mix design, strength, durability and heat insulation characteristics', *International Journal of Physical Sciences*, vol. 1, no. 1, pp. 005-016.

ISO834 1975, *Fire Resistance Tests Elements of Building Construction*, International Organisation for Standardisation.

Johansen, K.W. 1949, 'Theory of Timber Connections', *International Association of Bridge and Structural Engineering*, vol. 9, pp. 249-262.

Johnsson, H. 2004, 'Plug Shear Failure in Nailed Timber Connection', Lulea University of Technology, Lulea.

Jorge, L.F., Lopes, S.M.R. & Cruz, H. 2011, 'Interlayer Influence on Timber-LWAC Composite Structures with Screw Connections', *Journal of Structural Engineering*, vol. 137, no. 5, pp. 618-624.

Jorge, L.F.C., Schänzlin, J., Lopes, S.M.R., Cruz, H. & Kuhlmann, U. 2010, 'Time-dependent behaviour of timber lightweight concrete composite floors', *Engineering Structures*, vol. 32, no. 12, pp. 3966-3973.

Jorissen, A.J.M. 1998, *Double shear timber connections with dowel type fasteners*, Delft University Press.

Karacabeyli, E. & Ceccotti, A. 1996, 'Quasi-static reversed-cyclic testing of nailed joints', *Proceedings of the 29th CIB-W18 Meeting, Universität Karlsruhe, Karlsruhe, Germany, Paper*, pp. 29-27.

Kavaliauskas, S. & Kvedaras, A. 2010, 'The Predictive Model for Load-Carrying Capacity of Inclined Screws as Connecting-Links in Timber-Concrete Composite Beams', *modern building materials,structures and techniques*, Vilnius Lithuania.

Kavaliauskas, S., Kvedaras, A. & Valiunas, B. 2007, 'Mechanical behaviour of timber-to-concrete connections with inclined screws', *JOURNAL OF CIVIL ENGINEERING AND MANAGEMENT*, vol. 8, no. 3, pp. 193–199.

Khorsandnia, N., Valipour, H.R. & Crews, K. 2012, 'Experimental and analytical investigation of short-term behaviour of LVL–concrete composite connections and beams', *Construction and Building Materials*, vol. 37, no. 0, pp. 229-238.

Kieslich & Holschemacher 2010, 'Composite constructions of timber and high-performance concrete', *Advanced material research*, vol. 133 - 134, pp. 1171-1176.

Kim, J., Yoon, J. & Kang, B. 2007, 'Finite element analysis and modeling of structure with bolted joints', *Applied Mathematical Modelling*, vol. 31, no. 5, pp. 895-911.

Kotinda, T.I. 2004, 'Modelagem numérica de vigas mistas aço-concreto simplesmente apoiadas: ênfase ao estudo da interface laje-viga', The University of São Paulo (USP) Brazil.

Kuenzi, E.W. 1955, *Theoretical design of a nailed or bolted joint under lateral load*, USDA forest products lab, Madison.

Kuhlmann, U. & Aldi, P. 2008, 'Simulation of grooved connections in timber-concrete composite beams considering the distribution of the material properties', paper presented to the *World Conference on Timber Engineering WCTE*.

Kuhlmann, U. & Michelfelder, B. 2004, 'Grooves as shear-connectors in timber-concrete composite structures', paper presented to the *World Conference on Timber Engineering WCTE*, Lahti, Finland.

Kuhlmann, U. & Michelfelder, B. 2006, 'Optimised design of grooves in timber-concrete composite slabs ', paper presented to the *World Conference on Timber Engineering WCTE*, Portland USA.

Küng, R. 1987, *Verbunddecke Holz-Leichtbeton* Technische Universitat Graz, Germany.

Larsen, H.J. 1975, 'Determination of Load-Slip Curves for Bolts and Nails', *Rep. Presented at IUFRO Wood Engrg. Group*, vol. 3.

Leborgne, M.R. & Gutkowski, R.M. 2010, 'Effects of various admixtures and shear keys in wood-concrete composite beams', *Construction and Building Materials*, vol. 24, no. 9, pp. 1730-1738.

Lukaszewska, E. 2009, 'Development of Prefabricated Timber-Concrete Composite Floors', Universitetstryckeriet, Luleå, Lulea.

Lukaszewska, E., Fragiacomo, M. & Johnsson, H. 2010, 'Laboratory Tests and Numerical Analyses of Prefabricated Timber-Concrete Composite Floors', *Journal of Structural Engineering*, vol. 136, no. 1, pp. 46-55.

Lukaszewska, E., Johnsson, H. & Fragiacomo, M. 2008, 'Performance of connections for prefabricated timber–concrete composite floors', *Materials and Structures*, vol. 41, no. 9, pp. 1533-1550.

Mackerle, J. 2005, 'Finite element analyses in wood research: a bibliography', *Wood Science and Technology*, vol. 39, no. 7, pp. 579-600.

Martin, S., Mungwaa, U., J., J.-F.o., Amos, F. & Guy, H. 1999, 'Experimental study of a composite wood concrete beam with the INSA Hilti new flexible shear connector', *Construction and Building Materials*, vol. 13, no. 1999, pp. 371-382.

Mascia, N.T. & Santana, C.L.O. 2009, 'Remarks on the slip modulus of nailed connections for linear analysis of plywood timber beams', *Construction and Building Materials*, vol. 23, no. 8, pp. 2731-2737.

Mascia, N.T., Santana, C.L.O. & Cramer, S.M. 2008, 'Evaluation of the equivalent slip modulus of nailed connections for application in linear analysis of plywood timber beams', *Materials Research*, vol. 11, pp. 151-157.

McCullough, C.B. 1943, 'Oregon tests on composite (timber-concrete) beams', *Journal of the American Concrete Institute*, vol. 14, no. 5, pp. 429-440.

McLain, T. & Thangjitham, S. 1983, 'Bolted Wood-Joint Yield Model', *Journal of Structural Engineering*, vol. 109, no. 8, pp. 1820-1835.

Mehta, P.K. & Monteiro, P.J.M. 2005, *Concrete: Microstructure, Properties, and Materials*, 3rd edn, McGraw-Hill Professional.

Meierhofer, U. 1992, 'a new efficient system for timber/concrete composite structural elements. Test, research and development', *the IUFRO S5.02 Timber Engineering Conference*.

Miled, K., Le Roy, R., Sab, K. & Boulay, C. 2004, 'Compressive behavior of an idealized EPS lightweight concrete: size effects and failure mode', *Mechanics of Materials*, vol. 36, no. 11, pp. 1031-1046.

Miotto, J.L. 2009, 'Composite structures of wood-concrete: evaluation of glued laminated timber beams reinforced with glass fibers', The University of São Paulo (USP), São Carlos.

Miotto, J.L. & Dias, A.A. 2011, 'Glulam-concrete composites: experimental investigation into the connection system', *Materials Research*, vol. 14, no. 1, pp. 53-59.

Miotto, J.L. & Dias, A.A. 2012, 'Evaluation of perforated steel plates as connection in glulam–concrete composite structures', *Construction and Building Materials*, vol. 28, no. 1, pp. 216-223.

Möhler, K. 1956, 'Über das Tragverhalten von Biegeträgern und Druckstäben mit zusammengesetztem Querschnitt und nachgiebigen Verbindungsmitteln', Habilitation TH Karlsruhe.

Molina, J. 2008, 'Análise do comportamento dinâmico da ligação formada por barras de aço coladas para tabuleiros mistos de madeira e concreto para pontes', Universidade de São Paulo.

Moses, D.M. 2000, 'Constitutive and analytical models for structural composite lumber with applications to bolted connections', University of British Columbia.

Moss, P.J. 1997a, 'Multiple-Bolted Joints in Wood Members', *General Technical Report FPL-GTR-97, US Department of Agriculture, Forest Products Laboratory*.

Moss, P.J. 1997b, 'Multiple-bolted joints in wood members: a literature review'.

Muller, P. 1922, 'Decke aus hochkantig stehenden Holzbohlen oder Holzbrettern und Betondeckschicht', *Patentschau aus dem Betonbau und den damit verwandten Gebieten. Auszuge aus den Patentschriften. Beton und Eisen, H. XVII, S*, vol. 244.

Natterer, J., Hamm, J. & Favre, P. 1996, 'Composite wood-concrete floors for multi-story buildings', paper presented to the *World Conference on Timber Engineering WCTE*, New Orleans, Louisiana.

Natterer, J.K. 2002, 'New technologies for engineered timber structures', *Progress in Structural Engineering and Materials*, vol. 4, no. 3, pp. 245-263.

Nauta, F. 1984, 'New Zealand forest service timber bridges', *Pacific timber engineering conference*, Auckland, New Zealand.

NDS 1997, *National Design Specification for wood construction*, *National Forest Products Association*, Washington D.C., USA.

Negrão, J.H.J.D.O., Leitão de Oliveira, C.A., Maia de Oliveira, F.M. & Cachim, P.B. 2010a, 'Glued Composite Timber-Concrete Beams. I: Interlayer Connection Specimen Tests', *Journal of Structural Engineering*, vol. 136, no. 10, pp. 1236–1245.

Negrão, J.H.J.d.O., Maia de Oliveira, F.M., Leitão de Oliveira, C.A. & Cachim, P.B. 2010b, 'Glued Composite Timber-Concrete Beams. II: Analysis and Tests of Beam Specimens', *Journal of Structural Engineering*, vol. 136, no. 10, pp. 1246-1254.

Nishiyama, N. & Ando, N. 2003, 'Analysis of load-slip characteristics of nailed wood joints: application of a two-dimensional geometric nonlinear analysis', *Journal of Wood Science*, vol. 49, no. 6, pp. 505-512.
Nolan, G. 2009, *Experience with concrete overlayed bridges in Tasmania*.
NSW, R.a.T.A. 2008, *Timber bridge manual*, Roads and Traffic Authority NSW, Australia, Sydney, NSW.
O'Neill, J.W. 2009, 'The Fire Performance of Timber-Concrete Composite Floors', University of Canterbury, Christchurch, New Zealand.
Ooi, C. 2011, 'Study on Pre and Post Peak Expression of Different Connection Performance for Timber-Concrete Composite System', Universiti Tun Hussein Onn, Malaysia.
Oudjene, M., Meghlat, E.M., Ait-Aider, H. & Batoz, J.L. 2013, 'Non-linear finite element modelling of the structural behaviour of screwed timber-to-concrete composite connections', *Composite Structures*, vol. 102, no. 0, pp. 20-28.
Parmanen, J., Sipari, P. & Uosukainen, S. 1999, 'Sound insulation of multi-storey houses: Summary of impact sound insulation', *VTT PUBLICATIONS*.
Patton-Mallory, M. 1996, 'The three-dimensional mechanics and failure of single bolt wood connections', Colorado State University.
Patton-Mallory, M. & Cramer, S.M. 1997a, 'Nonlinear material models for analysis of bolted wood connections', *Journal of Structural Engineering*, vol. 123, no. 8, p. 1063.
Patton-Mallory, M., Pellicane, P.J. & Smith, F.W. 1997b, 'Modeling Bolted Connections in Wood: Review', *Journal of Structural Engineering*, vol. 123, no. 8, pp. 1054-1062.
Patton-Mallory, M., Pellicane, P.J. & Smith, F.W. 1998a, 'Qualitative assessment of failure in bolted connections: maximum stress criterion', *Journal of testing and evaluation*, vol. 26, no. 5, pp. 489-496.
Patton-Mallory, M., Pellicane, P.J. & Smith, F.W. 1998b, 'Qualitative assessment of failure in bolted connections: Tsai-Wu criterion', *Journal of testing and evaluation*, vol. 26, no. 5, pp. 497-505.
Persaud, R. & Symons, D. 2006, 'Design and testing of a composite timber and concrete floor system ', *Journal of the Structural Engineering Society of New Zealand*, vol. 19, no. 1, pp. 30-43.
Piazza, M. & Ballerini, M. 2000, 'Experimental and numerical results on timber-concrete composite floors with different connection systems', paper presented to the *World Conference on Timber Engineering WCTE*, Whistler Resort, British Columbia, Canada.
Pincus, G. 1969, 'Bonded wood-concrete T-beams', *Journal of the Structural Division*, vol. 95, no. 10, pp. 2265-2279.
Pincus, G. 1970, 'Behaviour of wood-concrete composite beams', *Journal of the Structural Division*, vol. 96, no. 10, pp. 2009-2019.
Postulka, J. 1983, 'Strengthening of wooden ceiling constructions', *IABSE Symposium Strengthening of Building Structures-Diagnosis and Therapy, Venezia*.
Postulka, J. 1997, 'Holz-Beton-Verbunddecken-36 Jahre Erfahrung', *Bautechnik*, vol. 74, no. 7, pp. 478-479.
Quenneville, P. 2009, 'Design of Bolted Connections: A Comparison of a Proposal and Various Existing Standards', *Journal of the Structural Engineering Society (SESOC) New Zealand Inc*, vol. 22, no. 2, pp. 57-62.
Ramezanianpour, A., Samadian, M. & Mahdikhani, M. 2012, 'Engineering properties and durability of self-consolidating concretes (SCC) containing volcanic pumice

ash', *Asian journal of civil engineering (building and housing)*, vol. 13, no. 4, pp. 521-530.
Ravindrarajah, R., DiFalco, V. & Surian, S. 1997, 'Effects of Binder Materials on the Properties of Polystyrene Aggregate Concrete', pp. 1-16.
Richart, F. & Williams, C. 1943a, 'Tests of composite timber-concrete beams', *American Concrete Institute*, vol. 39, pp. 253-276.
Richart, F.E. & Williams Jr, C.B. 1943b, 'Tests of composite timber-concrete beams', *ACI Journal Proceedings*, vol. 39, ACI.
Ronca, P., Gelfi, P. & Giuriani, E. 1991, 'The behaviour of a wood-concrete composite beam under cyclic and long term loads', in, *Structural repair and maintenance of historical buildings II. Vol. 1: general studies, materials and analysis.*, Computational Mechanics Publications, pp. 263-275.
Sabaa, B. & Ravindrarajah, R.S. 1997, 'Engineering properties of lightweight concrete containing crushed expanded polystyrene waste', *Materials Research Society, 1997, Fall Meeting, Symposium MM, Advances in Materials for Cementitious Composites December*, pp. 1-3.
Santos, C., De Jesus, A., Morais, J. & Lousada, J. 2010, 'A Comparison Between the EN 383 and ASTM D5764 Test Methods for Dowel-Bearing Strength Assessment of Wood: Experimental and Numerical Investigations', *Strain*, vol. 46, no. 2, pp. 159-174.
Schober, K. & Rautenstrauch, K. 2006, 'Upgrading and repair of timber structures with polymer concrete facing and strengthening', paper presented to the *World Conf. on Timber EngineeringWCTE* Portland, Ore.
Selle, R., Holschemacher, K. & Heiden, B. 2010, 'An alternative approach for hybrid floors made of timber and concrete (TCCs)', *modern building materials,structures and techniques*, Vilnius Lithuania.
Shrestha, R., Mak, J. & Crews, K. 2012, 'Experimental investigation on epoxy bonded shear connection for timbers concrete composites', paper presented to the *world conference on timber engineering (WCTE)*.
Smith, I. 1994, 'The Canadian approach to design of bolted timber connections', *Wood Des. Focus*, vol. 5, no. 2, pp. 5-8.
Smith, I., Craft, S.T. & Quenneville, P. 2001, 'Design capacities of joints with laterally loaded nails', *Canadian journal of civil engineering*, vol. 28, no. 2, pp. 282-290.
Soltis, L.A. & Wilkinson, T.L. 1987, *Bolted-connection design*, US Department of Agriculture, Forest Service, Forest Products Laboratory.
Steinberg, E., Selle, R. & Faust, T. 2003, 'Connectors for Timber–Lightweight Concrete Composite ', *Journal of structural engineering*, vol. 129, no. 11, pp. 1538-1545.
STIC, L. 2009, viewed 15.04.2014 2014.
Symons, D., Persaud, R. & Stanislaus, H. 2010a, 'Slip modulus of inclined screws in timber–concrete floor', *Structures and Buildings*, vol. 16, no. 4, pp. 245–255.
Symons, D., Persaud, R. & Stanislaus, H. 2010b, 'Strength of inclined screw shear connections for timber and concrete composite construction', *The Structural Engineer*, vol. 88, no. 1, pp. 25-32.
Tan, D. & Smith, I. 1999, 'Failure In-the-Row Model for Bolted Timber Connections', *Journal of Structural Engineering*, vol. 125, no. 7, p. 713.
Tomasi, R., Crosatti, A. & Piazza, M. 2010, 'Theoretical and experimental analysis of timber-to-timber joints connected with inclined screws', *Construction and Building Materials*, vol. 24, no. 9, pp. 1560-1571.
Topçu, I.l.B. 1997, 'Semi lightweight concretes produced by volcanic slags', *Cement and Concrete Research*, vol. 27, no. 1, pp. 15-21.

Turrini, G. & Piazza, M. 1983, *Una tecnica di recupero statico dei solai in legno*.
Van der Linden, M.L.R. 1999, 'Timber-Concrete Composite Floor Systems', Delft University Press.
Winkler, E. 1867, 'Theory of elasticity and strength', *Dominicus Prague, Czechoslovakia*.
Yasar, E., Atis, C.D., Kilic, A. & Gulsen, H. 2003, 'Strength properties of lightweight concrete made with basaltic pumice and fly ash', *Materials Letters*, vol. 57, no. 15, pp. 2267-2270.
Yeoh, D. 2010, 'behaviour and design of timber concrete composite floor system', University of Canterbury, Chrischirch.
Yeoh, D., Fragiacomo, D., De Franchesch, M. & Heng Boon, K. 2010, 'The state-of-the-art on timber-concrete composite structures – a literature review', *Journal of Structural Engineering*.
Yeoh, D., Fragiacomo, M., Buchanan, A. & Gerber, C. 2009, 'Preliminary research towards a semi-prefabricated LVLconcrete composite fl oor system for the Australasian market', *Australian Journal of Structural Engineering*, vol. 9.
Yeoh, D., Fragiacomo, M. & Deam, B. 2011, 'Experimental behaviour of LVL-concrete composite floor beams at strength limit state', *Engineering Structures*, vol. 33, no. 9, pp. 2697-2707.
Yeoh, D.E.C., Fragiacomo, M., Buchanan, A., Crews, K., Haskell, J., Deam, B. 2008, 'Development of Semi-Prefabricated Timber-Concrete Composite Floors in Australasia', paper presented to the *WCTE*, Japan.
Yttrup, P. & Nolan, G. 1996, 'Performance of Timber Beam Bridges in Tasmania, Australia', *International Wood Engineering Conference*, vol. 1, pp. 75-80.
Zabihi, Z. & Gerber, C. 2012, *Interim report on experimental results and the proposed design methods for timber only floors*, University of Technology, Sydney, Sdyney.
Zahn, J.J. 1991, 'Design equation for multiple-fastener wood connections', *Journal of Structural Engineering*, vol. 117, no. 11, pp. 3477-3486.

APPENDICES

Appendix A (Chapter 4)

A.1 CONCRETE

All coarse aggregates used in mix designs were sourced from Dunmore, NSW, which include 10mm and 20mm crushed latite gravel whilst 50/50 blended fine/coarse sand was sourced from Kurnell natural river sand. Scoria light-weight aggregates were provided by Aerolite Quarries in Victoria. The grading of conventional and Scoria light-weight aggregates were carried out in compliance with AS2758.1 (1998) specifications and limits as depicted in Tables A-1 and A-2, respectively.

Table A-1 Particle distribution for coarse and fine aggregates

Sieve size	Fine aggregate		Coarse aggregate			
			10 mm(nominal size)		20 mm(nominal size)	
	Limits[1]	Passing	Limits	Passing	Limits	Passing
[mm]	[%]	[%]	[%]	[%]	[%]	[%]
26.50	-	-	-	-	100	100
19.00	-	-	-	-	85 to 100	95
13.20	-	-	100	100	-	51
09.50	100	100	85 to 100	87	0 to 20	14
06.70	-	100	-	-	-	6
04.75	90 to 100	98	0 to 20	11	0 to 5	4
02.36	60 to 100	81	0 to 5	3	-	3
01.18	30 to 100	65	0 to 2	2	0 to 2	2
0.600	15 to 80	55	-	-	-	-
0.300	5 to 40	36	-	-	-	-
0.150	0 to 25	8	-	-	-	-
0.075	0 to 20	4	-	-	-	-
Absorption [%][+]	1.2		1.8		1.6	
SSD density[kg/m³][+]	2650		2700		2710	

[*]Limits defined in accordance with AS2758.1 (1998)
[+] Test performed in accordance with AS1141.5 (2000)

Table A-2 Particle distribution for Scoria coarse and fine aggregates

Sieve size	Fine aggregate		Coarse aggregate	
			14 mm(nominal size)	
	Limits*	Passing	Limits	Passing
[mm]	[%]	[%]	[%]	[%]
26.50	-	-	100	100
19.00	-	-	85 to 100	100
13.20	-	-	-	77
09.50	100	100	0 to 20	15
06.70	-	100	-	7
04.75	90 to 100	100	0 to 5	6
02.36	60 to 100	91	-	6
01.18	30 to 100	69	0 to 2	-
0.600	15 to 80	46	-	-
0.300	5 to 40	35	-	-
0.150	0 to 25	9	-	-
0.075	0 to 20	3	-	1
Absorption [%]+	12%		9	
Uncompacted mass per unit volume of dry aggregate[kg/m³]^	850		2710	

*Limits defined in accordance with AS2758.1 (1998)
+, ^ Test performed in accordance with AS1141.5 (2000) and AS1141.4 (2000)

A maximum nominal size of 20mm aggregate was used in CC and HSC mixes whilst maximum nominal size was reduced to 10mm for other mixes with the exception of Scoria LWC mix which contained a nominal 14mm Scoria light-weight aggregate as its maximum aggregate size. All aggregates were prepared to saturated surface dry condition prior to mixing.

Shrinkage limited Portland cement and fly ash were used as the binder for some of the concrete mixes. Drinkable grade tap water was added to all mixes after conditioning to room temperature (23±2 °C). Furthermore, in order to improve the workability of the mixes a high range water reducing admixture was employed.

Mix proportioning of the raw material ingredients was carried out by mass. The mixing sequences were carried out in compliance with AS1012.5 (1999). The standard mixing process proposed by Australian standard for conventional concrete was slightly modified for LWC mixes due to the presence of the light-weight aggregate. Fresh concrete was poured into moulds and compacted utilising an external vibrating table.

The fresh properties of SCC including flowability, passing ability and filling ability of the SCC mix were measured using different test methods such as slump-flow, J ring and L box funnel as demonstrated in Figure A-1.

The slump flow test gives an indication on the flowability, passing ability and yield stress of SCC. The test involves filling an Abram's Cone with the SCC and placing it in the centre of a slump flow board complying with ASTMC143 (2012). The Abram's Cone was lifted to a height of approximately 230mm in 3 Sec and allowed the concrete to flow out onto the slump flow board in a circular shape. The slump flow diameter is then measured as the diameter of the circle of concrete within two directions (d_1 / d_2) as shown in Figure A-1a. The mix was required to reach a slump diameter of 680 mm and the mix was determined to be in compliance after the slump flow test was completed.

The J Ring test was carried out to measure the passing ability of the SCC mix through blockage. The J Ring test is very similar to the slump-flow test, the only difference being the incorporation of the J Ring which is placed in the centre of the slump-flow board and in which the Abram's Cone sits inside. The Abram's Cone is lifted to a height of approximately 230mm over 3 Sec and the mix flows outwards through the reinforcing bars on the J Ring. Slump-flow diameter is again measured along with the time the mix takes to flow to its final testing position. The testing procedure for the J Ring test is depicted in Figure A-1b. The concrete reached a diameter of 655mm in the J Ring test with no bleeding or aggregate segregation. This was compared with the slump flow test diameter of 680mm, creating a difference of 25mm. Appropriate passing ability is indicated by a diameter difference of less than 25mm which means the SCC mix was determined to have adequate passing ability.

The L box test assesses the flowability and passing ability of SCC where the concrete is subjected to blockage by reinforcement (EFNARC 2005). The L box consists of a vertical column connected to a long horizontal section, and the two are separated by a gate and a set of rebar as shown in Figure A-1c. Each of the sections has approximately the same volume; the test starts by closing the gate and then filling the vertical column with SCC to the top. Once the column in filled the gate is opened and the concrete is allowed to flow through the gate and the rebar to fill the horizontal section.

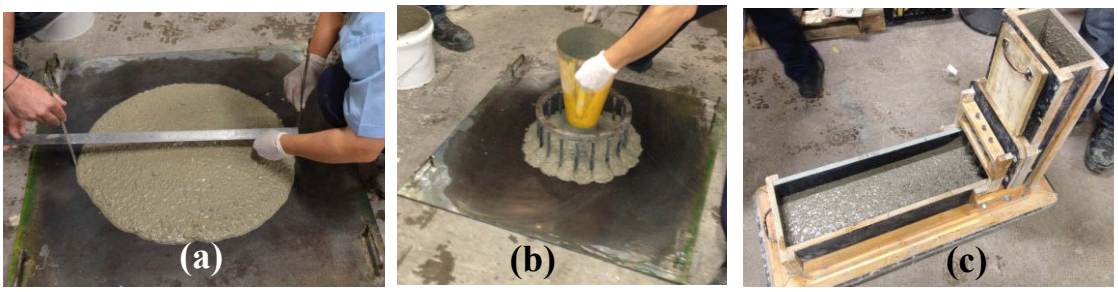

Figure A-1 (a) Slump-flow (b) J ring and (c) L box tests to measure workability of SCC

The flowability is determined by the ratio of height of the concrete at the end of the horizontal section to height of the concrete next to the vertical column. EFNARC (2005) proposed that a mix with adequate flowability has a ratio of 0.8-1.0 or greater. In the test, the ratio was approximately 0.94. Hence, the mix had adequate flowability. The passing ability was also determined to be adequate by carrying out a visual inspection which showed an even distribution of the aggregate around the rebar. Moreover, SCC exhibits much higher workability as measured by flow instead of slump. The typical value of the flow test is between 650mm-700mm.

Various specimens such as 100 and 150mm cylinders and MOR and shrinkage prisms were cured based on AS1012.8.1 (2000). The specimens were removed at 1 day and then were placed in lime-saturated water at a temperature of 20±2°C until the testing date.

A.1.1 Testing methods

Uniaxial compression and splitting tensile tests were carried out on cylindrical specimens of 100 × 200 mm in compliance with AS1012.9 (1999) and AS1012.10 (2000), respectively (Figure A-2 a and b).

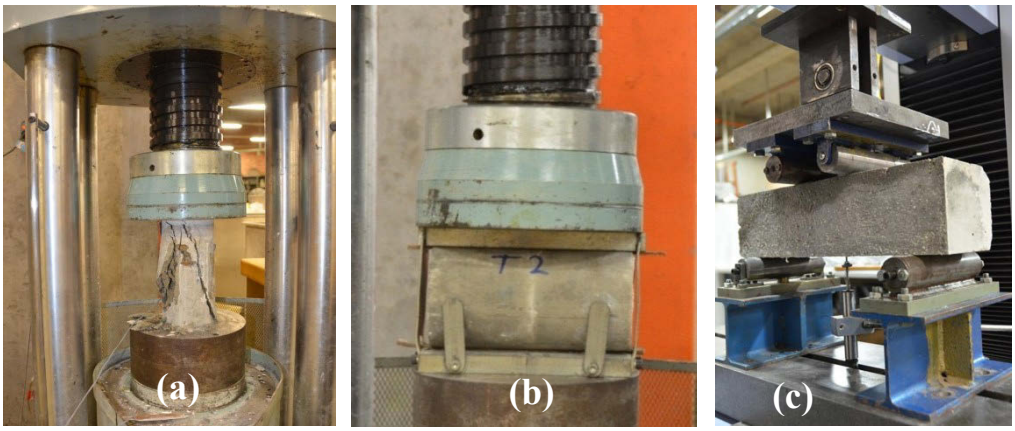

Figure A-2 (a) Uniaxial compression, (b) indirect tensile and (c) four-point bending test

Three cylindrical specimens were tested under force control in an 1800kN universal testing machine with a load rate of 20±2MPa/min and 1.5±0.15MPa/min for compressive and splitting tensile tests, respectively. Flexural tensile strength or modulus of rupture (MOR) was measured utilising a four-point bending test on three 100 × 100 × 400mm prisms at a loading rate of 1±0.1MPa/min until fracture based on AS1012.11 (2000) as depicted in Figure A-2c. Static chord modulus of elasticity (MOE) test was also obtained from three 150 × 300mm cylinders in accordance with AS1012.17 (1997). The hardened material properties tests were carried out at 3, 7 and 28 days from pouring the concrete.

A.1.2 Concrete results

The concrete matrixes of different concrete types obtained from indirect tensile test were depicted in Figures A-3 and A-4. Compressive and indirect tensile strength developments from 3 to 7 and 7 to 28 days of different concrete types are illustrated in Figure A-5. The pre-peak compressive stress-strain graphs of the series at different ages were plotted utilising the compression test as illustrated in Figure A-6.

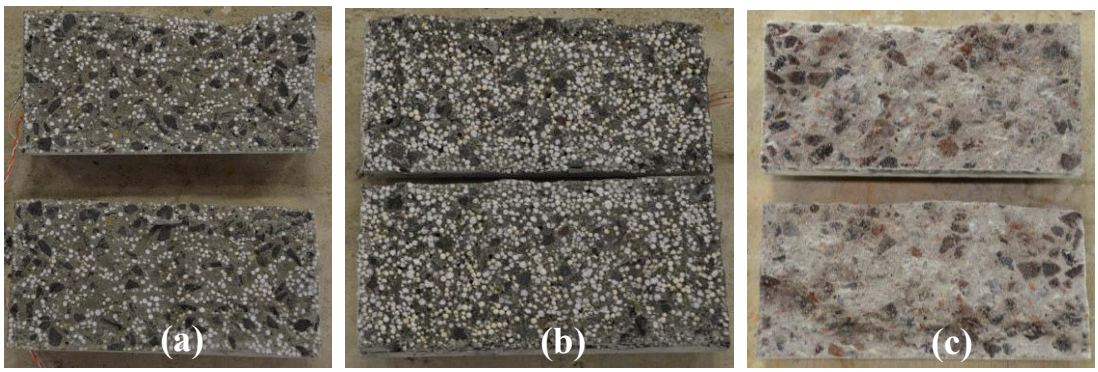

Figure A-3 Concrete matrix (a) EPS LWC2000, (b) EPS LWC1600 and (c) Scoria LWC

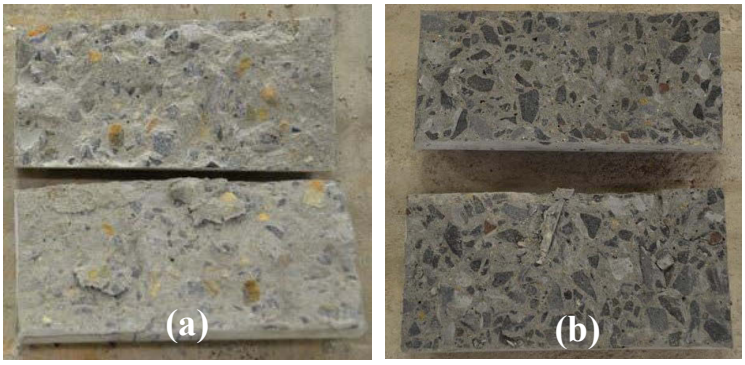

Figure A-4 Concrete matrixes (a) CC and (b) HSC series

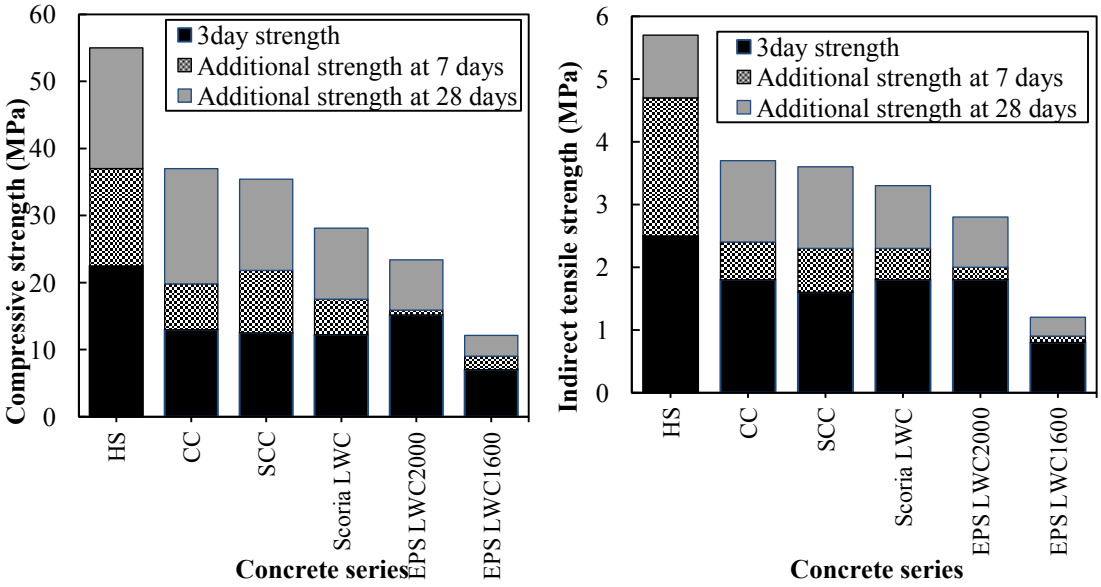

Figure A-5 Compressive and tensile strengths development of different series

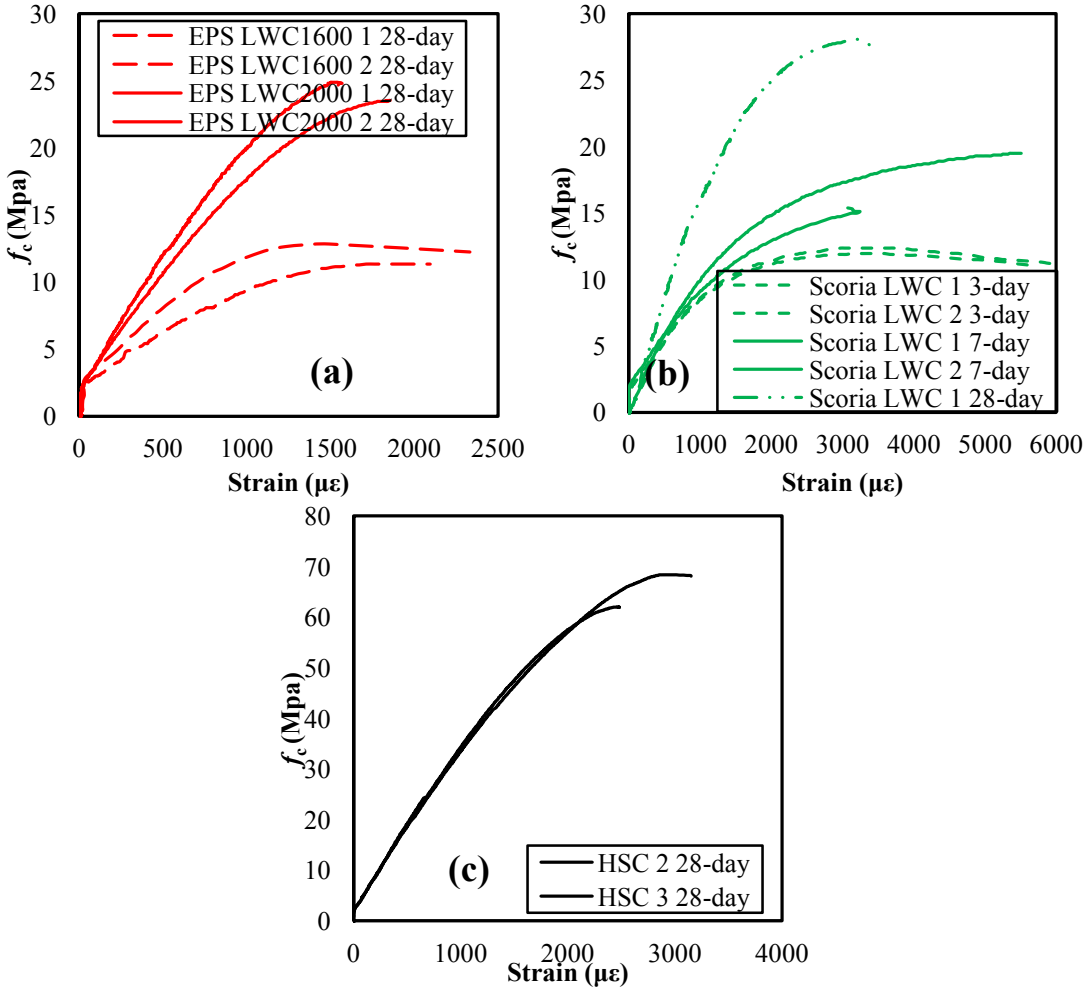

Figure A-6 Pre-peak compressive stress-strain of (a) EPS LWC1600 and 2000 series, (b) Scoria LWC and (c) HSC concrete series

It is noteworthy to mention that strain gauges used in the test were broken after experiencing the peak load. As a result the pre-peak responses were obtained from the compressive test.

Concrete represents a complex failure mode under different types of loading and this is attributed to various sizes and shapes of the voids in the concrete matrix and also the presence of micro cracks at the interfacial transition zones (Mehta & Monteiro 2005).

Comparing indirect tensile and compression tests, it was observed that higher energy is needed to initiate and extend cracks in the concrete matrix in compression. Hence, concrete failure under compression is less brittle compared to its failure in tension.

In the compressive test of EPS LWC1600 and 2000, no crack was initiated in the matrix up to about 50% of compressive strength whilst in the presence of coarse aggregate in the rest of mixes, a stable system of shear-bond cracks already was evident and their size and length grew as the compressive load increased and initiated a failure surface at an angle of approximately 20°- 30° from the vertical direction as shown in Figure A-7a, b and c.

Observations of the compressive strength test exhibited major differences such as the shape and angle of cracks in the test series under compression failure as depicted in Figure A-7.

In concrete mixes utilising 20mm coarse aggregate such as high-strength and conventional concretes (Figure A-7a and b) failure was brittle whereas EPS LWCs showed much higher ductility with many cracks on the surface (Figure A-7d and e).

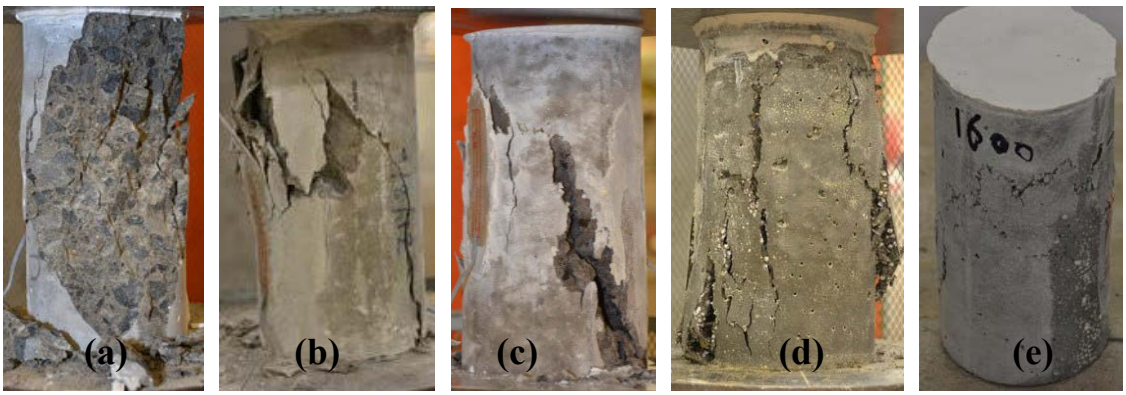

Figure A-7 Failure mode of (a) HSC, (b) CC, (c) Scoria LWC, (d)EPS LWC2000 and (e) EPS LWC1600 in compression

A.1.3 Drying shrinkage

The shrinkage of different concrete types was measured up to 112 drying days using three samples of 75x75x280mm in compliance with AS1012.13 (1992) as depicted in Figure A-8.

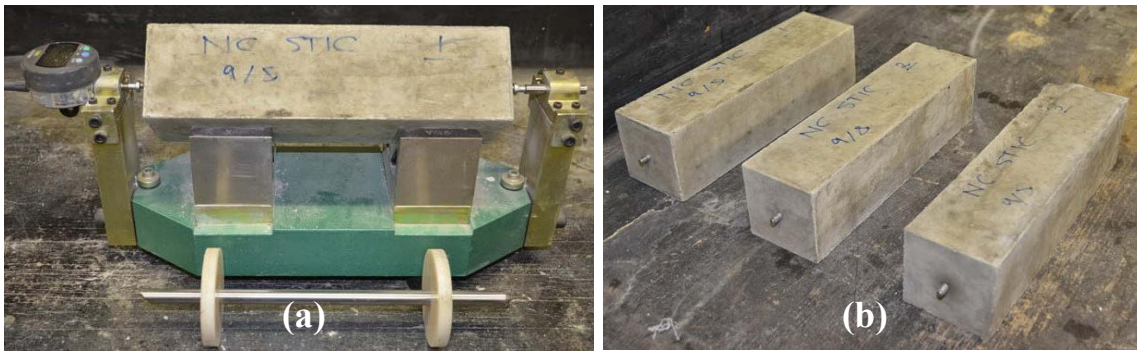

Figure A-8 (a) Shrinkage measurement and (b) shrinkage samples

Figures A-9:A-15 illustrate the shrinkage-age and weight-age graphs for different test series to provide an indication of their suitability for use in TCCs where shrinkage is an important consideration. The shrinkage results of high performance concrete series were compared to those of conventional series as a reference.

A significant part of the shrinkage occurred in the first 50 days. The EPS LWC mixes were repeated utilising shrinkage limited cement which resulted in 25% lower shrinkage at 112 drying days compared to a similar series of conventional cement.

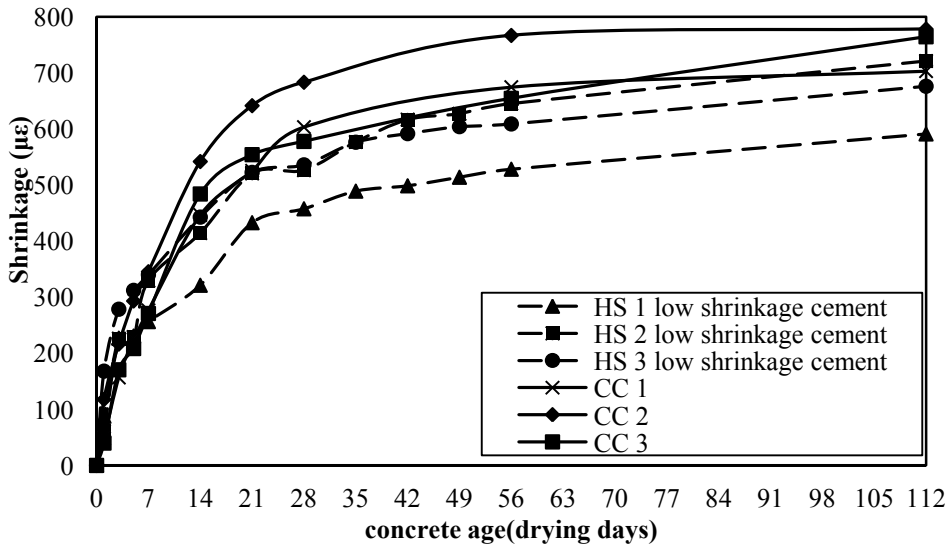

Figure A-9 Shrinkage-drying ages diagram of CC and HSC test series

HSC and CC samples displayed consistent 112-day shrinkage between the samples. The early age shrinkage of the HSC series occurred during the first 7 days and exhibited the highest shrinkage rate, reaching a value of 308.8$\mu\varepsilon$. The short-term shrinkage up to 28 days continued to decrease the shrinkage rate, reaching a value of 506.7$\mu\varepsilon$. The long-term shrinkage between 28 and 56 days continued to decrease the shrinkage rate, eventually reaching a 112 day shrinkage of 663$\mu\varepsilon$ as depicted in Figure A-10.The 56-day shrinkage results of CC mix was lower than the maximum 56 day shrinkage of 1000 micro strain stated by AS1379 (2007).

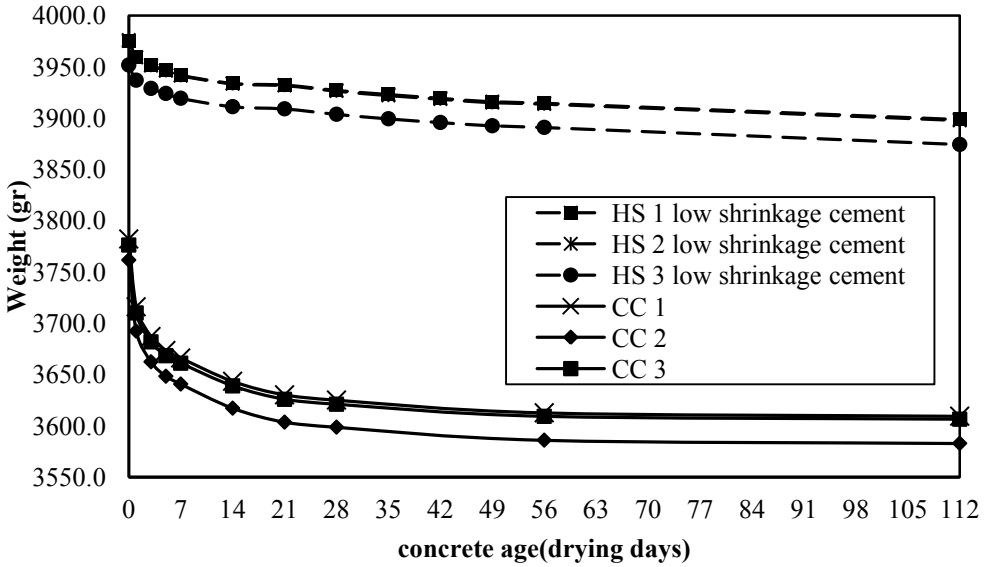

Figure A-10 Weight-drying ages diagram of CC and HSC test series

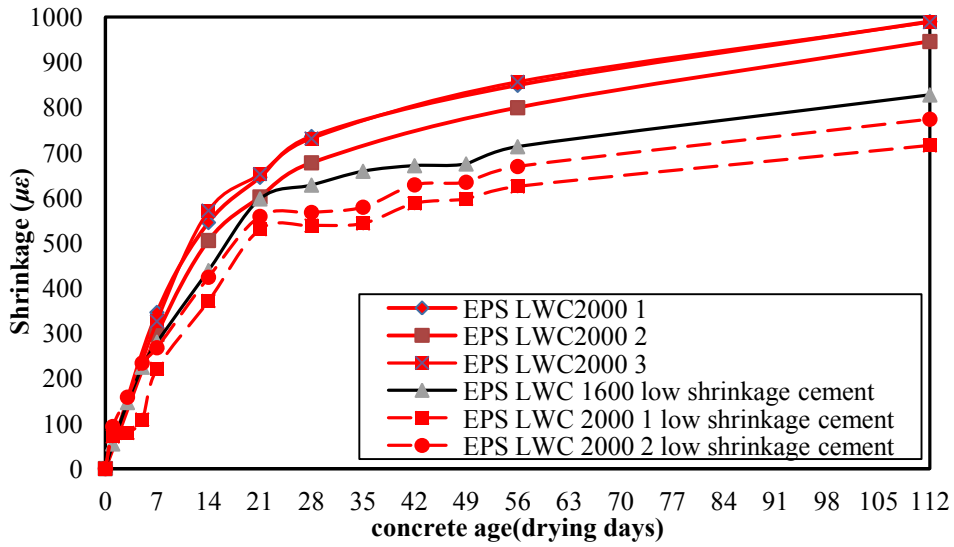

Figure A-11 Shrinkage-drying ages diagram of EPS LWC test series

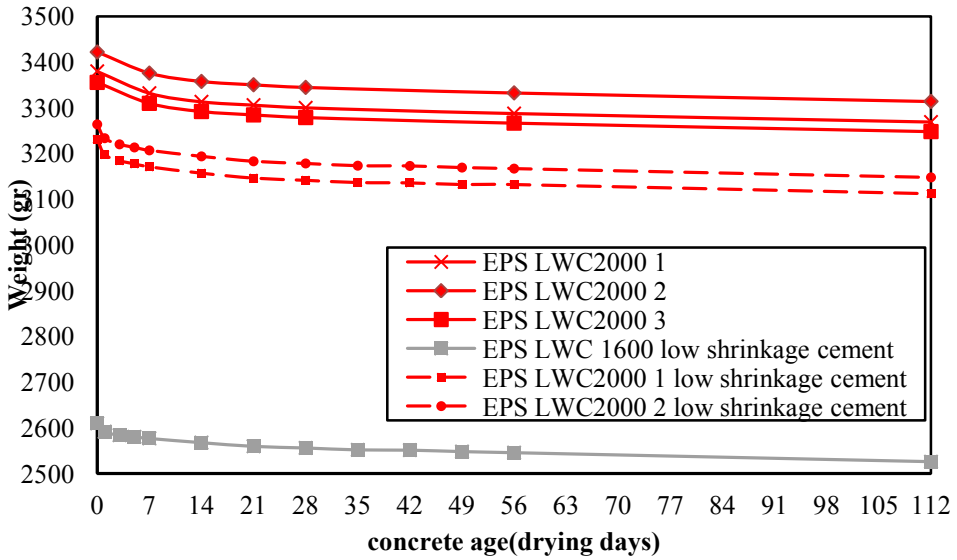

Figure A-12 Weight-drying ages diagram of EPS LWC test series

Two EPS LWC2000 samples with shrinkage limited cement mixes experienced consistent 112-day shrinkage results and EPS LWC1600 samples utilising shrinkage limited cement exhibited very similar shrinkage results which were slightly higher than EPS LWC2000 with shrinkage limited cement results as shown in Figure A-11.

Similar to CC and SCC series, the EPS LWC 2000 and 1600 series represented the highest rate of shrinkage during the early age period in the first 7 days, reaching values of 244.3 and 279.93$\mu\varepsilon$, respectively. Similarly, for both mixes the rate of shrinkage decreased in the short-term, with EPS LWC2000 and 1600 with low shrinkage cement series reaching values of 552.5 and 627.7$\mu\varepsilon$ at the end of 28 days.

The long-term shrinkage of the EPS LWC2000 and 1600 series with low shrinkage cement highlighted a further decrease in shrinkage rate, eventually reaching 112 day shrinkage results of 744 and 827.3$\mu\varepsilon$, respectively. It is evident that EPS LWC2000 series exhibited about 20% and 30% higher drying shrinkage compared to CC series at 56 and 112 drying days, respectively. Higher shrinkage of EPS LWC compared to CC is attributed to high cement content and lack of coarse aggregate.

However, EPS LWC experiences higher shrinkage than conventional concrete. There is a significantly lower tendency for drying shrinkage cracks to form in EPS LWC. The shrinkage stress of EPS LWC is approximately 25% to 50% lower than that of CC series.

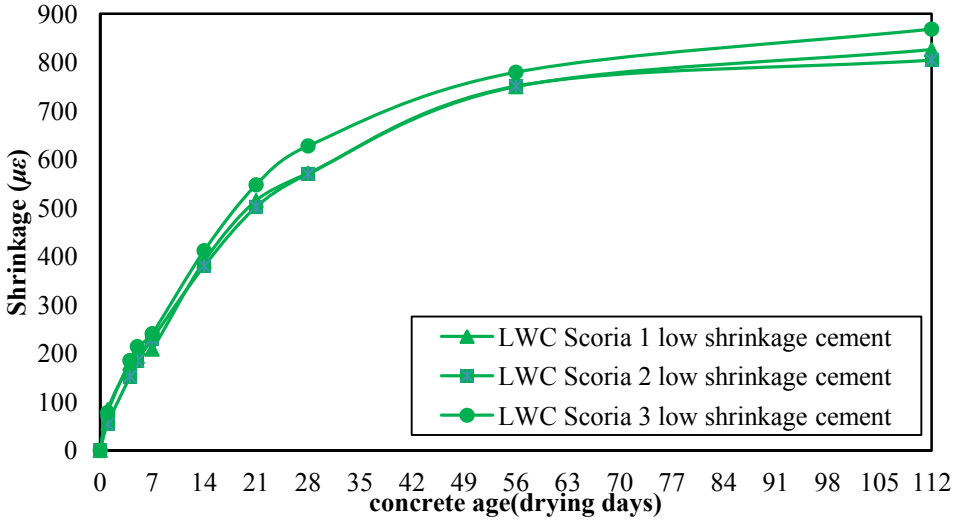

Figure A-13 Shrinkage-drying ages diagram of Scoria LWC test series

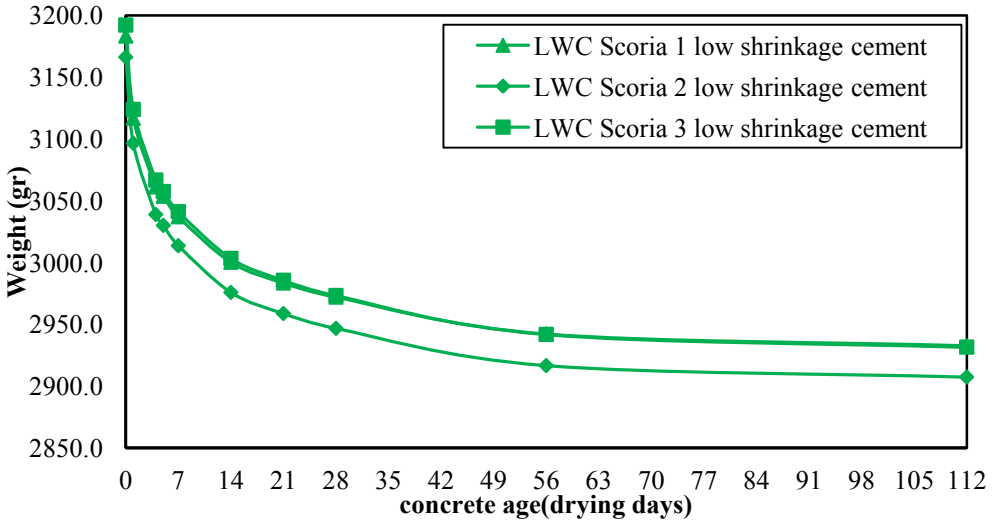

Figure A-14 Weight-drying ages diagram of Scoria LWC test series

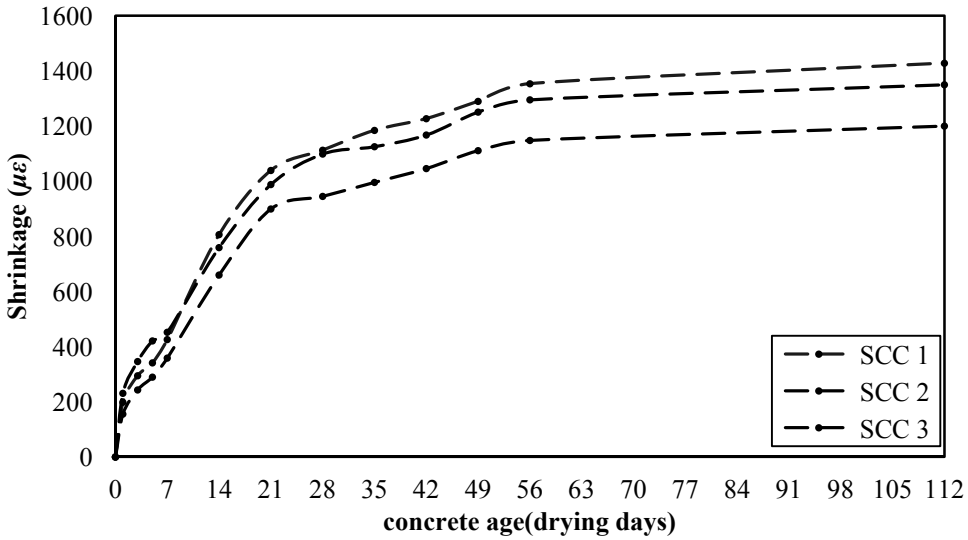

Figure A-15 Weight-drying ages diagram of SCC test series

Scoria samples exhibited lower drying shrinkage comparing to EPS LWC or SCC as graphed in Figure A-13. The early age shrinkage of the Scoria series which occurred during the first 7 days exhibited the highest shrinkage rate, reaching a value of 240$\mu\varepsilon$. The short-term shrinkage up to 28 days continued to decrease in shrinkage rate, reaching a value of 598$\mu\varepsilon$. The long-term shrinkage between 28 and 56 days continued to decrease in shrinkage rate, eventually reaching a 112 day shrinkage of 836$\mu\varepsilon$.

SCC experienced a relatively consistent 112-day shrinkage results. Similar to the CC mix, the early age shrinkage displayed the highest rate of shrinkage reaching a value of 412.2$\mu\varepsilon$. Similarly, the short-term shrinkage showed this decrease in shrinkage rate, gaining a value of 1052.2$\mu\varepsilon$ at 28days. The long-term shrinkage showed a further decreased shrinkage, eventually reaching a 112 day shrinkage of 1326$\mu\varepsilon$ (Figure A-14).

The HSC mix displayed the least amount of shrinkage with an average of 663$\mu\varepsilon$ after 56 days whilst the EPS LWC 1600 and 2000 series indicated slightly increased shrinkages achieving 56-day shrinkage of 744 and 827.3$\mu\varepsilon$, respectively. SCC samples experienced much higher shrinkage rates than other concrete types, reaching an average of 1326$\mu\varepsilon$ after 112 days with 87% higher shrinkage at 112 days compared to similar CC series.

A.2 TIMBER (LVL)

In addition to the material tests carried out by the timber supplier or Zabihi and Gerber (2012), quasi-static compressive tests parallel to the grain direction were carried out on four hySPAN project LVL specimens of 220x193x45 in compliance with AS4357.0 (2005) and an axial compression load was applied to the specimens at a uniform loading until failure occurred (Figure A-16). All the results are listed in Chapter 4. hySPAN project LVL indicates a significant compressive strength, parallel to grain of 53.4MPa. The relatively low CoV of 6.8% highlighted the consistency of the results. The test set up and failure modes of the specimens are shown in Figure A-16.

Figure A-16 Test set-up and compressive failure of LVL loaded parallel to the grain

Appendix B (Chapter 5)

B.1 PUSH-OUT TEST RESULTS: CONVENTIONAL CONCRETE

Two types of SFS VB and SPAX screws were tested to quantify the difference between crossed screws connections at different angles with and without interlayer. Moreover, two innovative connectors of L and U profiles in combination with three small SPAX screws were designed and tested to identify alternative connection solutions in TCCs.

Tables B-1 and B-2 present the load capacity and ductility of the test series utilising conventional concrete. Tables B-3 and B-4 list different slip moduli of the test series obtained from EN26891 and the modified methods, respectively. Moreover, the mean, standard deviation and coefficient of variation (CoV) of the test data were tabulated.

Table B-1 Load capacity of different series utilising conventional concrete

series	No.	Load capacity(kN)			
		Range	Ave	σ	CoV
SFSWI30	4	39.0-41.6	40.1	1.2	2.9
SFSWI45	5	31.7-35.8	33.2	1.6	4.8
SFSWI60	5	30.9-36.6	33.8	2.2	7.0
SFSI45	5	30.0-32.3	31.0	0.9	3.0
SSFSWI45	5	26.7-28.3	27.6	0.6	2.2
SSFSI45	5	19.5-23.2	21.0	1.8	8.8
SPAX WI30	5	37.3-43.0	40.7	2.3	5.6
SPAX WI45	5	35.6-39.8	38.3	1.8	4.8
SPAX WI60	5	32.9-37.8	35.4	2	5.6
SPAX I45	5	28.1-32.6	29.5	2.3	7.9
coach 45	5	25.3-27.6	26.1	1.0	4.0
L+3 SPAX	5	52.6-59.8	54.6	3.0	5.5
U+3 SPAX	5	38.6-42.6	40.0	1.5	3.9

Table B-2 Ductility of different test series utilising conventional concrete

series	u_y(mm)	u_u(mm)	u_f(mm)	D_u		D_f	
	Ave(CoV)	Ave(CoV)	Ave(CoV)	Range	Ave(CoV)	Range	Ave(CoV)
SFS WI30	0.7(33.2)	1.9(20.5)	3.0(21.8)	1.5-3.6	2.8(35.7)	3.2-5.0	4.4(19.0)
SFS WI45	0.5(29.6)	2.1(11.0)	3.2(7.3)	2.7-4.8	3.9(23.1)	4.1-7.8	6.1(26.4)
SFS WI60	0.4(33.0)	2.2(9.0)	3.4(11.1)	3.4-7.1	5.2(27.1)	5.0-11.3	7.9(30.0)
SFSI45	1.4(13.0)	3.6(16.5)	4.9(15.8)	2.0-3.0	2.5(18.2)	2.6-4.4	3.4(21.5)
SSFSWI45	0.7(15.0)	1.9(9.4)	2.7(8.1)	2.4-3.3	2.8(13.4)	3.1-4.5	4.0(14.0)
SSFSI45	1.5(21.5)	3.0(9.5)	3.5(11.7)	1.5-2.7	2.1(27.2)	2.0-3.6	2.5(29.3)
SPAX WI30	0.7(25.2)	1.7(19.4)	3.2(18.7)	1.7-3.2	2.5(21.8)	3.6-5.5	4.6(15.7)
SPAX WI45	0.9(10.9)	2.4(8.2)	3.9(8.9)	2.6-3.2	2.8(8.7)	4.0-5.2	4.4(10.1)
SPAX WI60	0.8(16.5)	2.1(9.5)	3.3(4.6)	2.3-3.6	2.8(18.5)	4.0-5.6	4.4(15.7)
SPAX I45	1.9(22.6)	4.4(55.8)	5.2(18.5)	1.4-7.2	2.8(90.7)	2.0-4.9	2.9(39.9)
coach 45	0.4(24.8)	2.9(29.7)	5.6(19.2)	4.4-11.3	6.9(40.3)	9.3-20.5	13.2(33.9)
L+3 SPAX	0.3 (37.9)	2.5(9.1)	2.8(9.8)	5.2-15.4	9.0(43.4)	5.6-17.7	10.1(45.6)
U+3 SPAX	0.2(31.4)	5.3(14.1)	8.5(8.4)	28.8-62.5	38.5(35.6)	43.7-112	63.0(44.2)

Table B-3 Slip moduli of different series utilising CC based on EN26891

Series	Slip moduli (kN/mm)								
	$K_{s,0.4}$			$K_{s,0.6}$			$K_{s,0.8}$		
	Range	Ave	σ(CoV)	Range	Ave	σ(CoV)	Range	Ave	σ(CoV)
SFSWI30	33.7-40.3	36.8	3.7(10.1)	30.7-38	34.5	3.7(10.6)	25.6-32.1	29.3	3.2(10.9)
SFSWI45	16.8-54.1	28.8	14.7(51)	18.1-43.5	26.6	10.1(38.0)	16.9-35.4	23.4	7.2(31)
SFSWI60	22.4-58.7	34.2	14(41.3)	22.1-39.3	29.1	6.2(21.5)	19.8-27.7	24.1	3.6(14.8)
SFSI45	13.7-17.8	15.2	1.5(10.1)	14.0-16.8	15.4	1.1(7.0)	12.7-15.4	14.2	1.0(7.0)
SSFSWI45	21.6-31.6	26.3	3.9(14.7)	21.1-30.6	24.8	3.5(14.1)	18.7-25.5	21.8	2.4(11.1)
SSFSI45	7.5-12.9	10.5	2.0(18.6)	8.1-11.6	10.6	1.5(14.3)	8.3-11.2	10.0	1.3(12.9)
SPAX WI30	32.7-52.3	40.1	7.4(18.6)	34.5-45.6	38.4	4.5(11.6)	32.5-39.6	34.7	2.8(8.1)
SPAX WI45	20.9-29.4	25.3	3.8(14.9)	22.1-28.8	25.5	2.5(9.9)	20.2-25.6	22.8	2.0(8.8)
SPAX WI60	26.5-39.1	29.7	5.3(17.9)	26.1-37.6	28.8	4.9(17)	16.5-31.0	22.6	5.6(24.8)
SPAX I45	10.6-14.0	12.0	1.2(10.3)	11.4-13.3	12.6	0.8(6.0)	11.2	11.2	2.5(22.3)
coach 45	26.0-35.7	31.1	3.6(11.5)	28.1-35.5	30.8	3.1(10.0)	17.6-28.8	22.12	4.4(20.0)
L+3 SPAX	31.9-56.7	39.9	9.9(24.7)	31.2-44.7	35.5	5.4(15.3)	26.0-34.1	29.1	3.2(11.1)
U+3 SPAX	18.1-50.6	31.8	13.5(42.5)	20.6-31.3	25.0	4.1(16.5)	12.4-18.4	15.6	2.3(14.9)

Table B-4 Slip moduli of different series utilising CC based on the modified method

Series	Slip moduli (kN/mm)								
	$K_{s,0.4}$			$K_{s,0.6}$			$K_{s,0.8}$		
	Range	Ave	σ(CoV)	Range	Ave	σ(CoV)	Range	Ave	σ(CoV)
SFSWI30	43.0-71.4	55.7	11.9(21.5)	35.4-53.0	43.7	7.4(17.0)	27.9-38.8	33.9	4.8(14.1)
SFSWI45	31.2-88.8	55.8	22.1(39.6)	27.1-39.3	36.7	11.3(30.8)	22.1-40.6	27.8	7.6(27.4)
SFSWI60	49.9-77.6	60.5	11.6(19.1)	34.7-44.6	40.4	3.9(9.6)	26.1-29.9	27.9	1.6(5.8)
SFSI45	21.7-28.2	24.2	2.4(10.0)	18.7-22.4	20.6	1.5(7.4)	15.3-18.4	17.2	1.2(6.9)
SSFSWI45	35.3-52.1	44.4	7.7(17.3)	28.3-40.9	34.6	5.3(15.4)	22.6-30.4	26.9	3.3(12.1)
SSFSI45	14.1-20.5	17.6	2.4(13.4)	13.6-18.0	14.7	2.2(14.7)	11.2-15.0	12.6	1.7(13.5)
SPAX WI30	49.9-77.6	60.5	11.6(19.1)	34.7-44.6	40.4	3.9(9.6)	26.1-29.9	27.9	1.6(5.8)
SPAX WI45	52.4-80.7	62.2	11.9(19.2)	36.6-52.2	42.8	6.1(14.2)	19.4-35.0	26.7	6.3(23.7)
SPAX WI60	45.9-55.1	50.0	4.2(8.4)	35.4-46.2	39.1	4.3(11.0)	19.4-35.0	26.7	6.3(23.7)
SPAX I45	18.9-31.0	22.5	4.8(21.8)	17.2-20.1	18.5	1.3(7.2)	8.0-17.0	14.3	3.6(25.5)
coach 45	63.3-93.1	76.9	12.0(15.7)	41.3-63.7	51.8	10.1(19.6)	20.7-39.4	28.5	7.5(26.3)
L+3 SPAX	82-134.4	105	20.6(19.6)	46.2-65.9	57.1	7.8(13.6)	32.6-40.6	38.0	3.2(8.5)
U+3 SPAX	88-135.8	113	19.8(17.5)	32.6-79.7	49.9	20.0(40.2)	14.3-26.2	20.3	4.7(23.0)

B.1.1 CC SFS VB screws series

The load-slip response and analytical model of conventional concrete series utilising crossed short and long SFS VB screws at 30°, 45° and 60°, I and WI interlayer series are plotted in Figure B-1. The mathematical descriptive models and sample correlation coefficients, R^2 of CC series are given in Equations (B-1):(B-6).

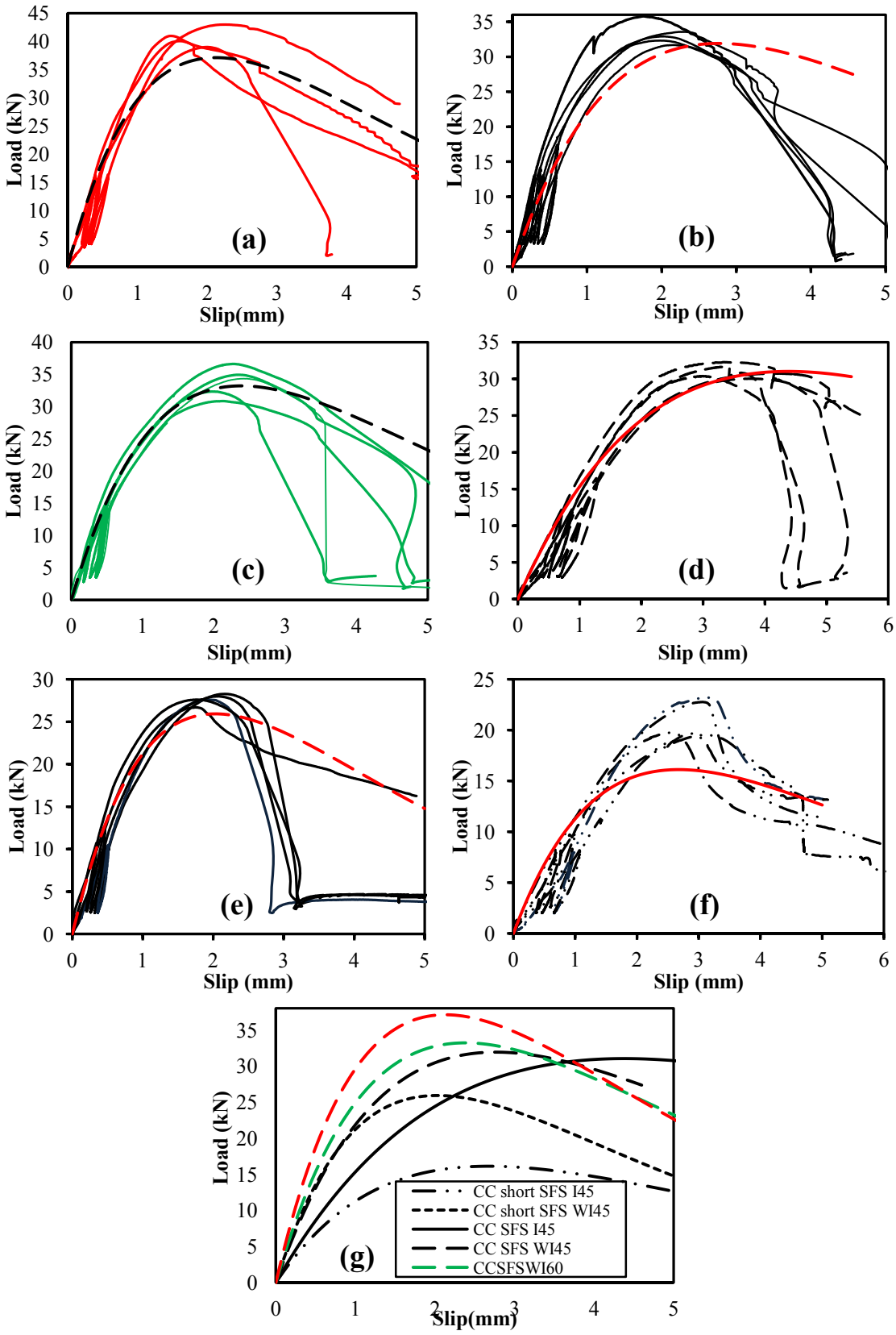

Figure B-1 Load-slip and analytical model of CC SFS series(a) WI30, (b) WI45, (c) WI60, (d) I45, (e) short SFS WI45, (f) short SFS I45 and (g) comparison of models

$$P = 1573(e^{-0.45\upsilon} - e^{-0.48\upsilon}) \ , (R^2 = 0.94) \qquad \text{[SFS WI30]} \qquad \text{(B-1)}$$

$$P = 864.5(e^{-0.34\upsilon} - e^{-0.38\upsilon}) \ ,(R^2 = 0.92) \qquad \text{[SFS WI45]} \qquad \text{(B-2)}$$

$$P = 873.4(e^{-0.4\upsilon} - e^{-0.44\upsilon}) \ ,(R^2 = 0.99) \qquad \text{[SFS WI60]} \qquad \text{(B-3)}$$

$$P = 1235(e^{-0.22\upsilon} - e^{-0.24\upsilon}) \ ,(R^2 = 0.97) \qquad \text{[SFS I45]} \qquad \text{(B-4)}$$

$$P = 2871(e^{-0.49\upsilon} - e^{-0.50\upsilon}) \ ,(R^2 = 0.97) \qquad \text{[SSFS WI45]} \qquad \text{(B-5)}$$

$$P = 2481(e^{-0.37\upsilon} - e^{-0.38\upsilon}) \ ,(R^2 = 0.83) \qquad \text{[SSFS I45]} \qquad \text{(B-6)}$$

Figures B-2:B-6 show the failure mode and opened specimens of different CC series.

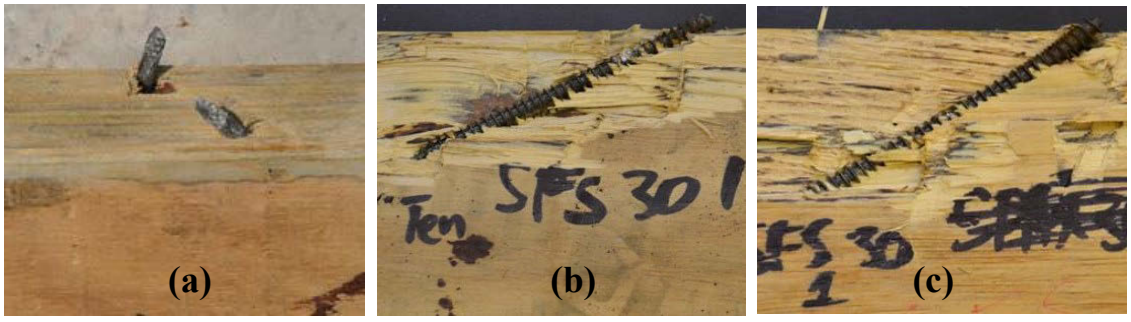

Figure B-2 (a) failure of tensile screws and opened specimens of screws in (b) tension and (c) compression in CC SFSWI30 series

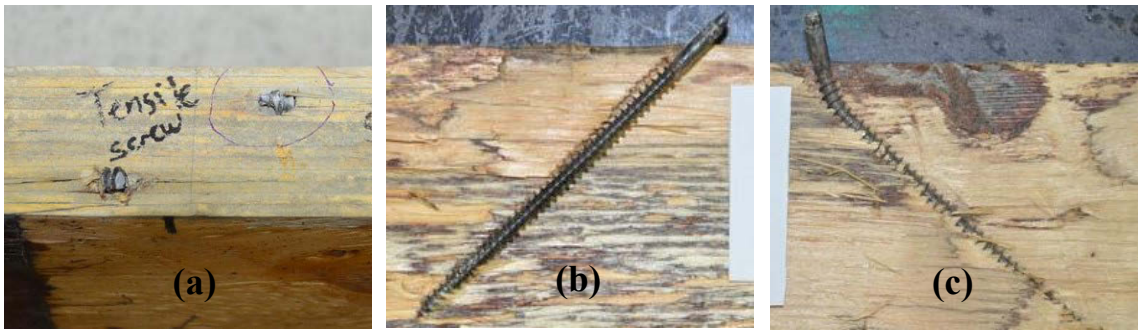

Figure B-3 (a) failure of tensile screws and opened specimens of screws in (b) tension and (c) compression in CC SFSWI45 series

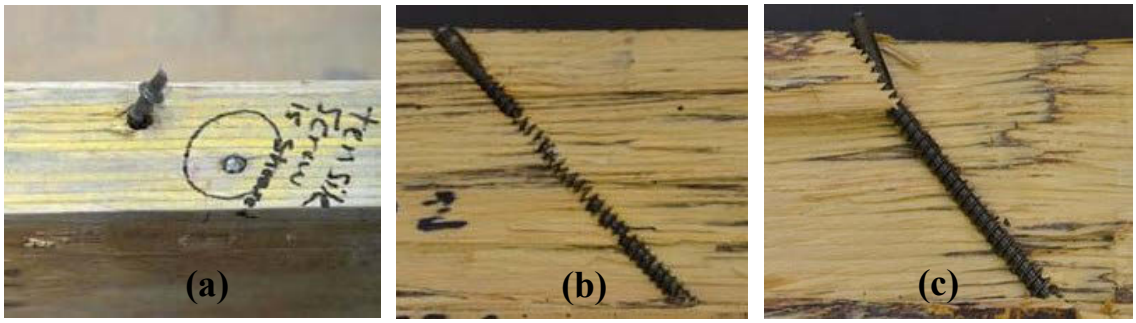

Figure B-4 (a) Failure of tensile screws and opened specimens of screws in (b) tension and (c) compression in CC SFSWI60 series

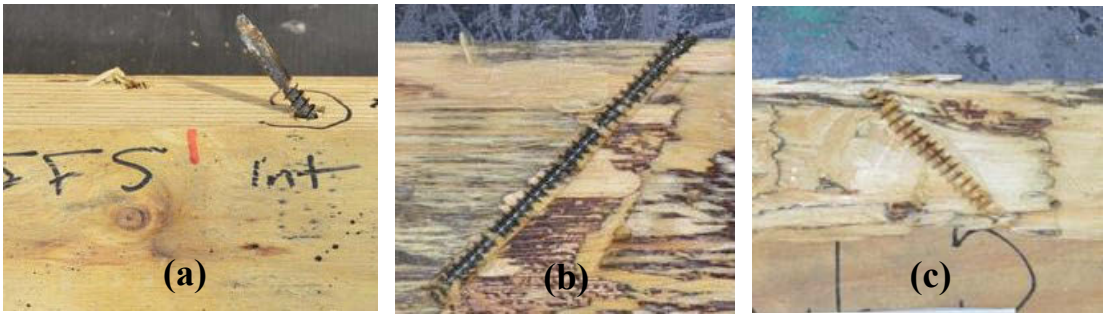

Figure B-5 (a) Failure of tensile screws and opened specimens of screws in (b) tension and (c) compression in CC SFSI45 series

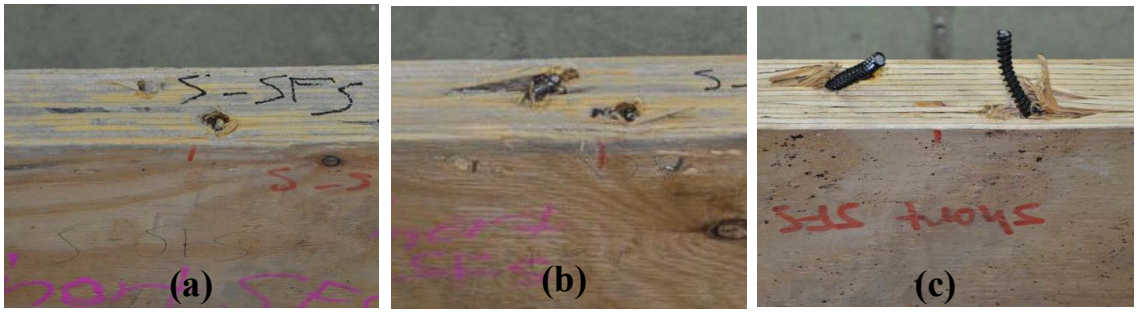

Figure B-6 (a) Failure of tensile screws in CC short SFS samples 2:5 WI45 series (b) bent screws with formation of plastic hinge in sample1 CC short SFSWI45 series and (c) bent screws with formation of plastic hinge for CC short SFSI45 series

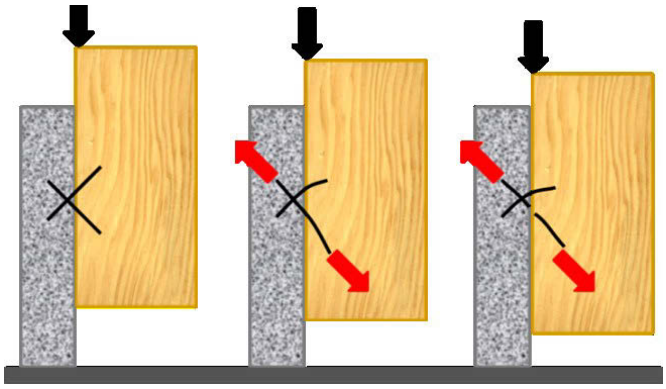

Figure B-7 Tensile failure of the screw placed in tension

Generally, in the case of tensile failure of screws, a loud distinct sound corresponding to tensile failure of the screw in tension was heard as the screw failed. Moreover, no embedding failure and plastic hinge was observed in the screw placed in tension. The timber surrounding the tensile screws did not crush in any of the specimens. CC SFS series exhibited a single peak at maximum load. There was no initial drop of load due to a lesser amount of localised concrete failure at the connection.

CC SFS WI30 series represented a single failure mode as tensile failure of the screws placed in tension (Figure B-2a). There was no timber crushing around the tensile screw as depicted in Figure B-2b. CC SFS WI30 series represented a strength range of 39-41.6kN, with an average of 40.1kN. The minimal strength dispersion with CoV of 2.9% demonstrates consistent results.

The behaviour of the CC SFS 45 specimens (WI and I series) was fairly consistent. CC SFS WI45 series represented a strength range of 31.7-35.8kN with an average of 33.8kN. The minimal strength dispersion with CoV of 4.8% shows consistent results.

CC SFS WI45 series initially exhibited a linear behaviour and the load increased quite steadily, slowing slightly before reaching the peak load at around 31.7-35.8kN and when the load reached F_{max}, the samples showed signs of a non-linear response. Following the peak load, the load gradually reduced to approximately 75-90% F_{max} before a sudden tensile failure of screw occurred as depicted in Figure B-1b. CC SFS WI45 series showed a small, localised failure in the concrete slab directly around the shear connection. Small cracking was caused by the deformation of the screw at the interface. In all specimens, failure was likely a tensile failure of the screw, with shear contributing as shown in Figure B-3a. Necking was evident on failed screws, and

screws failed at their narrowest point, located 20-30mm above the thread as shown in Figure B-3b.

All specimens of CC SFS WI60 series failed by tensile failure of the screw placed in tension as shown in Figure B-4a and b. There was some timber crushing in front of the compressive screw on all samples due to deformation of screws (Figure B-4c). CC SFS WI60 series represented a strength range of 30.9-36.6kN, with an average of 33.8kN. The minimal strength dispersion with CoV of 7.0% demonstrates consistent results.

Application of an interlayer in CC SFS I45 series resulted in a similar behaviour to the CC SFSWI45series. There was slightly higher deflection (3-4mm) before F_{max} which resulted in lower ductility than the series without interlayer. A total deflection of 4.4 - 5.2mm was recorded across the specimens.

CC SFS I45 series represented a strength range of 30.0-32.3kN, with an average of 31.8kN. The minimal strength dispersion with CoV of 3.0% indicates consistent results. However, there was some variation in the slip at F_{max} results. Slip at F_{max} value varied between 2.6-3.7mm and the average slip at F_{max} was 3.2mm with a CoV of 12.5%.Initially all five samples displayed linear behaviours and the samples behaviour changed as the load reached F_{max}, experiencing a ductile response. After reaching F_{max}, the load reduced to approximately 80-90%F_{max} highlighting a continuation of the ductility of the connections, before a sudden and tensile failure occurred (Figure B-1d). CC SFS I45 series demonstrated multiple modes of failure. Specimens 1, 3, 4 and 5 failed in tensile failure of screw in tension at its narrowest point suddenly after F_{max}(Figure B-5a) whilst sample 4 showed formation of a plastic hinge in both intact screws.

The load-deflection behaviour of the CC SSFS WI45 series utilising short SFS screws was similar to that of the specimens utilising long SFS screws. The F_{max} and the corresponding slip values obtained were very consistent in this case with CoV values of 2.1% for F_{max} and 9.4% for slip at F_{max}. These specimens showed a slip of around 2mm before a F_{max} of around 28kN was reached. After peaking, load decreased until a sudden failure occurred at 2-3mm slip at around 90% F_{max} as shown in Figure B-1e.

Failure in CC short SFS WI45 series with the exception of specimen 1 occurred in the tensile screw and the point of failure was located just above the anchor on the concrete side. Necking was also present at the point of failure (Figure B-6a), however not to the

extent which was experienced in the long SFS screws. Specimen 1 experienced large ultimate slip of 5mm corresponding to a load of approximately 60% of F_{max}. A large torsional twist due to the formation of a plastic hinge in the bent screw was observed in specimen 1 (Figure B-6b). The observed failure modes agreed with the failure mode of short SFS series reported by Van der Linden (1999).

The behaviour of the CC short SFS I45 series was slightly different from the CC short SFS WI45specimens. The F_{max} values were relatively consistent with a CoV value of 8.8%, however they were less consistent than other CC SFS 45 series. Conversely, the slip at F_{max} values were the most consistent out of all the specimens with a CoV value of 8.3%.These specimens experienced approximately 2.5-3.0mm slip at F_{max} which was at around 21kN. As the load decreased after F_{max}, ultimate failure occurred at approximately 75% F_{max} with a slip value of around 4mm as depicted in Figure B-1f. CC short SFS I45 series experienced large torsional twist which occurred as the connectors had failed by plastic hinge in screw. Due to the inclusion of the interlayer, the timber was more susceptible to crushing. The twisting occurred as there was localised crushing of the timber in the interlayer and surrounding the compression screw.

The decrease in the length of the SFS screws used in the connections led to 17% and 32% reduction in strength of CC short SFS WI45 and I45, respectively compared to that of long SFS screw series. The failure observation agreed with Van der Linden (1999) who reported the same failure mode in the presence of 19mm interlayer. In contrast,Van der Linden (1999) reported that by increasing the interlayer thickness to 28mm, the dominant failure mode changed to the withdrawal of short SFS screws. The decrease in the length of the SFS screws reduced different slip moduli of shear connector approximately 8% and 31% for CC short SFS WI45 and I45 compared to that of long SFS series, respectively.

The ductility of long SFS series varied within 3.4-7.9. Increasing of the inclination angle from 30° to 60° increased the ductility whereas inclusion of the interlayer led to 44% ductility reduction compared to similar series without interlayer. Short SFS exhibited 40% lower ductility compared to the similar series of long SFS series.

B.1.2 CC SPAX screws series

The load-slip response and analytical model of conventional concrete series utilising crossed SPAX screws inclined at 30°, 45° and 60°, with and without interlayer series are plotted in Figure B-8. The mathematical descriptive models and sample correlation coefficients, R^2 of CC series are given in Equations (B-7):(B-10).

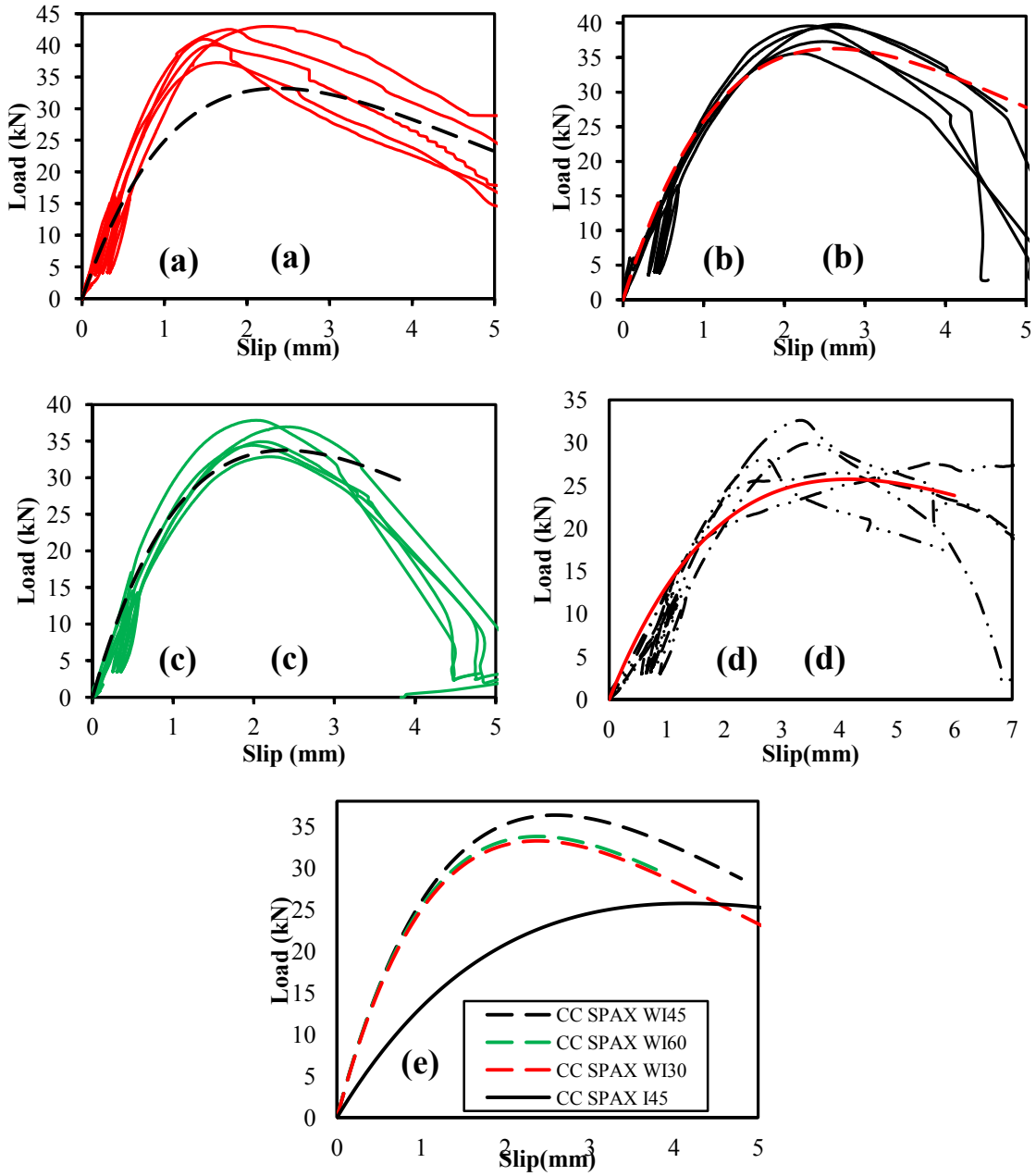

Figure B-8 Load-slip of CC SPAX series(a) WI30, (b) WI45, (c) WI60, (d) I45 and (e) comparison of analytical graphs

$$P = 177.7(e^{-0.35\upsilon} - e^{-0.62\upsilon}) \ , (R^2 = 0.89) \qquad \text{[SPAX WI30]} \qquad \text{(B-7)}$$

$$P = 990.5(e^{-0.37v} - e^{-0.41v}) \ ,(R^2 = 0.98) \qquad \text{[SPAX WI45]} \qquad \text{(B-8)}$$

$$P = 1496(e^{-0.41v} - e^{-0.43v}) \ ,(R^2 = 0.97) \qquad \text{[SPAX WI60]} \qquad \text{(B-9)}$$

$$P = 725.2(e^{-0.22v} - e^{-0.25v}) \ ,(R^2 = 0.93) \qquad \text{[SPAX I45]} \qquad \text{(B-10)}$$

Figures B-9:B-12 show the failure mode and opened specimens of different CC series utilising SPAX screws.

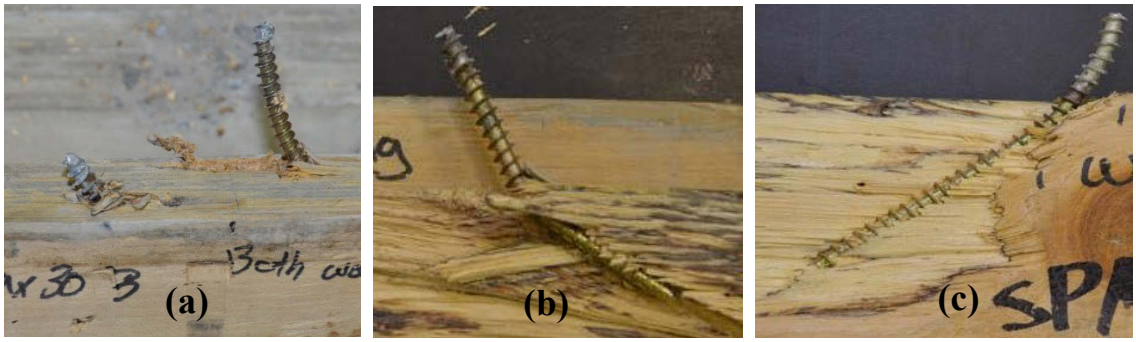

Figure B-9 (a) Intact screws and opened specimens of screws in (b) tension and (c) compression in CC SPAX 30WI series

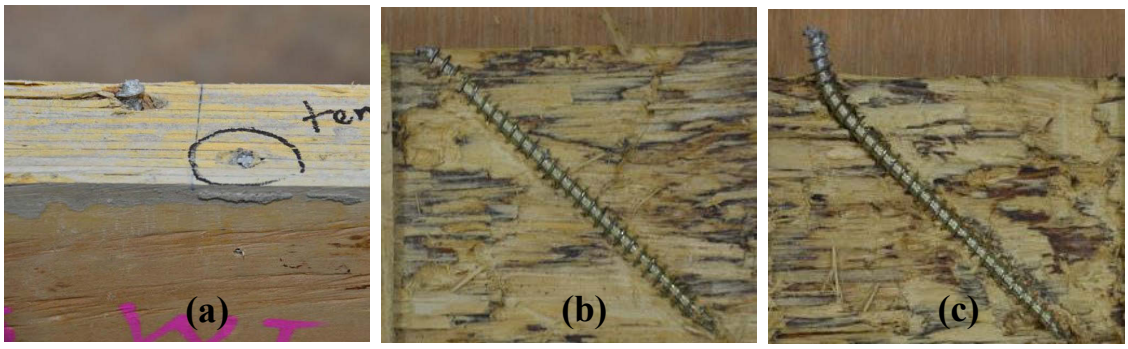

Figure B-10 (a) Failure of tensile screw and opened specimens of screws in (b) tension and (c) compression in CC SPAX 45WI series

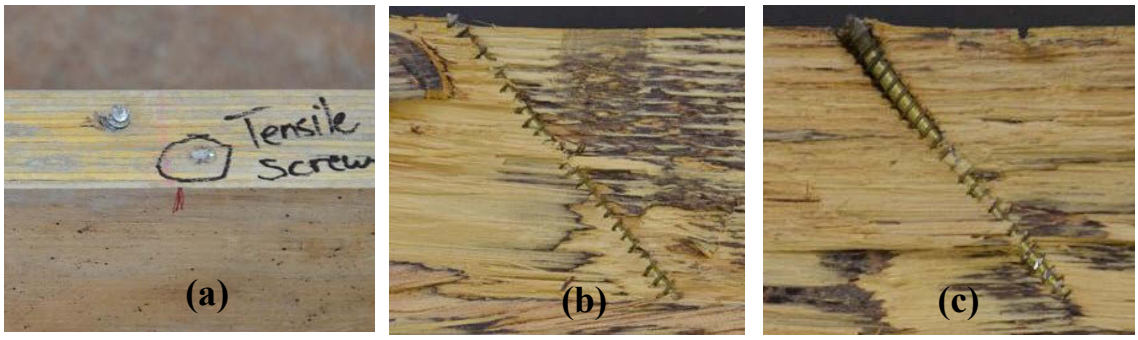

Figure B-11 (a) Failure of tensile screw and opened specimens of screws in (b) tension and (c) compression in CC SPAX 60WI series

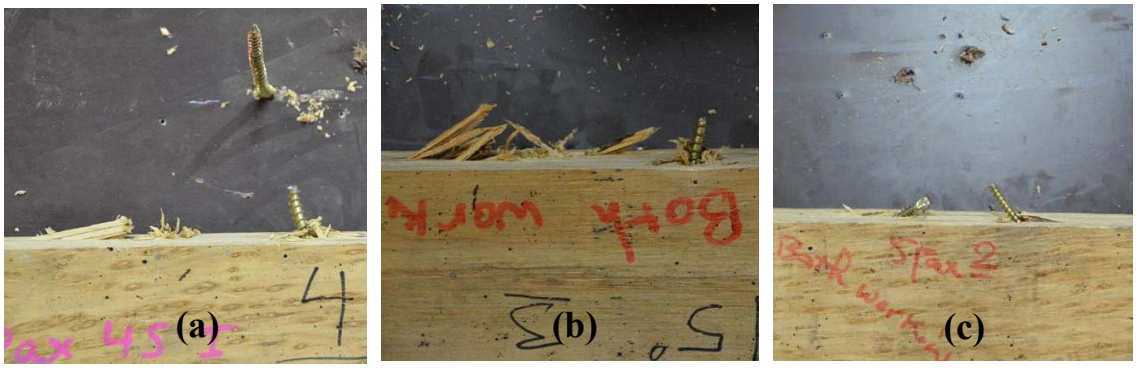

Figure B-12 Intact screws for different specimens of CC SPAX 45I series

CC SPAX WI30 series demonstrated a single mode of failure. All specimens failed with both screws intact (Figure B-9). In all samples crushing of timber in both the tension and compression screws were observed (Figure B-9a and b). There was lateral displacement of screw with formation of a plastic hinge in both screws. In this case the load carrying capacity of the shear connector was governed by the embedding strength of the surrounding timber and bending capacity of the screw. CC SPAX WI30 demonstrated strength range of 37.3-43.0kN, with an average value of 40.7kN. This is minimal strength dispersion with CoV of 5.6%.

CC SPAX WI45 series had a strength range of 35.5-39.8kN, with an average of 38.3kN. The minimal strength dispersion with CoV of 4.8% demonstrates consistent results. CC SPAX WI45 series initially exhibited a linear behaviour, similar to the CC SFS WI45 series. As the load reached F_{max}, the samples showed signs of a non-linear response. After reaching F_{max} the samples displayed ductile response by maintaining load until a sudden tensile failure of screw in tension at approximately 70% F_{max}. On all samples, the SPAX screw placed in tension failed in tension with no lateral movement as shown in Figure B-10a and b.

CC SPAX WI60 series demonstrated single failure mode. On all samples, the SPAX screw placed in tension failed in tension with no lateral movement as depicted in Figure B-11a and b. Slight crushing of timber was observed in front of the screw placed in compression as shown in Figure B-11c. CC SPAX WI60 series represented a strength range of 32.9-37.8kN, with an average of 35.4kN. The minimal strength dispersion with CoV of 5.6% demonstrates consistent results.

CC SPAX I45 demonstrated considerable dispersion for average slip with quite consistent F_{max} results as highlighted in the CoV results. CC SPAX I45 exhibited multiple failure modes as three samples (2, 3 and 4) experienced a single peak failure and both bent screws were intact with formation of plastic hinge whereas the other two samples (1 and 5) reached F_{max} after experiencing far greater slip and failed in tensile failure of screw placed in tension (Figure B-8d).

All samples experienced linear behaviours over the initial stages of the test. After reaching F_{max}, all samples experienced a ductile response before failure. After reaching F_{max} the load reduced in a range of 54 - 97%F_{max} before a sudden and complete failure occurred (Figure B-8d).

CC SPAX I45 series represented a strength range of 26-31kN, with an average of 28.8kN. The minimal strength dispersion with CoV of 7.6% demonstrates consistent results. A highly consistent stiffness result was observed as shown by the significantly low CoV values. The strength of CC SPAX WI45 series was 15% higher than the similar SFS series. However, SPAX I45 series produced 5% less strength than similar SFS series.

In the case of tensile failure of the screw, the tensile failure mode occurred when the load carrying capacity of the connection exceeded the tensile strength of the screw. Hence, the strength of the TCC connection is highly dependent on the tensile capacity of the screw. The necking of the screws was evident in the failed samples and the failure of screws occurred at the narrowest point of the screw.

The ductility of SPAX series varied between 2.9 and 4.6. Increasing of the inclination angle from 30° to 60° has a minor impact on ductility whereas inclusion of the interlayer led to 35% reduction compared with the similar series without the interlayer.

B.1.3 L profile and U profile connection and inclined coach screws series

The load-slip responses and analytical model of CC L and U profiles and coach screws inclined at 45°series are plotted in Figure B-13. The mathematical descriptive models and sample correlation coefficients, R^2 of CC series utilising L and U profiles and coach screw 45 degree are given in Equations (B-11):(B-13).

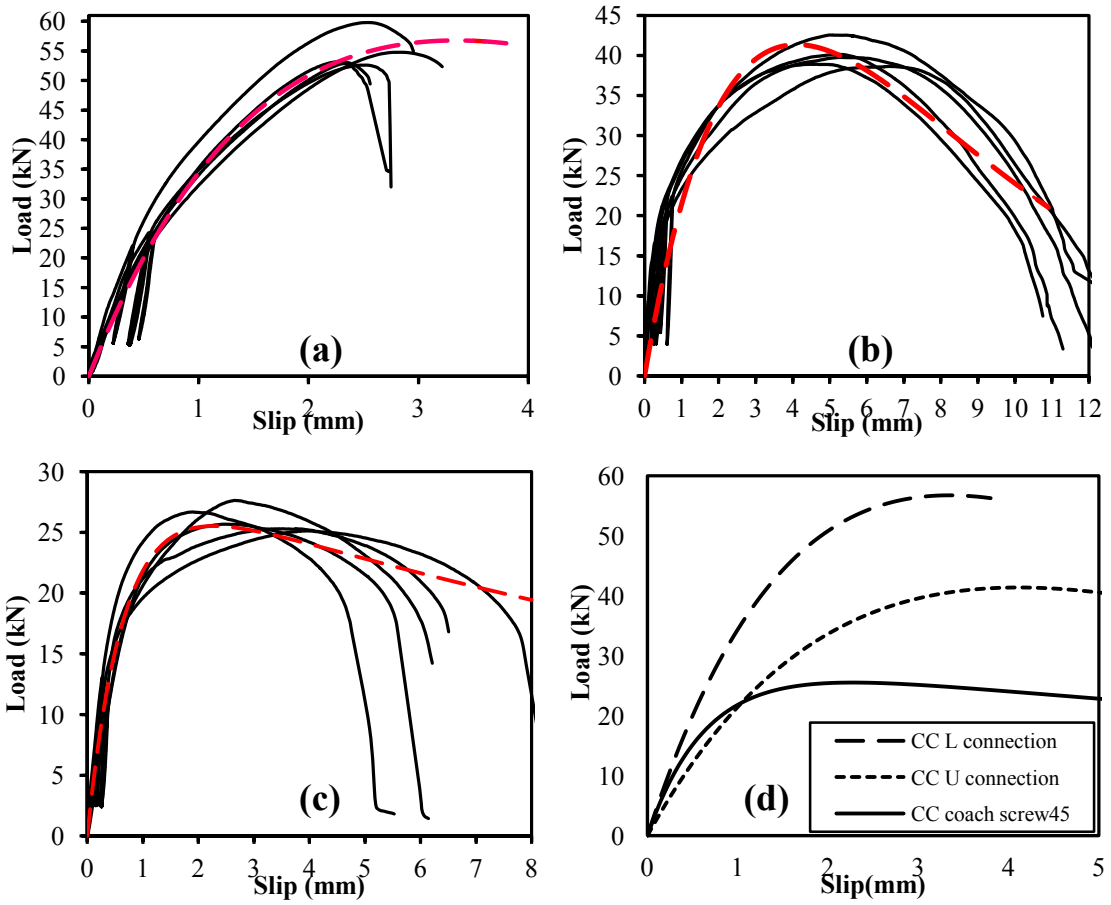

Figure B-13 Load-slip and analytical model of (a) CC L profile and 3 short SPAX screws series, (b) CC U profile and 3 short SPAX screws series, (c) coach45 series and (d) comparison of analytical graphs

$$P = 323.6(e^{-0.23\upsilon} - e^{-0.38\upsilon}) \ , (R^2 = 0.96) \qquad \text{[L profile]} \qquad \text{(B-11)}$$

$$P = 1221(e^{-0.23\upsilon} - e^{-0.25\upsilon}) \ , (R^2 = 0.90) \qquad \text{[U profile]} \qquad \text{(B-12)}$$

$$P = 29.92(e^{-0.05\upsilon} - e^{-1.52\upsilon}) \ , (R^2 = 0.97) \qquad \text{[coach45]} \qquad \text{(B-13)}$$

The L series of connectors exhibited the highest average strength of 54.6kN which was 36.6% higher than the U series and 109% higher than the coach screw series. This was anticipated as the L connector was the most rigid design being fabricated from a structural section with a relatively high moment of inertia compared to the U connector, and thus it was less susceptible to bending and deflection. Additionally, 3 small SPAX screws used increased load capacity than a single coach screw.

All 5 L series specimens failed in a combined tensile and shear failure of the SPAX screws. The failure surface had a very clean finish with very little necking evident which resulted in a brittle failure mode due to the high carbon content of the screws.

There appeared to be no deformation to the L connector itself with no surface cracks or other evident signs of stress to the steel. The LVL joist for all the L series specimens showed no visible signs of crushing, with no splitting. The LVL surrounding the timber remained undamaged highlighting that the SPAX screws did not experience an embedment mode of failure as illustrated in Figure B-14b and c.

The concrete also remained undeformed with no localised failure (Figure B-14a). Two opened LVL joists along the timber grain demonstrated that the SPAX screws remained straight along the shank with no visible plastic hinges and signs of embedment as depicted in Figure B-14.

Figure B-13 illustrates the brittle behaviour of the L connector compared to the U and coach screw series which is evident from the abrupt termination of the load-slip diagram of the L series. Whilst the L series connector has a high strength, the brittle behaviour is highly undesirable as it provides very little warning to the occupants of the structure and as a result may be termed as a catastrophic failure.

The L series connectors had the highest average serviceability and ultimate slip moduli. Compared to the other connection designs in literature, the L connector exhibited a relatively high serviceability slip modulus; however it does not achieve the same stiffness values such as the perforated steel plate connector system tested by Miotto and Dias (2011) and Miotto and Dias (2012) or concrete notches investigated by Yeoh (2010). It is noteworthy that direct comparison of TCC connectors is not valid due to different geometry, arrangement and material properties of the TCC specimens.

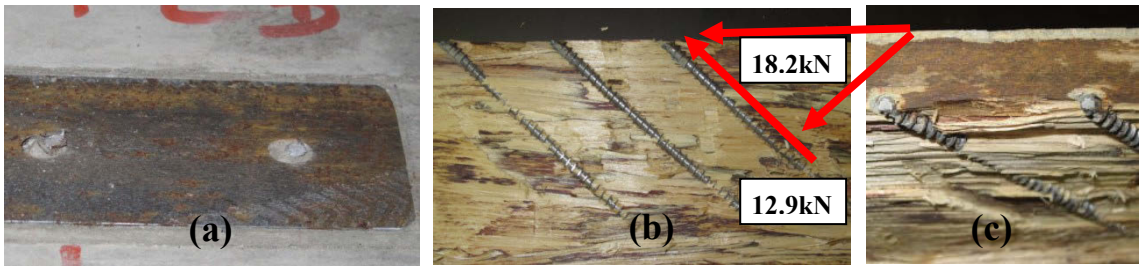

Figure B-14 Failure of (a) head of screw in concrete (b) opened specimen and (c)tensile and shear failure of the SPAX screws

The L profile series showed relatively reliable slip moduli, shown by low CoV of 10-25%. L connectors were placed evenly along the length of the LVL joist. Hence, direct shear force loading resulted in an eccentricity in the TCCs. Thus during the push out test, the right LVDT should have demonstrated less slip, due to the restraint provided from the unequal angle being embedded on that side. However a stiffness analysis of all the load-slip diagrams from the L series comparing the readings between the left and the right LVDT showed no trends for lower stiffness of the unrestrained side.

The strength of each SPAX screw in the L series was calculated as 18.2kN in shear (54.6kN/3). Resolving the shear strength into two components, the component of the shear force along the screw, 12.9kN is close to the tensile strength of the small SPAX screw at 13.4kN, obtained from the uni-axial tensile tests as reported in Chapter 6.

The U series connector demonstrated the second highest strength with an average strength of 40.0kN. The U connector demonstrated a 36.6% lower strength than the L connector and 53.3% higher strength than the coach screw. It was anticipated that the U connector would have a similar failure load to the L connector due to the use of the 3 SPAX screws to fix the U connector to the LVL.

Figure B-13b illustrates that the U connector failed in a very ductile manner with a ductility of 63 and this is attributed to the plastic deformation of the thin wall thickness of the U connector and thus, the SPAX screw head was allowed to be slowly pulled through the bottom section of the U connector and remained firmly intact whilst the steel in the U connector around the screws experienced a plastic deformation as illustrated in Figure B-15a.

This result attributed to the fact that the U connectors were produced from low carbon steel with a yield stress of 210MPa whilst the SPAX screws were made from high carbon steel with an ultimate tensile stress of 1063MPa as reported in Chapter 6.

Although the U connector did not achieve the same strength as the L connector, this ductile behaviour is desirable. A slight plastic hinge of the SPAX screw was visible just below the head with crushing of the LVL whilst the concrete slab remained undamaged and this ductile failure was consistent for all 5 U specimens as shown in Figure B-15b. Steel with a minimum yield stress of 491MPa is required to avoid plastic failure around the screw perforation at the bottom section of the U connector.

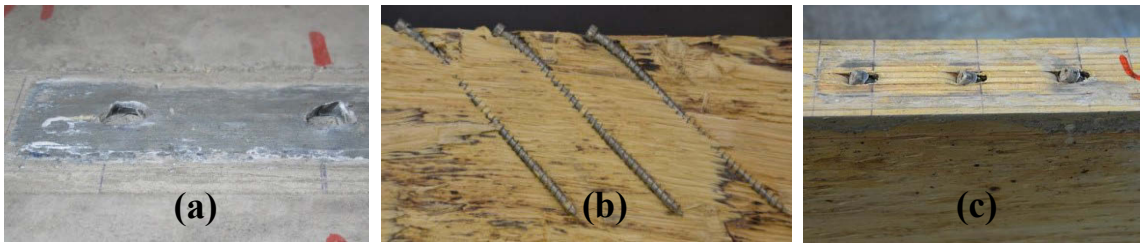

Figure B-15 (a) Plastic deformation of the screw holes in the U connector, (b) opened specimen and (c) screw head being pulled through the U connector and timber crushing

Additionally, both the U and L connector utilised 3 SPAX screws and thus under this loading arrangement they exhibit similar behaviour. However, the serviceability slip modulus of the U connector was close to that of the coach screws series. The ultimate slip modulus was the lowest across all series which is explained by plastic deformation of the U connector near the screw holes resulting in large slip behaviour.

Figure B-16c shows that the average strength of 26.1kN for the coach screw series is resolved into two components and the tension component of the shear force is close to the value achieved in the uni-axial tensile tests, 19.3kN as reported in Chapter 6. The coach screw series exhibited the lowest serviceability slip modulus. However ultimate slip modulus of the coach screw series indicated the second highest average slip modulus. This is due to the coach screw connector exhibiting greater slip resistance when loaded at 60%F_{max}. Overall the slip moduli calculated are reliable, as shown by the relatively low CoV varying on average between 10% and 25%.

Figure B-13c highlights that the coach screw failed in a ductile manner with a ductility of 13, possibly because the coach screws were made from a mild carbon steel. It was observed that the coach screws failed in a combination of shear and tension at the TCC interface with no signs of a plastic hinge. The failure surface has a rougher pattern than that observed in the SPAX screws and there are signs of ductile failure in the screw with some areas of necking (Figure B-14b).

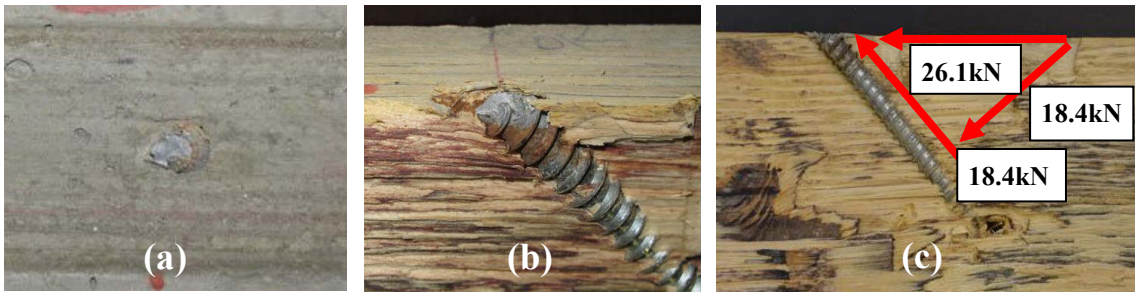

Figure B-16 Tensile and shear failure in the coach screw

No splitting or embedment of the timber was observed (Figure B-14b) whilst the concrete remained undamaged (Figure B-14a).

B.2 PUSH-OUT TEST RESULTS: EPS LIGHT-WEIGHT CONCRETE

Tables B-5 and B-6 present the load capacity and ductility of the EPS LWC test series. Tables B-7 and B-8 list the load capacity and different slip moduli of the test series obtained from EN26891 and modified methods, respectively. Moreover, the mean, standard deviation and coefficient of variation (CoV) of the test data were tabulated.

Table B-5 Load capacity of different series utilising EPS LWC

series	No.	Load capacity(kN)			
		Range	Ave	σ	CoV
SFSWI30	5	33.1-37.7	34.9	2.0	5.8
SFSWI45	10	26.5-34.7	30.8	2.3	7.5
SFSWI60	5	22.4-27.8	25.3	2.0	7.8
SSFSWI45	5	13.5-21.0	17.3	2.7	15.4
SFSI45	5	24.4-29.6	27.6	2.0	7.2
SPAX WI30	5	28.6-36.1	32.3	3.2	10.0
SPAX WI45	5	33.8-36.9	35.2	1.3	3.6
SPAX WI60	5	31.6-33.5	32.3	0.7	2.2
SPAX I45	5	27.4-32.0	29.3	1.8	6.3
SFSWI45EPS1600	5	22.7-26.8	24.9	2.0	8.1
SFSI45EPS1600	5	19.1-24.7	21.1	2.1	10.0

Table B-6 Ductility of different test series utilising EPS LWC

series	u_y(mm)	u_u(mm)	u_f(mm)	D_u		D_f	
	Ave(CoV)	Ave(CoV)	Ave(CoV)	Range	Ave(CoV)	Range	Ave(CoV)
SFSWI30	0.3(43.8)	1.9(77.1)	4.4(32.9)	2.6-8.3	5.4(45.7)	5.9-29.4	15.5(59.1)
SFSWI45	0.6(16.9)	2.8(35.9)	4.6(22.4)	2.9-8.2	5.1(40.2)	5.5-13.0	8.3(28.7)
SFSWI60	0.5(12.7)	5.4(17.5)	6.5(13.4)	8.1-11.6	9.7(13.3)	10.3-13.0	11.7(9.0)
SSFSWI45	0.3(19.9)	1.8(21.2)	3.3(35.2)	3.8-9.1	6.4(31.5)	3.8-17.4	11.7(42.5)
SFSI45	1.0(13.1)	2.4(18.7)	5.5(27.6)	2.0-2.6	2.4(11.1)	3.4-7.6	5.5(28.0)
SPAX WI30	0.4(23.6)	1.4(12.3)	2.4(11.3)	2.9-3.8	3.5(9.7)	3.3-6.9	5.9(24.9)
SPAX WI45	0.6(20.7)	2.4(18.7)	3.8(25.7)	3.1-4.6	4.1(15.2)	4.8-8.1	6.4(20.9)
SPAX WI60	0.7(8.5)	2.2(28.7)	3.4(12.6)	2.1-4.7	3.4(31.1)	4.5-5.7	5.1(9.7)
SPAX I45	1.2(33.7)	3.7(10.9)	5.3(14.3)	2.0-4.2	3.3(29.9)	2.7-7.0	4.8(33.3)
SFSWI45 EPS1600	0.7(21.0)	1.2(21.6)	6(0)	1.6-1.8	1.7(3.9)	6.7-10.5	9.1(18.6)
SFSI45 EPS1600	1.1(16.2)	1.4(14.3)	6(0)	1.2-1.7	1.3(14.2)	4.6-6.5	5.6(15.6)

Table B-7 Slip moduli of series utilising EPS LWC based on EN26891

Series	Slip moduli (kN/mm)								
	$K_{s,0.4}$			$K_{s,0.6}$			$K_{s,0.8}$		
	Range	Ave	σ(CoV)	Range	Ave	σ(CoV)	Range	Ave	σ(CoV)
SFSWI30	46.5-73	59.9	14.4(24.0)	40.9-65.5	50.0	9.3(18.7)	14.3-51.7	36.9	138(37.5)
SFSWI45	30.6-62.0	43.0	9.7(22.5)	28.3-43.5	35.4	4.6(13.0)	18.1-33.9	28.4	4.5(15.7)
SFSWI60	23.6-29.8	27.0	2.6(9.6)	25.5-28.9	26.5	1.4(5.4)	7.2-25.4	19.6	8.0(40.7)
SSFSWI45	22.1-40.5	28.5	7.3(25.7)	19.8-41.5	30.1	7.7(25.6)	15.1-33.8	21.2	7.6(35.9)
SFSI45	18.5-24.8	21.0	2.6(12.6)	16.8-23.0	19.4	2.4(12.2)	15.4-20.9	17.5	2.1(11.8)
SPAX WI30	41.1-77.2	53.9	14.5(27.0)	36.5-64.1	48.9	10.1(20.6)	33.4-50.7	42.1	6.6(15.7)
SPAX WI45	27.9-61.2	39.5	13.4(33.8)	25.9-54.8	35.6	11.5(32.3)	24.6-40.8	30.6	6.6(21.7)
SPAX WI60	31.0-69.7	38.1	18.9(49.8)	19.2-35.6	28.2	5.9(20.8)	18.6-25.7	24.0	3.0(12.6)
SPAX I45	13.4-19.5	16.2	2.2(13.4)	13.7-19.3	16.4	2.1(12.6)	12.9-17.0	14.4	1.8(12.2)
SFSWI45 EPS1600	28.3-34.5	31.6	3.1(9.9)	25.5-30.3	28.2	2.4(8.7)	23.2-27.1	25.5	2.0(8.0)
SFSI45 EPS1600	13.6-24.7	18.2	4.1(22.3)	13.8-21.7	17.3	2.9(16.9)	13.8-19.5	16.4	2.3(13.8)

Table B-8 Slip moduli of series utilising EPS LWC based on modified method

Series	Slip moduli (kN/mm)								
	$K_{s,0.4}$			$K_{s,0.6}$			$K_{s,0.8}$		
	Range	Ave	σ(CoV)	Range	Ave	σ(CoV)	Range	Ave	σ(CoV)
SFSWI30	57-121.1	87.9	30.1(34.3)	45.8-81.8	61.1	15.5(25.3)	14.7-58.6	42.0	17.8(42.3)
SFSWI45	48.1-86.9	60.1	11.1(18.4)	36.4-56.4	42.6	5.9(13.9)	18.1-40.0	32.0	5.9()18.3
SFSWI60	47.5-80.0	63.2	12.2(19.2)	37.9-48.6	42.3	4.1(9.7)	7.8-36.2	25.8	12.2(47.2)
SSFSWI45	23.2-84.0	64.5	24.7(38.4)	28.1-56.0	47.0	15.5(33.1)	16.7-40.1	25.8	9.4(36.6)
SFSI45	20.4-27.9	24.9	2.8(11.4)	17.9-24.7	21.5	2.4(11.3)	16.0-21.9	18.7	2.1(11.3)
SPAX WI30	55-100.2	82.4	17.4(21.1)	43.0-70.7	62.4	11.0(17.7)	37.2-54.5	48.9	6.9(14.1)
SPAX WI45	61.8-146	89.4	33.0(36.9)	47.3-69.0	54.5	8.6(15.7)	33.3-42.3	38.0	4.1(10.7)
SPAX WI60	31.0-85.4	57.6	24.4(42.4)	25.0-43.2	35.3	8.4(23.7)	20.7-32.3	27.9	5.2(18.8)
SPAX I45	24.8-51.7	35.5	9.9(27.8)	19.9-33.5	25.8	5.0(19.3)	16.6-23.0	18.9	2.8(14.6)
SFSWI45 EPS1600	33.6-44.9	37.5	6.4(17.2)	28.3-34.8	31.0	3.4(11.0)	24.9-29.7	27.1	2.4(9.1)
SFSI45 EPS1600	22.6-28.2	25.4	2.4(9.3)	19.3-23.7	21.1	1.7(7.8)	16.7-21.2	19.0	1.7(9.1)

B.2.1 EPS LWC 2000 SFS VB screws series

The load-slip response and analytical model of EPS LWC series utilising SFS screws with and without plywood interlayer are plotted in Figure B-17. The mathematical descriptive models and sample correlation coefficients, R^2 of EPS LWC2000 series utilising crossed SFS screws are given in Equations (B-14):(B-18).

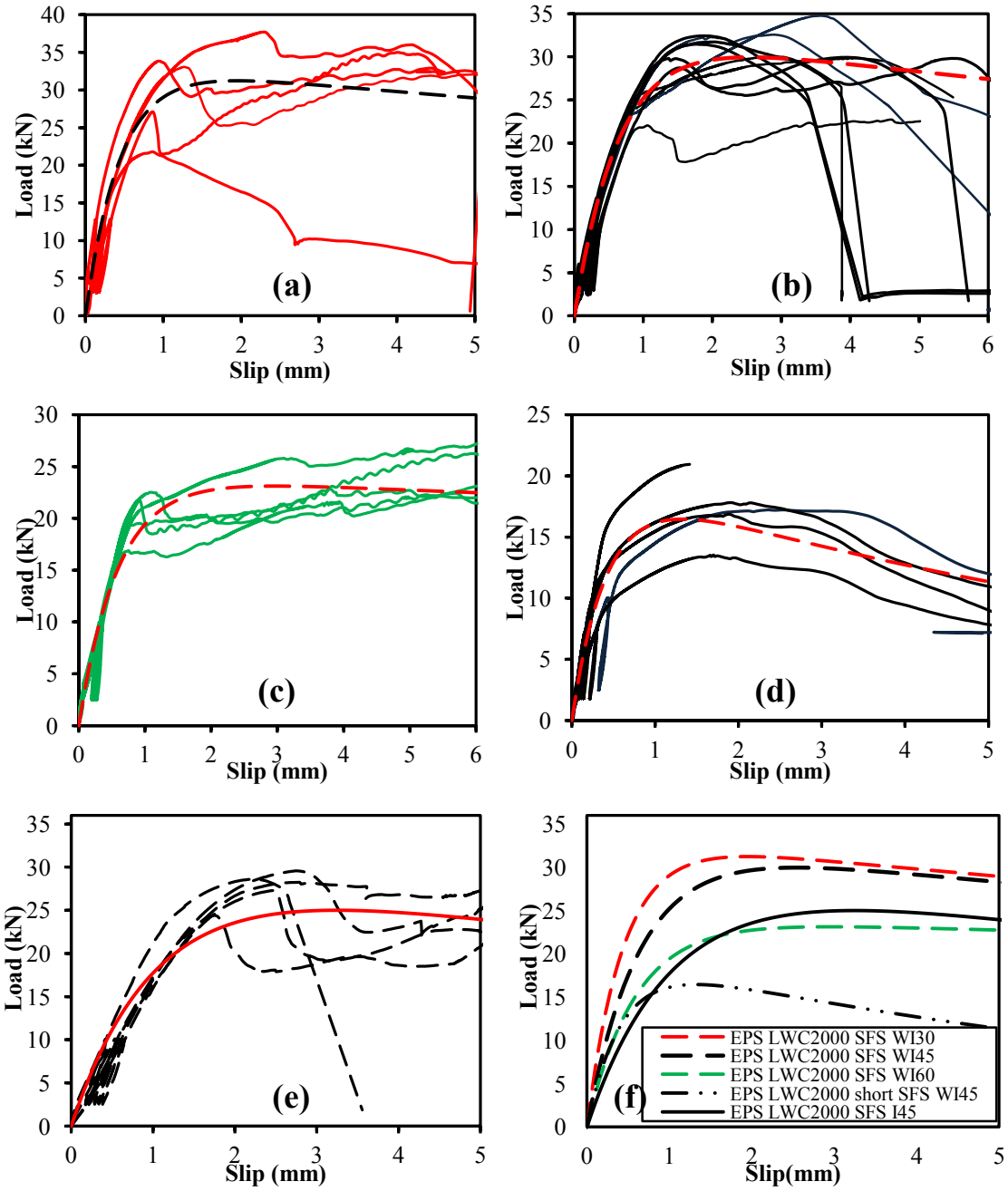

Figure B-17 Load-slip and analytical model of LWC2000 EPS SFS series (a) WI30, (b) WI45, (c) WI60, (d) WI45 short SFS, (e) I45 and (f) comparison of analytical graphs

$$P = 33.5(e^{-0.03\upsilon} - e^{-0.3\upsilon}) \ ,(R^2 = 0.89) \qquad \text{[SFSWI30]} \qquad \text{(B-14)}$$

$$P = 33.10(e^{-1.57\upsilon} - e^{-0.03\upsilon}) \ ,(R^2 = 0.98) \qquad \text{[SFSWI45]} \qquad \text{(B-15)}$$

$$P = 24.07(e^{-0.01\upsilon} - e^{-1.7\upsilon}) \ ,(R^2 = 0.93) \qquad \text{[SFSWI60]} \qquad \text{(B-16)}$$

$$P = 20.1(e^{-0.11\upsilon} - e^{-2.42\upsilon}) \ ,(R^2 = 0.87) \qquad \text{[SSFSWI45]} \qquad \text{(B-17)}$$

$$P = 30.6(e^{-0.98v} - e^{-0.05v}) \ ,(R^2 = 0.88) \qquad \text{[SFSI45]} \qquad \text{(B-18)}$$

Figures B-18:B-22 show the failure mode and opened specimens of different EPS LWC2000 series utilising SFS screws.

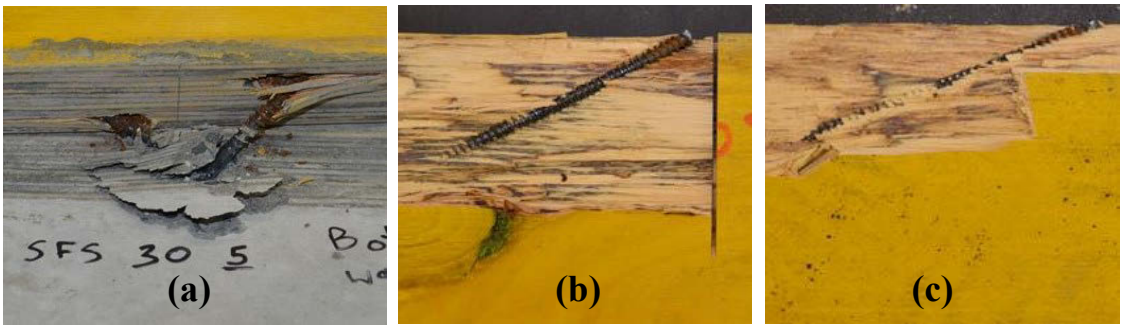

Figure B-18 (a) Intact screws and opened specimens of screws in (b) tension and (c) compression in EPS LWC 2000 SFS WI30 series

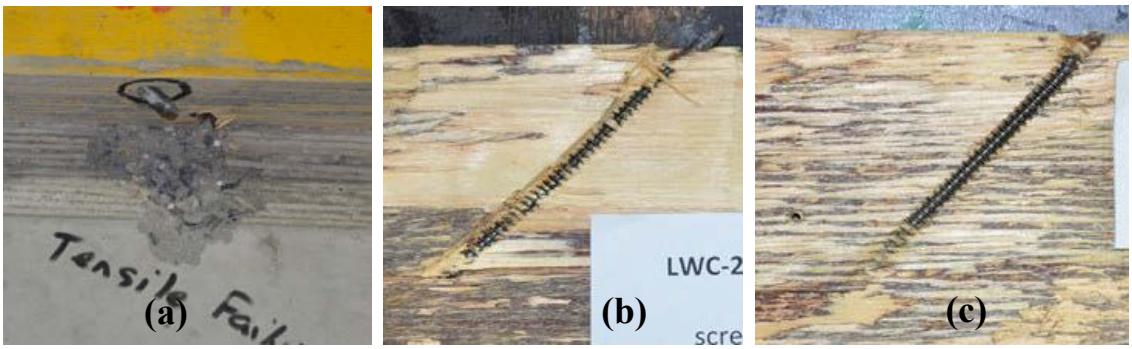

Figure B-19 (a) Failure of tensile screw and opened specimens of screws in (b) tension and (c) compression in EPS LWC 2000 SFSWI45 series

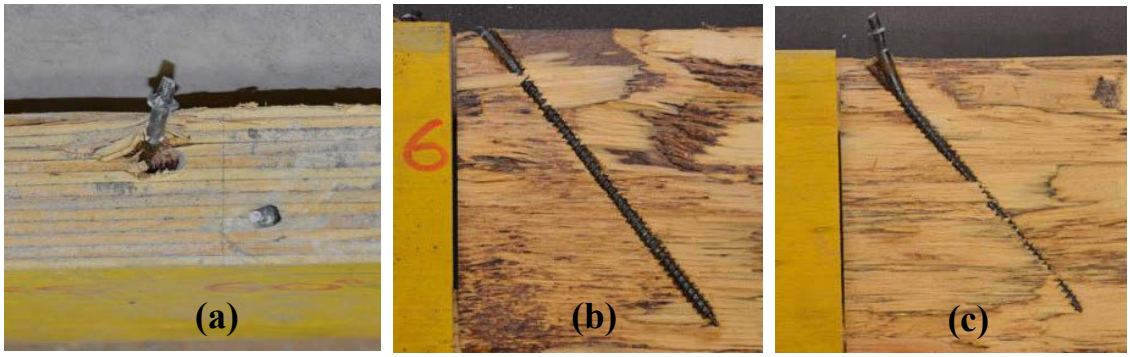

Figure B-20 (a) Failure of tensile screws and opened specimens of screws in (b) tension and (c) compression in EPS LWC 2000SFSWI60 series

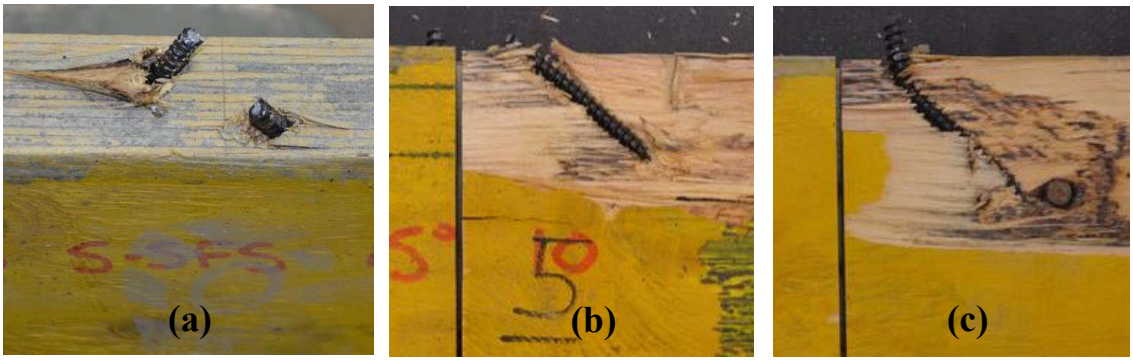

Figure B-21 (a) Intact screws and opened specimens of screws in (b) tension and (c) compression in EPS LWC 2000short SFS WI45 series

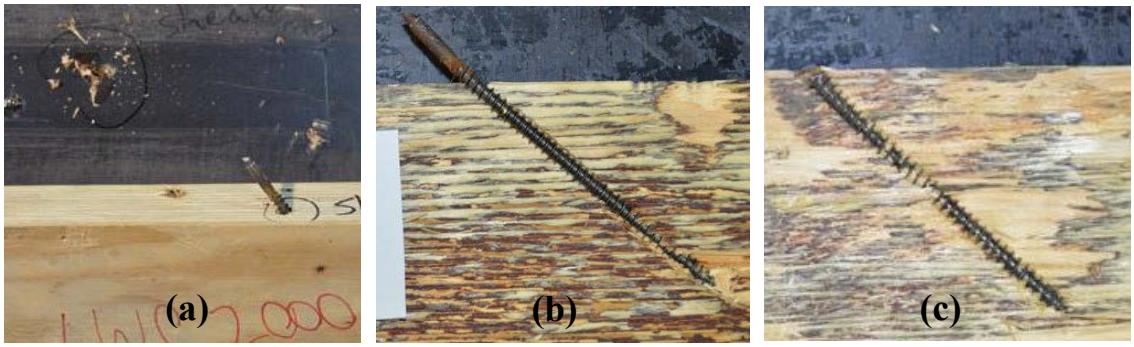

Figure B-22 (a) Failure of tensile screw and opened specimens of screws in (b) tension and (c) compression in EPS LWC 2000 SFS I45 series

Generally, in the case of tensile failure of screws, a loud distinct sound corresponding to tensile failure of the screw in tension was heard as the screw failed. Moreover, no embedding failure and plastic hinge was observed in the screw placed in tension. The timber surrounding the tensile screws did not crush in any of the specimens.

EPS LWC SFS WI30 series demonstrated multiple failure modes. For specimens 1 and 2, the tensile screw failed, and for the remaining specimens the screws were intact. EPS LWC SFS WI30 series exhibited localised concrete failure around the shear connection due to deformation of the screws at the interface (Figure B-18a). Sample 3 experienced a lower F_{max}; the tensile screw was slightly protruding from the side of the LVL. With the exception of specimen 3, all samples exhibited maximum loads of 33.1-37.7kN with CoV of 5.8% which represents minimal dispersion and demonstrates consistent results.

EPS LWC SFS WI45 series represented a single failure mode as tensile failure of the screws placed in tension. There was some localised concrete failure and localised timber failure around the compressive screw due to the tensile and compressive screw

deformation which cracks the surface of the concrete (Figure B-19). There was no timber crushing around the tensile screw as depicted in Figure B-19. The tensile screw failed when the load carrying capacity of TCC sample exceeded the tensile strength of the SFS screw. In this case, the strength of TCC sample is dependent on the tensile capacity of the screw.

The behaviour of this series was split as some samples exhibited a single peak behaviour similar to the CC SFS WI45 series. The other samples exhibited a dual peak behaviour, with the first peak followed by a small drop before load increased again and then ultimate failure. In these cases, an initial localised failure in the concrete at the connection is likely to have caused the first drop, before the ultimate failure of the screws. Failure in all cases was more ductile than similar series utilising CC series, with a greater deflection following F_{max} before failure. EPS LWC2000 SFS WI45 series represented a strength range of 26.5-34.7kN, with an average of 30.8kN. The minimal strength dispersion with CoV of 7.5% demonstrates consistent results.

All specimens of EPS LWC2000 SFS WI60 series failed by tensile failure of screw placed in tension. There was some localised failure of concrete around the tensile screw on all samples due to deformation of screws. EPS LWC2000 SFS WI60 series demonstrated a strength range of 22.4-27.8kN, with an average of 25.3kN. The minimal strength dispersion with CoV of 7.8% demonstrates consistent results.

All specimens of EPS LWC2000 short SFS WI45 failed by plastic hinge in compression screw. There was torsional twist experienced on all specimens. This has occurred as there was localised crushing/deformation of the timber surrounding the compression screw. This behaviour shortened the length of the compression screw in the vertical plane, increasing its length in the horizontal plane causing the specimen to twist. There was no concrete failure experienced with localised failure of the timber in both the tension and compression screws. This has occurred as the screw has not entered the timber as deeply, and is not as secure in the timber. This type of failure is very ductile.

EPS LWC2000 short SFS WI45 series demonstrated a strength range of 13.5-21.0kN, with an average of 17.3kN with CoV of15.4% which demonstrated lower consistency of the results. The lower consistency of these results is attributed to a mechanical machine error with test specimen 2 which was pre-loaded to 18kN before testing.

EPS LWC2000 SFS I45 series demonstrated a strength range of 24.4-29.6kN, with an average of 27.6kN with CoV of 7.2% which demonstrated consistent results. Specimen 5 exhibited a sudden failure, with both screws failing. Four of the samples 1-4 of EPS LWC2000 SFS I45 exhibited a similar dual peak pattern to some EPS LWC2000 SFSWI45 specimens. This coincided with slip between the concrete and plywood interlayer of around 2-5mm, and some detachment between layers. This was likely to be due to localised failure of the concrete at the connection which allowed the deformation of the screws. This coincided with slip between the concrete and interlayer of around 2-5mm, and some detachment between layers.

Typical behaviour of LWC short SFS observed by Jorge, Lopes and Cruz (2011) included an initial peaking of load, which was generally followed by some recovery of load, and in many cases a later maximum load. This was attributed to local crushing of the concrete due to the low compressive strength of light-weight aggregate.

However, Jorge, Lopes and Cruz (2011) noted that the mortar matrix in LWC is stronger than in CC and this may result in a higher anchor strength after the initial crushing of aggregate, leading to the recovery of load level after an initial drop. Similar behaviour was observed in the EPS LWC2000 SFS series of the tests in this study,, likely for these same reasons.

EPS LWC series exhibited highest ductility among the test series. The ductility of long SFS series varied between 5.5-11.7. The EPS LWC2000 SFS series exhibited no obvious trend between inclination angle and ductility whilst inclusion of interlayer led to 35% ductility reduction compared to similar series without interlayer.

Short SFS led to an increasing of 40% compared to similar series utilising long SFS series.

B.2.2 EPS LWC 2000 SPAX screws series

The load-slip responses of LWC EPS2000 SPAX screws at different angles with and without interlayer series are plotted in Figure B-23. The mathematical descriptive models and the sample correlation coefficients, R^2 of EPS LWC2000 series utilising crossed SPAX screws are given in Equations (B-19):(B-22).

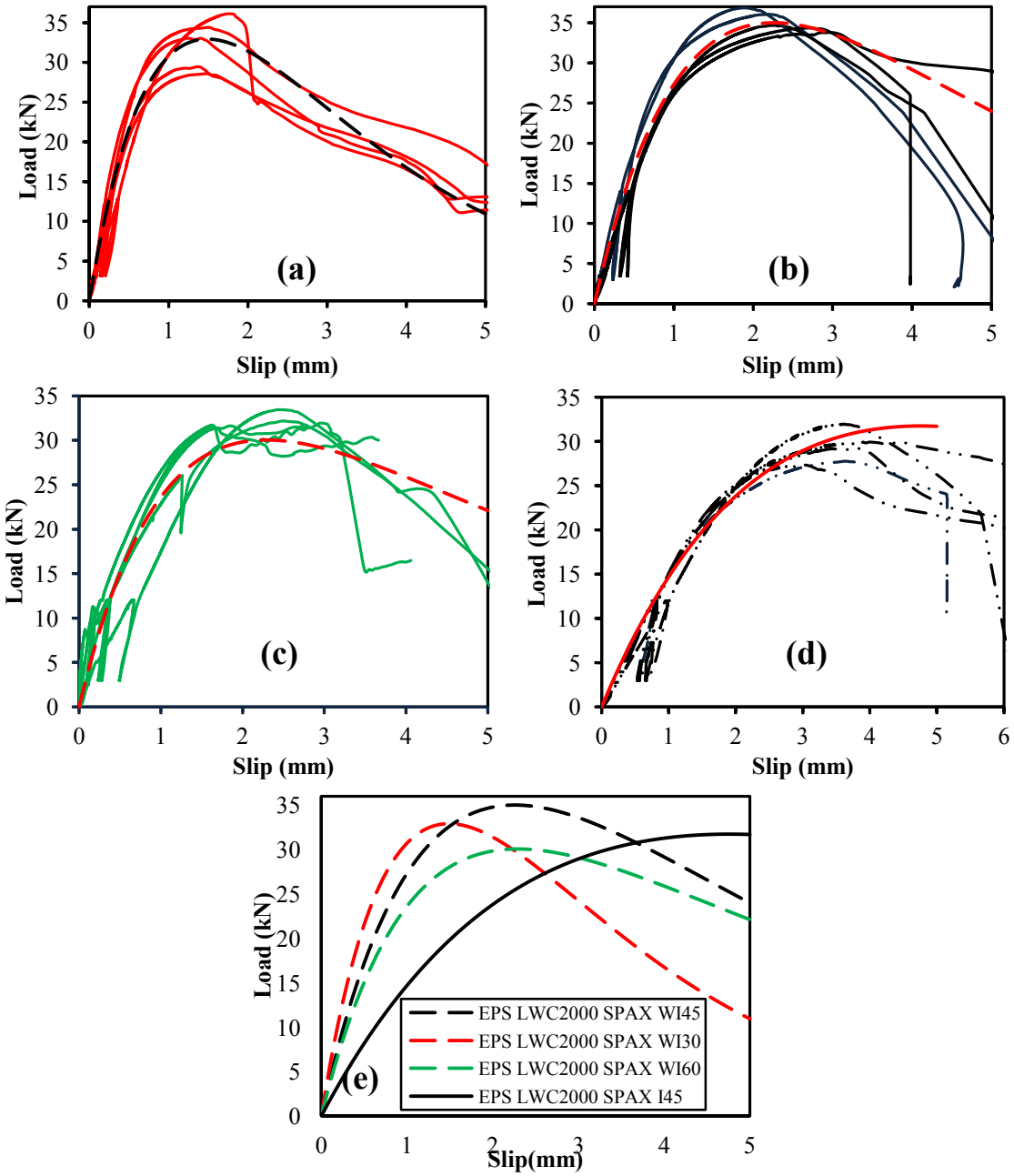

Figure B-23 Load-slip and analytical model of LWC EPS 2000 SPAX series(a) WI30, (b) WI45, (c) WI60, (d) I45 and (e) comparison of analytical graphs

$$P = 114.9(e^{-0.28\upsilon} - e^{-0.66\upsilon}) \ ,(R^2 = 0.97) \qquad \text{[SPAX WI30]} \qquad \text{(B-19)}$$

$$P = 114.9(e^{-0.28\upsilon} - e^{-0.66\upsilon}) \ ,(R^2 = 0.97) \qquad \text{[SPAX WI45]} \qquad \text{(B-20)}$$

$$P = 63.2(e^{-0.20\upsilon} - e^{-0.81\upsilon}) \ ,(R^2 = 0.90) \qquad \text{[SPAX WI60]} \qquad \text{(B-21)}$$

$$P = 488.8(e^{-0.19\upsilon} - e^{-0.23\upsilon}) \ ,(R^2 = 0.98) \qquad \text{[SPAX I45]} \qquad \text{(B-22)}$$

Figures B-24:B-27 show the failure mode and opened specimens of different EPS LWC2000 series utilising SPAX screws.

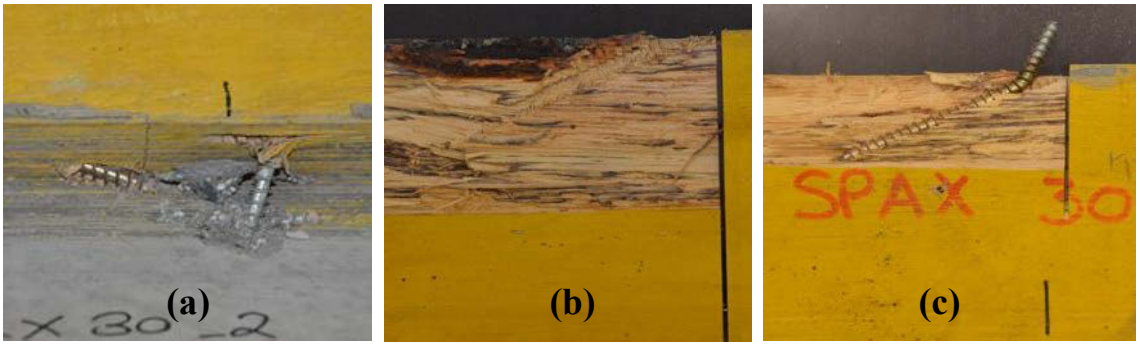

Figure B-24 (a) Intact screws and opened specimens of screws in (b) tension and (c) compression in EPS LWC2000 SPAX WI30 series

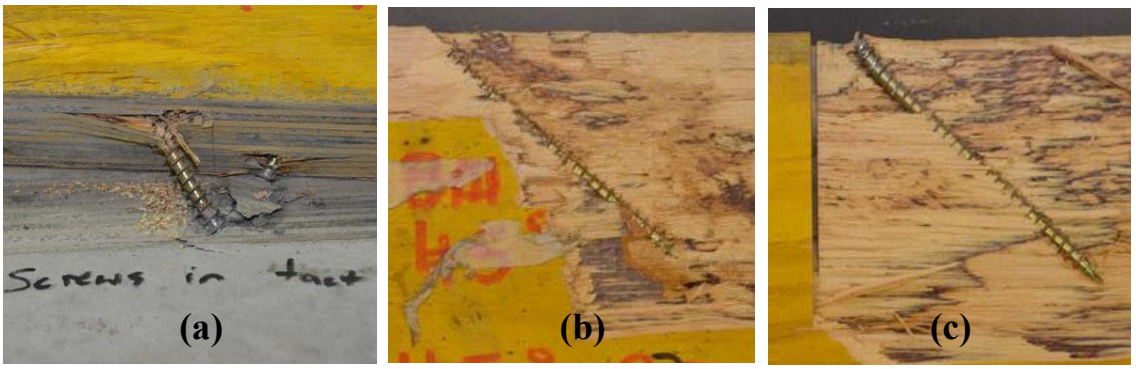

Figure B-25 (a) Tensile failure and opened specimens of screws in (b) tension and (c) compression in EPS LWC2000 SPAX WI45 series

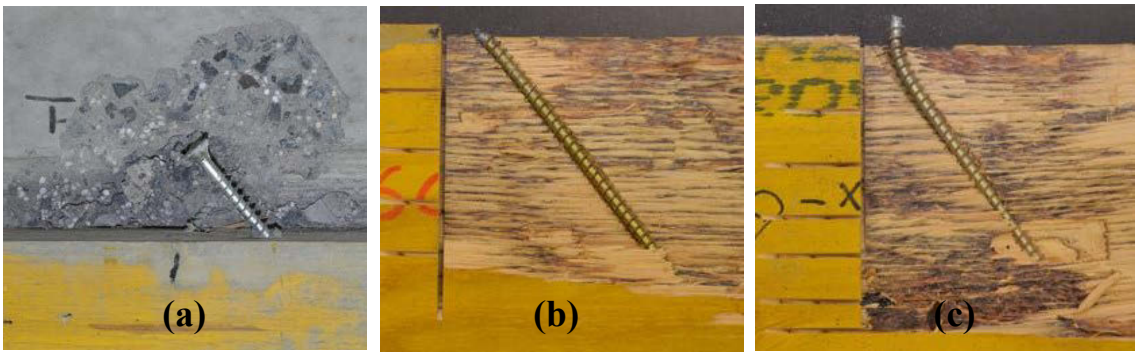

Figure B-26 (a) Tensile failure and opened specimens of screws in (b) tension and (c) compression in EPS LWC2000 SPAX WI60 series

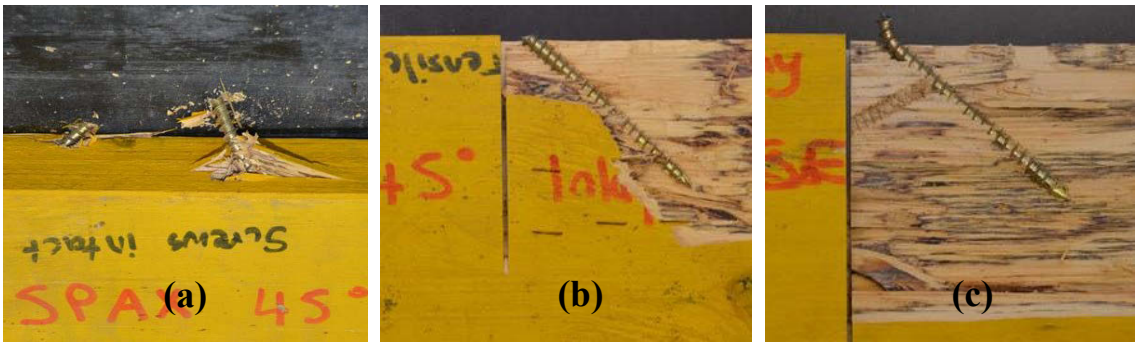

Figure B-27(a) Intact screws and opened specimens of screws in (b) tension and (c) compression in EPSLWC2000 SPAX I45 series

EPS LWC SPAX WI30 series demonstrated a single mode of failure. All specimens failed with both screws intact (Figure B-24a). In all samples localised failure of concrete around the shear connector as well as localised crushing of timber in both the tension and compression screws were observed (Figure B-24b and c).

There was lateral displacement of screws with formation of a plastic hinge in the screw placed in compression. In this case the load carrying capacity of the shear connector was governed by the embedding strength of the surrounding timber and bending capacity of the screw. EPS LWC 2000 SPAX WI30 series represented a strength range of 28.6-36.1kN, with an average of 32.3kN. The minimal strength dispersion with CoV of 10.0% demonstrates relatively consistent results.

EPS LWC2000 SPAX WI45 series demonstrated multiple modes of failure. All specimens 1-4 failed in tensile failure of screw placed in tension, however specimen 5 had both bent screws intact with formation of a plastic hinge (Figure B-25a).

There was some localised failure of concrete and timber around the shear connectors and it is attributed to deformation of the tensile and compression screw in concrete and deformation of compressive screw in timber. EPS LWC2000 SPAX WI45 series represented a strength range of 33.8-36.9kN, with an average of 35.2kN. The minimal strength dispersion with CoV of 3.6% demonstrates consistent results.

EPS LWC2000 SPAX WI60 series demonstrated multiple modes of failure. Specimens 1, 2, 3 and 5 failed in tensile failure of screw, however specimen 4 experienced large localised concrete failure and the screws were both intact with no localised failure of the timber (Figure B-26a).

Poor compaction of connection area in specimen 4 might be the reason for large concrete failure as no other specimens failed in this manner. For all specimens some localised failure of concrete around the shear connectors was observed and it is attributed to the deformation of tensile and compression screw in concrete before failure whilst there was some crushing in front of compressive screw in timber. EPS LWC2000 SPAX WI60 series represented a strength range of 31.6-33.5kN, with an average of 32.3kN. The minimal strength dispersion with CoV of 2.2% demonstrates consistent results.

EPS LWC SPAX I45 series demonstrated multiple modes of failure. Specimens 1, 2, 3 and 5 failed with screws intact and specimen 4 failed in tensile failure of screw. For specimens 1, 2, 3, and 5 there was very large torsional twist observed. This has occurred as the shear connectors have failed as plastic hinge in screw. Because of the presence of an interlayer made of plywood, the timber is more susceptible to crushing.

The twisting occurred as there was localised crushing of the timber in the interlayer and surrounding the compression screw as displayed in Figure B-27a. This behaviour shortened the length of the compression screw in the vertical plane, increasing its length in the horizontal plane (parallel to the interface) causing the specimen to twist. The failure coincides with the rotation of the fastener about some point along the screw.

EPS LWC SPAX I45 series represented a strength range of 27.4-32.0kN, with an average of 29.3kN. The minimal strength dispersion with CoV of 6.3% demonstrates consistent results. The presence of interlayer significantly reduced the stiffness of the EPS LWC2000 SPAX 45 series. EPS SPAX series I45 experienced 59% and 53% lower serviceability and ultimate slip moduli compared to the results with the interlayer series.

It is noted that tensile failure of screw in tension occurred when the load carrying capacity of the joint exceeded the tensile strength of the SPAX screw and the strength of the specimen depends on the tensile capacity of the screw.

The ductility of SPAX series varied between 4.8-6.4. The EPS LWC2000 SPAX series exhibited no obvious trend between inclination angle and ductility whilst inclusion of interlayer led to 25% ductility reduction compared to similar series without interlayer.

B.2.3 LWC-EPS1600 SFS VB screw series

The load-slip responses of LWC EPS1600 SFS45 with and without interlayer are plotted in Figure B-28.

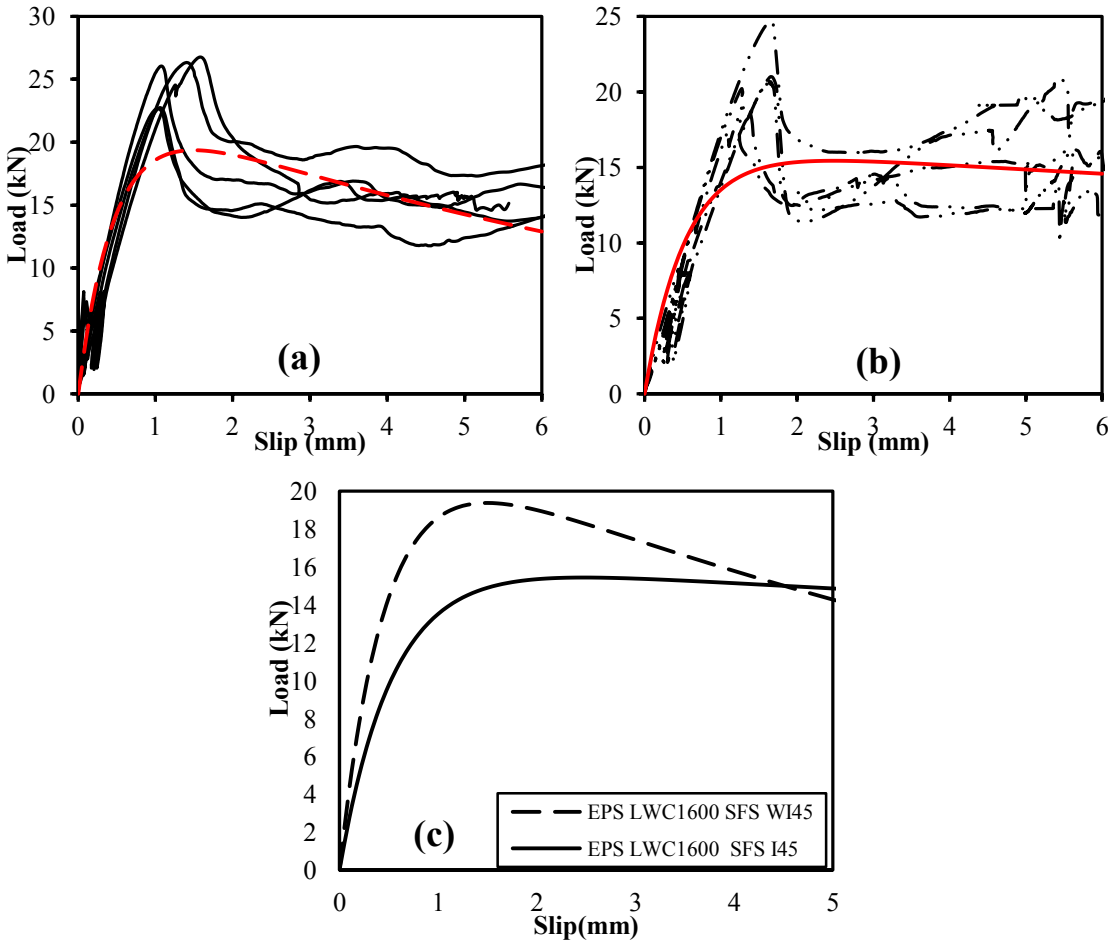

Figure B-28 Load-slip and analytical model of EPS LWC1600 SFS (a) WI45, (b) I45 and (c) comparison of analytical graphs

The mathematical descriptive model and the sample correlation coefficient, R^2 of EPS LWC1600 series utilising crossed SPAX screws are given in Equations (B-23) and (B-24).

$$P = 23.6(e^{-0.10v} - e^{-2.41v}) \ ,(R^2 = 0.80) \qquad \text{[EPS1600SFSWI45]} \qquad \text{(B-23)}$$

$$P = 16.36(e^{-0.02v} - e^{-1.87v}) \ ,(R^2 = 0.74) \qquad \text{[EPS1600SFSWI45]} \qquad \text{(B-24)}$$

The LWC1600 SFS series also showed single peak behaviour, but not a complete failure as observed in the CC series. The initial failure was caused again by localised concrete failure; however it was also accompanied by the failure of the compression screw, leading to a more significant reduction in load where load was not significantly recovered before final failure as depicted in Figure B-29.

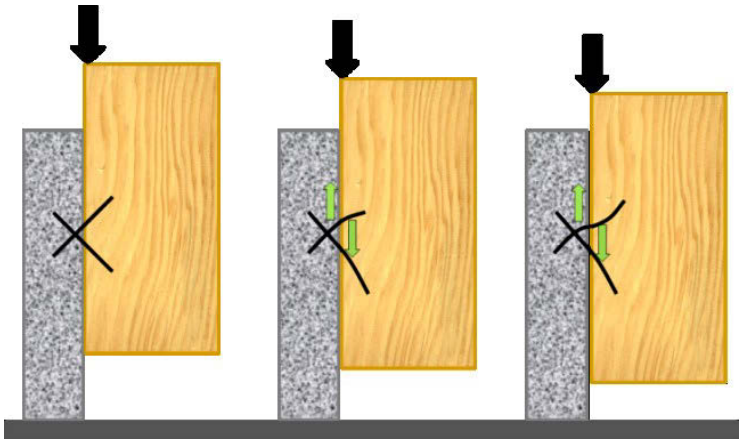

Figure B-29 Failure of compressive screws in EPS LWC1600 SFS45 test series

F_{max} for the EPS LWC 1600 SFSWI45 was reduced compared to similar series utilising EPS LWC2000. EPS LWC 1600 SFSWI45series also behaved and failed in a different manner to previous EPS LWC2000 series with ultimate failure of screw in compression. These samples reached a peak, and then the load had a relatively sudden decline before plateauing at around 60-80% of F_{max}. Localised concrete failure at the connection allowed additional deformation of the screws whilst the load remained constant.

Similar to the EPS LWC2000 series, a reduction in the compressive strength of the concrete allowed the localised failure of the concrete around the SFS screws. In these specimens, due to a further reduced compressive strength compared to the EPS LWC2000 concrete, the localised failure of the concrete led to the deformation of the compressive screw, which allowed it to become perpendicular to the direction of loading. Hence, the compressive screws were subjected to only shear force, and the screws failed under this increased shear force relative to the cross-section (or reduced section relative to the direction of shear) as schematically shown in Figure B-29.

The subsequent plateauing of the force was the result of continued tension in the tensile screw; however slip became large as loading continued (15-30mm). This behaviour demonstrates the value of the compression screw in resisting the shear force.

The increase in slip of these specimens, while maintaining a relatively constant load was due to the continued tension in the tensile screw until the compressive screw eventually reached shear failure.

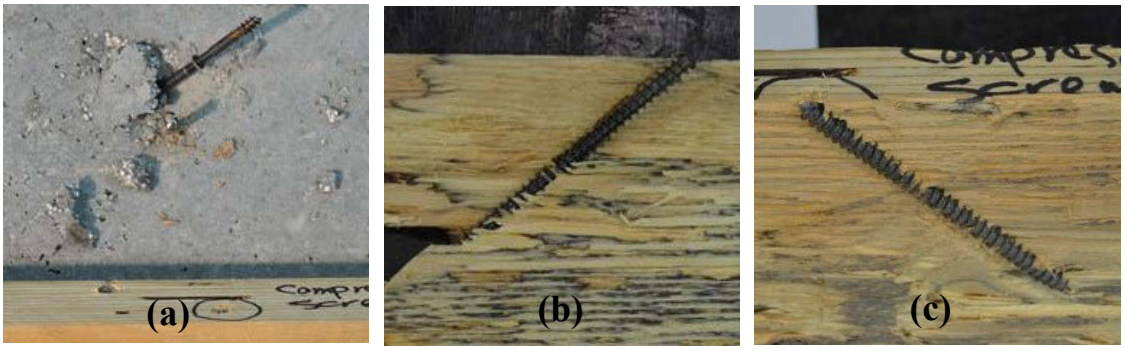

Figure B-30 (a) Failure of compressive screw and opened specimens of screws in (b) tension and (c) compression in LWC EPS1600 SFS I45 series

The EPS LWC1600I45 series behaved similarly to the EPS LWC1600WI45 series, though with reduced load capacity. Initial failure was due to shear failure of the compressive screw in most samples as depicted in Figure B-30.

Samples with EPS LWC2000 and EPS LWC1600 concrete showed 20-25% and 40-60% less slip at F_{max} were observed EPS LWC2000 and EPS LWC1600 SFS series experienced respectively than similar samples constructed from CC series. Lower strength samples failed at lower loads and hence it was expected the slip at failure would be lower. Load-slip graphs show a relatively linear relationship up to the maximum load as depicted in Figures B-17, B-23 and B-28. The reductions in slip are greater than the reductions in failure load and hence, EPS LWC series experienced higher stiffness at different load level rather than that of the HSC, CC and SCC series.

It is also worth noting that low strength samples, EPS LWC1600 series experienced significant slip after initial failure, while the connection was at partial capacity before total failure.

B.3 PUSH-OUT TEST RESULTS: SCORIA LIGHT-WEIGHT CONCRETE

The load-slip response and analytical model of LWC Scoria series utilising SFS VB and SPAX crossed screws at ±45° with and without interlayer series are plotted in Figure B-31. The mathematical descriptive models and sample correlation coefficients, R^2 of Scoria LWC test series are given in Equations (B-25):(B-28).

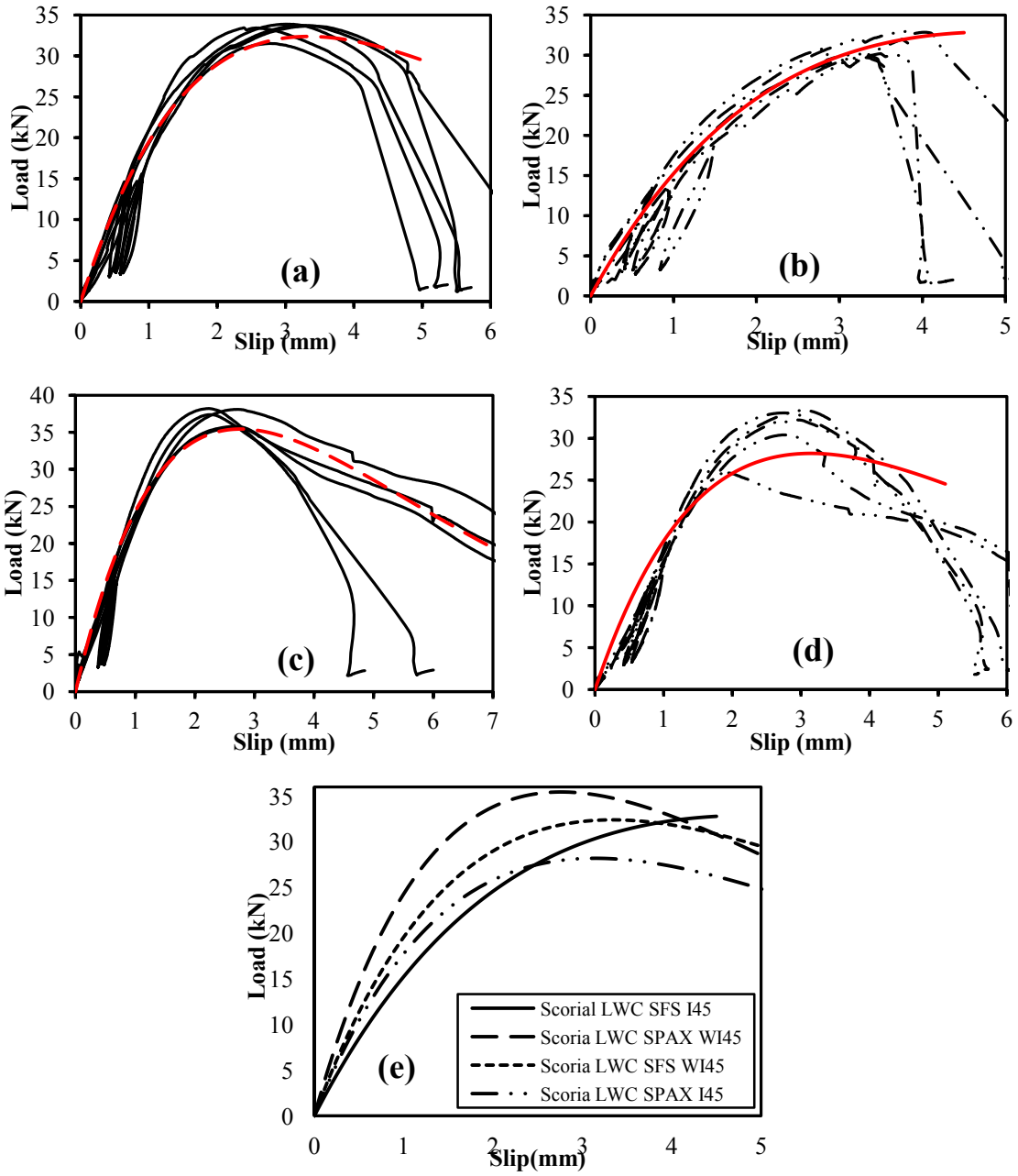

Figure B-31 Load-slip and analytical model of Scoria LWC series(a)SFS WI45, (b) SFS I45, (c) SPAX WI45, (d) SPAX I45 and (e) comparison of analytical graphs

$$P = 862.3(e^{-0.28v} - e^{-0.32v}) \ ,(R^2 = 0.98) \quad \text{[SFS WI45]} \quad \text{(B-25)}$$

$$P = 101.2(e^{-0.13v} - e^{-0.31v}) \ ,(R^2 = 0.98) \quad \text{[SFS I45]} \quad \text{(B-26)}$$

$$P = 1615(e^{-0.35v} - e^{-0.37v}) \ ,(R^2 = 0.98) \quad \text{[SPAX WI45]} \quad \text{(B-27)}$$

$$P = 1418(e^{-0.31v} - e^{-0.33v}) \ ,(R^2 = 0.93) \quad \text{[SPAX I45]} \quad \text{(B-28)}$$

Tables B-9 and B-10 present the load capacity and ductility of the test series utilising Scoria LWC. Tables B-11 and B-12 list the load capacity and different slip moduli of the test series obtained from EN26891 and the modified methods, respectively. Moreover, the mean, standard deviation and coefficient of variation (CoV) of the series were listed.

Table B-9 Load capacity of different series utilising Scoria LWC

series	No.	Load capacity(kN)			
		Range	Ave	σ	CoV
SFSWI45	5	31.5-33.9	33.2	1.0	2.9
SFSI45	5	29.7-34.2	31.6	1.9	6.1
SPAX WI45	5	35.6-38.2	37.1	1.3	3.5
SPAX I45	5	25.9-33.3	30.8	2.9	9.5

Table B-10 Ductility of different test series utilising Scoria LWC

series	u_y(mm)	u_u(mm)	u_f(mm)	D_u		D_f	
	Ave(CoV)	Ave(CoV)	Ave(CoV)	Range	Ave(CoV)	Range	Ave(CoV)
SFSWI45	1.0(21.2)	3.0(12.0)	4.6(6.4)	2.6-3.8	3.0(17.3)	3.8-5.5	4.6(15.9)
SFSI45	1.0(11.3)	3.5(13.5)	3.9(7.2)	3.7-4.4	3.4(17.8)	3.6-4.7	3.9(16.2)
SPAX WI45	1.0(16.5)	2.5(11.6)	4.2(15.8)	1.7-3.2	2.5(23.8)	2.9-5.2	4.2(23.6)
SPAX I45	1.4(4.1)	2.6(18.1)	4.1(5.8)	1.3-2.2	1.9(18.9)	2.5-3.1	2.9(9.0)

Table B-11 Slip moduli of series utilising Scoria LWC based on EN26891

Series	Slip moduli (kN/mm)								
	$K_{s,0.4}$			$K_{s,0.6}$			$K_{s,0.8}$		
	Range	Ave	σ(CoV)	Range	Ave	σ(CoV)	Range	Ave	σ(CoV)
SFSWI45	18.4-23.4	19.8	2.0(10.2)	19.3-22.5	20.4	1.3(6.4)	17.3-19.1	18.1	0.8(4.5)
SFSI45	14.2-16.8	15.7	1.2(7.6)	13.1-18.3	15.8	1.9(12.1)	10.3-14.2	13.0	1.7(12.7)
SPAX WI45	20.1-26.7	23.9	2.7(11.3)	21.4-27.3	24.1	2.3(9.5)	19.7-25.5	22.1	2.3(10.4)
SPAX I45	15.0-17.9	16.2	1.2(7.5)	15.8-26.3	18.8	4.2(22.5)	15.0-23.1	17.6	3.2(18.0)

Table B-12 Slip moduli of series utilising Scoria LWC based on the modified method

Series	Slip moduli (kN/mm)								
	$K_{s,0.4}$			$K_{s,0.6}$			$K_{s,0.8}$		
	Range	Ave	σ(CoV)	Range	Ave	σ(CoV)	Range	Ave	σ(CoV)
SFSWI45	41.5-68.2	52.4	11.2(21.5)	30.7-40.6	35.5	3.6(10.2)	22.9-30.7	25.5	3.1(12.1)
SFSI45	21.6-33.0	26.5	4.1(15.5)	16.1-30.5	22.2	5.5(24.9)	11.6-18.4	15.8	2.8(17.9)
SPAX WI45	52.9-68.2	59.6	6.6(11.2)	36.2-48.9	41.1	5.0(12.3)	28.7-36.1	30.7	3.1(10.1)
SPAX I45	13.6-27.9	23.1	5.5(23.9)	20.9-25.6	22.6	2.0(8.9)	18.3-23.6	20.2	2.0(10.2)

Figures B-32:B-34 show the failure mode and opened specimens of different Scoria LWC series utilising SFS and SPAX screws. Scoria LWC SFS WI and I series revealed consistent strength and stiffness, however not so consistent for slip at F_{max} and ductility as shown by the CoV values. Similar to the CC series, the Scoria LWCSFS WI series initially exhibited a linear behaviour and load increased quite steadily, slowing slightly before reaching the peak load at 31.5-33.9kN whilst as the load reached F_{max}, the samples showed a non-linear response. Following the peak load, the load gradually reduced to about 80% F_{max} before a sudden tensile failure of screw as shown in Figure B-31a.

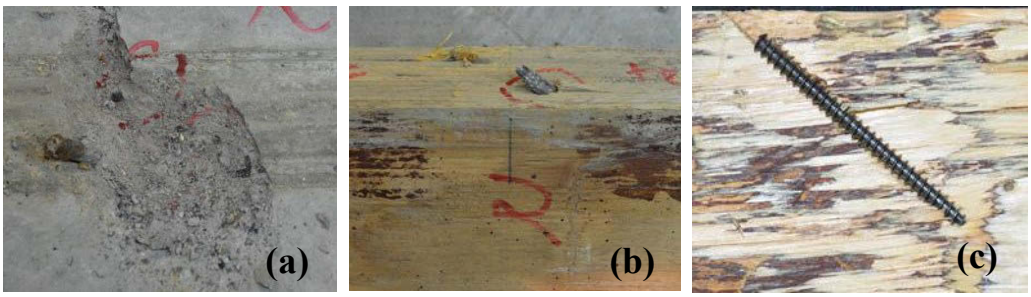

Figure B-32 (a) Localised concrete crushing in Scoria LWC, (b) tensile failure of tensile screw and (c) opened specimens of screws in tension in LWC SFS WI45 series

Figure B-33 (a) Failure of tensile screw (b) tensile failure of screw Scoria LWC SFS I45

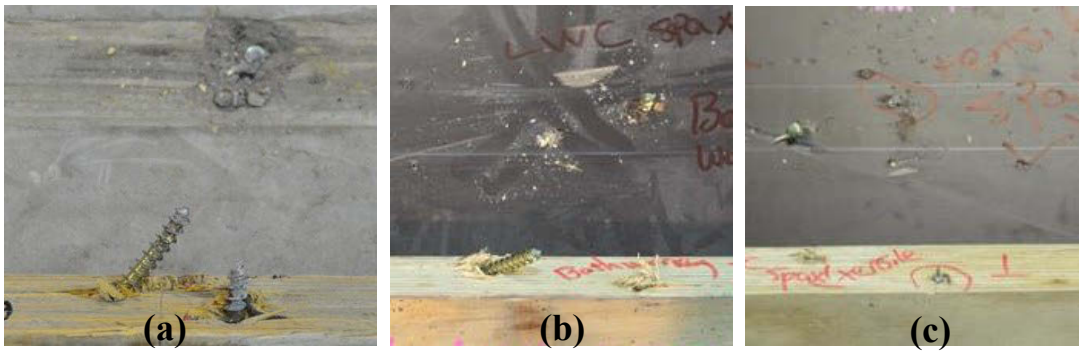

Figure B-34 (a) Intact screws, LWC Scoria SPAX WI45 series (b) intact screws, Scoria LWC SPAX I45 series and (c) failure of tensile screw in Scoria LWC SPAX I45 series

Scoria LWC SFS WI45 series indicated signs of small, localised failure in the concrete around the shear connections. Such cracking was caused by the deformation of the screw at the interface as depicted in Figure B-32a. All specimens experienced a tensile failure of the screw placed in tension, with shear contributing as shown in Figure B-32. Necking was evident on failed screws, and screws failed at their narrowest point, located 20-30mm above the thread and embedded in concrete as shown in Figure B-32b. The average slip at F_{max} results of the series is 2.6mm with a CoV of 15.9%. The results show a minor difference, which adds to the consistency of the results.

Similar to LWC SFS WI45 series, samples of LWC SFS I45 series initially experienced a linear behaviour, and then changed to a non-linear response as the load moved towards F_{max}. After reaching F_{max}, samples displayed ductile responses, until a sudden tensile failure was encountered. There were some fluctuations and wave type pattern in in the load-slip response of the three samples. This pattern was achieved by pieces of aggregate caught in the testing rig, causing fluctuations to occur as the aggregate withstood load until it broke and fell as depicted in Figure B-31b.

Necking of the screws in tension was evident and the failure of each screw occurred at its narrowest point (Figure B-33). Scoria LWC SFSI45 series showed signs of small, localised failure in the concrete around the shear connections. Scoria LWC SFSI45 series indicated the lowest stiffness among Scoria series result with approximately 20% reduction compared to similar series without interlayer.

Scoria LWC SPAX WI45 series demonstrated multiple modes of failure. The initial part of response displayed a linear behaviour followed by a ductile response as the load reached F_{max}. After reaching F_{max}, specimens 1 and 5 experienced tensile failure of

screw in tension, failing at approximately 75%F_{max}. However specimens 2,3 and 4 maintained the load up until 50%F_{max} with higher slip values and both bent screws were intact which formed a plastic hinge (Figure B-31c). There was some localised failure of concrete and timber around the shear connectors and this is attributed to the deformation of screws in concrete and timber as displayed in Figure B-34a.

Scoria LWC SPAX WI45 series represented a strength range of 35.6-38.2kN with an average of 37.1kN. The minimal strength dispersion with CoV of 3.5% indicates consistent results. Scoria LWC SPAX WI45 series exhibited an average of slip at F_{max} of 2.3mm with CoV of 6.5%.

Similar to Scoria LWC SPAX WI45 series, Scoria LWC SPAX I45 series demonstrated multiple failure modes with a linear behaviour upon reaching F_{max}. After reaching F_{max} the nonlinear ductile behaviour was continued until a sudden tensile failure occurred at approximately 75% F_{max} in samples 1, 3 and 4. In contrast, samples 2 and 5 experienced a more ductile behaviour with formation of plastic hinge in screw as they continued to hold load up until approximately 37- 67% F_{max} as depicted in Figure B-31d. A very large torsional twist was observed in these samples.

Scoria LWC SPAX I45 series represented a strength of ranging 25.9-33.3kN, with an average of 30.9kN. The minimal strength dispersion with CoV of 9.5% demonstrates relatively consistent results. The average slip at F_{max} of LWC Scoria SPAX I45 series was 2.4mm with a CoV of 33.6%.

Comparison of Scoria SFS and SPAX series implies that the SPAX series had a F_{max} of 37.0kN, 11.3% greater than the similar SFS series. However, comparing CC SFS45 and SPAX 45 series, CC SPAX I45 produced the lowest F_{max} overall. Similar to CC series, Scoria LWC SPAX I45 presents the lowest strength of the Scoria series. Serviceability and ultimate stiffness of Scoria LWC WI and I series were less than similar CC series. Scoria LWC series showed a higher non-linear response than the CC series.

The presence of interlayer was shown to affect the strength of Scoria LWC SPAX 45 series much more severely than Scoria LWC SFS45 samples, as shown by the large differences of 17% compared to 5%.

The average slip results at F_{max} indicated that the presence of the interlayer had a significant effect on the CC SFS45 and CC SPAX 45 series, demonstrated by a high difference 35– 42% higher slip. Therefore, the average slip at F_{max} is significantly

influenced by the interlayer. However, the Scoria LWC series presented marginal differences, Scoria LWC WI series had less slip at F_{max} whilst maintaining a comparable average F_{max}.

The presence of the interlayer reduced the stiffness of Scoria LWC SPAX 45 series. Scoria SPAX series I45 experienced 32% and 22% lower serviceability and ultimate slip moduli compared to with interlayer series.

Scoria LWC test series showed that the shear connector has made a difference and Scoria LWC SPAX 45 series has outperformed Scoria LWC SFS 45 by on average 4.7% in terms of strength where the highest strength was experienced by Scoria LWC SPAX WI45 with a value of 37kN. The SPAX screw has a slightly larger diameter, 8.1mm compared to 7.6mm and 5mm at the bottom section of the SFS screw. This larger diameter and different material properties of steel in SPAX screw compared to SFS VB screw accounts for its greater axial strength and yield moment.

Scoria LWC SPAX WI45 series indicated serviceability and ultimate stiffness of 20.7% and 18.1% greater than Scoria LWC SFSWI45 series, and Scoria LWC SPAX I45series exhibited serviceability and ultimate stiffness of 3.2% and 19% higher than Scoria LWC SFS I45 series. Scoria SPAX WI45 series exhibited the most effective connection with highest serviceability and ultimate stiffness. This is evident as Scoria LWC SPAX WI45 series indicated the lowest average slip at F_{max}, 8-13% lower than SFS WI45 (Table B-10), and the highest average F_{max}, 11-15% more than SFS WI45 (Table B-9). Hence, SPAX screws can be identified as a potential practical alternative for TCC construction.

The ductility of Scoria LWC varied within 2.9-4.6. The Scoria LWC SFS series exhibited 10%-35% higher ductility compared to that of SPAX series whilst inclusion of interlayer in SFS and SPAX series led to 15% and 30% lower ductility, respectively.

B.4 PUSH-OUT TEST RESULTS: HIGH STRENGTH CONCRETE

The load-slip responses of high-strength concrete, HSC series utilising SFS VB and SPAX screws inclined at 45° with and without interlayer are plotted in Figure B-35. The mathematical descriptive models and sample correlation coefficients, R^2 of HSC series are given in Equations (B-29):(B-31).

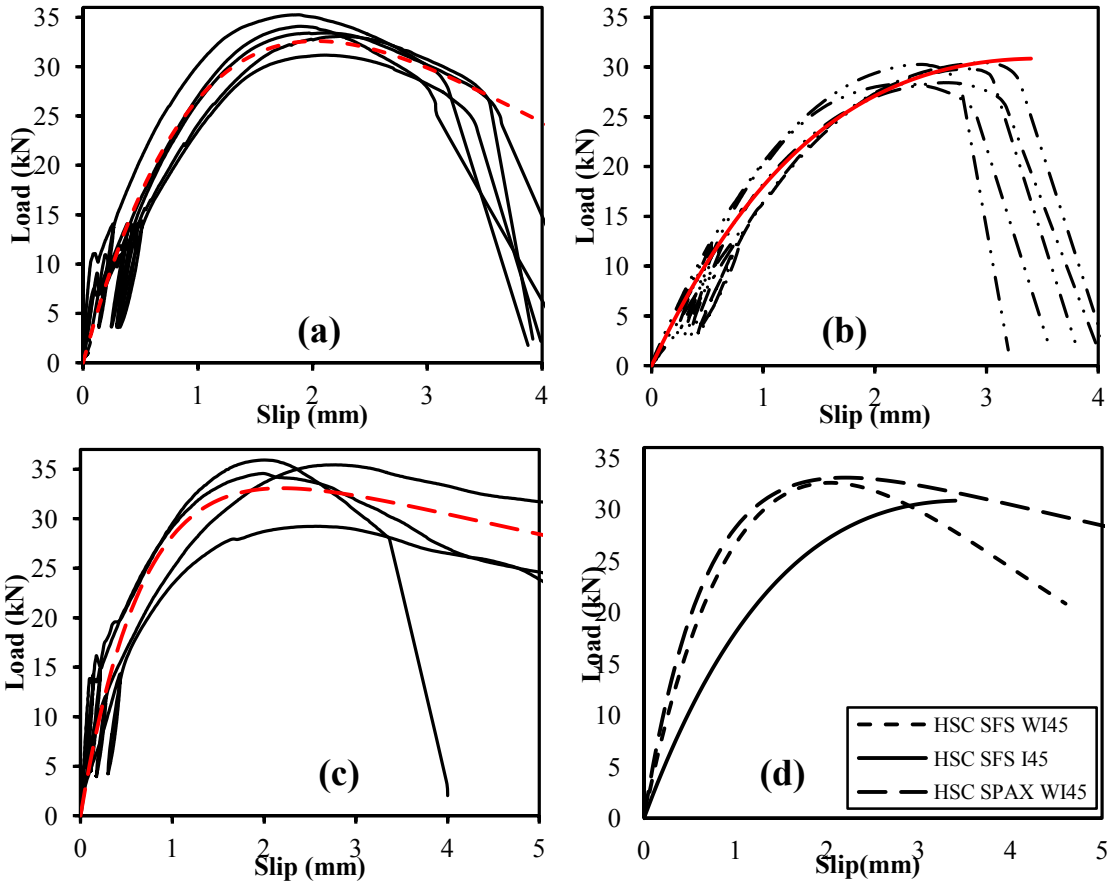

Figure B-35 Load-slip and analytical model of high strength concrete series(a) SFS WI45, (b) SFS I45, (c) SPAX WI45 and (d) comparison of analytical graphs

$$P = -634.7(e^{-0.53v} - e^{-0.46v}) \ ,(R^2 = 0.96) \quad \text{[SFSWI45]} \quad \text{(B-29)}$$

$$P = 924.5(e^{-0.27v} - e^{-0.30v}) \ ,(R^2 = 0.98) \quad \text{[SFSI45]} \quad \text{(B-30)}$$

$$P = 40.8(e^{-0.07v} - e^{-1.43v}) \ ,(R^2 = 0.93) \quad \text{[SPAX WI45]} \quad \text{(B-31)}$$

Tables B-13 and B-14 present the load capacity and ductility of the test series utilising high-strength concrete. Tables B-15 and B-16 list the load capacity and different slip moduli of the test series obtained from EN26891 and the modified methods, respectively. Moreover, the mean, standard deviation and coefficient of variation (CoV) of the test data were tabulated.

Table B-13 Load capacity of different series utilising high strength concrete

series	No.	Load capacity(kN)			
		Range	Ave	σ	CoV
SFSWI45	5	31.2-35.3	33.4	1.5	4.5
SFSI45	5	28.3-30.4	29.5	1.0	3.4
SPAX WI45	5	29.2-35.9	34.1	2.8	8.1

Table B-14 Ductility of different test series utilising high-strength concrete

series	u_y(mm)	u_u(mm)	u_f(mm)	D_u		D_f	
	Ave(CoV)	Ave(CoV)	Ave(CoV)	Range	Ave(CoV)	Range	Ave(CoV)
SFSWI45	0.8(13.5)	2.0(9.9)	3.3(6.9)	2.4-2.8	2.7(6.0)	3.8-4.8	4.4(8.6)
SFSI45	0.9(22.3)	2.7(10.1)	3.2(7.8)	2.5-3.4	2.9(13.7)	2.9-4.1	3.6(15.7)
SPAX WI45	0.6(23.7)	2.6(14.4)	5.2(27.3)	3.9-5.0	4.2(31.8)	3.9-8.9	8.5(38.0)

Table B-15 Slip moduli of series utilising high strength concrete based on EN26891

Series	Slip moduli (kN/mm)								
	$K_{s,0.4}$			$K_{s,0.6}$			$K_{s,0.8}$		
	Range	Ave	σ(CoV)	Range	Ave	σ(CoV)	Range	Ave	σ(CoV)
SFSWI45	24.4-42.6	30.7	7.0(22.8)	24.5-36.5	28.6	4.7(16.5)	22.2-30.3	25.1	3.3(13.0)
SFSI45	16.6-22.9	19.7	2.9(14.9)	16.7-22.6	19.4	2.5(13.1)	15.2-19.9	17.2	2.0(10.0)
SPAXWI45	29.5-62.5	47.1	16.6(35.2)	30.3-48.0	37.3	8.2(21.9)	23.4-33.0	27.4	4.8(17.6)

Table B-16 Slip moduli of high strength concrete series based on the modified method

Series	Slip moduli (kN/mm)								
	$K_{s,0.4}$			$K_{s,0.6}$			$K_{s,0.8}$		
	Range	Ave	σ(CoV)	Range	Ave	σ(CoV)	Range	Ave	σ(CoV)
SFSWI45	57.7-77.2	68.0	7.6(11.1)	39.2-49.4	43.9	4.4(10.0)	29.1-36.0	32.6	2.9(9.0)
SFSI45	26.5-34.1	30.3	3.5(11.5)	22.2-28.9	25.1	2.8(11.0)	18.3-23.2	20.3	1.9(9.4)
SPAX WI45	55.6-140	98.7	35.5(35.9)	33.2-55.9	46.2	9.4(20.4)	24.1-33.2	30.5	4.3(14.2)

Figures B-36:B-38 show the failure mode and opened specimens of different HSC series utilising SFS and SPAX screws.

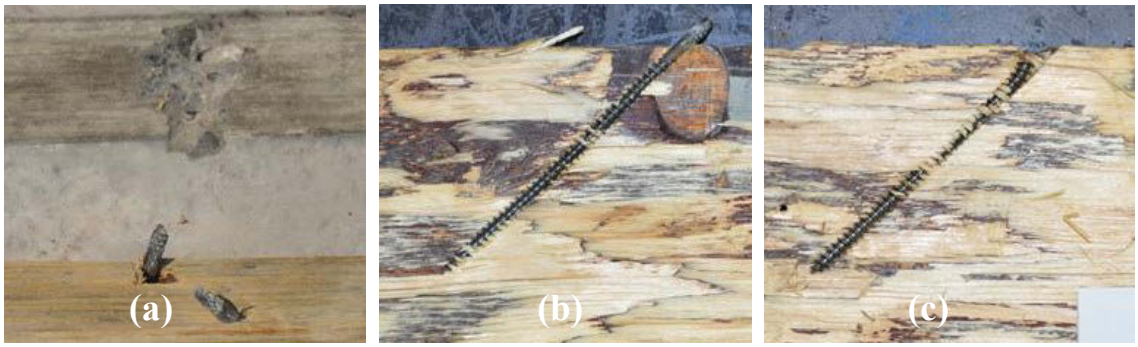

Figure B-36 (a) Failure of tensile screw and opened specimens of screws in (b) tension and (c) compression in HSC SFS WI45 series

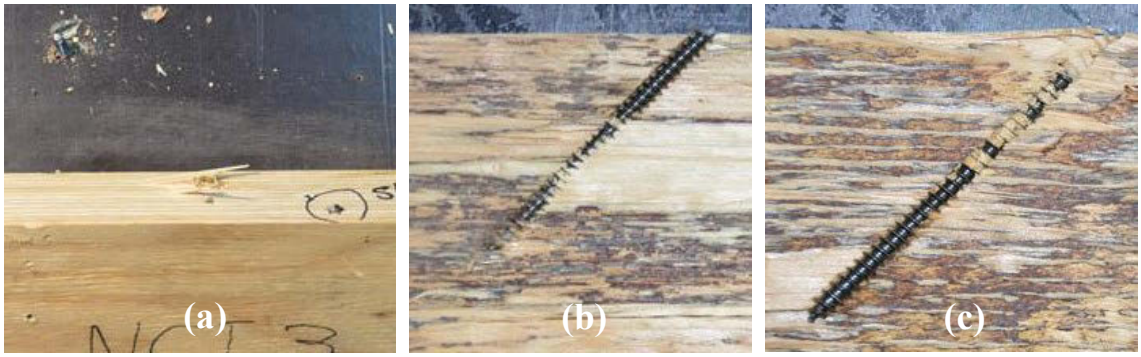

Figure B-37 (a) Failure of tensile screw and opened specimens of screws in (b) tension and (c) compression in HSC SFS I45 series

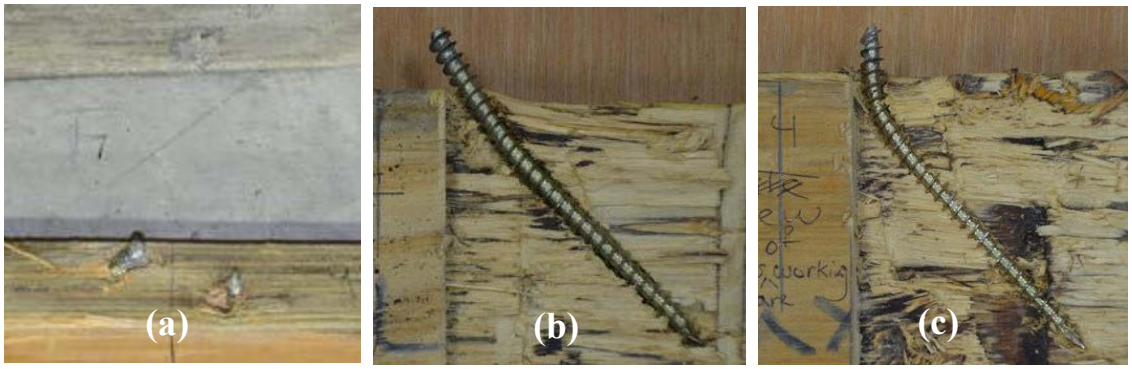

Figure B-38 (a) Intact screws and opened specimens of screws in (b) tension and (c) compression in HSC SPAX WI45 series

Opened specimen indicated that the composites failed due to a tensile failure in the screw, with plastic deformation of screw placed in compression and localised damage in surrounding concrete. Necking was evident in the tension screw in all test series, further highlighting a tensile failure after undergoing plastic deformation. HSC series exhibited

higher serviceability and ultimate slip moduli compared to CC series whereas a similar trend was not observed in strength.

The ductility of HSC series varied within 3.6-8.6. The HSC SPAX series exhibited approximately two times higher ductility compared to that of SFS series whilst inclusion of interlayer in SFS series led to 20% ductility reduction.

B.5 PUSH-OUT TEST RESULTS: SELF-CONSOLIDATING CONCRETE

The load-slip of SCC series utilising SFS screws at 45° with and without interlayer are plotted in Figure B-39. The mathematical descriptive model and the sample correlation coefficient, R^2 of SCC series are given in Equations (B-32) and (B-33).

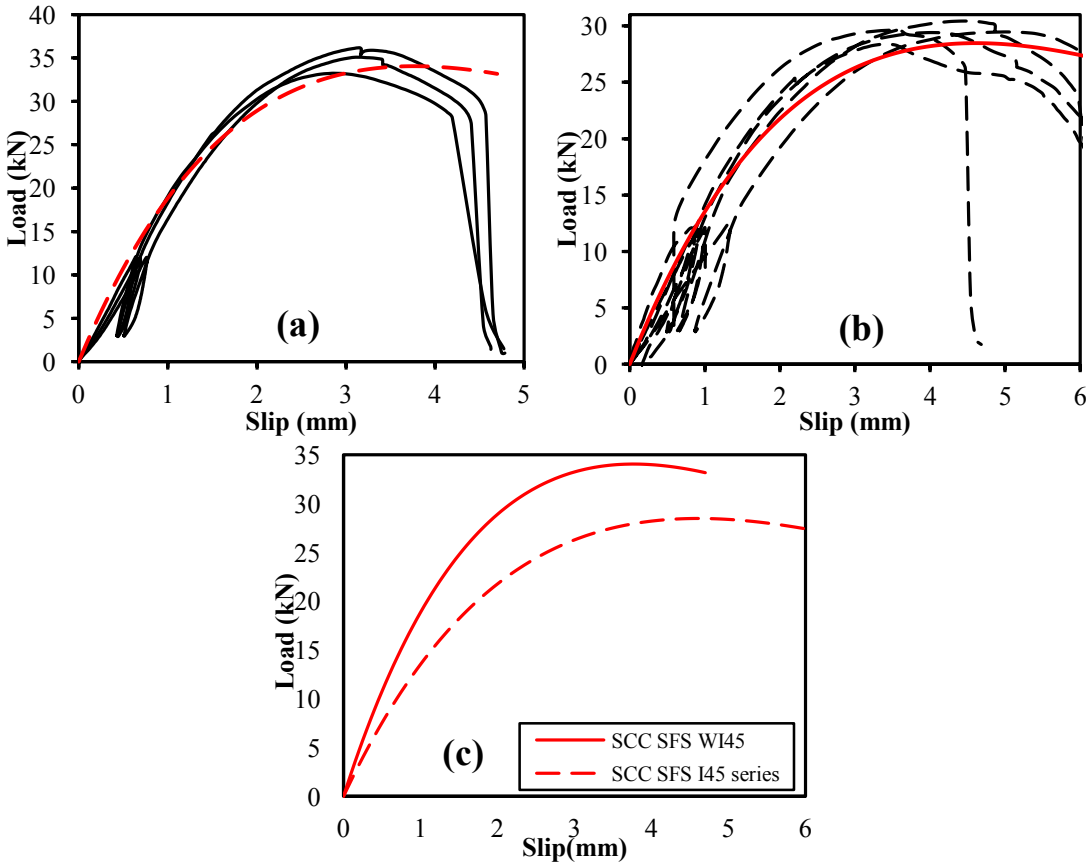

Figure B-39 Load-slip and analytical model of SCC SFS series(a) WI45, (b) I45 and (c) comparison of analytical graphs

$$P = 725.3(e^{-0.25v} - e^{-0.28v}) \ ,(R^2 = 0.95) \qquad \text{[SFSWI45]} \qquad \text{(B-32)}$$

$$P = 861.7(e^{-0.20v} - e^{-0.23v}) \ ,(R^2 = 0.98) \qquad \text{[SFSI45]} \qquad \text{(B-33)}$$

Tables B-17 and B-18 present the load capacity and ductility of the test series utilising SCC, respectively. Tables B-19 and B-20 list the load different slip moduli of the test series obtained from EN26891 and the modified methods, respectively. Moreover, the mean, the standard deviation and coefficient of variation (CoV) of the test data were tabulated.

Table B-17 Load capacity of different series utilising self-consolidating concrete

series	No.	Load capacity(kN)			
		Range	Ave	σ	CoV
SFSWI45	5	33.2-36.2	34.6	1.6	4.7
SFSI45	5	28.4-30.4	29.5	0.7	2.5

Table B-18 Ductility of different test series utilising SCC

series	u_y(mm)	u_u(mm)	u_f(mm)	D_u		D_f	
	Ave(CoV)	Ave(CoV)	Ave(CoV)	Range	Ave(CoV)	Range	Ave(CoV)
SFSWI45	1.1(14.8)	3.1(5.6)	4.4(4.1)	2.5-3.0	2.7(9.4)	3.3-4.3	3.8(12.7)
SFSI45	1.4(26.0)	4.2(19.0)	5.7(14.6)	2.6-3.3	3.0(8.7)	3.4-4.9	4.1(14.0)

Table B-19 Slip moduli of series utilising SCC based on EN26891

Series	Slip moduli (kN/mm)								
	$K_{s,0.4}$			$K_{s,0.6}$			$K_{s,0.8}$		
	Range	Ave	σ(CoV)	Range	Ave	σ(CoV)	Range	Ave	σ(CoV)
SFSWI45	21.5-24.4	22.7	1.5(6.7)	17.5-19.7	19.0	1.2(6.4)	16.4-17.6	17.1	0.6(3.5)
SFSI45	9.7-15.5	12.6	2.2(17.3)	9.8-14.8	12.5	2.0(15.7)	9.2-12.9	11.2	1.4(12.5)

Table B-20 Slip moduli of series utilising utilising SCC based on the modified method

Series	Slip moduli (kN/mm)

	$K_{s,0.4}$			$K_{s,0.6}$			$K_{s,0.8}$		
	Range	Ave	σ(CoV)	Range	Ave	σ(CoV)	Range	Ave	σ(CoV)
SFSWI45	43.4-48.1	45.9	2.3(5.1)	25.0-28.9	26.7	2(7.5)	20.3-21.9	21.1	0.8(3.9)
SFSI45	21.8-27.5	23.7	2.3(9.8)	16.2-20.4	18.0	1.8(9.8)	12.9-15.8	14.1	1.1(8.1)

Application of an interlayer in SCC series increased the slip at F_{max} about 51%. Comparing CC and SCC series, application of SCC decreases the strength about 4% and 6% in the specimens without and with interlayer, respectively. Application of SCC instead of CC in WI series reduced different slip moduli including $K_{s,0.4}$, $K_{u,0.6}$ and $K_{u,0.8}$ about 20%, 40% and 30%, respectively.

As demonstrated in Figure B-39, the behaviour of the SCC specimens (WI and I series) was fairly consistent. The load increased quite steadily, slowing slightly before peaking. Most of the specimens reaching a maximum load of around 30-35kN and the load gradually reduced to around 80-90% F_{max} before a sudden failure occurred. This means that the connector failed due to a tensile failure of the screw in all cases, with shear being a contributor. Necking was evident in the tension screw in all cases, further highlighting a tensile failure after undergoing plastic deformation. A total slip of 2.8 - 4.2mm was measured across the specimens. Furthermore, the screws failed at their narrowest point, located 10-20mm above the thread and embedded in the concrete. Figures B-40 and B-41 show the failure and opened samples of different SCC series.

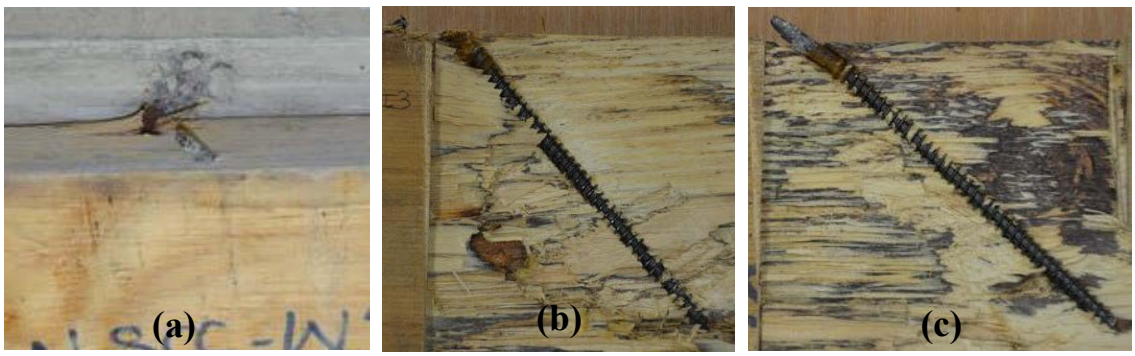

Figure B-40 (a) Failure of tensile screw and opened specimens of screws in (b) tension and (c) compression in SCC SFS WI45 series

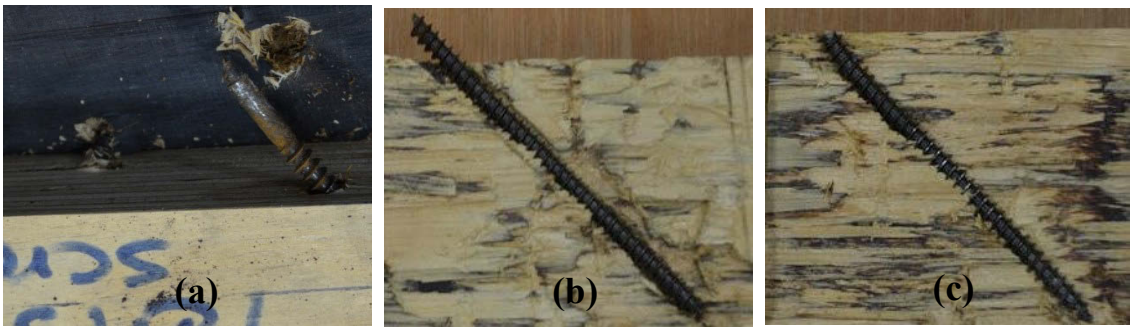

Figure B-41 (a) Failure of tensile screw and opened specimens of screws in (b) tension and (c) compression in SCC SFS I45 series

A reductions ranging from 20%-27% were observed in slip moduli of SCC I series rather than CC I series. Inclusion of an interlayer led to a significant reduction in slip modulus of CC and SCC test series (ranging from 35-47%). Moreover, the inclusion of an interlayer reduced the load capacity of CC and SCC test series about 7% and 15%, respectively.

B.6 PUSH-OUT TEST

Once the TCC was loaded in the steel frame, it was then placed directly underneath the hydraulic jack of the testing machine. It was crucial that the alignment was correct, so that the applied shear force was acting directly on the shear connection.

A timber screw was drilled into the LVL joist-end to limit splitting along the LVL joist-end due to excessive load. The loading plate and top of timber joist were contacted tightly before commencing the test.

Two light-weight metal brackets were mounted on the concrete or interlayer (where present) using double sided adhesive tape. The contact tip of the LVDT rested against the surface of the metal bracket and as the timber joist displaced relative to the concrete, the contact tip moved and thus the slip was measured by the LVDT.

For the first TCC specimen of each series, the maximum load was approximated and this value was used to carry out the loading procedure. After the first TCC specimen test, the recorded maximum load value was used to determine the loading procedure for subsequent specimens within that series. It also must be noted, that the testing machine had to be manually controlled during the application of the load in some of the test series (all test series except EPS LWC 2000 series) and as a result, a slight deviation from the idealised loading procedure was present in those series.

Appendix C (Chapter 6)

C.1 SERVICEABILITY TESTS OF TIMBER-ONLY MODULES

The load-deflection at third and mid-spans responses of timber-only modules, linear regressions and R^2 values are plotted in Figures C-1:C-5.

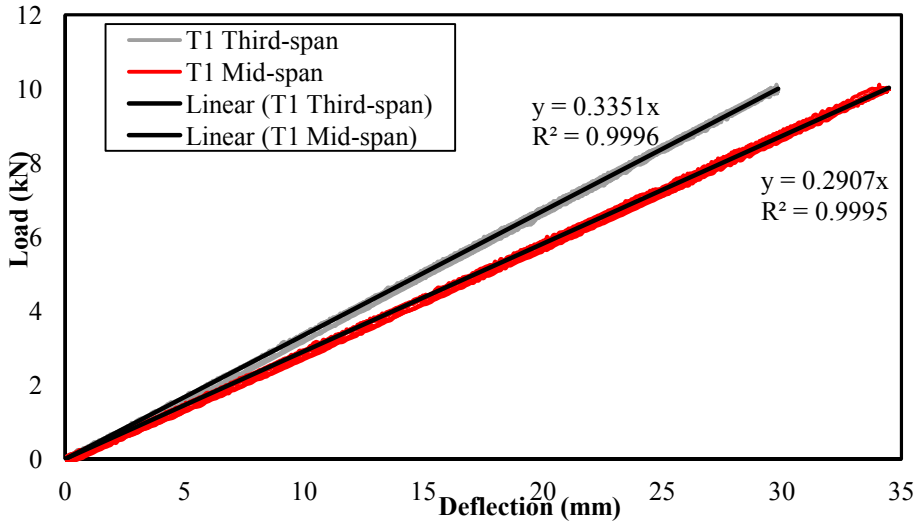

Figure C-1 Serviceability load-deflection response for timber module1 used in CC1

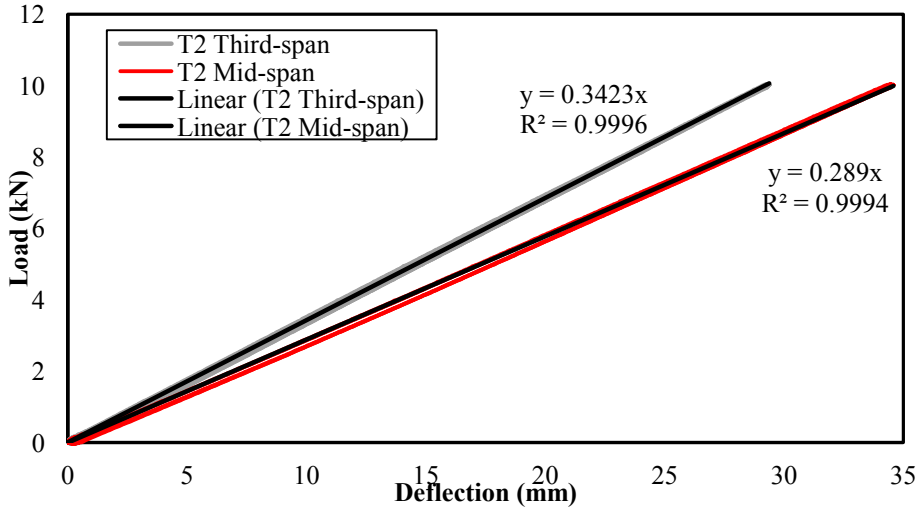

Figure C-2 Serviceability load-deflection response of timber module2 used in CC2

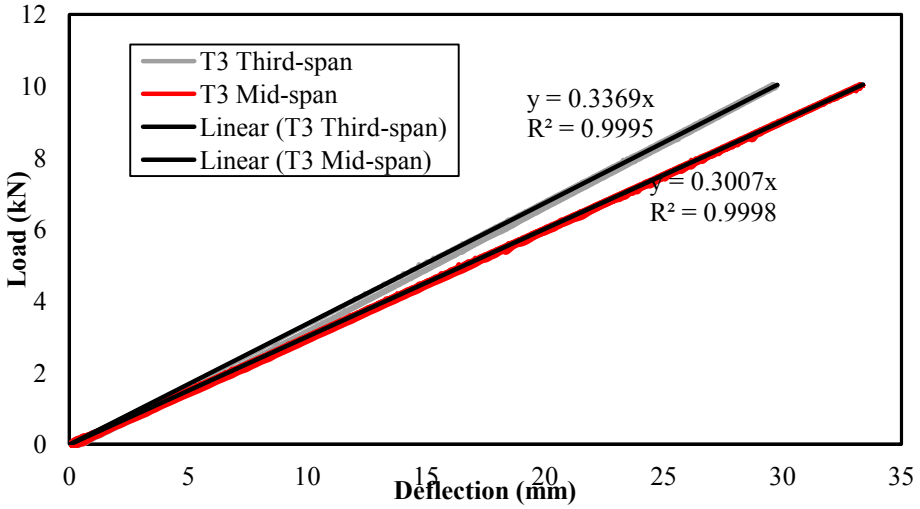

Figure C-3 Serviceability load-deflection response of timber module3 used in CC3

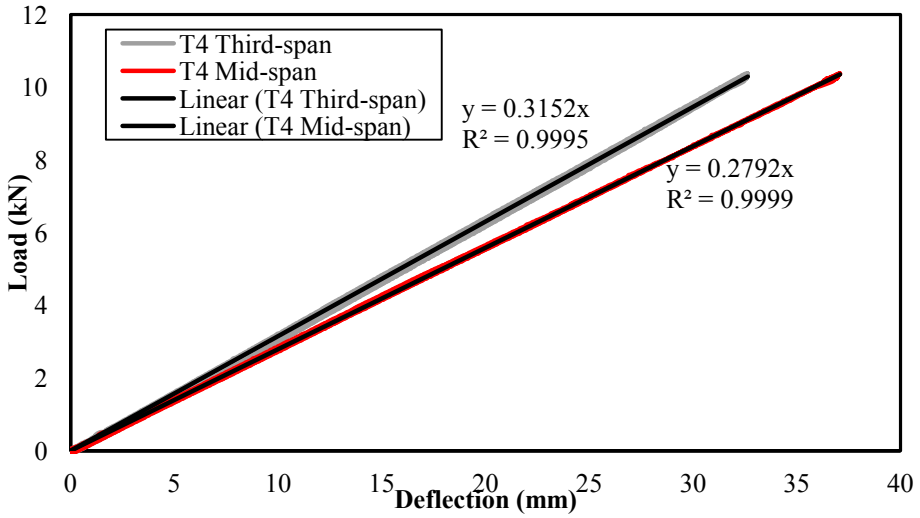

Figure C-4 Serviceability load-deflection response of timber module4 used in LWC1

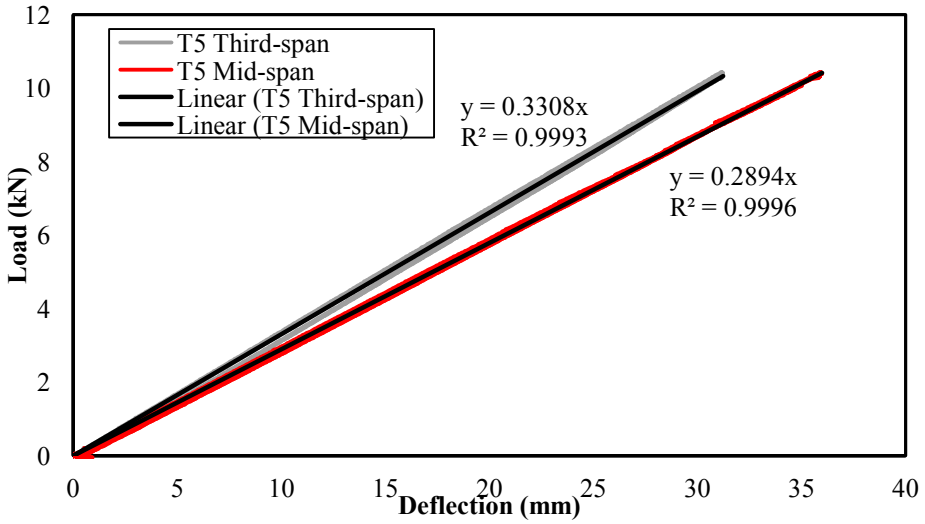

Figure C-5 Serviceability load-deflection response of timber module5 in LWC2

R^2 indicates how strongly the beams behave linearly. The results are all very close to 1 highlighting that the beams have performed linearly under the service loads.

C.2 SERVICEABILITY TESTS OF TCC MODULES

The load-deflection responses at third and mid-spans, linear regression and R^2 values for TCC modules subjected to serviceability load are plotted in Figures C-6:C-10. The curve fitting should cover a minimum range of 20 % of data (for example, between 10% and 30 % or between 20 % and 40 % of SR). The stiffness results for module CC1 are noticeably lower than that of modules CC2 and CC3 due to this being the first beam that was exposed to the testing procedure.

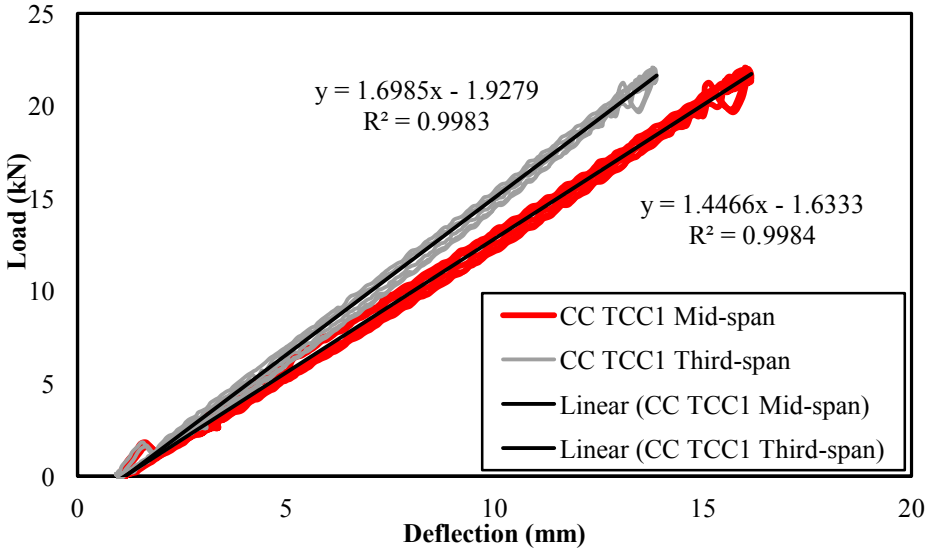

Figure C-6 Serviceability load-deflection response of TCC CC1 module

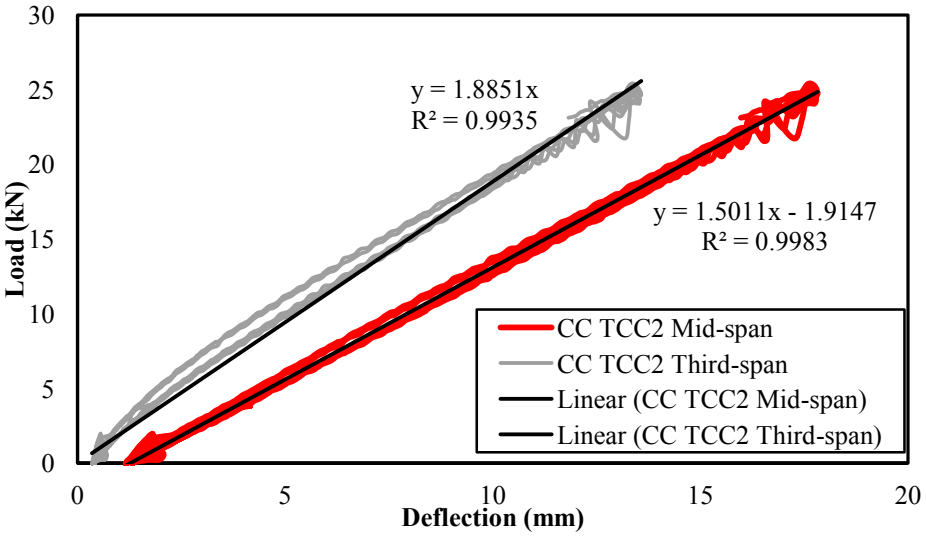

Figure C-7 Serviceability load-deflection response of TCC CC2 module

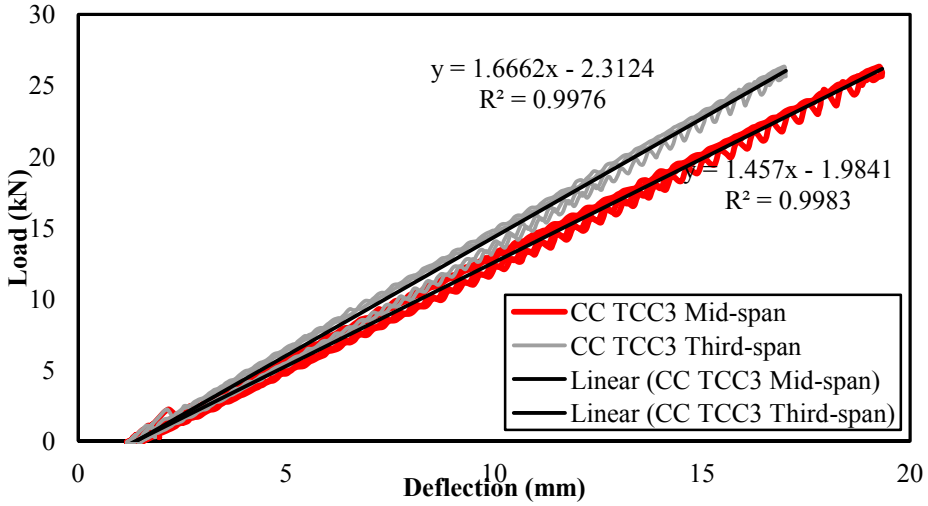

Figure C-8 Serviceability load-deflection response of TCC CC3 module

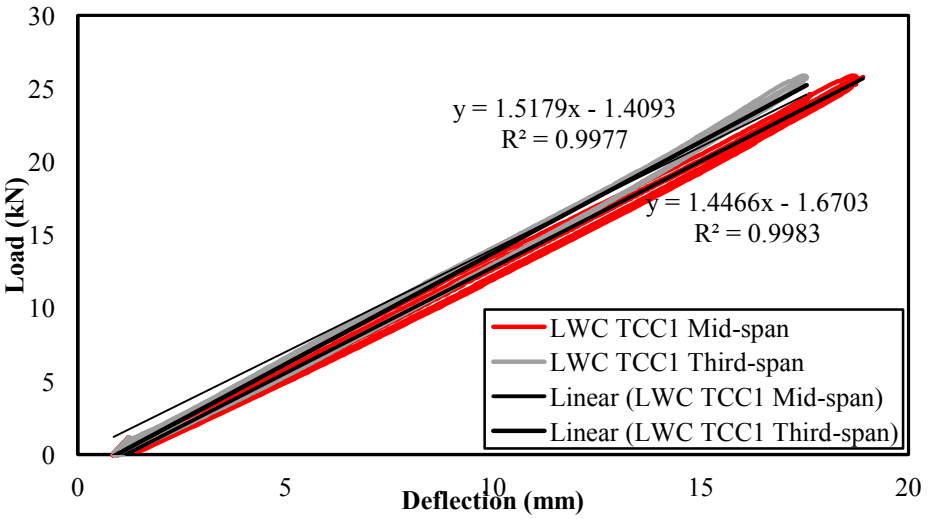

Figure C-9 Serviceability load-deflection response of TCC LWC1 module

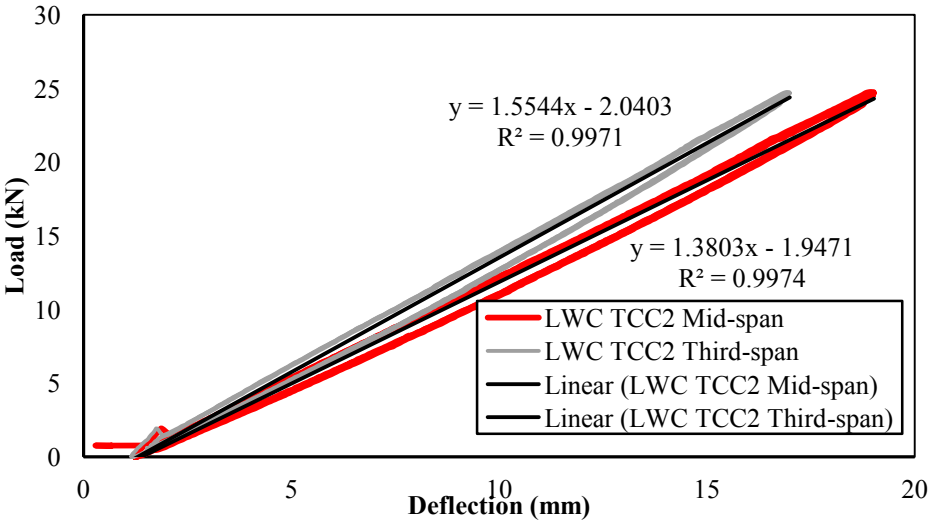

Figure C-10 Serviceability load-deflection response of TCC LWC2 module

C.3 ULS TEST OF TCC MODULES

C.3.1 Slip at shear connections and beam-ends of TCC modules

Throughout the ultimate load tests, it was noted that a relative displacement was evident between the concrete slab and LVL flanges. The slip was evident at both ends. Slip readings reported in this chapter follow the sign convention illustrated in Figure C-11.

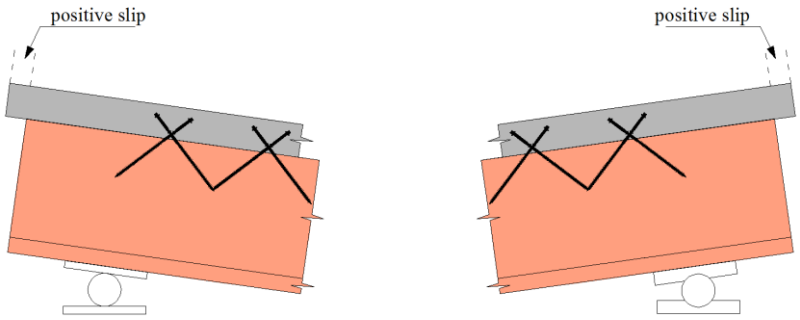

Figure C-11 Sign convention for slip measurement

The slips between the concrete and the LVL joists at the supports and the first three pairs of screws placed at symmetric locations of the two beam-ends were monitored as plotted in Figures C-12 and C-13. Slip at interface of LVL bottom flange and LVL webs at supports were also measured in timber modules as shown in Figures C-14 and C-15. It is noted that relative slips between the slab and timber joist due to self-weight, creep and shrinkage was neglected. The slip due to shrinkage is in the opposite direction to the one the composite module experiences under self-weight or external bending load. Hence, for a beam subjected to shrinkage, shear connections had to recover the slip due to shrinkage before contributing to the load carrying (Al-deen, Ranzi & Vrcelj 2011).

The slip at different load levels of SLS, ULS and $0.8F_{max}$ was shown. All load–slip responses exhibited a high initial stiffness - which softened at higher load levels. Due to the contribution of different parameters such as non-linear load-slip response of shear connection in non-linear behaviour of TCC modules, this curve softened at higher loads. Comparing CC and LWC series, LWC series experienced higher slip at interface of timber webs and flange. The maximum slip at interface of concrete and timber observed at peak load were 1.8mm for CC1, 2.3mm for CC2 and 2.5mm for CC3 whilst LWC1 and LWC2 indicated 1.5mm and 4mm slips at the interface of composite materials, respectively. The slip for CC exhibited symmetric initial deformations at the two beam ends whereas LWC series showed slightly higher slip on one side of the beam.

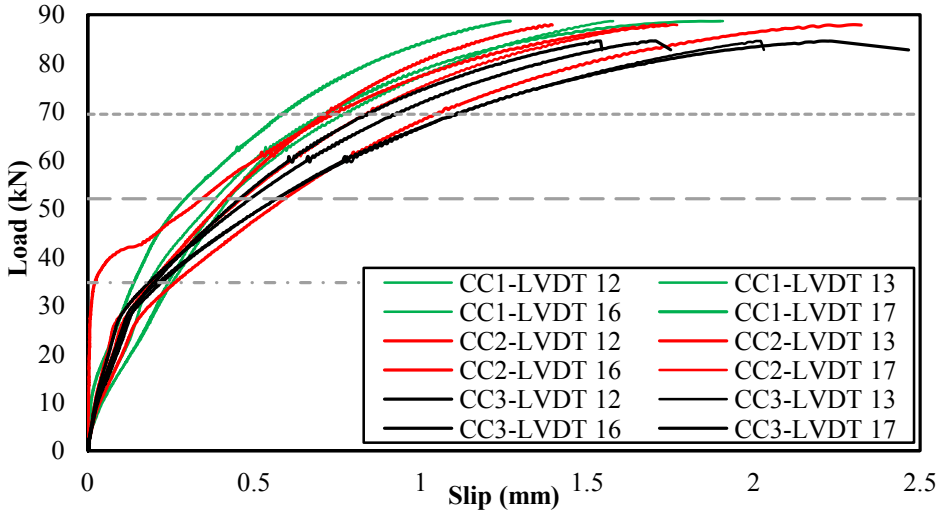

Figure C-12 Slip at interface of timber and concrete and load in each jack for CC series

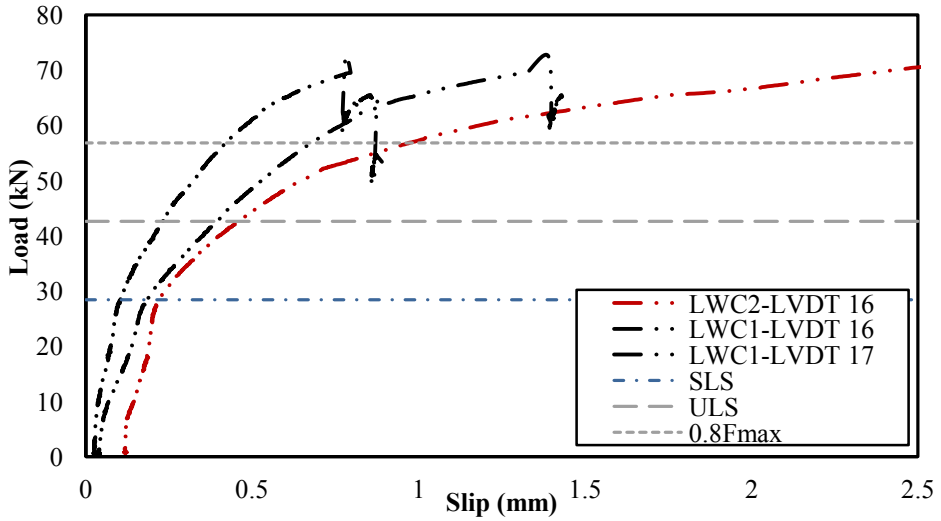

Figure C-13 Slip of timber and concrete and load in each jack of LWC series

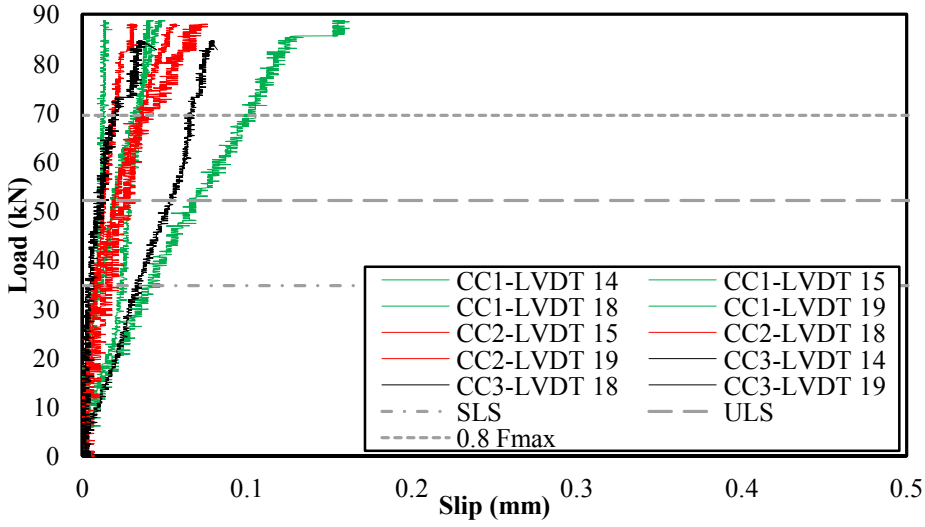

Figure C-14 Slip of LVL bottom flange and LVL web and load for CC series

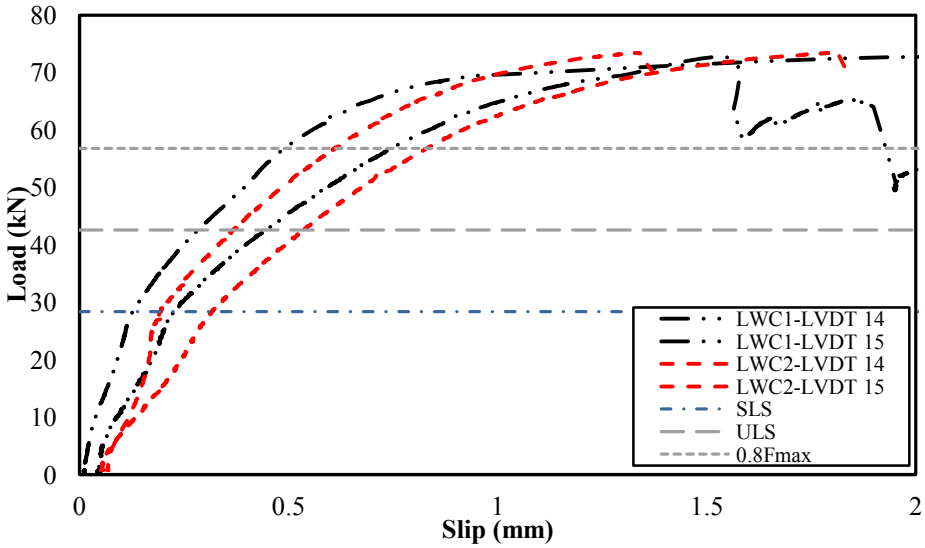

Figure C-15 Slip of LVL bottom flange and LVL web and load for LWC series

Figures C-16:C-18 depict the slip measurements for the first three pairs of crossed shear connections placed at symmetric locations of the two beam ends in LWC TCC modules.

All three pairs of crossed shear connections exhibited similar load-slip response as a high stiffness starting part, softening at higher load levels in both LWC1 and LWC2 but the first and second pairs of connections exhibited slightly higher initial stiffness. The slip values observed near the peak loads were similar for the three samples.

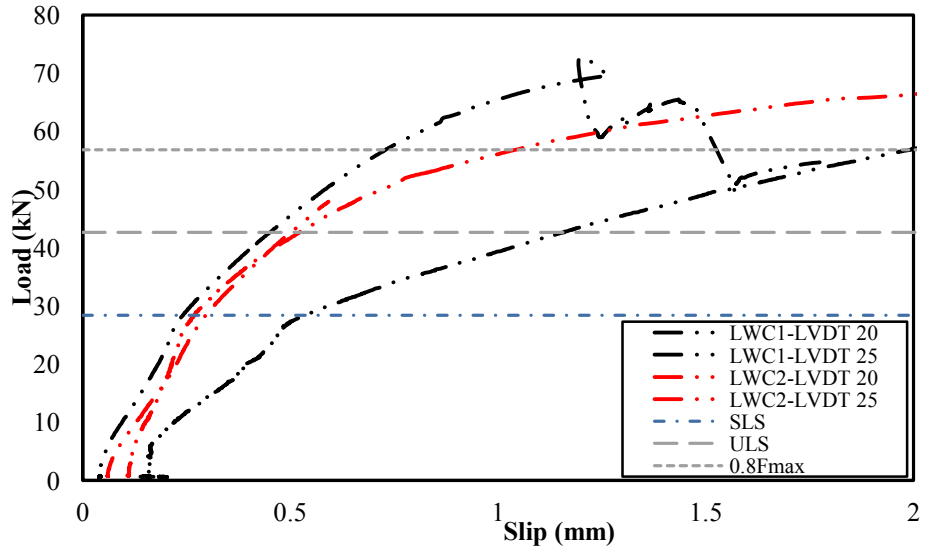

Figure C-16 Slip at first pair of connection from beam-ends in LWC series

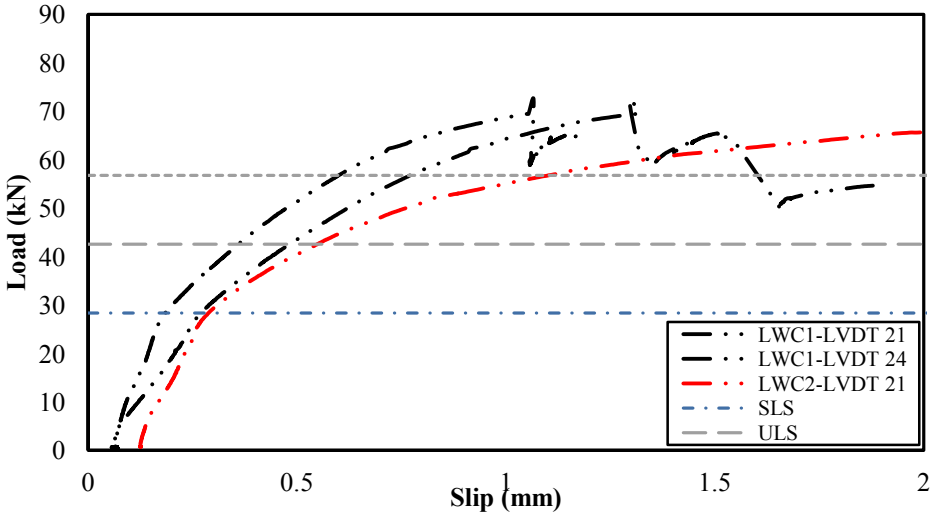

Figure C-17 Slip at second pair of connection from beam-ends in LWC series

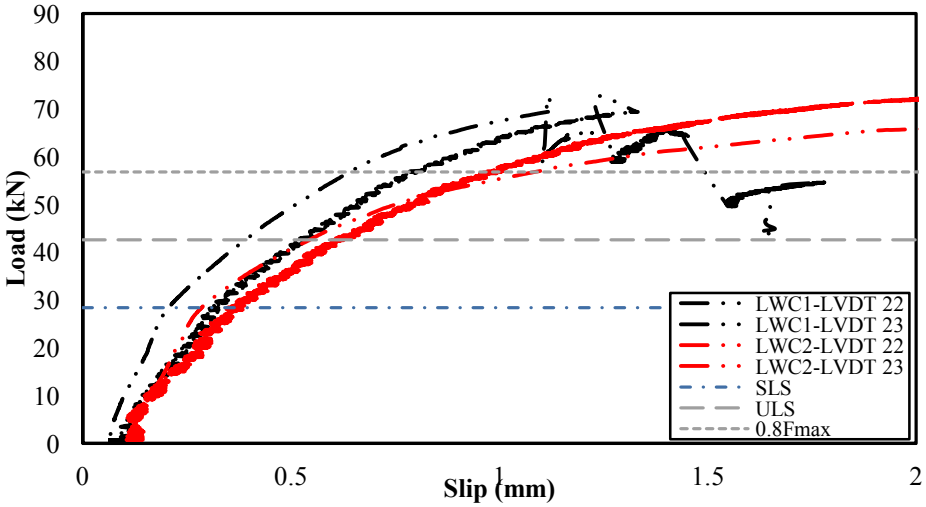

Figure C-18 Slip at third pair of connections from beam-ends in LWC series

All three pairs of crossed shear connections exhibited similar load-slip response as a high stiffness starting part, softening at higher load levels in both LWC1 and LWC2 but first and second pairs of connections exhibited slightly higher initial stiffness. The slip values observed near the peak loads were similar for the three samples. Slip measurements of LWC1 along the beam length for first three pairs of screw corresponding to different load levels are shown in Figure C-19. This provides a better overview of the development of the relative movement between slab and joist. It was observed that the magnitude of the slip between concrete and LVL was proportional to the distance from the beam-end and the largest slip among the measured ones occurred at the inner connectors nearest to the point load. Some of the LVDTs at the left part of

the beam measured the slip greater than the expected trend observed in the right part of the modules.

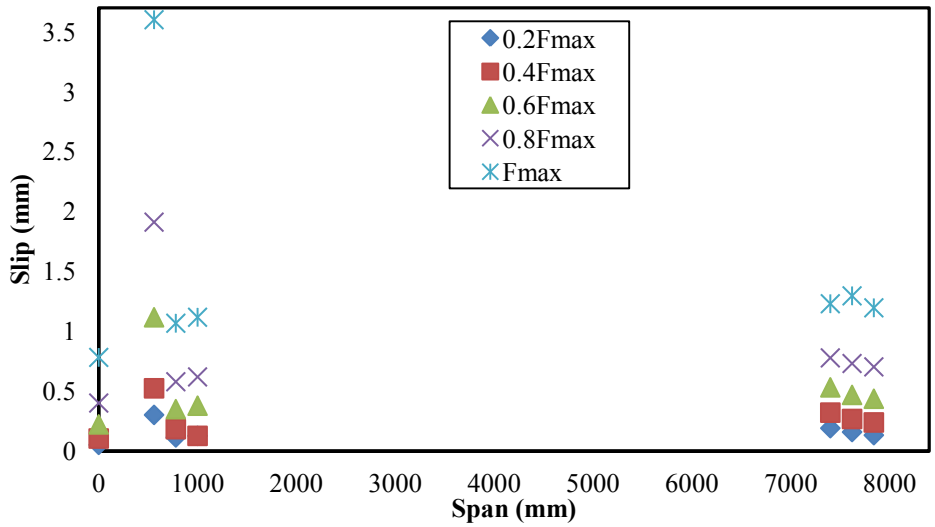

Figure C-19 Slip measurement along the beam length at different load level for LWC1

C.3.2 **Strain gauge data analysis of TCC modules**

Strains of timber-only and TCC modules at mid-span cross-sections were recorded by strain gauges and data taker during the serviceability and ultimate experiments as shown in Figures C-20:C-26.

The strain gauges were located on the top and underside of the concrete slab and on the top, middle and underside of the LVL webs and top and underside of LVL bottom flange as illustrated in Chapter 5.

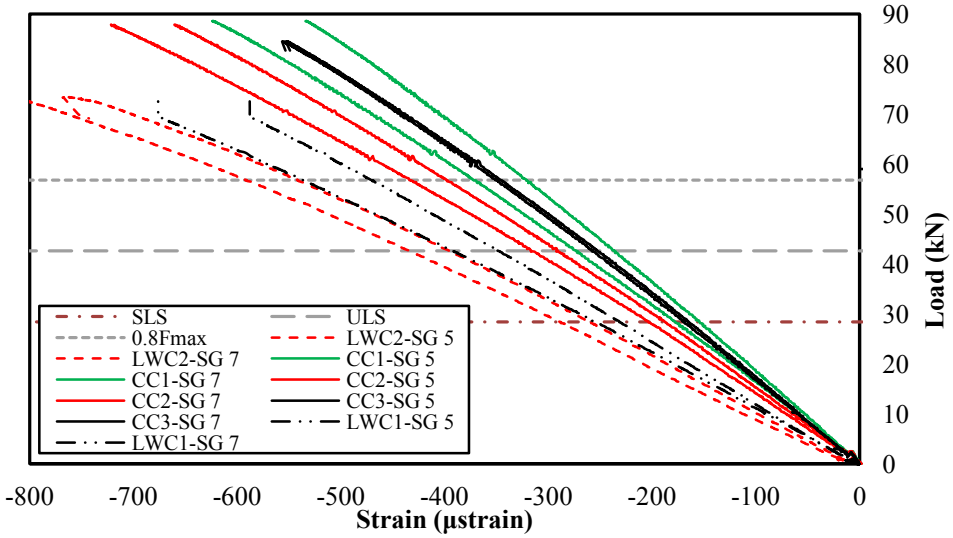

Figure C-20 Strain reading measured at the top of concrete slabs

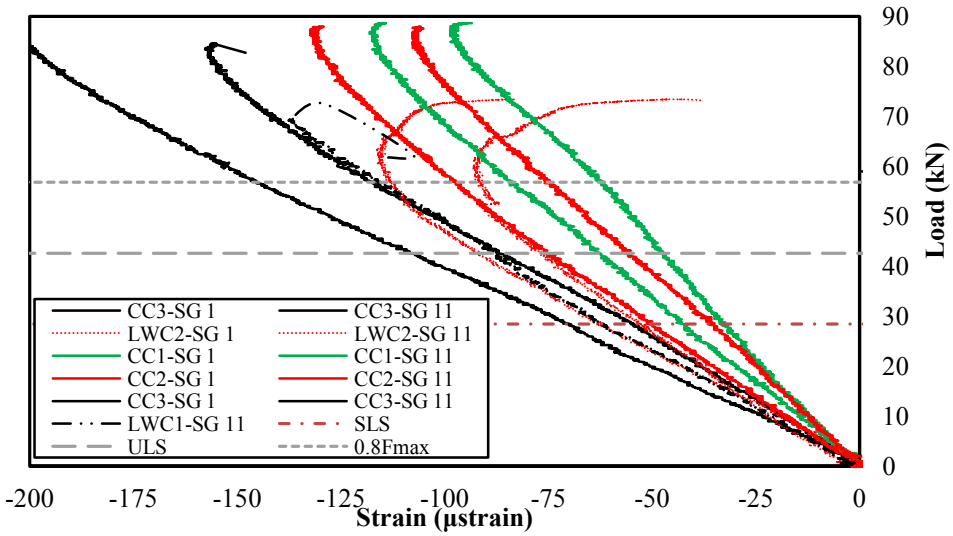

Figure C-21 Strain reading measured at the underside of concrete slabs

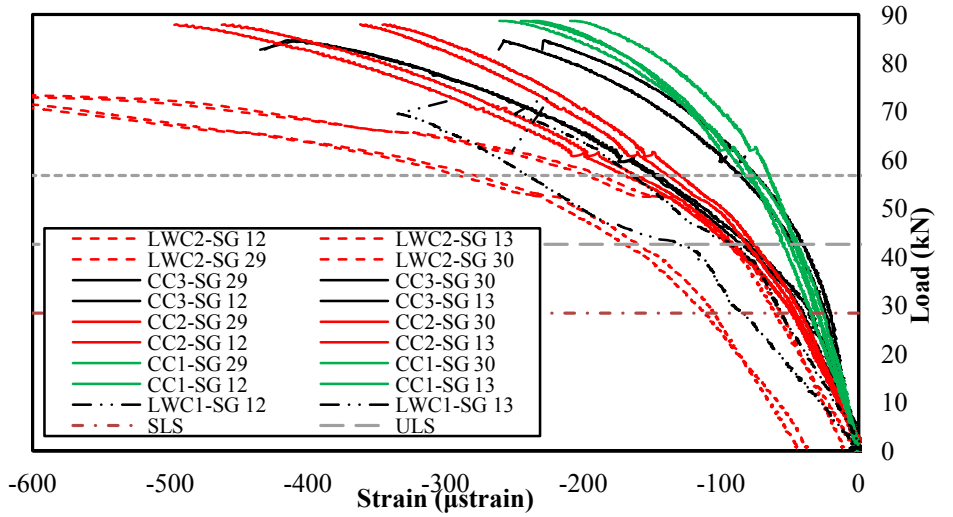

Figure C-22 Strain reading measured at the top of LVL webs

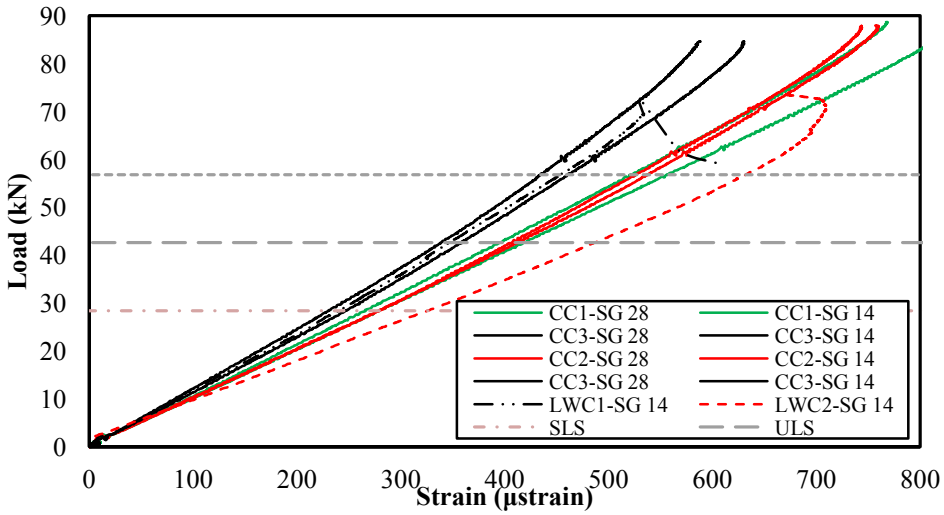

Figure C-23 Strain reading measured at the mid-height of LVL webs

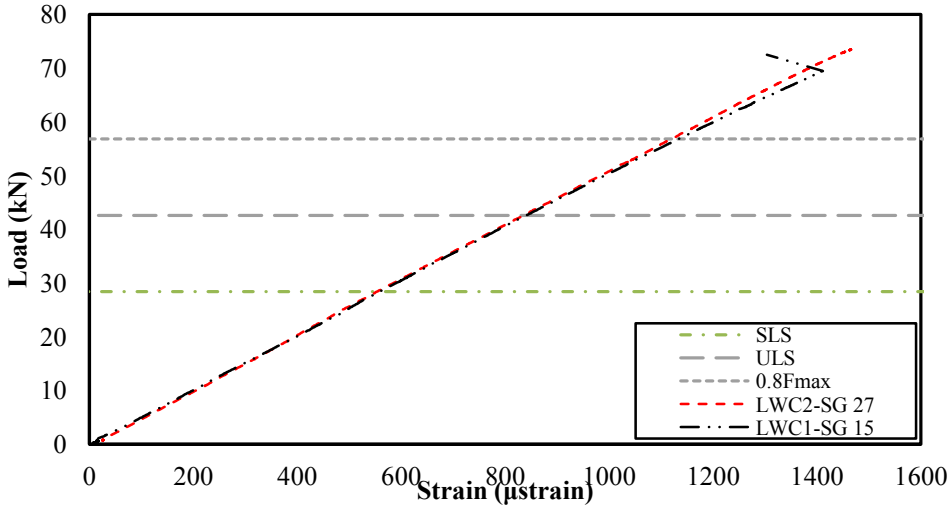

Figure C-24 Strain reading measured at the underside of LVL webs

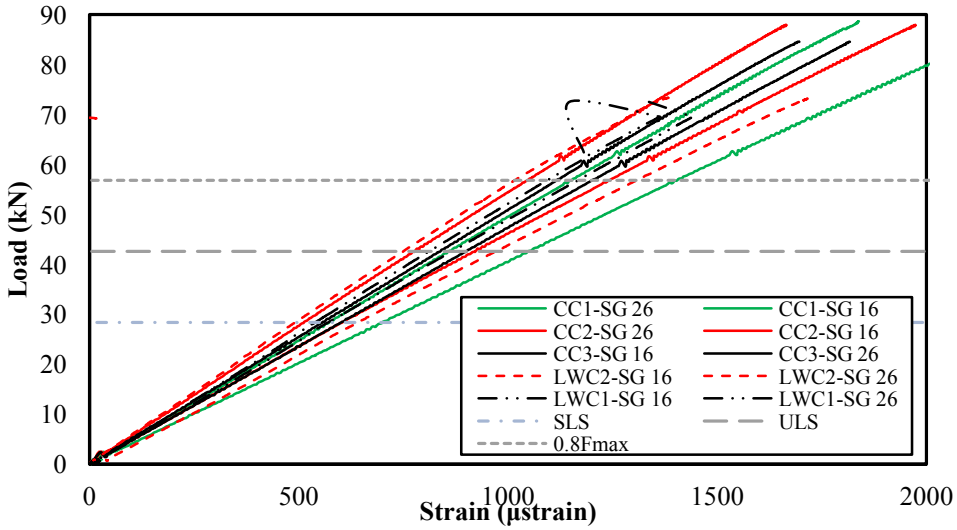

Figure C-25 Strain reading measured at the top of LVL bottom flanges

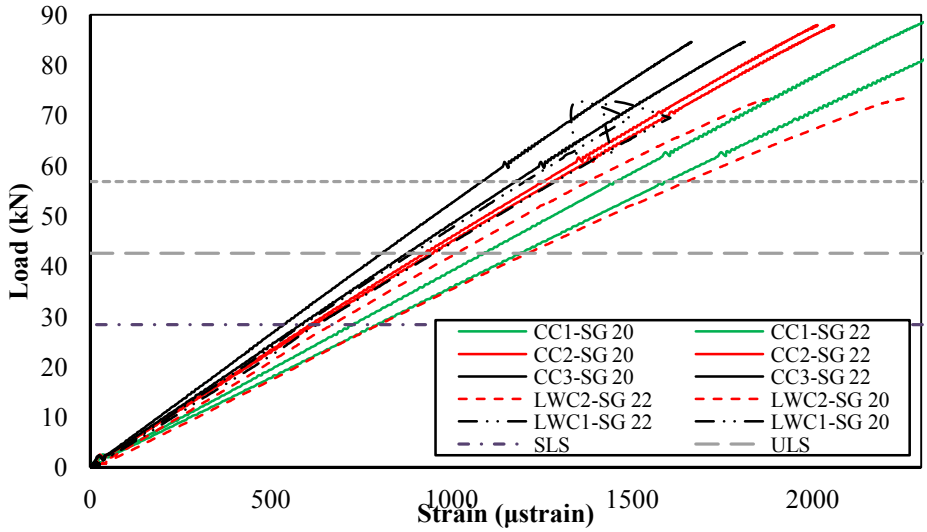

Figure C-26 Strain reading measured at the underside of LVL bottom flanges

Appendix D (Chapter 8)

D.1 EXPERIMENTAL TESTS USED IN ANALYTICAL MODELS

The experimental tests used in the analytical model of stiffness and strength (Chapter 6) consisted of embedment test carried out by Franke and Quenneville (2011), uni-axial tensile and yield moment tests to characterise the input parameter of the models. This Appendix reviews the methodology of the experimental tests and their results.

D.1.1 Uni-axial tensile test

The characteristic tensile capacity of screws, f_{uk} (head pull-off or shank tensile capacity) is calculated by testing in compliance with EN1383 (1999) using a steel plate to replace the head side timber member as shown in Figure D-1. The steel plate must have a sufficient thickness to induce either a pull-off failure of the head, or a tensile failure of the shank. Different screws used as connectors in TCCs were tested in a uni-axial tensile test to determine their ultimate tensile strengths using a 500kN universal testing machine. The setup of the uni-axial tensile test procedure involved feeding each screw shank through a perforated plate. The diameter of the hole in the plate was selected relative in size to the head of the screw. Thus the head of the screws were restrained using a thick steel plate and the threaded shank of the screw was fixed into a threaded clamp. A constant loading rate of 0.1kN/Sec was applied throughout the testing.

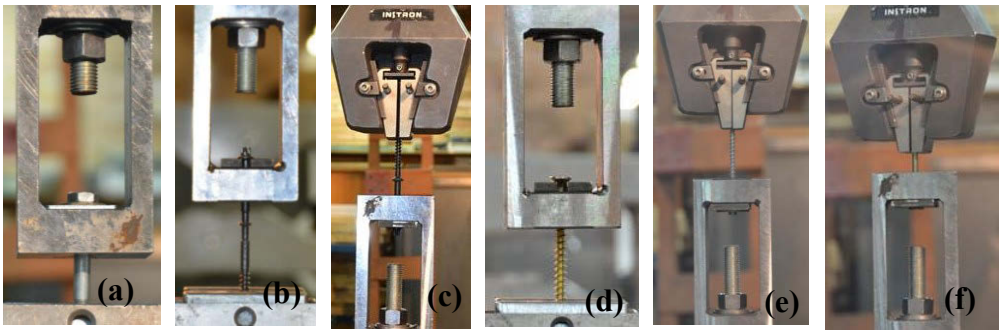

Figure D-1 Uni-axial tensile test set-up of (a) medium coach, (b) long SFS VB, (c) short SFS VB, (d) SPAX, (e) small SPAX screws and (f) type17 wood screws used in TCCs

Figure D-2 Tensile failure of (a)medium coach, (b)long SFS, (c)short SFS, (d) SPAX, (e)small SPAX screws and(f)pull-off failure of type17 wood screw used in TCCs

Figure D-2 illustrates the failure patterns of the screws used in the experiment. The failure modes included tensile failure of the threaded part (Figure D-2a, b, c, d and e) or a pull-off failure of the head (Figure D-2f).

It is concluded that the tensile failure of threaded part governs the failure of all screw types with the exception of wood screws which experienced a pull-off failure of the head at the interface between the head of screw and the smooth shank. Table D-1 lists the tensile strength and CoV and standard deviation of screw test series.

Table D-1 Tensile strength of the screws

Seriers	No.	F_u(N)	Area (mm^2)	f_u^*(N/mm^2)	σ	CoV(%)
coach	3	19324.3	41.9	461.2	26.9	5.8
Long SFS	3	20268.6	16.6	1221	19.8	1.6
short SFS	3	16334.4	16.6	984	8.6	0.9
Long SPAX	3	22890.8	19.6	1167.9	6.3	0.4
small SPAX	3	13401.4	12.6	1063.6	6.4	0.6
Wood 17	3	17064.7	18.1	942.8	43.6	4.6

* core diameter of screw was used for calculation of f_u

Lower ultimate tensile strength of coach screw compared to the other screws with visible necking at the interface between the smooth shank and thread (Figure D-2a) exhibited a ductile failure whilst other screws exhibited a relatively brittle failure with no visible necking and this is consistent with high carbon steel composition of the screws. The low CoV of the series shows the consistent quality of the screws.

D.1.2 Embedding test

The embedment or dowel-bearing strength and foundation modulus of timber for dowel-type fasteners can be determined using different standards such as ASTM5764 (1997) and EN383 (2007).

To minimise the bending of fastener in the embedding tests, specific specimen geometries and loading conditions are proposed in the standards. Herein, the experimental data of embedment test carried out by Franke and Quenneville (2011) on the same LVL product (hySPAN Radiata pine LVL) as used in this investigation was adopted to calculate the foundation moduli of 6 and 8mm diameter screw embedded parallel and transverse to the grain of LVL. The experimental embedment test in Franke and Quenneville (2011) was accomplished in compliance with ASTM5764 (1997) utilising a half-hole testing as indicated in Figure D-3.

ASTM5764 (1997) specifies the dimension of specimens to be 38mm or 2*d* as minimum thickness and 50mm or 4*d* as maximum width where *d* is fastener diameter. Moreover, a constant loading rate of 1.0mm/min is proposed which leads to achieving the maximum force within 1 to 10min. The yield loads were measured using the 5%-offset method. The embedment strength of specimens was determined in compliance with ASTM5764 (1997) by dividing the yield load by the thickness of timber specimens and fastener diameter.

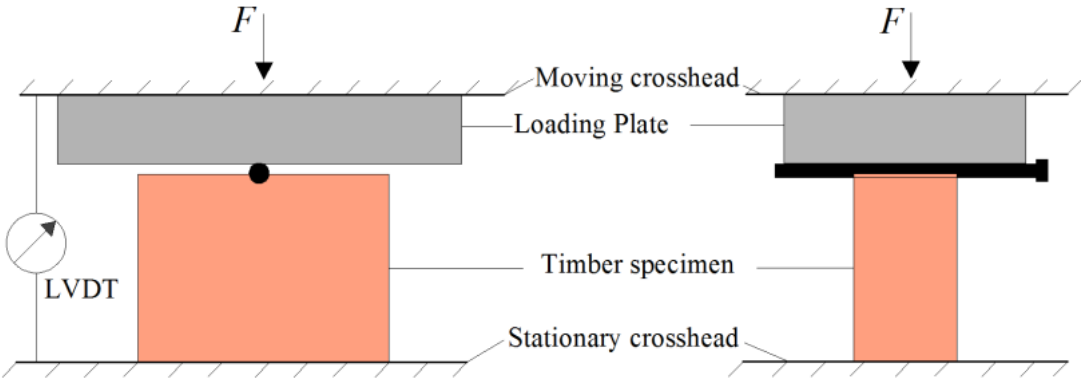

Figure D-3 Test configuration half-hole test in accordance with ASTM5764 (1997)

The applied load versus the relative deformation of specimen measured by linear variable differential transducers (LVDTs) was plotted. The initial slope of the load-deformation curve indicates the foundation modulus of fastener in timber k_f using:

$$k_f = \frac{0.4F_{max}}{\frac{4}{3}(v_{04} - v_{01})} \quad \text{(D-1)}$$

where, v_{01} and v_{04} are deformation measurements at 0.1 and 0.4 of F_{max}. The embedment stress-deformation of 6 and 8mm diameter screw embedded parallel to the grain of LVL are shown in Figure D-4.

The foundation moduli of screw parallel and transverse to the grain, k_p and k_t were calculated utilising the stress-displacement graphs reported in Franke and Quenneville (2011).

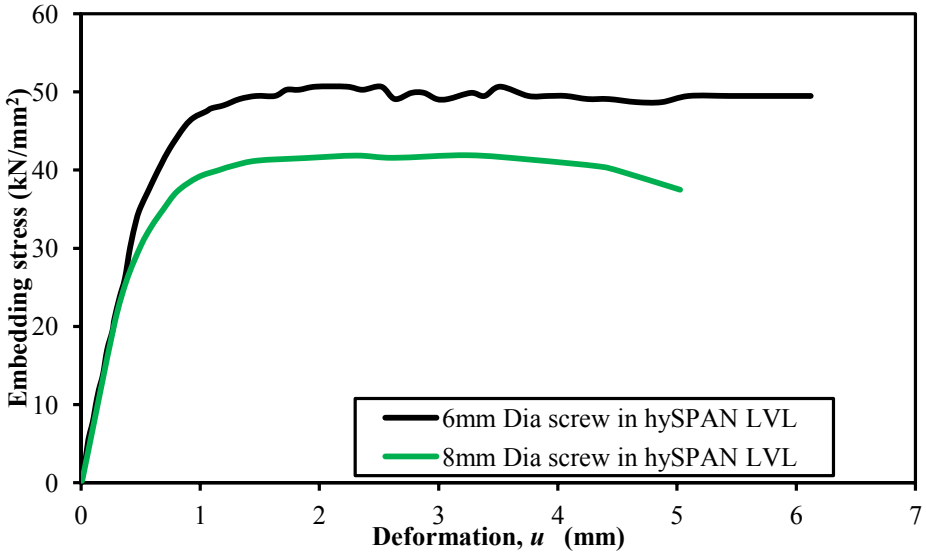

Figure D-4 Embedding stress-deformation of 6 and 8mm dowels (Franke & Quenneville 2011)

D.1.3 Characteristic yield moment

The characteristic yield moment of the screw is essential to estimate the failure modes associated with flexural deformation of screw and formation of plastic hinges in the load capacity models proposed by Johansen's theory and Eurocode 5 EN (2004).

The plastic capacity of fastener or characteristic yield moment ($M_{y,Rk}$) can be determined by either four-point bending experimental tests in compliance with EN409 (2009), or alternatively, by the means of analytical equations using characteristic

ultimate strength of the fastener as given by the codes such as EN (2004) and DIN1052 (2004) as:

$$M_{y,Rk}=0.3 f_{uk} d^{2.6} \qquad \text{(D-2)}$$

where, d is 0.75 times the diameter of screw and f_{uk} is characteristic ultimate strength of fastener. This study compares characteristic yield moment of 100mm wood screws determined by both methods. Three wood screws were tested in tension to determine their ultimate tensile strength.

The four point bending test was carried out in compliance with EN409 (2009) to measure characteristic yield moment of normal wood screws as shown in Figure D-5. EN409 (2009) limits the bend angle of screw, α to a maximum value of $45/d^{0.7}$ degrees where d is the fastener diameter in mm. The dimensions l_1 and l_3 (Figure D-5) need to be at least 2 times of the fastener diameter, d. The free length of the dowel type fastener, l_2 varies between d and $3d$. The characteristic value for the yield moment, $M_{y,Rk}$ is determined by:

$$\mathrm{M}_{y,Rk}=\max\begin{cases} F_1 l_1 \\ F_3 l_3 \end{cases} \qquad \text{(D-3)}$$

where, dimensions l_1, l_2, l_3 and forces F_1 and F_2 are shown in Figure D-5. The ultimate loads and tensile strength of wood screw were used in the characteristic yield moment calculations. The experimental results of the characteristic yield moment in accordance with EN409 (2009) are listed in Table D-2. The analytical characteristic yield moment proposed by Eurocode 5 model (Equation (D-2)) are also compared to the experimental results as tabulated in Table D-2.

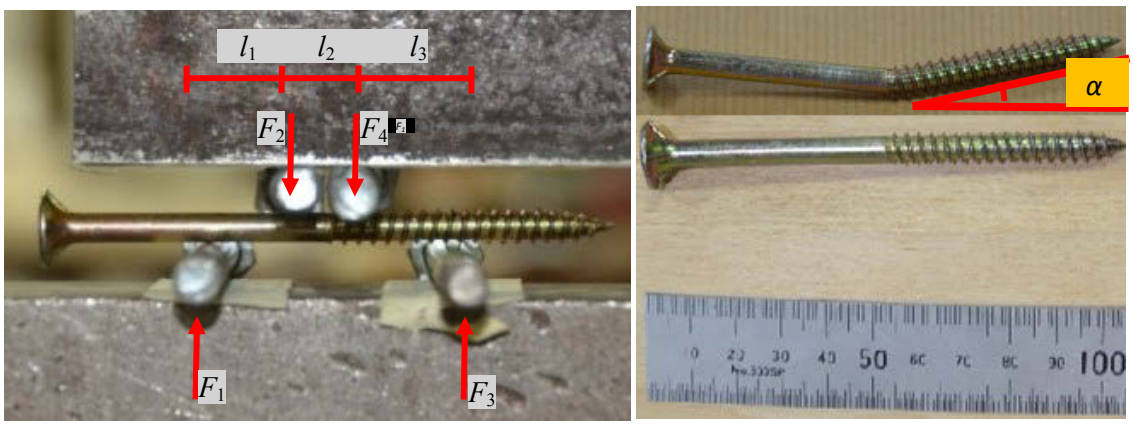

Figure D-5 Test configuration of four point bending test and bent screw

Table D-2 Characteristic yield moment of normal wood screw

Specimen	F(N)	l_1 and l_3 (mm)	$M_{y,Rk}$ (N.mm)	$M_{y,Rk}$(N.mm) (Eurocode 5)
specimen 1	567.5	15	17025	-
specimen 2	637.5	15	19125	-
specimen 3	587.5	15	17640	-
Mean	597.5		17930	18093.2
Σ	36.1		1079.6	
CoV(%)	6		6	
% Error(%)				0.9